

WL-TR-97-4054

**PROCEEDINGS OF THE 1996 USAF
AIRCRAFT STRUCTURAL INTEGRITY
PROGRAM CONFERENCE**



VOLUME I

ASIP

Gary K. Waggoner
WL/Materials Directorate
Wright-Patterson AFB, Ohio

John W. Lincoln
ASC/Deputy for Engineering
Wright-Patterson AFB, Ohio

James L. Rudd
WL/Flight Dynamics Directorate
Wright-Patterson AFB, Ohio

**USAF Aircraft Structural Integrity Program Conference
Hyatt Regency San Antonio
San Antonio, Texas**

June 1997

FINAL REPORT FOR PERIOD 3-5 DECEMBER 1996

Approved for public release; distribution unlimited

**MATERIALS DIRECTORATE
WRIGHT LABORATORY
AIR FORCE MATERIEL COMMAND
WRIGHT-PATTERSON AFB OH 45433-7734**

DTIC QUALITY INSPECTED 3

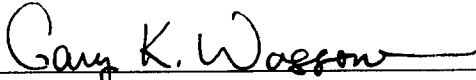
19970708 075

NOTICE

When government drawings, specifications, or other data are used for any purpose other than in connection with a definitely related government procurement operation, the United States Government thereby incurs no responsibility or any obligation whatsoever; and the fact that the government may have formulated, furnished, or in any way supplied the said drawings, specifications, or other data, is not to be regarded by implication or otherwise as in any manner licensing the holder or any other person or corporation, or conveying any rights or permission to manufacture use, or sell any patented invention that may in any way be related thereto.

This report has been reviewed by the Office of Public Affairs (ASC/PA) and is releasable to the National Technical Information Service (NTIS). At NTIS, it will be available to the general public, including foreign nationals.

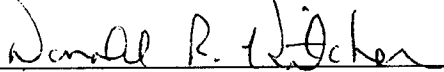
This technical report has been reviewed and is approved for publication.



GARY K. WAGGONER

Chief

Systems Support Division



DONALD R. KITCHEN

Acting Director

Materials Directorate

If your address has changed, if you wish to be removed from our mailing list, or if the addressee is no longer employed by your organization, please notify WL/MLS Bldg 652, 2179 Twelfth St Ste 1, Wright-Patterson AFB, Ohio 45433-7718 to help us maintain a current mailing list.

Copies of this report should not be returned unless return is required by security considerations, contractual obligations, or notice on a specific document.

REPORT DOCUMENTATION PAGE			Form Approved OMB No. 0704-0188	
Public reporting burden for this collection of information is estimated to average 1 hour per response, including the time for reviewing instructions, searching existing data sources, gathering and maintaining the data needed, and completing and reviewing the collection of information. Send comments regarding this burden estimate or any other aspect of this collection of information, including suggestions for reducing this burden, to Washington Headquarters Services, Directorate for Information Operations and Reports, 1215 Jefferson Davis Highway, Suite 1204, Arlington, VA 22202-4302, and to the Office of Management and Budget, Paperwork Reduction Project (0704-0188), Washington, DC 20503.				
1. AGENCY USE ONLY (Leave blank)		2. REPORT DATE June 1997	3. REPORT TYPE AND DATES COVERED Final, 3-5 December 1996	
4. TITLE AND SUBTITLE Proceedings of the 1996 USAF Aircraft Structural Integrity Program Conference, Volume I			5. FUNDING NUMBERS PE 62102F PR 4349 TA LA WU BR	
6. AUTHOR(S) 1-Gary K. Waggoner, Compiler & Editor; 2-John W. Lincoln, ASC/ENF; and 3-James L. Rudd, WL/FIB, Editors				
7. PERFORMING ORGANIZATION NAME(S) AND ADDRESS(ES) 1-Materials Directorate and 3-Flight Dynamics Directorate, Wright Laboratory; 2-Aeronautical Systems Center, Deputy for Engineering, all three of the Air Force Materiel Command Wright-Patterson AFB OH 45433			8. PERFORMING ORGANIZATION REPORT NUMBER WL-TR-97-4054	
9. SPONSORING/MONITORING AGENCY NAME(S) AND ADDRESS(ES) Materials Directorate (POC: Gary Waggoner, WL/MLS, 937-255-2282) Wright Laboratory Air Force Materiel Command Wright-Patterson AFB OH 45433-7734			10. SPONSORING/MONITORING AGENCY REPORT NUMBER WL-TR-97-4054	
11. SUPPLEMENTARY NOTES Volume II - WL-TR-97-4055				
12a. DISTRIBUTION AVAILABILITY STATEMENT Approved for public release; distribution is unlimited.			12b. DISTRIBUTION CODE	
13. ABSTRACT (Maximum 200 words) This report contains the proceedings of the 1996 USAF Structural Integrity Program Conference held at the Hyatt Regency Hotel in San Antonio, Texas, from 3-5 December 1996. The conference, which was sponsored by the Aeronautical Systems Center's Engineering Directorate and the Wright Laboratory's Flight Dynamics and Materials Directorates, was hosted by the San Antonio Air Logistics Center Aircraft Directorate, Aircraft Structural Integrity Branch (SA-ALC/LADD). This conference, as in previous years, was held to permit experts in the field of structural integrity to communicate with each other and to exchange views on how to improve the structural integrity of military weapon systems. Sessions were primarily focused on analysis and testing, engine structural integrity, structural materials and inspections, structural repair, and force management. This year, as in previous years, our friends from outside the U.S. borders provided the audience with outstanding presentations on activities within their countries. It is anticipated this conference will include their contributions in the agenda of future meetings. This year, 18 countries were represented in the audience.				
14. SUBJECT TERMS			15. NUMBER OF PAGES 578	
			16. PRICE CODE	
17. SECURITY CLASSIFICATION OF REPORT UNCLASSIFIED	18. SECURITY CLASSIFICATION OF THIS PAGE UNCLASSIFIED	19. SECURITY CLASSIFICATION OF ABSTRACT UNCLASSIFIED	20. LIMITATION OF ABSTRACT SAR	

GENERAL INSTRUCTIONS FOR COMPLETING SF 298

The Report Documentation Page (RDP) is used in announcing and cataloging reports. It is important that this information be consistent with the rest of the report, particularly the cover and title page. Instructions for filling in each block of the form follow. It is important to *stay within the lines* to meet *optical scanning requirements*.

Block 1. Agency Use Only (Leave blank).

Block 2. Report Date. Full publication date including day, month, and year, if available (e.g. 1 Jan 88). Must cite at least the year.

Block 3. Type of Report and Dates Covered. State whether report is interim, final, etc. If applicable, enter inclusive report dates (e.g. 10 Jun 87 - 30 Jun 88).

Block 4. Title and Subtitle. A title is taken from the part of the report that provides the most meaningful and complete information. When a report is prepared in more than one volume, repeat the primary title, add volume number, and include subtitle for the specific volume. On classified documents enter the title classification in parentheses.

Block 5. Funding Numbers. To include contract and grant numbers; may include program element number(s), project number(s), task number(s), and work unit number(s). Use the following labels:

C - Contract	PR - Project
G - Grant	TA - Task
PE - Program Element	WU - Work Unit Accession No.

Block 6. Author(s). Name(s) of person(s) responsible for writing the report, performing the research, or credited with the content of the report. If editor or compiler, this should follow the name(s).

Block 7. Performing Organization Name(s) and Address(es). Self-explanatory.

Block 8. Performing Organization Report Number. Enter the unique alphanumeric report number(s) assigned by the organization performing the report.

Block 9. Sponsoring/Monitoring Agency Name(s) and Address(es). Self-explanatory.

Block 10. Sponsoring/Monitoring Agency Report Number. (If known)

Block 11. Supplementary Notes. Enter information not included elsewhere such as: Prepared in cooperation with....; Trans. of....; To be published in.... When a report is revised, include a statement whether the new report supersedes or supplements the older report.

Block 12a. Distribution/Availability Statement.

Denotes public availability or limitations. Cite any availability to the public. Enter additional limitations or special markings in all capitals (e.g. NOFORN, REL, ITAR).

DOD - See DoDD 5230.24, "Distribution Statements on Technical Documents."

DOE - See authorities.

NASA - See Handbook NHB 2200.2.

NTIS - Leave blank.

Block 12b. Distribution Code.

DOD - Leave blank.

DOE - Enter DOE distribution categories from the Standard Distribution for Unclassified Scientific and Technical Reports.

NASA - Leave blank.

NTIS - Leave blank.

Block 13. Abstract. Include a brief (*Maximum 200 words*) factual summary of the most significant information contained in the report.

Block 14. Subject Terms. Keywords or phrases identifying major subjects in the report.

Block 15. Number of Pages. Enter the total number of pages.

Block 16. Price Code. Enter appropriate price code (*NTIS only*).

Blocks 17. - 19. Security Classifications. Self-explanatory. Enter U.S. Security Classification in accordance with U.S. Security Regulations (i.e., UNCLASSIFIED). If form contains classified information, stamp classification on the top and bottom of the page.

Block 20. Limitation of Abstract. This block must be completed to assign a limitation to the abstract. Enter either UL (unlimited) or SAR (same as report). An entry in this block is necessary if the abstract is to be limited. If blank, the abstract is assumed to be unlimited.

TABLE OF CONTENTS

Volume I

	Page
FOREWORD	vii
AGENDA	ix
INTRODUCTION	xv
<u>SESSION I - OVERVIEWS</u>	
Economic Life Evaluation of the T-38-29 Wing	3
<i>H. Burnside and W. Wang</i>	
C-141 Systems and Structural Assessment Program	31
<i>H. Huggins, G. Weitz and R. Alford</i>	
Aging Aircraft Structures Database	63
<i>R. Perez and M. Van Dernoot</i>	
An Overview of the Wright Laboratory Structural Integrity of Aging Aircraft Core Area	85
<i>M. Zeigler, Capt J. Denney, C. Paul and L. Hutsell</i>	
Aging Aircraft Management - A Practical Analytical Approach for Effective Sustainment	109
<i>J. Cochran and R. Alford</i>	
F117-PW-100 Tailored ENSIP for Five Peacetime C-17 Missions	127
<i>S. Patel</i>	
ASIP and the Air Force Aging Aircraft Fleet	155
<i>R.N. Hadcock</i>	
<u>SESSION II - LIFE ENHANCEMENT</u>	
Material Characterization of Laser-Shock Peened Titanium for Turbine Engine Applications	179
<i>S. Thompson, J. Ruschau and T. Nicholas</i>	
The Effect of Laser Shock Peening (LSP) on Airfoil FOD and High Cycle Fatigue	205
<i>S. Mannava, W. Cowie and A. McDaniel</i>	
Evaluation of Shear Tears Found at Cold Expanded Holes in 7178-T6 Extrusions - KC-135 Laboratory Teardown Inspection	237
<i>E. Easterbrook and L. Reid</i>	

SESSION III - REPAIR

Composite Patch Repairs of Cracked Metal Structures: Effects of Adhesive Nonlinearity, Thermal Cycling and Debonding	249
<i>W. Chow and S. Atluri</i>	
Repair Substantiation Fatigue Testing Including Temperature and Frequency Effects for a Bonded Composite Repair to an F-111 Lower Wing Skin.....	291
<i>K. Walker and R. Boykett</i>	
The Probabilistic Assessment of Aircraft Subjected to Widespread Fatigue Damage	305
<i>M.C. Shiao, J. Bakuckas Jr., and C. Bigelow</i>	
Experimental Verification of Rose's Constant K Solution in Bonded Crack Patching	319
<i>R. Muller, R. Fredell, J. Dally and C. Guijt</i>	

SESSION IV - CORROSION/FATIGUE

Prediction of the Intergranular Corrosion/Fatigue Interaction Effect in Thin-Webbed Stiffening Members	337
<i>R. Bush, A. Hinkle, R. Bucci and M. Kulak</i>	
Advantageous Applications of Bonded Repairs for Corrosion Damage	359
<i>A. Kerr</i>	
Damage Tolerance Implications of Corrosion Pillowing on Fuselage Lap Joints	383
<i>N. Bellinger and J. Komorowski</i>	
Full Scale AV-8B Wing Test with Known Delaminations	411
<i>T. Hullander</i>	
GLARE®, Reducing Weight and Improving Structural Integrity	467
<i>J. Gunnink and B. Voegesang</i>	
An Experimental Evaluation of Fatigue Crack Growth Prediction Models	477
<i>L. Lazzeri and A. Salvetti</i>	
Lower Wing Disassembly and Inspection Results of Two High Time USAF B707 Aircraft	509
<i>J. Luzar and A. Hug</i>	
Thoughts on Risk Analysis of an Aging Aircraft.....	529
<i>R.P. Bell, K.M. Jones and R.E. Alford</i>	

Volume II

SESSION V - DYNAMICS/MECSIP

Risk Analysis of Fatigue Cracking in IAF F-16 Aircraft	559
<i>R. Halevi, J. Weihs, H. Cohen and D. Bar-Shalom</i>	
Sonic Fatigue - A Problem Requiring Special Handling	597
<i>T. Beier</i>	
Application of the MECSIP Process to the B-2 Ground Refueling System	613
<i>E. Wells</i>	

SESSION VI - WIDESPREAD FATIGUE DAMAGE

Controlling Multi-Site Damage by Means of Design and Inspection Trade-offs	641
<i>A. Brot</i>	
Analysis of Stiffened Panels with Multiple Site Damage	655
<i>M. Heinimann, H. Wang and A. Grandt Jr.</i>	
A Proposed Engineering Approach to Assessing the Residual Strength of Aircraft Containing a Lead Crack Interacting with Multiple Site Damage	683
<i>G. Chell, M. Ferrell, R. McClung and S. Hudak Jr.</i>	
Enhanced Repair Assessment Procedure and Integrated Design (RAPID)	711
<i>M. Shaio, J. Bakuckas Jr., and C. Bigelow</i>	
The Onset of Multiple Site Damage and Widespread Fatigue Damage in Aging Airplanes	729
<i>D. Jeong and P. Tong</i>	

SESSION VII - ENGINES

A Probabilistic Approach to Aircraft Turbine Rotor Material Design	753
<i>G. Leverant, D. Littlefield, R. McClung, H. Hillwater and J. Wu</i>	
Engine Health Monitoring System for Gas Turbine Engines	793
<i>M. Roemer</i>	
The Role of Residual Stress in Low Cycle Fatigue of Gas Turbine Engine Disks	807
<i>E. Bradley, S. Berkley and R. Fairbanks</i>	
Quantification of Process Margin for Robust Engine Components	825
<i>P. Domas and H. Popp</i>	
Structural Integrity of Composite Containment Structures	837
<i>C. Chamis and P. Gotsis</i>	
A Probabilistic Life Method for a Two-Lobed Turbine Disk Attachment	867
<i>C. Date, C. Balis, D. Greving, J. Musgrave, D. Langefels and K. Richardson</i>	
PT6A-68 JPATS Engine Structural Integrity Program	879
<i>B. Wilkinson</i>	
The Future Direction and Development of Engine Health Monitoring (EHM) Within the United States Air Force	901
<i>Sqn Ldr A.J. Green</i>	

SESSION VIII - NDE/I

Computer Monitored Shot Peening, An Update	913
<i>J.R. Harrison</i>	
Freeze-Frame Imaging of Operating Turbine Engines Using Synchronous Multiplane Tomography (SMT)	917
<i>T. Kirchner and P. Burstein</i>	
Orthogonal-Axis Eddy Current Probes for High Sensitivity/High Productivity Inspection of Aircraft Structure	931
<i>G. Burkhardt, J. Fisher, J. Stolte, S. Kramer and K. Cobble</i>	
Eddy Current Inspection of Engine Blade Slots	951
<i>W. Hoppe</i>	

SESSION IX - FORCE MANAGEMENT

F-14 Fatigue Tracking	983
<i>R. Dalrymple, T. Fallon and T. Chappell</i>	
Achieving an Integrated Usage Based Maintenance Program for the Canadian Forces C-130	1003
<i>T. Padfield, A. McCray and Capt A. van den Hoeven</i>	
Aging Aircraft Usage Monitoring in the Royal Australian Air Force	1025
<i>Sqd Ldr M. Wilkin</i>	
A Review of a Strain and Flight Parameter Data Based Aircraft Fatigue Usage Monitoring System	1035
<i>L. Molent</i>	
ATTENDANCE LIST	1055

FOREWORD

This report was compiled by the Systems Support Division, Materials Directorate, Wright Laboratory, Wright-Patterson Air Force Base, Ohio. It was initiated under Task 24180704 "Corrosion Control & Failure Analysis" with Gary K. Waggoner as the Project Engineer.

This technical report was submitted by the editors.

The purpose of this 1996 Conference was to bring together technical personnel in DoD and the aerospace industry who are involved in the various technologies required to ensure the structural integrity of aircraft gas turbine engines, airframes and other mechanical systems. It provided a forum to exchange ideas and share new information relating to the critical aspects of durability and damage tolerance technology for aircraft systems. The conference was sponsored by the Air Force Materiel Command (AFMC), Aeronautical Systems Center, Deputy for Engineering and Materials and Flight Dynamics Directorates of the Wright Laboratory, Wright-Patterson Air Force Base, Ohio. It was hosted and co-sponsored by the Aircraft Structural Integrity Branch, Aircraft Directorate of AFMC's San Antonio Air Logistics Center, Kelly Air Force Base, Texas.

1996 USAF Aircraft Structural Integrity Program Conference

AGENDA

MONDAY, 2 DECEMBER 1996

5:00 PM - 7:00 PM PRE-REGISTRATION

TUESDAY, 3 DECEMBER 1996

7:30 AM - 5:30 PM REGISTRATION

7:30 AM - 8:15 AM CONTINENTAL BREAKFAST

8:15 AM - 8:30 AM OPENING COMMENTS
J. Lincoln, ASC/EN

SESSION I - OVERVIEWS

Chairman - *J. Rudd, WL/FIB*

8:30 AM - 9:00 AM Economic Life Evaluation of the T-38-29 Wing
H. Burnside and W. Wang
Southwest Research Institute
Jon Dubke
SA-ALC

9:00 AM - 9:30 AM Systems and Structural Assessment Program
H. Huggins and G. Weitz
Lockheed Martin, Marietta, GA
R. Alford
WR-ALC/LJLEA, Robins Air Force Base, GA

9:30 AM - 10:00 AM Aging Aircraft Structures Database
R. Perez and M. Van Dernoot
McDonnell Douglas Aerospace, St. Louis, MO

10:00 AM - 10:30 AM REFRESHMENT BREAK

10:30 AM - 11:00 AM An Overview of the Wright Laboratory Structural Integrity of
Aging Aircraft Core Area
M. Zeigler, Capt J. Denney, C. Paul and L. Hutsell
WL/FIB, Wright-Patterson AFB, OH

11:00 AM - 11:30 AM Aging Aircraft Management - A Practical Analytical Approach for
Effective Sustainment
J. Cochran
Lockheed Martin Aeronautical Systems Company, Marietta, GA
R. Alford
WL-ALC/LJLE, Robins Air Force Base, GA

11:30 AM - 12:00 PM F117-PW-100 Tailored ENSIP for Five Peacetime C-17 Missions
S. Patel
Pratt & Whitney, East Hartford, CT

12:00 PM - 1:30 PM LUNCH AND PRESENTATION
ASIP and the Air Force Aging Aircraft Fleet
R.N. Hadcock
RNH Associates, Huntington, NY

SESSION II - LIFE ENHANCEMENT

Chairman - *C. Harris*, NASA/LRC

1:30 PM - 2:00 PM Material Characterization of Laser-Shock Peened Titanium for
Turbine Engine Applications

S. Thompson

WL/MLSE, Wright-Patterson AFB, OH

J. Ruschau

University of Dayton Research Institute

T. Nicholas

WL/MLLN, Wright-Patterson AFB, OH

2:00 PM - 2:30 PM The Effect of Laser Shock Peening (LSP) on Airfoil FOD and High
Cycle Fatigue

S. Mannava, W. Cowie and A. McDaniel

GE Aircraft Engines, Cincinnati, OH

2:30 PM - 3:00 PM Evaluation of Shear Tears Found at Cold Expanded Holes in
7178-T6 Extrusions - KC-135 Laboratory Teardown Inspection

E. Easterbrook and L. Reid

Fatigue Technology Inc., Seattle, WA

3:00 PM - 3:30 PM REFRESHMENT BREAK

SESSION III - REPAIR

Chairman - *G. Waggoner*, WL/MLS

3:30 PM - 4:00 PM Composite Patch Repairs of Cracked Metal Structures: Effects of
Adhesive Nonlinearity, Thermal Cycling and Debonding

W. Chow and S. Atluri

Georgia Institute of Technology, Atlanta, GA

4:00 PM - 4:30 PM Repair Substantiation Fatigue Testing Including Temperature and
Frequency Effects for a Bonded Composite Repair to an F-111
Lower Wing Skin

K. Walker and R. Boykett

Aeronautical and Maritime Research Laboratory, Australia

- 4:30 PM - 5:00 PM The Probabilistic Assessment of Aircraft Subjected to Widespread Fatigue Damage
M.C. Shiao
 Galaxy Scientific Corporation
J. Bakuckas Jr. and C. Bigelow
 Federal Aviation Administration, William J. Hughes Technical Center, Atlantic City International Airport, NJ
- 5:00 PM - 5:30 PM Experimental Verification of Rose's Constant K Solution in Bonded Crack Patching
R. Muller, R. Fredell J. Dally, and C. Guijt
 United States Air Force Academy
- 6:00 PM - 7:30 PM RECEPTION

WEDNESDAY, 4 DECEMBER 1996

- 7:30 AM - 5:30 PM REGISTRATION
- 7:30 AM - 8:00 AM CONTINENTAL BREAKFAST

SESSION IV - CORROSION/FATIGUE

Chairman - *D. Nieser*, OC-ALC/LACRA

- 8:00 AM - 8:30 AM Prediction of the Intergranular Corrosion/Fatigue Interaction Effect in Thin-Webbed Stiffening Members
R. Bush, A. Hinkle, R. Bucci and M. Kulak
 Aluminum Company of America, Alcoa Center, PA
- 8:30 AM - 9:00 AM Advantageous Application of Bonded Repairs for Corrosion Damage
A. Kerr
 Advanced Repair Technology International, Ft. Worth, TX
- 9:00 AM - 9:30 AM Damage Tolerance Implications of Corrosion Pillowing on Fuselage Lap Joints
N. Bellinger and J. Komorowski
 National Research Council Canada, Ottawa, Canada
- 9:30 AM - 10:00 AM Full Scale AV-8B Wing Test with Known Delaminations
T. Hullander
 National Aviation Depot, Cherry Point, NC
- 10:00 AM - 10:30 AM REFRESHMENT BREAK
- 10:30 AM - 11:00 AM GLARE®, Reducing Weight and Improving Structural Integrity
J. Gunnink
 Structural Laminates Company, Delft, The Netherlands
B. Voegesang
 Delft University of Technology, The Netherlands

11:00 AM - 11:30 AM An Experimental Evaluation of Fatigue Crack Growth Prediction Models
L. Lazzeri and A. Salvetti
University of Pisa, Pisa, Italy

11:30 AM - 12:00 PM Lower Wing Disassembly and Inspection Results of Two High Time USAF B707 Aircraft
J. Luzar and A. Hug
Boeing Defense & Space Group - Product Support Division, Wichita, KS

12:00 PM - 1:30 PM LUNCH AND PRESENTATION
Thoughts on Risk Analysis of an Aging Aircraft
R.P. Bell and K.M. Jones
Lockheed Martin Aeronautical Systems, Marietta, GA
R.E. Alford
WR-ALC/LJLE, Robins Air Force Base, GA

SESSION V - DYNAMICS/MECSIP

Chairman - *K. Leikach*, Naval Air Systems Command

1:30 PM - 2:00 PM Risk Analysis of Fatigue Cracking in IAF F-16 Aircraft
R. Halevi, J. Weihs, H. Cohen and D. Bar-Shalom
Israel Air Force

2:00 PM - 2:30 PM Sonic Fatigue - A Problem Requiring Special Handling
T. Beier
McDonnell Douglas Corporation, St. Louis, MO

2:30 PM - 3:00 PM Application of the MECSIP Process to the B-2 Ground Refueling System
E. Wells
ASC/YSDF, Wright-Patterson AFB, OH

3:00 PM - 3:30 PM REFRESHMENT BREAK

SESSION VI - WIDESPREAD FATIGUE DAMAGE

Chairman - *T. Swift*, FAA

3:30 PM - 4:00 PM Controlling Multi-Site Damage by Means of Design and Inspection Trade-offs
A. Brot
Israel Aircraft Industries, Ben-Gurion Airport, Israel

4:00 PM - 4:30 PM Analysis of Stiffened Panels with Multiple Site Damage
M. Heinemann, H. Wang and A. Grandt, Jr.
Purdue University, West Lafayette, IN

- 4:30 PM - 5:00 PM A Proposed Engineering Approach to Assessing the Residual Strength of Aircraft Containing a Lead Crack Interacting with Multiple Site Damage
G. Chell, M. Ferrell, R. McClung and S. Hudak, Jr.
Southwest Research Institute, San Antonio, TX
- 5:00 PM - 5:30 PM Enhanced Repair Assessment Procedure and Integrated Design (RAPID)
M. Shaio, J. Bakuckas Jr., and C. Bigelow
Federal Aviation Administration, William J. Hughes Technical Center, Atlantic City International Airport, NJ
- 5:30 PM - 6:00 PM The Onset of Multiple Site Damage and Widespread Fatigue Damage in Aging Airplanes
D. Jeong
U.S. Department of Transportation, Volpe National Transportation, Cambridge, MA
P. Tong
The Hong Kong University of Science and Technology, Hong Kong
- 7:30 PM - 9:00 PM Open Session on NASGRO Development
R. Forman
NASA Johnson Space Center, Houston, TX

THURSDAY, 5 DECEMBER 1996

7:30 AM - 5:30 PM REGISTRATION

7:30 AM - 8:00 AM CONTINENTAL BREAKFAST

SESSION VII - ENGINES

Chairman - *C. Pomfret*, RAF (Retired)

- 8:00 AM - 8:30 AM A Probabilistic Approach to Aircraft Turbine Rotor Material Design
G. Leverant, D. Littlefield, R. McClung, H. Hillwater and J. Wu
Southwest Research Institute, San Antonio, TX
- 8:30 AM - 9:00 AM Engine Health Monitoring System for Gas Turbine Engines
M. Roemer
Stress Technology Incorporated, Rochester, NY
- 9:00 AM - 9:30 AM The Role of Residual Stress in Low Cycle Fatigue of Gas Turbine Engine Disks
E. Bradley and S. Berkley
Fatigue Management Associates LLC, Jupiter, FL
R. Fairbanks
United Airlines, San Francisco, CA

9:30 AM - 10:00 AM	Quantification of Process Margin for Robust Engine Components <i>P. Domas and H. Popp</i> GE Aircraft Engines, General Electric Company, Cincinnati, OH
10:00 AM - 10:30 AM	REFRESHMENT BREAK
10:30 AM - 11:00 AM	Structural Integrity of Composite Containment Structures <i>C. Chamis and P. Gotsis</i> NASA Lewis Research Center, Cleveland, OH
11:00 AM - 11:30 AM	A Probabilistic Life Method for a Two-Lobed Turbine Disk Attachment <i>C. Date, C. Balis, D. Gréving, J. Musgrave, D. Langefels and K. Richardson</i> AlliedSignal Engines, Phoenix, AZ
11:30 AM - 12:00 PM	PT6A-68 JPATS Engine Structural Integrity Program <i>B. Wilkinson</i> Pratt & Whitney Canada, Longueuil, Quebec
12:00 PM - 1:30 PM	LUNCH AND PRESENTATION The Future Direction and Development of Engine Health Monitoring (EHM) Within the United States Air Force <i>Sqn Ldr A.J. Green</i> WL/POTC, Wright-Patterson AFB, OH
SESSION VIII - NDE/I Chairman - <i>R. Paglia</i> , AF NDI Program Office, WL/MLS-OL	
1:30 PM - 2:00 PM	Computer Monitored Shot Peening, An Update <i>J.R. Harrison</i> Metal Improvement Co., Inc.
2:00 PM - 2:30 PM	Freeze-Frame Imaging of Operating Turbine Engines Using Synchronous Multiplane Tomography (SMT) <i>T. Kirchner and P. Burstein</i> Foster Miller, Inc., Waltham, MA
2:30 PM - 3:00 PM	Orthogonal-Axis Eddy Current Probes for High Sensitivity/High Productivity Inspection of Aircraft Structure <i>G. Burkhardt, J. Fisher and J. Stolte</i> Southwest Research Institute, San Antonio, TX <i>S. Kramer and K. Cobble</i> Raytheon E-Systems Aerospace Division, Greenville, TX
3:00 PM - 3:30 PM	REFRESHMENT BREAK

3:30 PM - 4:00 PM Eddy Current Inspection of Engine Blade Slots
 W. Hoppe
 Systems Research Laboratories, Dayton, OH

SESSION IX - FORCE MANAGEMENT

Chairman - *J. Turner*, SA-ALC/LADD

4:00 PM - 4:30 PM F-14 Fatigue Tracking - Methodology and Lessons Learned
 R. Dalrymple and T. Fallon
 Naval Air Warfare Center, Aircraft Division, Warminster, PA
 T. Chappell
 SEMCOR, Inc., Arlington, VA

4:30 PM - 5:00 PM Achieving an Integrated Usage Based Maintenance Program for
 the Canadian Forces C-130
 T. Padfield and A. McCray
 CAE Aviation Ltd., Edmonton, Alberta, Canada
 Capt A. van den Hoeven
 NDHQ Ottawa, Canada

5:00 PM - 5:30 PM Aging Aircraft Usage Monitoring in the Royal Australian Air Force
 Sqd Ldr M. Wilkin
 Laverton, Victoria, Australia

5:30 PM - 6:00 PM A Review of a Strain and Flight Parameter Data Based Aircraft
 Fatigue Usage Monitoring System
 L. Molent
 Aeronautical and Maritime Research Laboratory, Melbourne,
 Victoria, Australia

EXHIBITORS

- ARTI/DYNCORP
- BOMBARDIER INC
- CSA ENGRG INC/BOEING/USAF
- FAA DEPT OF TRANS
- FATIGUE TECHNOLOGY INC
- GEORGIA TECH
- HQ USAFA/DFEM
- KARTA TECHNOLOGY INC
- MCDONNELL DOUGALS AERO
- MEASUREMENT SYS INC
- METAL IMPROVEMENT CO INC
- MOOG ESPRIT
- MTS SYSTEMS CORP
- NATIONAL TECHNICAL SYSTEMS
- NTIAC TRI
- SMITHS INDUSTRIES
- SOUTHWEST RESEARCH
- STRUCTURAL LAMINATES CO
- SYS & ELECTRONICS INC
- USAF/ANALYTICAL SERV & MATLS
- WEST COAST INDUSTRIES

INTRODUCTION

This report contains the proceedings of the 1996 USAF Structural Integrity Program Conference held at the Hyatt Regency San Antonio in San Antonio, Texas from 3-5 December 1996. The conference, which was sponsored by the Aeronautical Systems Center's Engineering Directorate and the Wright Laboratory's Flight Dynamics and Materials Directorates, was hosted and co-sponsored by the San Antonio Air Logistics Center Aircraft Directorate, Aircraft Structural Integrity Branch (SA-ALC/LADD). This conference, as in previous years, was held to permit experts in the field of structural integrity to communicate with each other and to exchange views on how to improve the structural integrity of military weapon systems. Sessions were primarily focused on life enhancement, repair, corrosion/fatigue, dynamics/MECSIP, widespread fatigue damage, engines, NDE/I, and force management. This year, as in previous years, our friends from outside the U.S. borders provided the audience with outstanding presentations on activities within their countries. It is anticipated that this conference will include their contributions in the agenda of future meetings. This year 18 countries, plus NATO, were represented in the audience.

The sponsors are indebted to their hosts for their support of the conference. The sponsors are also indebted to the speakers for their contributions. In particular, thanks are due to the three luncheon speakers for their informative presentations, Mr. R.N. Hadcock on ASIP and the Air Force Aging Aircraft Fleet; Messrs. R.P. Bell, K.M. Jones, and R.E. Alford on Thoughts on Risk Analysis of an Aging Aircraft; and Squadron Leader A.J. Green, on The Future Direction and Development of Engine Health Monitoring (EHM) Within the United States Air Force.

As usual, much of the success of the conference is due to the efforts of Jill Jennewine and her staff, including Lori Kilian and Esther Burnett, from Universal Technology Corporation. Their cooperation is greatly appreciated.

JOHN W. LINCOLN
ASC/ENF

GARY K. WAGGONER
WL/MLS

DONALD B. PAUL
WL/FIB

JIMMY TURNER
SA-ALC/LADD

SESSION I

OVERVIEWS

Chairman: *J. Rudd*, WL/FIB

Economic Life Evaluation of the T-38 -29 Wing

Dr. Hal Burnside*

Dr. Wei Wang

Southwest Research Institute

6220 Culebra Road

San Antonio, Texas 78238-5166

Mr. Jon Dubke

San Antonio Air Logistics Center

Bldg 179, 404 Greig Street

Kelly AFB, Texas 78241-5944

1.0 INTRODUCTION

For over 35 years the T-38 has been used by the United States Air Force (USAF) as an advanced fighter trainer. No other aircraft in aviation history has fulfilled this mission over such a long period of time. More remarkably, the USAF would like to fly the T-38 until the year 2020, and possibly beyond, and the T-38 is currently undergoing an upgrade to modernize its avionics. Not only is the future service time much longer than originally expected, but the training environments represent fighter missions that are more severe than that for which the T-38 was originally designed. This has required that the USAF maintain an active structural integrity program for the T-38. Reference 1 reviewed the development and evolution of the T-38 structure and addressed programs being undertaken by the USAF to ensure structural integrity over its remaining life.

As part of one such Air Force Structural Integrity Program (ASIP) initiative, the San Antonio Air Logistics Center (SA-ALC) in July 1993 initiated a durability test of the T-38 -29 wing with Southwest Research Institute (SwRI). The purpose of the test was to assess the -29 wing's long-term fatigue behavior in

meeting anticipated future fleet usage requirements. The wing was subjected to a loading spectrum that represented T-38 Euro-NATO Joint Jet Pilot Training (ENJJPT) usage flown at Sheppard Air Force Base during 1988 through 1991. That usage was thought to be representative of the new Specialized Undergraduate Pilot Training (SUPT) being utilized by the Air Education Training Command (AETC) to train its pilots. However, after a SUPT Flight Loads Data Recorder Program was completed in May 1994, the SUPT usage was proven to be more severe than the ENJJPT test spectrum.

During the durability test, periodic inspections were made in accordance with the Aircraft Scheduled Inspection and Maintenance Requirements (Technical Order (T.O.) 1T-38A-6) until the test was terminated at 26,500 test hours of ENJJPT usage. The durability test wing was then destructively torn down, and a complete analytical condition inspection (ACI) was performed. The predominate fatigue cracking in the wing lower skin fastener holes occurred outboard of Wing Station (WS) 64.8. Large wing skin cracks were also found in the milled pockets at WS 21.7 and 38.6 on the left and right wings.

The purpose of the effort described in this paper, documented in SwRI's engineering report for SA-ALC (Reference 2), was to assess the long-term economic life of the -29 wing and to predict future wing replacement rates. This economic life evaluation drew upon results from the completed -29 wing durability test and teardown inspection, existing durability and damage tolerance analyses, aircraft usage surveys, and a coupon test program (Reference 3) that evaluated fatigue life issues associated with coldworking -29 wing skin fastener holes.

2.0 EVALUATION OF WING TEARDOWN RESULTS

Statistical Analysis Rotoscan/Eddy-Current Indications Found During Test

During the conduct of the wing durability test, certain wing fastener holes were periodically inspected by rotoSCAN and eddy-current. The holes were assigned to six inspection areas, designated per T.O. 1T-38A-6, as shown in Figure 1. Table 1 lists the number of holes in each area and the initial inspection times and recurring inspection intervals. The procedure per T.O. 1T-38A-36 was to first inspect the hole by rotoSCAN, and if an indication was found, the fastener was removed and a bolt-hole eddy-current inspection was performed. If the bolt-hole eddy-current inspection confirmed the rotoSCAN finding, the fastener hole was

reamed until the indication was removed, and an oversize fastener was installed. Table 1 summarizes the confirmed roscan/eddy-current indications initially found in each area during the test, and the number of repeat indications, i.e., the number of indications found in subsequent periodic inspections after the holes were reworked.

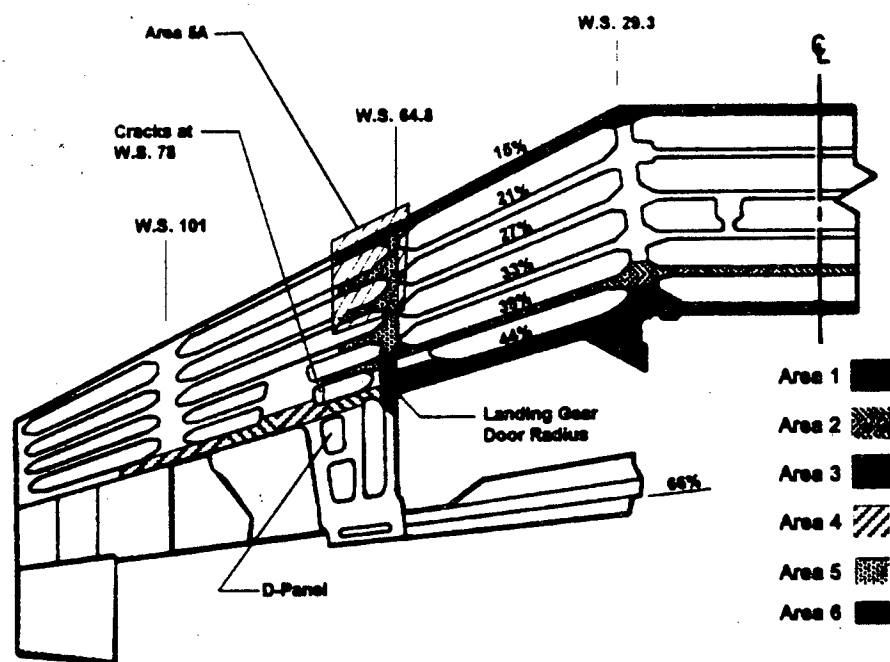


Figure 1. T.O. 1T-38A-6 Inspection Areas

As shown in Table 1, Areas 1-4 and Area 6, consisting of 550 fastener holes, had only a total of five confirmed indications found during the conduct of the test. Area 5, consisting of 160 fastener holes, had a total of 52 confirmed indications. Because of the large number of confirmed indications found in Area 5 after the second inspection at 15,000 flight hours, SA-ALC and SwRI divided Area 5 into two areas (5A and 5B) for inspection purposes. Area 5A was then subsequently inspected every 500 flight hours, and Area 5B continued to be inspected at 7,000 flight hours intervals. As indicated in Figure 1, holes in Area 3 on the 15% spar outboard of WS 64.8 were reassigned to Area 5A.

Table 1. Confirmed Indications by Rotoscan/Eddy-Current

Area	Inspection Times (Hrs) (Initial/Recurring)	Number of Holes (Right + Left)	Number of Initial Indications	Number of Repeat Indications
1	9,000/2,000	158	0	0
2	10,000/4,000	150	0	0
3	5,000/3,000	164	1	0
4	6,000/4,000	86	3	1
5A	8,000/7,000 (500*)	90	43	22
5B	8,000/7,000	70	9	0
6	6,000/500	16	1	0
Total		710	57	23

*Subsequently reduced to 500 hours

A Weibull evaluation of the rotoscan/eddy-current indications found during the durability test was performed to provide an estimate of the number of fastener holes projected to experience fatigue cracking as a function of flight hours. The small number (5 total) of indications in Areas 1-4 and Area 6 precluded obtaining any reliable statistical results from those areas. Therefore, the analysis was confined to Area 5. Furthermore, in Area 5B, eight of the nine initial indications were found at the 22,000 (15,000+7,000) flight hour inspection, and the other indication was found at the 15,000 hour inspection. Because of the uncertainty when the cracks in Area 5B actually occurred, it was decided to limit the statistical analysis to Area 5A which had a shorter (500 hour) inspection interval.

Area 5A has 90 fastener holes, and Figure 2 shows the cumulative distribution of confirmed indications plotted on Weibull probability scale. The straight line was fitted, by eye, to the Area 5A data points after 15,000 hours. The data points before 15,000 hours were included in estimating the cumulative probability, but the recorded times-to-indication were not used directly in fitting the equation. The reason was that had the inspections been performed more frequently (e.g., every 500 hours) before the 8,000 and 15,000 hour inspection

times, the times-to-indication would have been shorter than recorded.

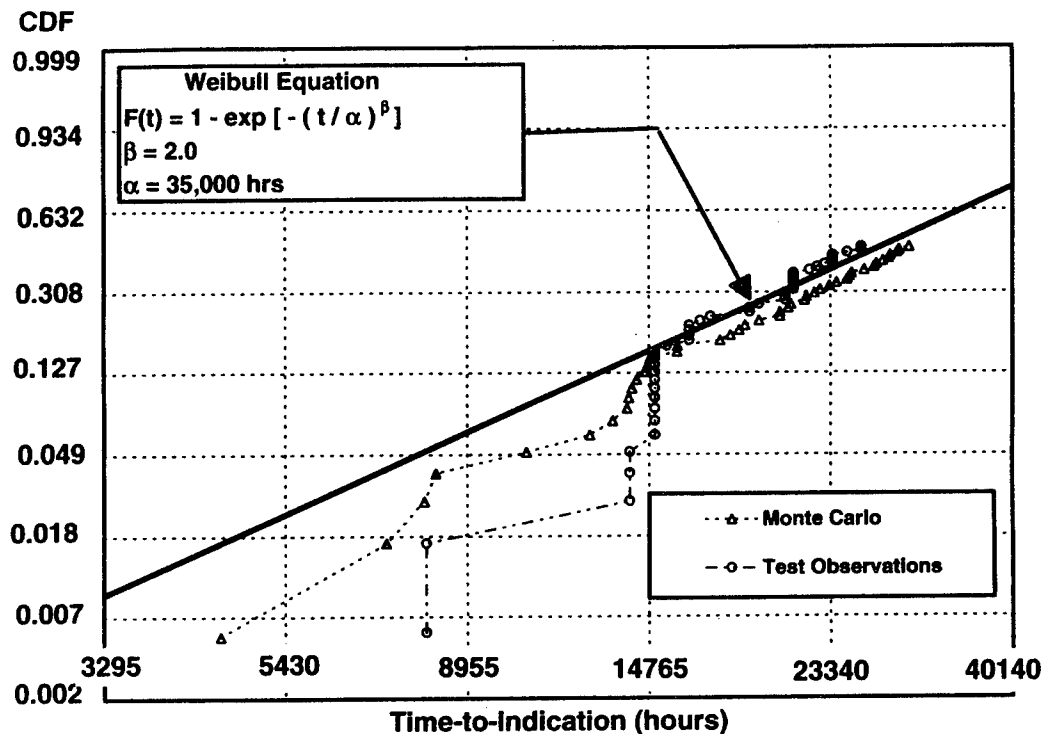
From the straight line fit of the test data given by circles in Figure 2, the Weibull equation for the cumulative probability, $F(t)$, of having a confirmed indication is

$$F(t) = 1 - \exp(-(t/\eta)^\beta) \quad (1)$$

where t = time-to-indication

$\beta = 2.0$ (shape parameter, slope of straight line)

$\eta = 35,000$ hours (characteristic life)



**Figure 2. Comparison of Inspection Data in Area 5A
with 5A Monte Carlo Simulation Results**

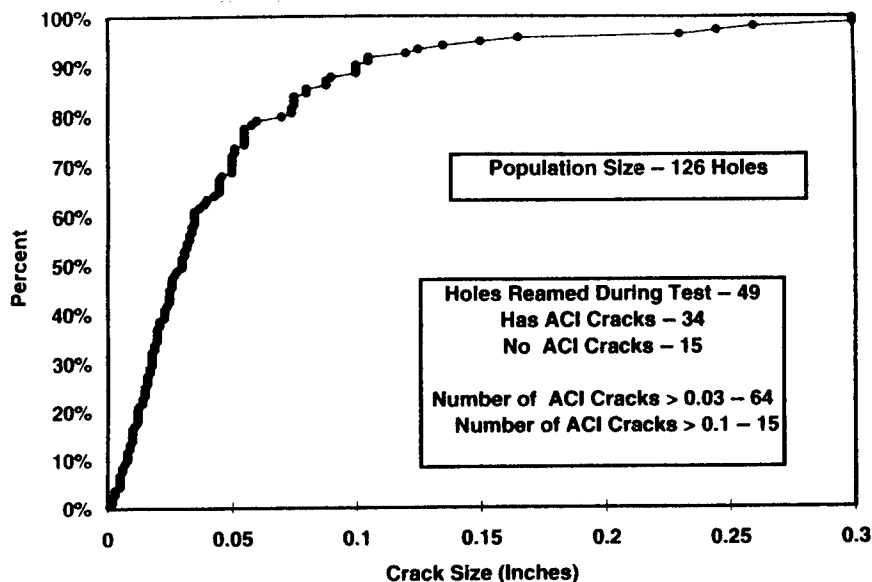
Reference 4 indicates that $1.0 < \beta < 4.0$ implies an early wear-out and that many mechanical failure modes are in this class. The characteristic life is the life at

which the model predicts that 63.2 percent of the holes in Area 5A would have confirmed indications. The above Weibull model can be used to project the number of holes having indications by multiplying the cumulative probability by the total number of holes in the population (i.e., 90 holes in Area 5A for one T-38 wing).

To validate the above Weibull model, particularly for time less than 15,000 flight hours, a Monte Carlo simulation was performed based on the Weibull probability distribution. The results of the simulations is also shown in Figure 2. Simulation results are shown as triangles, assuming continuous inspection (i.e., zero inspection intervals). As expected, there is a good agreement between the simulations and observations for time greater than 15,000 hours. For time less than 15,000 hours, there is a large difference between the simulations and observations. However, this difference is also to be expected since the plotted simulation data assumed zero inspection intervals. If the simulation-generated samples were "inspected" based on the actual inspection intervals used in the test, the simulation points occurred before the next inspection time would need to be shifted to the right to match the inspection time. After these adjustments, the agreement between the simulations and observations is good, thus confirming the validity of the Weibull model.

Flaw Size Distribution Found in Post-Test ACI

To support the economic life analysis to be performed in Section 4 for the wing lower skin, an evaluation was made of the distribution of crack sizes found during the post test ACI. Figure 3 shows the distribution for 126 fastener holes in the wing lower skin. This includes 49 holes that were reamed during the test, of which 34 holes still had fatigue cracks that were found during the ACI. The crack size refers to the radial depth of the crack. If more than one crack was found at a fastener hole, the dominant crack size was taken for the analysis. Figure 3 also shows that 64 cracks had a depth greater than 0.03 inch and 15 holes had cracks greater than 0.1 inch. An analysis was also made of the crack sizes found in the 95 holes that were not reamed. The distribution is quite similar to that shown in Figure 3. Forty-six holes had cracks greater than 0.03 inch in depth, and 12 holes had cracks greater than 0.1 inch.



**Figure 3. ACI Crack Size Distribution — Skin Cracks
Includes Unreamed and Reamed Holes**

3.0 FRACTURE MECHANICS CRACK GROWTH ANALYSES

The economic life assessment for the wing lower skin, as will be discussed in the next section, was based upon the cracking experience found in the -29 wing durability test and the service experience cracking found in aircraft flying the Lead-In Fighter (LIF) and Introduction to Fighter Fundamentals (IFF) usages. Because the durability test was conducted for ENJJPT usage, the test results had to be adjusted for other usages of interest. The economic life analysis also used the equivalent initial flaw size (EIFS) concept to establish a measure of manufacturing quality. Both the adjustment in usage and the EIFS analysis were made using fracture mechanics crack growth analyses. The remainder of this section summarizes the approach used in the crack growth analyses and the results.

Stress Spectra for Crack Growth Analyses

For the fracture mechanics crack growth analyses, stress spectra were needed at each fastener hole location where the analysis was conducted. This

includes stresses along each wing spar from about WS 60 to about WS 83. During the durability test, strain gages were located at the WS 64.8/15% and WS 64.8/21% spars and near the D-Panel. Using previously developed stress-to-load ratios, stress sequences for the crack growth analyses were created for these three strain gage locations. To compute the stresses at individual fastener holes, stress results from a coarse grid NASTRAN model were interpolated between neighboring grid points. Stress spectra for individual fastener holes were obtained by multiplying the stress spectra at one of the three gage locations that is closest to the hole with the stress scale factor for that hole (Reference 2).

Fracture Mechanics Models

Stress intensity factors (SIF) for the retardation and equivalent initial flaw size (EIFS) crack growth analyses were taken from the following sources:

- Corner Cracks: NASGRO SIF solutions for a straight hole with no countersink (Reference 5).
- Bore Cracks: SIF solutions from Newman and Raju (Reference 6).
- Countersunk Cracks: Corner crack solution compounded with a stress concentration factor (Reference 7).

The Forman crack growth equation with the modified Willenborg retardation model in the SUPERCRAKES computer program (Reference 8) was used for the crack growth analyses. Crack growth at one location was assumed not to be influenced by crack growth at any other locations.

Retardation Parameters for ENJJPT, SUPT and LIF/IFF Usages

Before the EIFS distribution could be established, an estimate of crack growth retardation for the ENJJPT test usage had to be made. The modified Willenborg retardation model was selected to be used for the crack growth analyses. The retardation parameter in the model was determined by matching crack growth predictions obtained using the SUPERCRAKES computer program with the coupon test results performed under ENJJPT usage in the accompanying test program (Reference 3). Similarly, coupon test results were used to establish the retardation parameters for the other usages of interest, and the parameters ranged between 2.7 and 3.0. Details regarding retardation can be found in Reference 2.

Determination of Equivalent Initial Flaw Sizes

The EIFS is not the actual manufacturing initial flaw size, but rather the initial flaw size which, if used in a fracture mechanics crack growth analysis, would result in the crack size found during the post-test ACI. Therefore, the candidate cracks for the EIFS analysis should reasonably be distributed over the area of interest. The candidate holes should not have been reamed during the test, as small cracks would have been removed by the reaming process. As a practical matter, cracks in the fastener holes should also be amenable to standard fracture mechanics analysis. This means that candidate holes should not contain multiple cracks or cracks with very large or small aspect ratios.

To meet the above criteria, 24 holes were ultimately selected for the EIFS analysis, including 12 bore cracks and 12 corner cracks. Countersunk cracks were not selected for the EIFS analyses, since there were very few countersunk cracks found in the ACI and no satisfactory retardation factors were found for the countersunk cracks. These 24 holes were reasonably spread over the wing area of interest, and therefore, the EIFS distributions should be representative of the wing.

A bore or a corner crack is characterized by two parameters: crack length c (radial dimension) and crack depth a (along the hole's axis). To determine the equivalent initial flaw sizes, c_0 , for an observed crack, the *actual* aspect ratio of the crack observed from the teardown inspection was assumed to remain constant during the growth of the crack. A trial initial crack size, c_0 , was selected, and the program SUPERCRAKES was used to grow the crack. If the observed crack size was reached at about 26,500 hours (the wing durability test time for ENJJPT usage), the trial c_0 was the desired initial size. Otherwise, a new c_0 was chosen, and the procedure was repeated until the correct c_0 was found.

Figure 4 is a histogram for the equivalent initial flaw lengths for the 24 holes that were analyzed. It can be seen that the distribution of the initial crack sizes for corner cracks and for bore cracks are quite similar. The best distribution fit of the data was found to be Weibull with parameters $\beta = 0.996$ and $\eta = 0.0061$. Since the slope, β , is essentially equal to unity, the distribution is exponential, a special case of the Weibull. In this case, the mean initial crack size is equal to $\eta = 0.0061$ inch. The solid line in Figure 5 shows the EIFS data plotted using a Weibull scale.

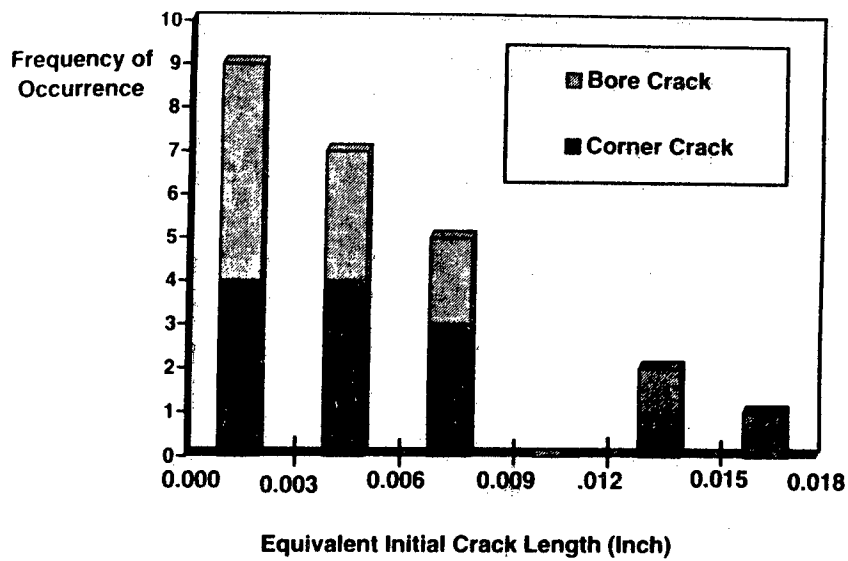


Figure 4. Histogram of Equivalent Initial Flaw Sizes

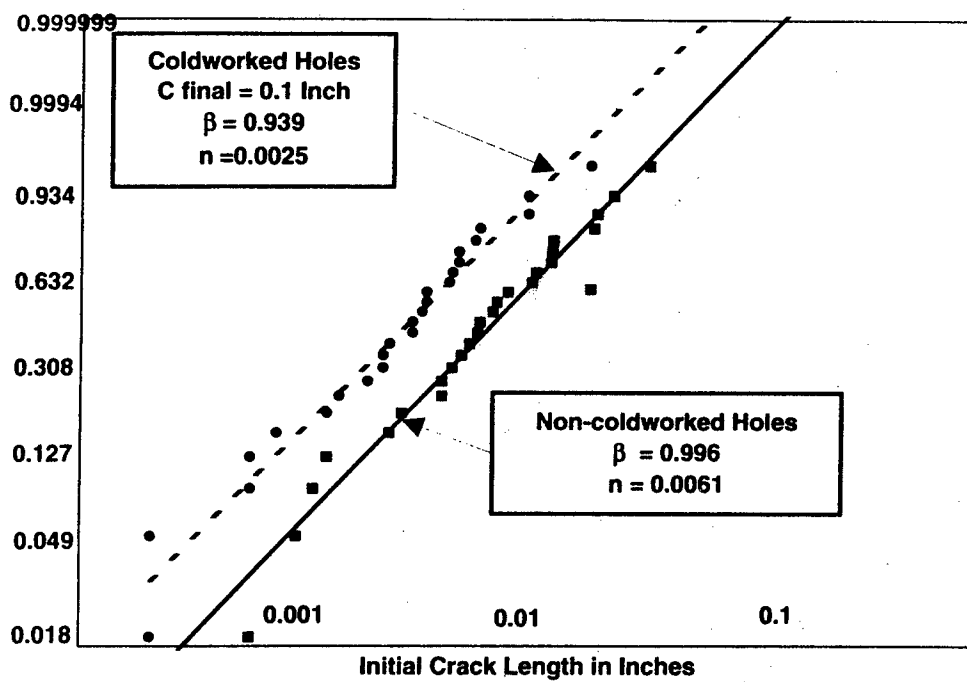


Figure 5. EIFS Weibull Distribution for Non-Coldworked and Coldworked Holes

Adjustment of Durability Test Results to Other Usages

All elements are now in place to conduct fracture mechanics analyses for the training usages of interest. Although the T-38 is currently flying the Introduction to Fighter Fundamentals (IFF) usage, the IFF usage spectrum, as measured from flight data recorders, was not yet available for the analyses. Therefore, the IFF and Lead-In Fighter (LIF) spectra were assumed to be the same in severity. Furthermore, the AETC anticipates flying a mixed SUPT and IFF usage in the future, and the mission mix was assumed to be 61% SUPT and 39% IFF. This usage is designated as MIXED SUPT/IFF.

Crack growth calculations were conducted at a variety of locations for the SUPT, ENJJPT, LIF/IFF and MIXED SUPT/IFF usages to obtain the time, in flight hours, required to grow a crack from its EIFS to the following two specified final sizes: (1) c (radial crack size) = 0.03 inch, and (2) c = the detectable size taken to be 0.1 inch. The ratios of mission severities were obtained by normalizing the crack growth to the SUPT usage, and it was observed that the ratios are reasonably constant for the various crack locations and for the two final crack sizes. Table 2 lists the mission severity ratios obtained. Table 2 also gives the ratios of mission severity for a crack in the wing skin at WS 38.6. These results will be used in Section 4 when wing skin cracking found in service is analyzed.

Table 2. Mission Flight Hour Ratios (Normalized to SUPT)

Usage	Fastener Holes	Milled Radii (WS 38.6)
SUPT	1.00	1.00
ENJJPT	1.30	1.90
LIF/IFF*	0.31	0.35
MIXED SUPT/IFF	0.60	0.64

*IFF = Introduction to Fighter Fundamentals. A new AETC usage, taken to be the same as LIF.

4.0 WING ECONOMIC LIFE EVALUATION

Background

To predict the economic life or durability of the wing for the various usages of interest (i.e., SUPT, ENJJPT, LIF/IFF and MIXED SUPT/IFF), the durability test results, as well as field cracking experience found in the LIF/IFF fleet at the WS 92.5/44% spar fastener holes and the WS 78 milled pocket radius in the lower wing skin, were considered. A number of -29 wings flying the LIF/IFF usage have been condemned because of cracking at the WS 92.5 and WS 78 locations.

The most recent predicted economic lives for the -29 wing are given in (Northrop Aircraft) NOR 77-19 (Reference 9). The economic lives were based on the time for a corner crack in the most critical fastener hole in the lower wing skin to grow from an equivalent initial flaw size of 0.0001 inch to a detectable crack size of 0.100 inch. The economic lives given in NOR 77-19 were: Air Training Command (ATC) Usage >50,000 hours; Lead-In Fighter (LIF) Usage: 8,100 hours; Dissimilar Air Combat Training (DACT) Usage: 10,800 hours.

Economic Life Criteria

It is first necessary to establish economic life criteria before the economic life of T-38 wings can be established. A general definition of economic life is quoted from MIL A-008866B, Paragraph 6.2.2 Economic Life, (Reference 10):

. . . . It will be assumed that the economic life of the test article has been attained with the occurrence of widespread damage which is uneconomical to repair and, if not repaired, could cause functional problems affecting operational readiness. This can be characterized by a rapid increase in the number of damage locations or repair costs as a function of cyclic test time.

The above definition of economic life is qualitative, and a more quantitative measure of economic life is needed. A multi-year program to develop durability methods was conducted from 1978-1984 under the direction of the Structures and Dynamics Division at Wright-Patterson Air Force Base. Results are documented in a nine volume report (Reference 11). This report provides some guidance in defining economic life as it pertains to the T-38 wing.

The economic (repair) limit has been defined as "...the most opportune time for economic repair or modification of the structure (e.g., the time when fastener hole oversizing should be accomplished)..."[Reference 12]. The economic repair limit for a fastener hole is reached when the largest radial crack in the hole reaches a size that can still be cleaned up by reaming the hole to the next fastener size (e.g., 0.030" - 0.050"). Since fatigue cracks frequently originate at fastener holes, this philosophy could be useful for defining durability damage limits during the design stage.

Fatigue cracks are also likely to originate at cutouts, radii and other structural discontinuities. However, there is no well defined criterion for the economic repair limit for such details.

For the T-38 -29 wing, it is SA-ALC's current policy to permit field maintenance to oversize a fastener hole by up to 1/16 inch (0.0625) without special disposition from SA-ALC engineering. This will remove a 0.03125 inch radial crack. Radial cracks larger than 0.03125 inch must be reviewed and, perhaps, analyzed on a case-by-case basis.

This 0.03125 inch radial crack size is consistent with that quoted above from the WP-AFB Durability Methods Development (Reference 11). Therefore, for the economic life evaluation, a 0.03 inch radial crack will be assumed as a lower bound. The upper bound will be taken as a 0.1 inch radial crack, which is the usual detectable crack size for a fastener hole and the size used in NOR 77-19 (Reference 9) for the original economic life evaluation of the -29 wing.

Economic Life Approach

Reference 11 evaluated two fracture mechanics based methods, the Deterministic Crack Growth Approach (DCGA) and the Probabilistic Crack Growth Approach (PCGA), for evaluating economic life. The DCGA was the method used in NOR 77-19 for the original economic life analyses of the -29 wing. One advantage the PCGA has over the DCGA is the ability to take into account the stochastic nature of initial manufacturing quality. Since an EIFS distribution was determined from the wing teardown, the PCGA is the method of choice for the T-38 wing. Table 3 summarizes the elements in the PCGA

procedure that was used to evaluate the economic life of the wing lower skin fastener holes.

Table 3. Probabilistic Crack Growth Analysis Implementation

PCGA Concepts	Implementation of PCGA Concept
Initial Fatigue Quality	<ul style="list-style-type: none"> ● Determine Equivalent Initial Flaw Size (EIFS) distribution from ACI and crack growth analyses.
Structural Damage Measure	<ul style="list-style-type: none"> ● Determine Mission Severity Ratios for SUPT, MIXED SUPT/IFF, IFF and ENJJPT usages. ● Set economic life criteria: <ul style="list-style-type: none"> – Lower Bound = 0.03 inch radial crack – Upper Bound = 0.1 inch radial crack ● Conduct crack growth analyses at EIFS locations. ● At each EIFS location, determine the initial crack sizes $c_i(t)$ to reach $c_f = 0.03$ and $c_f = 0.1$ as a function of flight hours.
Dominant Crack Population	<ul style="list-style-type: none"> ● Let the EIFS locations represent the 133 skin fastener holes believed to have fatigue cracks. (Found by ACI and/or reamed during test.)
Statistically Independent Cracks	<ul style="list-style-type: none"> ● Assume that crack growth at one location is not influenced by crack growth at an adjacent location.
Probabilistic Format	<ul style="list-style-type: none"> ● At each EIFS location determine the probability of an initial crack reaching $c_f = 0.03$ and $c_f = 0.1$ using the EIFS distribution. ● Conduct Monte Carlo simulations to determine the probability of the number of holes (i.e., 1, 2, 5, 10, 20,...) having cracks larger than $c_f = 0.03$ and $c_f = 0.1$.

Probabilistic Evaluation of Wing Skin Fastener Holes

Crack growth analyses were performed at the 24 EIFS locations plus five non-EIFS locations. The additional five fastener holes were included to represent the cracking experience found during the durability test and in the field at the D-

Panel and at WS 92.5/44% spar locations. At each location, analytical expressions were developed for $c_i(t)$ by fitting curves to the crack growth numerical results, where $c_i(t)$ is the initial crack size required to reach $c_f = 0.03$ or $c_f = 0.1$ at time t . All analyses were performed for SUPT usage since most of the T-38 fleet is currently flying SUPT. The time scales for mission hours were scaled for other usages according to the mission severity ratios shown in Table 2. From the Weibull EIFS distribution established in Section 3 and the $c_i(t)$ curves, it is possible to determine the probability of a crack at any one of the 29 fastener holes exceeding $c_f = 0.03$ and $c_f = 0.1$ as a function of flight hours.

The final step in the PCGA process involved determining the probability that more than a given number of holes (i.e., 1, 2, 5, 10, 20,...) have cracks larger than $c_f = 0.03$ or $c_f = 0.1$ inch. The population of crack sites was taken as the fatigue crack locations observed in the durability test. A fatigue crack location was assumed at either where a fatigue crack was found during the post-test ACI or where there was a confirmed roscan/eddy-current (and the hole was subsequently reamed) indication. A total of 133 fastener holes fall into these categories and, thus, the 29 analysis locations were mapped into the set of 133 holes based upon the similarity of the holes in location, size and expected stress field.

Using the model representing the 133 fastener holes, Monte Carlo simulations were conducted to determine the probability of the number of holes having cracks larger than $c_f = 0.03$ and $c_f = 0.1$. A sample size of 2000 was found to be adequate for the simulations. The dashed lines in Figure 6 shows the simulation results for the SUPT usage for $c_f > 0.1$ inch. A complete set of plots for all usages can be found in Reference 2. Probability curves for the ENJJPT, LIF/IFF and MIXED SUPT/IFF usages were obtained from the SUPT results by scaling the flight hours according to the usage severity ratios given in Table 2.

To use these probability curves for economic life predictions requires a definition of the economic life limit. For example, is the economic life of the wing reached when there are 30 fastener cracks reaching $c\{\text{Final}\} = 0.03$ inch? Or is the economic life of the wing reached when there are 15 fastener cracks reaching $c\{\text{Final}\} = 0.1$ inch? Obviously, to establish such economic life criteria requires: (1) knowledge of the T-38 wing structure, (2) past field and depot maintenance experience in repairing -29 wings with small (e.g., 0.03 inch) cracks and repairing/condemning wings with larger (e.g., 0.1 inch) cracks, and (3) the depot's and field's ability to provide the greater levels of engineering and maintenance support required when the number of cracks found in the wing increases. Once

the criterion is established, the appropriate probability curves in Figure 6 can be multiplied by the fleet size to obtain the wing replacement rates as a function of flight hours.

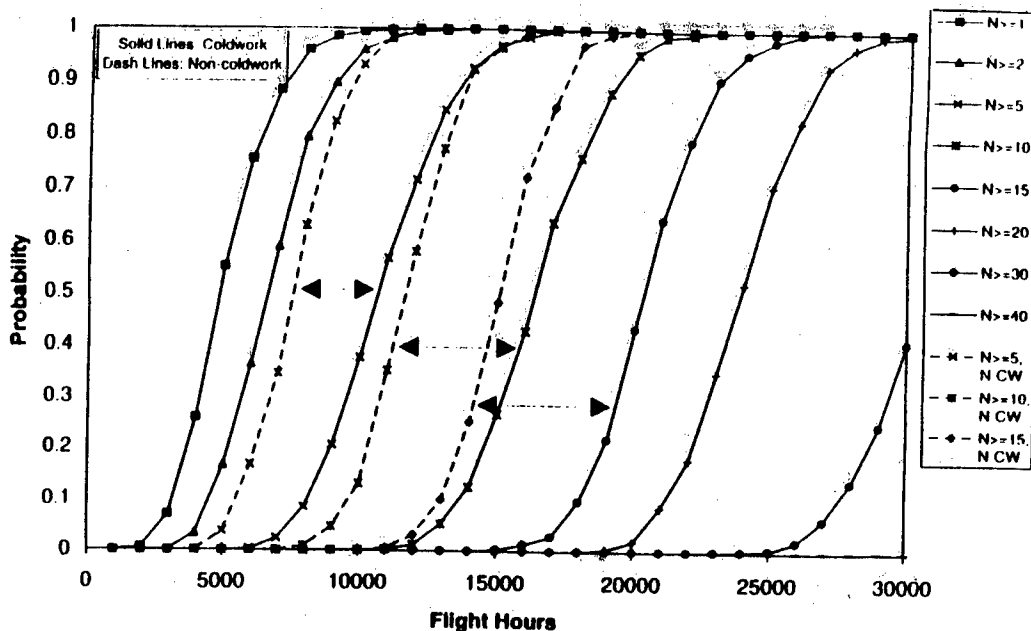


Figure 6. Probability that N or More Holes will have a Crack Greater Than 0.1 Inch for SUPT Usage (Arrows Illustrate Difference in Non-Coldworked and Coldworked Holes)

Validation of the Probabilistic Model

Using the ACI teardown results and the results of the periodic inspections performed during the durability test, it was possible to evaluate the validity of the probabilistic model. For example, Table 4 compares the probabilistic predictions with the cracking experience found in the wing durability test. The analytical predictions were adjusted for the ENJJPT test usage. The test and analytical predictions shown in the table compare favorably, especially if one considers that 49 fastener holes were reamed during the durability test, and cracks of unknown sizes were removed by the reaming process

Table 4. Comparison of Probabilistic Model Predictions with Durability Test Results

No. of Cracks Exceeding 0.03 (Durability Test ACI)	Avg. No. of Cracks Exceeding 0.03 (Predicted)
64	58
No. of Cracks Exceeding 0.1 (Durability Test ACI)	Avg. No. of Cracks Exceeding 0.1 (Predicted)
15	25

A second validation was made by comparing the probabilistic predictions with the crack indications found by roscan and eddy-current. The test data and the associated Weibull fit to those fastener holes that had to be reamed larger than 1/16 inch to remove a 0.03125 inch radial crack are re-plotted in Figure 7 along with Monte Carlo simulation results. The hole population used in the probabilistic analysis were the 52 holes in Area 5A that either has a confirmed crack found during the post-test ACI or a confirmed roscan/eddy-current indication. The simulation, adjusted for ENJJPT usage, shows the expected number of holes reaching 0.03 inch as a function of flight hours. Results are given in terms of the cumulative percent of the total population of 52 holes. The analytical predictions provide an upper bound to the test results. The analysis should bound the test results from above since not all the cracks could be found in an inspection.

Economic Life for Wing Skin Fastener Holes

After considerable discussion with SA-ALC personnel and evaluation of the wing durability test data, SwRI recommended that the economic life criteria for the wing skin fastener holes be taken as when there is a 50% probability that 15 fastener or more holes reach $c = 0.1$ inch. Therefore, the cumulative distribution function (CDF) corresponding to the $N \geq 15$ curve in Figure 6 was used for the economic life evaluation of the skin fastener holes without coldworking. For example at this 50% probability level ($P_r = 0.5$), Figure 6 indicates that the economic life for SUPT usage is 15,000 flight hours.

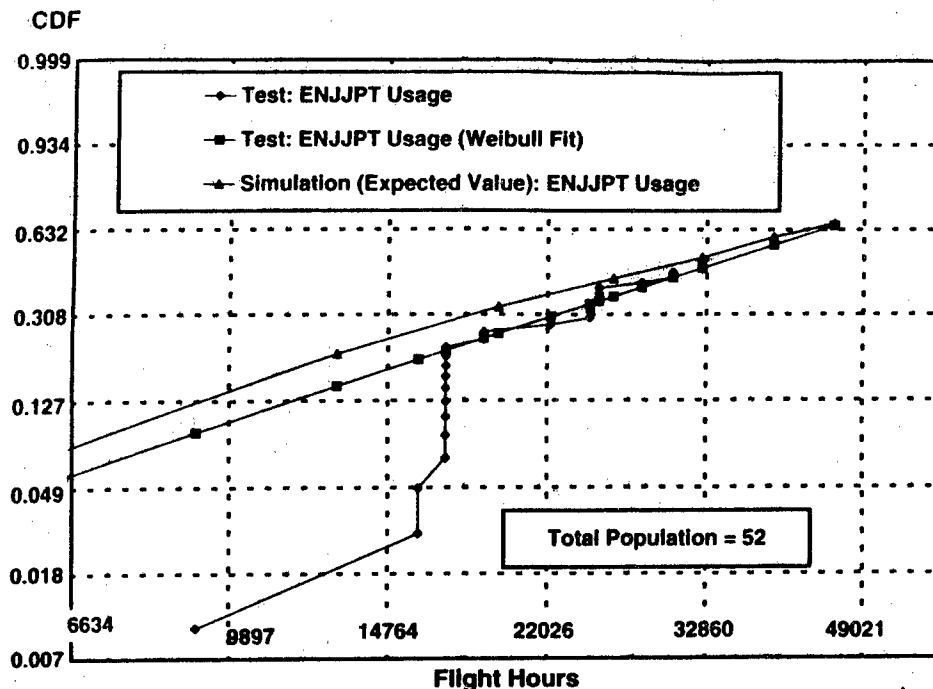


Figure 7. Comparison of Probabilistic Simulation with Durability Test Experience

Using curves similar to those in Figure 6 for $c = 0.03$ inch, the criterion for 15 or more wing skin fastener holes reaching $c = 0.1$ inch is approximately the same as 45 or more fastener holes reaching $c = 0.03$ inch. From Table 4, the number of cracks exceeding 0.03 and 0.1 inch in radial depth for the unreamed and reamed holes found during the durability test ACI was 64 and 15, respectively. Although the test was concluded at 26,500 ENJJPT flight hours, if the cracking experienced during the durability test had been found on a service wing, the wing would probably have been condemned before 26,500 flight hours. Using the mission severity ratios given in Table 2, 26,500 ENJJPT flight hours would be equivalent to about 20,000 SUPT hours. Therefore, the criteria of 15 holes having cracks greater than 0.1 inch, appears to be compatible with the wing durability test results.

Economic lives at the 50% probability level for the ENJJPT, LIF/IFF, and MIXED SUPT/IFF usages were obtained by scaling the SUPT life using the

mission flight hour ratios given in Table 2. These lives can be interpreted as the number of flight hours when 50% of the wings in the fleet would be expected to have to be replaced because of cracking in fastener holes similar to the hole cracking found from the -29 durability test.

Effect of Coldworking Selected Fastener Holes

SA-ALC plans to coldwork a number of the fastener holes outboard of WS 64.8 that experienced cracking in the wing durability test. One purpose of the T-38 Lower Wing Skin Coupon Test (Reference 3) was to quantify the effect on fatigue life of coldworking existing countersunk fastener holes. The results of that testing indicated that only about an 1.5 increase in fatigue life was obtained when existing countersunk fastener holes were coldworked. Effects of coldworking in the probabilistic analysis were accounted for by establishing a new EIFS distribution that would result in a 1.5 increase in fatigue life corresponding to a final crack size of 0.1 inch. The dashed line in Figure 5 shows the new EIFS distribution plotted on Weibull probability paper together with the non-coldworked distribution. The mean initial equivalent flaw size decreases to about 0.0025 inch for the coldworked holes.

The probabilistic simulations were re-conducted using the new EIFS distribution, and the results are shown as solid lines in Figure 6. The increase in life at the 50% probability level was 1.35 using the $c_f = 0.03$ inch criterion and 1.4 using the $c_f = 0.1$ inch criterion. The full 1.5 increase in life was not realized because not all of the fastener holes in the 133 hole analysis set were coldworked. Using the 50% probability level, the economic life for the coldworked wing skin under SUPT usage increases from 15,000 to 20,500 flight hours when the selected fastener holes are coldworked.

Inclusion of LIF/IFF Service Cracking Experience

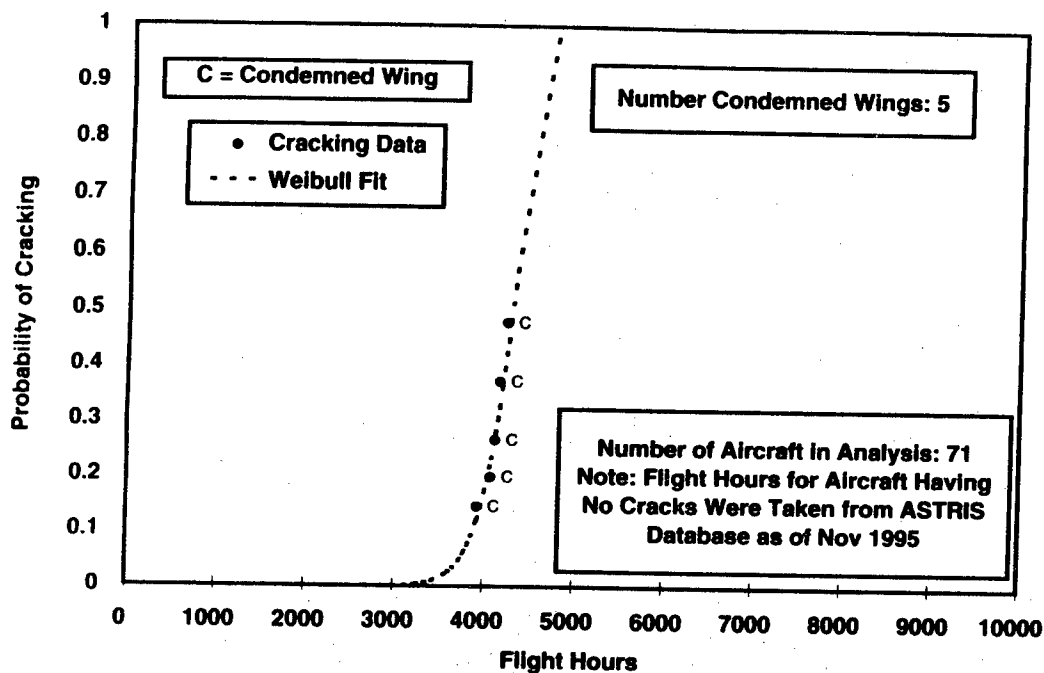
As mentioned at the beginning of this section, a number of cracks have been found in -29 wings flying the LIF/IFF usage. The majority of the wing cracking is located at the:

- Landing Gear Door Radius at WS 64.8
- D-Panel
- Skin in the Milled Pockets Areas at WS 78
- WS 92.5 Fastener Holes at the 44% Spar

Cracking at the landing gear door radius and at the D-Panel can be

repaired and have not caused any wings to be removed from service. However, cracks in the milled pockets of the wing's skin are not repairable, and when a crack is found the wing must be removed from service.

As of November 1995, five wings flying the LIF/IFF usage were condemned because of cracks found in the skin at WS 78 during field inspections. A separate Weibull analysis of cracking at WS 78 was performed for the 71 aircraft flying the LIF/IFF usage for the entire life of the wing. Figure 8 shows the probability of cracking given by the Weibull analysis. The data points for the five condemned wings fall very close to the Weibull curve. Another Weibull analysis was performed for the cracking at the WS 92.5 fastener holes. For this case the USAF had condemned eight wings, and cracks in 20 other wings has been stopped drilled and placed on a 25 hour recurring eddy-current inspection. For the economic life evaluation, all 28 wings were assumed to have reached their economic life. Figure 9 shows the Weibull fit to the cracking experienced at WS 92.5



**Figure 8. WS 78 — Cracking Experience
IFF/LIF Usage**

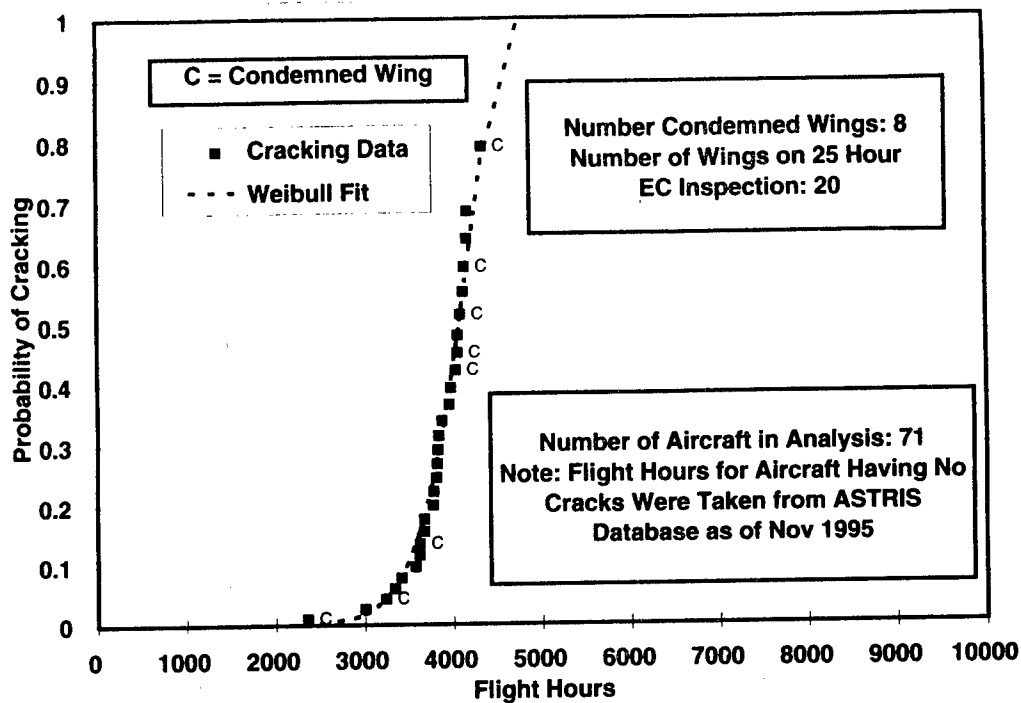


Figure 9. WS 92.5 — Condemned and 25 Hours Eddy Current Inspected Wings - IFF/LIF Usage

At the 50% probability level the economic lives for these two locations for the SUPT usage is given in Table 5. Since the USAF is planning to install a rivetless nutplate at WS 92.5, the corresponding increase in fatigue life was taken to be a factor of 1.5 based upon the coldworked coupon tests. No increase in fatigue life was assumed at WS 78, since no life enhancement method has been demonstrated to alleviate cracking in the skin's milled pockets.

Economic Life Based Upon Wing Durability Test and LIF/IFF Cracking Experience

The previous sections discussed the cracking experience found in the LIF/IFF fleet at WS 92.5 and WS 78, as well as the cracking experienced in the wing lower skin durability test. These three modes were combined to estimate the reliability and replacement schedule for the complete wing. This was accomplished as follows:

Table 5. Wing Economic Lives (50% Probability Level) Considering Individual and Combined Replacement Modes, SUPT Usage

Replacement Modes	Economic Life (Flight Hours)	Economic Life with Coldworking (Flight Hours)
Wing Skin	15,000	20,500
WS 92.5	13,150	19,725
WS 78	12,290	None
Combined	12,000	12,300

Let $P_r(t)_{\text{Skin}}$ represent the probability that the wing will have to be replaced by time, t , because of the cracking in the wing skin. $P_r(t)_{\text{Skin}}$ can be obtained from Figure 6. The reliability of the wing at time t , considering only cracks in the skin, then becomes

$$R(t)_{\text{Skin}} = 1 - P_r(t)_{\text{Skin}} \quad (2)$$

Similar expressions for the reliability associated with WS 78 and WS 92.5 can be developed from the curves given in Figures 8 and 9. Assuming that each replacement mode is independent, then the wing reliability at time t , $R(t)$, is the product of the individual reliabilities for $R(t)_{\text{WS 92.5}}$, $R(t)_{\text{WS 78}}$ and $R(t)_{\text{Skin}}$. Therefore, the probability of wing replacement at time t now becomes

$$P_r(t)_{\text{Wing}} = 1 - R(t)_{\text{Wing}} = 1 - [1 - P_r(t)_{\text{WS 92.5}}][1 - P_r(t)_{\text{WS 78}}][1 - P_r(t)_{\text{Skin}}] \quad (3)$$

where $P_r(t)_{\text{Skin}}$, $P_r(t)_{\text{WS 92.5}}$, and $P_r(t)_{\text{WS 78}}$ are given respectively in Figures 6, 8 and 9.

The predicted number of wing replacements by time, t , in flight hours is given by the fleet size times the probability of wing replacement.

At a 50% probability level, the economic lives for the combined replacement modes for the skin, WS 92.5 and WS 78 are given in Table 5. For the combined replacement modes, little increase in life is obtained from coldworking. Although coldworking the selected fastener holes and installation of the rivetless nutplates do have an effect on the economic life of the wing skin and the WS 92.5 fastener holes, cracks in the milled skin at WS 78 dominate the

economic life of the entire wing. No life improvement at WS 78 was assumed since a repair of a crack in the wing skin is not currently available.

5.0 WING REPLACEMENT SCHEDULE

In this section, the probability of wing replacement given by Equation (3) will be used to predict the replacement schedule for the T-38 -29 fleet. This schedule provides the anticipated wing replacement requirements so that adequate lead times are available for obtaining funding, establishing the appropriate procurement contracts, and manufacturing the wings.

Table 6 shows the numbers of T-38A and T-38B aircraft in the Air Education Training Command (AETC) and is divided into three time frames:

- Prior to January 1996
- From January 1996 to Avionics Upgrade
- Past the Avionics Upgrade

Similar information was obtained for the Air Combat Command (ACC) and Air Force Materiel Command (AFMC). As shown in Table 6, all T-38As in the AETC are assumed to have flown the ENJJPT usage from the time of wing manufacture until January 1996. The 65 T-38B aircraft flying the LIF usage are assumed to have flown this mission over the entire wing life. The term "duration (hrs)" in the table is the average number of fleet flight hours for that particular usage. All economic life predictions are based on average fleet flight hours for a given usage, rather than individual aircraft hours.

From January 1996 to the time of installation of the avionics upgrade in the year 2000, the 51 Instructor Pilot Training (IPT) aircraft are assumed to be flown 300 hours per year and will accumulate 1200 flight hours. The 92 aircraft which had flown ENJJPT usage prior to 1996 have now transitioned to SUPT usage and will accumulate an additional 1680 hours each by the time the avionics upgrade is installed in the year 2000. The other 220 aircraft are now flying SUPT at 348 hours per year and are assumed to have accumulated 1392 SUPT hours each by the year 2000. It is further assumed that the avionics upgrade is applied to the AETC IFF fleet in the year 2002, after which time the fleet will be drawn down to 41 aircraft and continued to fly the combined SUPT/IFF usage. Beyond the time of the avionics upgrade, the 51 IPT and 92 SUPT (formerly ENJJPT) aircraft will continue to fly at 300 and 420 hours per year, respectively.

Table 6. Assumptions for T-38 Wing Replacement — AETC Usage

Command	Time Frame	Prior to Jan '96		Jan '96 to Avionics Upgrade		Past Avionics Upgrade	
		T-38A	T-38B	T-38A	T-38B	T-38A	T-38B
AETC (IPT)	Fleet Size Usage Hrs/Year Duration (Hrs)	51 ENJPT 4247	0	51 ENJPT 300 1200	0	51 ENJPT 300 6000	0
AETC (ENJPT)	Fleet Size Usage Hrs/Year Duration (Hrs)	92 ENJPT 5298	0	92 SUPT 420 1680	0	92 SUPT 420 16800	0
AETC (IFF)	Fleet Size Usage Hrs/Year Duration (Hrs)	20 ENJPT 4904	65 LIF 3642	20 LIF 312 2496	65 LIF 312 1940	N/A	N/A
AETC (SUPT)	Fleet Size Usage Hrs/Year Duration (Hrs)	220 ENJPT 4440	0	220 SUPT 348 1392	0	N/A	N/A
AETC (SUPT/IFF)	Fleet Size Usage Hrs/Year Duration (Hrs)	N/A	N/A	N/A	N/A	185 SUPT/IFF 348 13920	41 SUPT/IFF 348 12528

The adjustments in equivalent flight hours from other usages to the SUPT usage were based upon the mission severity ratios given in Table 2. The number of predicted wing replacements at a given number of flight hours was obtained by multiplying the probability of wing replacement in Equation (3) by the fleet size. Results are shown in Figure 10 for the various usages. It is assumed that all aircraft, except the IFF T-38Bs, have life enhancement applied to the wing lower skin (coldworking) outboard of WS 64.8 and at the WS 92.5/15% spar fastener hole (rivetless nutplate). Figure 10 projects that two wing replacements will be required, one starting in about 2012 and a second replacement of the SUPT/IFF wings in about the year 2035.

The analysis assumption that probably has the greatest effect on the fatigue crack growth, and hence, economic life, is the assumed future MIXED SUPT/IFF usage. The wing replacement schedule was based upon an assumed mission mix 61% SUPT and 39% IFF. To provide an estimate as to what effect variations in the SUPT/IFF usage could have on the wing replacement schedule, an analysis was conducted for the 185 aircraft that will be flying SUPT/IFF after the year 2000. Assuming a variation of plus or minus 15% in usage severity from the baseline (assumed usage) case, the differences in usage severity could account for a change in the wing replacements times of about plus or minus three years.

It is noted that the actual wing replacement schedules shown in Figure 10 were developed by using the entire probability curves in Figures 6, 8 and 9. The economic lives given in Table 5 were at the 50% probability level.

6.0 SUMMARY AND RECOMMENDATIONS

This paper has provided an economic life assessment of the T-38 -29 wing to predict wing replacement rates from the present time to the year 2040. Such anticipated wing replacement requirements were needed by the USAF to allow adequate lead times for obtaining funding, establishing the appropriate procurement contracts, and manufacturing the wings.

The assessment used a probabilistic approach that combined results from a full-scale durability test of the -29 wing with in-service fatigue cracks found in aircraft flying the LIF/IFF usage. The economic life evaluation also considered the effects of fatigue life enhancements to the -29 wing by coldworking selected lower wing skin fastener holes outboard of WS 64.8 and applying rivetless nutplates to specific fasteners at WS 92.5.

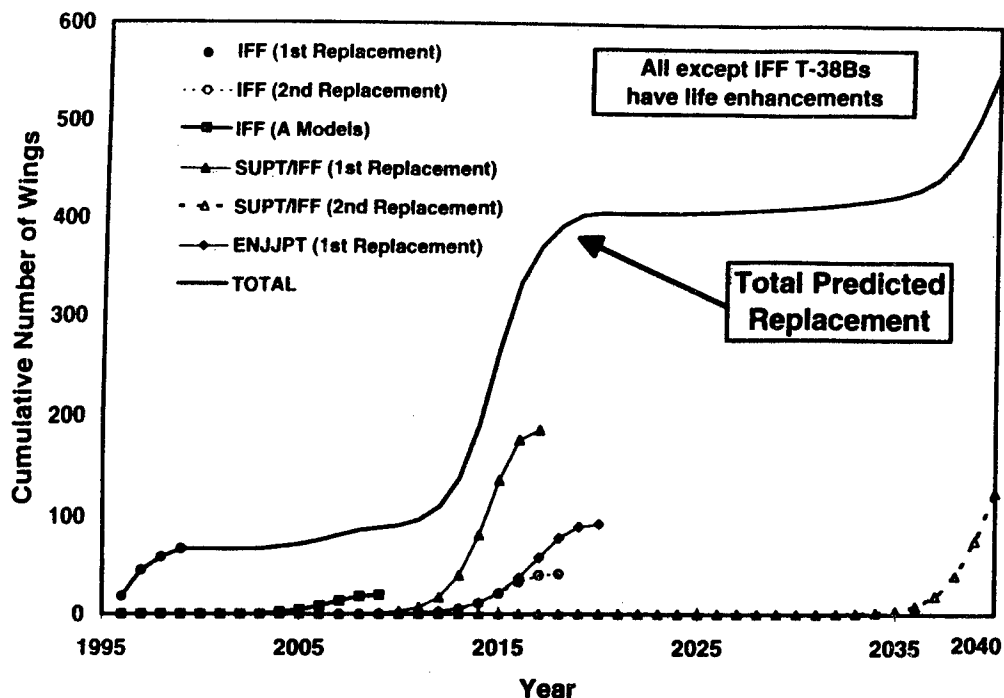


Figure 10. T-38 Projected Wing Replacement Schedule

The evaluation made certain assumptions that should be reviewed as updated information concerning T-38 fleet operations becomes available. For example, the structural severity of a recently introduced usage, Introduction to Fighter Fundamentals (IFF), was taken to be the same as the Lead-In Fighter (LIF). When new IFF data are obtained from ongoing flight usage assessment programs, the equivalency of the LIF/IFF usages and the impact on economic life should be reviewed. After completion of the avionics upgrade in about the year 2000, the AETC anticipates flying a combined SUPT/IFF syllabus. This analysis assumed a mission mix of 61% SUPT and 39% LIF. However, after the MIXED SUPT/IFF usage is introduced, a new flight usage survey program should be conducted, and the effects of the new MIXED SUPT/IFF usage on both flight safety and economic life should be updated.

SA-ALC's cracked/condemned -29 wing database was valuable in predicting, with a Weibull analysis, future cracking rates at the Landing Gear Door Radius, D-Panel, Wing Skin at WS 78, and the WS 92.5/44% Spar Fastener Holes.

This database should be actively maintained, and the Weibull analyses should be periodically updated to reflect current aircraft usage and cracking experience.

Furthermore, since skin cracks in the milled pocket at WS 78 appear to be the dominate reason for condemning the wing, the USAF should evaluate methods to extend the fatigue life at these milled pockets in the current -29 wing. For future wing production, the USAF should consider redesign of those areas or improvements in the manufacturing process.

As discussed in this paper, the SA-ALC has a number of completed and ongoing programs addressing the durability of the -29 wing. As the T-38's new avionics upgrade program matures, similar economic life assessments for the fuselage should be conducted to ensure that the fuselage's durability behavior will meet future Air Force training requirements.

REFERENCES

1. "ASIP Initiatives for the T-38 Aircraft," by O.H. Burnside and J. Dubke, Wright Laboratory WL-TR-96-4030, *Proceedings of the 1994 USAF Structural Integrity Program Conference*, San Antonio, Texas, December 6-8, 1994.
2. "Evaluation of T-38 Using Wing Durability Test Results," by O.H. Burnside, C.E. Kimball, K.H. Schrader, W. Wang D.H. Wieland, and Y-T Wu, Final Report, SwRI Project 06-7257, SA-ALC Contract No. F41608-90-D-2060-0039, April 1996.
3. "Lower Wing Skin Coupon Testing," by P.C. McKeighan, Final Report, SwRI Project 06-7256, SA-ALC Contract No. F41608-90-D-2060-0041, March 1996.
4. *The New Weibull Handbook*, R. B. Abernathy, Gulf Publishing Company, Houston, Texas, October 1994.
5. Fatigue Crack Growth Computer Program "NASA/FLAGRO" Version 2.0, Structures and Mechanics Division, NASA Johnson Space Center, Houston, Texas, May 1994.
6. Newman, Jr. and I.S. Raju: "Stress-Intensity Factor Equations for Cracks in Three-Dimensional Finite Bodies Subjected to Tension and Bending Loads," NASA Technical Memorandum 85793, April 1984.
7. "Durability and Damage Tolerance Analysis (DADTA)," by D. Wieland and J. Cutshall, Final Report, SwRI Project 06-5041, SA-ALC Contract No. F41608-90-D-2060-0014, Draft Final Report, June 1994.
8. Carter, "SUPERCRAKS (NORCRACK) - A Crack Growth Program," referenced in NOR 77-18 and NOR 83-107, revisions and corrections by SwRI in 1992 and 1993.
9. NOR 77-19, "Summary Report, T-38 Damage Tolerance Assessment Program NPN

- 3347," Northrop Aircraft Corporation, February 1979.
10. MIL A-008866B (USAF), Airplane Strength and Rigidity Ground Tests, 1975.
 11. AFFDL-TR-79-3118, "Durability Methods Development," Air Force Flight Dynamics Laboratory, Wright-Patterson Air Force Base: Phase I, April 1978 - June 1979 and Phase II, June 1979 - January 1984,
 12. Tiffany, "Durability and Damage Tolerance Assessments of United States Air Force Aircraft," AIAA Structural Durability and Damage Tolerance Workshop, Washington, D.C., April 1978.

C-141

Systems and Structural Assessment Program

**Presented At The 1996 Aircraft Structural Integrity
Program (ASIP) Conference, San Antonio, Texas**

3-5 December 1996

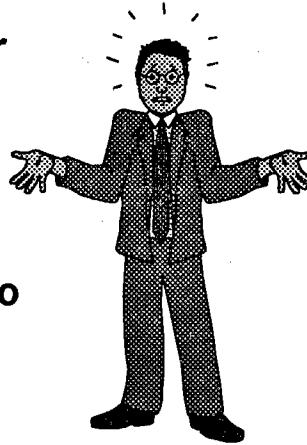
**H. D. Huggins
G. M. Weitz
Lockheed Martin
Marietta, Georgia**

**R.E. Alford
WR-ALC/LJLEA
Robins AFB, Georgia**

Managing a fleet of aircraft without knowing each aircraft's present condition is very difficult. Even though the C-141 has an extensive data base of cracks and repairs, there is still other data that needs to be added to effectively manage a large group of aircraft. This is particularly true for the C-141 systems data. This presentation will show how the System and Structural Assessment Program (SSAP) was performed. Although this program is being performed on the C-141 it can also be applied to any aircraft system. I would like to thank Russ Alford the C141 ASIP Manager for making this program possible and assisting me on this presentation.

What Is the Purpose of the SSAP ?

- **Assess the structural repair configuration of selected aircraft**
- **Gather system data for individual aircraft and add to the existing database**



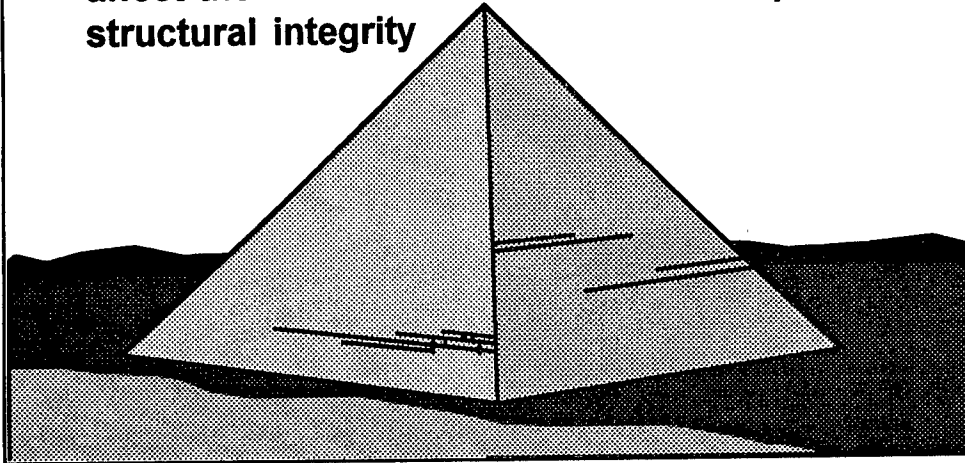
The purpose of the SSAP is to verify existing structural repairs that exists in the present C-141 database and document any additional repairs not in that database. This is an integral part of the repair tracking program and is used to help establish inspection intervals.

The C-141 aircraft systems are being inspected to establish a database to depict the overall system integrity, thus making it easier to establish trends in the degradation of particular systems.

Aging Aircraft

- Numerous repairs on aging aircraft affect the structural integrity

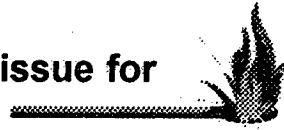
- It is very important to know the extent of these repairs



With increasing pressure on both military and commercial fleets due to aging of their aircraft, the area of repair tracking is becoming increasingly important. It is necessary to be able to establish the risk of flying high time aircraft on an individual aircraft basis. The number, location and size of existing repairs is an essential part of this structural analysis. The information gathered will significantly enhance the safe management of operational aircraft.

Condition of Systems

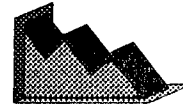
- Deterioration of systems critical issue for aging aircraft



- Aircraft systems are high maintenance items

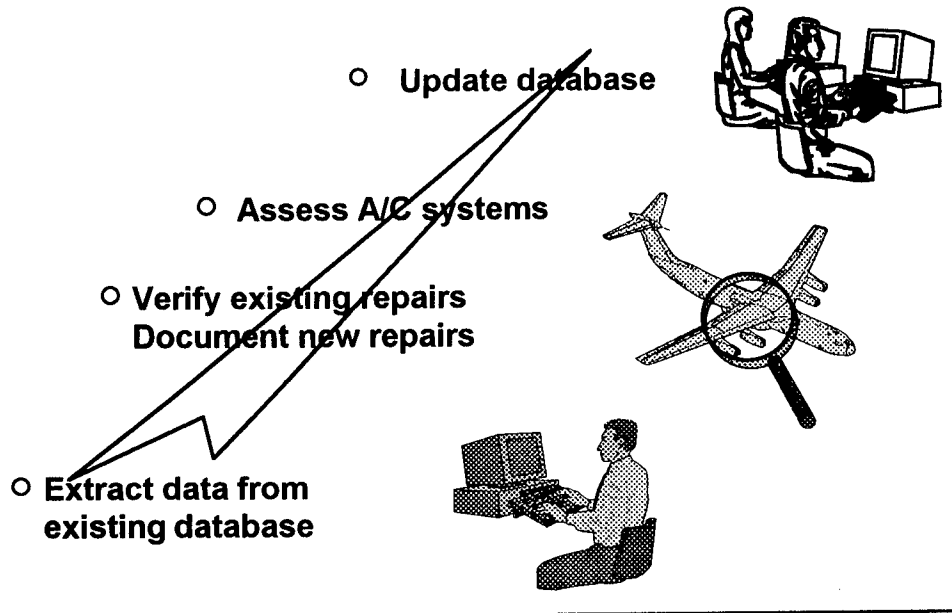


- Develop discrepancy trend patterns and form a statistical data base



The degradation of systems on an aging aircraft is a major concern of the Air Force. Systems are high maintenance items and if not inspected on a regular basis can increase the maintenance cost and put the aircraft at a higher risk while flying. The SSAP assesses the systems and creates a statistical database that may show patterns or trends in the degradation of particular systems. This information can not only be used to lower maintenance cost and decrease down time but also to increase safety.

Program Scenario



The SSAP scenario begins with each team extracting existing data on an individual aircraft from the C-141 repair tracking database. This data consists of the discrepancy, location, repair description, inspection intervals and date repair was documented. Teams also get a systems checklist with specific areas and particular types of discrepancies to be assessed.

Teams then travels to bases where the ISO inspection is being performed on that aircraft. The aircraft systems are inspected and existing structural repairs are verified or documented along with identifying numbers and photographs. All the system and structural data is input into computer programs, while on location. All the data for the individual aircraft is sent by modem to the Data Control Center for uploading into the main database.

Assessment Performed at Isochronal Inspections

- **4 Teams traveling to 11 different bases**

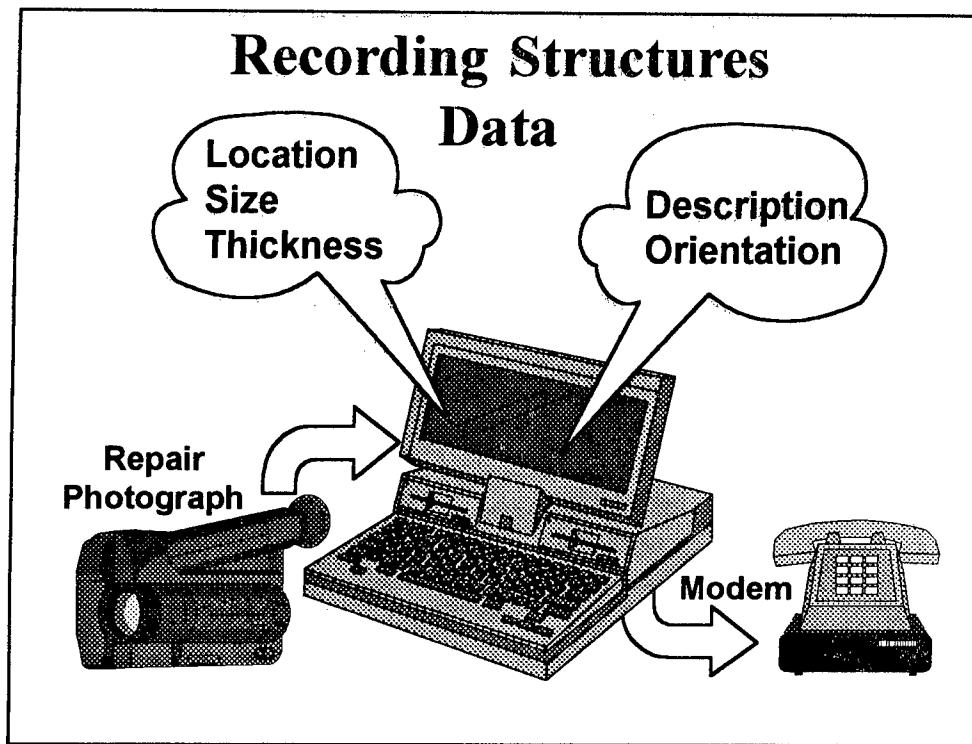


- **Work performed on a non-interference basis**

The SSAP program consisted of 4 teams of 2 engineers per team that traveled to 11 Air Force Bases.

There were 135 selected aircraft to receive the assessment. The Air Force selected these aircraft based on retirement date, total damage hours and other factors. The bases are notified to confirm the ISO inspection date of the selected aircraft. The assessment teams are then scheduled to be present during the ISO inspection. These assessments usually take 3 days and are being accomplished on a non-interference basis with the normal ISO inspection (5 to 7 days).

Structures



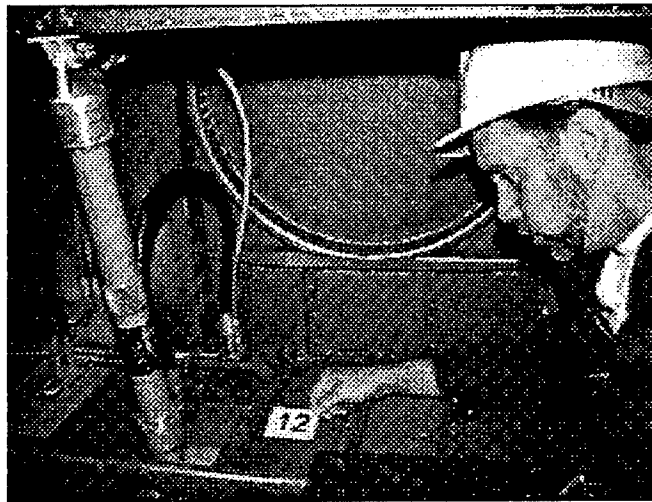
The input of a new structural repair consist of the following: a/c tail number, description of the part that is repaired, description of the repair, repair picture number, location (FS, WL, ect.) and length, width, thickness and orientation of repair. Also included are the inspection intervals associated with the repairs.

The repair is then videoed and a digital picture is captured and saved on the computer using the repair picture number as the file name. The video tape containing the repairs for each aircraft is also stored in the SSAP library.

For a repair that is already in the database, the repair information is verified to be accurate. If there are erroneous entries, the record will be corrected to agree with the repair installed.

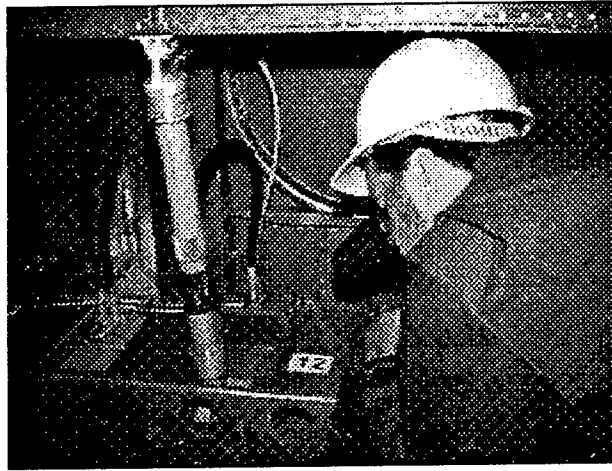
After all structural repairs have been verified and documented the data is sent via modem to Lockheed Martin to be uploaded to the main database.

Identifying the Repair



Each repair is identified by a number. Shown here is an engineer numbering a structural repair in the hayloft area of the aircraft. Some repairs are standard and have already been defined with standard repair numbers. These repairs are not photographed.

Photographing the Repairs



In confined spaces a small digital camera is used as shown here.

SSAP Structures Results for 100 Aircraft

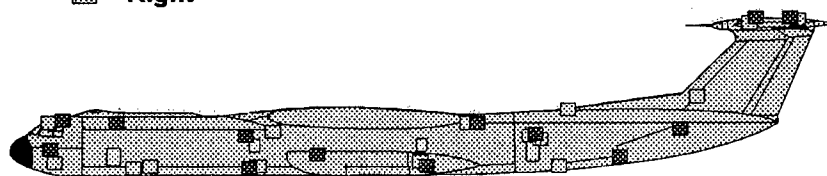
- **19617 Total repairs**
- **3943 New repairs added to database**

<u>Area</u>	<u>New Repairs</u>
Fuselage	3249
Wing	622
Empennage	72

The structural results for 100 aircraft are shown on this slide. The total number of repairs are shown compared to the additional repairs found during SSAP. This shows that 20% of the repairs were not in the database, and most of those were on the fuselage.

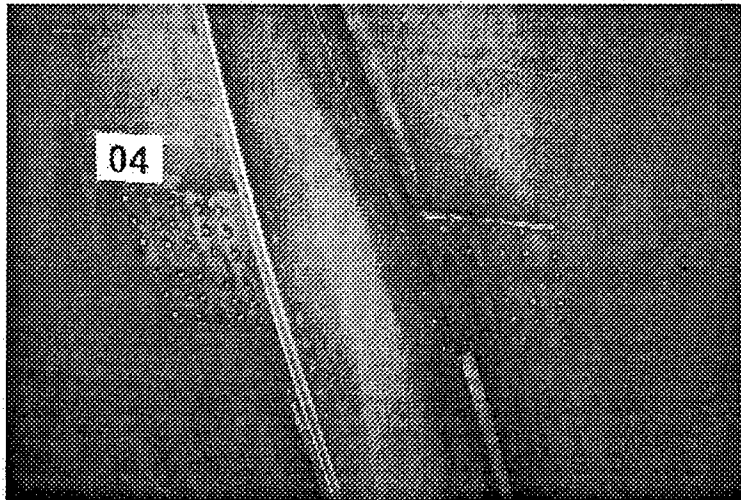
Plot of Repairs on Fuselage

■ Left
▨ Right



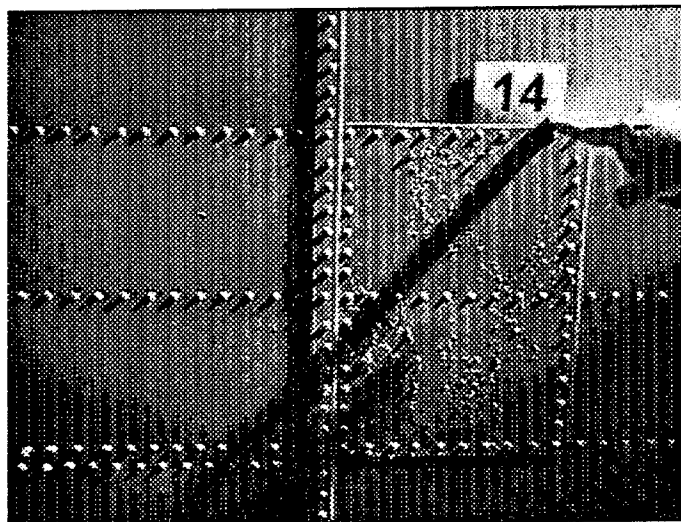
The above slide shows a fuselage plot of a typical aircraft. This plot is computer generated from the repair tracking database which includes records input during the SSAP. Each repair symbol represents a repair, and may be selected (double-clicked) to see repair description, crack growth analysis for the zone and photograph or drawing of the specific repair.

Photo of Repair



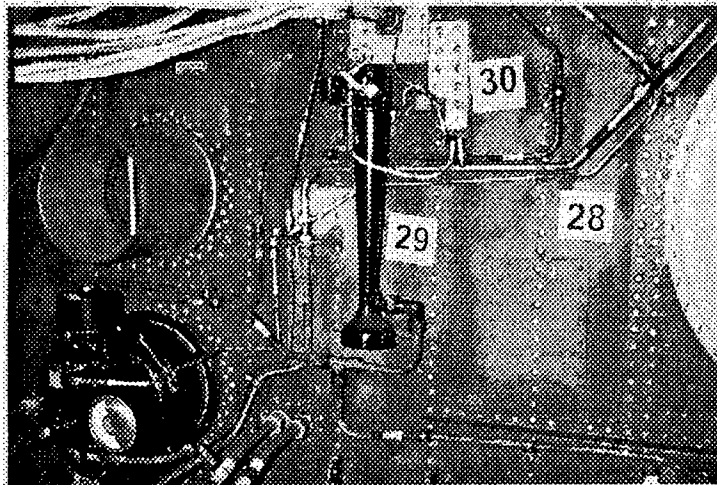
Shown above is a typical 'E' point repair install on the no. 2 pylon left wing.

Photo of Repair



Shown on this slide is a doubler installed on the hayloft floor.

Photo of Repair



Shown on this slide are 3 adjacent repairs located on the FS 1398 pressure bulkhead.

**Systems
and
Secondary Structure**

Recording Systems Data

- Visual Inspection



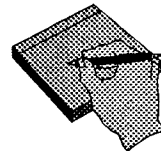
- General Condition



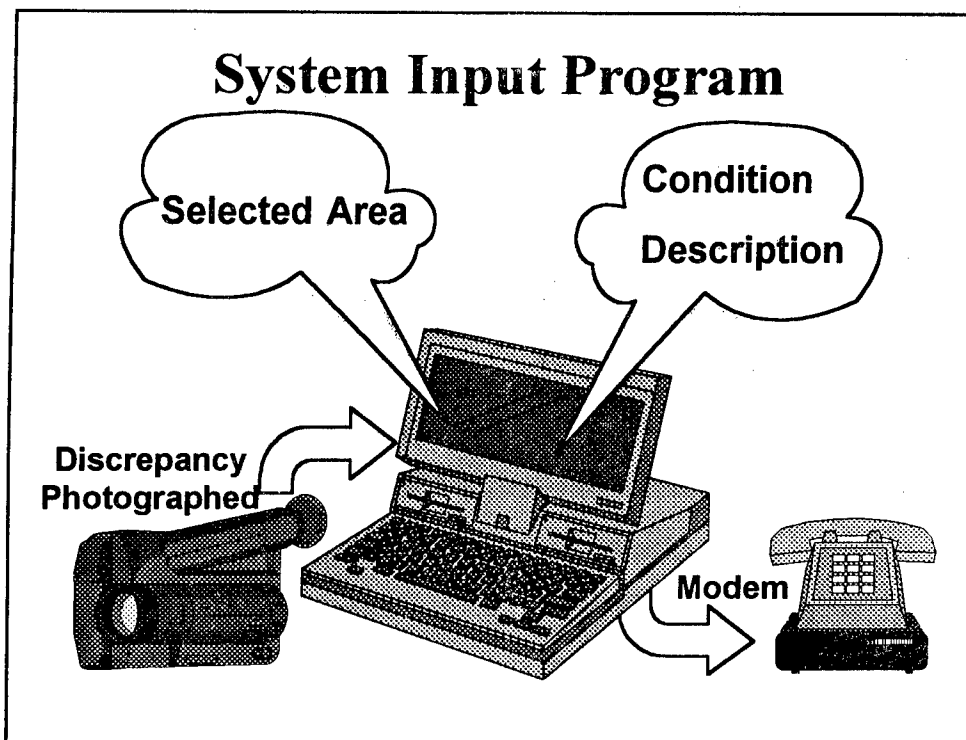
- Specific Items



- Record Discrepancies



For the systems assessment, which also includes secondary structure, 53 general areas of the aircraft were visually inspected. The systems checklist also contain a total of 898 specific items which are common discrepancies usually found in these areas. When these discrepancies or ones not on the list were found they were recorded.



All items on check list are in the systems input program. Each individual system item has 3 choices; no discrepancies found, unable to inspect or discrepancy found. When a discrepancy is found, comments may be entered describing the findings.

If a major discrepancy is noted (bare wire in hydraulic area or engine disconnect, etc..) it is digitally photographed and the identifying picture file entered into the comments.

Each individual area is rated on a scale from 1 to 10 (10 being excellent) after all items for that area are inspected. Also the percent of new wiring present is noted if applicable to that area.

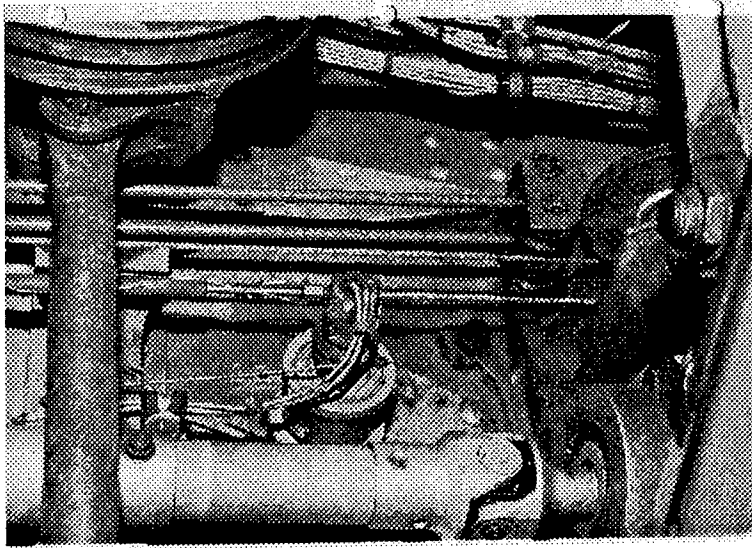
After all system items have been input the data is sent via modem to Lockheed Martin to be uploaded to the main database.

System Results

<u>Area</u>	<u>Discrepancy</u>	<u>% Discrepant</u>
Fuel boost pump wiring	Worn, frayed Insulation	85 %
APU start accumulator	Corrosion	79 %
Flap tracks	Corrosion	73 %

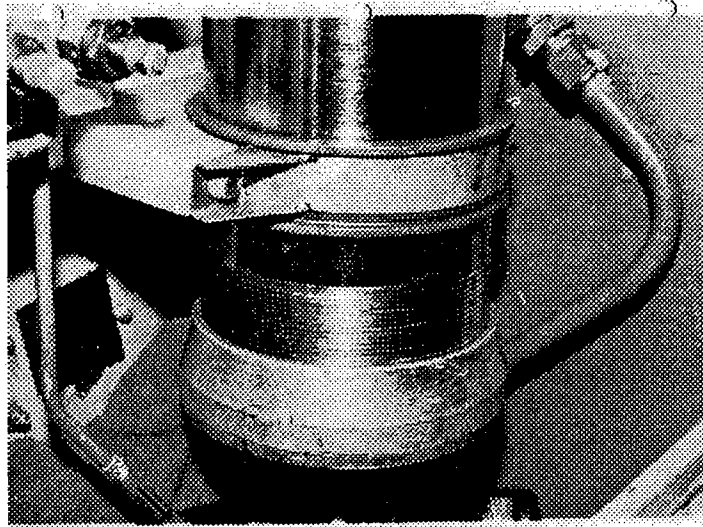
The top three discrepant system items are shown above.

System Check



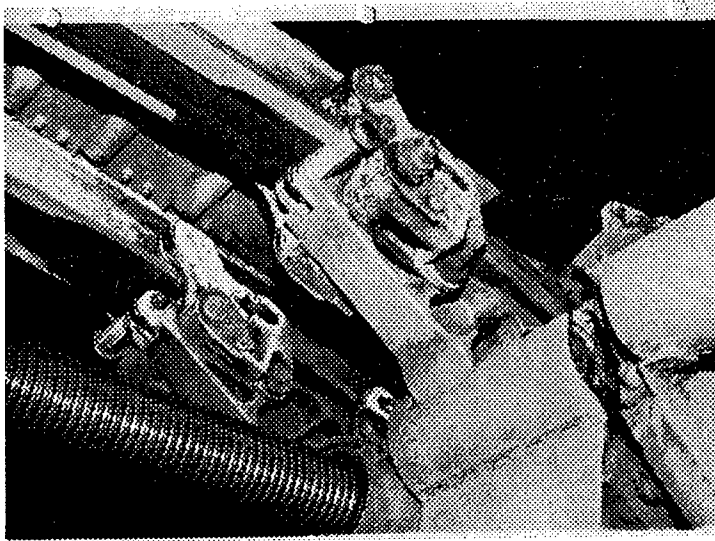
Shown in this photograph is the fuel boost pump wiring.

System Discrepancy



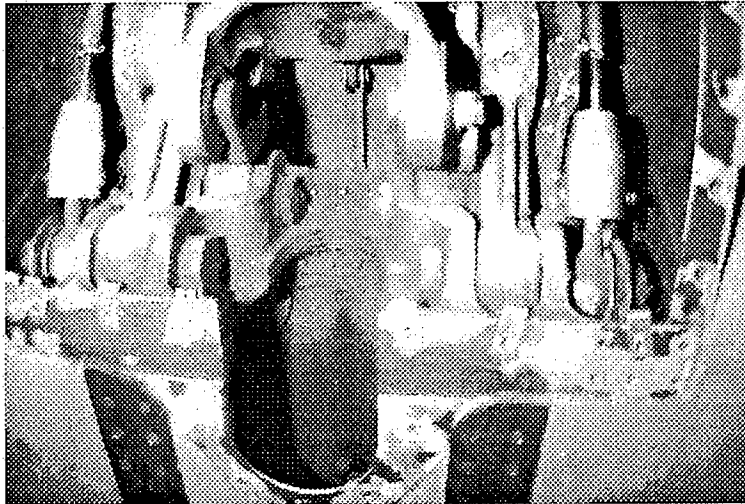
This is the APU start accumulator, mild corrosion is on the cylinder threads.

System Discrepancy



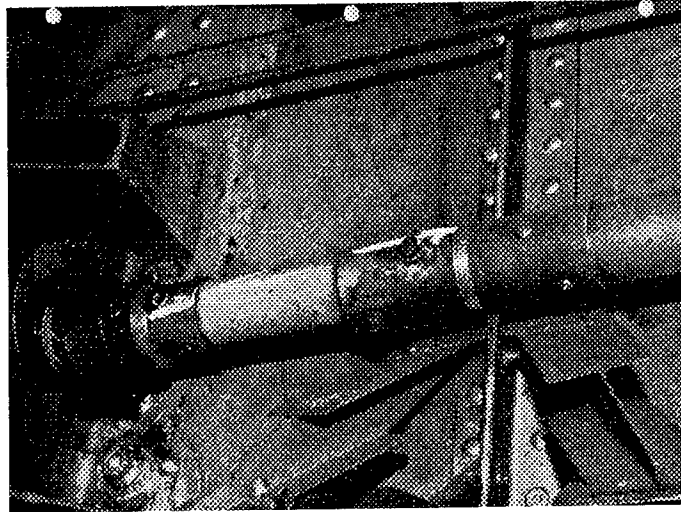
This photograph shows two system items, the flap track rib with mild corrosion and the flap jackscrew. Also shown is a secondary structure item, a flap carriage containing moderate corrosion.

System Discrepancy



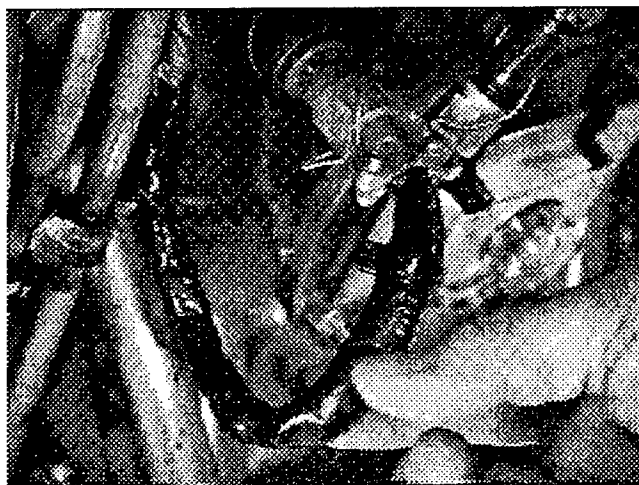
This photo shows where a jackscrew has cut into a closure fitting inside the flap. This situation occurs when the flap carriage is mis-located.

System Discrepancy



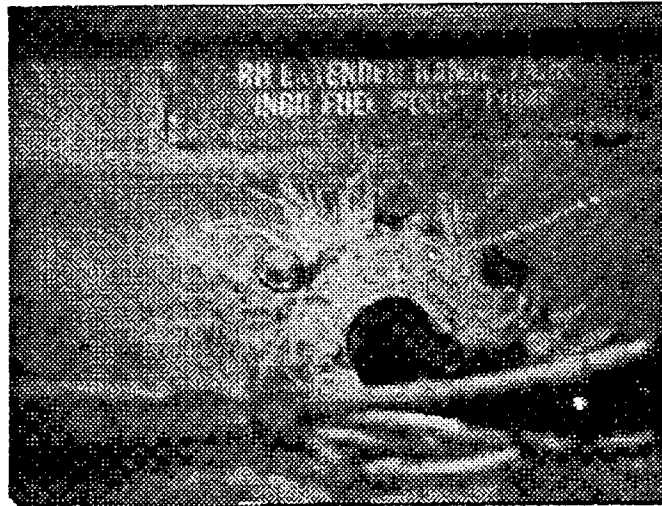
This photograph shows the flap track drive torque tube rubbing against a stiffener on the rear beam. Notice the witness mark indicating that the torque tube rotated and rubbed against the stiffener. This was caused by the rubber bushing coming out of the gear box support, shown on the left of the photograph.

System Problem



Black tape shown here, indicates the wrong type of electrical tape for the engine compartment.

System Check



A potentially serious area is where the wire for the fuel boost pump connector passes through the rear beam of the wing.

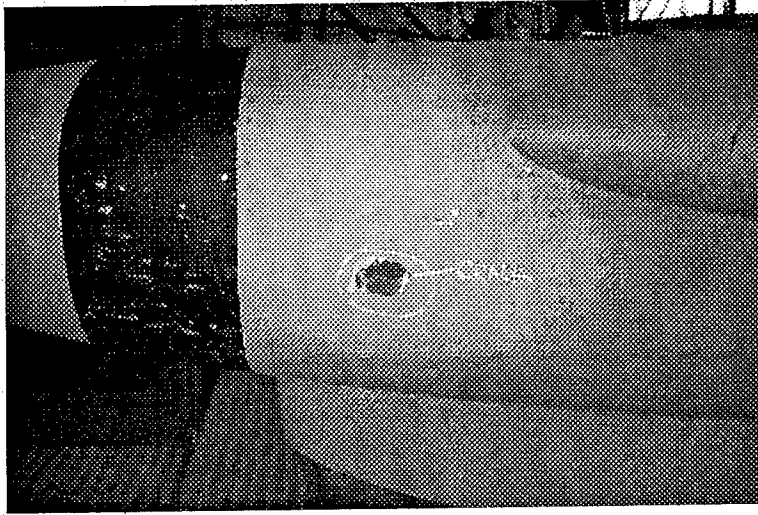
This photo is shot from the aft side of the wing rear beam. The connection is made within the wing box and is sealed by a housing. If the housing leaks and the hole is filled with sealant, fuel will be trapped at the connection. The hole should be clear of sealant as shown above.

Secondary Structure Results

<u>Area</u>	<u>Discrepancy</u>	<u>% Discrepant</u>
Flap carriage	Corrosion	72 %
Aileron trailing edge	Repairs	64 %
Pylon blowout doors	Repairs	63 %

Shown on this slide are the top three discrepancies in the secondary structure.

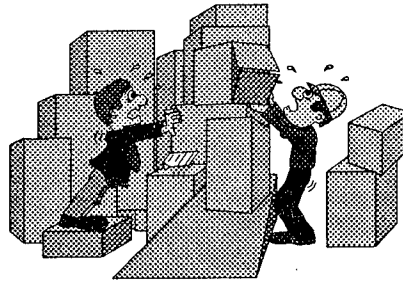
Secondary Structure Discrepancy



The above slide shows a large puncture/crack in the secondary structure of the bullet on the horizontal stabilizer.

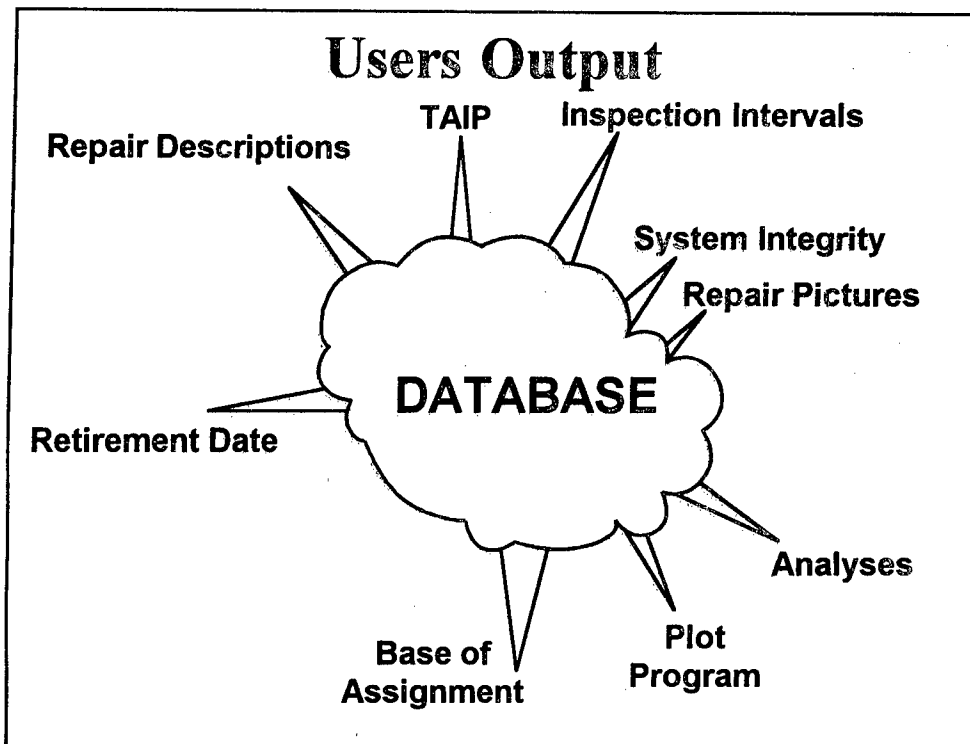
What Are We Doing With All the Results ?

- Define inspection intervals
- Optimize inspections
- Statistical summary
- Risk analysis



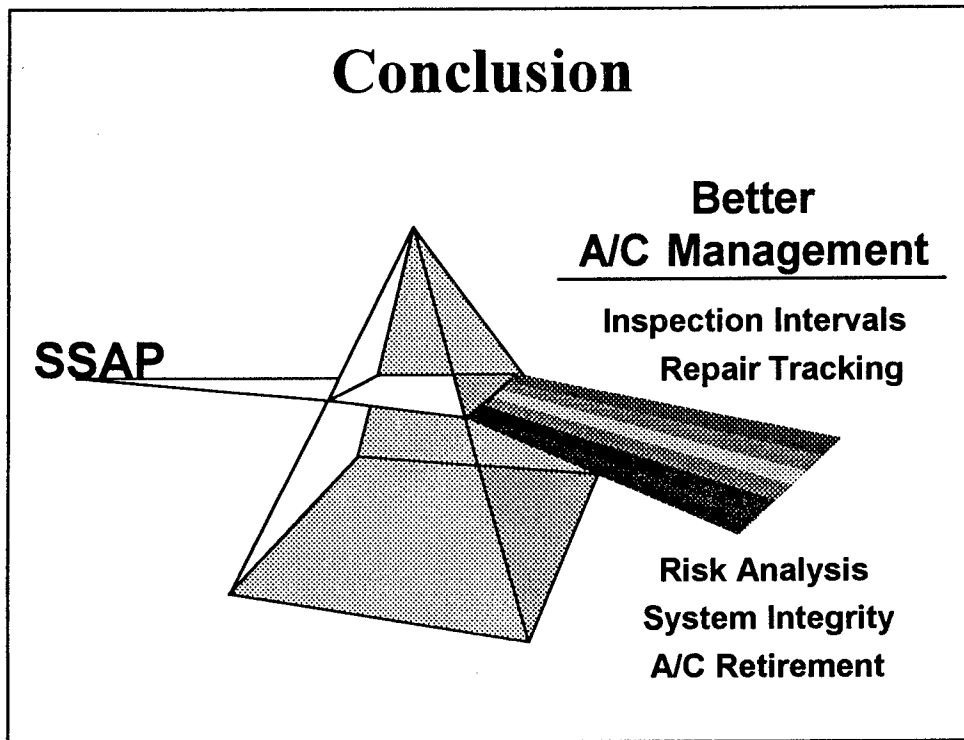
The data for both systems and structures is added to the existing database to be used to effectively manage individual aircraft. The structures database is used to schedule inspections and perform analyses to maintain flight safety. The systems and secondary structure database is used to statistically perform forecast/trend analyses for various components.

Tailored Aircraft Inspection Program (TAIP) is presently being developed so that structural repairs or system inspections will be optimized for an individual aircraft based on a combination of considerations. These considerations include, damage hours, usage, number of repairs or discrepancies along with already scheduled inspections.



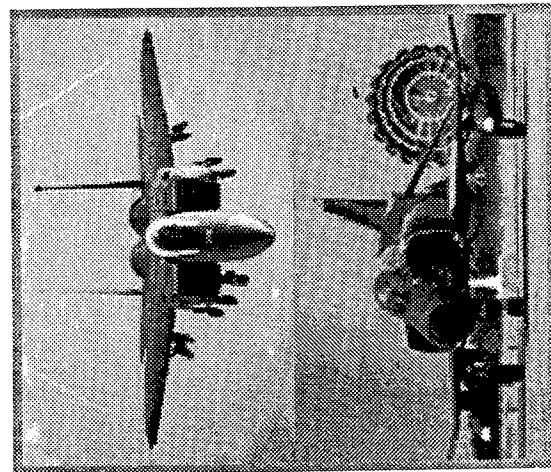
With the additional information collected during the SSAP on both the systems and structures the user may access the information shown above. This information helps manage the aging fleet effectively, efficiently and safely. This data also will help predict problems that may arise later in the fleet.

Conclusion

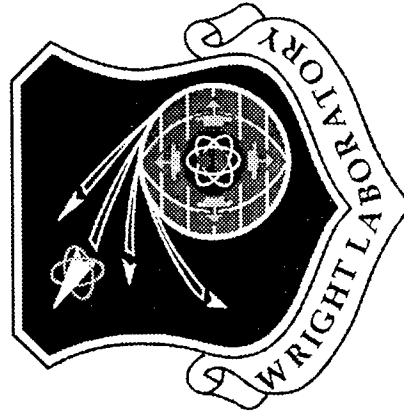


As shown the SSAP is adding to an already valuable database. By filling in missing pieces and verifying known repairs the database is made more useful and accurate. It also is creating a database of important system findings that did not exist prior to the program. This data aids in repair tracking by re-defining inspection intervals and predicting life expectancy of structures and systems. This database is essential to managing an aging aircraft at the most critical phase of its life.

Aging Aircraft Structures Database



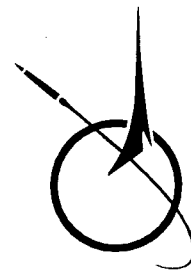
by Rigo Perez and Michael VanDernoot
McDonnell Douglas Aerospace
St. Louis, MO



1996 USAF Structural Integrity Program Conference

3 - 5 December 1996
San Antonio, TX

C60503.001



Aging Aircraft Structures Database

Agenda: Background

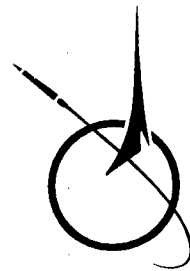
Objective

Database Examples

Database Operations

Interaction With AFGROW

Data Collection Status



C60903 002

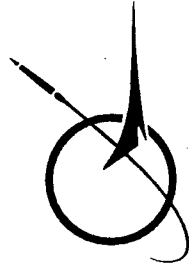
Aging Aircraft Structures Database

Background:

- Fatigue, Corrosion, and Life Enhancement Data Is Fragmented
- Data Needed for New Model Development Is Not Easily Available To Wright Laboratory (WL)
- WL Sponsored Program

Objective:

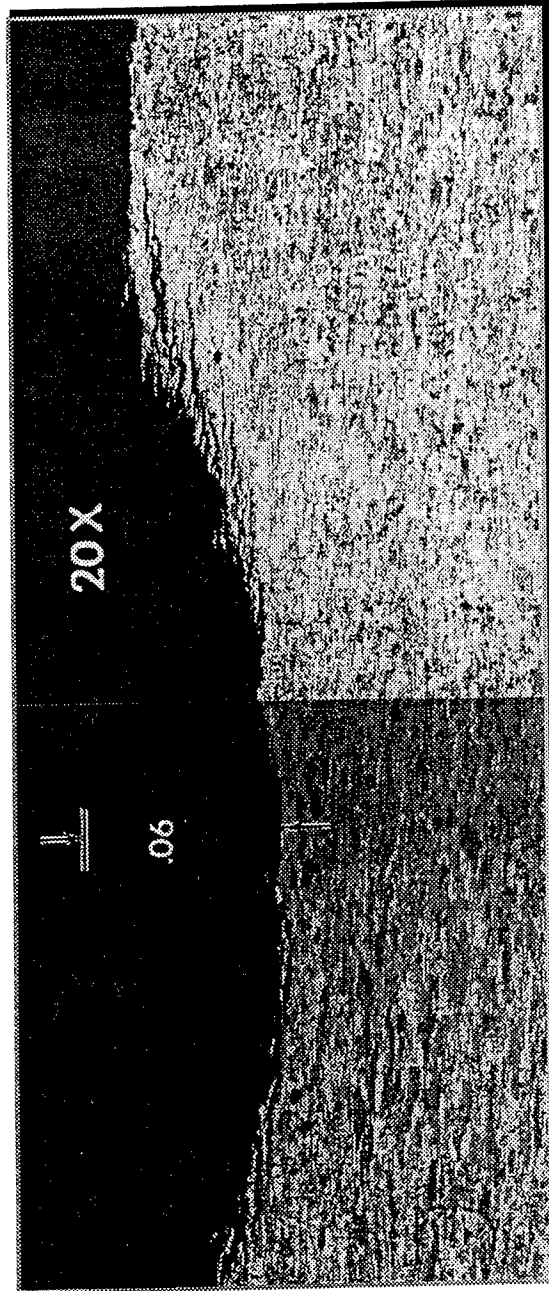
- Develop a Database for Storing Aging Aircraft Data at WL
- Link the Database With EXCEL and AFGROW To Analyze Data
- Collect Representative Data



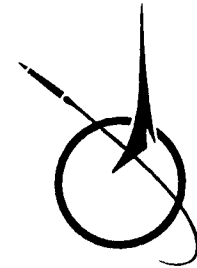
C66909 003

Aging Aircraft Structures Database

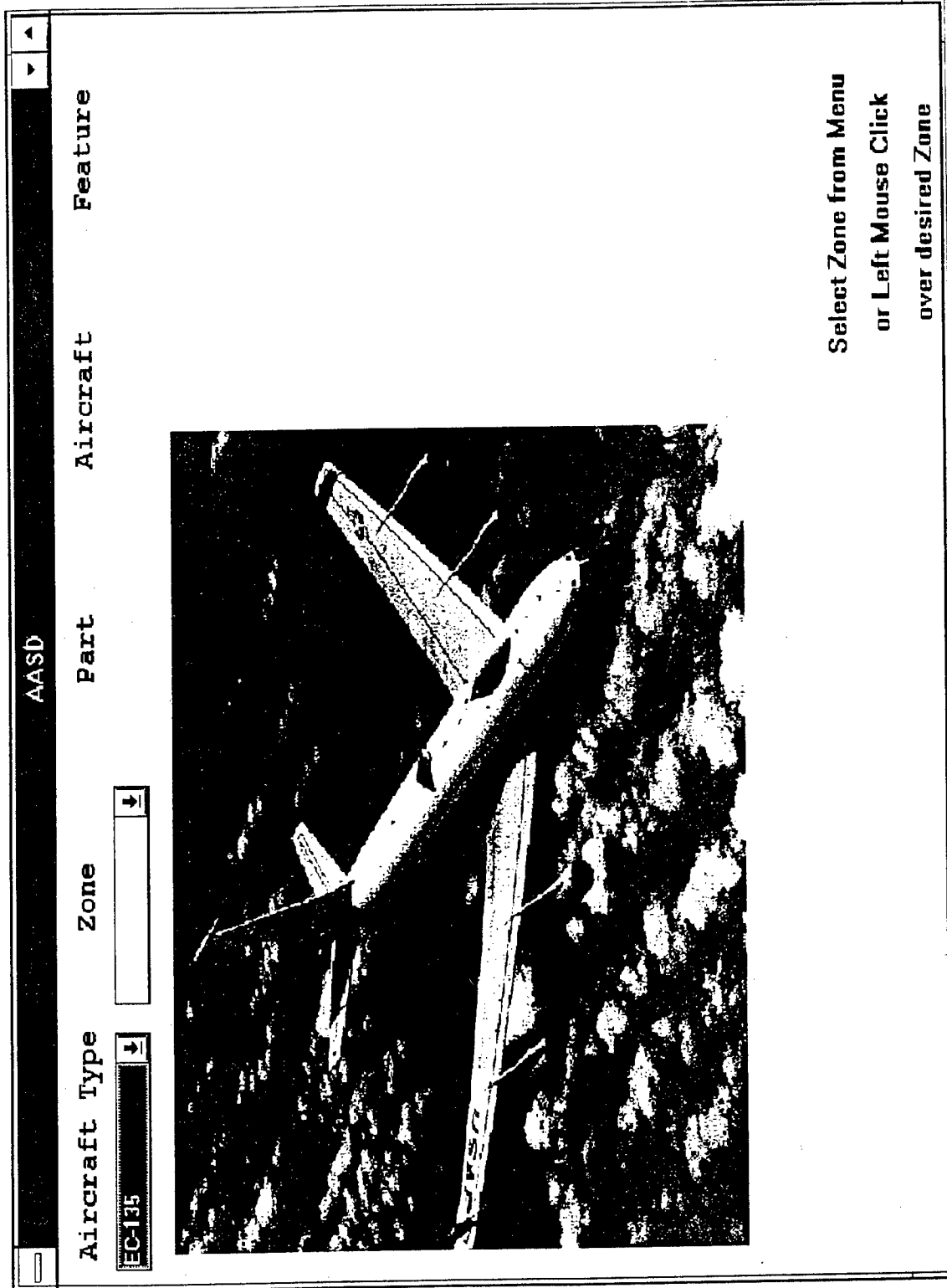
Database Example: Corrosion



Reference: R. Frank, Boeing Document No. D500-12641-6, 1 February 1994



C60909.005



AASD				
Aircraft Type	Zone	Part	Aircraft	Feature
EC-135	forward fuselage	BS 420 Frame near		

Part Number:

na

Part Section Number:

287

Part Material:


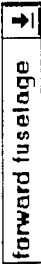



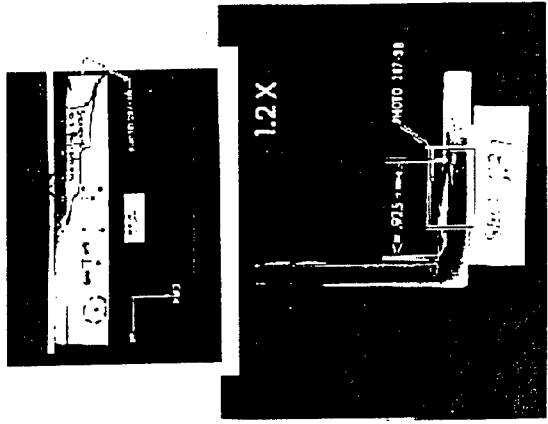
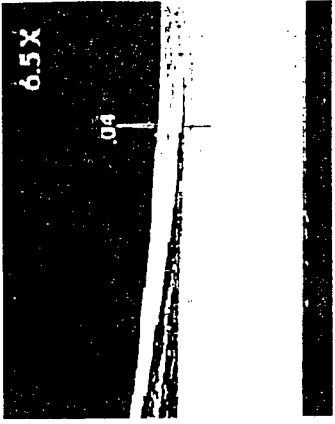
7xxx, plate

Select Specific Aircraft
from Menu

or Left Mouse Click
over a Feature

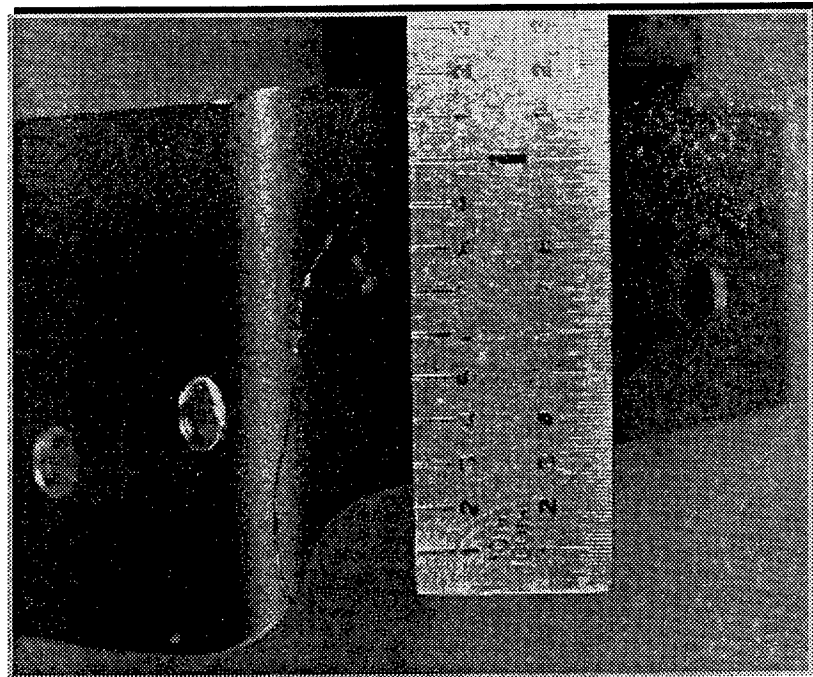
or Right Mouse Click
to De-Select

Part BS 420 Frame near

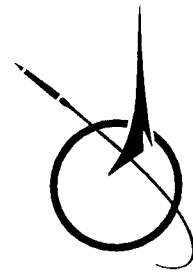
AASD			
Aircraft Type	Zone	Part	Aircraft
EC-135	forward fuselage	BS 420 Frame nea	All EC-135s
<div> <div>  </div> <div>  </div> <div>  </div> <div>  </div> </div>			
<div> <div>  </div> </div>			
<div> <div> <div>Source Reference:</div> <div>R. Frank, Boeing</div> </div> <div> <div>Part Thickness:</div> <div></div> </div> </div>			
<div> <div> <div>Surface Description:</div> <div>non-faying</div> </div> <div> <div>Total Area:</div> <div></div> </div> </div>			
<div> <div> <div>Corrosion Area:</div> <div>.75</div> </div> <div> <div>Corrosion Minimum Depth:</div> <div>.002</div> </div> <div> <div>Corrosion Maximum Depth:</div> <div>.04</div> </div> </div>			
<div> <div>  </div> <div>  </div> </div>			
<div> <div>Plot</div> </div>			

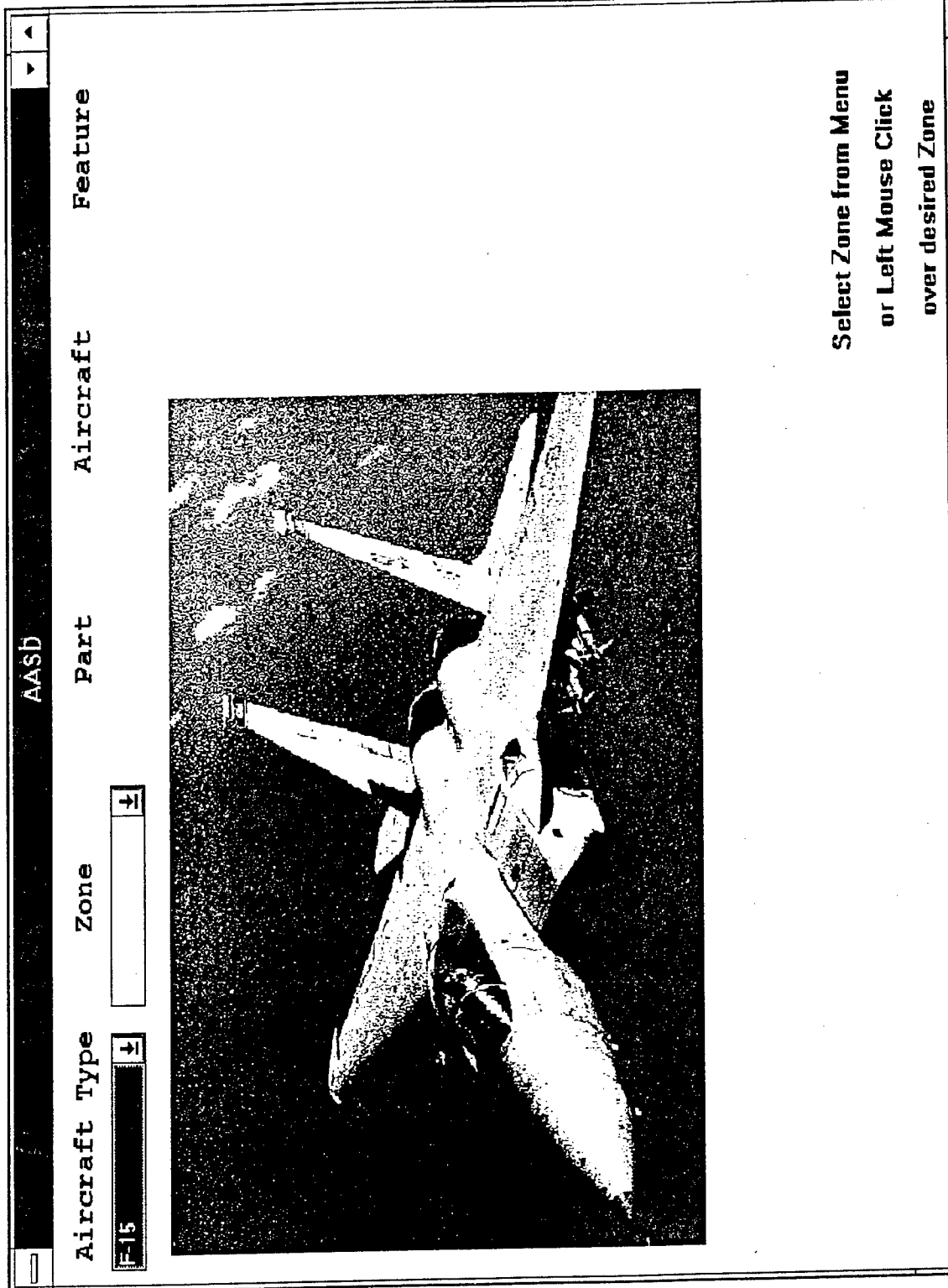
Aging Aircraft Structures Database

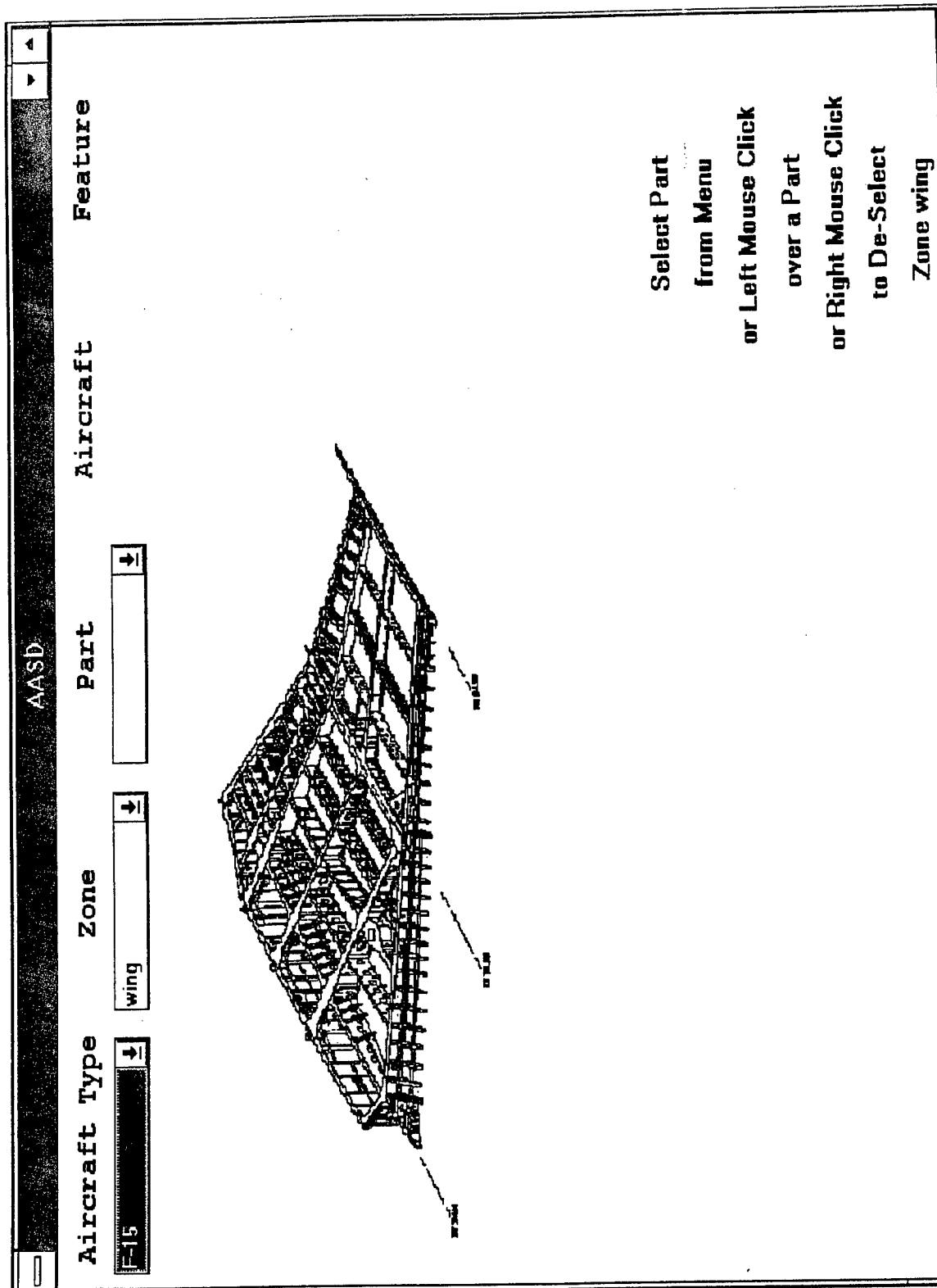
**Database Example:
Fatigue Cracks**



C60905 004







Aircraft Type	Zone	Part	Aircraft	Feature
15	wing	Outb. Front Spar (L)		

Part Number:
na

Part Section Number:
na

Part Material:
7075-T7352

Select Specific Aircraft
from Menu
or Left Mouse Click
over a Feature
or Right Mouse Click
to De-Select

The diagram illustrates a cross-section of an aircraft wing. Key components labeled include the 'Front Spar' running horizontally, the 'Door 171 UR' at the top, and a 'Wire Conduit Hole Where Crack Occurred' on the upper surface. A 'Fib Attachment' is shown on the lower surface. The part number 'XW 165.024' is also indicated.

Part BS 420 Frame near

Aircraft Type	Zone	Part	Aircraft	Feature
F-15	wing	Outb. Front Spar (1)		Wire Bundle Hole

**FRONT SPAR WIRE BUNDLE ROUTING HOLE
TYPICAL CRACK LOCATIONS**

Source Reference:
J.S.Sermersheim, MDC

Hole Number:
Wire Bundle Routing Hole

Hole Diameter:
1.52

Part Thickness:
.12

Crack Clock Position:
2

Crack Dimension(s):
.375

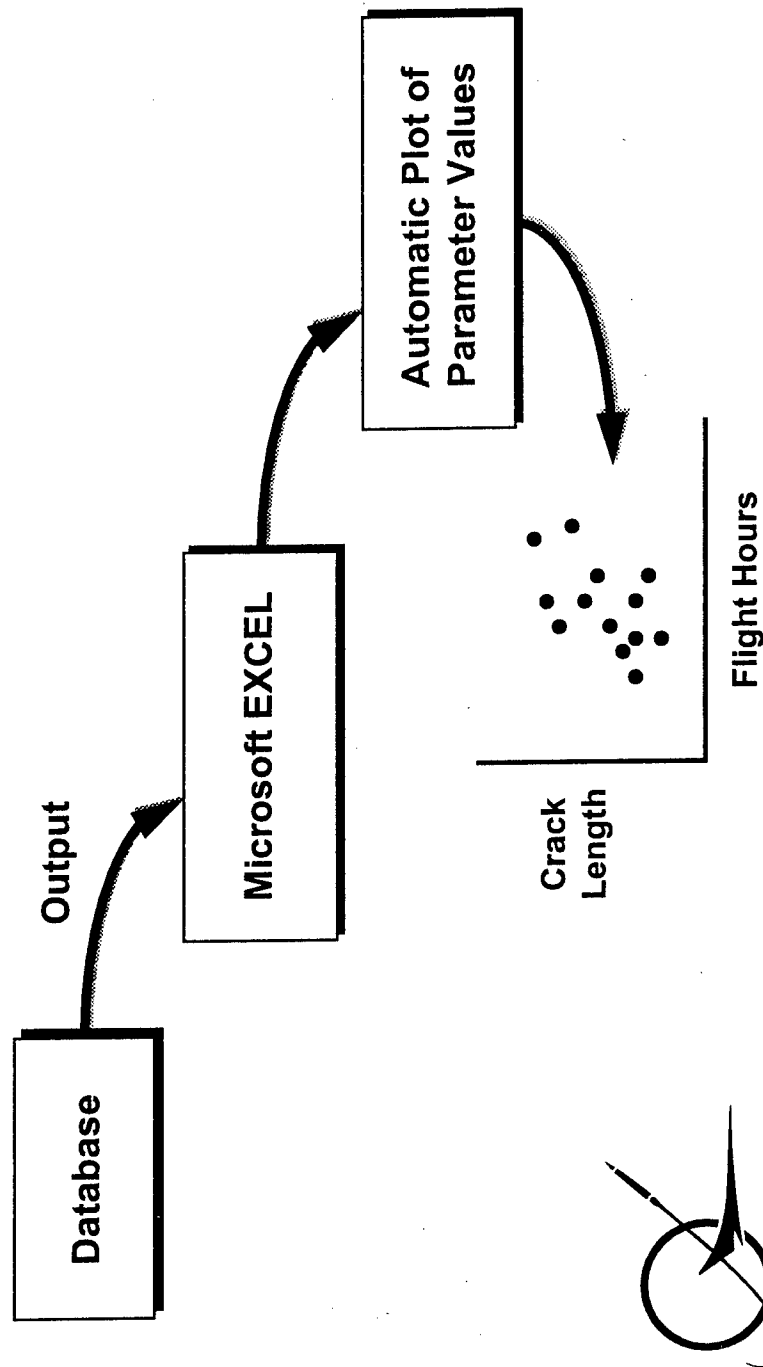
Plot

AASD			
Aircraft Type	Zone	Part	Aircraft
F-15	wing	Outb. Front Spar (L)	All F-15s
			W/B Hole Repair
<p>Feature</p>			
<p>Source Reference:</p> <p>J.S. Sermersheim, MDC</p>			
<p>Description:</p> <p>Two 0.063 in. titanium doublers installed with 23 0.1895 in. diameter interference fit HI-LOK fasteners.</p> <p>Filler is installed in the hole.</p> <p>Up to 0.50 in. of material can be blended out to remove cracks.</p>			
<p>Plot</p>			



Aging Aircraft Structures Database

Database Operation Example



C60903 006

Select Plot Type

Data Analysis

Horizontal Axis:

Actual Flight Hours

Vertical Axis:

Fatigue Crack Dimension

Sample Points:

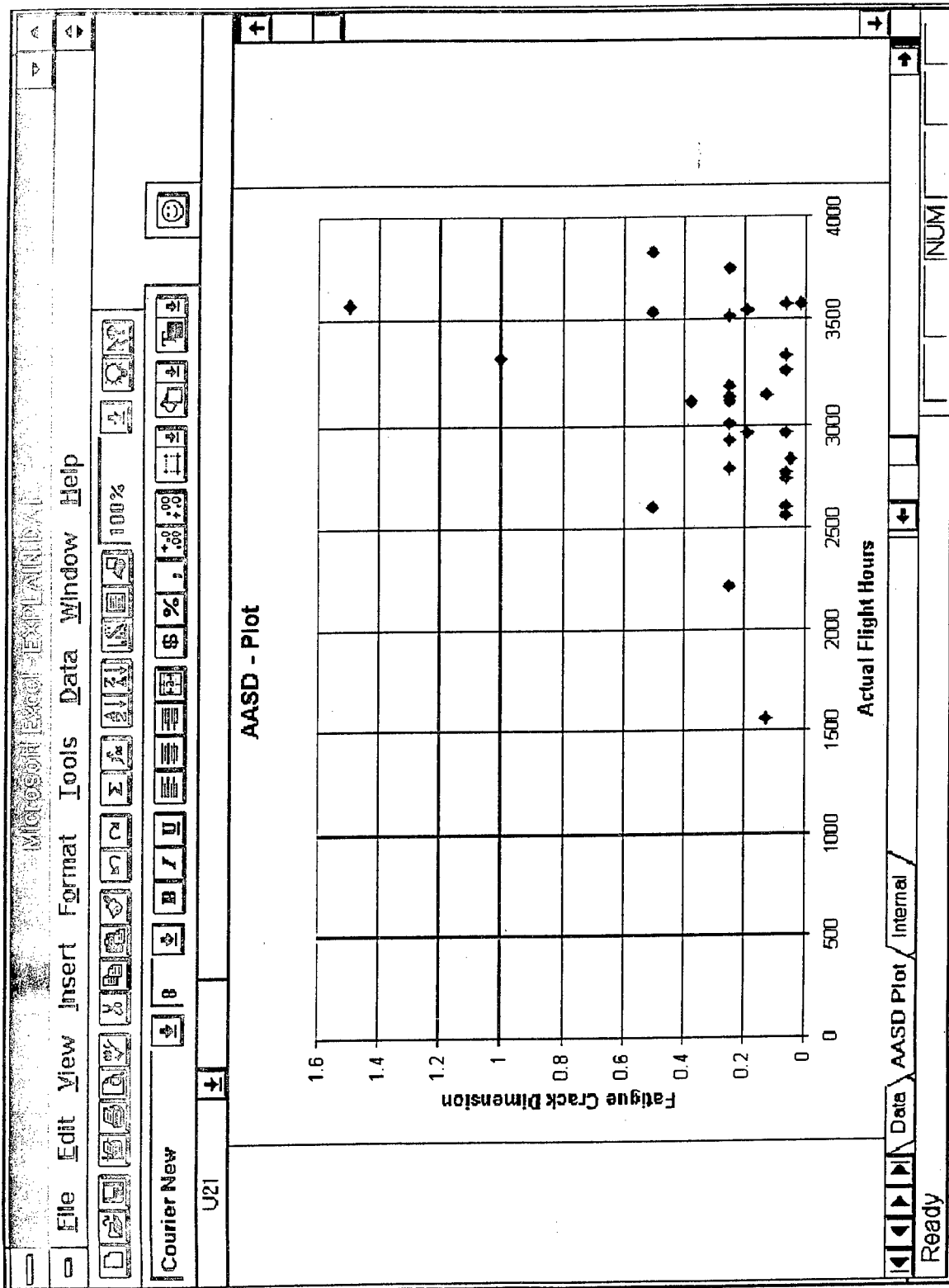
All F-15s

Plot

Material Properties

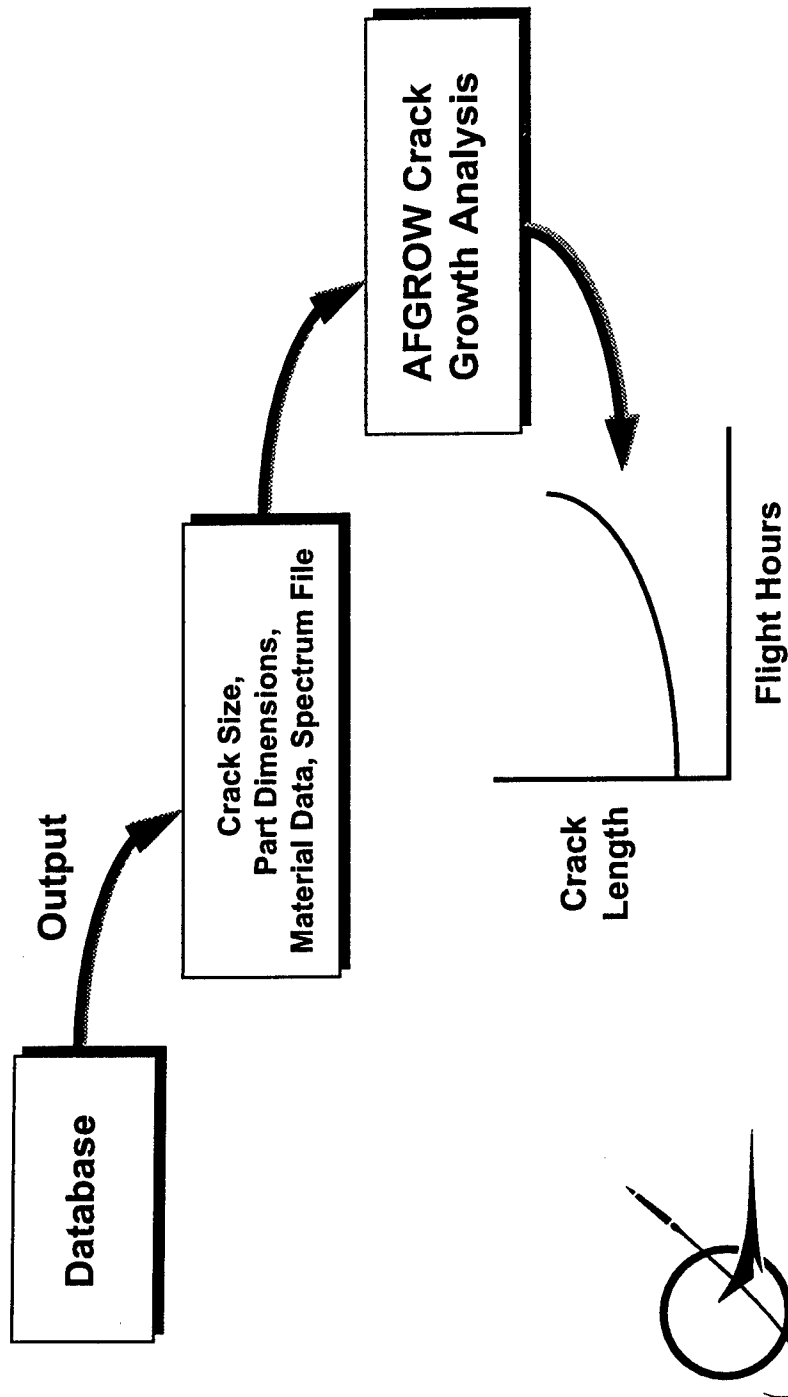
Spectrum

Exit



Aging Aircraft Structures Database

Database Interaction With AFGROW



CS0903 007

Aging Aircraft Structures Database

Data Collection Status

The Following Representative Data Has Been Entered in the Database:

Aircraft	Type of Data	Source
F-15	Fatigue and Repair	McDonnell Reports
C/KC-135	Fatigue and Corrosion	OC-ALC Invasive Disassembly
C-141	Fatigue	WR-ALC Weep Hole Data, AIRS, EDCARS
C-130	Fatigue	Brown, Greenhaw, 1987



C60909 008

Aging Aircraft Structures Database

Summary

- The Database Provides a Way of Storing Fatigue, Corrosion and Repair Information at WL
- Provides a Way of Analyzing Stored Data Rapidly With EXCEL
- Data Can Be Used for New Model Development at WL
- Linked To AFGROW Crack Growth Analysis



CE0903.009

An Overview of the Wright Laboratory Structural Integrity of Aging Aircraft Core Area

“Today's Aircraft Flying Tomorrow”

1996 ASIP Conference
3 December 1996

Michael L. Zeigler, Principal Engineer
Structural Integrity Branch
Wright Laboratory

Structural Integrity of Aging Aircraft

Wright Laboratory

Outline

- Background
- Need
- Approach
- Products

Structural Integrity of Aging Aircraft

Wright Laboratory

Background

- Flying farther, heavier, longer
 - Reduction in overseas bases - Global Reach
 - Mission changes - weight growth
 - Fewer replacements planned
- Aging aircraft structures impact
 - Increased costs
 - Reduced mission effectiveness
 - Safety of flight

Reduce Support Costs while Increasing Fatigue Life

Structural Integrity of Aging Aircraft

Wright Laboratory

Background

- Air Force S&T Response
 - 1993 - AFOSR URI
 - 1994 - SAB Aging Aircraft Summer Study
 - AFMC/ST
 - Aging Aircraft Initiative
 - Aging Aircraft Structures Emphasis Area
 - 6.2 and 6.3 Plus-up
 - New 6.4 PE to accelerate S&T/ALC transition

Structural Integrity of Aging Aircraft

Wright Laboratory

Need

- Strategy for need identification
 - Technology Master Process, TPIPT
 - Impacts MAJCOM Mission Area Plan
 - Air Logistic Centers - Tech Needs
 - WL Customer Focus IPT
 - Structural Integrity Working Group
 - People

Structural Integrity of Aging Aircraft

Wright Laboratory

Approach

- Focus Areas
 - Corrosion/Fatigue
 - Repairs
 - Widespread Fatigue Damage
 - Dynamics
 - 6.1/6.2/6.3 programs
- Collaborative Teaming



STRUCTURAL INTEGRITY OF AGING AIRCRAFT

WEB OF ALLIANCES



AGING AIRCRAFT

UDRI, AS&M
MDA, FAA, NASA
AFOSR, Purdue, Can,
Aust, UK, Battelle

STRUCTURAL INTEGRITY OF AGING AIRCRAFT

- Widespread Fatigue Damage
- Repairs
- Dynamics
- Corrosion/Fatigue

AS&M, R-Tech
USAF, MDA, ML, FAA
FMV, Navy, Boeing
Can, Aust, UK, KSI
Georgia Tech, AFIT,
AFOSR

AFOSR, Boeing
Lockheed Martin
FIM, NLR,
Seek Eagle
Can, Aust, UK,
Calspan, AFIT,
CFDRC, GTRI,
Israeli AF, F-16 SPO

OC-ALC, AMC
MDA, UDRI, ARINC
Navy, AFOSR, NASA,
Honeywell, FAA
Northrop Grumman
Can, Aust, UK

Structural Integrity of Aging Aircraft

Wright Laboratory

Corrosion/Fatigue

PROBLEM

The impact of corrosion damage on structural integrity is not well understood

GOAL

Provide the necessary tools to determine the effects of corrosion/fatigue on structural integrity

- Interaction with WFD

Structural Integrity of Aging Aircraft

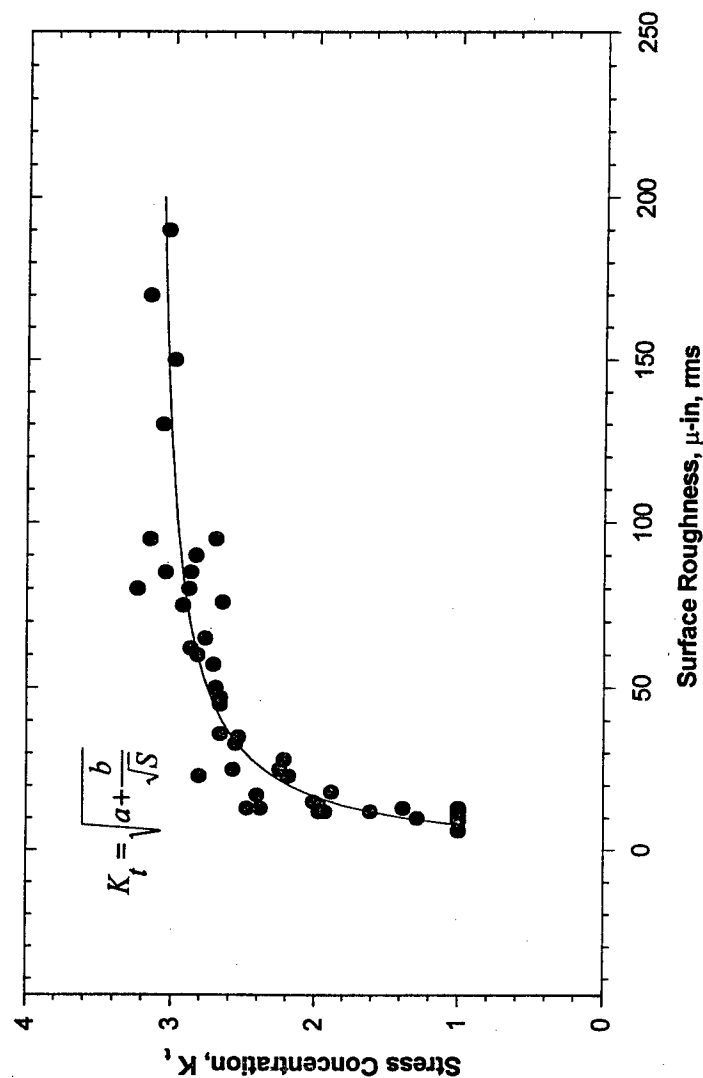
Wright Laboratory

- Corrosion/Fatigue
 - Structural integrity issues
 - Identification/Quantification
 - Metrics/Transformations
 - Test Protocol/Validation
 - Contribution to widespread fatigue damage
 - Pitting
 - Pillowing

Metrics and Transformations Development

CORROSION/FATIGUE

K_t as a Function of Surface Roughness



The data was generated in an effort by Clayton L. Harmsworth, Wright Laboratory, ASD Technical Report 61-121, July 1961

1. 85 rotating beam specimens were used in the program.
2. The corrosive solution was a 20% (by weight) salt-spray at 95F.
3. The unexposed specimens were polished to a 5-10 m-in, rms surface roughness.

Structural Integrity of Aging Aircraft

Wright Laboratory

Repairs

PROBLEM

Bonded composite repair technology is not fully developed

-Design criteria, durability/damage tolerance

GOAL

Develop and validate design/analysis tools

- Design criteria, structural integrity

Structural Integrity of Aging Aircraft

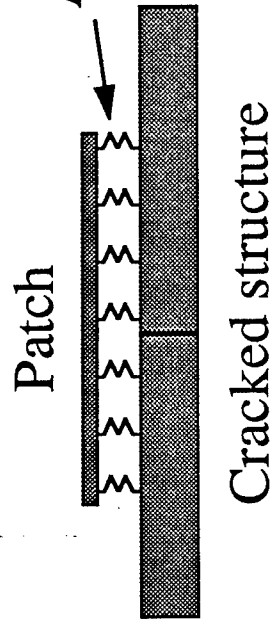
Wright Laboratory

- Repairs
 - Design criteria
 - Develop design and analysis tools for bonded repairs - User oriented
 - FEM-based to Engineering solutions
 - Damage Tolerance Analysis
 - Experimental verification
 - Identify M&P needs, NDI/E requirements

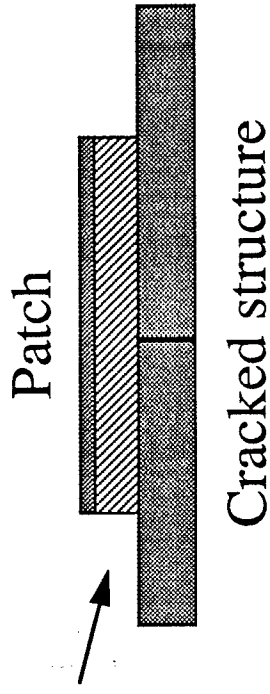
Structural Integrity of Aging Aircraft

Wright Laboratory

Common FEM Approach



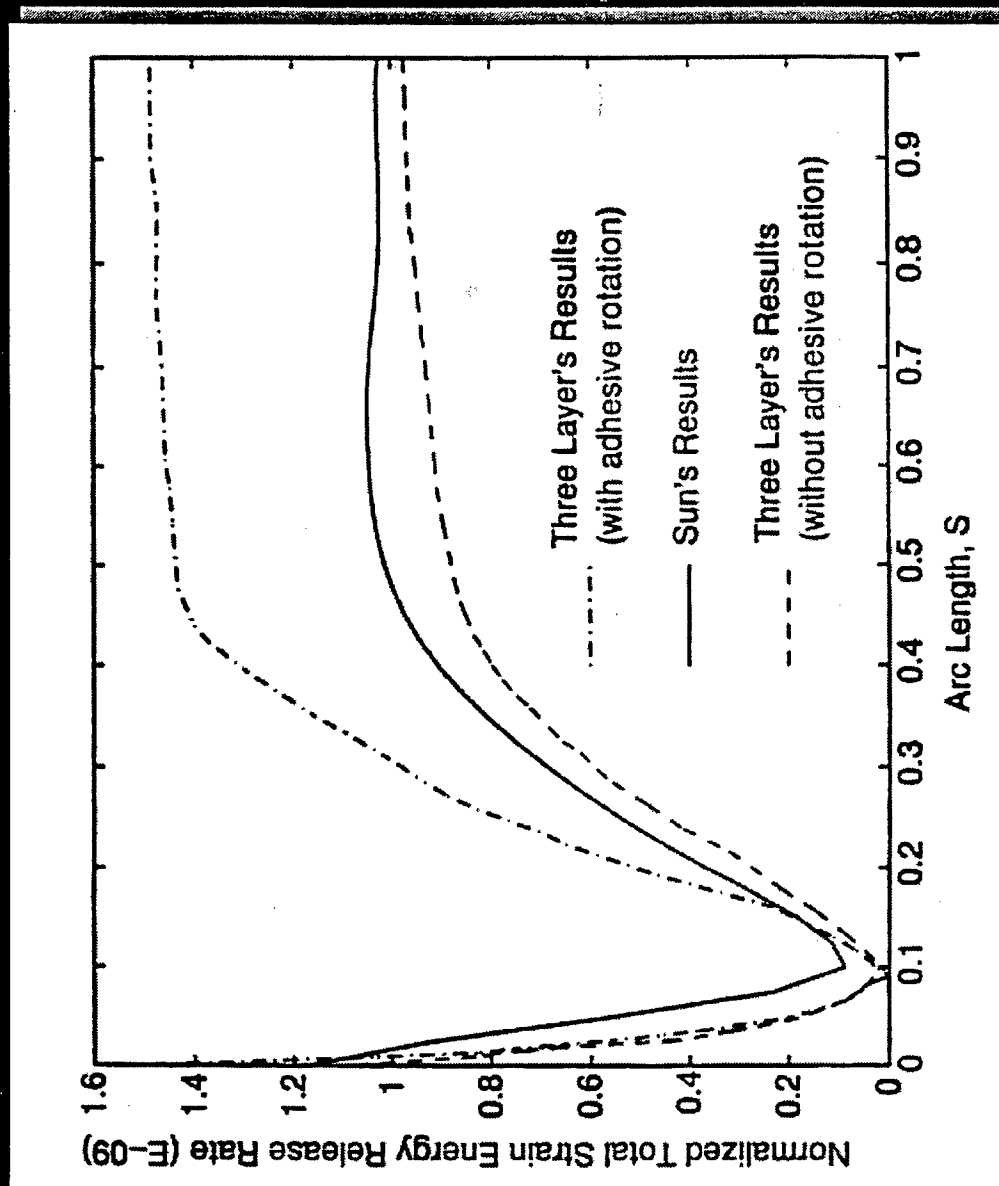
FEM using 3-layer technique



- Modeling adhesive as continuum provides accurate analyses of:
 - Thermal effects
 - Nonlinear adhesive
 - Progressive damage

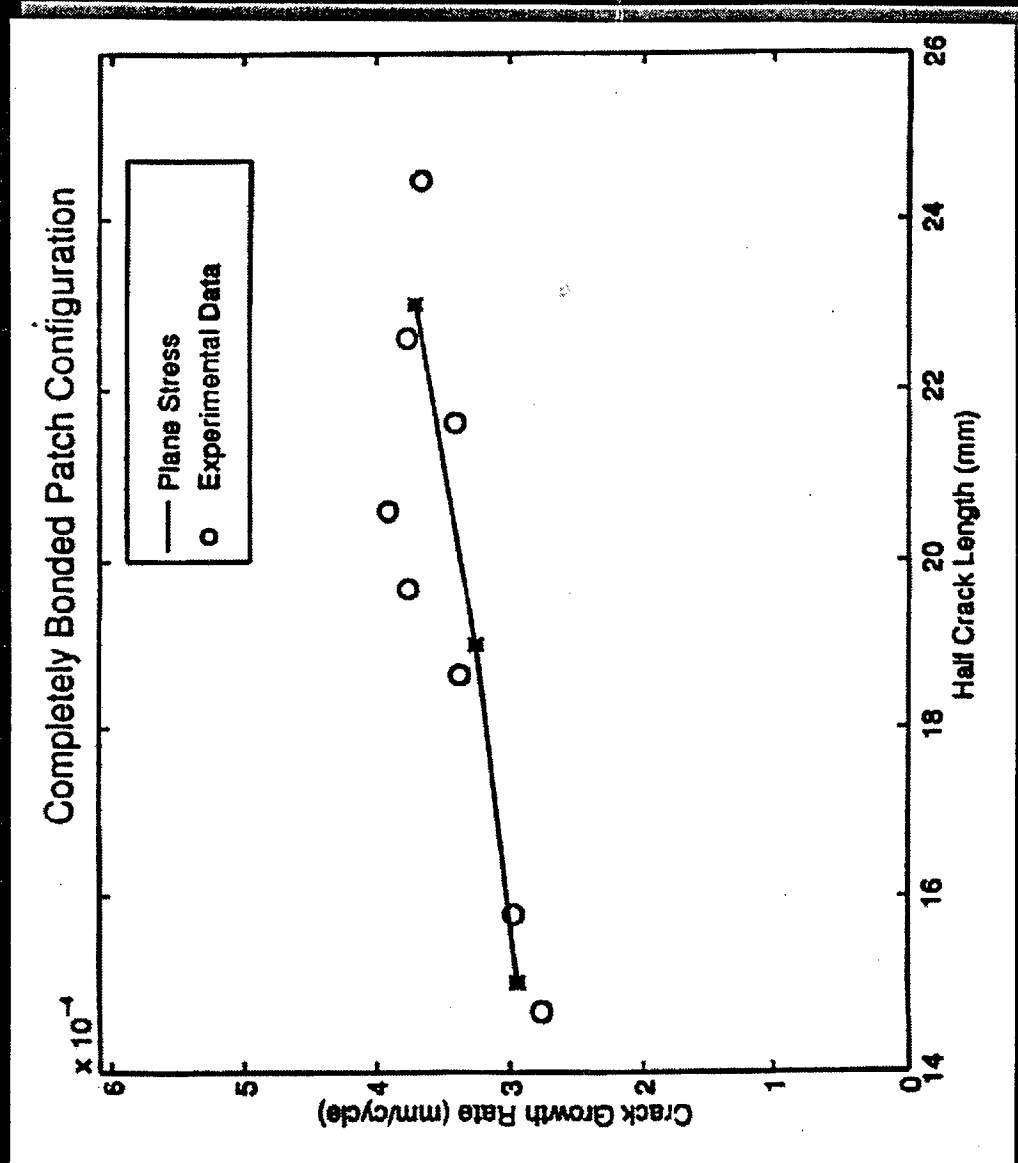


3-LAYER TECHNIQUE COMPARED WITH COMMON FEM APPROACH





COMPARISON OF EXPERIMENTAL AND ANALYTICAL FATIGUE CRACK GROWTH



Structural Integrity of Aging Aircraft

Wright Laboratory

Widespread Fatigue Damage

PROBLEM

The onset of widespread fatigue damage due to multisite damage degrades aircraft structural integrity

GOAL

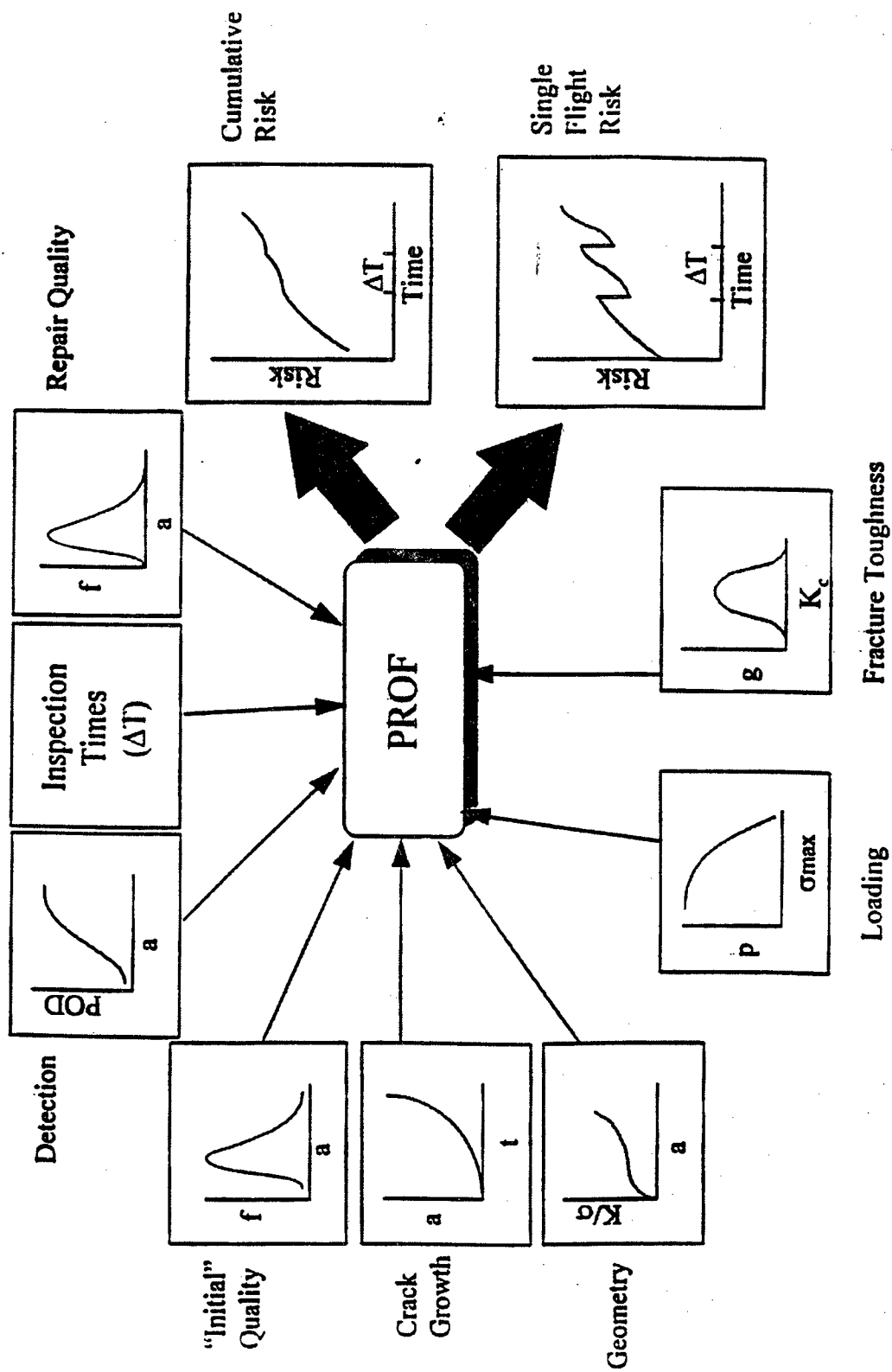
Provide probabilistic tools for risk assessment

Structural Integrity of Aging Aircraft

Wright Laboratory

- Widespread Fatigue Damage
 - AF is collaborating with FAA/NASA
 - Deterministic analysis/validation
 - Probabilistic analysis
 - WL/AFOSR/Purdue

RISK ANALYSIS FOR AGING AIRCRAFT



Structural Integrity of Aging Aircraft

Wright Laboratory

- PROF - Near-term plans
 - WFD scenarios
 - Multi-Element Damage
 - Discrete Source Damage
 - Validation

Structural Integrity of Aging Aircraft

Wright Laboratory

Dynamics

PROBLEM

Damage due dynamic loads interacting with structures

-Buffet, Limit cycle oscillation, cavity acoustics

GOAL

Develop/validate analysis methods

Demonstrate suppression techniques

Structural Integrity of Aging Aircraft

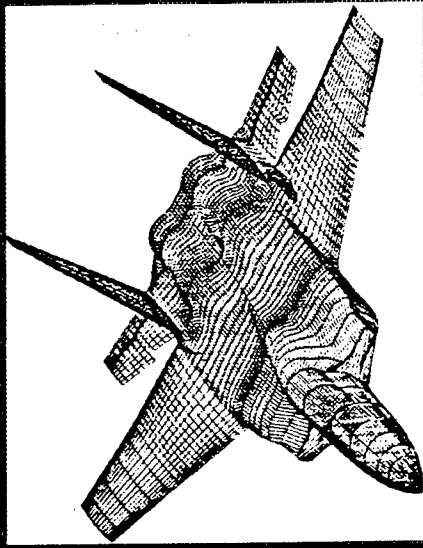
Wright Laboratory

- Dynamics
 - Excessive/repeated dynamic loads - Cracking
 - Premature aging leads to costly repair/replacement
 - Prediction and Suppression
 - Aeroelasticity, buffet, LCO, Acoustics

DYNAMICS - AEROELASTICITY

Solutions

- **Computational Aeroelasticity (ENS3DAE)**
 - Unsteady aerodynamics, aeroelasticity code
 - One of the most advanced codes available
 - Enhancing and validating capabilities
 - Collaborate with WL/FIM
 - Demonstrate analysis on F-15 and on F-5 wing
- **Limit Cycle Oscillation**
 - Wind tunnel testing with flow visualization
 - Develop general LCO prediction method
- **Twin Tail Buffet**
 - Measure dynamic response (F-18 twin-tails/AOA range)
 - Investigate buffet alleviation on F-15 model
 - Collaborate with Navy

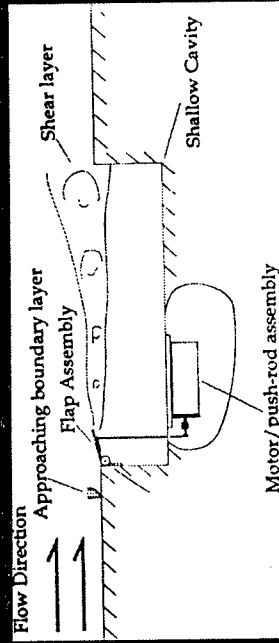


9519/DIG/13

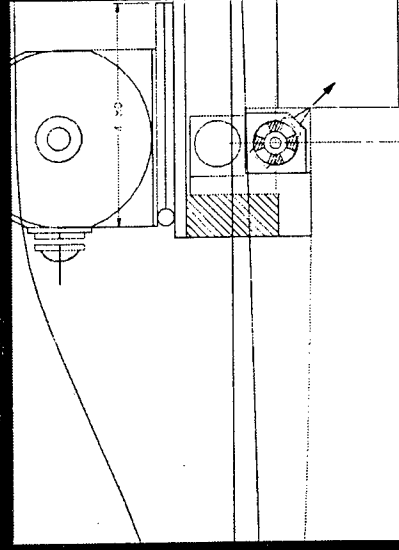
DYNAMICS - ACOUSTICS

Solutions

- **Long History in Field:**
 - 60's - prediction of frequencies/pressure amplification
 - 70's - reduction of pressure oscillations in cavities
 - 80's - supersonic flow
 - 90's - active control concepts
- **Develop Analytical Prediction**
 - Subsonic/supersonic free stream flow
 - PC based code to predict frequency, amplitude



Oscillating Flap



Blown Air

- **Evaluate Active Suppression Methods**
 - Analytical study
- **Wind Tunnel Tests - evaluate most promising**
 - Oscillating Flap (in tunnel now!)
 - Blown Air
- **Flight Test Best Concept**

Structural Integrity of Aging Aircraft

Wright Laboratory

Summary

- Technology development necessary
- Strategic collaboration required
- Product-oriented approach

Aging Aircraft Management

A Practical Analytical Approach For Effective Sustainment

**Presented At The 1996 USAF Structural Integrity
Program Conference, San Antonio, Texas**

3-5 December 1996

**J.B. Cochran
Lockheed Martin
Marietta, Georgia**

**R.E. Alford
WR-ALC/LJLEA
Robins AFB, Georgia**

Aging aircraft management in terms of safe operations is probably one of the primary concerns of both civilian and military users today. This presentation today deals with an analytical approach that provides maintainers with a tool that will aid the decision making process. Although presented in a generic sense, it is fair to say that it draws heavily on the last twenty (20) years of C-141 Starlifter force management experience.

I wish to thank my colleague Mr. Russ Alford, who is the C-141 ASIP Manager, for assisting me in putting together this presentation.

Acknowledgment

This presentation would not be possible without the full support and cooperation of the C-141 Engineering Branch at WR-ALC, Robins AFB , Georgia. The initiative to establish an analytical approach to aging aircraft force management during its sustainment years is a product of the long history and experience in managing the C-141 Starlifter.

The C-141 is the most heavily used aircraft in the large aircraft inventory of the Air Force and is the third oldest in years. With a service life goal of 45,000 hours, by the time it achieved 36,000 hours it was becoming increasingly apparent that force management during the remaining years of its service life was going to be a challenge. Over the last five (5) years, the C-141 Engineering Branch at Warner Robins Air Logistics Center, supported by the C-141 Structural Integrity Division at Lockheed Martin, have gained a great deal of experience in managing an aircraft that has exceeded its original design life. There have been pitfalls and successes, but out of it all has come an initiative to establish an analytical approach to managing an aging aircraft. We call it the Aging Aircraft Management Plan (AAMP).

The Need

An individual Aging Aircraft Management Plan (AAMP) that forecasts cost effective maintenance actions during the remaining 20% of the aircraft's service life, and at the same time, assures that a high level of confidence in operational safety is maintained until retirement.

In today's atmosphere of reduced budgets and increased world tensions, performing a "Global Reach" policy as adapted by the Air Mobility Command is heavily dependent upon aircraft availability. Available aircraft must be fully mission capable, safe to operate and ready to respond when called upon. This may sound good, but it does not happen without timely, proactive maintenance, and the full understanding of how past maintenance actions and aircraft usage affect the overall structural integrity and the aircraft's operational capability. To ensure that these goals are met in a cost effective manner, an individual Aging Aircraft Management Plan is imperative.

Why The Need

- Force Structural Maintenance Plan (FSMP) of the "mature years" not sufficiently adequate.
- Usage and user requirements tend to dictate shorter inspection/maintenance intervals, but the opposite occurs.
- Database required for rapid analytical response generally not readily available or non-existent.
- Unscheduled downtimes that could be avoided.

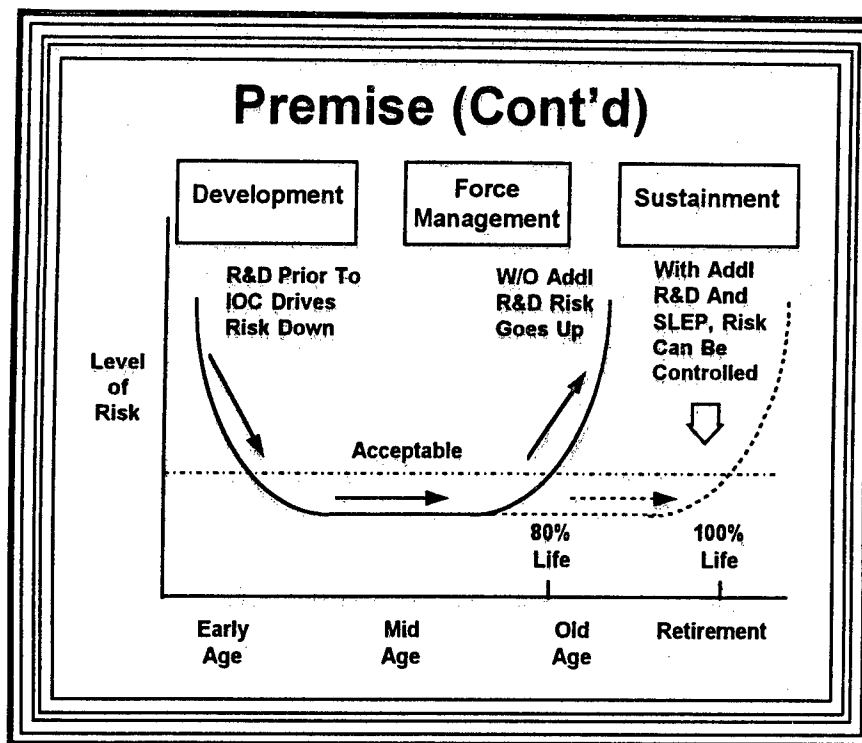
An Aging Aircraft Management Plan can provide for those actions that are dictated by increased usage, increased inspection intervals, lack of a comprehensive historical database and reduced funding. One may think of it as an extension or enhancement of the Mil-Std-1530 Force Structural Maintenance Plan (FSMP) to provide guidance in inspections, repairs and modifications in the latter years of an aircraft's service life.

Premise

The basis for this novel approach is the assumption that an aircraft enters into the aging aircraft environment at eighty percent of its estimated service life (at an acceptable risk) that takes Mil-Std-1530 Task 5 into a sustainment era until aircraft retirement.

This premise is not without some validity based on the findings of the 1994 Scientific Advisory Board Summer Study.

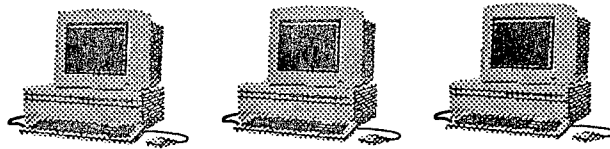
The second law of thermodynamics (or the Law of Entropy) states that although the total energy of a system is always the same, over time, more and more of that energy becomes less available for useful work. This is equally true of an aircraft. If we have learned anything in our past experiences, it is that the older a thing gets, the more attention it requires if it is to continue a useful function. With this in mind, and based on real experience with the C-141, as well as insight given by the 1994 Scientific Advisory Board (SAB) Summer Study on Aging Aircraft, we have selected the eighty (80) percent of service life point as the transition from a day-to-day FSMP to one that addresses the peculiarities of aircraft aging, i.e., the AAMP.



This chart is given to pictorially represent what has already been said. This chart is also taken from the 1994 SAB report that documents the findings of the Summer Study on Aging Aircraft.

Objective


Provide the user with a computerized logic analysis that results in recommended Force (or individual aircraft) Management actions commensurate with aircraft usage and maintenance experience, both past and forecasted.




Most, if not all, information required to make sound, logical decisions regarding force management actions resides in some electronic database. The inefficiency of the collation of this data for a specified problem rests in the current lack of an organized (electronic) approach to data retrieval, manipulation, and outputting of logical conclusions and/or recommendations.

The objective of the AAMP analysis program is to computerize the required assessments and analyses through use of some form of "artificial intelligence" or "neural network" programming that will give the user a systematic approach to addressing real or potential problem areas.

Requirements







- Historical database of usage, utilization, repairs, modifications, inspections, corrosion experience, system R&M data, and component/full scale test data that is readily accessible. 

- Thorough understanding and interpretation of statistical & probabilistic analyses as related to real experience and practical application thereof. 

- Proficiency in NDI reliability. 

The accuracy and reliability of the AAMP analysis program will be no better than the input data that drive the answers to the variety of "logic" questions and actions contained in the AAMP. The more comprehensive, accessible, accurate, and reliable the historical database of aircraft usage and maintenance related data is, the higher the confidence level the user will have in the statistical and probabilistic analyses results as they relate to real experience and practical application. One of the underlying factors of the recommended actions from the AAMP is and will be the reliability of Non-Destructive Inspections (NDI).

Influencing Factors

- Usage 
- Maintenance 
- Corrosion 
- NDI proficiency 
- Material properties 
- Policy/procedure changes 

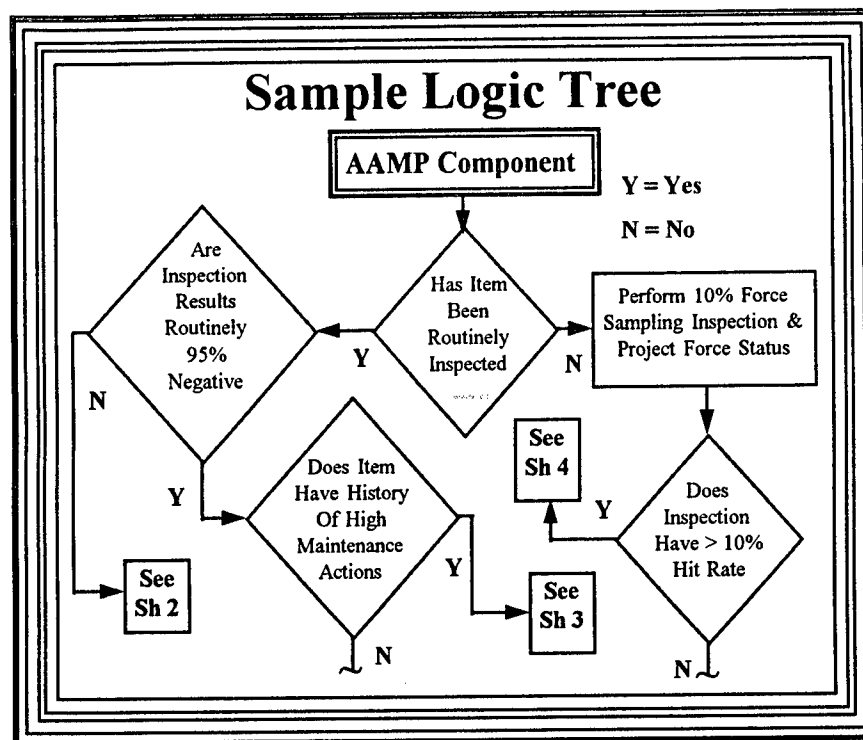
The list of factors shown above may not be all, but they are the most prominent with which any force management plan must contend. This is nothing new, as these factors are already very much a part of the Force Structural Maintenance Plan (FSMP). However, in the "aging" years of the weapon system, these same influencing factors usually become more pervasive in the overall force management decision process.

Solution-- "Geriatric Geritol"

(A prescription for an Aging Aircraft Management Plan)

- **Construct a logic tree for systematic actions.**
 - **Construct a database to support the systematic actions.**
 - **Establish statistical & probabilistic analysis routines consistent with existing analysis tools such as DTA and FEM.**
 - **Computerize the logic tree "logic" with interactive capability to analysis routines.**
- (The AAMP analysis program)**

Managing an aging aircraft in the latter years of its service life is challenging to say the least. Seemingly, the day-to-day modus operandi of force management intensifies with an increasing frequency of problems that threaten aircraft availability. This presentation has set the tone for an enhanced means of dealing with these increasing threats, and now it's time to formulate a solution. Although the title of this chart is humorous, it nonetheless is appropriate for aging aircraft management. As stated earlier in our objective, the "geriatric" prescription calls for a computerized process having interactive capability with established analysis routines. In other words, construct an AAMP analysis program.



This chart is shown only to give an example of constructing a logic tree to address problems that affect structural and systems integrity (to what degree yet to be determined). The key is to construct the logic tree in a systematic approach that begins with a rhetorical question and proceeds through an ever expanding series of questions and actions until a final solution is achieved.

The next four (4) charts are really a continuation of this chart to give an idea how an analysis program might address the prescribed actions.

Logic Tree Analysis

Has
Item Been
Routinely
Inspected

The "yes" or "no" answer to this question requires the AAMP analysis program to access the historical inspection records for frequency of inspections and compare with a pre-defined "routine" interval.

In the above question, the user may use his or her engineering judgment for the "yes" or "no" answer. However, if the AAMP analysis program is to be substantiated by the accuracy of input data, then it is appropriate to allow the program to access the documented records to determine the answer based on a predefined and programmed "routine" interval.

Logic Tree Analysis

**Are
Inspection
Results
Routinely 95%
Negative**

**AAMP again accesses the database and
calculates the number of positive findings
versus the total inspections to answer this
question.**

Again, the AAMP analysis program will access the appropriate database and calculate the answer.

Logic Tree Analysis

**Perform 10% Force
Sampling Inspection &
Project Force Status**

**With insufficient information for continued
analysis, AAMP recommends a force
management action before proceeding with
the analysis to obtain a final action.**

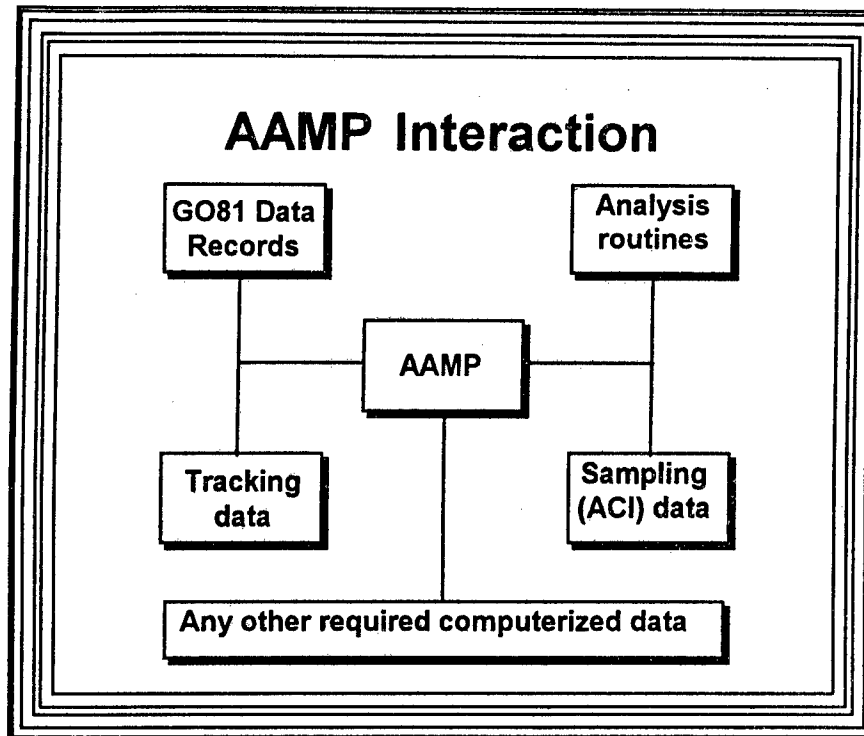
When the AAMP analysis program encounters "insufficient" data to continue its calculations, it will provide a recommendation aimed at obtaining the needed information. The above statement is a sample of a pre-programmed recommendation.

Logic Tree Analysis

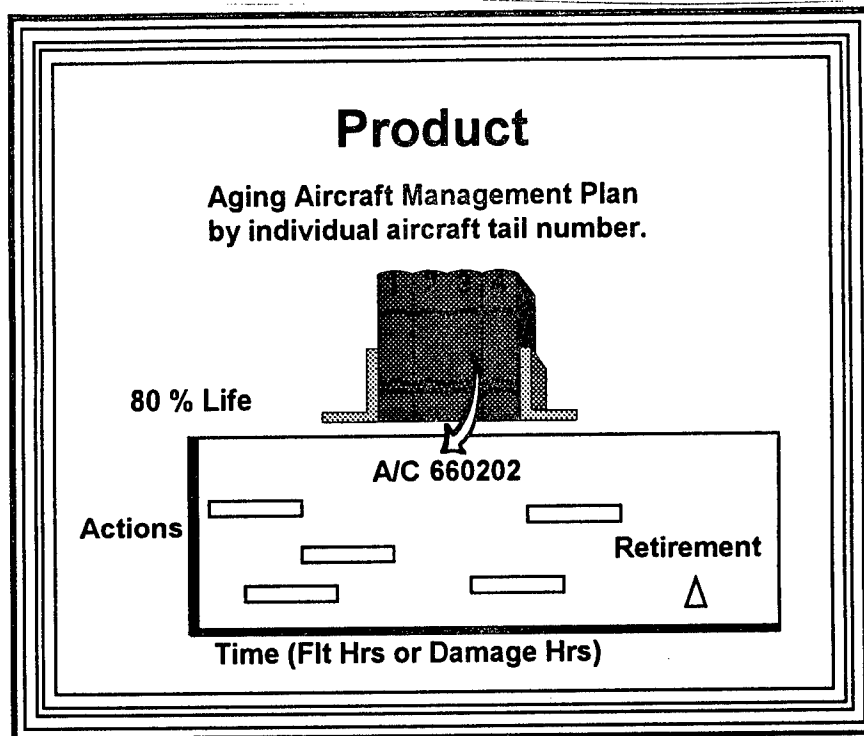
Does
Inspection
Have > 10%
Hit Rate

Based on number of inspections and findings,
AAMP calculates the hit rate and continues its
analysis appropriately.

This is an example analysis continuation based on results of a recommendation that was implemented. Calculating the appropriate answer, the program then continues the logic progression to final solution.



As depicted in the above chart, the AAMP analysis program will have interactive capability with required source data as well as specialized analysis routines. For the C-141, it is envisioned that AAMP will be another analysis tool under the umbrella of the Automated Readiness Integrated Engineering System (ARIES).



Although the AAMP analysis program is not in itself an Aging Aircraft Management Plan, it nonetheless provides a methodology needful for the formulation of such a plan. As the weapon system ages, averages (in terms of usage and maintenance actions) tend to lose their meaning. What becomes important is those things that affect the individual aircraft. Appropriate utilization of the AAMP analysis program will significantly aid in the development of an individual aircraft timeline of proactive events that minimize aircraft downtime and maximize aircraft availability.

AAMP Future Plans

- Continue development throughout 1997.
- Have a working model by end of 1997.
- Setup instructions and users guide by mid 1998.
- Export technology to other weapon systems.

That's all folks!



The AAMP analysis program is in no way operational at this time. What we have attempted to do with this presentation is bring an awareness of this initiative to the audience. We think it will be a very beneficial tool for the ASIP manager. We will continue to develop this concept throughout 1997 with a goal of having a working model by the end of the year. If all goes well, set up instructions and a user's guide should be available by mid 1998. It is the intent of the C-141 ASIP manager to make the AAMP analysis program available to anyone that wishes to incorporate it into their respective force management plans.

1996 USAF Structural Integrity Program Conference

3-5 December 1996

San Antonio, TX



F117-PW-100 TAILORED ENSIP for FIVE PEACETIME C-17 MISSIONS

**Presenter: Subhash Patel
Pratt & Whitney**

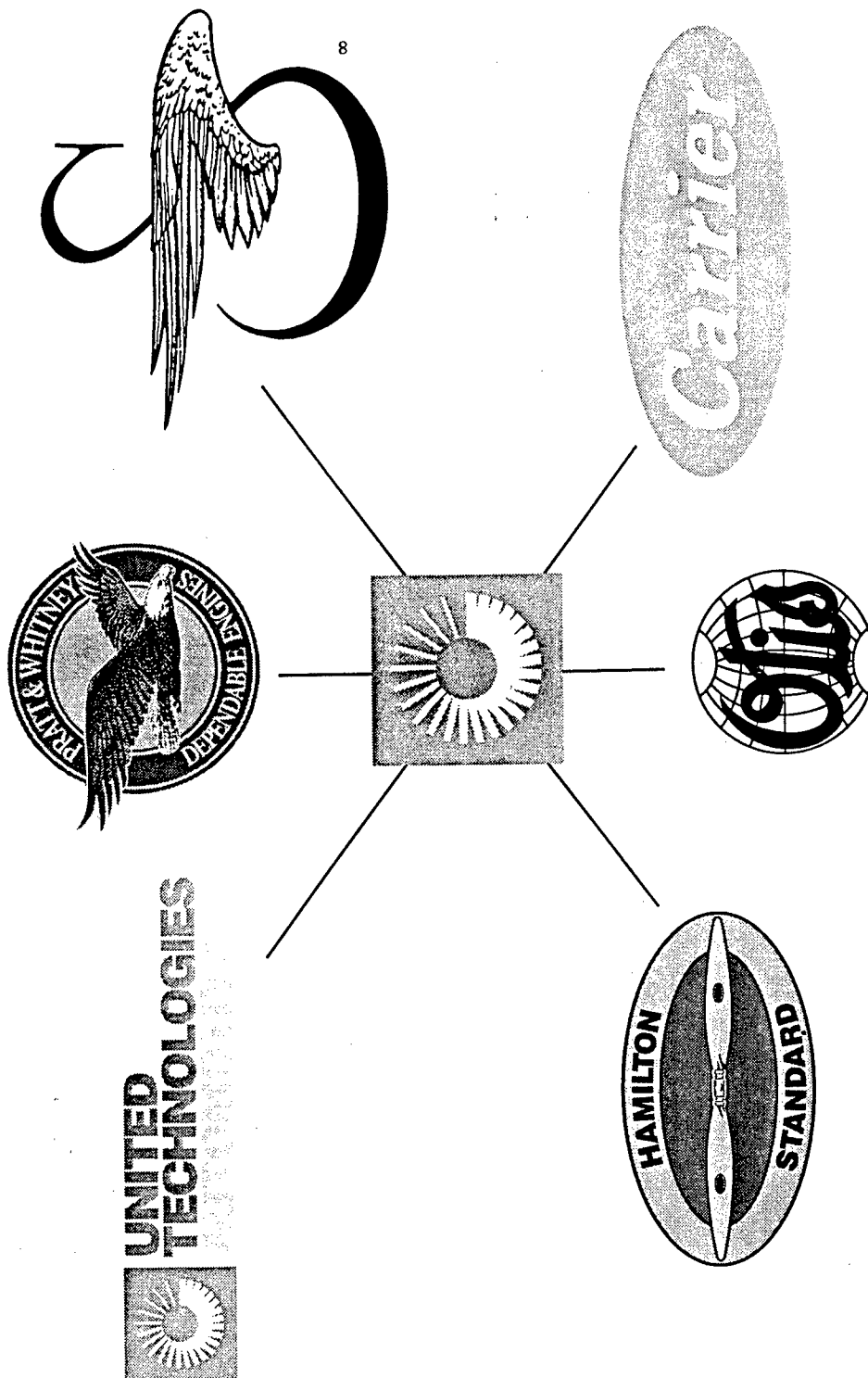
Authors: Subhash Patel, Herman Johnson

PRESENTATION OVERVIEW

- Background
- Tailored ENSIP Assessment
 - Program Goals and Schedules
 - P&W/USAF Teams
 - Design Criteria
 - Manufacturing and Quality Control (NDI assessment)
 - Material Characterization
 - Component Testing
 - Engine Life Management Plan
 - Life Tracking System
- Program Status
- Summary

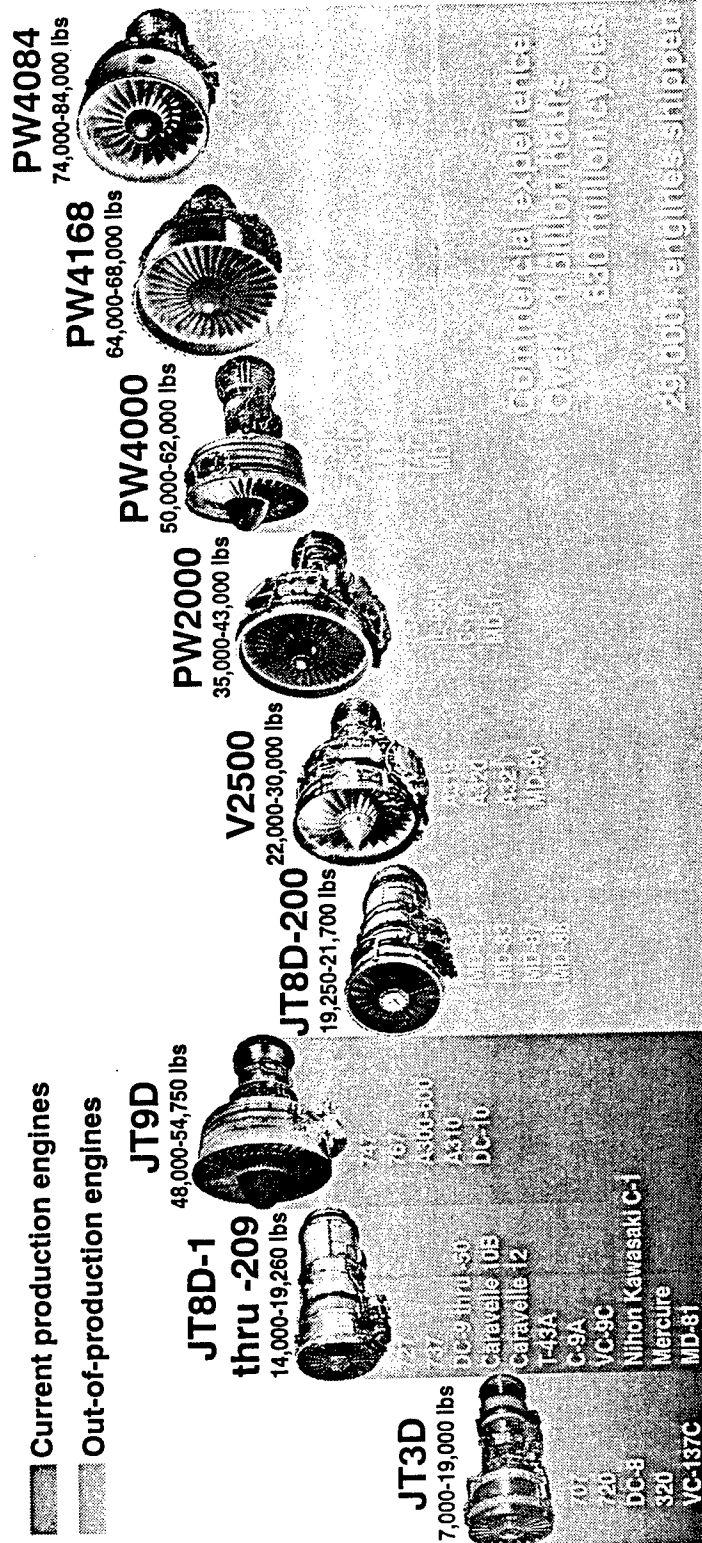


UNITED TECHNOLOGIES CORPORATION (UTC)

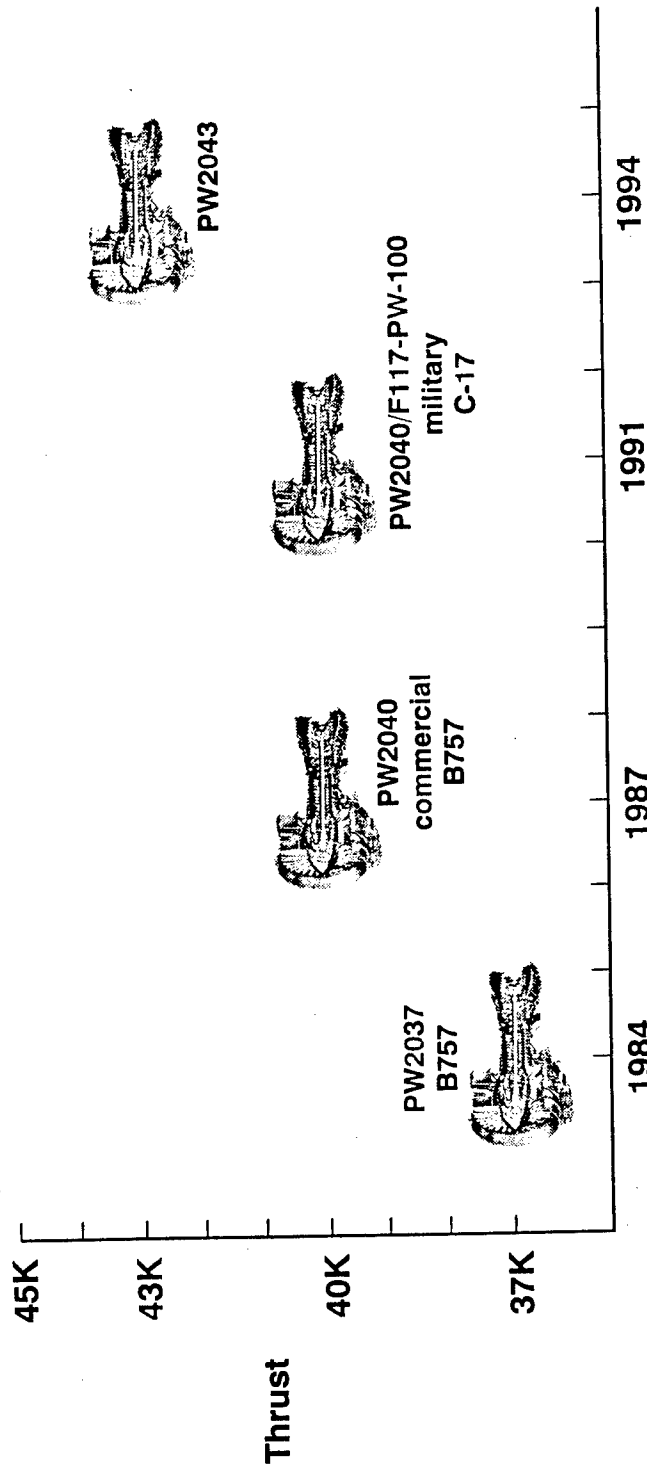


PRATT & WHITNEY PRODUCTS

POWER FOR THE WORLD'S COMMERCIAL AIRCRAFT



PW2000/F117 ENGINE FAMILY

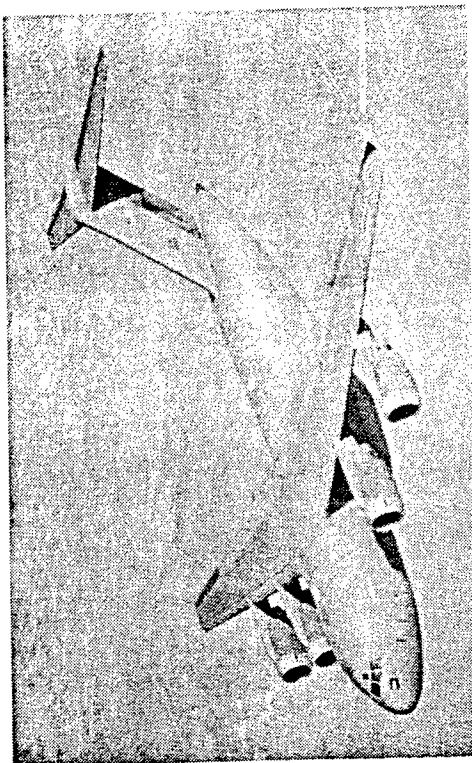


- USAF purchased off-the-shelf commercially FAA certified engine
- Advantages to the USAF
 - No engine development funds required from USAF
 - Preferred customer status for the USAF (cost/engine)
 - Commercial upgrades automatically included in C-17/F117



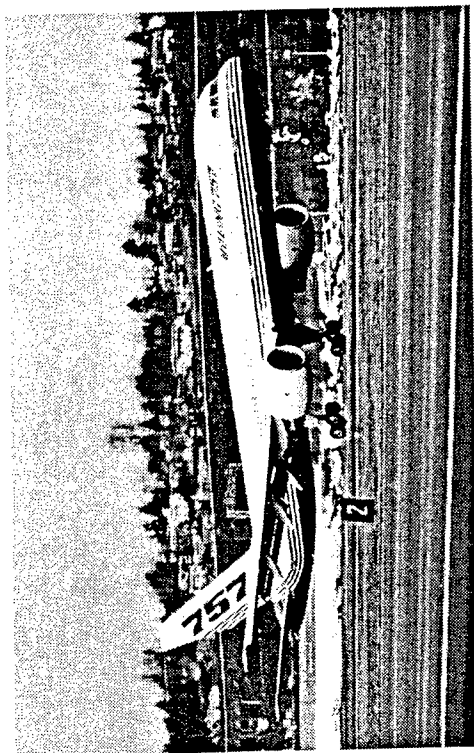
COMMERCIALLY PROVEN ENGINE FOR GLOBEMASTER III

F117-PW-100



C-17 Globemaster III

PW2000



Boeing 757

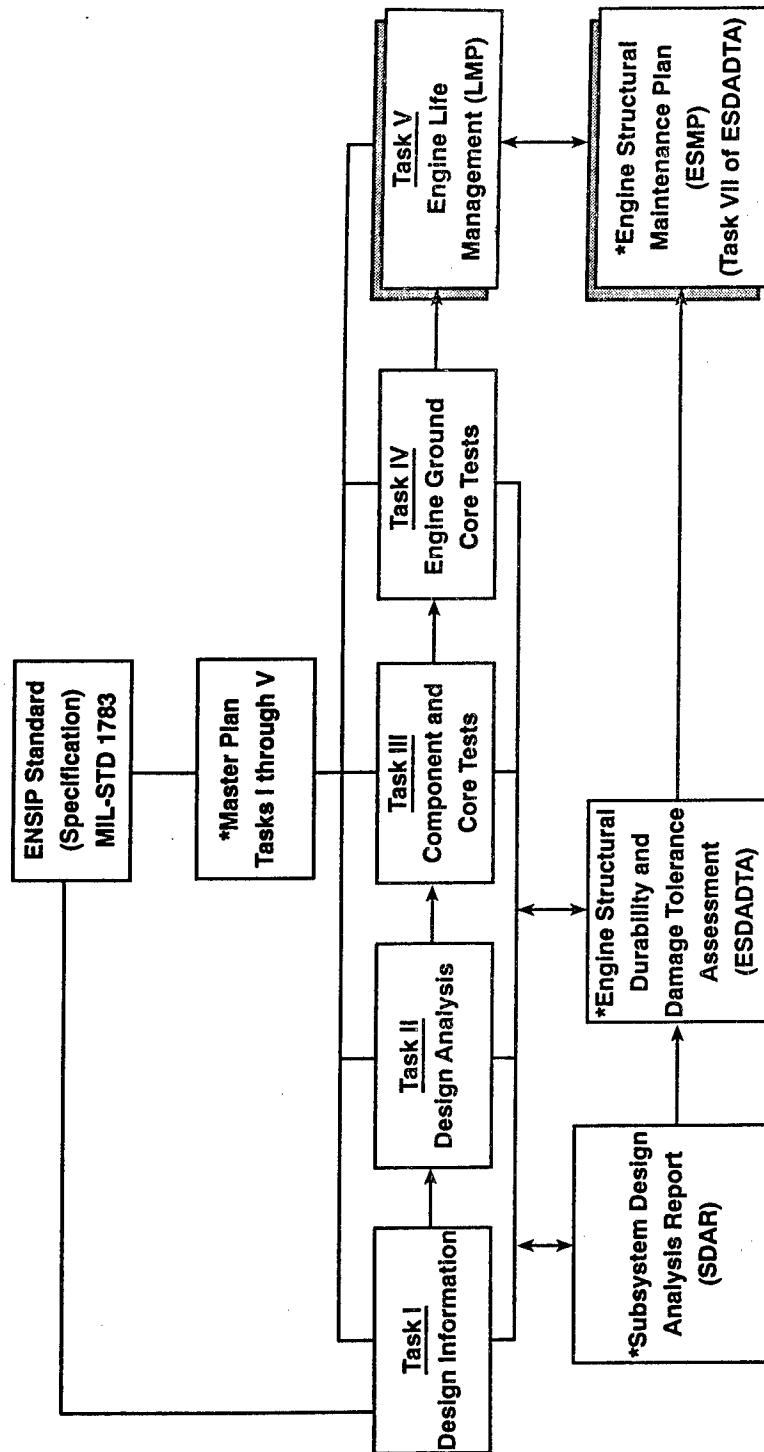


**F117-PW-100 (DO-3)
TAILORED ENSIP ASSESSMENT
for
'94 IMPROVEMENT PACKAGE
ENGINE**



F117-PW-100 ENSIP

PROGRAM TASKS



*Deliverable Documents



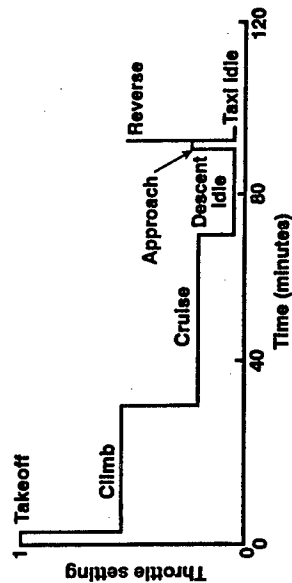
F117-PW-100 ENSIP

TAILORED ENSIP ASSESSMENT

- PW2000 service experience documented for initial benchmark
- PW2000 FAA tests and reports used for ENSIP as applicable
- ENSIP assessment limited to five peace time C-17 missions defined by USAF
- Damage tolerance verification tests performed on selected components
 - HPT rotor hot cyclic spin test
 - Diffuser case hot cyclic pressure test
- X-664-13 engine telemetry test utilized to verify latest HPT thermals
- No accelerated mission engine testing performed
 - Commercial testing done for FAA certification
- Conceptual design improvement options considered
 - Detailed Design/Implementation outside the scope of this program

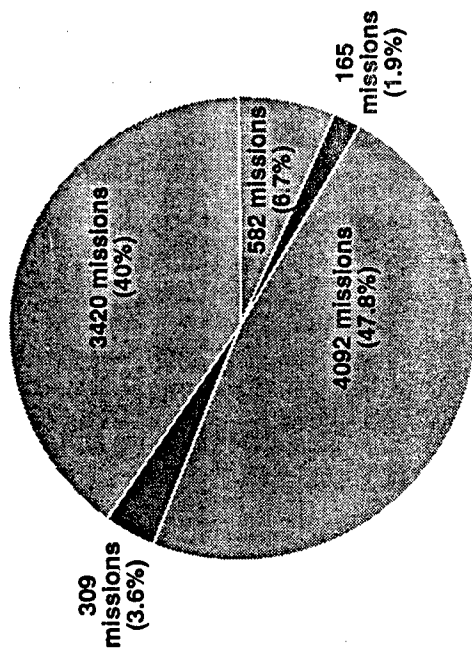
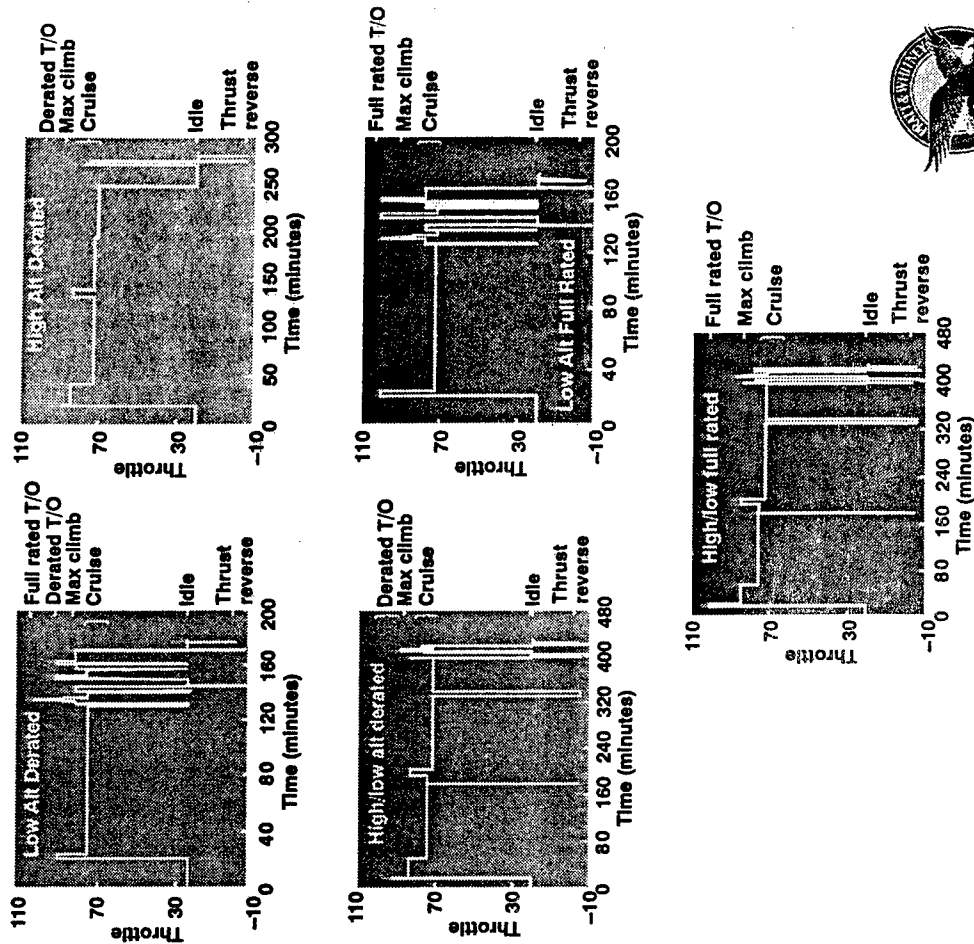


Commercial Mission



Typical commercial mission full rated takeoff

Military Missions for ENSIP Assessment



8568 missions in 30,000 EFH

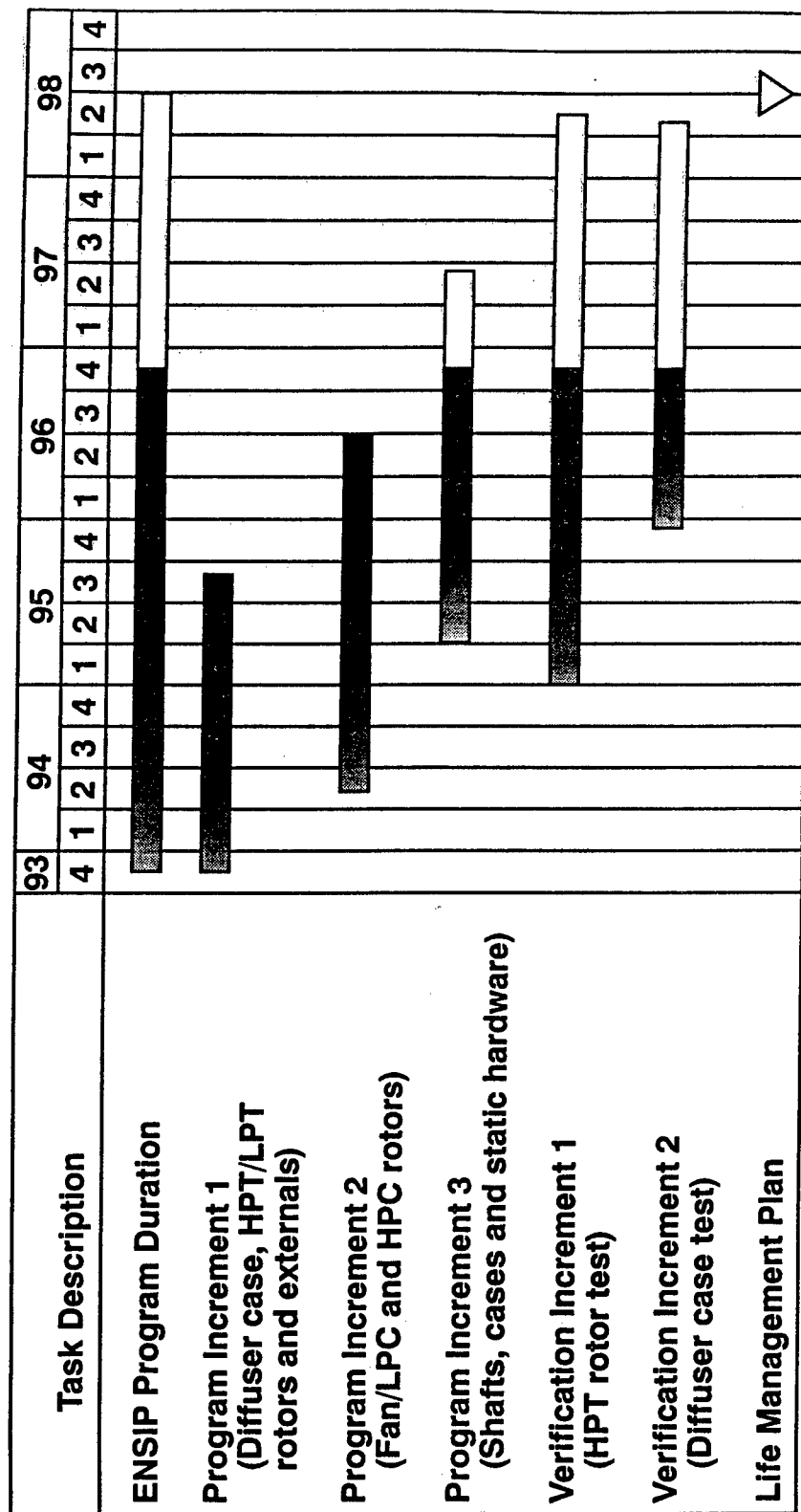
F117-PW-100 ENSIP

PROGRAM GOALS

- Durability and damage tolerance analysis for five peace time C-17 missions that meets the intent of Mil-Std-1783 for '94 package F117-PW-100 (DO-3) engine
- Integrate PW2000 service experience and ENSIP analysis to establish recommended inspection interval/maintenance requirements
- Life Management Plan at program end provides for safe engine operation and maximizes fleet life



OVERALL PROGRAM SCHEDULE



F117-PW-100 ENSIP

PROGRAM DELIVERABLES

- Master plan – annual update
- Engine Structural Durability And Damage Tolerance Assessment (ESDADTA) plan – annual update
- Subsystem Design Analysis Report (SDAR) – semi-annual update
- Engine Structural Maintenance Plan (ESMP) – annual update
- Engine Life Management Plan (LMP) at program end



F117-PW-100 ENSIP TEAMS

PRATT & WHITNEY/USAF ENSIP EXPERIENCE INTEGRATED

- Pratt & Whitney/USAF Technical Steering Committee
 - Provides a forum for detailed technical reviews
- Pratt & Whitney Internal Review Team
 - Internal technical reviews/consistent ENSIP application
- Pratt & Whitney Materials Test and Characterization Team
 - Monthly status reviews
- Pratt & Whitney ENSIP Analysis Teams
 - Dedicated teams for Fan/LPC, HPC, IC/Fn mount, Diffuser/Combustor, HPT, LPT and engine External
 - Weekly status reviews



F117- PW-100 ENSIP

DESIGN CRITERIA

Fracture critical and durability critical components identified for analysis

F117-PW-100 design usage requirements

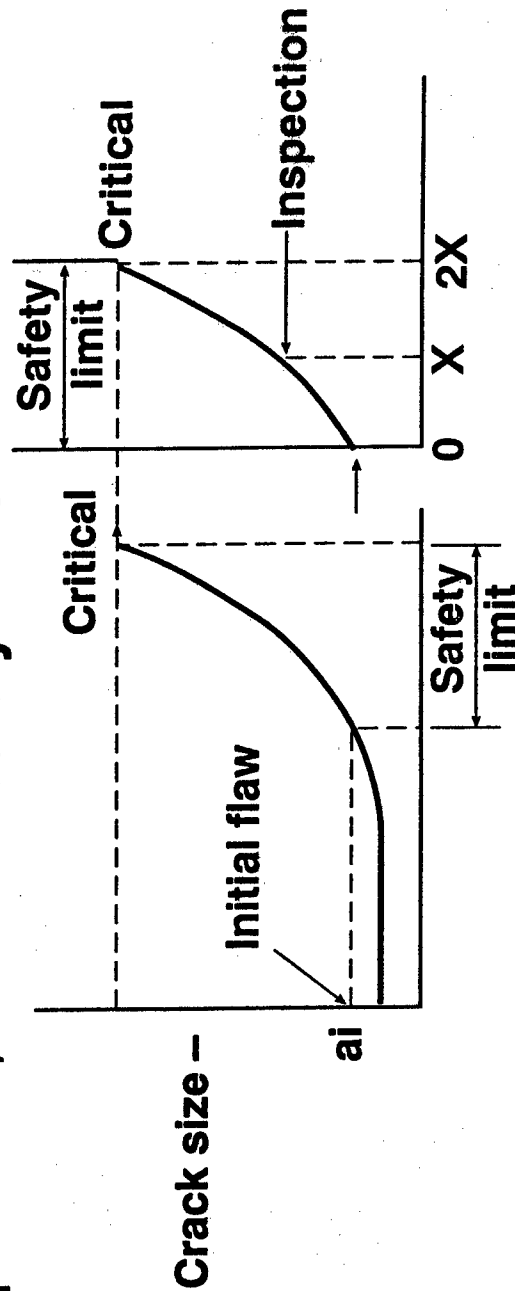
<u>Parameter</u>	<u>Quantity</u>
Engine Flight Hours (EFH)	30,000
Total accumulated missions	8568
Total low-altitude, full rated takeoff missions	309
Total low-altitude, derated takeoff missions	4092
Total high-/low-altitude, full rated takeoff missions	165
Total high-/low altitude, derated takeoff missions	582
Total high-altitude derated takeoff missions	3420



F117- PW-100 ENSIP

INSPECTION INTERVAL

- Assume initial flaws at critical locations (depends on inspection capabilities)
- Determine life to critical crack size (safety limit)
- Inspect at $1/2 \rightarrow 1X$ safety limit



Usage – (hrs/missions) Usage – (hrs/missions)



F117-PW-100 ENSIP

MANUFACTURING AND QUALITY CONTROL NDI ASSESSMENT

- F117-PW-100 recommended embedded and surface flaw sizes are based on F100-PW-229 NDI reliability experience
- Embedded flaw size based on demonstrated sonic capability
- Surface flaw size assumptions for damage tolerance calculations are consistent with F100-PW-229 demonstrated capability
- Enhanced depot inspection requirements are based on F100-PW-229 eddy current capability



F117-PW-100 ENSIP

NDI DEVELOPMENT/CAPABILITY DEMONSTRATION ACTIVITY

- Improved Sonic NDI Capabilities for Embedded Flaw detection
 - Demonstrated acceptable signal/noise ratio \approx # 1 FBH for fine grain Inco 718 LPT disks
 - Enhanced capability for Powder Nickel IN100 (PWA1100) to \leq # 1 FBH for HPT disks
- Developed Enhanced NDI for EB welded titanium drum rotor unmachined weld ID surface
 - “Bubbler Probe” Shear Wave Sonic (SWS) inspection from weld OD machined surface
 - Demonstrated capability to detect active 0.020" x 0.040" cracks from ID surface weld spatter
 - SWS inspection can detect surface or embedded weld anomalies



F117-PW-100 ENSIP

INITIAL SURFACE FLAW SIZE RECOMMENDATIONS

- Based on F100-PW-229 reliability report, recommended F117-PW-100 initial flaw size is 0.020" x 0.040" for focused and 0.035" x 0.070" for normal FPI procedures
- Accepted alternative enhanced inspection technique for use at depot is eddy current
- 0.010" x 0.020" and 0.020" x 0.040" initial flaw size used for F117-PW-100 sensitivity studies



F117-PW-100 ENSIP

LCF AND FRACTURE MECHANICS TESTING PERFORMED TO SUPPORT F117 ASSESSMENT

Material	LCF	Fracture Mechanics
PWA 1100 (powder nickel)		
PWA 1085 (spheroidal Delta INCO 718)	Partial characterization	Full characterization
PWA 1469 (Cast + Hip INCO 718)	Partial	Full
	Partial	Full
PWA 1228 (Ti6-4)	Partial	Spot check
PWA 1224 (α -Beta Ti6-2-4-2)	Partial	Partial
PWA 1225 (Beta Ti6-2-4-2)	Partial	Full
PWA 1085 EB weld	Spot check	Partial
PWA 1224/1225 EB welded	Partial	Partial
AMS 5616 (Greek ascology)	Spot check	Partial
PWA 1262-1 (Cast + Hip Ti6-4)	Spot check	Partial



F117-PW-100 ENSIP

LCF AND F/M TEST PROGRAM

Materials test:

Incorporates existing data base from CEB and expands data base to cover requirements of complex military missions

- Screening tests to establish equivalency
- Additional R-ratio, temperature, frequency (dwell) tests
- Subelement verification tests to correlate life system models
 - Constant amplitude tests
 - Simulated duty cycle tests

Component test:

- Preflawned component verification tests
 - Verify component residual life capability
 - Correlate analysis models against actual component feature cyclic capabilities



F117-PW-100 ENSIP

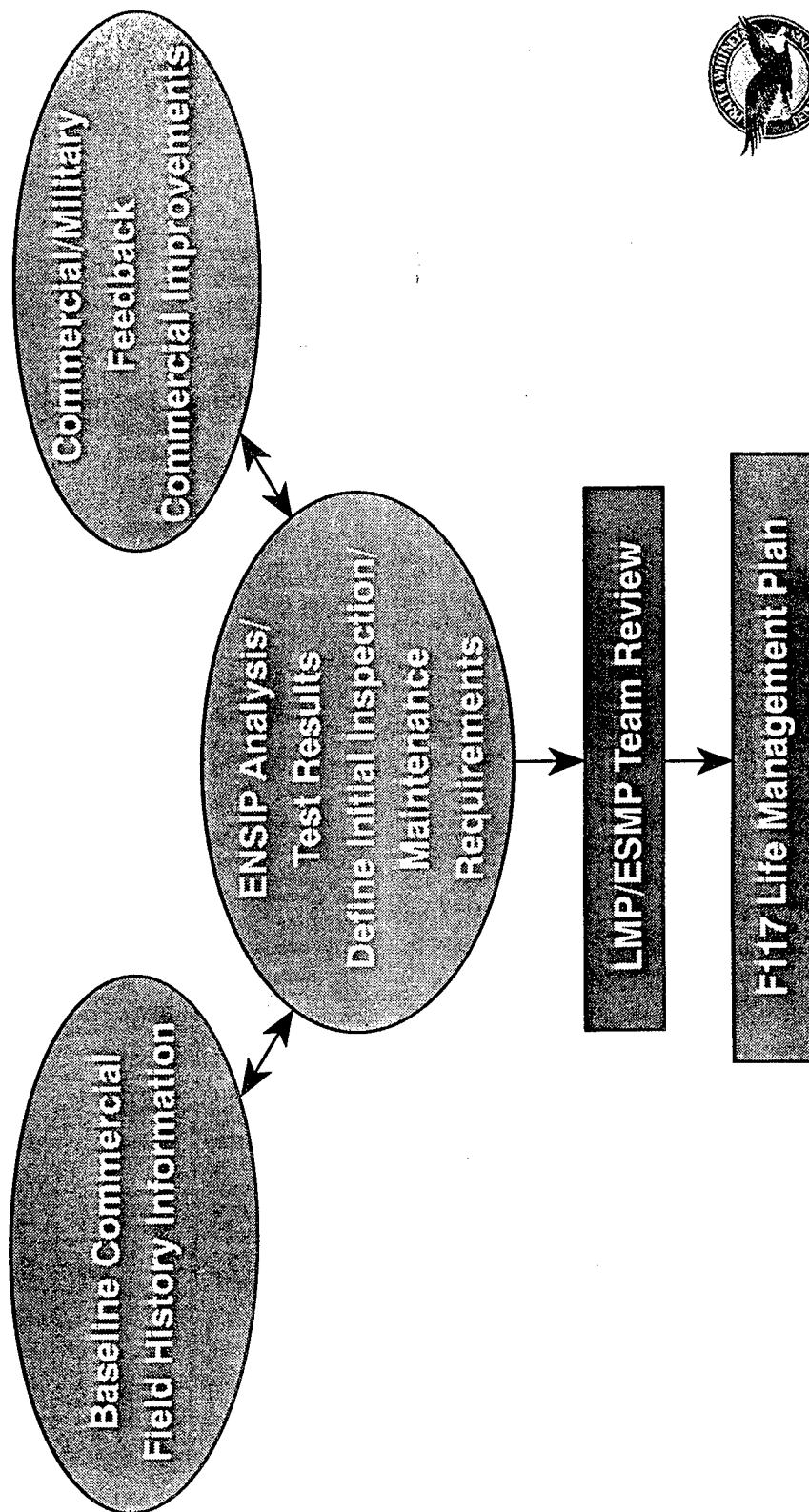
COMPONENT TESTING

- Damage tolerance verification test performed on selected components
 - HPT rotor hot cyclic spin test
 - Diffuser case hot cyclic pressure test
- Remaining components by analysis/similarity to other Pratt & Whitney military programs
 - HPC drum rotor per F100-PW-229
 - Welded Fan/LPC 3 stage drum per F100-PW-220/229



F117-PW-100 ENSIP

ENGINE LIFE MANAGEMENT PLAN LMP PROCESS UTILIZES SEVERAL DATA SOURCES



F117-PW-100 ENSIP

LIFE TRACKING SYSTEM

- Critical components tracked individually via tape downloads to ground based data system (G081)
- Multiple life tracking equations used for critical components:
 - “K-factors” relate severity equivalency of major transients to on/off (Type I) cycle
 - Convert to “equivalent commercial cycle”
- Track against same LCF limits used by commercial operators



F117- PW-100 ENSIP

PROGRAM STATUS

- Increment I – Diffuser case, HPT and LPT rotors, and engine externals
 - Increment I is complete
- Increment II – Fan/LPC and HPC rotors
 - Increment II is complete
- Increment III – Cases, shafts, and static hardware
 - Analysis effort is on schedule
- Verification I – HPT rotor test
 - Hardware procurement is in process
 - Test is planned in 1997
- Verification II – Diffuser case test
 - Hardware procurement is in process
 - Test is planned in 1997



F117-PW-100 ENSIP

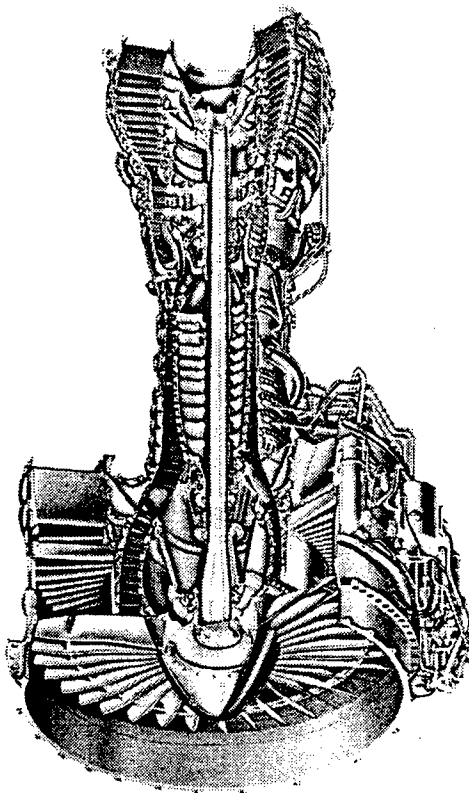
DEPOT INSPECTION INTERVAL

- Increment 1 and Increment 2 component analysis supports recommended inspection interval of 2000 composite missions/6000 N1 cycles
- Enhanced inspection areas and requirements identified
 - Improved NDI capability demonstrated
 - Supports inspection interval recommendations



F117-PW-100 ENSIP

ENHANCED INSPECTION REQUIREMENT



← Increment II →		← Increment I →	
Fan/LPC rotor		HPC rotor	
ECI	2 areas	ECI	12 areas
Re-sonic	4 areas	Re-sonic	3 areas
SWS	none	SWS	11 areas
Focused		Focused	
FPI	7 areas	FPI	17 areas
Diffuser case		HPT rotor	
Focused		ECI	10 areas
FPI	3 areas	Re-sonic	none
		Focused	
		FPI	21 areas
LPT rotor			
ECI	13 areas		
Re-sonic	1 area		
Focused			
FPI	19 areas		



ECI - Eddy Current Inspection
SWS - Shear Wave Sonic Inspection

F117-PW-100 ENSIP

SUMMARY

- Impact of five peace time C-17 missions on part lives have been quantified
- Detailed structural assessment results utilized to identify inspection/maintenance requirements
- Depot inspection interval 2000 missions/6000 cycles, equivalent to 6-7 years of field usage
- Application of ENSIP philosophy will maximize fleet life, minimize risk, and reduce life cycle cost



ASIP and the Air Force Aging Aircraft Fleet

Mr. Richard N. Hadcock
RNH Associates, Inc.
6 Sue Circle, Huntington, NY 11743-1979

1996 USAF Structural Integrity Program Conference
San Antonio, Texas, December 3-5 1996

Introduction

This paper was prepared from assessments and evaluations of the USAF aging aircraft fleet, which were undertaken at the request of Mr. Tobey Cordell, WL/MLLP, as part of the ML/WL Aging Systems Special Emphasis Area between March 1994 and November 1996.

Note: This paper has been prepared under U.S. Air Force Contract F33615-93-D-5326, Delivery Order 0001 "Engineering Assessment of Aging Systems" to Universal Technology Corporation, Dayton, Ohio, Subcontract 96-S401-01-36-C1 to RNH Associates, Inc. Richard N. Hadcock reports to Mr. Tobey M. Cordell, WL/MLLP. The paper was cleared for public release by ASC/PA on October 22, 1996, Reference No. ASC-96-2656.

Analyses of aircraft cost and price data included in this paper were performed under an in-house study at no cost to the contract.

Conclusions from this study are based on the author's personal assessments.

Summary

In 1995, the combined USAF Active-Duty, Air Force Reserve, and the Air National Guard aircraft fleet consisted of 6,624 aircraft with an average age of 17.5 years.

Of the total of 44 different types of aircraft in service, the structure of only eight were designed to the Air Force durability and damage tolerance requirements introduced in 1975. Thirteen other types were designed to prior USAF requirements, and the three types of helicopters in service were designed to U.S. Navy or U.S. Army requirements.

Of the other 20 types in the fleet, 16 are basically civil aircraft which were designed and certificated to FAA requirements prior to the introduction of the 1978 Structure Damage Tolerance and Fatigue Evaluation requirements. Two types are trainers based on foreign civil aircraft which were certificated to post-1978 FAA requirements, and two types are foreign military transports. Twenty-six percent of the fleet are over 30 years old, and many are scheduled to remain in service for an additional 20 to 30 years. Since many of these aircraft are made from aluminum alloys which suffer from corrosion and have poor fatigue resistance and fracture toughness, early detection and repair of corrosion and fatigue damage is essential.

It would take almost 100 years to replace the existing fleet at the current Air Force budget level for new aircraft procurement. It is therefore critical to maintain the airworthiness and operational capability of the aging aircraft in the fleet.

This paper includes information on the numbers and ages of the aircraft which made up the fleet as well as some estimates of replacement costs and service lives.

AGING AIRCRAFT ASSESSMENTS

Decisions whether or not to repair damage, replace components or retire individual aging aircraft are made after assessments are made from the three different considerations :

- **Structural Integrity;**
- **Operational Capability**
- **Continuing Life-Cycle and/or Aircraft Replacement Costs**

Structural Integrity

The USAF Aircraft Structural Integrity Program (ASIP) was established in 1958. The process, which has been very successful, consists of five tasks for each type of aircraft and is described together with task elements by Lincoln.^{1,2}

A critical component of the process is detection and definition of the extent of any fatigue cracks, particularly multi-site damage (MSD) or widespread fatigue damage (WFD) as well as various forms of surface, stress corrosion cracking (SCC) and exfoliation corrosion without disassembly of the structure. The Air Force Nondestructive Inspection program and the relationship of nondestructive inspection (NDI) and nondestructive evaluation (NDE) to Air Force aging aircraft is described by Cordell³. Cordell also describes the capabilities of various NDI/NDE systems to detect cracks and corrosion.

Operational Capability

Considerations affecting operational capability of individual aircraft and the fleet include:

- Effects of flight, payload and other restrictions
- Effects on Mission Capability Rates
- Effects of field and Programmed Depot Maintenance (PDM) schedules on aircraft availability
- Effects of aircraft retirements on overall fleet effectiveness

Some aircraft may be taken out of service for long periods of time if out-of-production replacement components or parts are unavailable and have to be fabricated, ordered from vendors or cannibalized from retired aircraft.

Life-Cycle Costs

Considerations used to assess aircraft life cycle costs include:

- Original R&D and acquisition costs
- Field and depot maintenance costs including NDI, repair, component replacement, and costs of equipment and training
- Costs of Engineering Change Proposals (ECPs) and major modifications
- Redesign and recertification, including selection and approval of new or substitute materials and processes

- Cost of extended or additional structural tests
- Current aircraft value and replacement costs

Maintenance costs, including the costs of corrosion and crack detection using NDI/NDE can be high, particularly if disassembly is required. Costs of new replacement components and parts, especially out-of-production forgings and machined parts, can be very high and delivery times can be many months or even years. Cannibalization or retrieving, inspecting and certifying old parts taken from aircraft in storage at Davis-Monthan AFB is expensive, but may save valuable time.⁴

A major consideration for the older aircraft is the effect of inflation during the past 20 to 40 years. As will be discussed later, inflation factors based on actual aircraft costs are much higher for military aircraft than standard rates: The flyaway cost of the C-130A was only \$2 million in 1957 whereas the cost of a C-130H is \$30 million in 1995.^{5,6}

Aircraft Costs and Prices

Various deflators have been developed for military aircraft costs and commercial aircraft prices. These include cost deflators are based on Federal Price Deflators for Defense Purchases, the Consumer Price Indices (CPI) for urban consumers, Producer Price Indices (PPI), as well as the deflators for Aircraft, Standard Industrial Classification (SIC) 3721, estimated by the Aerospace Industries Association (AIA) based on data from the Bureau of Labor Statistics, Producer Price Indices, Bureau of Economic Analysis, and the Commerce Department. Between 1950 and 1995 all these indices are of the same order as the CPI.

The average weekly wages for aircraft production worker has risen from \$68 in 1950 to \$770 in 1995.⁵ Aircraft production workers weekly wage deflators are slightly lower than the CPI and SIC 3721 deflators.

Inflators, which are the inverse of these deflators, have been used to convert then-year costs and prices to 1995 dollars. These are plotted in Figure 1.

Actual 1966 and 1995 costs of Lockheed C-130 military transport and prices of Boeing 737 airliners are listed in Figure 2. Actual inflation factors are 12 and 8.7 respectively when costs and prices are normalized to dollars per pound of aircraft empty weight to account for changes in operating empty weight (OEW). The comparable 1996-95 SIC and CPI inflation factors are very much lower at only 4.3 and 4.7 respectively. More than 2,100 C-130s and 2,500 Boeing 737s had been produced by 1995 and production of both aircraft will probably continue well into the next century.

Actual fly-away then-year costs and constant 1995 costs based on CPI inflators for the C-130 are shown in Figure 3. The constant 1995 dollars, C-130 costs increase by 140% between 1955-59 and 1990-94, whereas they should remain constant or decrease with the number of aircraft produced from the effects of learning curves. During the 1955-1995 time frame the percentage of flyaway cost of the airframe remained steady at 70% to 71%. The percentage of flyaway cost associated with avionics did increase from 2.4% for the C-130A to 4.5% for the C-130H but this is insufficient to cause the 140% cost increase.

These increases above general inflation have most been caused by the major reductions in the numbers of military aircraft procured, which have affected many of the cost elements listed in Figure 4. Other factors include implementation of more and more stringent government specifications and contractual and EPA regulations.

Over the 1950-95 time period, the number of military aircraft produced in the U.S. has dropped from a peak of 8,978 in 1952 to only 450 in 1995.⁵ Deliveries of military aircraft and fixed-wing commercial aircraft over 33,000 lb. are shown in Figure 5.

Then-year costs of military and prices of commercial aircraft are converted to 1995 costs and prices using the curves in Figure 6. The upper curve, titled "US Military Aircraft", was derived from analysis of the annual costs of 106 different types of USAF and USN aircraft produced between 1950 and 1995, based on the hypothesis that the flyaway costs (in constant 1995 dollars) of specific types of military aircraft should decrease with quantity, or, at worst, remain constant. Some of these aircraft (F-15, F-16, F/A-18, B-2, C-17, and C-130) were still in production in 1995, providing actual 1995 flyaway costs. The curve titled "US Commercial Aircraft" shown in Figure 6 was based on the hypothesis that prices (in terms of dollars/pound empty weight) of specific types of commercial aircraft should essentially remain constant with time, other than moderate increases caused by the introduction of derivative models. The database for commercial aircraft inflators included prices of 16 different turbojet airliner from 1958 through 1995. Aircraft still in production in 1995 include the Boeing 737, 747, 757, 767 and 777 and the McDonnell Douglas MD-80 and MD-11.

In Figure 7, the curve of "US Military Aircraft" cost inflators from Figure 6 is compared with an inflator curve based on the CPI multiplied by a function of the ratio of the number of military aircraft produced then-year to the number of military aircraft produced in 1995 (450 aircraft). The US Military Aircraft Replacement (MAR) cost inflators are which are plotted in the figure were obtained using the equation:

$$\text{Then-year Military Aircraft Replacement cost inflator} \approx \text{CPI}[N_m/450]^{0.6}$$

Where CPI = Then-year Consumer Price Index

N_m = Total then-year U.S. production of military aircraft

This global relationship is analogous to the equations derived in a 1972 Rand report by Levenson and others for cost estimates of specific aircraft airframes.⁷

Between 1950 and 1970, the inflator curve smoothes out the hills and valley of the curve derived from the equation: From 1970 to 1995 the curves are very similar. This supports the hypothesis that the total number of aircraft produced annually has a major influence on aircraft cost.

The actual fly-away then-year and constant 1995 costs based on CPI inflators for the C-130, shown in Figure 3, are compared with 1995 replacement costs based on the MAR cost inflators in Figure 8. In constant 1995 dollars, the C-130 costs now decrease between 1955 and 1974, then remain reasonably constant through 1995.

Then-year and 1996 replacement costs of some types which were in service in 1995 are listed in Figure 9.

The USAF Aging Aircraft Fleet

In the fall of 1995, the combined USAF fleet was composed of 6,624 aircraft, divided as follows:⁸

	Aircraft Type					Total
	A & F	B	C/KCT	T	Other	
Active-Duty (AD)	1898	183	1143	1200	267	4691
Air National Guard (ANG)	911	11	529	2	18	1471
Air Force Reserve (AFRES)	158	9	270	0	25	462
Total	2967	203	1942	1202	310	6624
Percent	44.8%	3.1%	29.2%	18.2%	4.7%	

Attack and fighter aircraft included the A-10, F-4, F-15, F-16, F-111, EF-111 and F-117. Transport, tankers and communication aircraft included C-130, KC/C/RC-135, C-141B, C-5A, C-5B, KC-10 and C-17 aircraft plus various commercial aircraft conversions. Bombers included B-52H, B-1B and B-2A. Most of the 1,202 trainers were T-37s and T-38s. The remaining 310 aircraft were electronic warfare (E-3, E-4, etc.) and surveillance airplanes and helicopters.⁸

The numbers and ages of the different types of aircraft in USAF service are listed in the annually in the May issues of Air Force Magazine.⁸

The different types of aircraft in the fleet may be divided into the four groups shown in Figure 10. The upper left group consists of aircraft designed to USAF

requirements prior to 1970 when the Air Force Aircraft Structural Integrity Program, MIL-STD-1530, were first implemented. Many of the aircraft designed prior to 1960 had no specified fatigue life requirements (e.g. B-52, C-130, KC-135, F-4) and aircraft designed between 1960 and 1970 failed to meet their original fatigue life requirements (e.g. C-5A). The lower left group were designed to the requirements of the Air Force Aircraft Structural Integrity Program.^{9, 10, 11}

Aircraft in the upper right hand group were designed to fail safe structural requirements, where the residual strength was required to equal 80% of limit load. The lower right group were designed to the structural requirements specified in 1978 in Federal Aviation Regulations Part 23 and 25 rule FAR 23.571 and 25.571, when Damage Tolerance and Fatigue Evaluation of the Structure was adopted, stating that "catastrophic failure due to fatigue, corrosion, or accidental damage will be avoided during the operational life of the airplane".^{12, 13}

Since more than half of the 1995 USAF aircraft fleet were designed to these earlier requirements, continued application of the ASIP is essential to structural integrity.

The numbers, ages and estimated replacement costs of 1585 aging transport and tanker aircraft designed to pre-1970 USAF requirements are shown in Figure 11. These include the C-130B through E, C-130H, KC-135, C-141B and C-5A. It should be noted that the wings of the entire fleet of C-5As were replaced with redesigned wings between 1980 and 1987. The redesign included conformance to the post-1970 requirements and substitution of the tougher and more stress corrosion-resistant, but lower strength 7075-T73511 for 7075-T6 material.

In 1994, many C-141B wings were found to have cracks in the weep holes in the lower wing plank risers. These were repaired using bonded boron/epoxy doublers.² However, fatigue life is running out and C-141Bs are being replaced by new C-17s.¹⁴ Some of the older C-130Bs will also be replaced by new C-130Js during the next few years.

Some of the aging trainer and communication aircraft are shown in Figure 12. The T-37 and T-38 were designed to the pre-1970 Air Force requirements: The T-39, T/CT-43 and C-12 were designed to pre-1978 FAR civil aircraft structural requirements. Not shown is the C-9, the military version of the DC-9. The Air Force operates 23 and their average age is 25 years. The T-37s will be replaced by the Beech MK 2 Joint Primary Trainer System (JPATS) aircraft during the next ten years. From 2000-2006 425 T-38s will be upgraded to extend service to 2020.

Aging bombers and miscellaneous aircraft are shown in Figure 13. These include the B-52H, which is expected to remain in service for at least 30 more years; the E-3 Advanced Warning and Control System (AWACS), which has a modified Boeing 707 airframe; the U-2R, the later version of the U-2 which originally flew in 1955; and the

HH/UH-1 and TCH/NCH-53 helicopters originally designed for the Army and Navy respectively.

The older fighter and attack aircraft designed to post-1970 Air Force structural requirements are shown in Figure 14. The A-10 was originally designed for an 8,000 hour life and this was extended to 12,000 hours because the flight spectrum was less severe than expected. This is expected to be further extended. In 1996., the A-10s average was 4,800 hours, so the A-10 will probably remain in service well into the 21st Century. Many of the older F-15As and Bs have been retired from service. However the F-15E is still in limited production, and is likely to remain in service for 20 more years, when it will have been replaced by F-22s. The older F-16As and Bs have also been retired or lost. F-16Cs and Ds are also still in production and will ultimately begin to be replaced by the Joint Strike Fighter (JSF), starting about 2010.

The F-15 and F-16 were designed for a fatigue life of 4,000 hours. This relates to 10 to 15 years A-D plus ANG or AFRES service. F-4E/G and RF-4Cs, which incorporate structural modifications for a 4,000 hour life, were finally retired from service in 1995 after 26 years without any structural failures, were supported throughout their lives by the ASIP. The lead RF-4C accumulated 7,300 hours.

Graphs showing the relationships between aircraft age and the percentage of aircraft remaining in service are plotted in Figure 15 for the F/RF-4, F-15 and F-16. The curves for the F-15A/B and the F-16A/B are similar, indicating that approximately one-third of the fleet have been retired, transferred or lost by the time the oldest aircraft reaches 20 years of service. The curve for the later model F-15C/D and the F-15E indicates that about 90% of these aircraft will still be in service at the 20-year mark. McDonnell Douglas advertised a 27-year structural life for the F-15E.

Figure 16 shows comparative plots for the A-7D, which was retired in 1993, and the A-10. The plot for the A-10 shows that retirements and losses has leveled off with about 380 (53%) of the original fleet of 713 still in service. Plots for the T-37 and T-38 are also shown in the Figure. The 425 T-38s which are to be modified, consist of 36% of the original production of 1189 aircraft produced by Northrop between 1959 and 1974. By 2020, when the T-38s will probably be retired, the oldest T-38 will be 55 to 60 years old.

Sustaining Costs

Costs associated with maintaining and modifying aging aircraft to extend their service life are high. The cost of rewinging the C-5A fleet was about \$10 million per aircraft between 1980-84, or about \$22 million in 1995 dollars.⁵ The cost of reengining KC-135s with F108 engines cost about \$16 million per aircraft in 1990, programmed depot maintenance (PDM) for the KC-135 costs about \$2 million per

aircraft every 6 years. The annual cost of corrosion for the KC-135 was \$147,900 per aircraft in 1990.^{15, 16}

Corrosion is the major contributor to the sustaining costs of aging aircraft airframes. The Air Force has initiated a program to solve corrosion problems before there are any catastrophic failures. The program includes detection of hidden corrosion using advanced NDI equipment, complete aircraft disassembly for corrosion documentation and mapping, corrosion data collection, and structural testing and analysis of corroded material.¹⁷

Annual corrosion costs for USAF aircraft listed in References 15 and 16 are plotted in Figure 17 against the year of initial operational capability (IOC) of the aircraft type. The data has been normalized to 1990 dollars per pound operating empty weight using weights from Jane's All the World's Aircraft.¹⁸ The plots show that corrosion costs have been reduced significantly for the more modern aircraft, particularly where the 7000-T6 alloys have been replaced by 7000-T73 and other more corrosion-resistant aluminum alloys: The annual corrosion cost in 1990 of the KC-135 (1957 IOC) was \$1.55/lb compared with \$0.30/lb for the C-5B (1986 IOC).

Fleet Replacement Costs

The total cost of replacing the entire current fleet of 6,624 aircraft is estimated at \$298 billion (in 1995 dollars). Figure 18 shows the distribution of these costs, of which 44% is for transports and tankers, 32% for fighter and attack aircraft, 16.5% is for bombers, and 2.5% is for trainers. Electronic aircraft and helicopters account for the remaining 5%.

The USAF budget associated with procurement of new aircraft and the numbers of aircraft procured annually is shown in Figure 19. In constant 1995 dollars, the budget is about \$2.4 billion for Fiscal Year 1997 and total procurement is only 32 new aircraft (F-15s, F-16s, C-17s). At these levels, it would take more than 100 years to replace the current USAF fleet of aircraft.

Budget levels will be increased significantly as the F-22 and Joint Strike Fighter (JSF) goes into production during the early part of the next century. Even so, budget restrictions will probably dictate that the life of many of the existing aircraft in the fleet must be extended well into the middle of the next century. The replacement value of the existing fleet is considerable and far outweighs the costs needed to continue to implement ASIP and to inspect, repair and refurbish existing aging aircraft.

An additional constraint to procurement of new aircraft types is the 12-to-15 year time span between program go-ahead and IOC.

Conclusions

The value of the existing USAF aircraft fleet, replacement costs and budget constraints will keep many aging aircraft in service through the first half of the next century

- Corrosion, fatigue, and the combined effects corrosion and fatigue are the primary causes of aging aircraft structural degradation
- Advanced NDE/NDI techniques are critical to identify and quantify corrosion and fatigue damage without disassembly of the structure
- ASIP is essential to the continued operational capability of the USAF fleet.

Acknowledgments

The author wishes to thank Mr. Tobey Cordell for his suggestion to present this paper and Dr. John Lincoln for my selection as a luncheon speaker at the 1996 ASIP Conference.

REFERENCES

1. Lincoln, John W. , *Aging Aircraft Issues in the United States Air Force*. SAMPE Journal, Sept/Oct 1996.
2. Lincoln, John W. , *USAF Aging Aircraft Program*. Aerospace Engineering., Nov 1994
3. Cordell, Tobey M., *Life management of Aging Air Force Aircraft: NDE Perspective*. SPIE, Oakland, CA, June 1995.
4. Grier, Peter, *Behind the High Readiness Ratio*. AF Magazine, March 1994.
5. Aircraft Year Books, Aviation Facts and Figures, and Aerospace Facts and Figures. 1946 through 1995-96. Published annually by Aerospace Industries of America (AIA), Washington, D.C.
6. Technical Manual: Unit Costs of Aircraft, Guided Missiles and Engines. USAF Publication 00-25-30. 1976.
7. Levenson, G.S. et al., *Cost Estimating Relationships for Aircraft Airframes*. RAND Report R-761-PR (Abridged), Rand, Santa Monica, CA. February 1972.
8. USAF Almanac 1996, Air Force Magazine, May 1996. (Also prior years)
9. Military Specifications for Airplane Strength and Rigidity: Flight Loads; Reliability Requirements; Repeated Loads and Fatigue, etc. MIL-A-8861 etc. Air Force Aircraft Structural Integrity Program, Airplane Requirements, MIL-STD-1530A, 1975. Air Force Guide Specification, Aircraft Structures, General Specification, AFGS-87221A, 1985.
10. Coffin, M.D. and Tiffany, C.F., *New Air Force Requirements for Structural Safety*. J. Aircraft, February 1976.
11. Lincoln, John W., *Damage Tolerance, USAF Experience*. 13th ICAF Symposium on Damage Tolerance in Aircraft Design, 1985.
12. Federal Aviation Regulations, Part 23 and Part 25, Airworthiness Standards. Particularly § 23.571 and § 25.571, Damage tolerance and fatigue evaluation of structures. CFR, 14, Space and Aeronautics. Department of Transportation, Washington, D.C.
13. Mar, James W., *Preserving Aging Aircraft*. Aerospace America, January 1996.
14. Lincoln, John W. , *Service Life Extension for the C-141*. Aerospace Engineering, November 1994.
15. Cook, Garth R. et al., *A Study to Determine the Annual Costs of Corrosion Maintenance*. Serial 3843. Systems Exploration , Inc., 1990 .
16. Cook, Garth R. et al. *Collection/Assessment of United States Air Force Corrosion Costs*. Final Report, Systems Exploration, Inc., 1992.
17. Groner, D.J. and Nieser, D.E., *U.S. Air Force Aging Aircraft Corrosion*. Canadian Air and Space Journal, June 1996.
18. Jane's All The World's Aircraft, 1950-51 through 1995-96. Published annually by Jane's Information Group, England.

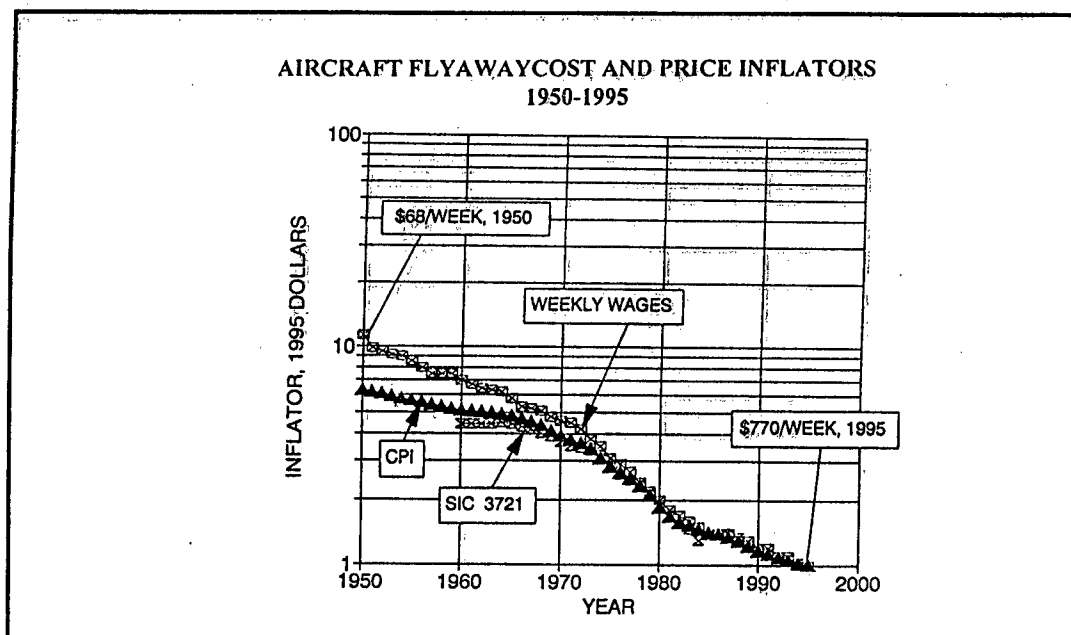


Figure 1. Aircraft Cost and Price Inflators.

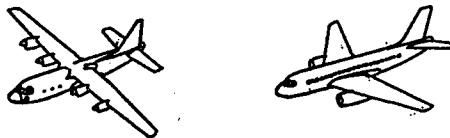
TRANSPORT AIRCRAFT COSTS & PRICES						
Year	Lockheed	OEW, lb	Cost, \$M	Boeing	OEW, lb	Price, \$M
1966	C-130E	72890	\$2.4	737-200	59235	\$3.2
1995	C-130H	76469	\$30.0	737-400	73700	\$35.0
\$/lb Inflation Factor: 1966-95			<u>11.9</u>	<u>8.8</u>		
Inflation Factors, 1966 to 1995 Dollars:						
SIC Factor		4.3				
CPI Factor		4.7				
Production Wages		5.7				

Figure 2. C-130 Costs and Boeing 737 Prices

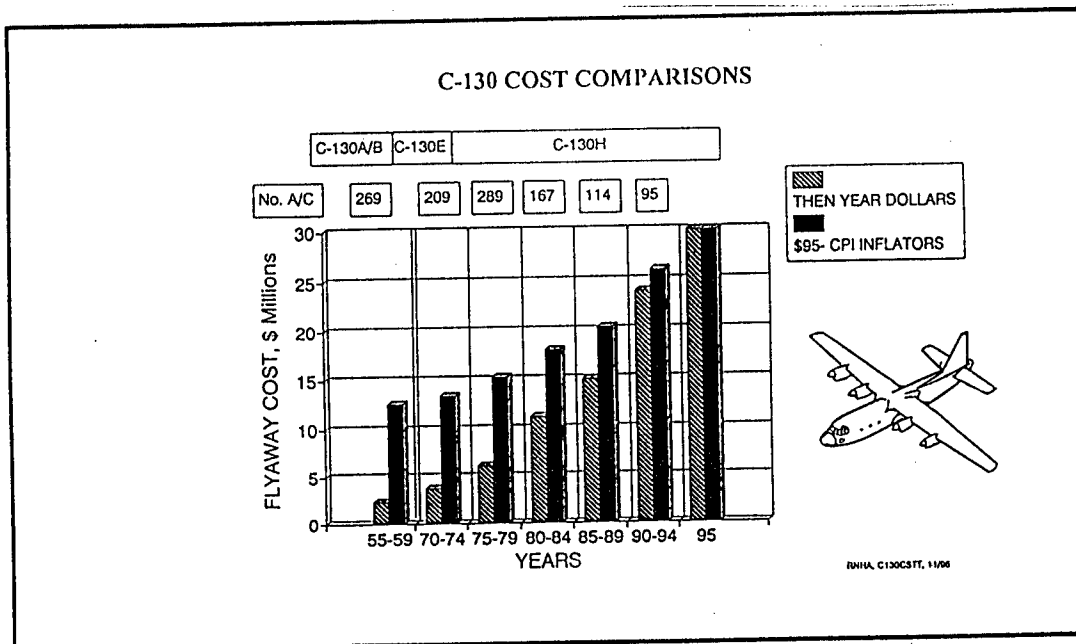


Figure 3. C-130 Flyaway Costs.

COST ELEMENTS:

- Manufacturing, Tooling, QC and Sustaining Engineering Labor Hours and Rates
- Materiel: Components, Forgings, Extrusions, Hardware, Material, Vendors, etc.
- GFE including Engine(s), Avionics and other Subsystems and Parts
- Manufacturing, Tooling and QC (Including NDE/I) Facilities and Equipment
- Supporting Operations (Procurement, Specifications, Subcontracts, etc.)
- Overheads and General and Administrative (G&A) Rates and Fee

COST FACTORS

- Production History (Learning Curves), Total Production, Annual Production Rates, Changes and Modifications, Facility and Equipment Utilization

TOTAL MILITARY AIRCRAFT ANNUAL PROCUREMENT

- Affects Materiel, GFE, Manufacturing & Facility Costs, Overhead Rates, etc.

Figure 4. Aircraft Flyaway Cost Elements

U.S. MILITARY & COMMERCIAL AIRCRAFT DELIVERIES 1950-1995

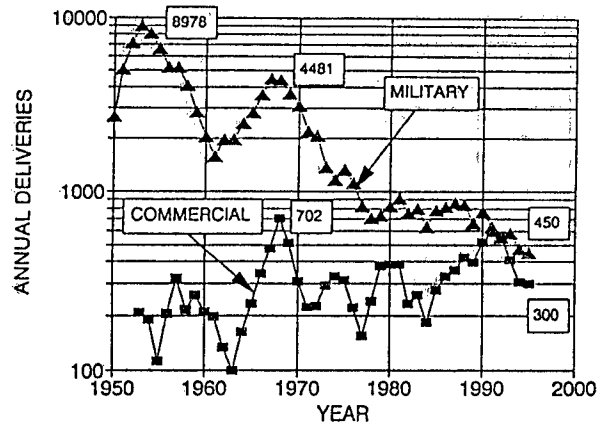


Figure 5. Military and Commercial Aircraft Deliveries.

AIRCRAFT COST AND PRICE INFLATORS 1950-1995

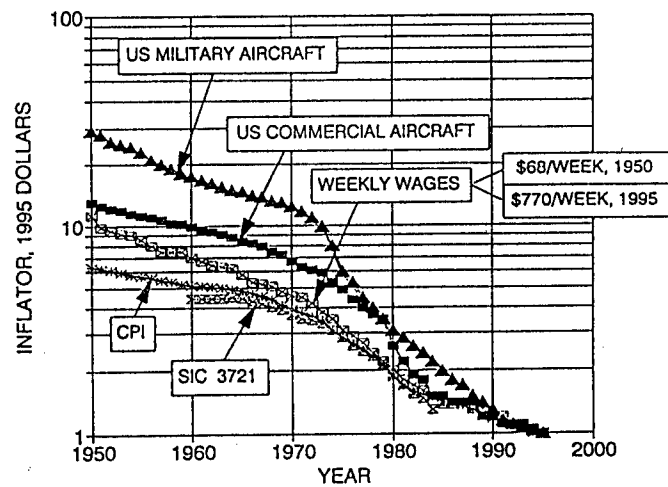


Figure 6. Cost and Price Inflators, 1950-1995.

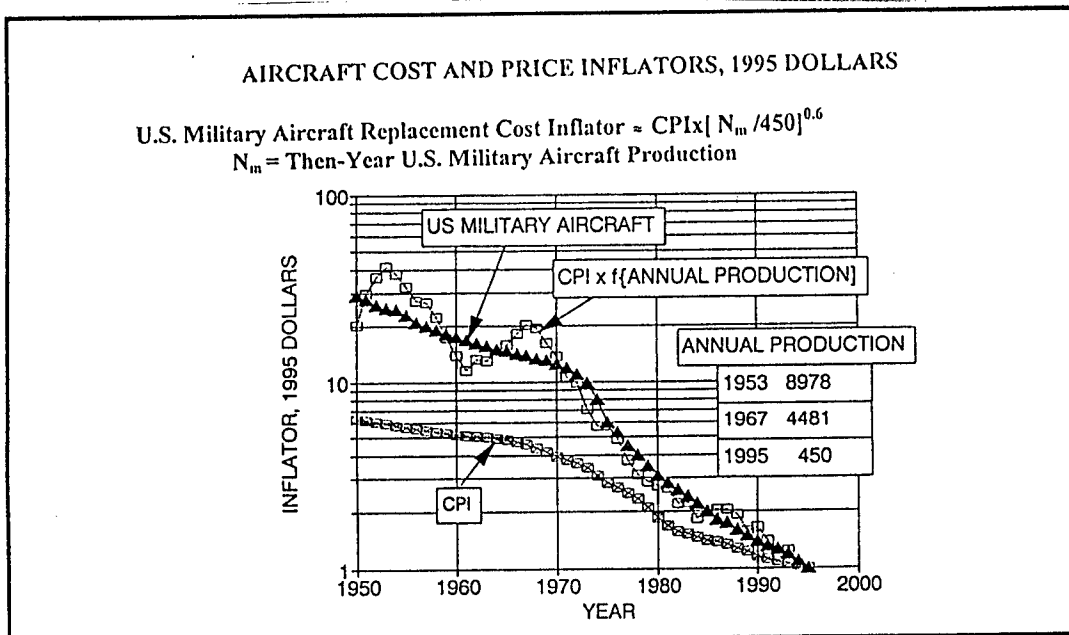


Figure 7. Military Aircraft Cost Inflatior Comparisons.

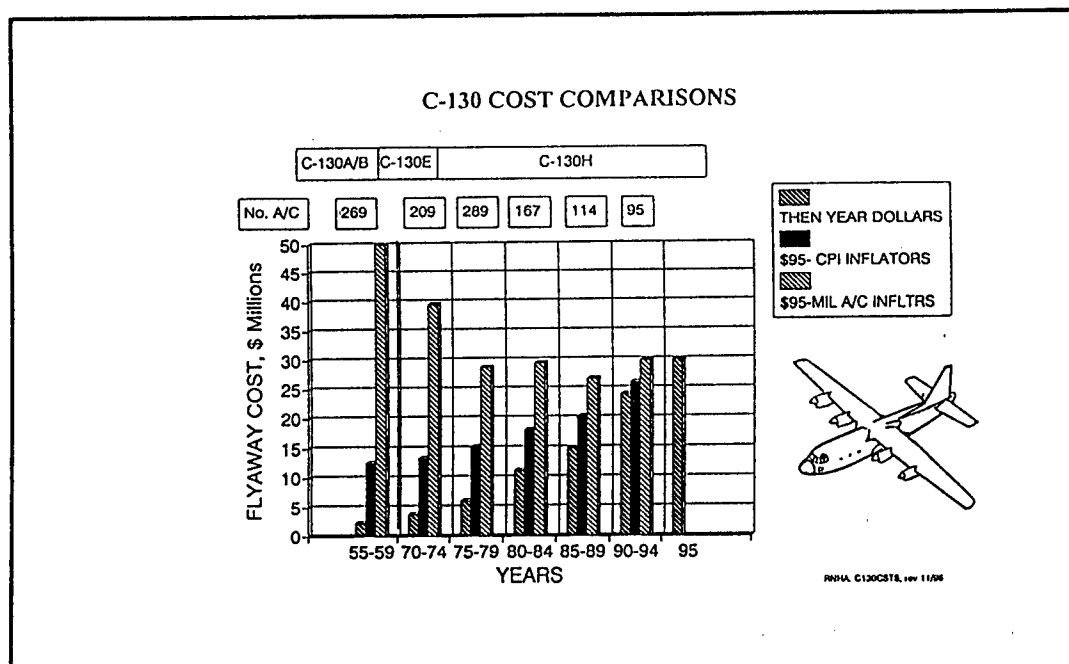


Figure 8. C-130 Flyaway Costs.

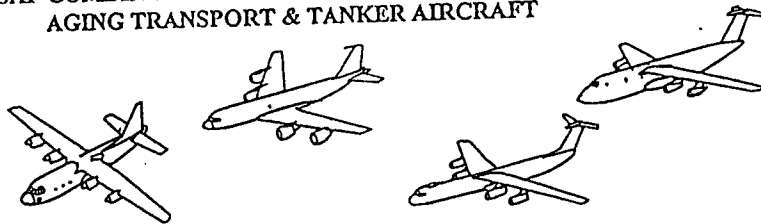
USAF AIRCRAFT FLYAWAY COSTS				
Then-Year and 1995 Dollars Based on US Military Aircraft Replacement Inflaters				
Aircraft	Year	Cost \$TY millions	Cost \$'95 millions	Remarks
A-10A	1978	\$5.3	\$21	
B-52H	1957	\$9.3	\$186	
C-130E	1963	\$2.06	\$32.0	C-130H: \$30m, '95
C-5A	1971	\$26.6	\$314	
C-5B	1988	\$136	\$204	C-5D: \$168m, '94 est.
F-4E	1967	\$2.4	\$16.2	
F-15A	1980	\$16.3	\$50	F-15C: \$36/50m, '91/2
F-16A	1982	\$8.6	\$25	F-16C: \$23m, '95
T-37A	1960	\$0.12	\$2.1	JPATS: \$2.5m, '96
T-38A	1965	\$0.75	\$8.3	T-45A: \$18m, '95

Figure 9. USAF Aircraft Flyaway Costs.

USAF COMBINED AIRCRAFT FLEET, 1995.							
6624 AIRCRAFT. AVERAGE AGE 17 YEARS							
STRUCTURAL DESIGN REQUIREMENTS							
USAF AND OTHER MILITARY AIRCRAFT REQUIREMENTS				FAA AND OTHER CIVIL AIRCRAFT REQUIREMENTS (FAR SECTION 23/25-571)			
Pre-1970	3063 Aircraft: 27 years old			Pre-1978	381 Aircraft: 13 years old		
AC-130	C-130	C-27	SR-71	C-9	C-21	C-26	E-8
B-52H	KC-135	T-37	UH-1	KC-10	C-22	VC-137	E-9
F/RF-4	C-141	T-38	MH-53	C-12	C-23	E-3	EC-18
F/EF-111	C-5	U-2		C-20	VC-25	E-4	T-43
Post-1970	2962 Aircraft: 9 years old			Post-1978	218 Aircraft: 1.3 years old		
A-10	F-15	C-17		T-1			
B-1B	F-16	HH-60		T-3			
B-2	F-117						

Figure 10. USAF Aircraft Structural Design Requirements

USAF COMBINED AIRCRAFT FLEET, SEPTEMBER 1995
AGING TRANSPORT & TANKER AIRCRAFT

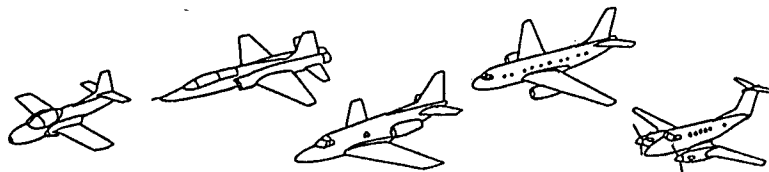


Aircraft	C-130B/E	C-130H	KC-135R	C-141B	C-5A
Deliveries	826	336	808	284	80
No. in Service	403	261	603	242	76
Ages	23-40	0-22	31-38	27-31	20-25
Replacement Cost 1995 Dollars	\$32m	\$32m	\$68m*	\$103m	\$292m

* Includes re-engine costs

Figure 11. USAF Aging Transport Aircraft.

USAF COMBINED AIRCRAFT FLEET, SEPTEMBER 1995
AGING TRAINER & COMMUNICATIONS AIRCRAFT



Aircraft	T-37	T-38	T-39	T/CT-43 (B737)	C-12 (King Air)
Deliveries	991	1189	149	19	48
No. in Service	461	471	3	14	48
Ages	25-38	23-35	30-35	21-22	12-20
Replacement Cost 1995 Dollars	\$2.8m	\$11m	\$7.5m	\$29m	\$3.8m

Figure 12 USAF Aging Trainer and Communication Aircraft.

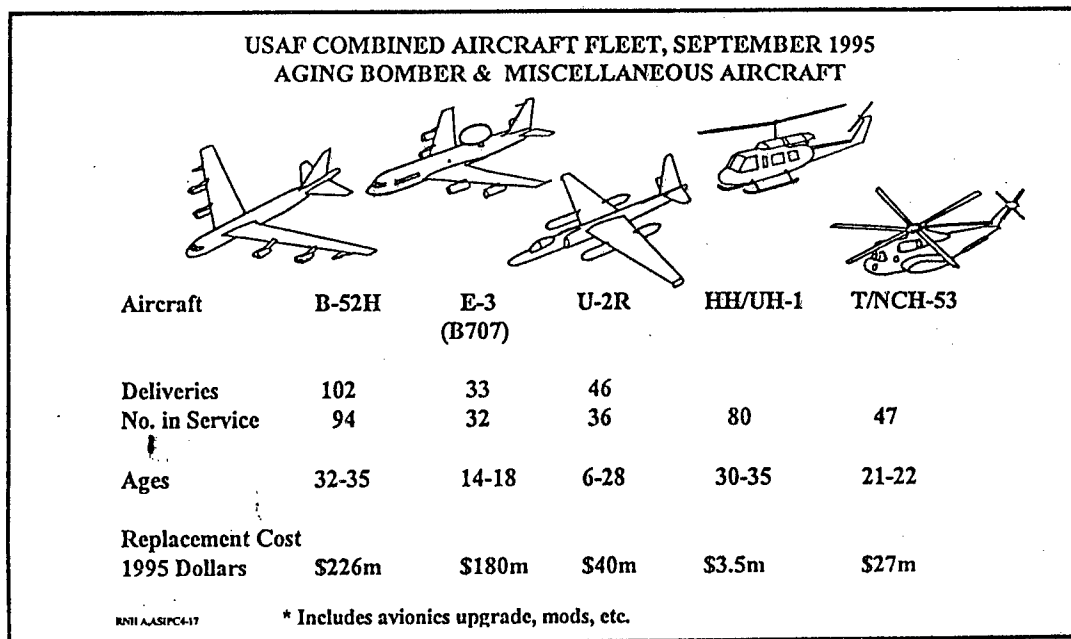


Figure 13. USAF Aging Bomber, Miscellaneous and Helicopter Aircraft

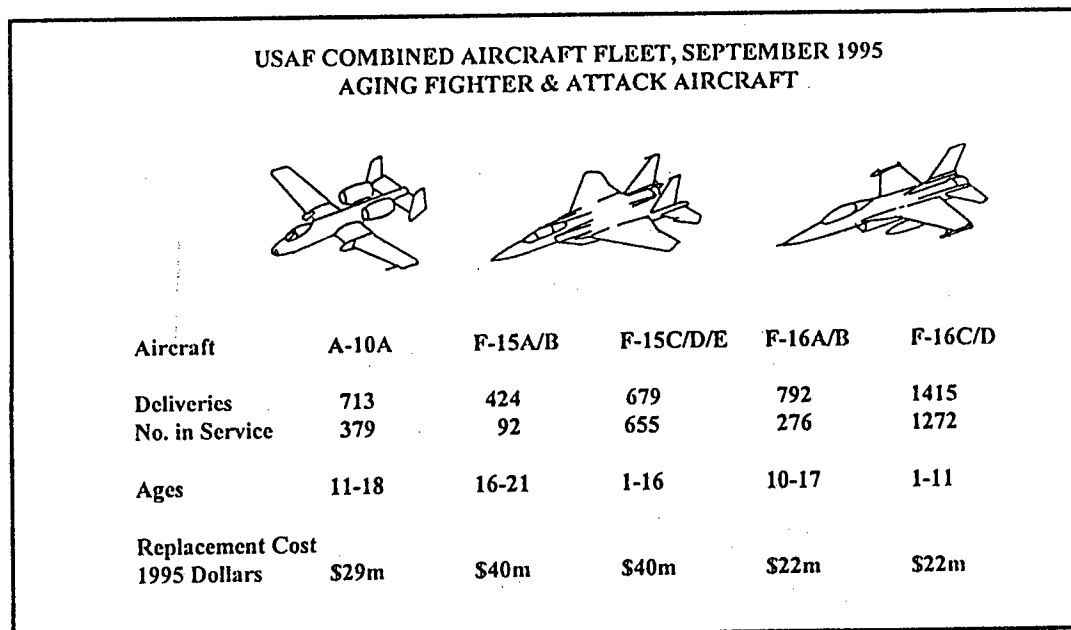


Figure 14. USAF Aging Fighter and Attack Aircraft

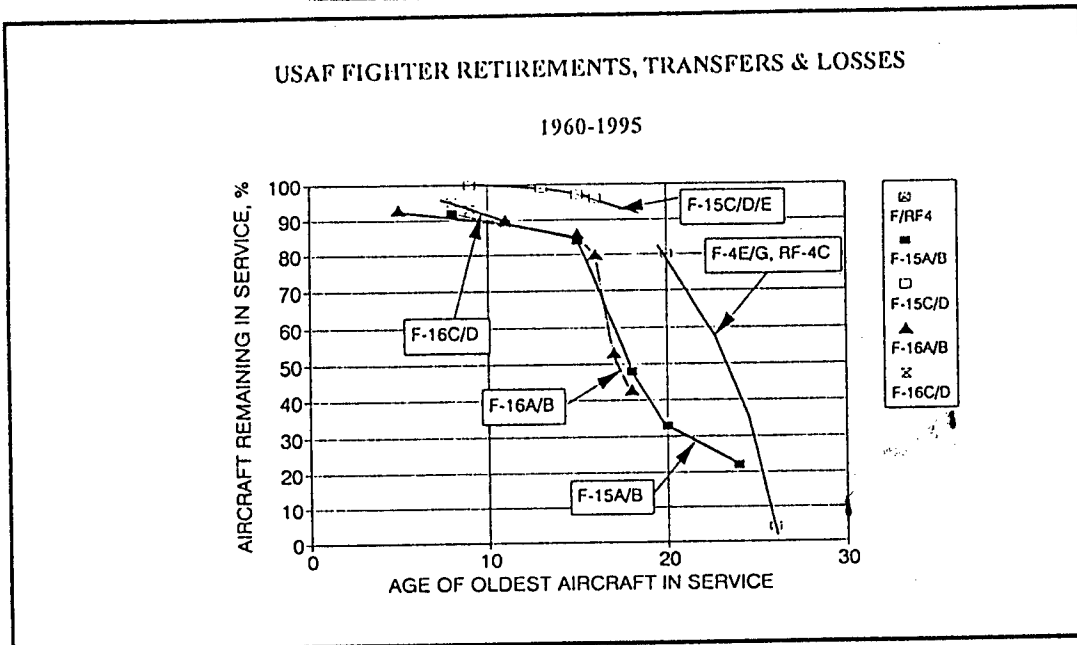


Figure 15. USAF Fighter Retirements, Transfers and Losses

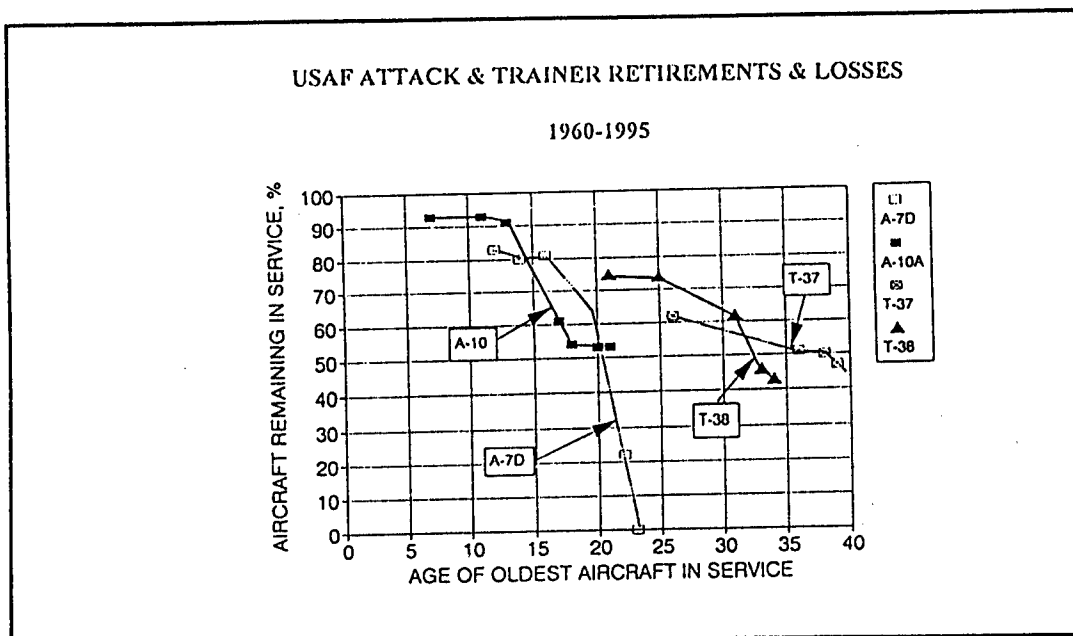


Figure 16. USAF Attack and Trainer Aircraft Retirements and Losses

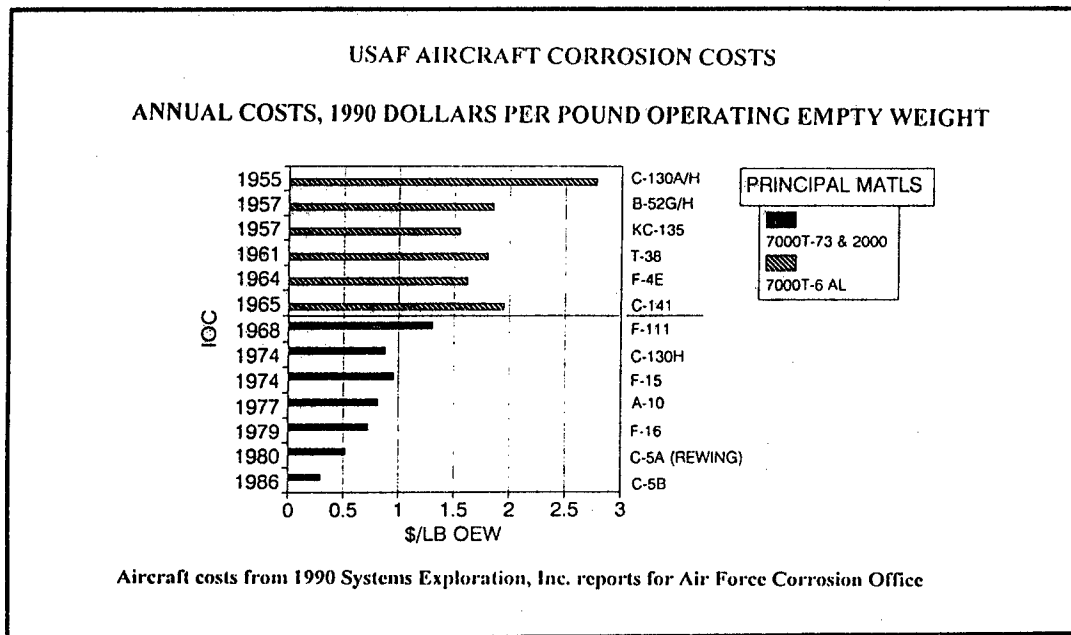


Figure 17. USAF Aircraft Corrosion Costs (1990)

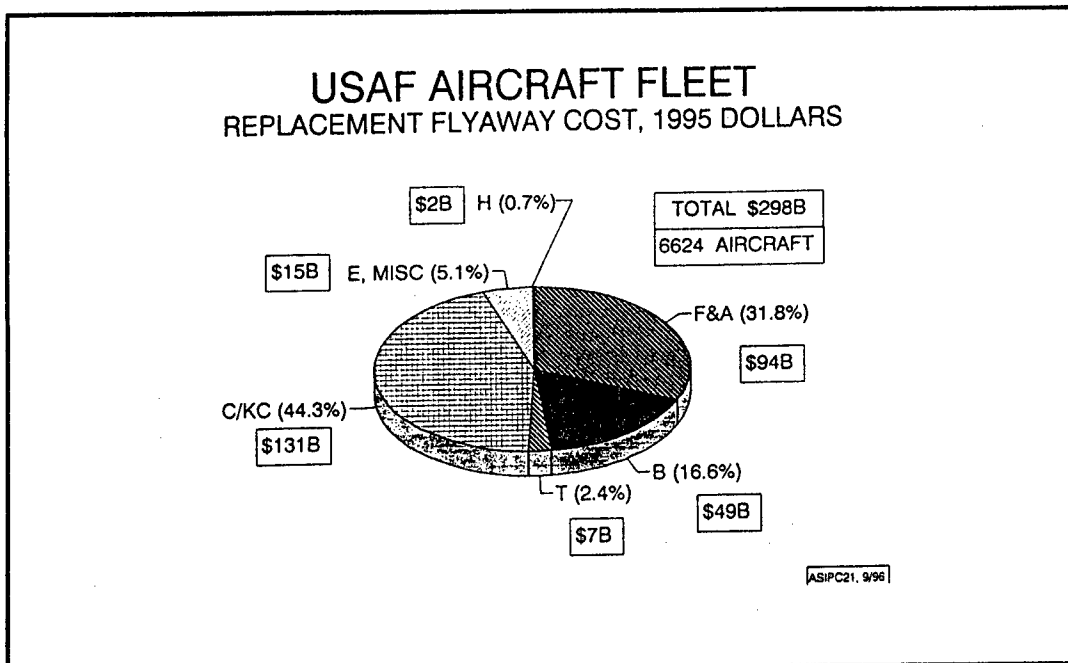


Figure 18. USAF Fleet: Replacement Aircraft Flyaway Costs.

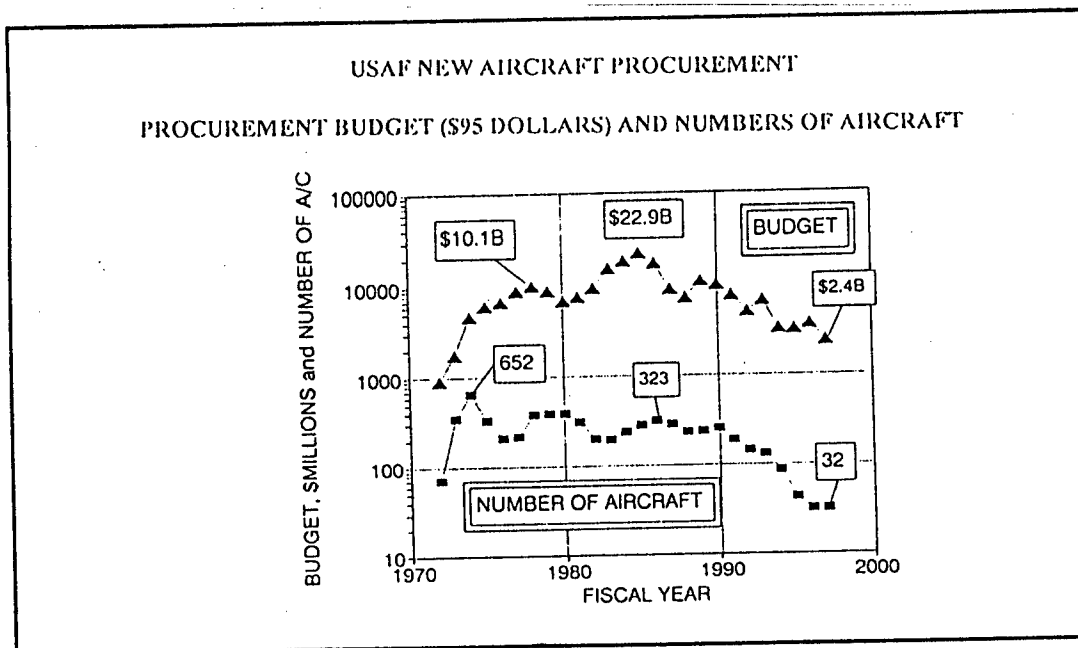


Figure 19. USAF New Aircraft Procurement: 1972-1995

SESSION II

LIFE ENHANCEMENT

Chairman: *C. Harris*, NASA/LRC

Material Characterization of Laser-Shock Peened Titanium for Turbine Engine Applications

Steven R. Thompson (WL/MLSC)

John J. Ruschau (UDRI)

Dr. Theodore Nicholas (WL/MLLN)

1996 USAF Structural Integrity Program Conference
3 December 1996

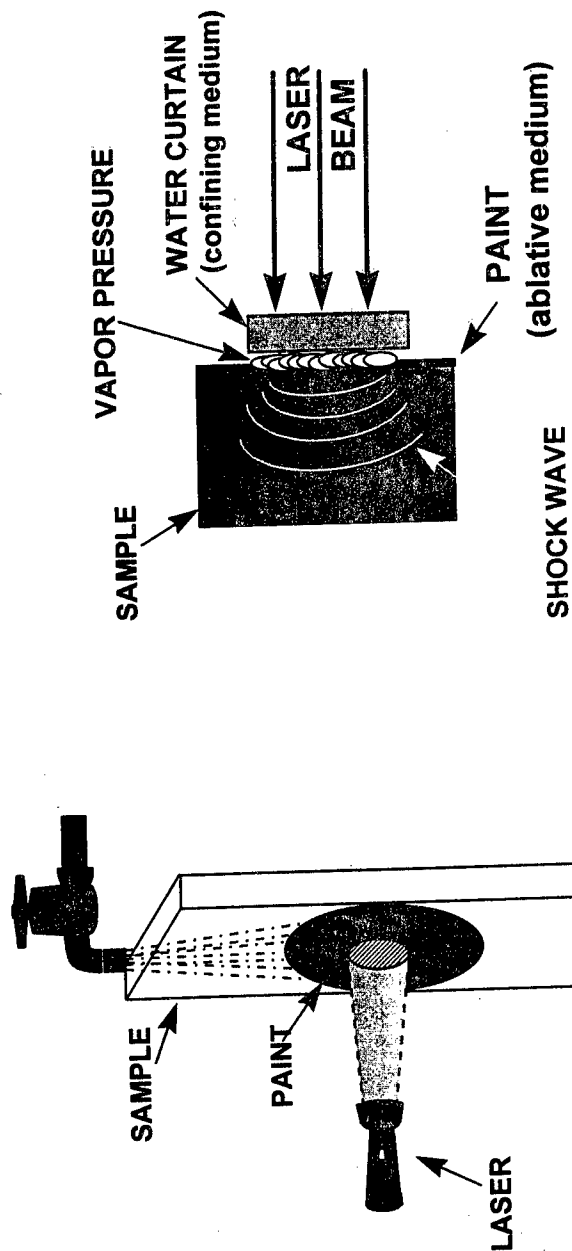
Objectives

- ◆ **Examine Fatigue Crack Initiation/Growth Characteristics of Laser-Shock Peened (LSP) Titanium**
- ◆ **Compare Fatigue Behavior of LSP Material with Dual Shot Peened (DSP) and Un-Peened (Baseline) Material**

Approach

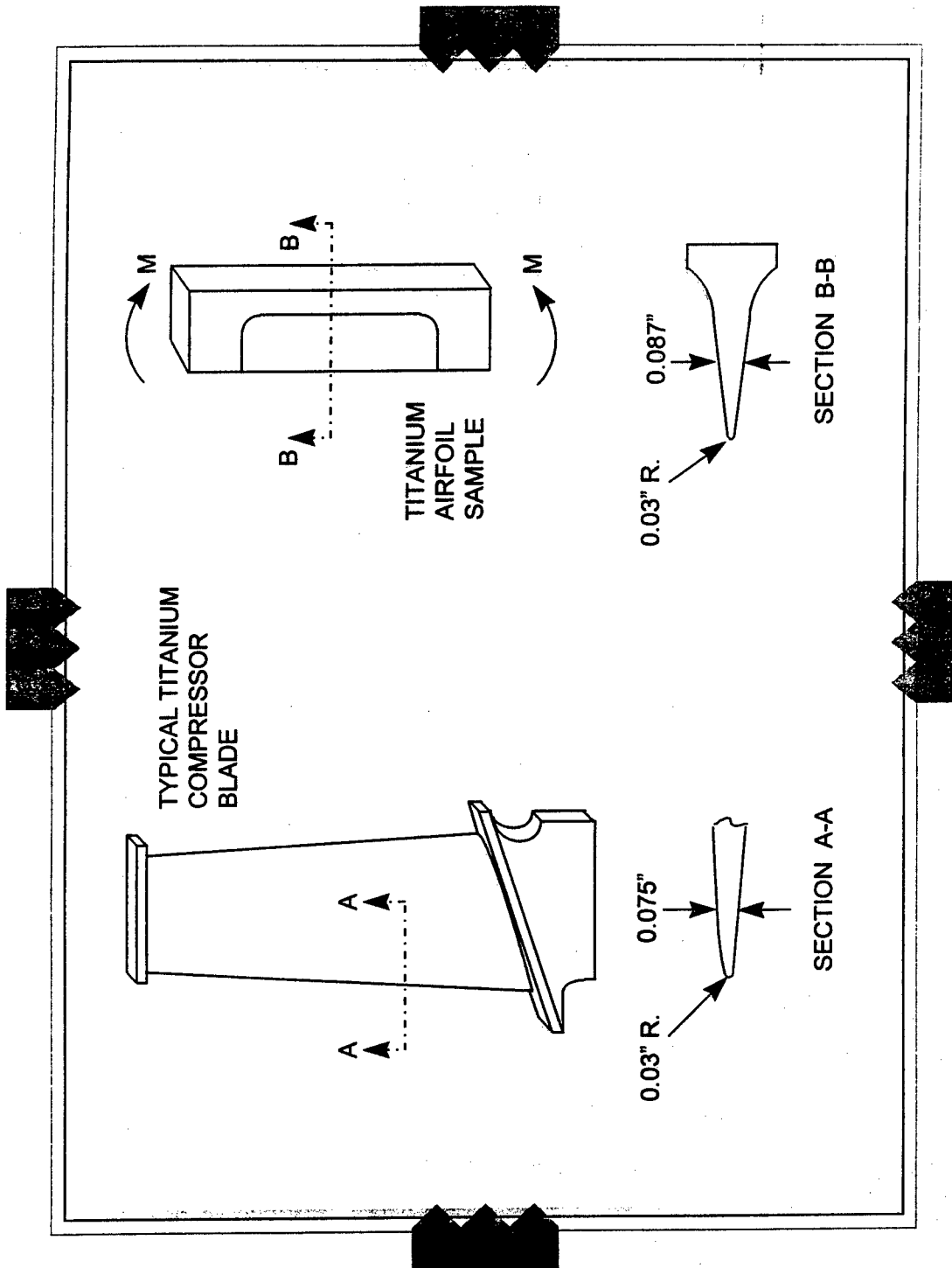
- ◆ **Fatigue Testing of 3-Point Bend Specimens**
 - LSP
 - DSP
 - Baseline
- ◆ **Compare Initiation With/Without Notch**
- ◆ **Measure Fatigue Crack Growth Rate**
- ◆ **Perform Metallography/Fractography Analysis**

Laser-Shock Peening - Concept



Test Specimen Design

- ◆ **Designed to Simulate Fan Blade Leading-Edge**
- ◆ **3-Point Bend (able to concentrate tensile loading in particular region)**
- ◆ **Mode I Cracking Only**



Stress Intensity Factor Analysis

- ◆ Stress Intensity Factor (SIF) derived by John & Kroupa (UDRI) using FEM

$$K = \sigma (\pi a)^{1/2} \cdot f(a/W),$$

where,

$$f(a/W) = \frac{1.1215 - 5.0402(a/W) + 14.4979(a/W)^2 - 22.0211(a/W)^3 + 12.927(a/W)^4}{(1 - a/W)^{3/2}}$$

Processing Parameters

◆ As-received (unprocessed)

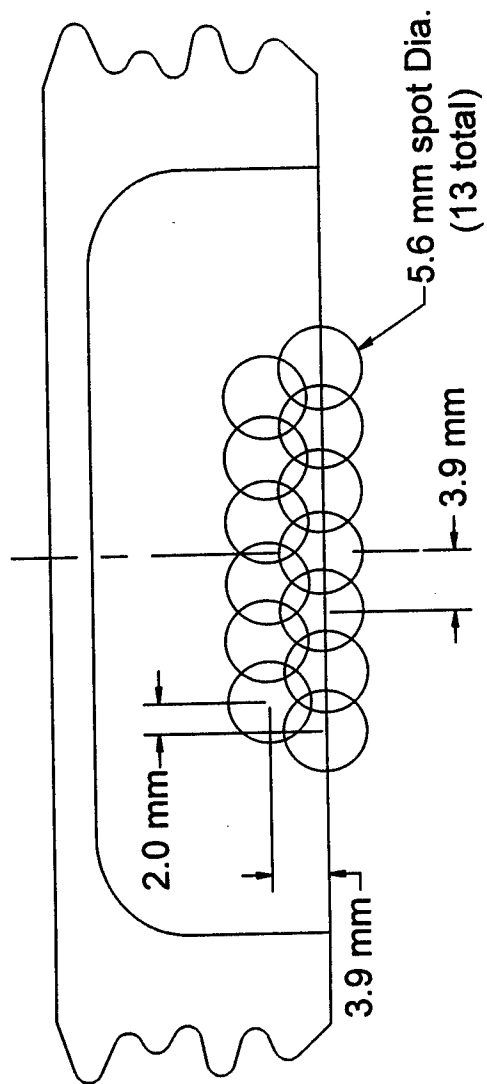
◆ Dual Shot-Peening (DSP)

- Step A: Shot peen with steel shot to 0.006-0.008A with 200% or more coverage
- Step B: Glass-bead peen to 0.005-0.007N with 400% or more coverage

◆ Laser Shock-Peening

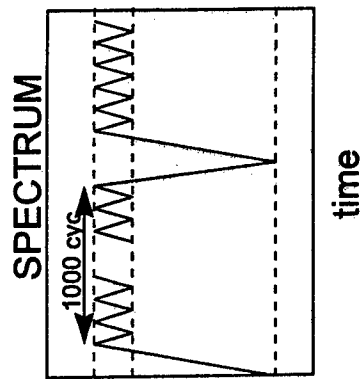
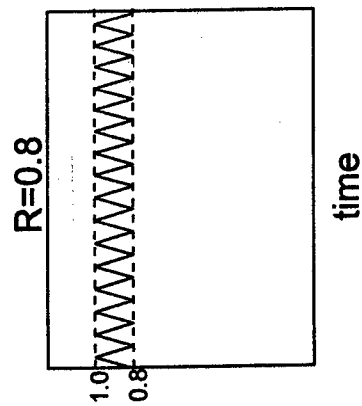
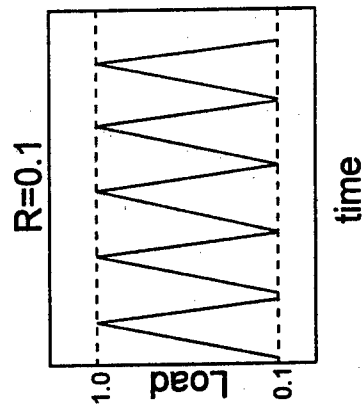
- 3 x 200 J/cm² (50 J pulse in each side)
- 30% spot overlap
- 5.6 mm circular spot

LSP Spot Pattern

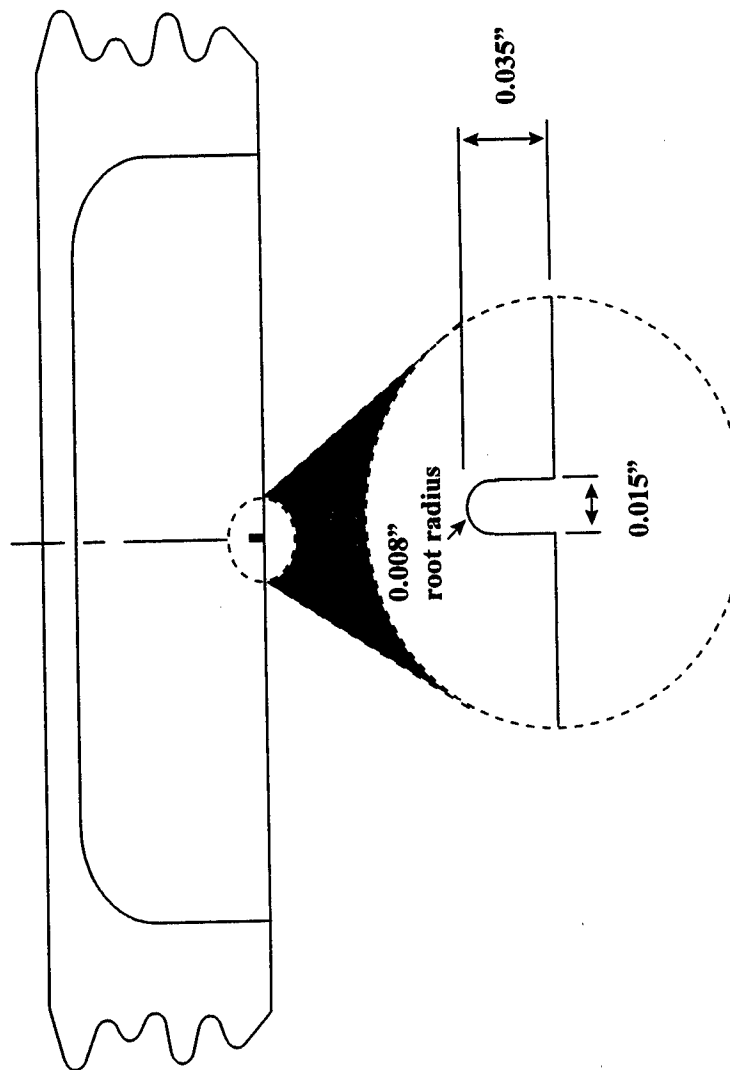


LOADING CONDITIONS

- 3-point Flexural
- Room Temperature
- 50-60 Hz (sinusoidal)



“Nicked” Specimen



Initiation Results - Smooth

Condition	Stress Ratio R	Maximum Stress for Crack Initiation ksi	Maximum Stress for Crack Initiation (MPa)
Baseline	0.1	$\leq 105^{\text{a}}$	$\leq (724)$
LSP (round spot)	0.1	96	(662)
LSP (elliptical spot)	0.1	92	(634)
DSP	0.1	96 ^e	(662)

^a - Average of three tests: 96, 118, and <101 ksi. For the latter case, the sample failed at the first stress level examined (101 ksi), thus initiation stress may have been lower.

^e - Average of two tests: each initiated at 96 ksi, max; process control questionable

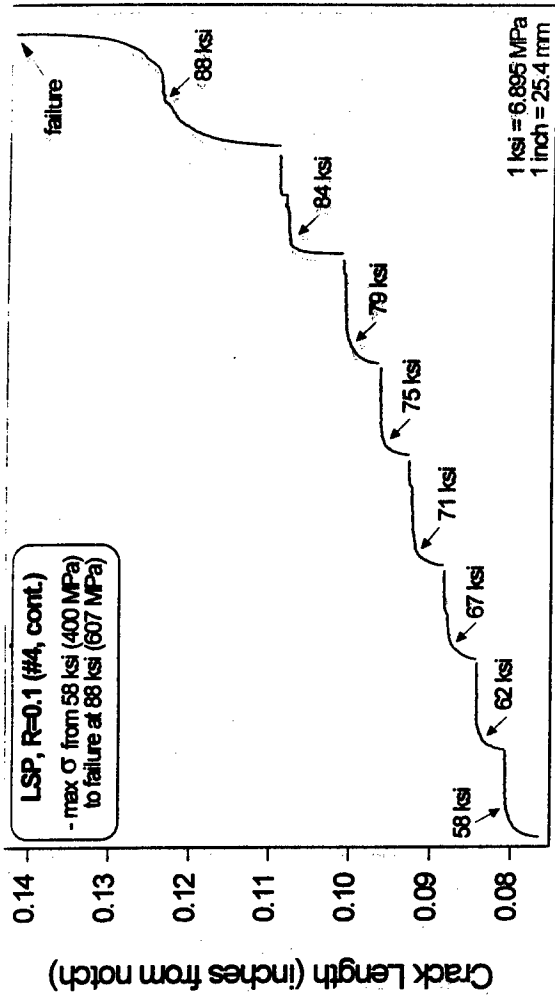
Initiation Results - Notched

Condition	Stress Ratio R	Maximum Stress for Crack Initiation ksi (MPa)	Maximum Stress to Cause Failure ksi (MPa)
Baseline	0.1	41 ^① (283)	41 ^① (283)
LSP (round spot)	0.1	41 ^① (283)	95 ^② (652)
LSP (elliptical spot)	0.1	50 (345)	88 (607)
DSP	0.1	41 (283)	41 (283)
Baseline	0.8	84 (579)	84 (579)
LSP (round spot)	0.8	75 (517)	88 (607)
LSP (elliptical spot)	0.8	96 (665)	96 (665)
DSP	0.8	84 (579)	84 (579)
Baseline	spectrum	54 (372)	54 (372)
LSP (round spot)	spectrum	84 (579)	88 (607)

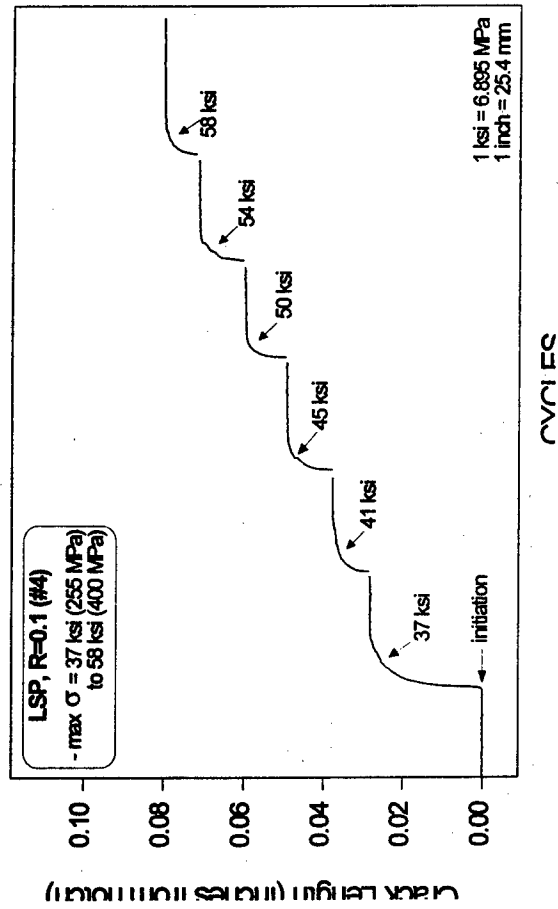
① - Average of two tests: both initiated and failed at 41 ksi.

② - Average of two tests: 37 and 45 ksi.

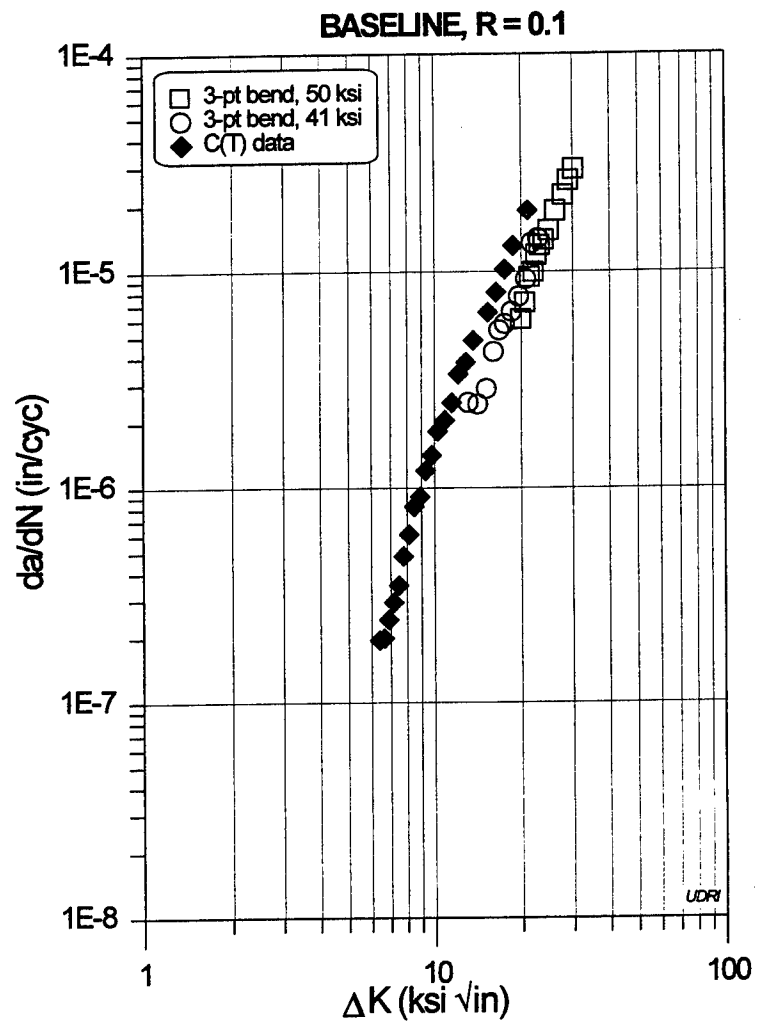
③ - Average of two tests: 88 and 101 ksi.

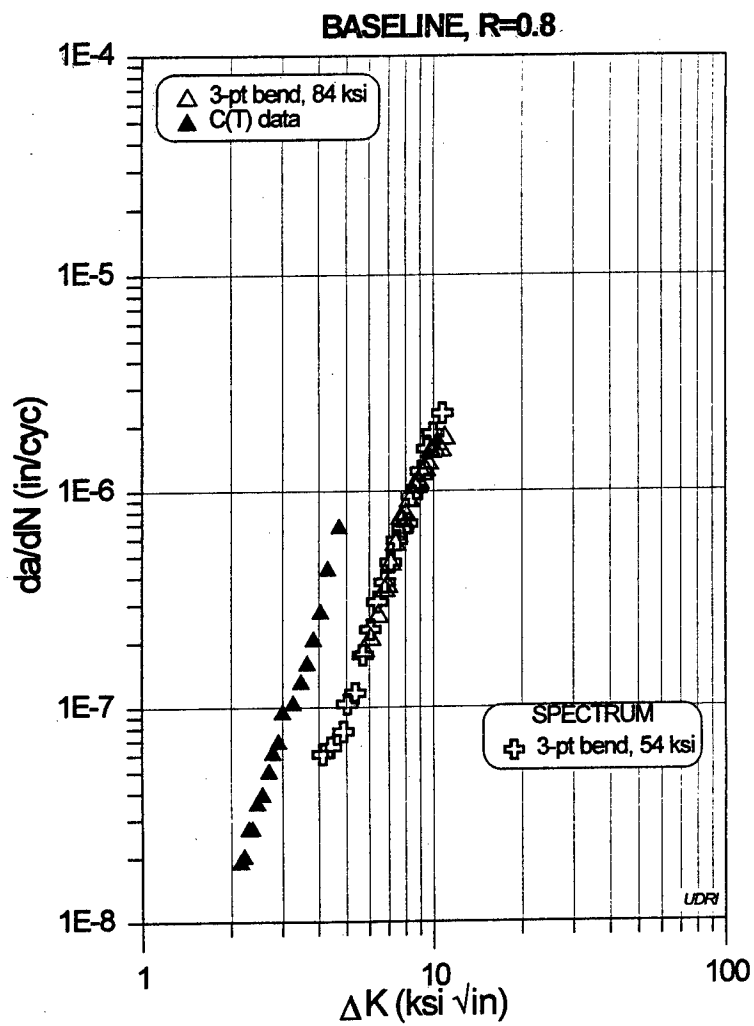


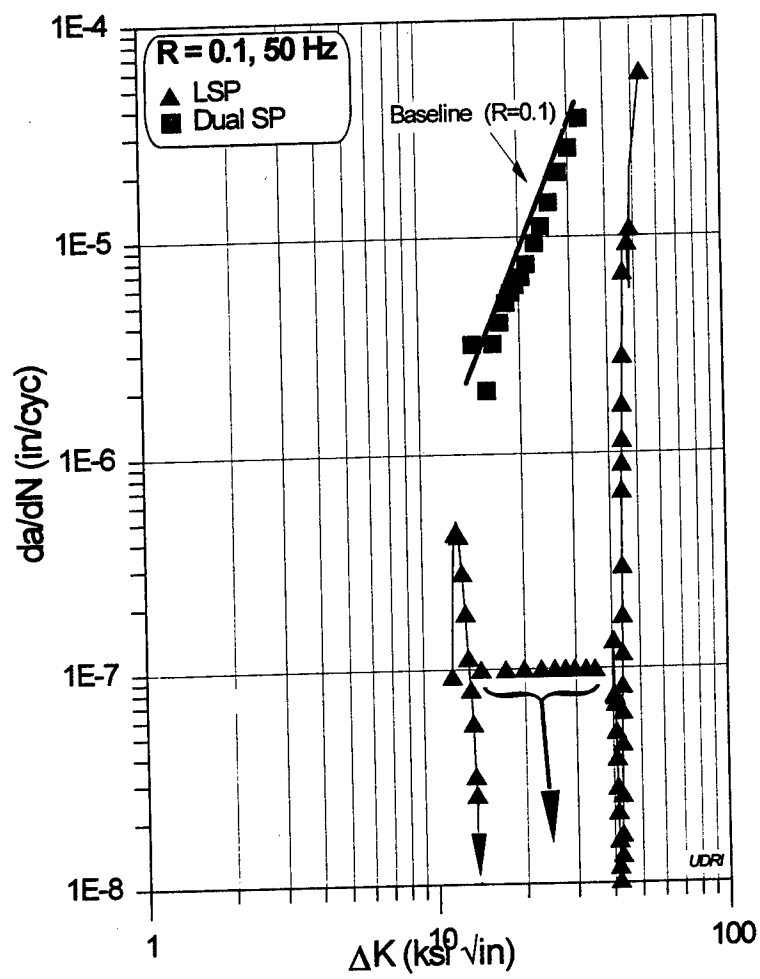
CYCLES

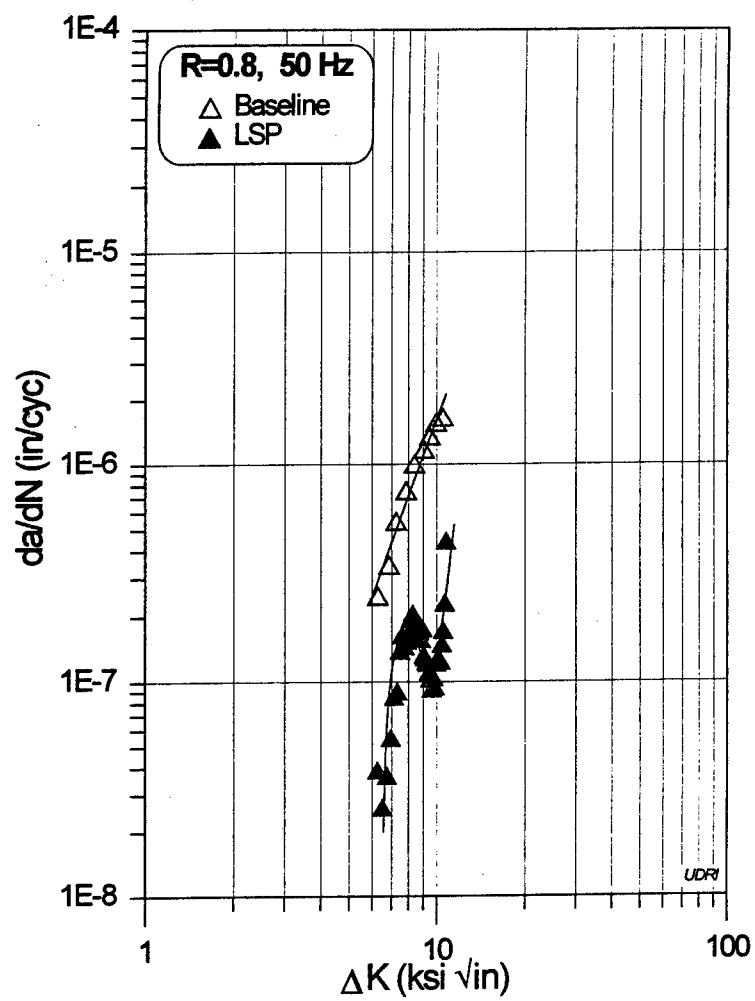


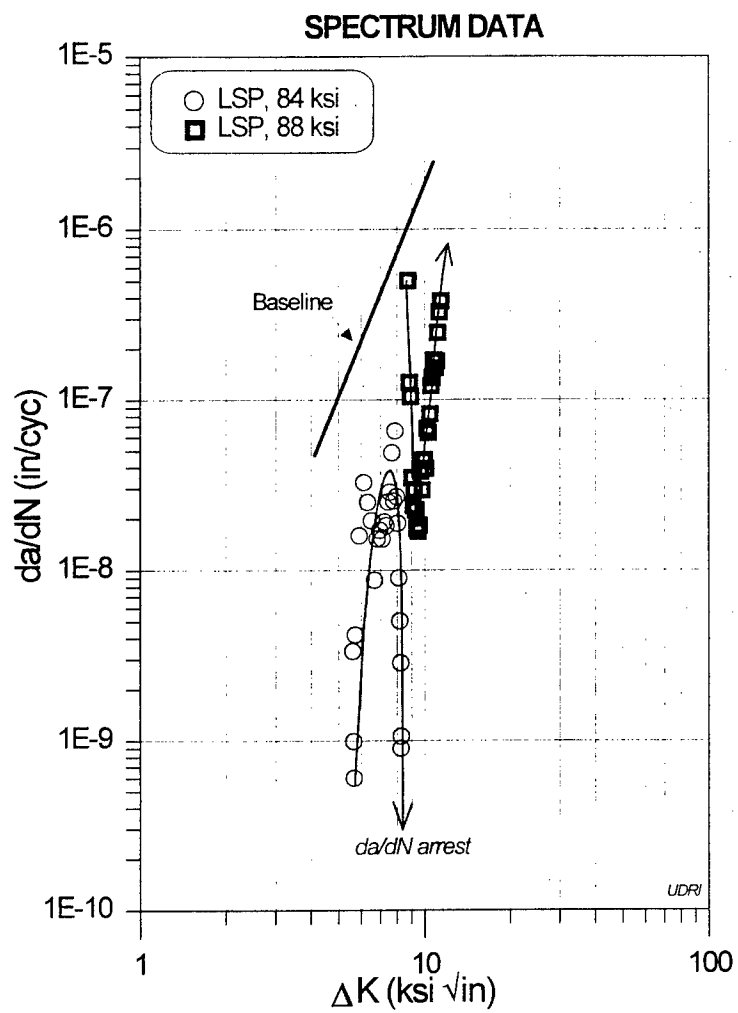
CYCLES







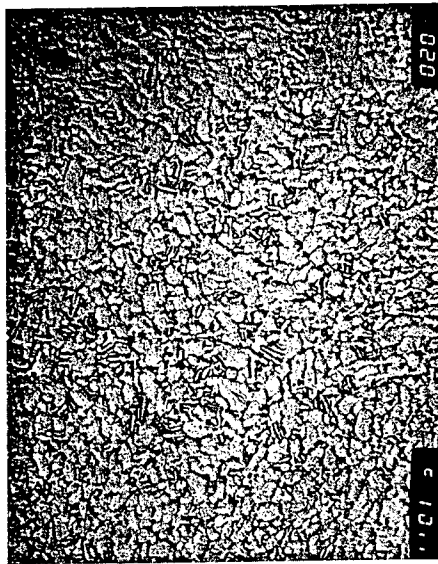




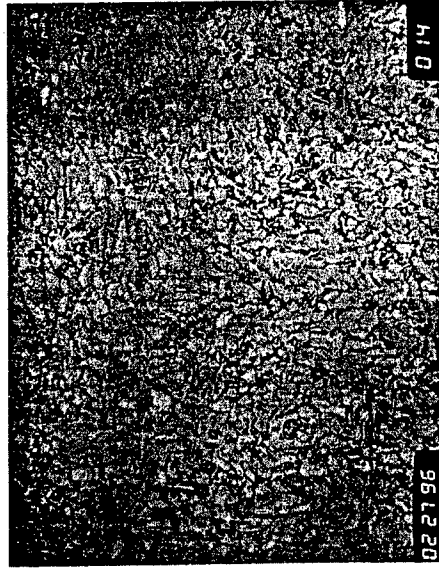
Metallography

◆ Microstructure of as-received and LSP

- Both microstructures consist of equiaxed grains of α and transformed β (Widmanstätten α)

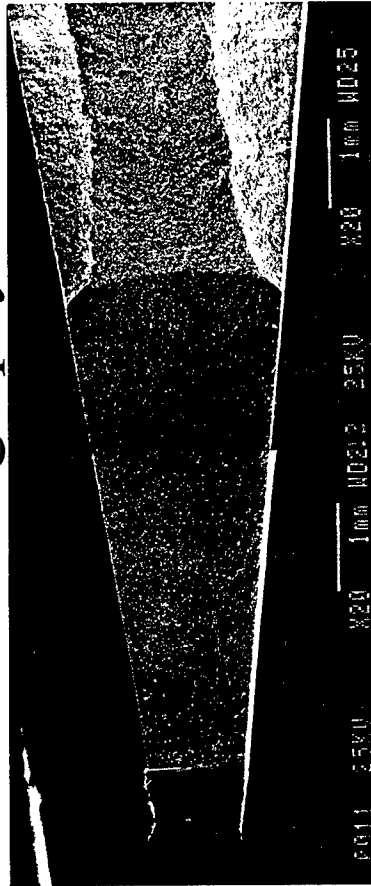


As-received (baseline)

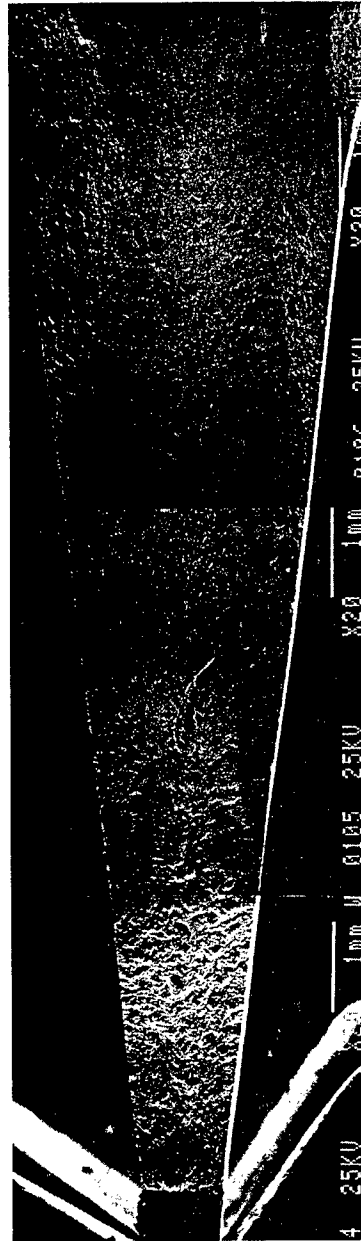


Laser-shock peened

Fractography



Baseline - R=0.1

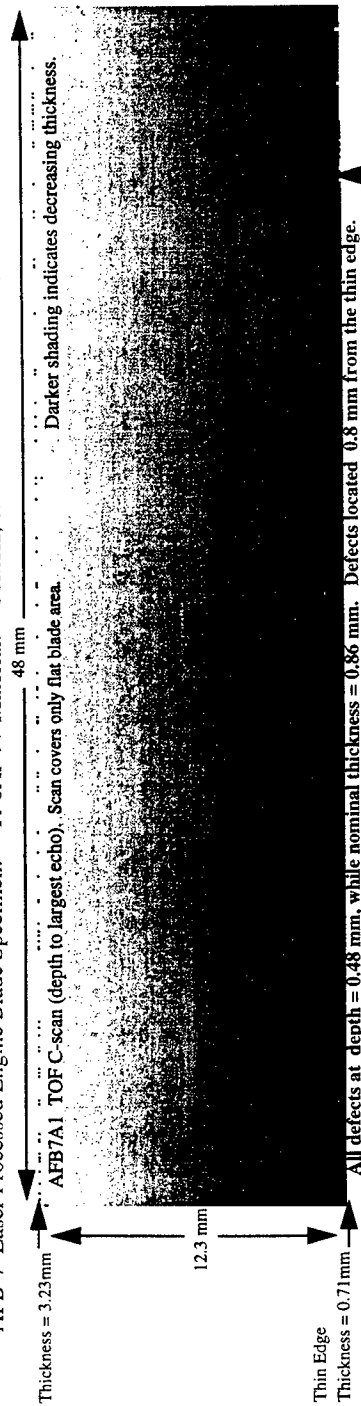


LSP - R=0.1

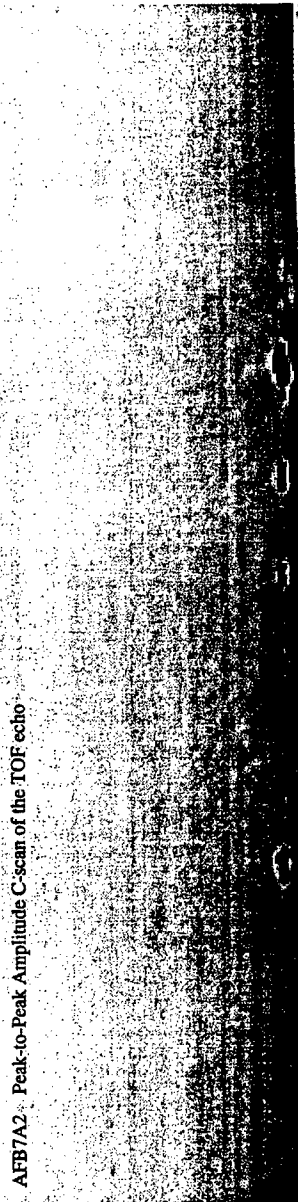
Non-Destructive Evaluation

- ◆ **As-received and LSP test samples, and fan blade which had been LSP'd were C-Scanned for flaws**
- ◆ **LSP sample was found to contain delaminations at the mid-plane of the thickness**
 - **The as-received specimen had none**
 - **Because of the curvature in the blade, proper inspection was impossible**

AFB-7 Laser Processed Engine Blade Specimen. Ti-6Al-4V Material. 50MHz, 0.5" Focused Transducer, 3-5-96 WL/MILLP



AFB7A2 Peak-to-Peak Amplitude C-scan of the TOF echo



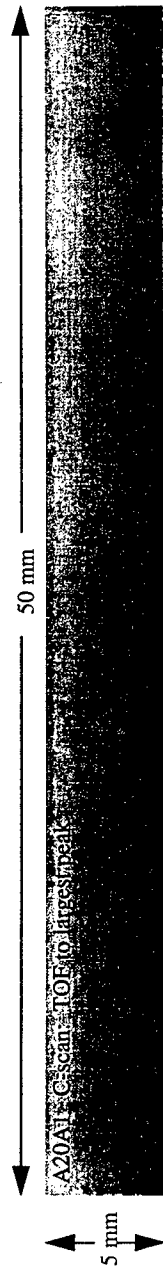
AFB7A3 Thresholded TOF C-scan. Depth to Threshold amplitude (higher sensitivity but increased noise)



Engine Blade Specimen #20

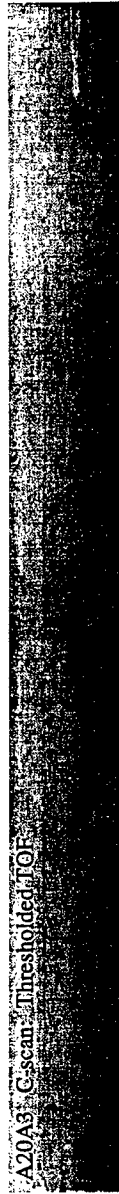
3-11-96 WL/MLLP

This specimen did not receive any laser shot peening. No defects were found by the UT C-scans.
Frequency: 50 MHz, Step size 50 μ m.



This side is the thin outer edge of specimen.

Darker shading indicates decreasing thickness.



Conclusions

- ◆ Similar initiation behavior although cracks arrest in LSP (at low R)
- ◆ Laser-shock peening resulted in substantial increase in threshold ΔK to produce stable da/dN at low R
 - Increase not as large at high R
- ◆ Mechanism behind this still not totally explained - residual stresses to be measured and calculated
- ◆ LSP can potentially produce damage in the material if process not adequately controlled

Future Work

- ◆ **Additional testing**
 - closure measurements
 - notch (damage) configuration
 - transition regions
- ◆ **Perform TEM investigation of microstructure**
- ◆ **Perform residual stress measurements**

THE EFFECT OF LASER SHOCK PEENING (LSP) ON AIRFOIL FOD AND HIGH CYCLE FATIGUE

S.R. Mannava, W.D. Cowie, A.E. McDaniel

**General Electric Aircraft Engines
Cincinnati, Ohio**

OUTLINE

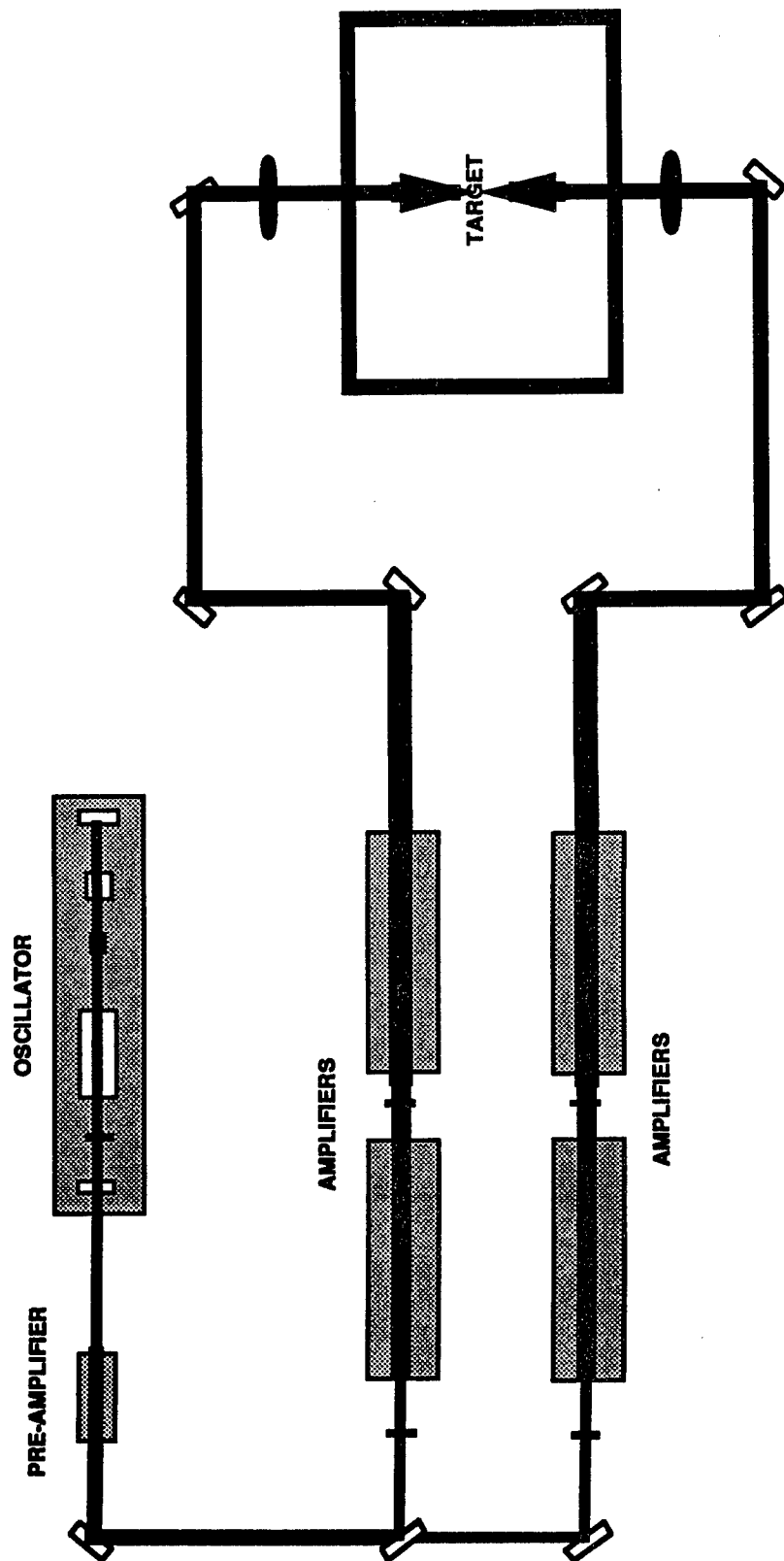
- **LSP History & Description of the Process**
- **GEAE LSP Airfoil Experience**
 - **FOD Simulation on Airfoils**
 - **HCF Testing**
 - **Preliminary Analysis of LSP Patch Residual Stress Distribution**
 - **Component Test Results**
 - **LSP Vs. Shot Peening**
- **Engine Test Results**
- **Summary**

LSP HISTORY AND DESCRIPTION OF THE PROCESS

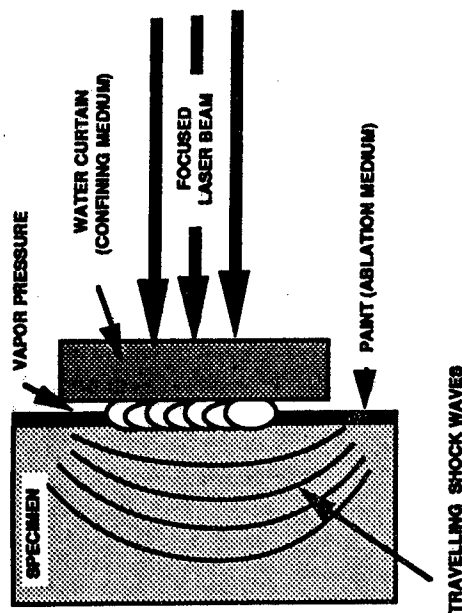
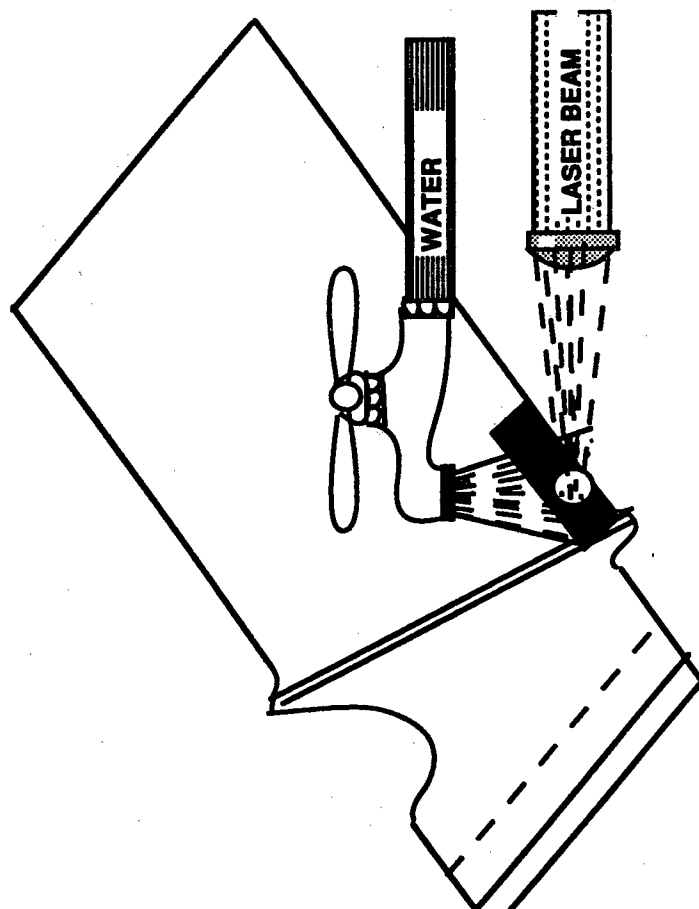
LSP History

- **Process Effect Discovered by Battelle Memorial Institute**
- **Wagner Laser Technologies (Sudbury Inc..) developed the proof of concept laser system**
- **GE Aircraft Engines is developing the Production laser equipment and the production Process for Airfoil Applications**

Typical LSP System for Airfoils

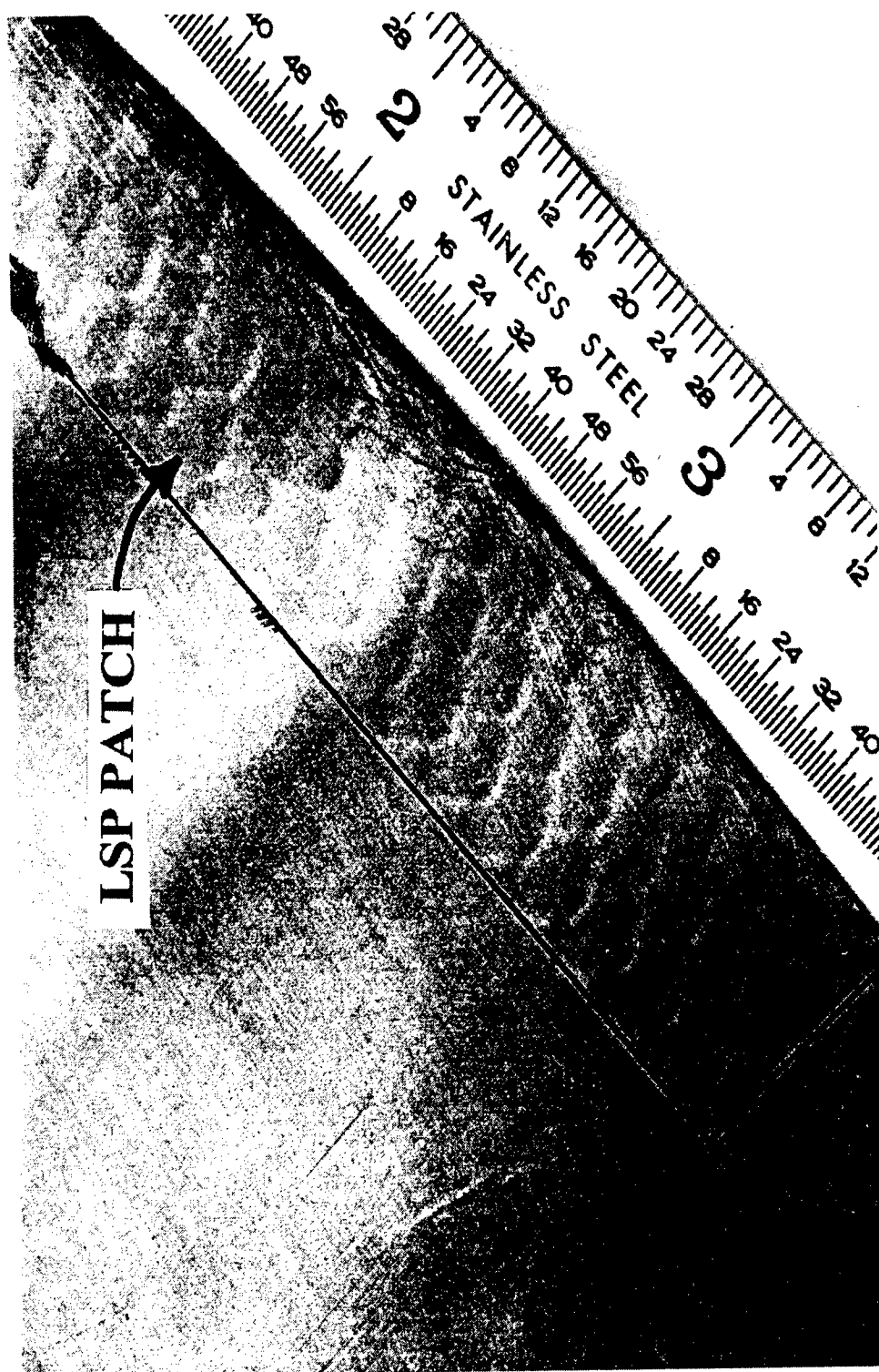


LSP CONCEPT

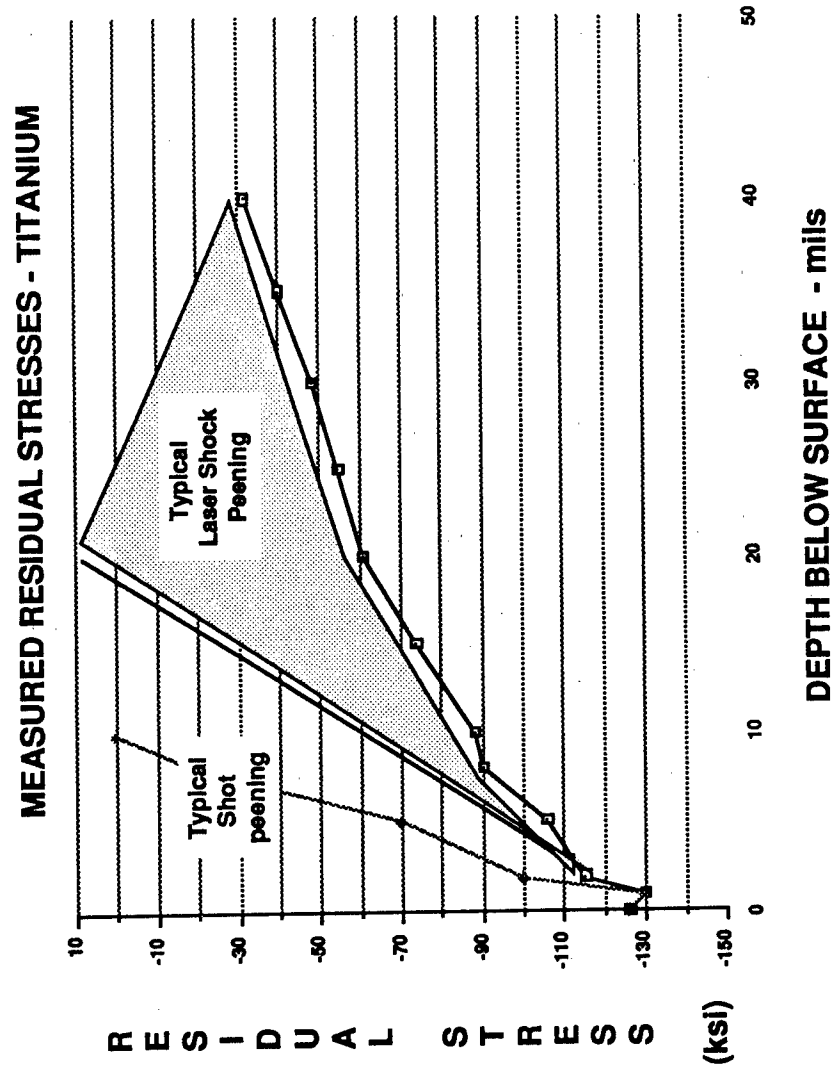


Residual stresses are generated by traveling shock waves created by rapidly expanding vapors due to absorption of high energy, ≈ 20 nanosecond laser pulses. Paint protects surface and water directs shock waves into the material.

LSP TREATED AREA



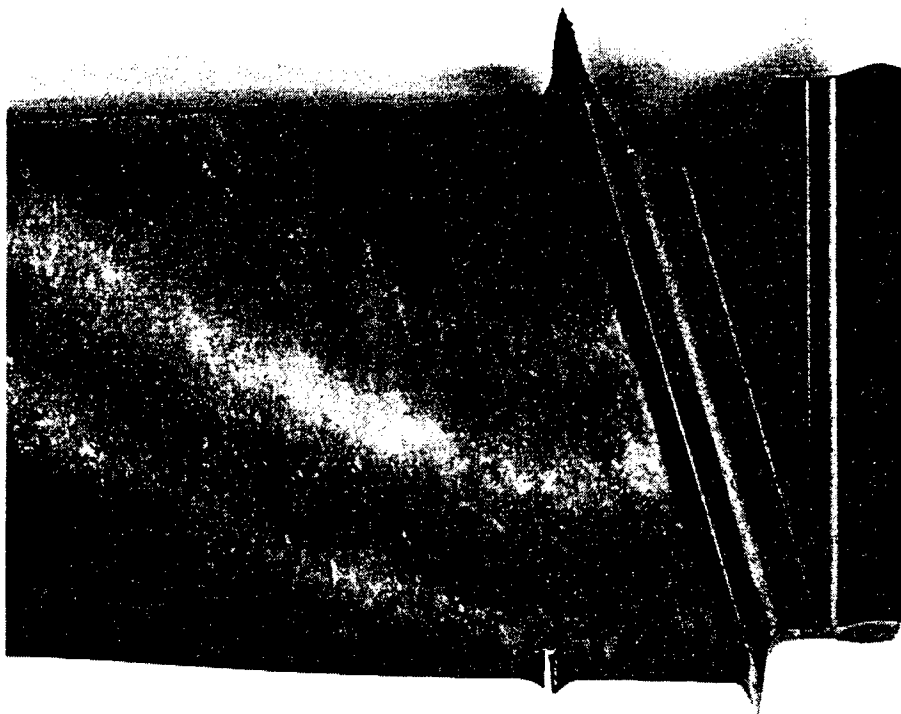
Advantages of LSP



GE Aircraft Engines LSP Experience

FOD Simulation on Airfoils

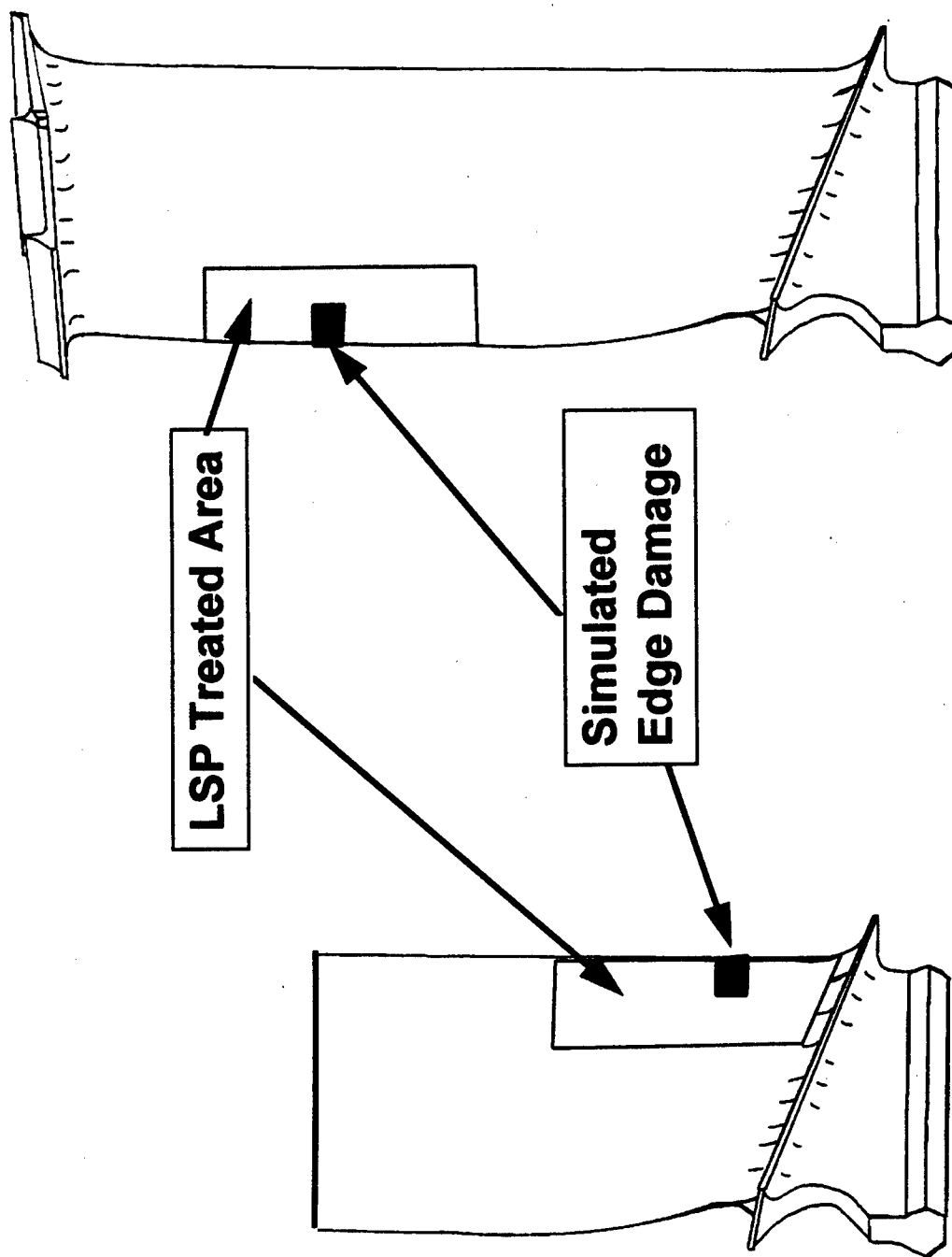
0.25" Deep Side Shear Damage With Chisel



High Cycle Fatigue Testing

SIREN HCF TEST FACILITY

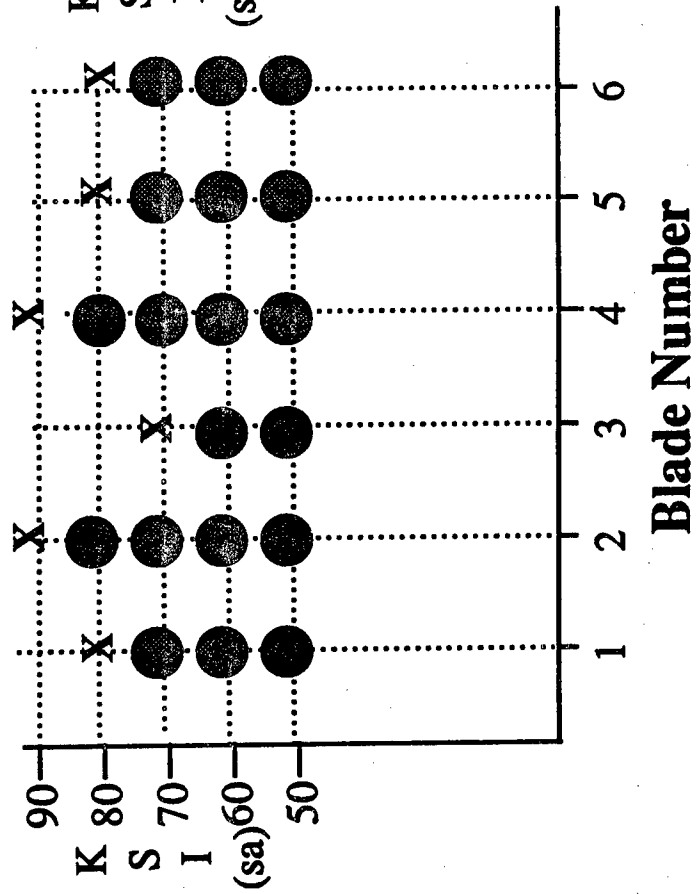




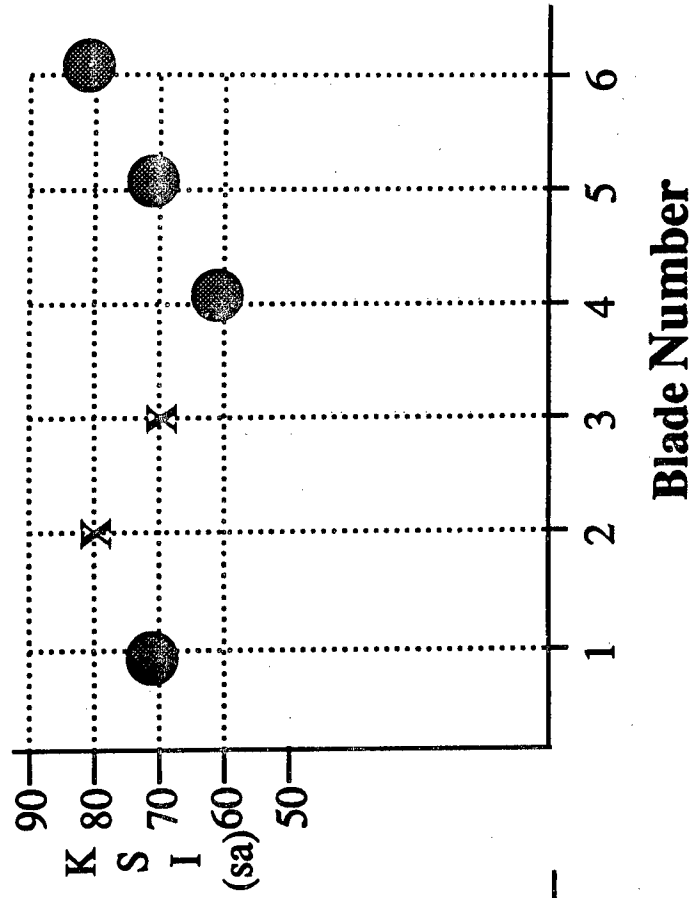
Flexural Blade Specimen Torsional Blade Specimen

HCF TEST METHODS

STAIR STEP



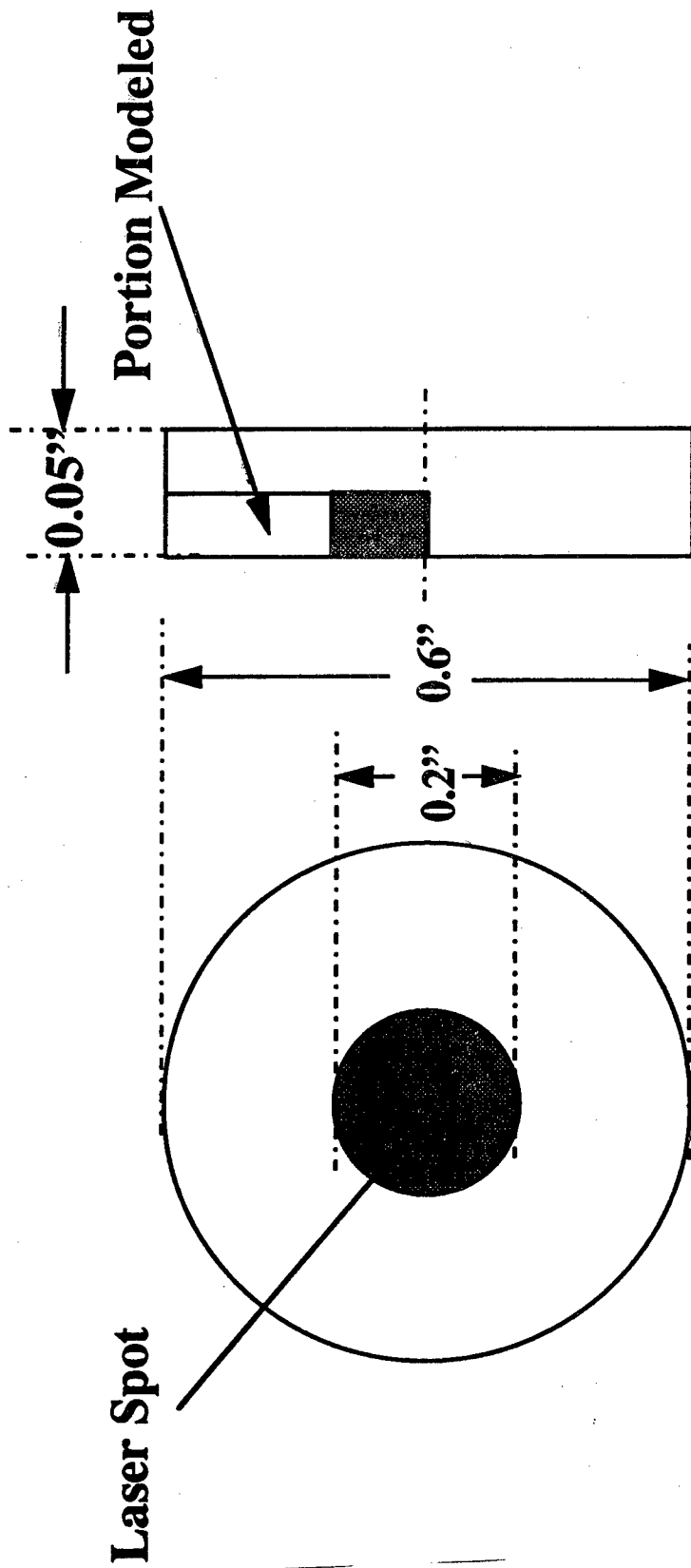
STAIR CASE



Preliminary Analysis of LSP Patch Residual Stress Distribution

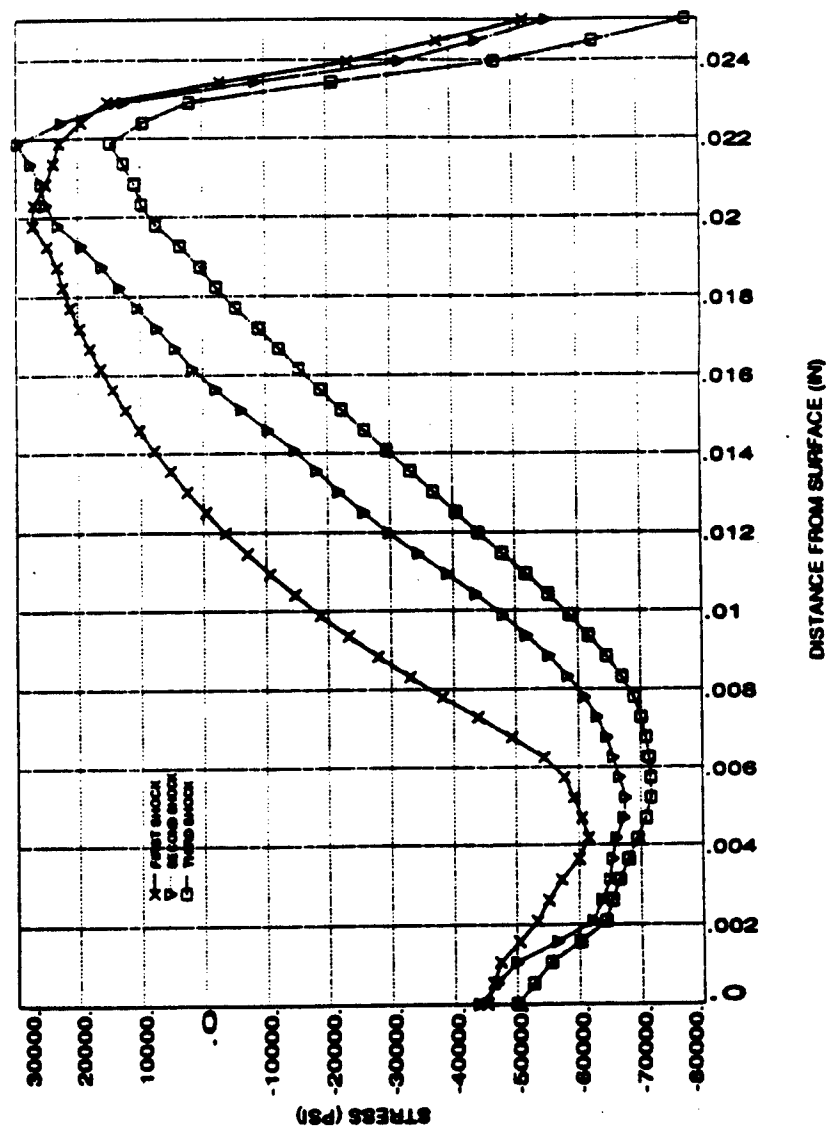
Axisymmetric Model

- Thickness approximates an airfoil
- Analysis of one shock takes about 5.8 hours on CRAY



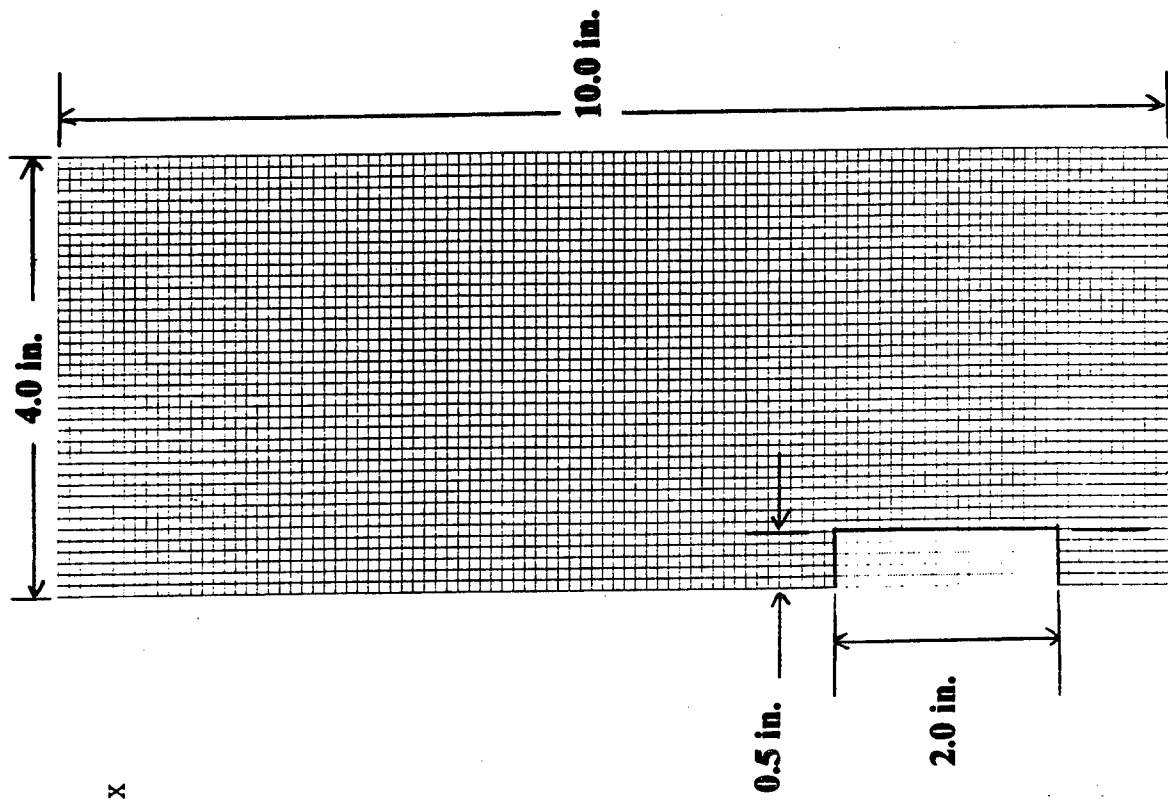
Axisymmetric Model

AXISYMMETRIC MODEL RESULTS
RESIDUAL STRESS AT CENTER OF SPOT



ANSYS 5.2
 OCT 2 1996
 08:23:54
 PLOT NO. 3
 ELEMENTS
 TYPE NUM
 ZV = 1
 DIST=5.5
 XF = 2
 YF = 5
 ZF = .025
 PRECISE HIDDEN

Date: Oct 2, 1996
 Time: 8:30 AM
 Filename: /users/mcclelliv/shock/plate/
 plate.grph
 GE
 Aircraft Engines



FLAT PLATE TEST CASE WITH LSP STRAINS

1
 Y
 Z X

ANSYS 5.2
 OCT 2 1996
 08:22:54
 PLOT NO. 1
 NODAL SOLUTION
 .STEP=1
 SUB =1
 TIME=1
 SY (AVG)
 RSYS=0
 DMX =.266E-06
 SMN =-1
 SMX =.776561
 -1
 -.802609
 -.605213
 -.407817
 -.21042
 -.013024
 .184372
 .381769
 .579165
 .776561



FLAT PLATE TEST CASE WITH LSP STRAINS

Date: Oct 2, 1996
 Time: 8:54 AM
 Filename: /Users/modan/ishock/plate/
 plate.grph



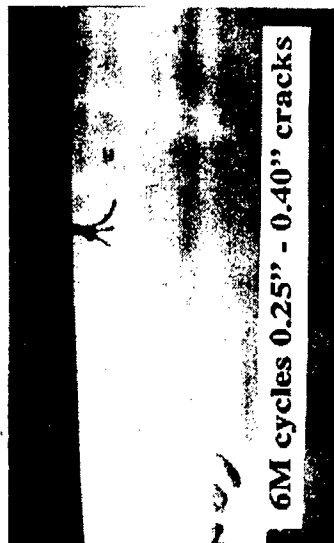
GE
 Aircraft Engines

Component HCF Test Results

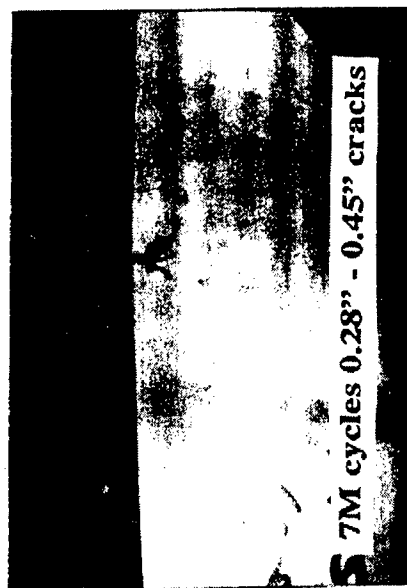
TORSIONAL HCF TEST OF NOTCHED LSP'D BLADE **Stairstep Test Starting @ 100ksida - 10⁶ Cycles**



S/N 37690
AFTER 120 KSI DA



S/N 37690
AFTER 200 KSI DA

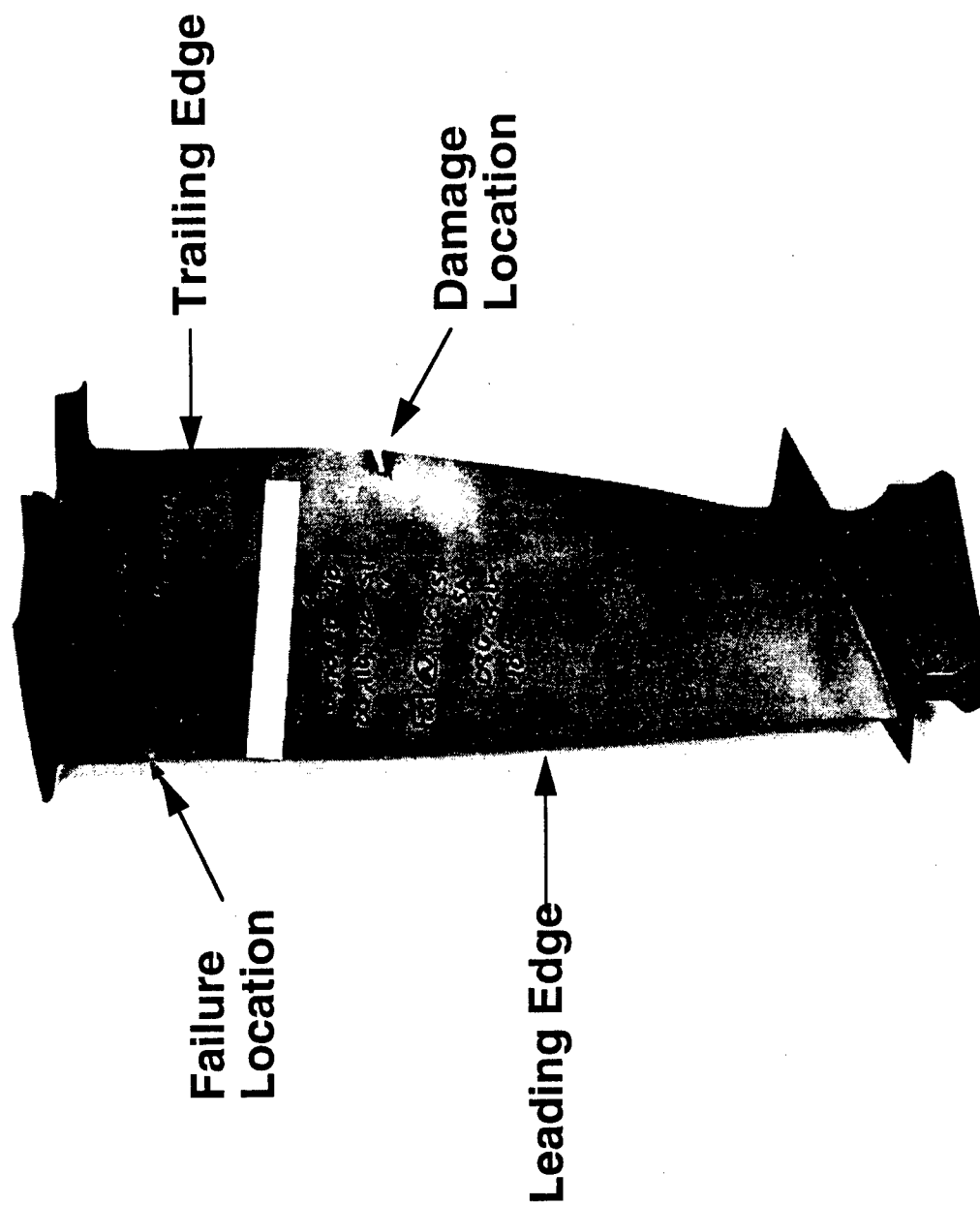


S/N 37690
AFTER 220 KSI DA

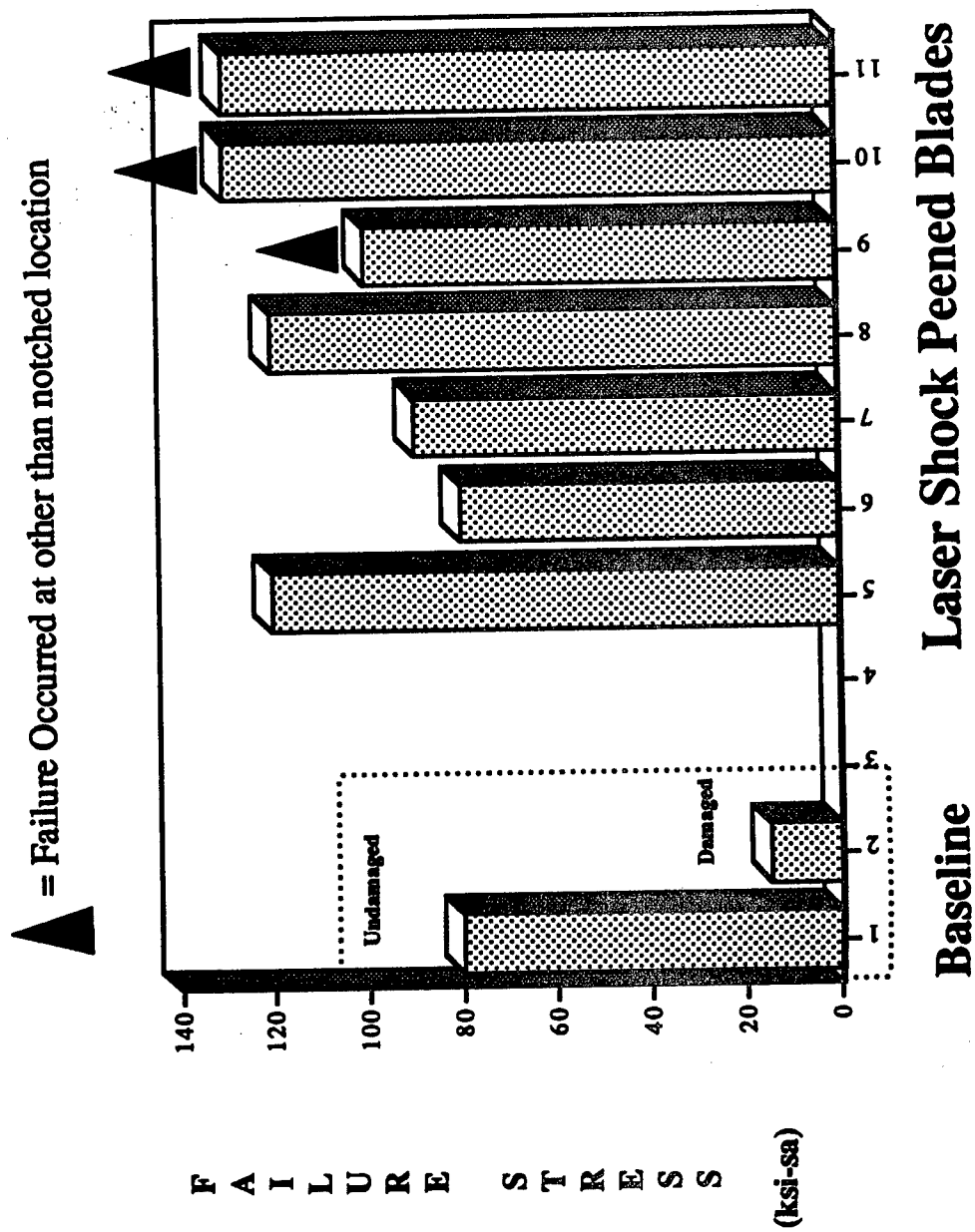


S/N 37690
FAILURE AT 240 KSI DA

TORSIONAL HCF TEST OF LSP'D BLADE WITH NOTCH



TYPICAL LSP FAN BLADE HCF TEST RESULTS (Torsional Mode with 1/4" side shear damage)



TORSIONAL TEST OF LSP'D BLADE WITH NOTCH

Staircase test - 10^7 cycles

- **Baseline with Damage**

- Runout @ 20 ksida
- Failure @ 30 ksida

- **LSP With Damage**

- Runout @ 200ksida
- Crack grew to 0.44" long and stopped growing
- Total crack length is 0.69" including damage

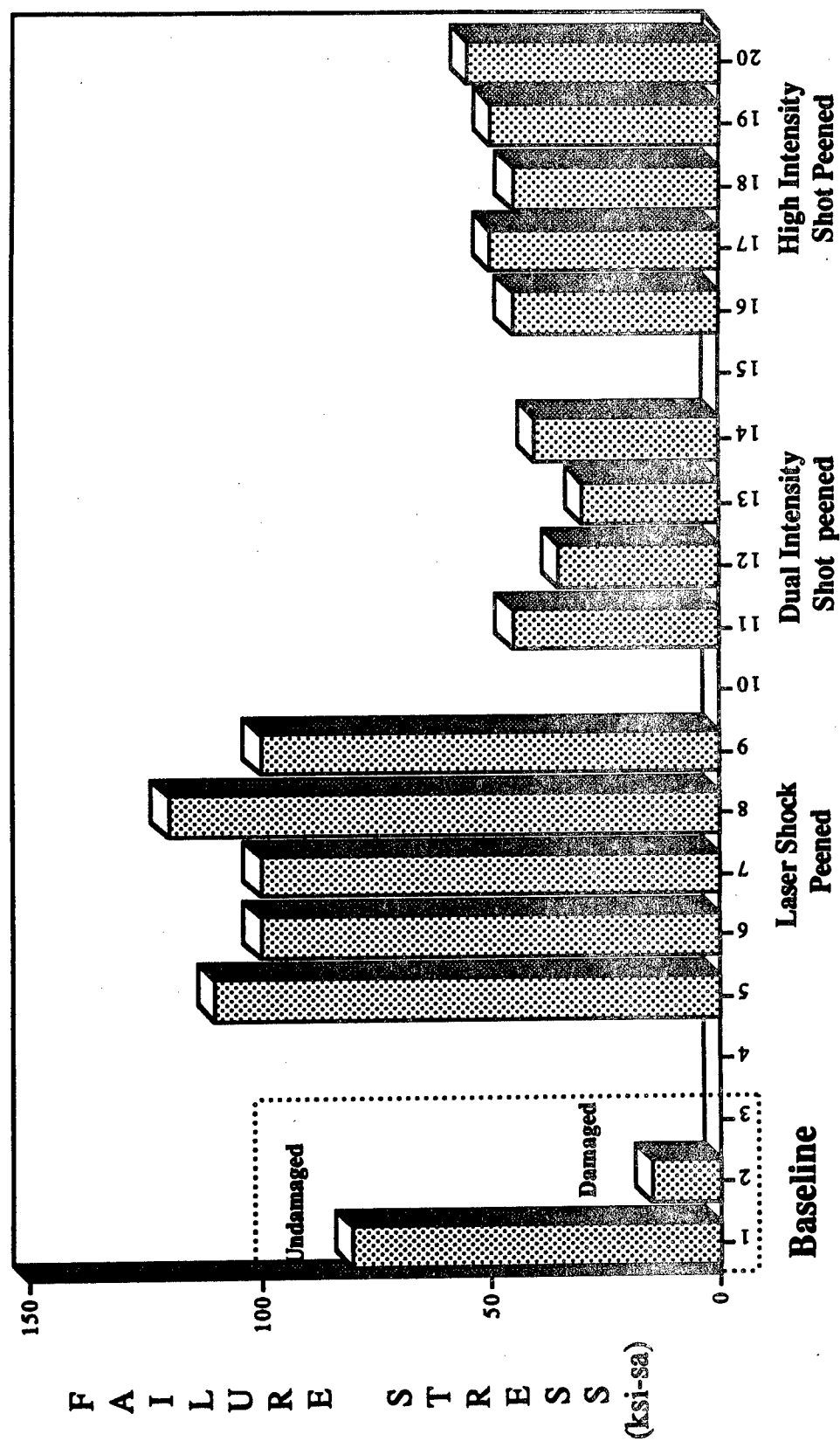


K S - S A

SPECIMENS

229

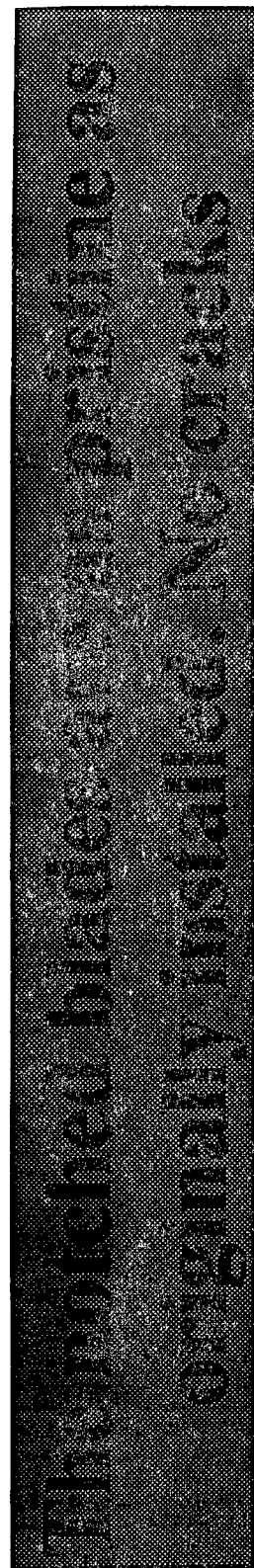
LSP Vs. SHOT PEENING HCF TEST RESULTS (0.25" side shear damage)



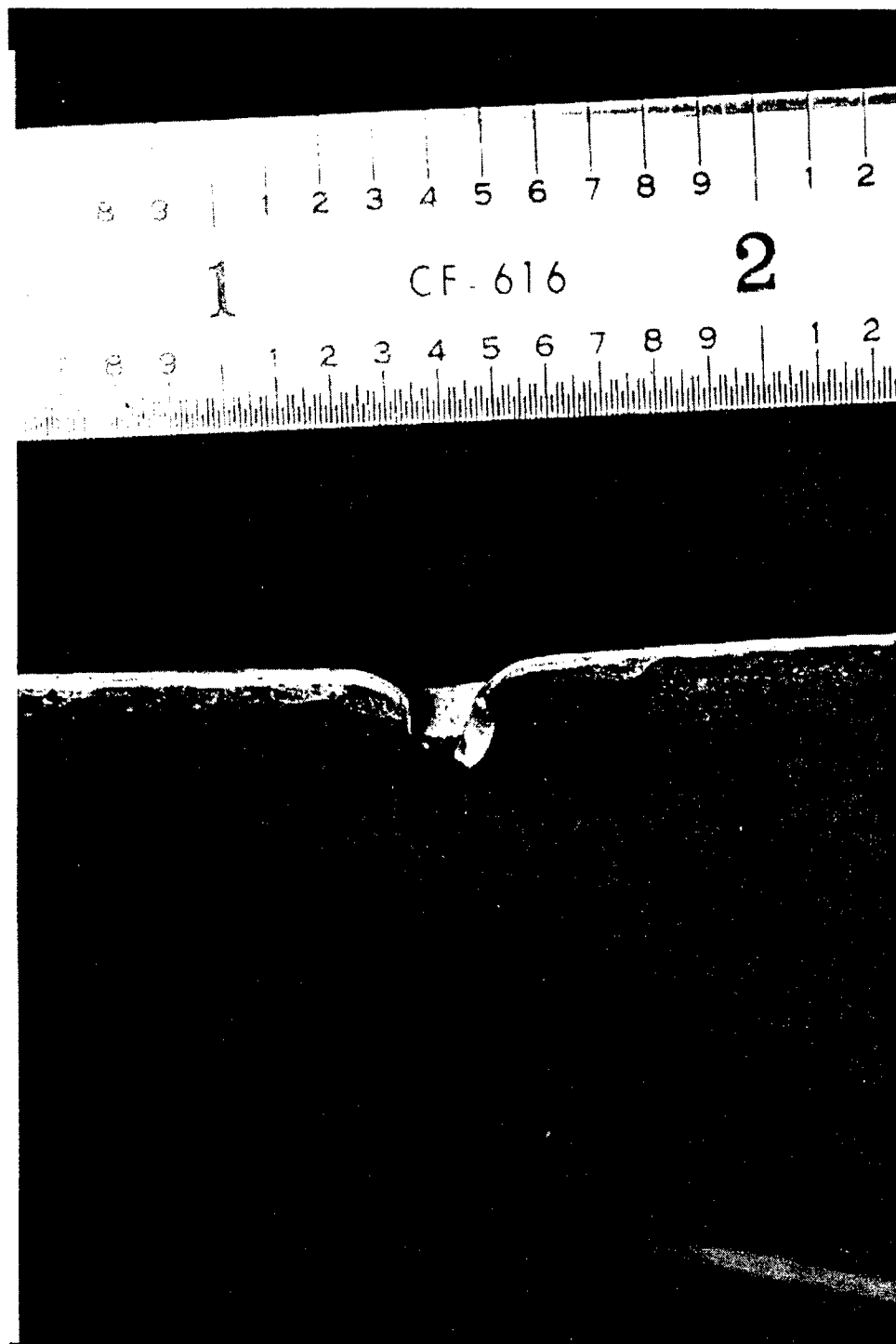
Engine Test Results

Engine Test of Notched Blades

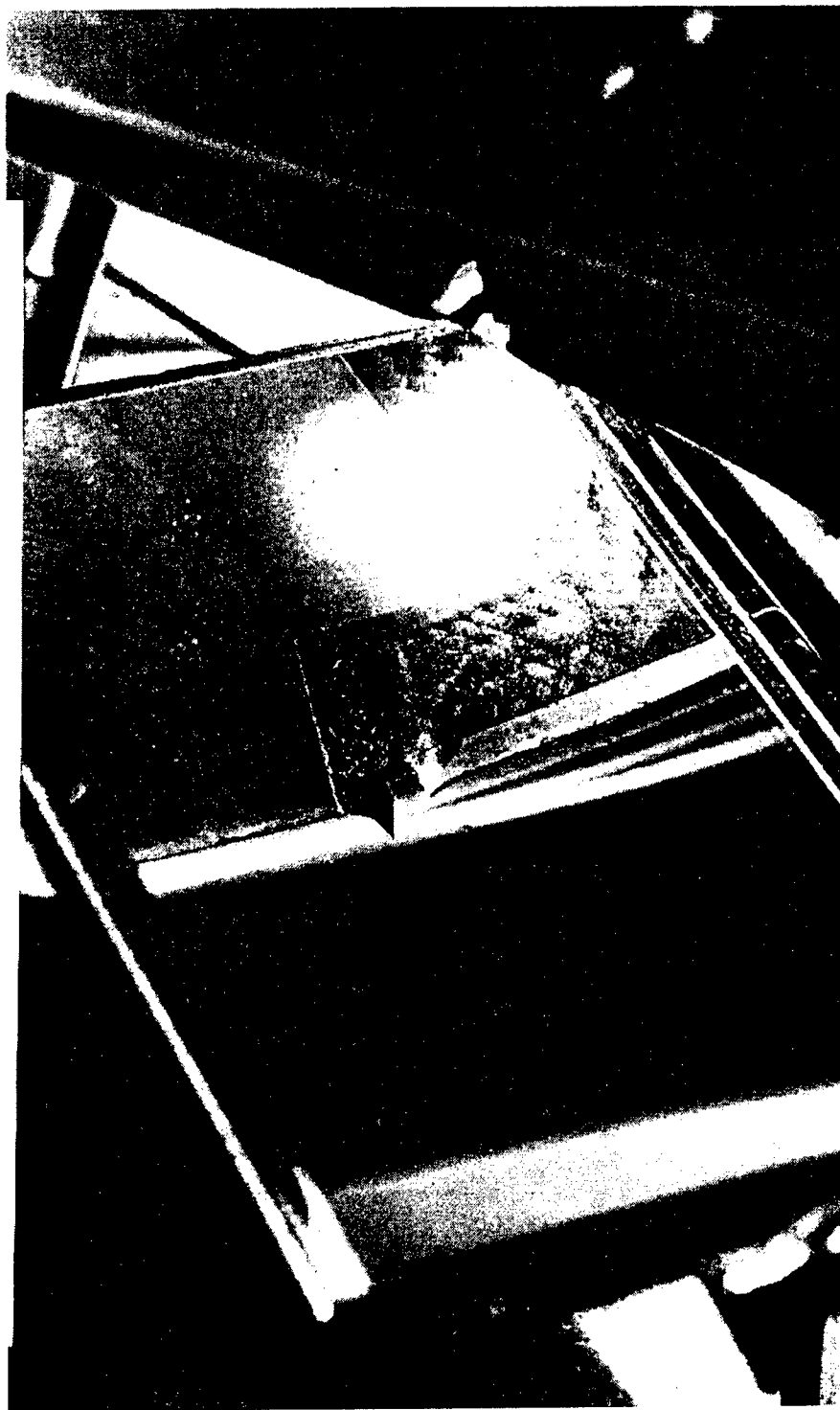
- Engine test was done at Arnold Engineering Development Center in Tennessee
- Two notched blades with 0.125" deep side shear damage were installed in the engine
- Maximum Maneuver distortion screen was installed to excite critical resonance conditions
- Ten Accels and Decels prior to resonance test
- Held for 30 minutes at peak resonance near max. power
- Five Accels and Decels before the engine was shut down



NOTCHED BLADE FOR ENGINE TEST



Notched Blade for Engine Test With Instrumentation



Summary

- **Laser Shock Peening is a Proven Method to Strengthen fan blade leading edges for FOD**
- **Dramatic results have been demonstrated in full scale component and engine test programs**
 - LSP treated blades increase tolerance to severe FOD
 - Eliminates special inspections for minor damage
 - Allows (as serviceable) generous FOD leading edge nicks
 - Permits blending of deep nicks instead of blade replacement
- **LSP has shown that it can both increase fatigue lives and significantly raise crack growth thresholds by locally changing the state of stress**
- **LSP is an exciting cutting edge technology that has wide implications that are just beginning to be explored**



100 Andover Park West • Seattle, WA 98188

**Evaluation of Shear Tears Found at Cold Expanded Holes in
7178-T6 Extrusions - KC-135 Laboratory Teardown Inspection**

By Len Reid, Vice President of Engineering, and
Eric Easterbrook, Engineering Manager

Paper presented at:
1996 USAF Aircraft Structural Integrity Program Conference
San Antonio, TX, USA
December 3-5, 1996

Evaluation of Shear Tears Found at Cold Expanded Holes in 7178-T6 Extrusions - KC-135 Laboratory Teardown Inspection

Mr. Len Reid, Vice President of Engineering
Mr. Eric Easterbrook, Engineering Manager
Fatigue Technology Inc.
100 Andover Park West, Seattle, WA 98188-2868

ABSTRACT

An evaluation was conducted to determine the cause and long-term effect of cracks or shear "tears" found at fastener holes in the lower outboard wing stringers of the KC-135 NASA Zero 'G' Aircraft. The tears were found during a recent teardown inspection conducted by the Boeing Defense and Space Group. The tears appeared to be associated with cold expansion performed on the holes during the implementation of ECP 484 that began in 1986. The investigation focused on the cold expansion process and its interaction with the 7178-T6 extrusion. A number of potential causes for the tears were examined including discrepant tooling, improper cold expansion procedure and the mechanical and fracture toughness properties of the stringer. Because the tears appeared in a large percentage of the holes, a fatigue test was conducted to determine the effect of the tears on the remaining fatigue life of the KC-135 outboard wing.

INTRODUCTION

In the ECP-484 Life Extension Modification of the C/KC-135, a number of fastener holes in the outboard wing lower surface were Split Sleeve Cold Expanded to Size (Cx2s_{SM}). The Cx2s process was targeted to improve the life of the 7178-T6 skin panels. The rework effort began in the summer of 1986 at Tinker AFB and continued for several years. Prior to the implementation of the ECP, Boeing Military Airplane Company (BMAC) conducted crack growth testing of Cx2s holes in 7178-T6 plate load-transfer type dogbone specimens. The results of these tests showed that pre-flawed Cx2s holes exhibited a cyclic test life five to ten times longer than pre-flawed, non-cold expanded holes [1]. Only the skin material (plate) was tested. The stringer (extrusion) was not tested even though it received cold expansion in the modification. This is one important observation that will be discussed later.

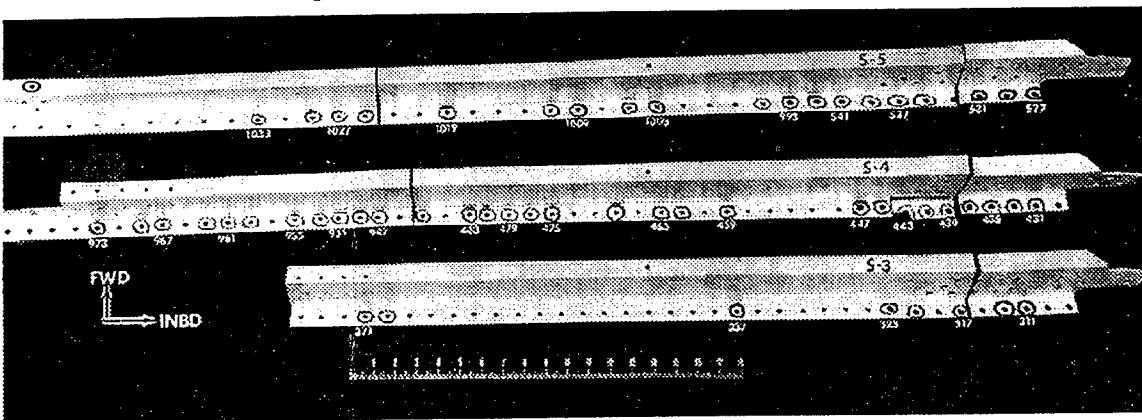


Figure 1
Representative Stringers from KC-135 Teardown

During a recent teardown inspection of the NASA Zero 'G' Airplane Left Hand Outboard Wing Lower Surface, cracks or tears were found extending from cold expanded holes in the lower wing skin stringers [2]. Holes with tears are circled in the Figure 1.

Of the 600 Cx2s holes inspected, 155 had shear tears. Some tears had actually broken through the ligament on a few of the larger (5/16 inch) short edge margin holes. All of the tears appeared to originate from a corner of the ridge left in the hole after Cx2s, i.e., the location corresponding to the split in the sleeve - see Figure 2. The tears were found only in the 7178-T6 extrusion stringers, and not in the wing skin (7178-T6 plate).

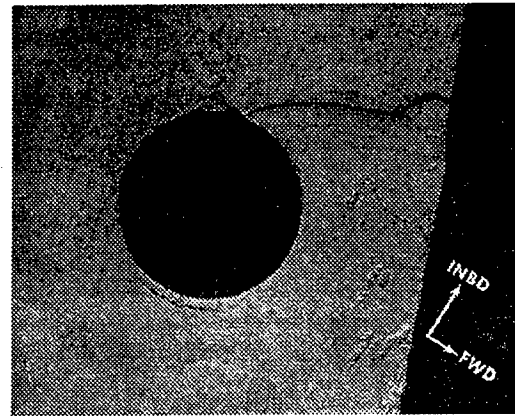


Figure 2
Typical Teardown Shear Tear
in KC-135 Stringer

To determine the cause of the KC-135 stringer tears, FTI examined the tooling setup, sleeve orientation and applied expansion as well as the mechanical properties of the material. Finite Element Analysis (FEA) was used to determine the local stress at the split during cold expansion. A brief analysis of the fracture toughness and the ability of the material to withstand a shear displacement was also performed. Finally, a fatigue test was run to see what effect the shear tears have on the long-term fatigue performance of the wing structure.

Cx2s PROCESS OVERVIEW

The Split Sleeve Cold Expansion to Size™ (Cx2s) process is accomplished by pulling a tapered mandrel, pre-fitted with a lubricated split sleeve through a hole, as shown in Figure 3. The function of the disposable split sleeve is to reduce mandrel pull force, ensure adequate radial expansion of the hole, preclude damage to the hole and allow one-sided processing. The process causes a radial plastic flow of material and produces an annular zone of residual compressive stress. This residual compressive stress created by cold expansion significantly increases fatigue and crack growth lives by reducing the stress concentration produced at the hole by in-service loads. The magnitude of the residual compressive stress zone is approximately equal to the compressive yield strength of the parent material. A balancing zone of tensile stress occurs adjacent to the circumferential compressive stress. This tensile stress is typically 10 to 15% of the tensile yield strength.

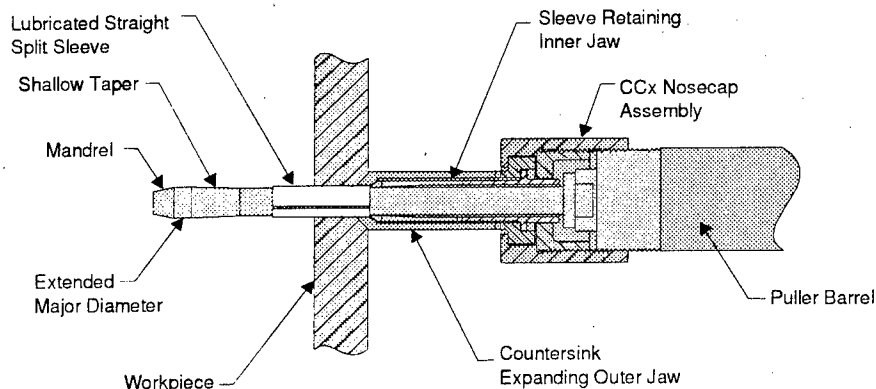


Figure 3
Cold Expansion to Size Tooling

The Cx2s process is designed so that the resulting cold expanded hole is sized to meet final hole requirements, thus eliminating the final ream process. This feature of the Cx2s process can provide a significant savings in labor time and cost when a large number of holes are being cold expanded. It also produces a consistent close tolerance hole; typically within 0.001 inch, not counting the dimension of the ridge. For applications in aluminum, the ridge is "flattened" during the fastener insertion.

SHEAR DISCONTINUITIES (TEARS)

Cold expansion has been known to cause a small shear discontinuity at the surface of the hole associated with the split in the sleeve as shown in Figure 4. In some 7000 series aluminum alloys, a small tear has been evident on the surface, but generally not to the magnitude witnessed in these KC-135 stringers.

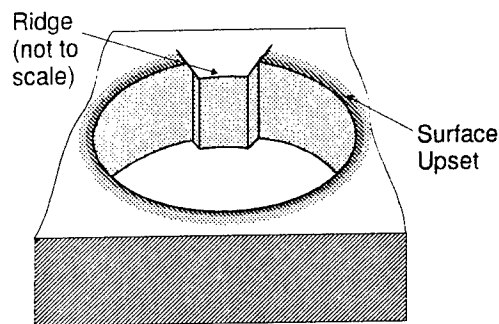


Figure 4
Schematic of Shear Discontinuity

Northrop evaluated shear discontinuities or tears in 7050 aluminum in a report published in 1982, [3]. The report showed that even with the presence of shear tears, life improvement was significant; three to eight times that of a non-cold expanded hole. None of the specimen failures in the Northrop test were associated with the shear tears as the crack actually initiated and propagated away from the tear(s). The tears observed in the test were typically less than 0.030 inch long and less than 0.008 inch deep; mainly a surface phenomenon.

FTI conducted an extensive investigation of shear tears and cracking associated with the hole cold expansion in 7050-T651 forged sections when the phenomenon was reported by a large aircraft manufacturer. In this case, the holes were drilled normal to the short transverse grain direction. The problem only occurred in holes greater than 3/8" diameter with the sleeve split orientation at 45 degrees to the grain direction (L-45-S). The cold expansion process is tailored to produce between 3% and 4% applied expansion to the hole. The S-L grain direction of some aluminum alloy products (particularly forgings) have low elongation percentage, less than 3% to 5% strain to failure, and low fracture toughness. This was clearly identified in the investigated problems when S-T grain direction percentage elongation in some samples were found to be less than 2%, highlighting a material property deficiency. The problem was corrected by controlling sleeve gap orientation and in some cases reducing the applied expansion level for larger diameter holes.

Cold expansion damage in these materials is probably caused by their inability to deform to the standard applied expansion levels without cracking. This occurs most frequently at the sleeve gap, due to the shear discontinuities acting as a stress concentration.

The Northrop and other reports about shear tears concluded that the tears were a harmless but annoying effect of the process, especially in 7000 series aluminum alloys. To eliminate concerns about the tears, users were directed to orient the split in the sleeve in line with the prevailing load path of the structure. By doing this, it was hoped that the ridge would not be a factor in the fatigue or crack growth life of the structure as cracks typically form normal to the load path. Ironically, it was this positioning of the sleeves that helped lead to the cracks observed in the teardown aircraft.

SHEAR TEAR VISUAL EXAMINATION AND COLD EXPANSION TRIALS

A visual and dimensional examination of the holes with the shear tears was performed on a removed stringer section. The holes showed evidence of cold expansion and displayed the shear tears much like the ones shown in Figure 5.

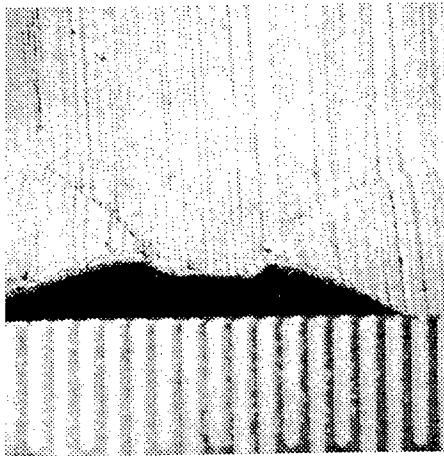


Figure 5
Shear Tears - Sleeve Ridge
Parallel to Extrusion
Direction and Loading

New holes were drilled into the upper flange of the stringer sample and cold expanded with KB2 100-2111 tooling (as specified in ECP 484). Shear tears were evident on the newly cold expanded holes, but not to the degree (less than 0.030 inch) found in holes in the teardown aircraft. Several attempts to induce larger tears including pre-loading the flange by poorly supporting the sleeve and other methods, were tried but were unsuccessful. The "poor support" simulated a gap between the stringer and skin that may have existed at the time of hole cold expansion. It was thought that unsupported material conditions during Cx2s may have caused the crack. After a number of attempts, it appeared that the KB2 100-2111 tooling could only induce small tears.

It was first thought that the large tears may have been the result of in-service loading or stress corrosion and that the hole "relieved" itself by extending the small shear tear. This hypothesis was subsequently dismissed when it was found that large tears were generated on the fatigue specimens being prepared for test. It is interesting to note

that no tearing occurred if the split was oriented in the transverse direction of the plate - shown in Figure 6.

This orientation was previously thought to be the worst position when maximizing fatigue life improvement. The ECP 484 instructions specified that the sleeve split was to be placed in the longitudinal direction (0 and 180 degrees), i.e., parallel to the spanwise load direction. It turns out that this orientation and the 45 degree orientation are the worst for producing shear tears. The total absence of tears in the 90 degree orientation was a striking contrast to the others. Obviously, conventional wisdom will need to be reevaluated.

Examination of the bore of the original holes on the stringer revealed that the fasteners were not installed into the holes with interference as specified. The fully formed ridge in the hole was practically undisturbed by the fastener. This was surprising considering that the subject Cx2s tooling was supposed to provide a hole giving 0.001 to 0.0035 inch interference with the fastener. A measurement of the holes showed that the hole diameter, after fastener removal, was up to 0.006 inch (.316 inch maximum diameter) larger than what would have been expected. The hole size could not be explained by the diameter of the installed fastener as it was nominally 0.312 inch. Typically, holes cold expanded in 7178-T6 at



Figure 6
No Shear Tears - Sleeve
Ridge 90° to Extrusion Grain
Direction and Loading

FTI using the KB2 100-2111 tooling resulted in 0.311 inch final hole, 0.001 inch over the targeted final hole of 0.3100 inch +0.0000, -0.0015.

Before, or just after, the ECP 484 rework started, FTI noticed that the sleeve originally supplied for the KB2 100-2111 tooling were 0.010 inch thick when they should have been 0.0080 inch thick. This discrepancy would result in a hole applied expansion range of 5.2 to 6.2% instead of the normal 3.9 to 4.9%. Approximately 11,000 sleeves were swapped out by FTI personnel between May 13 and 15, 1986. The larger thickness sleeve would go a long way toward solving the "large hole" mystery. However, attempts to duplicate the large crack and large hole phenomenon with a discrepant thicker sleeve were unsuccessful. The tear was about the same for the correct sleeve thickness, and the final hole diameters were not as large as those encountered in the stringer sample. At the time of this report, the large cold expanded hole diameter cannot be explained.

MECHANICAL TESTING

Mechanical testing was done to determine if the material properties were below specification and, therefore, responsible for the shear tears. This had been the case in other instances where large tears occurred. Testing was performed on an actual stringer piece in both the L and L-T grain directions. The test was conducted using ASTM E8 as a guideline. Tensile specimens were machined from the stiffener web instead of the flange. The flange had holes in it and was unsuitable for testing. It was thought that the flange and web would have similar properties. For the L specimens, the tensile properties met the BDM-4091 specification for 7178-T6 extrusion; $F_u = 99$ ksi, $F_y = 92$ ksi, elongation = 12.3% and modulus 10,300 ksi. The L-T specimens, because of their small size, were tough to grip and consequently did not make data collection easy. An offset in the LVDT setup negated an accurate modulus calculation, but the remainder of the data looked good except the F_y was a bit low; $F_u = 92$ ksi, $F_y = 65$ ksi, elongation = 5.5%. One of the specimens turned in an elongation of 4.85%. When compared to the normal applied expansion maximum of 4.9%, it is clear that the Cx applied expansion is near the threshold of this material in this grain direction.

FINITE ELEMENT ANALYSIS

Finite element analysis of the expansion has been completed for a limited two dimensional model. The results are somewhat inconclusive as they do not show the progression of the high strains through the thickness of the part. A three dimensional full contact model will be analyzed by FTI in 1997. The model will show the stresses generated by the mandrel as it passes through the part. Important elements such as contact surfaces and the effects of friction will be used. It is anticipated that this model will be refined such that it will predict the shear tears in any material.

FRACTURE ANALYSIS

Fracture analysis was performed to determine if the tears were caused by exceeding the fracture toughness. Both small and large shear tears have been observed at the area of shear discontinuity in the hole produced by the cold expansion process. For one hole examined, the relative sliding displacement between upper and lower crack surface at the tip of the shear discontinuity was about 4.16×10^{-3} inch. The measurement was taken from displaced surface scratches in a photo taken from a microscopic examination. If one assumes this value of the surface displacement to be an approximation of the crack-tip sliding displacement, the applied local stress intensity factor K_{II} during cold expansion process can be

estimated. If the estimated K_{II} is larger than the critical value of this material, fracture will take place. Holes with shear tears were sectioned to expose the tear area. The surface was examined using SEM to look for shear dimples; indicative of a shear failure. Evidence of dimples was not present in this specimen because of possible rubbing of the adjacent tear faces.

To reduce the possibility of rubbing, another specimen was cold expanded while it was held at a small tensile load. Once the tear initiated it broke through the remainder of the specimen by applying a load sufficient to pull it apart. Subsequent SEM observations revealed the presence of very fine dimples as shown in Figure 7. The actual mode of failure is quite complex, and further work is needed to determine the dominate mode, if indeed there is one.

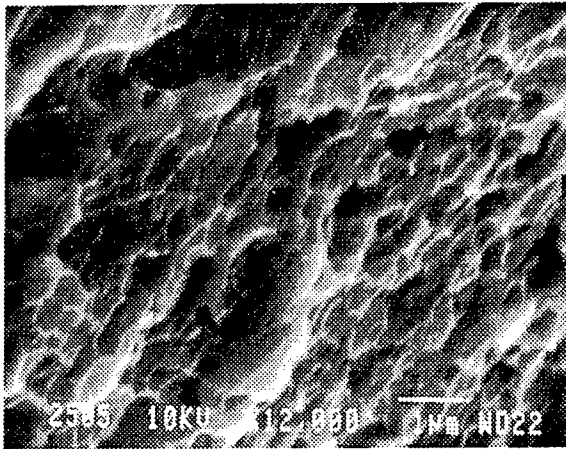


Figure 7
SEM Photograph of Shear Tear 12,000X

For small scale yielding, the crack tip sliding displacement (CTSD) is related to the applied K_{II} by the following relationship:

$$CTSD = \frac{K_{II}^2}{E' \tau_Y},$$

$$\text{or} \quad K_{II} = \sqrt{CTSD \cdot E' \cdot \tau_Y}$$

where $E' = E$ for plane stress, and $E' = \frac{E}{1-\nu^2}$ for plane strain; τ_Y = shear yield stress. For 7178-T6, $\tau_Y \approx 40 \text{ ksi}$, $E' = 10.3 \times 10^3 \text{ ksi}$, then

$$K_{II} = \sqrt{4.16 \times 10^{-3} \cdot 10.3 \times 10^3 \cdot 40} = 41.4 \text{ ksi} \sqrt{\text{in}}.$$

From the "Damage Tolerant Design Handbook," the critical fracture toughness of 7178-T6 sheet (thickness = 0.12 inch) in Mode I is:

$$\text{L-T: } K_{IC} = 50.4 \text{ ksi} \sqrt{\text{in}},$$

$$\text{T-L: } K_{IC} = 38.8 \text{ ksi} \sqrt{\text{in}}.$$

It is suggested that the critical fracture toughness in Mode II can be approximated by 80% of the value in Mode I. Therefore, one can obtain the critical Mode II fracture toughness as:

$$\text{L-T: } K_{IIc} = 40.3 \text{ ksi} \sqrt{\text{in}},$$

$$\text{T-L: } K_{IIc} = 31.0 \text{ ksi} \sqrt{\text{in}}.$$

The value of K_{II} during the Cx process is estimated at $41.4 \text{ ksi} \sqrt{\text{in}}$ for a split oriented along L-direction, which is much larger than the critical value $31.0 \text{ ksi} \sqrt{\text{in}}$. This may explain the cracking problem observed during the cold expansion of this material. In the same manner, the tears are not likely to occur when the sleeve is oriented toward the ligament as the estimated K_{II} for cold expansion is roughly equal to K_{IIc} . It appears, just like for the ductility of the material, that there is a problem of exceeding the threshold of a mechanical property.

To minimize the chance of cracking at the shear discontinuity for future applications, reducing the applied expansion may be a viable consideration.

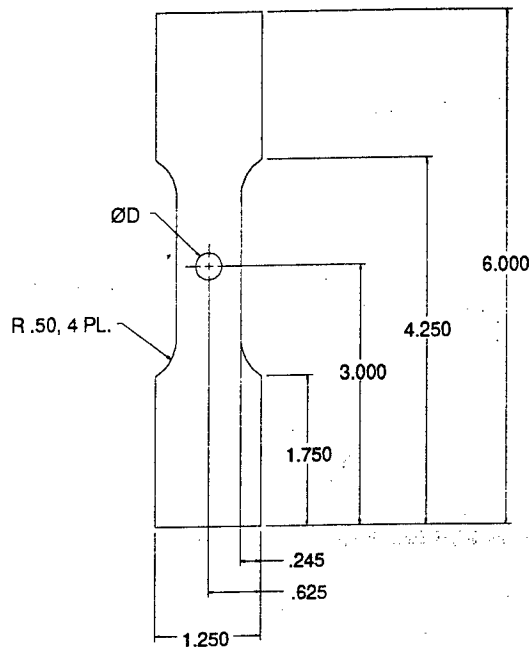


Figure 8
Fatigue Specimen Design

FATIGUE TESTING

Specimens

Web sections of several sections of scrapped 7178-T6 extrusion were used to manufacture 19 zero load transfer dogbone specimens shown in Figure 8. The specimen design has an edge margin (e/D) of about 1.23. This edge margin was selected as it represented the minimum edge margins of the holes in the stringers. The specimen's overall length dimension was in the direction of the material extrusion. The configurations were: 1) baseline, non-cold expanded (NCx) with a 0.3085/0.3100 inch hole, 2) Cold Expanded to Size (Cx2s) with the sleeve ridge oriented 0° to the load path, and 3) cold expanded with the sleeve ridge oriented 90° to the load path. Five repetitions of each configuration and four blank spares were manufactured. One specimen spare was used for a non-cold expanded specimen.

Test Plan

The specimens were cold expanded using KB2 100-2111-0 tooling where required. Post cold expansion measurements were made, and tear lengths were determined using a digital traveling microscope. The sleeve ridge location was photographed on both sides of each cold expanded specimen.

Testing was initially conducted at 20 ksi net section stress, R-ratio +0.05 and 13 Hz, but the stress level was increased to 25 ksi when one non-cold expanded specimen ran to over 750,000 cycles without a failure. Later, the frequency was reduced to 10Hz to reduce the occurrences of frame shutdowns during overpeak and underpeak trips. Specimens were generally run to about 600,000 cycles or two-piece failure.

TEST RESULTS AND DISCUSSION

The largest maximum tear length occurred on the mandrel entry side of the specimen; 0.143 inch. The average tear on the mandrel entry side was 0.075 inch. Tear lengths on the mandrel exit side averaged about 0.080 inch; not noticeably different than the entry side. Tears in 0 degree specimens were re-measured after having approximately 600,000 cycles applied. None of the tears showed any measurable growth. Additionally, no fatigue cracks were identified at the specimen hole or at the free edge away from the tear location. One of these specimens failed at just over 1,350,000 cycles.

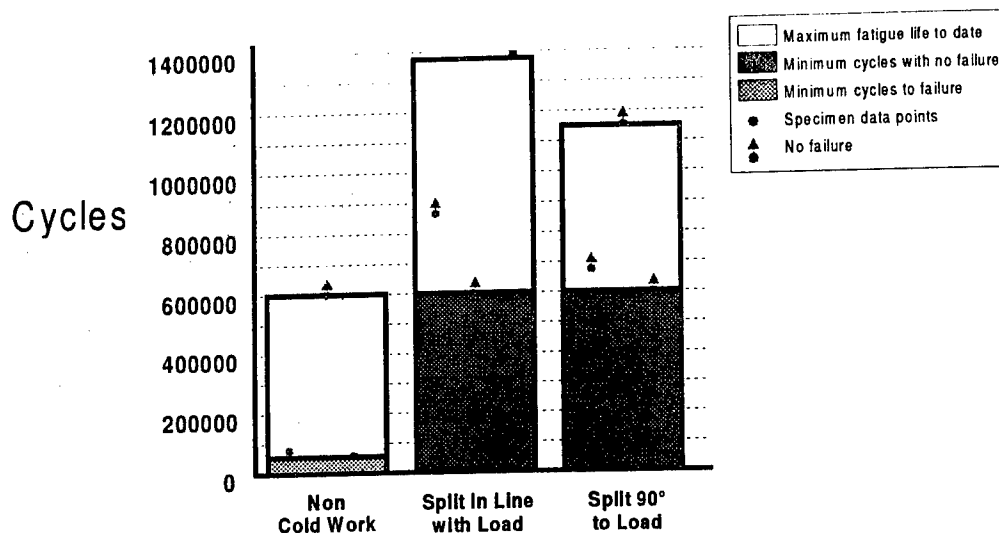


Figure 9
Fatigue Test Results

The fatigue data are shown graphically in Figure 9. There was a considerable amount of scatter in the non-cold expanded specimens. Two specimens failed at less than 100,000 cycles, while a third specimen ran to 600,000 cycles without failure. Since one of the non-cold expanded (NCx) and several Cx2s specimens were tested without failure, it was not possible to calculate a "true" average fatigue life for any of the specimen groups. Therefore, the technique of comparing specimen minimum failure lives was used. In general, the Cx2s process improved the lives of the specimens by a factor of nine.

For those specimens with the sleeve oriented at 0° to the load path (specified by ECP 484), approximately 20:1 life improvement has been demonstrated.

CONCLUSIONS AND RECOMMENDATIONS

From the observations, cold expansion trials, mechanical testing, finite element and fracture analysis, the following conclusions can be made about the nature and cause of the shear tears:

- The shear tears witnessed on the stringer are induced at the moment of cold expansion and are not a result of in-service loads or stress corrosion.
- Both small and large tears are produced by the Cx2s tooling at normal applied expansion levels.
- Tears occur most frequently when the sleeve is oriented in the longitudinal grain direction and are almost non-existent when oriented in the transverse direction, i.e., next to the ligament or web.
- Cracks occur because the expansion process is near or exceeds the limit of the values of elongation and K_{IC} for this material.
- The extensive overload generated by the cold expansion process produced such intense yielding at the tear end that stresses from the fatigue loading were not sufficient to promote significant growth of the tear in fatigue in a reasonably large number of cycles, i.e., 600,000.

The long-term effect of the shear tears, both small and large, can be predicted from the results of the open hole fatigue testing. The following is a summary of observations from testing:

- There were no failures in any of the specimens cold expanded 90° to the load path. One specimen was tested to over 1 million cycles without evidence of cracking. The minimum life improvement is projected to be substantially greater than 9:1.
- Although tears as long as 0.123 inch were present in the 0° specimens, the fatigue life improvement for that group was at least 20:1 using baseline minimum life of failed specimens. No degradation of fatigue life was observed for any cold expanded specimen.
- Only one Cx specimen failed from a fatigue crack extending from the initial tear. The other Cx specimen failure was at the hole edge, oriented 180°/90° to the load path away from the tears.
- The fatigue life improvement provided by the Split Sleeve Cold Expansion process typically increases as stress level decreases. The typical stress level encountered in the C/KC-135 lower wing outboard stringers is on the order of 12 ksi while the testing was run at 25 ksi. Therefore, greater life improvement can be expected from the in-service components.
- After approximately 600,000 cycles, none of the tears had any measurable growth in the 0° sleeve ridge orientation specimens, nor were fatigue cracks found to have initiated at the hole edge or specimen free edge.

Other general comments can be made from the study of this problem.

- Users must ensure that the split sleeve cold expansion process is safe for all elements of a stackup. On the KC-135 Program, only the skin material was tested. The extrusion not being the focus of the life improvement was not examined, but turned out to be the largest problem.
- Cold expansion is a robust process that is relatively unaffected by large initial cracks includes tears created in this application.

ACKNOWLEDGMENTS

The teardown inspection was conducted by Boeing Defense and Space Group, Wichita, under Air Force Contract No. F34601-90-C-1336. The authors wish to thank Bob Hammond and Joe Luzar of Boeing Defense and Space Group, Wichita, Kansas for their contributions.

REFERENCES

- [1] Boeing Report D500-10199-1
- [2] Boeing Report D500-12934-1, Jan. 31, 1996, "Laboratory Teardown Inspection of the LH Outboard Wing From The NASA Zero "G" Airplane"
- [3] "Split Sleeve Cold Worked Holes in 7050-T76351 Aluminum Plate for Improved Fatigue Life" by R. Hocker
- [4] FTI released Technical Brief #35444

SESSION III

REPAIR

Chairman: *G. Waggoner*, WL/MLS

Composite Patch Repairs of Cracked Metal Structures: Effects of Adhesive Nonlinearity, thermal Cycling & Debonding

Wai Tuck Chow,^{*} and Satya N. Atluri^{**}

*Computational Modeling Center
Georgia Institute of Technology, Atlanta, Georgia 30332-0356*

Comparison with the experimental data obtained by Denny¹ has been carried out to determine the ability of the finite element alternating method in predicting the fatigue response of a cracked metal panel with a partially debonded composite patch. There is a total of 15 different specimens considered in this comparison. Some of the parameters that are varied in these specimens include the disbond location, the disbond area, the initial crack length, the maximum stress loading and the stress ratio. For all these specimens, it has been found that the numerical results correlate very well with the experimental data, when the adhesive nonlinearity is properly accounted for in the analysis. In addition to this comparison with the experimental data, numerical studies have been carried out to examine the effect of the thermal cycling on the fatigue response of a bonded repair. It was found that due to the strong difference in the thermal expansion coefficient of the boron/epoxy patch and the aluminum panel, the fatigue life of a specimen which undergoes cycles of high-stress-at-low-temperature and low-stress-at-high-temperature loading is dramatically reduced. It was also found that the fatigue life of a specimen which undergoes a thermal-fatigue cycle is more sensitive to disbonds

^{*} Post-Doctoral Fellow

^{**} Institute Professor, Regents' Professor of Engineering and Director, Fellow AIAA.

in the adhesive layer than a similar specimen which undergoes fatigue loading at a constant temperature. In addition to this study, numerical analysis has been carried out to study the interaction between two nearby composite patches. The study found very little interactions between the two patches when these two patches lie horizontal to each other. On the other hand, when the two patches lie vertical to each other, the fatigue life of this specimen can increase substantially when these two patches are very close to each other; however this may lead to failure of the metal in between the patches, but this is not considered in the present study.

Introduction

Due to the high replacement costs and the shrinking budgets for aircraft acquisitions, many of the airplanes in the commercial as well as the military fleet are used beyond their original design lives. As a result, these aircraft undergo high cycles of repeated pressurization and loading, which in turn cause more fatigue cracks to be found emanating from local stress concentrations in the structure. Hence, to reduce the high cost of replacement for fatigue damages as well as possible accidental damages, the application of minor repairs using mechanical doublers or composite patches becomes an increasingly important option in the aerospace industry. While many of the repairs on an aircraft structure are still performed using mechanical doublers, various airlines as well as military facilities have begun experimenting with repairs using bonded composite patches (Jones and Callinan²). Repair using the mechanical doubler requires the cracked portion to be cutout and replaced with an undamaged sheet. In contrast, bonded repairs offer a wide range of advantages such as ease of application with no damage to the underlying

structure. In addition, bonded repairs using laminated composites offer high stiffness to weight ratio and such repairs can be readily formed into various complex shapes of different aircraft components. Nonetheless, some of the critical issues associated with the use of bonded repairs are still not fully resolved. These issues include the ability to predict the fatigue growth of cracks in bonded repairs as well as the effect of disbond on the effectiveness of the bonded repairs.

In general, the analysis of fatigue crack growth for composite repairs can be broadly categorized as either analytical or numerical. Based on the elastic inclusion analogy, Rose³ has obtained the solution for strip type patches by using a successive approximation method to deduce the asymptotic behavior of the modeled Fredholm integral equation. Rose⁴ further extended this method to obtain an approximate solution for a crack inside an elliptical patch. The solution for the elliptical patch is further extended by Fredell⁵ to include the effect of temperature. While the solution for Rose's model is simple and easy to implement, these solutions have strong limitations. Some of the limitations of the Rose's model include the assumptions that:

- the patch has to be either an infinite strip type or an elliptical shape type,
- the material behavior for the adhesive layer is linear elastic,
- the load transfer length must be significantly smaller than the patch size, i.e. the adhesive must be relatively stiff, or the size of the patch must be significantly large,
- the bonding of the patch is perfect without disbonds, and
- the size of crack is small compared to the size of the patch.

All of these assumptions limit the ability of the Rose's model to adequately analyze the effectiveness of most composite patches in reducing the fatigue crack growth. Therefore

to overcome these limitations, numerical methods have been employed in analyzing the effectiveness of repairs using composite patches. Jones and Callinan², Mitchell et al.⁶, and Chu and Ko⁷ have used the finite element method to study bonded patch repairs. Tarn and Shek⁸ have combined the boundary element method (for the plates) and finite element method (for the patch) to estimate the stress intensity factors. Park, Ogiso and Atluri⁹ have applied the integral equation approach in conjunction with the Schwartz-Neumann alternating method to calculate the stress intensity factors. In extending this work, the approach of the finite element alternating method was applied by Nagaswamy, Pipkins and Atluri¹⁰ to model a rectangular composite patch on a curved fuselage panel where the stress distributions due to curvature as well as the presence of stiffeners are accounted for. While these studies provide the methods to analyze a composite patch with perfect bonding, there have been few studies which concentrate on the verification of numerical analysis against experimental results especially when delaminations exist on bonded repairs.

Roderick¹¹ have examined the cyclic growth of a crack inside an elliptical disbond of a composite patch. Baker¹² has studied experimentally the effectiveness of composite repairs with disbond that occur during manufacturing. Denny¹ has experimentally investigated the fatigue life of composite patch with intentional disbond of various locations and size. This experiment also studies the effect of initial crack length, maximum applied fatigue stress and stress ratio. In this paper, analyses are performed using the finite element alternating method (FEAM) to study the fatigue life of partially bonded patches under different loading conditions. These numerical results are compared with the experimental data obtained by Denny¹ to determine the ability of FEAM in

predicting the fatigue life of partially bonded patches. Since debonds in bonded repairs are found frequently and the replacement of defective patches remains very difficult, the ability to predict the fatigue characteristic of partially bonded patches, and hence determining the safety of the repaired structure would be an extremely important issue to be resolved before bonded repairs can be used widely in the aerospace industry. In addition to the comparison with the experimental results, this paper also evaluates the effects of (i) temperature cycles, (ii) initial stresses due to the curing of the patch, and (iii) adhesive nonlinearity, on the fatigue characteristics of partially bonded patches. Furthermore, the interaction of two composite patches on fatigue life is also studied.

Finite Element Alternating Method

Through a series of papers written by Nishioka and Atluri¹³; Atluri and Nishioka¹⁴; Rajiyah and Atluri¹⁵; Park and Atluri¹⁶, and Wang and Atluri¹⁷, the alternating method has been established as an effective method in calculating the stress intensity factors for 2 and 3-dimensional linear elastic fracture mechanics. The cost-effectiveness of this method is achieved by combining the numerical methods such as boundary element method or finite element method with the analytical solutions of multiple collinear cracks. Since the analytical solutions for the cracks are incorporated directly into the alternating method, the cracks do not need to be meshed in the finite element model. Hence, very fine mesh which is typically required for linear elastic fracture mechanics would not be required. For this reason, the computational time as well as the time needed to prepare the finite element mesh are substantially reduced.

In the Schwartz-Neumann alternating method, two solutions are required:

Solution 1: A general analytical solution for an embedded crack in an infinite domain subjected to arbitrary crack surface traction.

Solution 2: A numerical scheme (the finite element method in this paper) to solve for the stresses in an uncracked finite body.

The general solution for an embedded crack is given by Muskhelishvili¹⁸ in terms of complex potential functions. To apply this solution to the alternating method, Park and Atluri¹⁶ used a set of Delta functions to represent the crack surface traction in order to analytically solve for the Cauchy integral required for the complex potential functions. To improve on the accuracy, Park¹⁹ used a set of approximate piecewise constant functions. In this paper, the crack surface traction is represented by a set of approximate linear basis functions developed by Wang and Atluri¹⁷. The stress intensity factors of the crack tips can then be directly calculated from the coefficients of the linear basis functions.

The finite element solution involves the analysis of the uncracked finite domain in order to calculate the stresses at the location of the actual cracks. Since the surface of each crack is traction free in the actual problem, these stresses are removed by applying the reverse stresses, and the analytical solution is then used to compute the K-factors corresponding to these reversed tractions. As explained below, this procedure will have to be repeated several times until convergence of the solution is achieved. The detailed steps involved in the finite element alternating method for an embedded crack in a finite body now follow with Steps 2 to 6 representing the iterative loop.

1. Solve the uncracked finite body under the prescribed tractions and displacements using the finite element method. This finite body has the same geometry as the original problem except the crack is ignored.
2. Using the finite element solution, a fit based on linear piecewise functions is made for the residual stresses at the crack surface location.
3. The residual stresses obtained in the previous step are reversed to create a traction free crack faces as in the given problem.
4. Using the reversed linear piecewise tractions, the analytical solution to the infinite body problem is solved.
5. The stress intensity factors for the current iteration are calculated using the above linear piecewise solution. If the magnitude of the stress intensity factors is less than a prescribed tolerance, then it is assumed that convergence has been achieved and the analysis is completed.
6. The tractions and displacements on the finite body are calculated. To satisfy the prescribed traction and displacement boundary conditions, the residual tractions and displacements on the external boundary are reversed. Using the reversed loading, the procedure would return to Step 2.

In practice, it has been found that this iterative procedure converges in less than 5 iterations in most cases. The overall stress intensity factors of the original problem are obtained by summing the stress intensity factors for all iterations. Note that the finite element method is used only to obtain a solution for the uncracked problem; hence the finite element alternating method is very efficient from the computational point of view particularly for fatigue growth analysis. This is because the finite element stiffness

matrix is decomposed only once and the decomposed matrix can be used repeatedly for all iterations as well as different crack lengths.

Implementation of Composite Patch Analysis

The composite patch analysis presented in this paper is to demonstrate the ability of the finite element alternating method in predicting the fatigue response of a cracked panel with partially bonded composite patch. For the present study, numerical analysis has been carried out to model the experiment performed by Denny¹ on partially bonded composite repairs. In his experiment, the patch (made of three plies of unidirectional boron/epoxy laminate) is bonded to a 2024-T3 aluminum panel with AF-163-2 film adhesive. The dimensions of the geometry for the composite patch and aluminum panel are given in Figure 1. The material properties of the boron/epoxy laminate, aluminum panel and adhesive layer are given in Table 1. In the current analysis, the patch and the panel are modeled with 8-noded isoparametric plane stress elements. The adhesive film is modeled with isoparametric 16-noded adhesive elements developed by Chu and Ko⁷. The adhesive element is based on a linear adhesive relationship between the shear stress and the difference of displacements between the patch and the panel:

$$\tau = K_{ADHE} (u_{patch} - u_{panel}) \quad (1)$$

where

$$K_{ADHE} = \left[\frac{t_{adhe}}{G_{adhe}} + \frac{3}{8} \left(\frac{t_{patch}}{G_{patch}} + \frac{t_{panel}}{G_{panel}} \right) \right]^{-1} \quad (2)$$

Here u is the displacement, t is the thickness and G is the shear modulus. In general, the shear modulus of an adhesive material is strongly nonlinear, but due to the lack of experimental data available, this nonlinear behavior can be approximated with an effective linear shear modulus. This effective modulus would be a function of the average shear strain on the adhesive layer.

The finite element mesh for the composite patch on the aluminum panel is shown in Figure 2. The mesh contains 4176 elements and 9337 nodes. To calculate the stress intensity factors of a cracked panel under a composite patch, two steps are involved. In the first step, the crack in the panel along with the composite patch and the adhesive layer are explicitly modeled in the finite element mesh. From the finite element solution, the shear stress on the adhesive layer is calculated using Eqn. 1. In the second step, the stress intensity factors of the cracked panel are solved using the finite element alternating method which uses the same finite element mesh except the crack is not modeled explicitly. The shear traction on the cracked panel (transferred through the adhesive layer) calculated in Step 1 is converted to nodal force to be applied in Step 2. Since this shear traction accounts for the "closing" force of the composite patch, only the cracked panel is required to be modeled in Step 2. Note that since finite element alternating method is used in Step 2, very fine mesh near the crack tip is not required.

The fatigue growth of a crack in general, can be calculated as a function of loading cycles. To take into account the effect of stress ratio, the Forman's crack growth equation (Forman, Kearney and Engler²⁰) is used. This equation is given as

$$\frac{da}{dN} = \frac{C (\Delta K)^n}{(1-R)K_c - \Delta K} \quad (3)$$

Here a is the crack length, N is the number loading cycles, ΔK is the range of the equivalent stress intensity factor, and R is the stress ratio in the cyclic loading. For 2024-T3 aluminum alloy, the values of $K_C = 91 \text{ MNm}^{-\frac{3}{2}} (83,000 \text{ psi}\sqrt{\text{in}})$, $C = 6.3 \times 10^{-21} \text{ Pa}^{-2} (3 \times 10^{-13} \text{ psi}^{-2})$ and $n = 3$ are used as given in Forman et al.²² In general, a fatigue calculation involves the calculation of the number of cycles for a crack to grow to a specified length. Using a simple linear integration scheme to solve for the Eqn. 3, the fatigue life cycle of the crack is subdivided into a number of interval steps based on the finite element mesh. The total number of cycles is obtained by summing the values from each step.

To account for the temperature effect during the curing process, two analyses are required for each interval step of the fatigue crack growth analysis; one for the load applied at σ_{\min} and the other is for the load applied at σ_{\max} . In the numerical model, it is assumed that the cure would fully solidify at 121°C and the specimen would undergo fatigue cycling between σ_{\min} at T_1 temperature and σ_{\max} at T_2 temperature. Due to the difference in the coefficient of thermal expansion, α_L , between the boron/epoxy patch and the aluminum panel, residual stresses would be induced on the repaired area when the temperature of the specimen differ from the cure temperature. And these residual stresses, which ^{are} dependent upon the temperature of the specimen, would be superimposed with the mechanical loading applied on the specimen. Hence, in this numerical model, both the mechanical loading as well as the loading induced by thermal cycling are accounted for in the fatigue crack growth analysis. It is to be noted here that even if the specimens were to undergo fatigue cycling at a constant temperature where $T_1 = T_2$ (which is the case

in the comparison analysis with the experiment performed by Denny¹), the drop in temperature after the curing process must be accounted for to properly model the fatigue crack growth of the specimens. Though ΔK is not effected by the temperature drop after the curing process (because the fatigue cycle is at a constant temperature), the ratio of stress intensity factor, $R = K_{\min}/K_{\max}$, would be affected by this temperature drop. Because of the boron/epoxy patch has a much smaller α_L than the aluminum panel, the patch contracts much less than the panel when the temperature drops. The residual stresses generated would cause the crack surface to open resulting a higher stress intensity factor and hence a higher stress ratio R . This higher stress ratio, R , would cause a faster crack growth in the Forman's crack growth equation (Eqn. 3).

Results

Comparison of Numerical Result with Experimental Data

This study involves the analyses of four different intentional disbond configurations as shown in Figure 3: (i) a completely bonded patch (CBP); (ii) crack tip disbonds (CTD) at both ends of the crack; (iii) a center disbond (CD) over the crack length; and (iv) a full width disbond (FWD) extending the full width of the patch and covering the crack. In some of the configurations listed above, disbond areas of 20%, 10%, and 5% of the total bond area of the patch were investigated. These specimens would undergo fatigue cycling at room temperature, 20 °C.

In the first configuration, there is no disbond on the patch repair. As has been determined from the Denny's experiment, the fatigue life of a perfectly patched specimen is about ten times longer than the unpatched specimen as shown in Figure 4. However, using the material data provided in Denny¹, it was found that the predicted fatigue life differs considerably from the experiment data for Specimen 20. In the numerical model of the completely bonded patch (CPB), the predicted fatigue crack growth is notably slower than the experimental result, approximately by a factor of five (shown in Figure 4 as linear model I). Since the material data for the boron/epoxy laminate and the aluminum panel are considered to be quite reliable, it would be easy to conclude that either the adhesive model or the material data for the adhesive film is not accurate. By simple trial and error, it was found that by reducing the shear stiffness, K_{ADHE} , of the adhesive layer, the predicted fatigue growth curve would correspond very well to the experimental result as shown in Figure 4 as linear model II. In this model, the adhesive stiffness, $K_{ADHE} = 0.2 \times 10^{12} \text{ Pa/m} (0.73 \times 10^6 \text{ psi/in})$, is an order of magnitude less than the adhesive stiffness calculated from the material data, $K_{ADHE} = 2.9 \times 10^{12} \text{ Pa/m} (10.6 \times 10^6 \text{ psi/in})$. The reason for the difference in the adhesive stiffness between these two models can be partly attributed to the fact that the shear modulus of a soft adhesive tends to be strongly nonlinear. In most cases, the shear modulus directly obtained from experiments is valid only for very small shear strain. However, the adhesive layer on the composite patch may undergo a much higher shear strain and hence has a much lower shear modulus as shown in Figure 5. Nonetheless, a simple linear approximation (to the slope of the nonlinear stress-strain level at the current

average operating stress level in the adhesive) seems to be sufficient in predicting the fatigue response of a bonded repair.

Unlike the Rose's model which is only valid when the crack is well within the size of the patch, the numerical model based on the finite element alternating method was able to predict the fatigue response when the crack grows within the size of the patch as well as when the crack grows outside of the patch. Figure 6 plots the stress intensity factor, ΔK , as a function of the crack length calculated (i) based on the finite element alternating method (FEAM) and (ii) based on the Rose's model. In this figure, both models are based on the same adhesive stiffness, K_{ADHE} (material model II). As shown in Figure 6, when the crack size is small relative to the patch, the difference between these two models is about 10%. However, as the crack grows longer, the difference between these two models increases substantially, especially when the crack tip grows beyond the boundary of the patch. The difference between these two models is magnified even greater on the fatigue curve plotted in Figure 7. It is to be noted here that one of the assumptions in Rose's model³ as is the characteristic load-transfer length, Λ , is not satisfied in this analysis. To obtain the asymptotic behavior of a crack under a composite patch, Rose had to assume that the load-transfer length has to be significantly smaller than the size of patch:

$$\Lambda = \left[\frac{G_{adhe}}{t_{adhe}} \left(\frac{E_{patch}t_{patch} + E_{panel}t_{panel}}{E_{patch}t_{patch}E_{panel}t_{panel}} \right) \right]^{1/2} \ll h_{patch} \quad (4)$$

where E is the elastic modulus and h_{patch} is the height of the composite patch.

As described in the earlier section, the curing process of the composite patch on the aluminum panel has been modeled. Due to the incompatibility of the coefficient of

thermal expansion between the boron/epoxy patch and the aluminum panel, residual stresses would be induced when the temperature is dropped after the curing process. Figure 8 shows the contour plot of the residual stress, σ_{22} , on the aluminum panel generated after the panel has been cooled from the cure temperature of 121 °C to the room temperature, 20 °C. The deformed shape in Figure 8 has been magnified by a factor of 100. Since the panel contracts much more than the composite patch, the crack surfaces would be opened by the residual stress generated and hence resulting high stress concentrations on the crack tips as shown in Figure 8.

Unlike the Rose's model where disbonds cannot be modeled, the FEAM is used to predict the fatigue response of partially bonded patches. Using the adhesive stiffness obtained from the perfect patched specimen, the fatigue response of a composite patch with crack tip disbonds (CTD) is analyzed. In this configuration, two specimens were tested; Specimen 6 and 7. In both specimens, the disbond area is 20% of the patch area. Figure 9 shows that the predicted fatigue curve correlates very well the experimental data from Specimen 6 and 7. Even though the disbond areas on both crack tips are quite large, both the analysis and the experiment show that the fatigue life of the specimens would be reduced by no more than 20%.

In the next analysis, the fatigue crack growth of specimens with a center disbond is evaluated. Specimen 16 has a disbond area of 10% and Specimen 17 has a disbond area of 5%. Figure 10 shows that the fatigue responses predicted with FEAM agree quite well with the experimental data from Specimen 16 and 17. The predicted number of cycles to failure for Specimens 16 and 17 are 99,411 and 114,707 respectively. These results correspond well with the experimental data where the number of cycles to failure

for Specimens 16 and 17 are found to be 92,624 and 116,817 respectively. Since the fatigue life of Specimen 16 (center disbond with disbond area of 10%) is less than the Specimen 6 or 7 (crack tip disbond with disbond area of 20%), it can be inferred that the effectiveness of the composite patch is more sensitive to the disbonds located at the center of the crack rather than the disbonds located at the crack tips.

Four full width disbond (FWD) specimens have been investigated by Denny; Specimens 4, 5, 11 and 14. These specimens have disbond areas of 20% (for Specimen 4 & 5), 10% (for Specimen 11), and 5% (for Specimen 14). The numerical analysis seems to provide good correlation with the experiment when the disbond area is small. However, for specimens with larger disbond area, the numerical solution seems to over predict the reduction in the fatigue life as shown in Figure 11. The predicted number of cycles to failure for Specimens 4, 5, 11 and 14 are 73,404, 73,404, 95,048 and 115,108 respectively. These results correspond with the experimental data where the number of cycles to failure for Specimens 4, 5, 11 and 14 are found to be 86,995, 82,324, 97,278 and 114,423 respectively.

To summarize the ability of finite element alternating method in predicting the fatigue response of partially bonded patch repair, the predicted results are displayed along with experimental data on a bar chart shown in Figure 12. The parameters that are varied in these specimens include the disbond shape, the disbond area, the initial crack length, the maximum applied stress, and the applied stress ratio. The details of each specimen are given in Table 2. Figure 12 shows that overall, FEAM can effectively predict the fatigue life of the aluminum panels with partial bonded composite patch. The overall error of prediction is found to be 7.5%.

Effect of Temperature Cycles

In general, an aircraft would undergo a thermal cycle during each single flight. As the aircraft climbs to the cruising altitude, the air temperature can drop to less than -50°C . However, when the aircraft is parked in a depot under a heated sun, the temperature can rise to 70°C . Since the boron/epoxy patch has a lower thermal expansion coefficient, the patch would contract much less than the aluminum panel when the air temperature drops. This induces a cyclic thermal tensile loading on the crack tip at a time when the mechanical stress is highest. In the current analysis, the sensitivity of the adhesive stiffness to the temperature is not considered, however as pointed out in the earlier section, the initial stresses due to the curing process (at 121°C) are accounted for in this numerical model. Figure 13 shows the fatigue response of a completely bonded patch (CBP) for Case I where the fatigue load is applied at room temperature, and Case II where the maximum load, σ_{\max} , is applied at -50°C and the minimum load, σ_{\min} , applied at 70°C . As shown in Figure 13, the fatigue life of the specimen undergoing the thermal cycles would be reduced by more than 60% when compared to the specimen loaded at room temperature. Furthermore, it was found that when crack tip disbond (CTD) is considered (where the disbond area is 20%), the fatigue life of the specimen undergoing the thermal cycles is further reduced by another 30% as shown in Figure 14. In contrast, the fatigue life of the CTD specimen loaded at room temperature is reduced by no more than 20% when compared with a perfect patched specimen. This model seems to indicate

that the specimen undergoing a typical thermal cycle would be more affected by partial disbond than the specimen loaded at constant temperature.

Interaction of Two Composite Patches

Given that cracks are sometimes found quite close to each other, it is important to study how two composite patches would interact with each other. In this paper, two types of patch interaction are considered. In both configurations, the two patches are considered to be perfectly patched. In the first configuration, both patches would lie on the same horizontal line as shown in Figure 15. When the patches are 100mm apart, there seems to be very little interactions between these two cracks. As shown in Figure 16, the fatigue response of the specimen with two patches is quite similar to the specimen with a single patch. When the distance between the two patches is reduced to 25mm, similar fatigue response is found in which there is very little interactions between these two cracks as shown in Figure 16.

In the second configuration, both patches would lie on the same vertical line as shown in Figure 17. When the patches are 100mm apart, there seems to be very little interactions between these two cracks as shown in Figure 18. However, when the distance between the two patches is reduced to 25mm, the fatigue crack growth is slowed by a factor of three as shown in Figure 18. Therefore, the specimen with two patches would have a longer fatigue life than the specimen with a single patch. However, it is possible that the metal in between the patches may fail in such situation; and this is not considered here.

Conclusion

Numerical analyses based on the finite element alternating method have been performed on several cracked panels with partially bonded composite patches. The numerical results are compared with the experimental data obtained by Denny¹ and the comparison indicates that the numerical results correlate quite well with the experimental data. Furthermore, a numerical study has been carried out to study the effect of high stress low temperature and low stress high temperature cycles. The result shows a very significant drop in the fatigue life when the specimen undergoes the thermal-fatigue cycle. This numerical result also shows that the specimen which undergoes the thermal-fatigue cycles is more sensitive to partial disbond than a specimen which undergoes the fatigue cycles at constant temperature. Furthermore, numerical study has been carried out to examine the interaction between two nearby patches. It has been found that the interactions between two nearby patches do not reduce the fatigue life of the specimen.

Acknowledgment

The technical assistance by Dr. Lehua Wang on finite element alternating method is greatly appreciated. This work was supported by AFOSR, with Dr. Jim Chang as the cognizant program official.

References

- ¹Denny, J. J., "Fatigue Response of Cracked Aluminum Panel with Partially Bonded Composite Patch," Master Thesis, 1995. Air force Institute of Technology.

- ²Jones, R., and Callinan, R. J., "Finite element analysis of patched cracks," *Journal Structural Mechanics*. Vol. 7, No. 2, 1979, pp.107-130.
- ³Rose, L. R. F., "A cracked plate repaired by bonded reinforcements," *International Journal of Fracture*, Vol. 18, No. 2, 1982, pp. 135-144.
- ⁴Rose, L. R. F., "Theoretical Analysis of Crack Patching," *Bonded Repair of Aircraft Structures*, pp. 77-105. A. A. Baker and R. Jones, editors. Dordrecht: Martinus Nijhoff Publishers, 1988.
- ⁵Fredell, R. S., "Damage Tolerant Repair Techniques for Pressurized Aircraft Fuselages," Ph.D. Dissertation, 1994. Faculty of Aerospace Engineering, Delft University of Technology.
- ⁶Mitchell, R. A., Wooley, R. M., and Chivirut, D. J., "Analysis of Composite Reinforced Cutouts and Cracks," *AIAA Journal*, Vol. 13, 1975, pp. 774-749.
- ⁷Chu, R. C., and Ko, T. C., "Isoparametric Shear Spring Element applied to Crack Patching and Instability," *Theoretical and Applied Fracture Mechanics*, Vol. 11, 1989, pp. 93-102.
- ⁸Tarn, J. Q., and Shek, K. L., "Analysis of Crack Plates with A Bonded Patch," *Engineering Fracture Mechanics* Vol. 40, 1991, pp. 1055-1065.
- ⁹Park, J. H., Ogiso, T., and Atluri S. N., "Analysis of Cracks in Aging Aircraft Structures, with and without Composite-Patch Repairs," *Computational Mechanics*, Vol. 10, 1992, pp. 169-201.
- ¹⁰Nagaswamy, V., Pipkins, D. S., and Atluri, S. N., "A FEAM-Based Methodology for Analyzing Composite Patch Repairs of Metallic Structures," *Computer Modeling and Simulation in Engineering*, Vol. 1, No. 2, 1996, pp. 263-288.

¹¹Roderick, G. L., "Prediction of Cyclic Growth of Cracks and Debonds on Aluminum Sheets Reinforced with Boron/Epoxy," *Fibrous Composite in Structural Design*, 1980, E. M. Lenoe, D. W. Oplinger, and J. J. Burke, editors, Plenum Press, New York, pp. 467-481.

¹²Baker, A. A., "Repair Efficiency in Fatigue Cracked Aluminum Components Reinforced with Boron/Epoxy Patches," *Fatigue and Fracture for Engineering Material and Structure*, Vol. 16, 1993, pp. 753-765.

¹³Nishioka, T., and Atluri, S. N. "Analytical Solution for Embedded Elliptical Cracks and Finite Element Alternating Method for Elliptical Surface Cracks, subjected to Arbitrary Loadings," *Engineering Fracture Mechanics*, Vol. 17, 1983, pp. 247-268.

¹⁴Atluri, S. N., and Nishioka, T., "Computational Methods for Three Dimensional Problems of Fracture," *Computational methods in the mechanics of fracture*, 1986, S. N. Atluri, editor, North Holland, pp. 230-287.

¹⁵Rajiyah, H., and Atluri, S. N., "Evaluation of K-factors and Weight Functions for 2-D Mixed-mode multiple cracks by the Boundary Element Alternating Method," *Engineering Fracture Mechanics*, Vol. 32, 1989, pp. 911-922.

¹⁶Park, J. H., and Atluri, S. N., "Fatigue Growth of Multiple-cracks near a Row of Fastener-holes in a Fuselage Lap-joint," *Computational Mechanics*, Vol. 13, 1993, pp. 189-203.

¹⁷Wang, L., and Atluri, S. N., "An implementation of the Schwartz-Neumann Alternating Method for Collinear Multiple Cracks with Mixed Type Boundary Conditions," *Computational Mechanics*, 1996 (in press).

¹⁸Muskhelishvili, N. I., "Some Basic Problems of the mathematical Theory of Elasticity," 1953, Noordhoo, Gronigen.

¹⁹Park, J. H., "Improvement of the Accuracy of Stress Fields in Multiple Hole Crack Problems," Internal report for Computational Modeling Center, Georgia Institute of Technology, 1993.

²⁰Forman, R. G., Kearney, V. E., and Eagle, R. M., "Numerical analysis for crack propagation in cyclic-loaded structures," *Journal of Basic Engineering* Vol. 89, 1967, pp. 459-464.

Table 1 Material properties for the aluminum panel, boron/epoxy patch, and adhesive layer.

Material	$E_L / E_T / G$ (GPa)	Poisson Ratio	CTE, α_L ($10^{-6} / ^\circ C$)	Thickness (mm)
2024-T3	72.4/72.4/27.2	0.33	22.7	1
Boron/Epoxy	210/25/72.4	0.168	4.5	0.127
AF-163-2	NA/NA/0.405	-	-	0.127

Table 2 Details of the specimens modeled.

Specimen	Configuration	Disbond Area (%)	Peak Load (MPa)	$R = \sigma_{\min} / \sigma_{\max}$
3	CBP	0	120	0.15
4	FWD	20	120	0.10
5	FWD	20	120	0.10
6	CTD	20	120	0.10
7	CTD	20	120	0.10
10	CBP	0	120	0.10
11	FWD	10	120	0.10
13	FWD	20	100	0.10
14	FWD	5	120	0.10
16	CD	10	120	0.10
17	CD	5	120	0.10
20	CBP	0	120	0.10
21	CBP	0	120	0.10
23*	CBP	0	120	0.10
24*	CBP	0	100	0.10

* Initial crack length = 12.7 mm instead of 25.4 mm in other specimens.

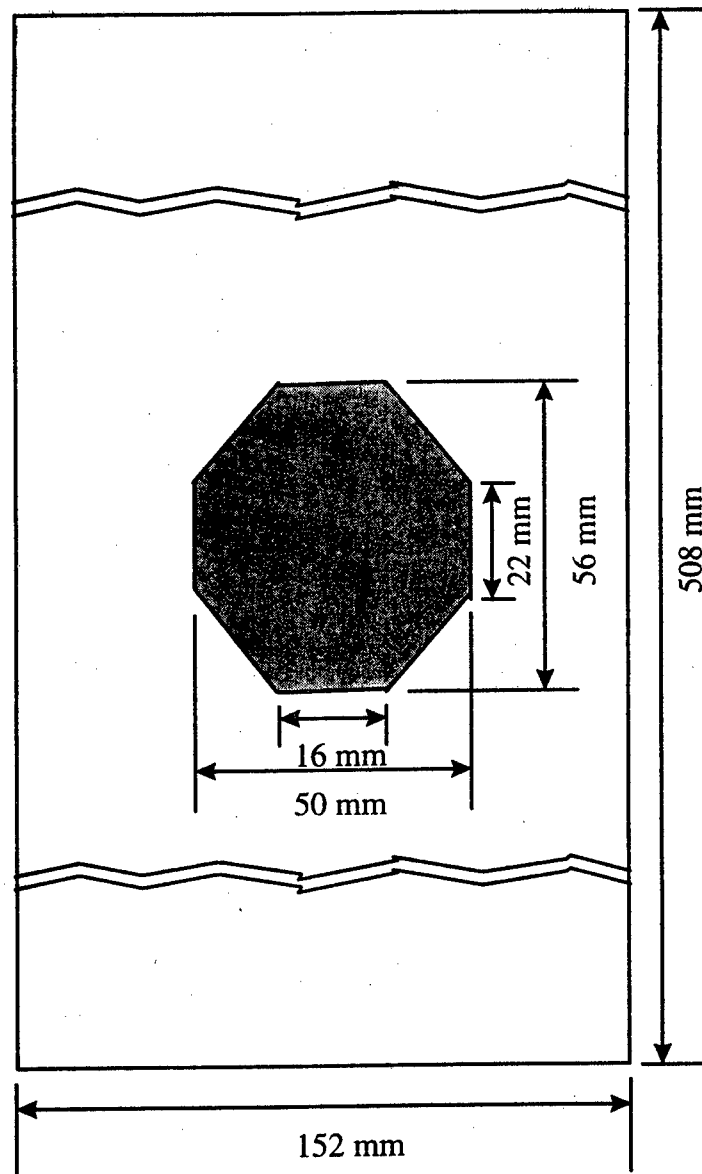


Figure 1 Geometry of the aluminum patch with the boron/epoxy patch.

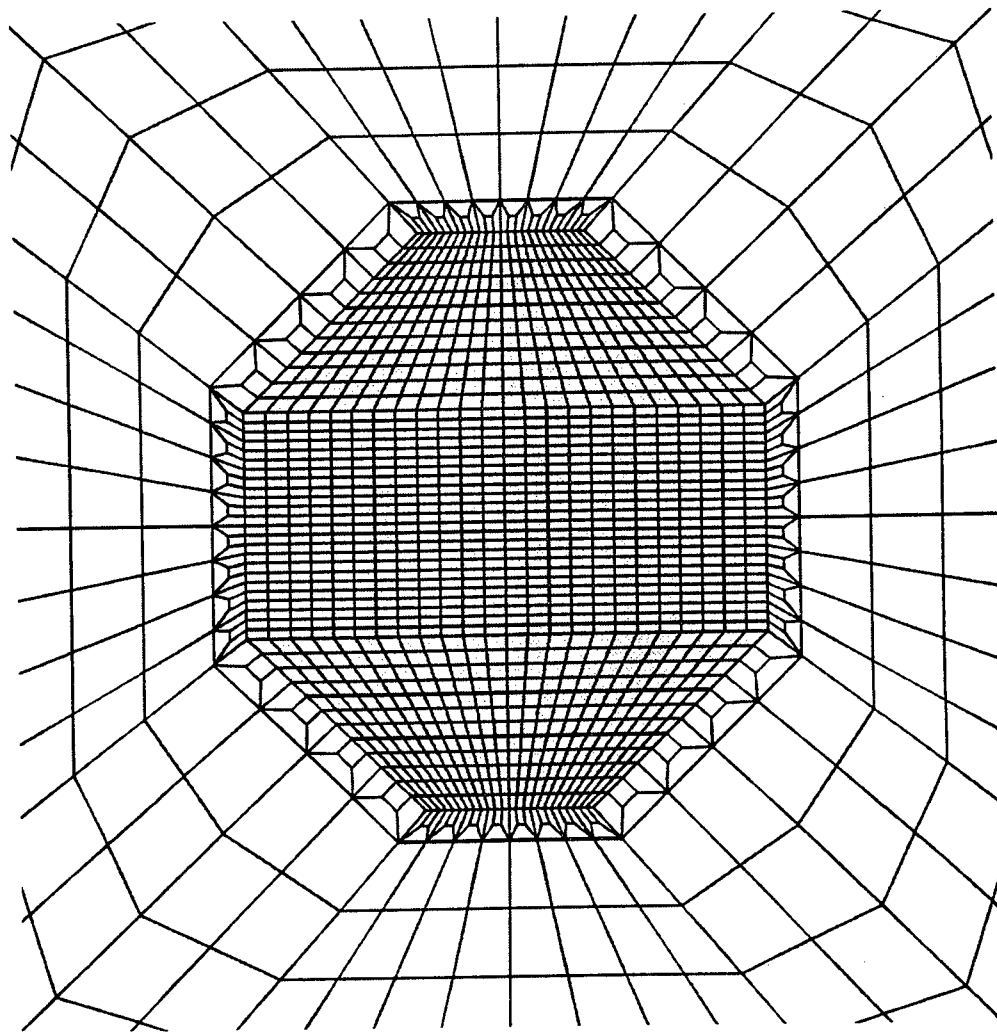
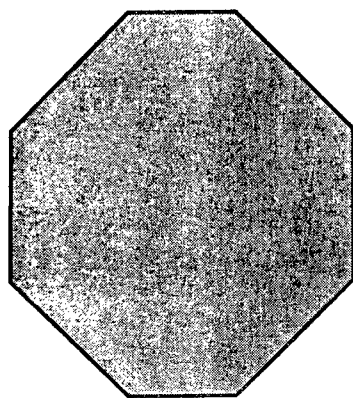
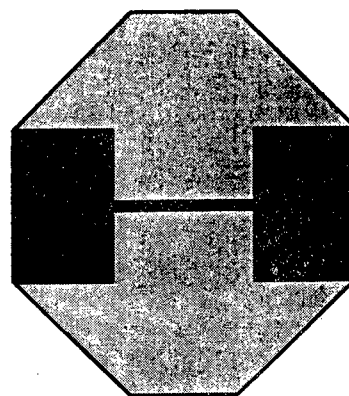


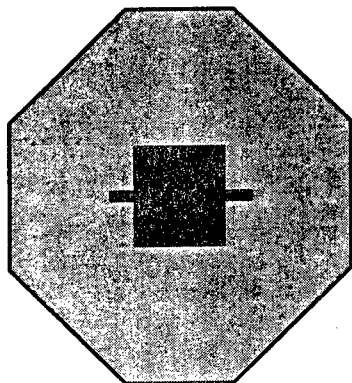
Figure 2 The finite element mesh of the composite patch on the aluminum panel.



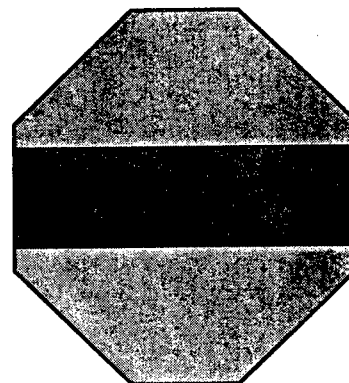
(i)



(ii)



(iii)



(iv)

Figure 3 Disbond configuration types (i) a completely bonded patch (CBP); (ii) crack tip disbonds (CTD); (iii) a center disbond (CD); and (iv) a full width disbond (FWD).

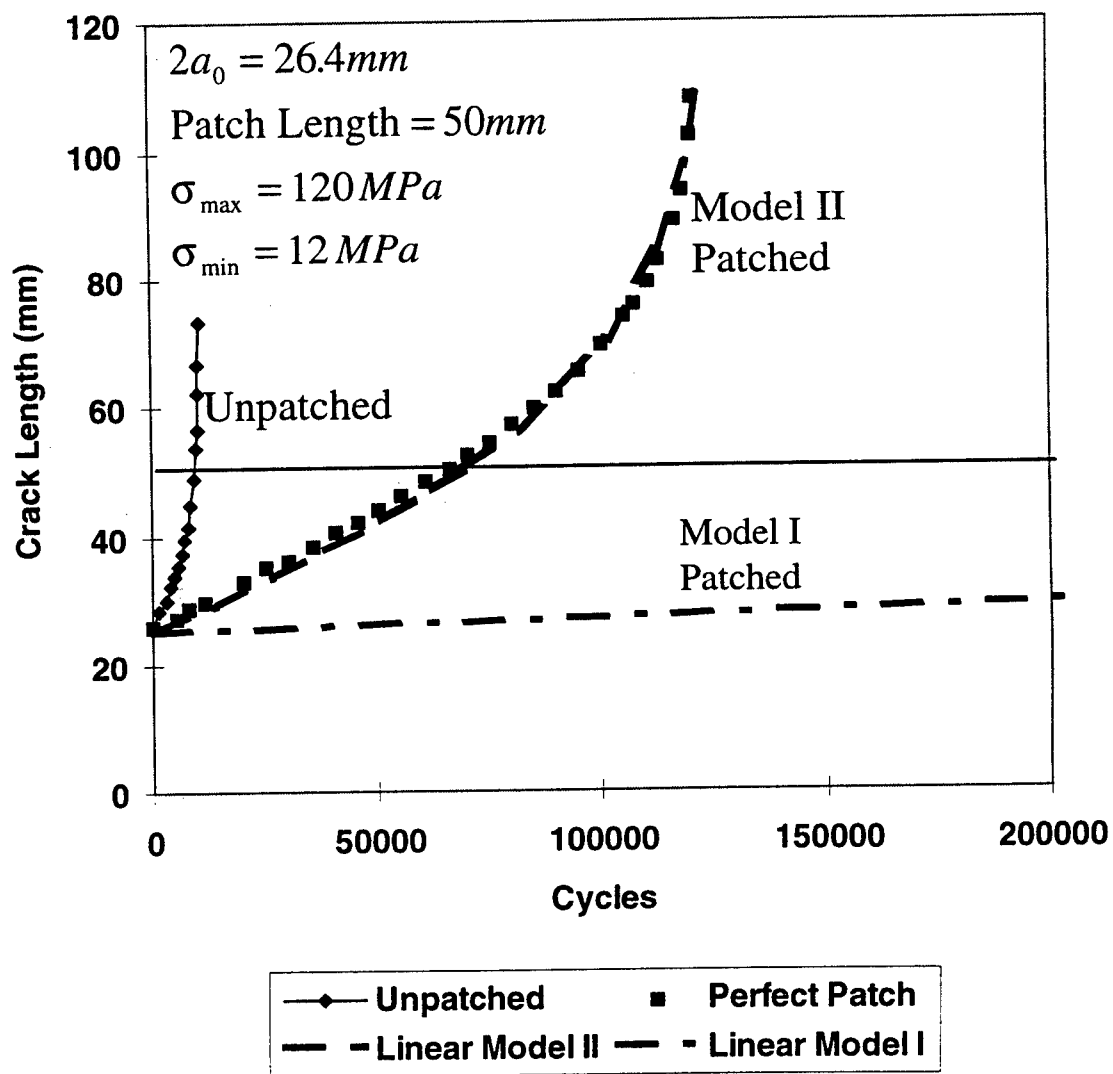


Figure 4 Comparison of results from numerical model I and II with the experimental data for completely bonded patch (CPB).

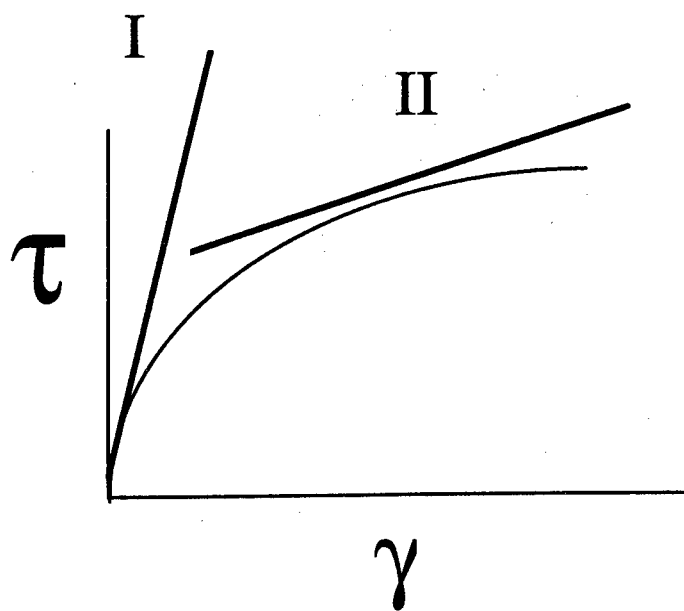


Figure 5 The nonlinear material behavior of adhesive layer where the shear modulus is strongly dependent on the shear strain.

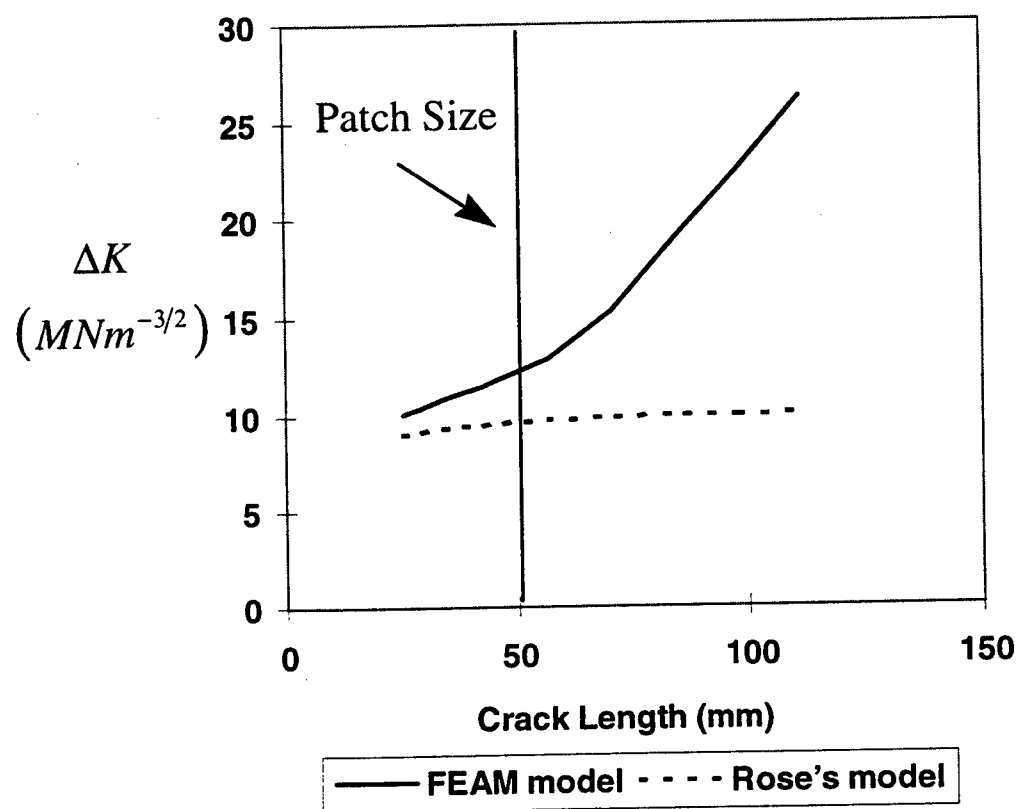
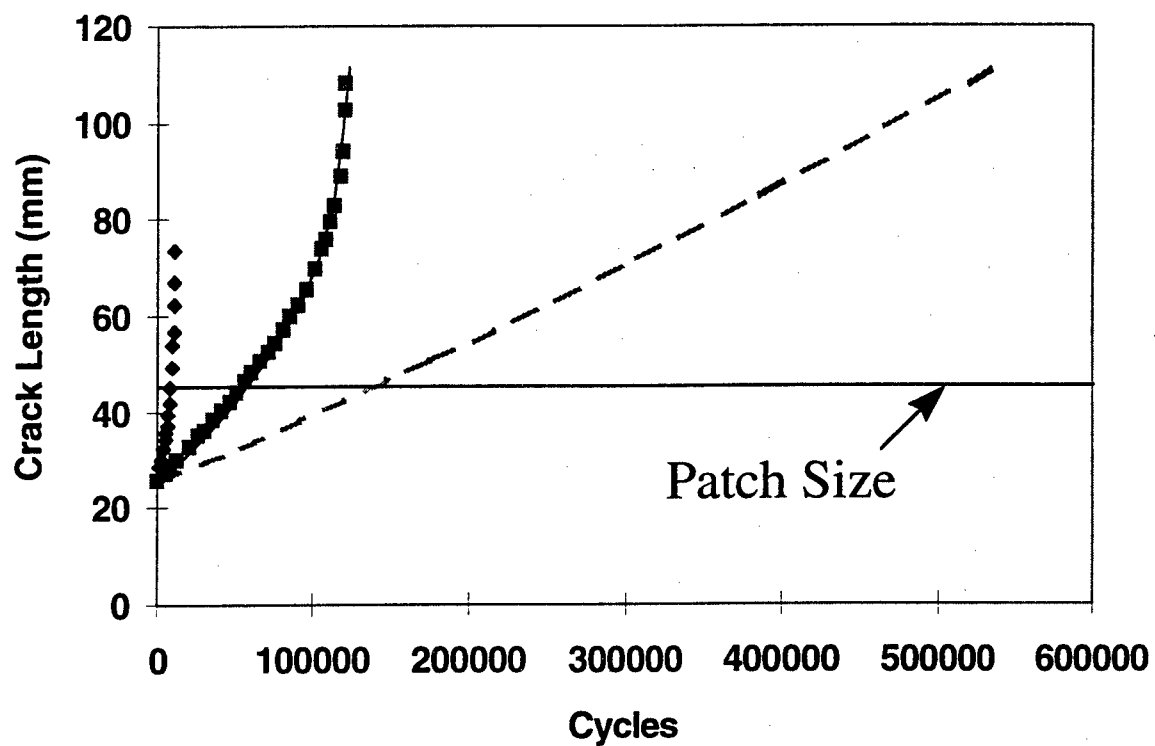


Figure 6 The stress intensity factor as a function of crack length for FEAM and Rose's models.



◆ Unpatched ■ Perfect Patch — FEAM Model - - Rose's Model

Figure 7 Fatigue response based on FEAM and Rose's models.

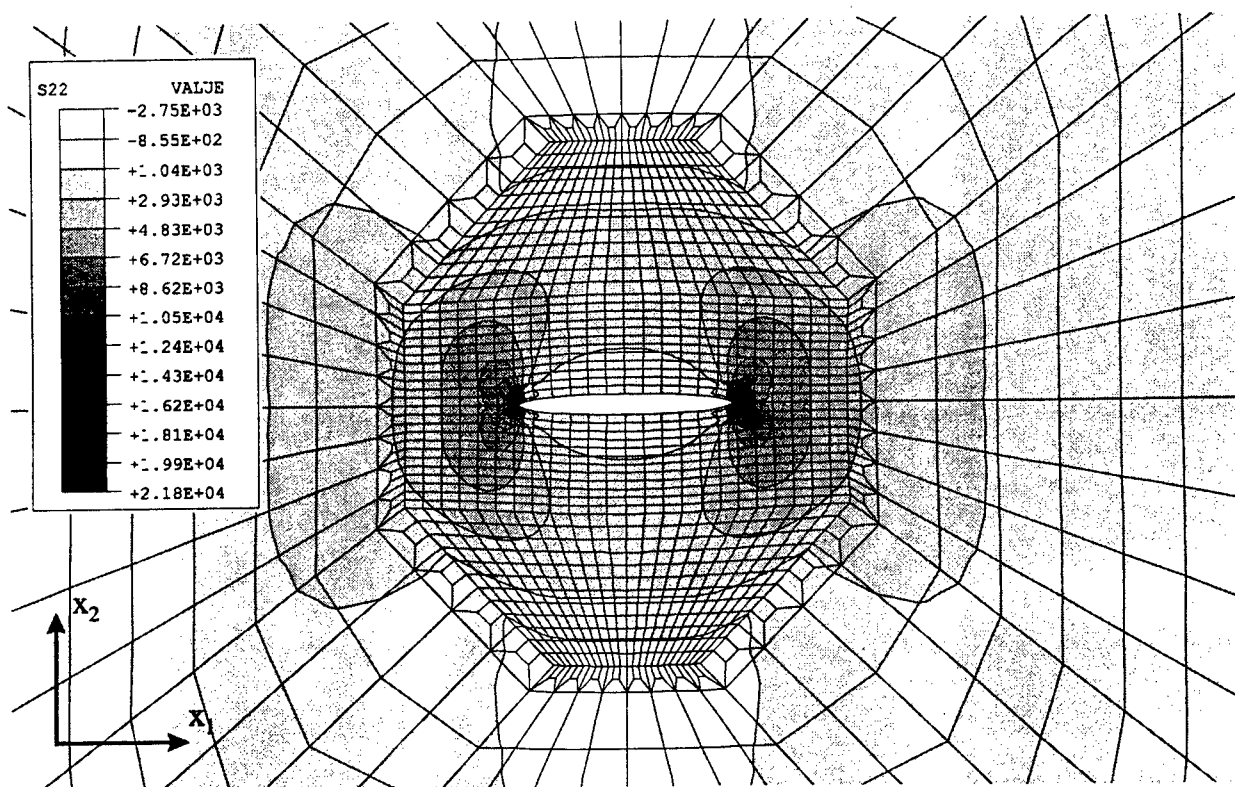


Figure 8 Contour plot of the residual stress, σ_{22} , due to the curing process.

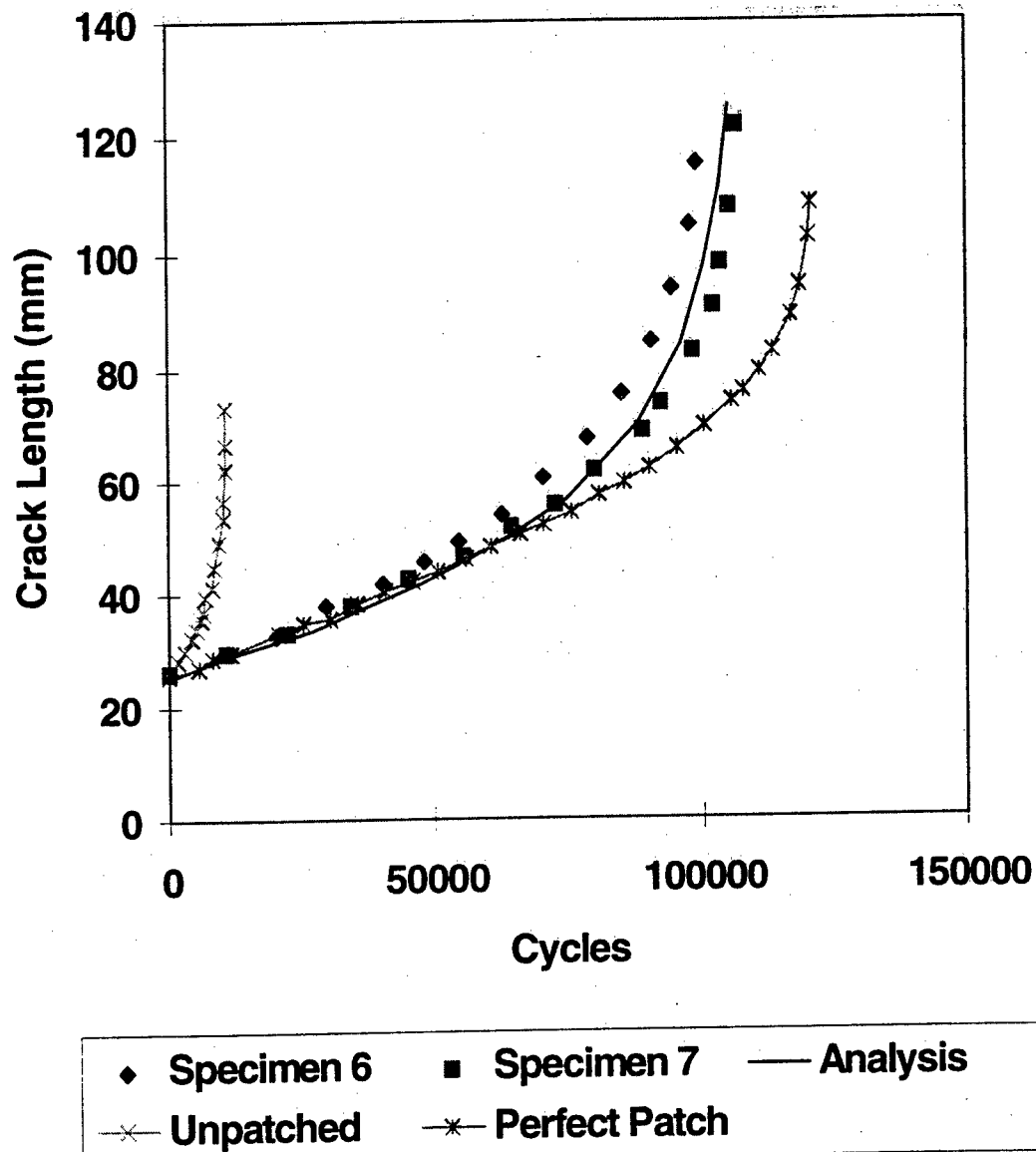


Figure 9 Comparison of numerical result with experimental data for Crack Tip Disbond (CTD)

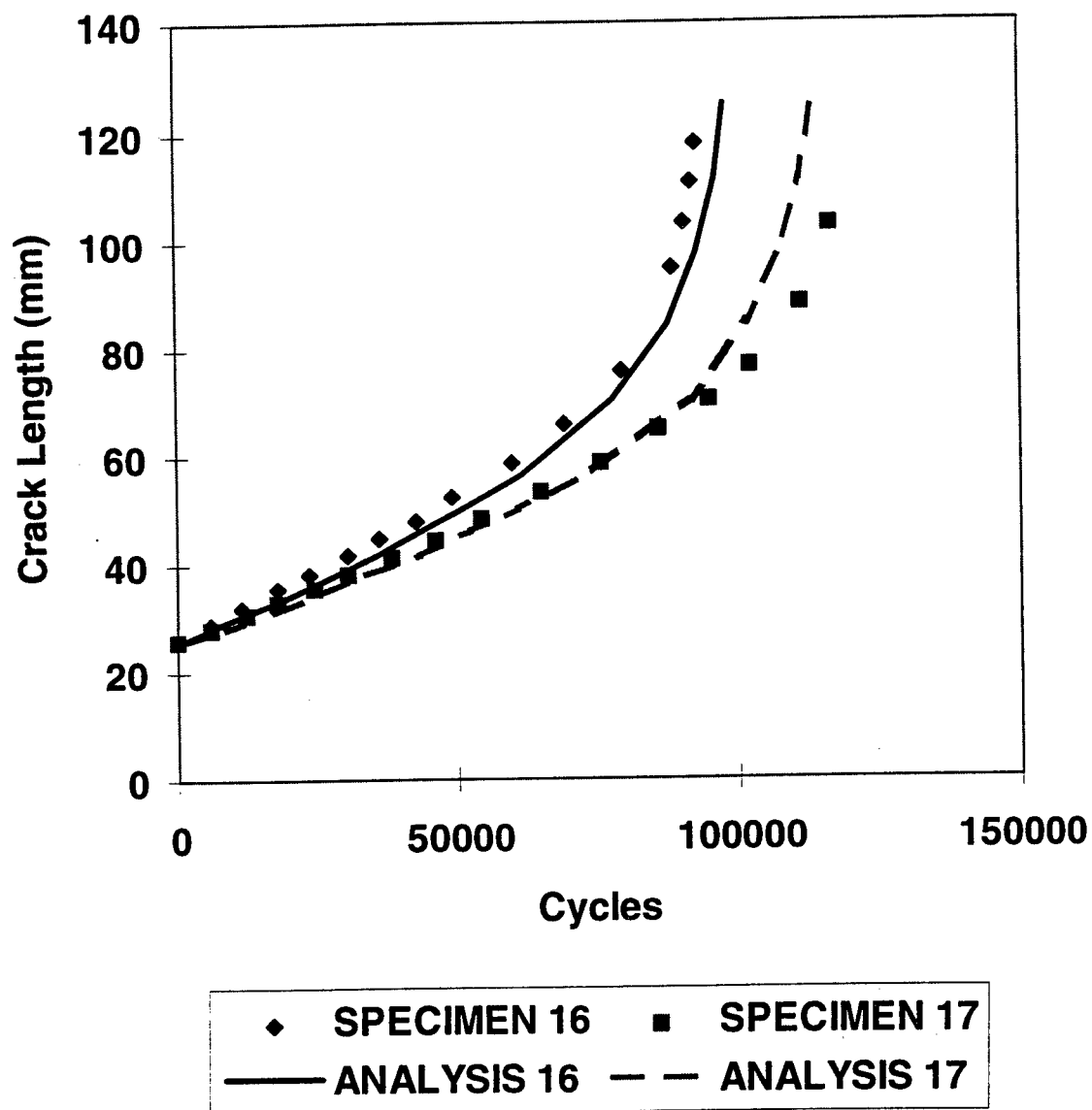


Figure 10 Comparison of numerical result with experimental data for Crack Disbond (CD).

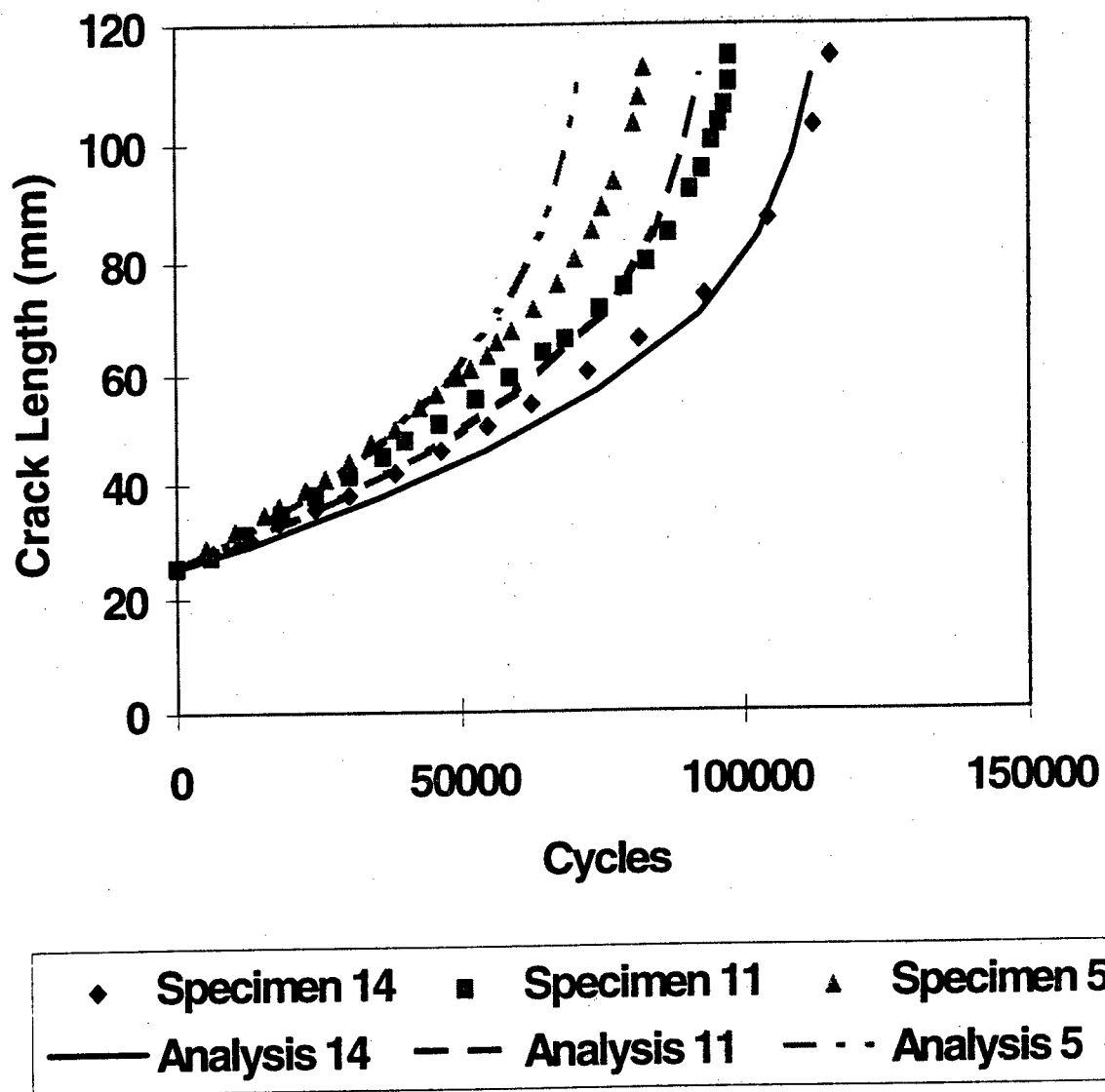


Figure 11 Comparison of numerical result with experimental data for full width disbond (FWD).

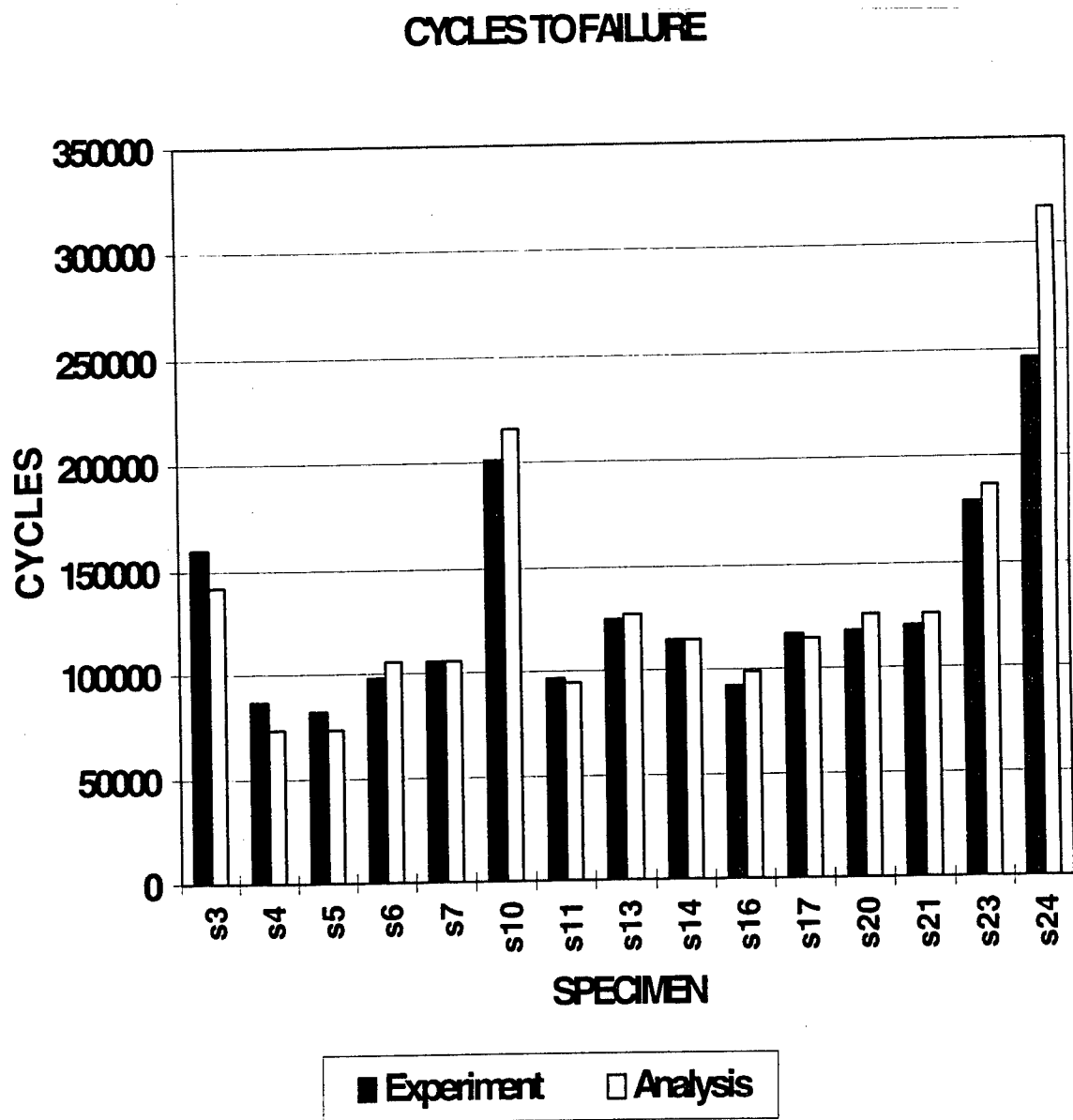


Figure 12 The predicted fatigue lifes against the experimental data.

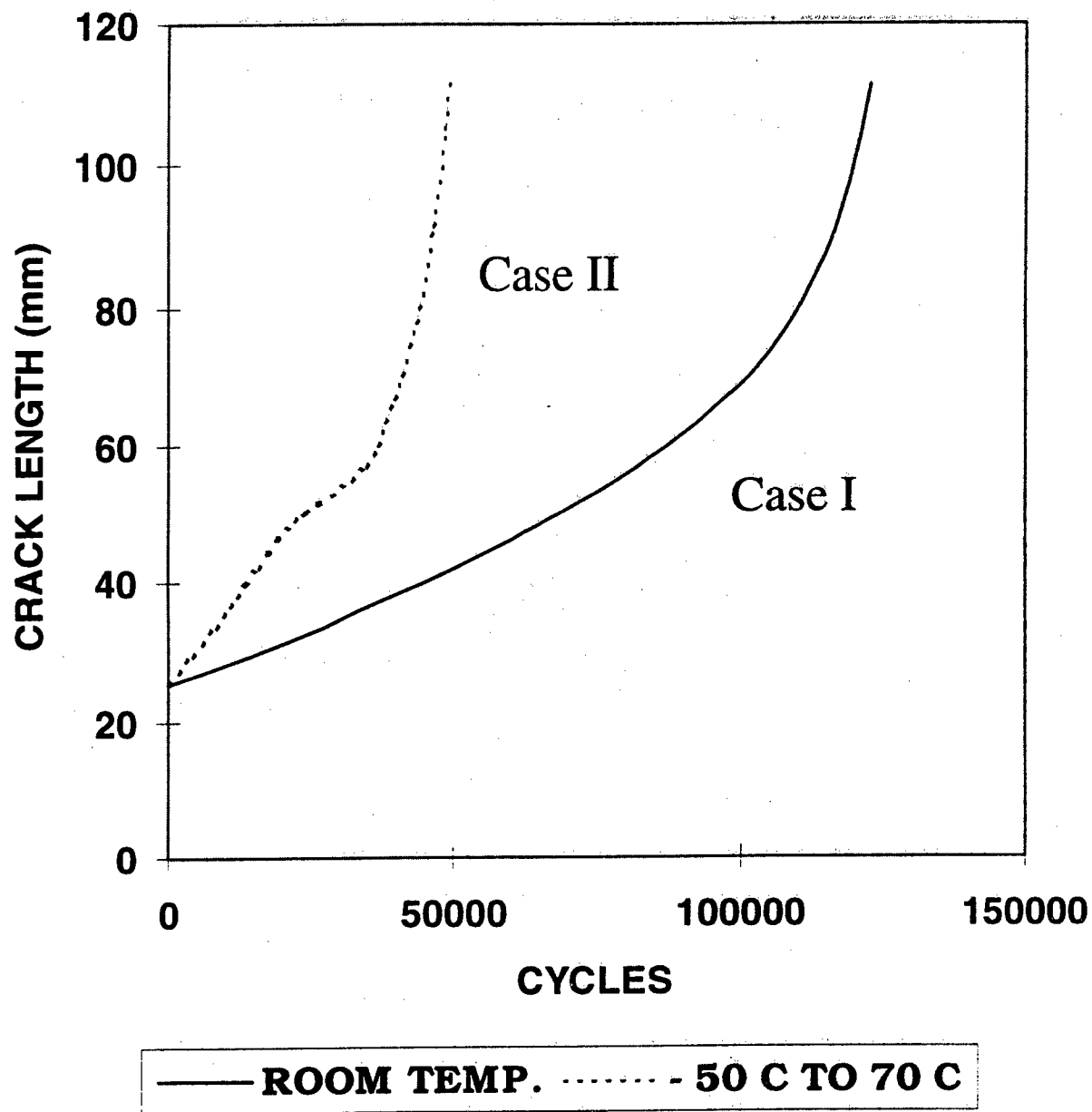


Figure 13 The fatigue response of a completely bonded patch (CBP) for Case I where the fatigue load is applied at room temperature, and Case II where the maximum load, σ_{max} , is applied at -50 C and the minimum load, σ_{min} , applied at 70 C.

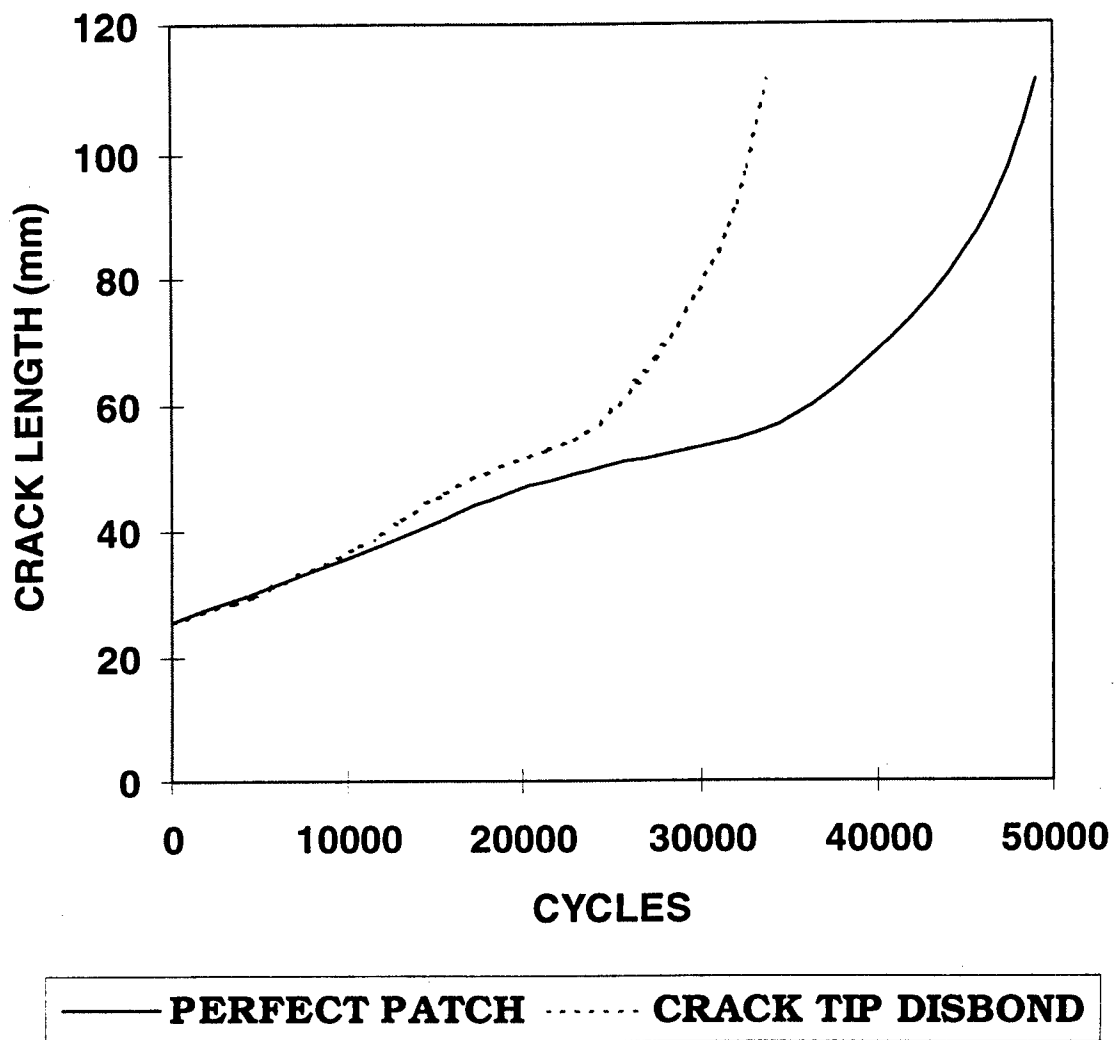


Figure 14 The fatigue life of the specimen undergoing the thermal cycles with Crack Tip Disbond (CTD).

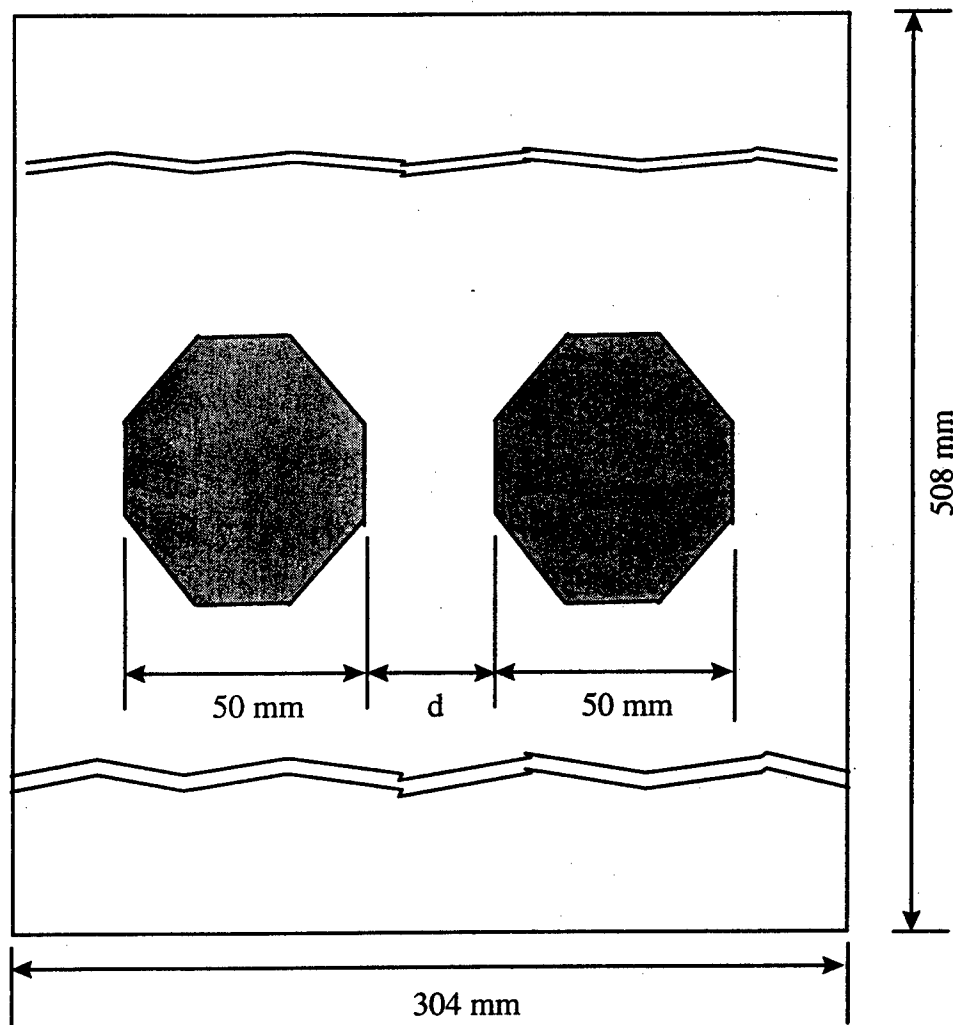


Figure 15 Geometry of the aluminum patch with two patches lying horizontally.

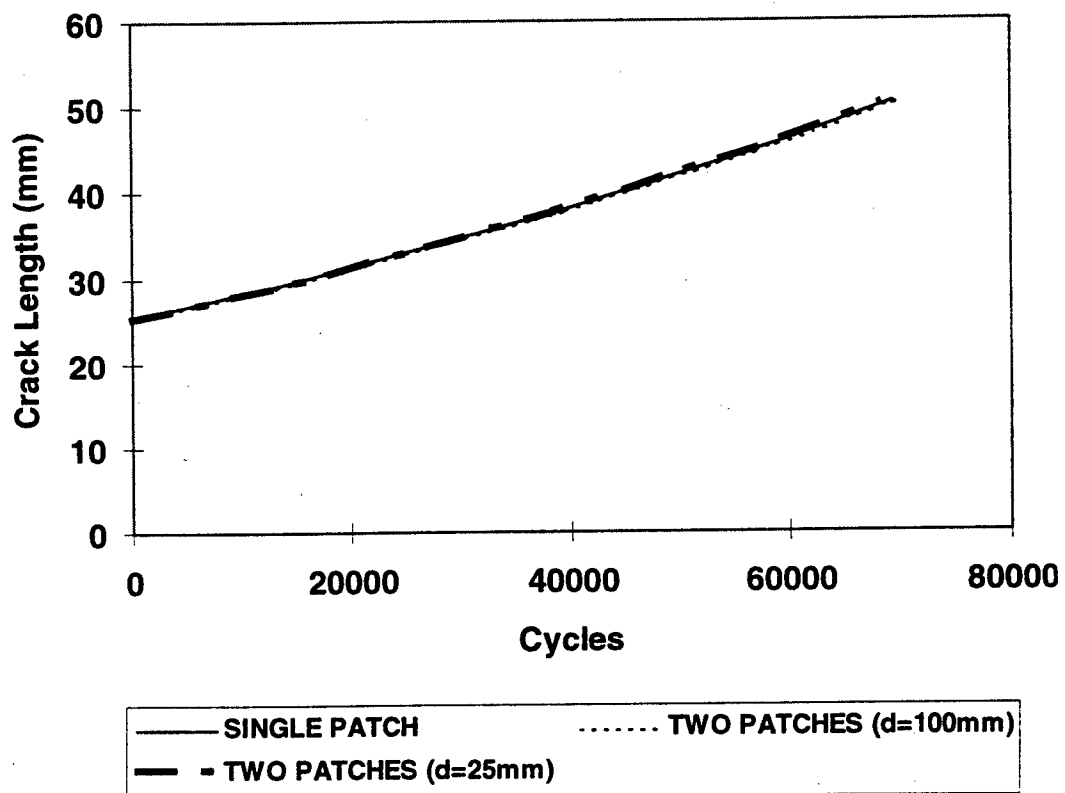


Figure 16 Interaction of two patches lying on a horizontal line.

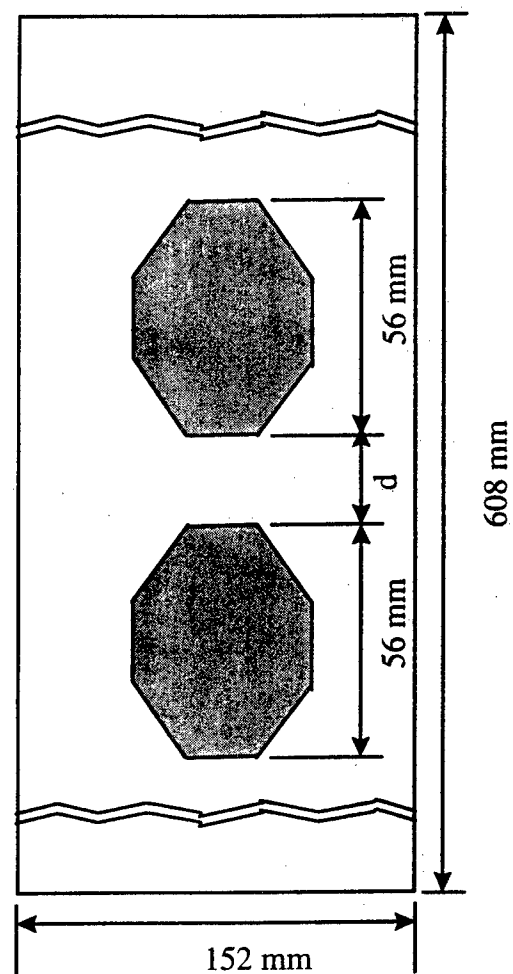


Figure 17 Geometry of the aluminum patch with two patches lying vertically.

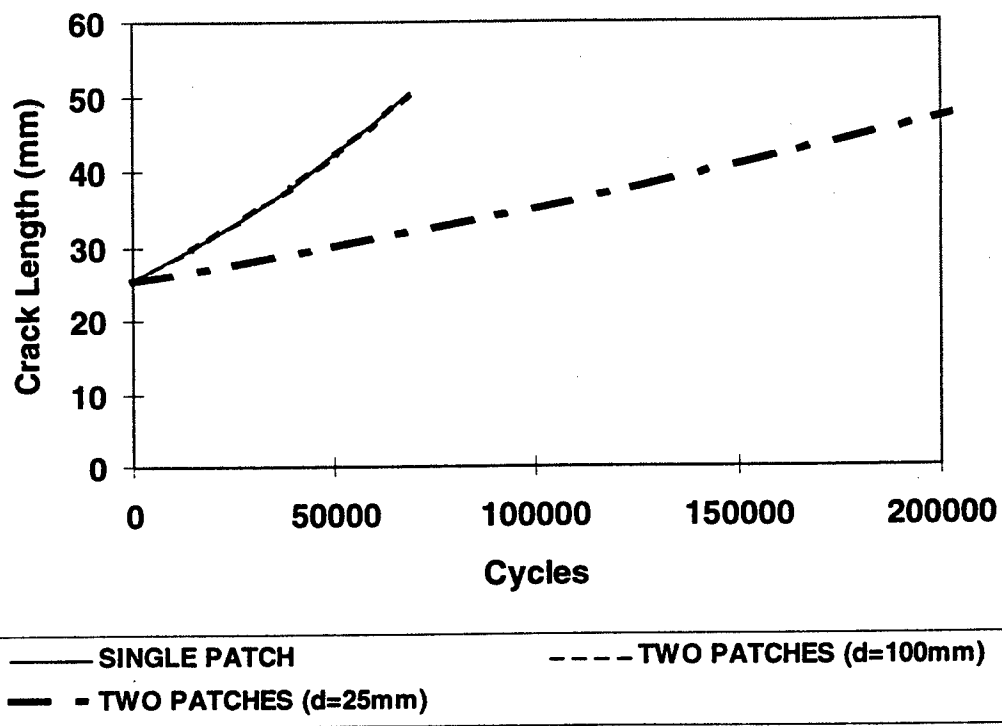


Figure 18 Interaction of two patches lying on a vertical line.

REPAIR SUBSTANTIATION FATIGUE TESTING INCLUDING TEMPERATURE AND FREQUENCY EFFECTS FOR A BONDED COMPOSITE REPAIR TO AN F-111 LOWER WING SKIN

by

K. Walker * and R. Boykett
(Senior Professional Officers)

DSTO, AERONAUTICAL AND MARITIME RESEARCH LABORATORY
Airframes and Engines Division
506 Lorimer St, Fishermens Bend, Victoria, Australia, 3207.
Ph: (61 3) 9626 7961 Fax: (61 3) 9626 7089

1. INTRODUCTION

The discovery of a 48 mm (tip to tip) chordwise, through thickness fatigue crack in the lower wing skin of an RAAF F-111C aircraft led to the development of a bonded composite repair. Fracture mechanics calculations predicted that the crack had degraded the residual strength to 150 MPa (21.7 ksi) which is considerably less than the Design Limit Stress of 256 MPa (37.1 ksi) which has been established for this area (Reference 1). The repair was therefore critical to flight safety and a comprehensive program of testing representative specimens was required to substantiate the repair. The testing program included both static and fatigue tests, and the effects of temperature and frequency of loading were investigated. This paper concentrates on the effect of temperature and loading frequency on the repair performance. These effects were found to be small, and certainly much less significant than that which is predicted by the conservative, simplified approach detailed in the RAAF Engineering Standard C5033 (Reference 2). The results indicate that the concern over thermal residual stress and thermal mis-match effects which arise from the C5033 analysis approach and which have been expressed elsewhere (eg Reference 3) are actually less of a problem than previously thought. That is not to say that the C5033 approach is invalid, but it is conservative and there may be scope to refine the analysis to remove unnecessary conservatism.

2. CRACK LOCATION AND RESIDUAL STRENGTH ESTIMATE

Figure 1 indicates the location of cracking on the lower wing-skin. The shaded areas indicate raised portions which serve as integral stiffeners and as attachment lands for the spars, McHenry et al. (Reference 4). The cracking occurred in an area lying below the forward auxiliary spar, at the spar station FASS 281.28, where the thickness of the integral stiffener is reduced from approximately 8 mm to the nominal skin thickness (at this location) of 3.7 mm (with the minimum acceptable thickness being 3.6 mm). The purpose of this depression in the stiffener is to allow full fuel flow and drainage between adjacent bays of the wing-box fuel tank. Two side-stiffeners are used to compensate for the loss of spanwise stiffness due to this fuel-flow passage, as indicated either side of the crack in Figure 1. The thickness variation in this region is more clearly illustrated in Figure 2. These geometrical features lead to a significant stress concentration factor and to out-of-plane secondary bending at the location of cracking, as discussed in Reference 5.

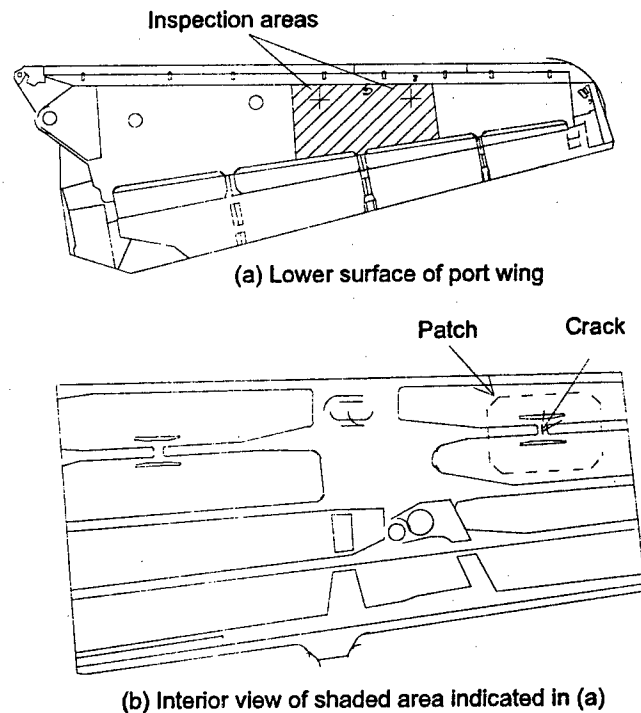


Figure 1 Location of cracking on the F-111 lower wing-skin, at FASS 281, showing also the outline of the repair patch.

The cracking occurs in the chordwise direction, normal to the direction of the nominal principal stress at that location. The presence of secondary bending results in faster crack growth along the wing-skin's inner surface relative to its outer surface. This discrepancy between the surface traces is further accentuated by the residual compressive stress at the outer surface caused by shot peening which is done at manufacture. For the purposes of assessing the residual strength, however, it is convenient to assume a straight-fronted through-crack, as indicated by the shaded area in Figure 2. This leads to the residual strength estimate of 150 MPa cited earlier. This estimate is conservative in at least two respects. First, the effective toughness for the skin material (2024-T851 aluminium alloy, 3.6 - 3.8 mm thick, LT orientation) has been found experimentally (Reference 6) to be in the range $57 - 62 \text{ MPa } \sqrt{\text{m}}$, which is significantly higher than the handbook value assumed earlier. Secondly, the beneficial effect of the spar bridging the crack has been ignored in deriving this estimate.

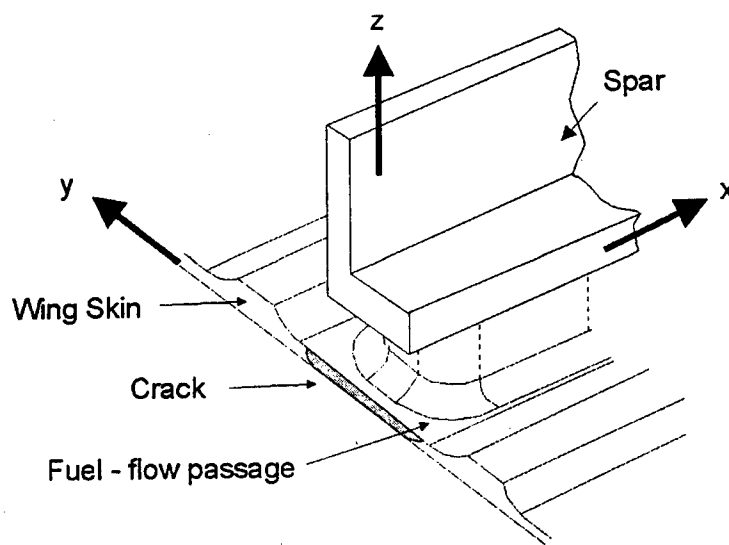


Figure 2: Local cross section geometry of the wing skin in the vicinity of the fuel-flow passage, showing the location of cracking.

3. REPAIR DESIGN

The repair consists of an externally applied 14 layer boron epoxy patch ($[0_3, \pm 45, 0_2]_s$) bonded with FM73 structural film adhesive. The patch is approximately 470 mm long and 320 mm wide. The ends and sides are tapered and the corners are chamfered in order to reduce the peel and shear stresses in the adhesive. Further details of the repair design and application procedures are given in Reference 7.

4. TEMPERATURE AND FREQUENCY EFFECTS

The influence of temperature on crack propagation behaviour after repair with a bonded composite patch is extremely complex. Factors include the following:

- a. The effective stress ratio, R , is increased due to the thermal residual stress. This will be tension in the aluminium and compression in the boron in the current F-111 example.
- b. The patching efficiency changes because the properties of the adhesive vary considerably with temperature. With an increase in temperature, the shear modulus, G , and the yield strength, τ_p , of the adhesive are reduced and thus the patching efficiency is also reduced.
- c. The crack propagation properties of the alloy itself may change with temperature.

Loading frequency is also a potential influencing factor because the time spent at high load is increased with a decrease in frequency and this is the point where the adhesive is loaded into the plastic region. Creep effects may occur, and the potential for this is higher at elevated temperature where the modulus and yield point for the adhesive are reduced. There is therefore a high potential for frequency to be a significant factor in crack patching performance.

5. SPECIMEN TESTING RESULTS

As detailed in References 8 and 9, three levels of structural testing were undertaken to substantiate the F-111 repair. The majority of the testing was performed on "panel" specimens and this paper concentrates on the panel specimen results. These specimens (working area approx. 300 mm x 190 mm) are intended to simulate the wing skin including the geometrical features shown earlier in Figure 2, *i.e.* an integral stiffener, machined out to provide a fuel-flow passage, with side stiffeners to restore the overall spanwise stiffness. The panels are wide enough that crack growth beyond the side stiffeners would not be significantly affected by edge effects, should crack growth occur after the application of patches to the (pre-cracked) specimens. Consistent with this width requirement, the panel specimens are also intended to be small enough to fit within a purpose-built environmental chamber providing a controlled temperature level. A sketch of the panel specimen is shown in Figure 3.

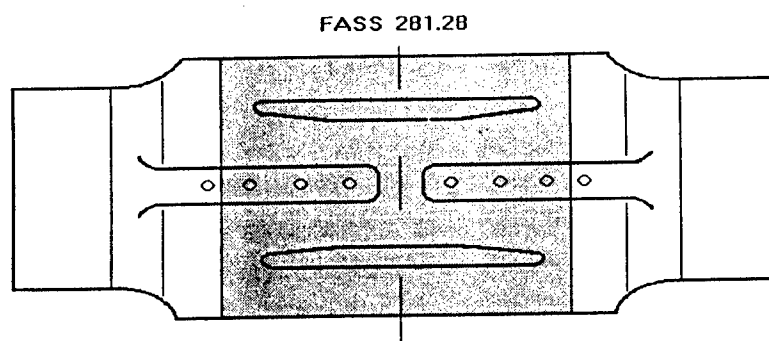


Figure 3: Panel specimen. View onto side representing upper surface of lower wing skin. Boron patch region is shown shaded.

The introduction of the crack defect into the specimens was achieved by creating an elliptical, part through notch in centre of the side representing the inner surface of the lower wing skin using Electro Discharge Machining (EDM). The specimen was then loaded under constant amplitude cyclic tension until a crack appeared at each end of the notch and grew to the required length.

Patching was done (after pre-cracking) to the specimen side representing the outer surface of the lower wing skin after it was carefully cleaned, grit blasted and treated with an adhesion promoter to ensure a good bond surface. Repair patches were made from Boron/Epoxy pre-preg fibre composite 5521-4. The patch designed for the panel specimen is not as long (reduced overlap) or wide (no taper) and is therefore a conservative version of that carried out for the actual repair on the aircraft. The pre-cured patch is bonded using FM-73 adhesive cured at 80° Celsius for 8 hours. Finally, Non Destructive Inspection (NDI) of the patched area was performed to confirm patch and bond integrity.

5.1 Static Strength

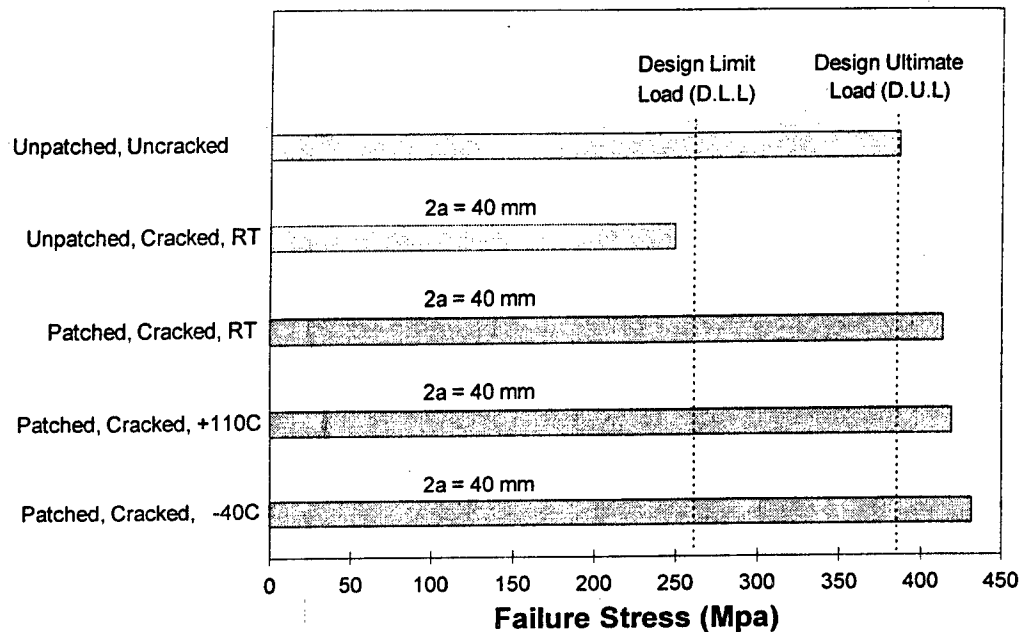


Figure 4: Results of static residual strength tests on panel specimens
(RT : Room Temperature)

Figure 4 summarises the static strength results on the panel specimens. The residual strength (stress in MPa) is calculated as the failure load divided by the nominal cross sectional area (829 mm^2 , ignoring the patch and crack). Notable points are as follows:

- The residual strength in the presence of a 40 mm crack is degraded to below the Design Limit Load, confirming the fracture mechanics prediction mentioned earlier.
- The repaired panels all exceed DUL, with little effect noted between the different temperatures. The temperature gradient was such that the temperature on the specimen during the hot test ($+110^\circ\text{C}$) ranged from 83.0°C to 119.4°C , and during the cold test (-40°C) from -16.3°C to -42.2°C . The maximum values were at the centre of the specimen due to heat transfer from the ends of the specimen into the grips of the testing machine. However, the hot test was repeated at a later date (August 1996) using a new environmental chamber. The specimen (FLTP-17) had already been used for fatigue loading (50,000 simulated flight hours) and the crack had grown to 69.4 mm. The

temperature range on the specimen was 105°C to 112°C, within the boundary of the boron patch, when it failed by the crack propagating to the edges at a load of 204.7 kN (247 MPa). Given that the Design Ultimate Stress for the high temperature load case is 214.5 MPa (Reference 8), the second high temperature test specimen also demonstrated that the repair restores sufficient static strength to survive the DUL applicable to the higher temperature design case. This is considered to be a remarkable achievement for FM73 adhesive because 110 °C is well in excess of the glass transition temperature T_G for the adhesive.

5.2 Fatigue Performance

Initial fatigue testing was performed on cracked, patched panel specimens tested at ambient conditions under a representative cycle by cycle spectrum at a frequencies of 3 and 5 Hz. Full details are given in References 8 and 9. The tests revealed an approximately constant crack growth rate of 0.7 mm per 1000 hours. Later testing investigated the effects of loading frequency and testing at a sustained, elevated temperature. Two frequencies were investigated (5 Hz and 0.5 Hz) and two temperatures (ambient and 80 °C). Crack growth results are shown in Figure 5 (ambient) and Figure 6 (80 °C). The specimens involved are numbered FLTP69-3 and FLTP 69-4. One load block represents 500 flying hours. The crack length and growth rates are always based on the total tip to tip length. The results of linear regression estimates of the growth rates from Figures 5 and 6 are summarised in Table 1.

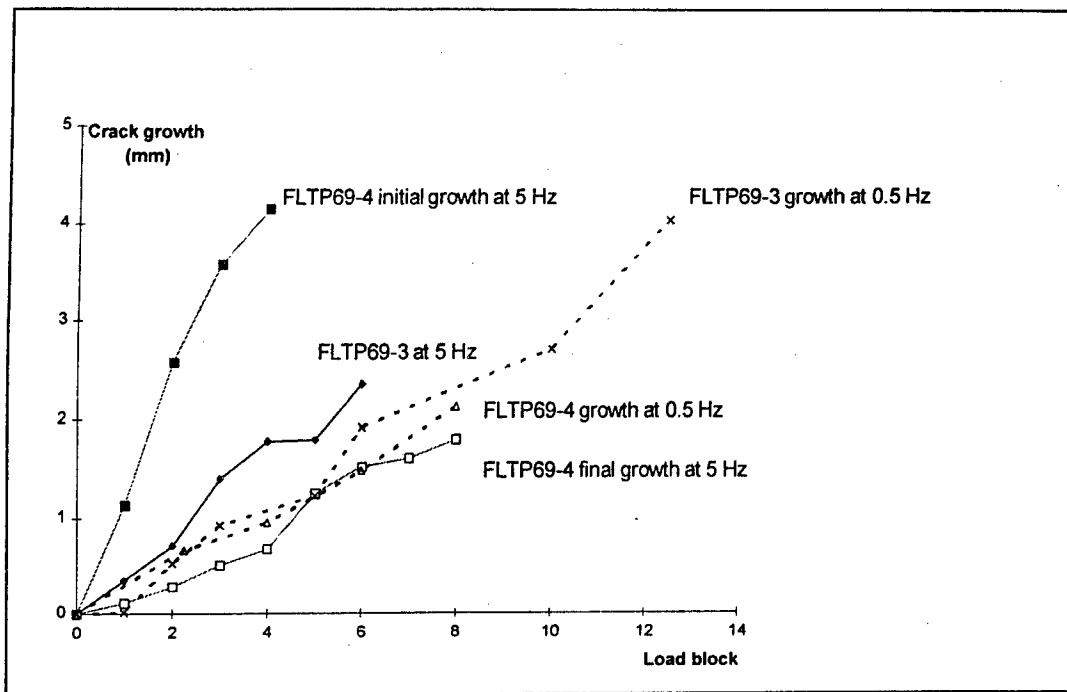


Figure 5: Panel Specimen crack growth comparisons at ambient temperature (end point is not necessarily the failure point)

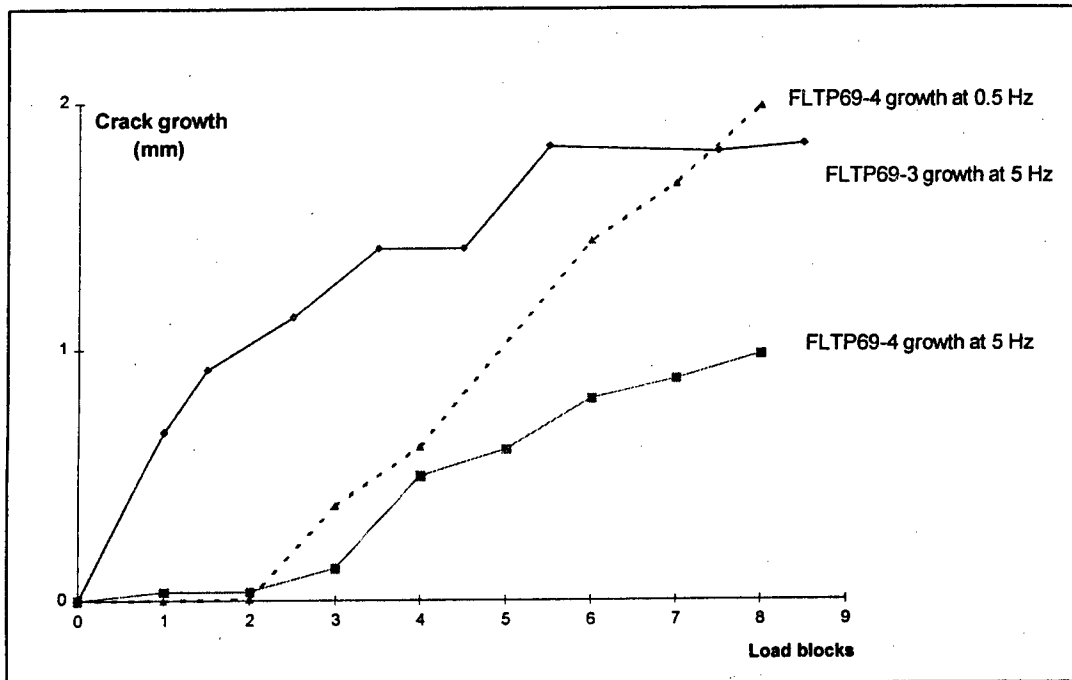


Figure 6: Panel specimen crack growth comparisons at 80 °C temperature (end point is not necessarily the failure point)

Specimen No	Temperature °C	Frequency Hz	Crack Growth Rate (mm per block)	Crack Growth Rate (mm per 1000 hrs)
FLTP69-3	Ambient	5	0.39	0.78
	Ambient	0.5	0.31	0.62
	80	5	0.19	0.38
FLTP69-4	Ambient	5	1.08	2.16
	Ambient	0.5	0.26	0.52
	80	5	0.14	0.28
	80	0.5	0.28	0.56
	Ambient	5	0.24	0.48

Average 0.72

Table 1: Summary of crack growth rates at various temperature and frequency combinations

From Table 1, the average of all the crack growth rates is 0.72 mm per 1000 hours. This is similar to the initial fatigue test results which showed a crack growth rate of 0.7 mm per 1000 hours for tests performed under ambient conditions at frequencies of 3 and 5 Hz. The results at Table 1 indicate that frequency of loading and test temperature do not have a significant or consistent effect on crack growth rate. The variability in crack growth rate is considered to be within that which could be reasonably be expected in any fatigue experiment. This insensitivity to testing temperature has been observed previously in patched, cracked specimens (Reference 10). Later work however (Reference 11) has shown a small increase in crack growth rate with an increase in test temperature. The increase however is considerably less than would be predicted by theory. This may be due to many factors including the fact that static rather than dynamic properties for the adhesive are used when performing the analysis.

5.3 Thermal Residual Stress

A series of experiments (Reference 9) were conducted to quantify the residual thermal stress which prevails in the panel specimens and this is compared with simple theory in this section. An investigation (Reference 12) was also conducted to quantify the actual coefficient of thermal expansion which would be expected in the repair area on the F-111 wing.

The experiments (Reference 9) included placing strain gauged pieces of 2024-T851 Aluminium Alloy (F-111 wing skin material) and the 14 layer boron epoxy laminate in an oven at a controlled temperature and measuring the expansion strain directly. The initial temperature was 23 °C and the oven was set to 80 °C.

Published values (Reference 2) for the coefficients of thermal expansion (α) for the aluminium and unidirectional boron epoxy are as follows:

- a. Aluminium, $\alpha = 23 \times 10^{-6}$ per °C
- b. Boron epoxy, $\alpha = 4.1 \times 10^{-6}$ per °C

The 14 layer boron epoxy laminate gave a strain increase of 168 $\mu\epsilon$ for the temperature increase of 57 °C (80-23). This equates to an effective α of 2.95×10^{-6} per °C. This compares well with the published value of 4.1×10^{-6} per °C for unidirectional boron. The ± 45 plies are expected to reduce the effective expansion.

The aluminium gave a strain increase of 1198 $\mu\epsilon$ for the 57 °C temperature increase. This equates to an effective α of 21×10^{-6} per °C which is in reasonable agreement with the published value of 23×10^{-6} per °C.

Another experiment was conducted where a panel specimen was gauged prior to bonding the patch. The actual residual strain in the patch after bonding at 80 °C, curing and returning to room temperature was measured. The "residual" strain was about 500 $\mu\epsilon$ (in compression as expected). The bonded, patched panel was then subjected to a temperature of about 80 °C (ie a ΔT of 57 °C) and the strain in the boron increased to approximately zero, ie the state of strain went from approximately 500 $\mu\epsilon$ in compression to the unbonded or free strain state. A similar strain increase (about 500 $\mu\epsilon$) was measured in the aluminium. This indicates that the adhesive bond remained intact throughout the temperature range and compatibility therefore ensured that the whole specimen behaved as a homogeneous item.

Another experiment (Reference 12) was conducted which included placing strain gauges in the repair area on an uncracked, unpatched F-111 test wing at AMRL. The area was subjected to an 80 °C temperature increase as per the cure cycle and method for applying the patch repair. The measured strain increase was used to compute an effective coefficient of thermal expansion for the repair area of 6×10^{-6} per °C. This is surprisingly low, and is significantly lower than FE predictions (Reference 13) and previous analytic work (References 14 and 15). It is also significantly lower than the values obtained

in earlier work on the F-111 Wing Pivot Fitting area (Reference 16), presumably because of differences in the level of constraint and/or heat flux in the area. The C5033 approach (References 2 and 14) allows for an effective coefficient of thermal expansion to be calculated as follows:

$$\alpha_{eff} = \frac{\alpha \times (1 + \nu)}{2}$$

where ν = poissons ratio

assuming $\nu = 0.3$ and $\alpha = 21 \times 10^{-6}$ per $^{\circ}\text{C}$, this gives

$$\alpha_{eff} = 13.7 \times 10^{-6} \text{ per } ^{\circ}\text{C}$$

This is still considerably higher than the experimentally obtained value, 6×10^{-6} per $^{\circ}\text{C}$.

6. DISCUSSION

The static mechanical properties of structural film adhesives such as FM73 are known to vary markedly with temperature. Also, the large difference in thermal coefficient of expansion between Aluminium Alloy and Boron Epoxy leads to an expectation of high residual stresses in bonded repairs. These factors would be expected to significantly influence the behaviour of a bonded composite repair such as the F-111 wing skin example. The experimental results however indicate a lack of sensitivity to both temperature (for the static and dynamic loading) and loading frequency (for the dynamic loading). This suggests that there may be scope to reduce the conservatism inherent in the current accepted and proven design analysis approach presented in RAAF Standard Engineering C5033.

In the case of the thermal mis-match problem, the measurements of actual expansion in a real wing indicate that the "problem" would be even less noticeable in a real repair than on test specimens. This may be because the actual level of constraint in a real structure is such that only a minimal amount of thermal mis-match occurs.

Reference 11 suggests that one difficulty with the models and analyses which currently over estimate the thermal effects (particularly under cyclic loading) may be the use of static rather than dynamic mechanical properties for the adhesive. This is currently under investigation at AMRL. The use of elastic formulae in the Reference 11 approach may also be a factor and this is being

investigated also. The aim is to improve the understanding of bonded composite repairs and develop more accurate analysis techniques to reduce excessive conservatism.

7. CONCLUSION

A series of static and fatigue tests were conducted to quantify the effects of test temperature and loading frequency on repair performance. The test results confirmed that the current analyses over estimate these effects. Further work to fully understand the complex mechanisms involved with these repairs under different temperature conditions is required. This will lead to improved analysis techniques which remove unnecessary conservatism.

8. ACKNOWLEDGMENTS

The authors wish to acknowledge the assistance and support provided by Drs F. Rose and A. Baker, and Messers. R. Callinan, L. Mirabella and L. Molent of the Airframes and Engines Division at AMRL.

9. REFERENCES

1. Walker, K., and Swanton, G., "Static and Fatigue Test Loading Development for an F-111 Bonded Composite Repair Substantiation", AMRL Technical Note, in preparation.
2. Anon, "Composite Materials and Adhesive Bonded Repairs", RAAF Engineering Standard C5033.
3. Fredell, R., "Damage Tolerant Repair Techniques for Pressurised Aircraft Fuselages", PhD Thesis, Delft University, The Netherlands, 1994.
4. McHenry, M.I., and Key, R.E., "The F-111 Logic: Familiar Materials; Proven Process", Metal Progress, 93, No3, 62-68 (1968).
5. Keeley, D., Callinan, R. and Sanderson, S., "A Validated Finite Element Model of an F-111 Lower Wing Skin Structural Detail at Forward Auxiliary Spar Station (FASS) 281.28", DSTO-TN-0046, in publication, 1996.
6. AMRL Structures Laboratory Report No 3/95, "Stress Intensity Factors for Thin Aluminium Alloy 2024-T851", May 1995.

7. Davis, M.J., Kearns, K.J., and Wilkin, M.O., "Bonded Repair to Cracking in Primary Structure : A Case Study", Proceedings PICAST2-AAC6 p 323-330, Institution of Engineers, Melbourne, Australia, March 1995.
8. Preston, P.F., Rose, L.R.F., Walker, K., and Wilson, E.S., "Repair Substantiation for a Bonded Composite Repair to Primary Aircraft Structure", presented at ISASTI '96, Jakarta, Indonesia, June 1996.
9. Boykett, R., and Walker, K., "F-111C Lower Wing Skin Bonded Composite Repair Substantiation Testing", DSTO Technical Note, in preparation.
10. Baker, A., "Repair Efficiency of Fatigue Cracked Aluminium Components Reinforced with Boron Epoxy Patches", Fatigue and Fracture of Engineering Materials and Structures, Volume 16, No7, pp. 753-765, 1993, Great Britain.
11. Baker, A., "Fatigue Studies Related to Certification of Composite Crack Patching for Primary Metallic Aircraft Structure", Presented at FAA-NASA Symposium on Continued Airworthiness of Aircraft Structures, Atlanta, Georgia, USA, 28-30 August 1996.
12. Mirabella, L., "Strain Gauge and Temperature Measurements of a Heated F-111 Wing", AMRL Laboratory Report in preparation.
13. Callinan, R.J., and Sanderson, S., "Finite Element Analysis of an F-111 Lower Wing Skin Fatigue Crack Repair", AMRL Technical Note, in preparation.
14. Rose, L.R.F., "Theoretical Analysis of Crack Patching", Bonded Repair of Aircraft Structures, Chapter 5, Martinus Nijhoff Publishers, 1988.
15. Callinan, R.J., Tran-Cong, T., and Walker, K., "Development and Validation of a Finite Element Based Method to Determine Thermally Induced Stresses in Bonded Joints of Dissimilar Materials", AMRL Technical Report, in preparation.
16. Molent, L., Ferrarotto, P., and Davis, M., "Thermal Strain Survey of an F-111C Wing Pivot Fitting", ARL-STRUC-TM-456, March 1987.

The Probabilistic Assessment of Aircraft Subjected to Widespread Fatigue Damage

**Dr. Michael C. Shiao
Galaxy Scientific Corporation**

**Dr. John G. Bakuckas, Jr.
Dr. Catherine A. Bigelow
William J. Hughes Technical Center
Federal Aviation Administration
Atlantic City International Airport, NJ**

**USAF Aircraft Structural Integrity Program Conference
San Antonio, Texas
December 3-5, 1996**

Outline of Presentation

- ◆ **Background**
- ◆ **Objective**
- ◆ **Probabilistic Modeling for WFD**
- ◆ **Preliminary Results**
- ◆ **Summary**
- ◆ **Future Work**

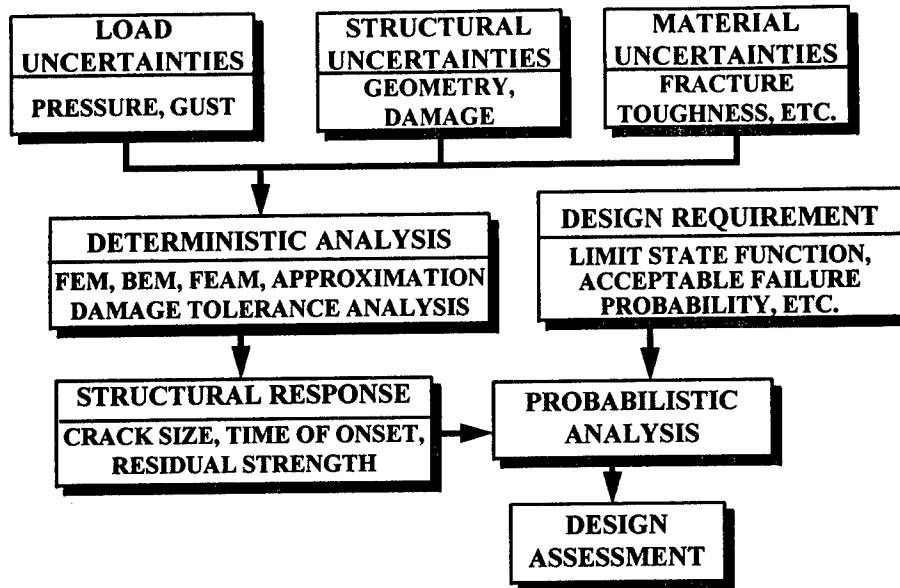
Background

- ◆ **Small undetected MSD cracks in several adjacent fastener holes can link together and reach a critical size in relatively few flights.**
- ◆ **WFD is a random phenomenon in nature.**
- ◆ **Better understanding of WFD behavior and its implications can be obtained with a comprehensive probabilistic assessment.**

Objective

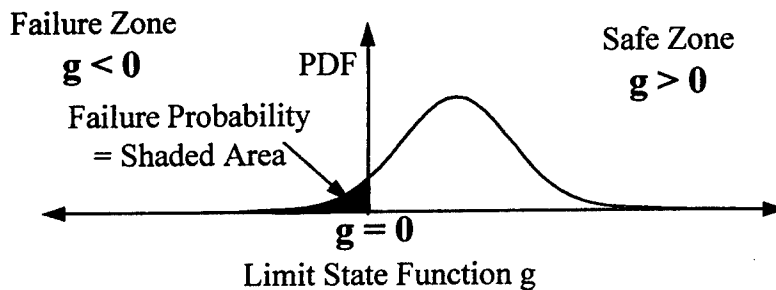
- ◆ **Demonstrate a computer code developed at FAA Technical Center which integrates existing deterministic and probabilistic codes for probabilistic WFD assessment**

SCHEMATIC OF RELIABILITY ANALYSIS FOR WIDESPREAD FATIGUE DAMAGE



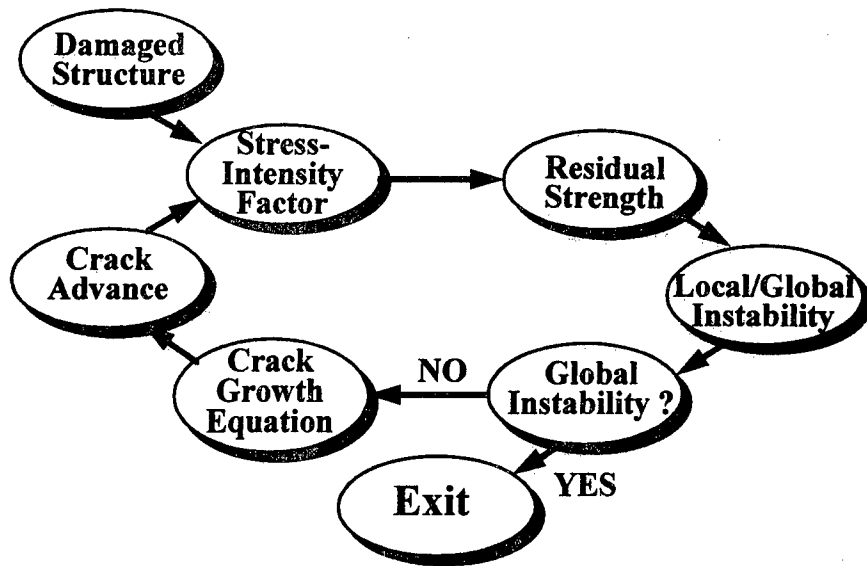
DEFINITION OF LIMIT STATE FUNCTION (OR SAFETY MARGIN)

LIMIT STATE FUNCTION g =
RESIDUAL STRENGTH AT CURRENT TIME -
CRITICAL RESIDUAL STRENGTH



Probability of Failure = Probability ($g < 0$)

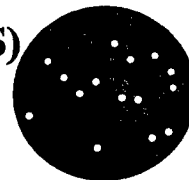
Deterministic Analysis



Probabilistic Analysis Methods

◆ Monte Carlo Simulation (MCS)

- ❖ Generates sampling points in entire domain

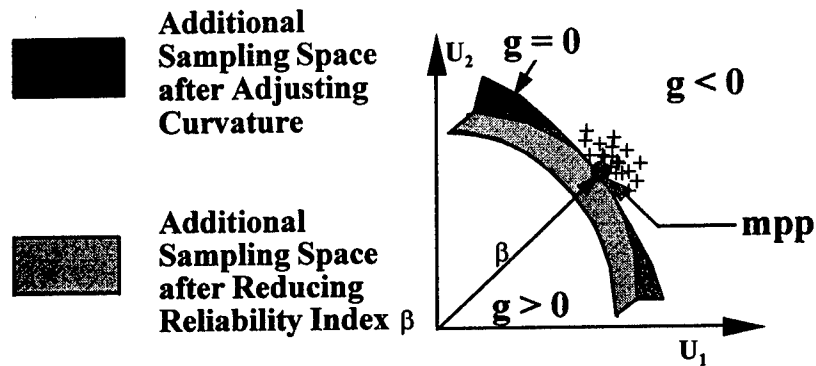


◆ Importance Sampling Method

- ❖ Identifies the failure region
- ❖ Generates sampling points in failure region only

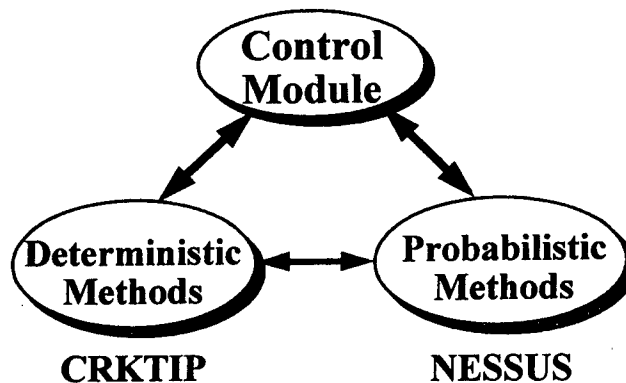


Adaptive Importance Sampling (AIS) (mpp-based)



mpp: most probable (failure) point

An Integrated Computer Code for Probabilistic WFD Analysis



CRKTIP

- ◆ **BEM Approach**
- ◆ **Use of Point Force and Dislocation Distribution for Crack Growth in 2D**
- ◆ **Accurate SIF Prediction with Relatively Coarse BEM Mesh**
- ◆ **Developed by Professor Denda of Rutgers University**
- ◆ **Funded by FAA Center of Excellence in Computational Modeling of Aircraft Structures**

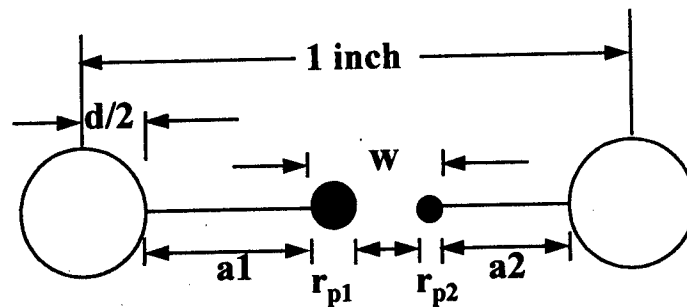
NESSUS

- ◆ **An Integrated Code for Probabilistic Structural Analysis**
- ◆ **A Suite of Probabilistic Methods**
- ◆ **Developed by Southwest Research Institute**
- ◆ **Funded by NASA Lewis Research Center**

Preliminary Results

- ◆ **Case I**
Flat Panel with Four Rivet Holes
- ◆ **Case II**
Flat Panel with Eight Rivet Holes
Considering Effect of Stiffeners

Local Instability/Crack Linkup



$$w = 1.0 - d - a1 - a2$$

$$w = r_{p1} + r_{p2}, \text{ linkup occurs}$$

Failure Criteria for Global Instability

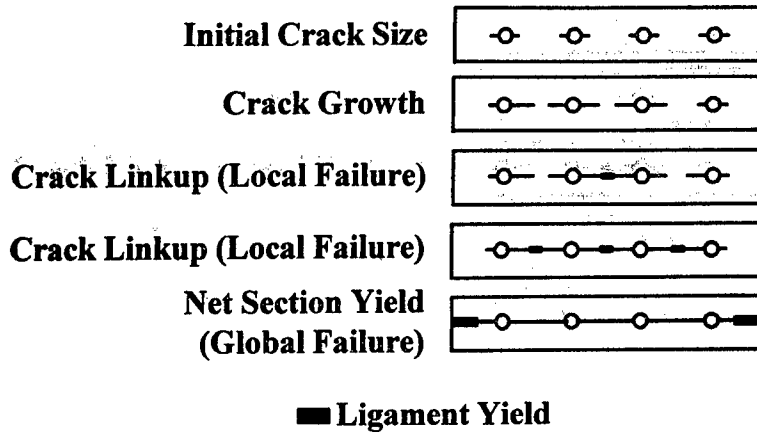
◆ Fracture

$$K_{Ic} \text{ (Fracture Toughness)} < K \text{ (Stress-Intensity Factor)}$$

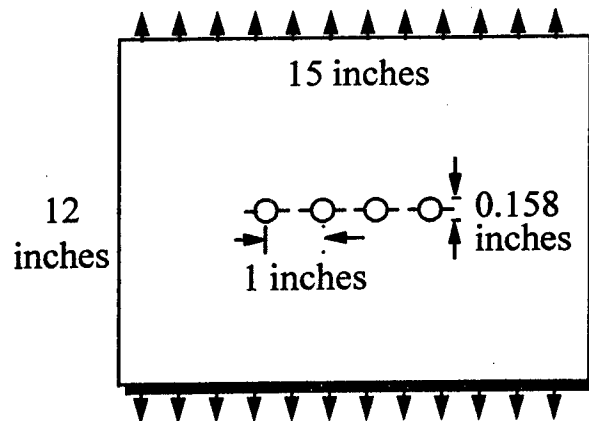
◆ Net Section Yield

$$\text{Yield Strength} < \frac{\text{Applied Traction} * \text{Width}}{\text{Remaining Ligament}}$$

Deterministic Analysis of A Flat Panel with WFD



Flat Plate with Open Holes (Case I)



Crack Growth Equation

$$da/dN = c \Delta K^m$$

c and m are input parameters

Uncertainties

- ◆ Applied Traction
- ◆ Structure
 - ❖ Initial Crack Size
- ◆ Material
 - ❖ Fracture Toughness
 - ❖ Yield Strength
- ◆ Crack Growth Parameters
 - ❖ c and m

Probabilistic Failure by AIS and MCS (95% Confidence Bound)

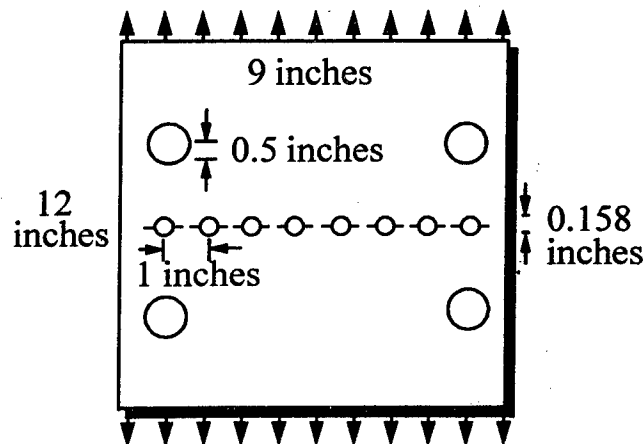
$$g \text{ (safety margin)} = N_f - 40000$$

AIS with 282 sampling points
 $0.0052 < P_f < 0.0064$

MCS with 1000 sampling points
 $0.0035 < P_f < 0.0155$

It requires **60,000** sampling points for MCS to achieve
the same level of accuracy predicted by AIS

Modeling of Stiffener Effect Using Four Corner Holes (Case II)



Crack Growth Equation

$$da/dN = c (\Delta K - \Delta K_{th})^m$$

where

$$\Delta K_{th} = 2.75 \text{ ksi } \sqrt{\text{in}}$$

$$\log(c) = b_0 + b_1 \log(m) - \log(F)$$

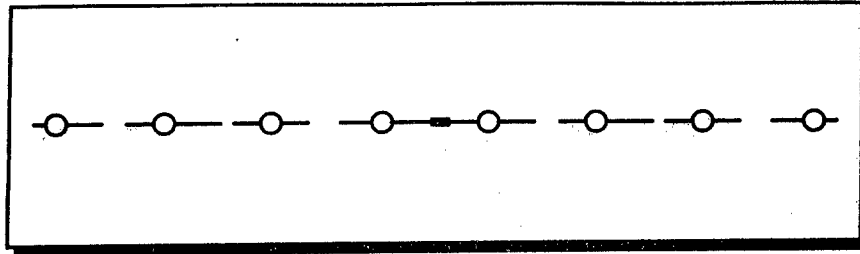
(m and F are input parameters,
b₀ and b₁ are constants)

Ref. Ostergaard and Hillberry, ASTM STP 798, 1983

Uncertainties

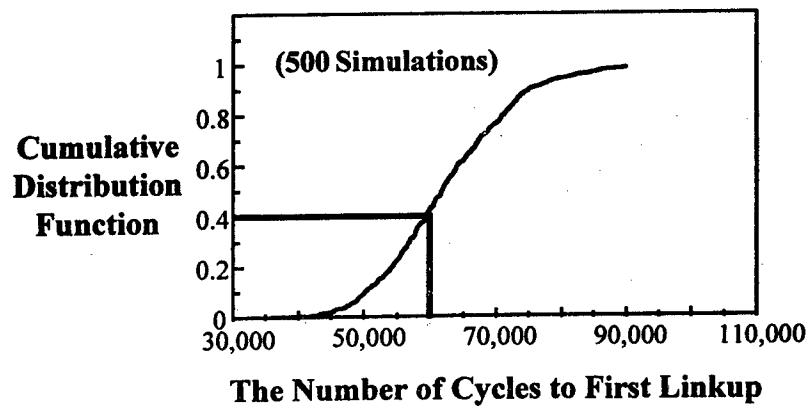
- ◆ Applied Load
- ◆ Structure
 - ❖ Initial Crack Size
- ◆ Material
 - ❖ Fracture Toughness
 - ❖ Yield Strength
- ◆ Crack Growth Parameters
 - ❖ F and m

Configuration for First Linkup (Local Failure)

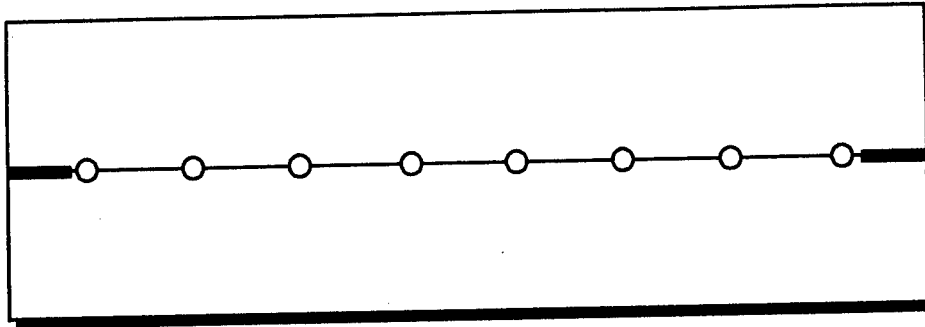


■ Ligament Yield

Cumulative Distribution Function of Number of Cycles to First Linkup

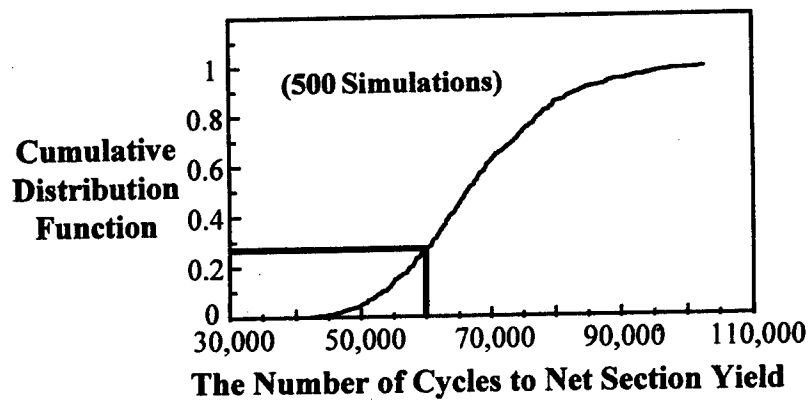


Configuration for Net Section Yield (Global Failure)



■ Ligament Yield

Cumulative Distribution Function of Number of Cycles to Net Section Yield



Summary

- ◆ **A prototype computer software for probabilistic WFD analysis has been developed which integrates CRKTIP with NESSUS.**
- ◆ **This software can integrate with any deterministic code for a comprehensive probabilistic analysis.**
- ◆ **The code has been exercised to demonstrate its ability to conduct probabilistic assessment of structures subjected to WFD.**
- ◆ **MPP-based importance sampling method is computationally feasible for WFD analysis.**

Future Work

- ◆ **Implement residual strength analysis**
- ◆ **Implement crack initiation life approach**
- ◆ **Conduct probabilistic risk assessment for discrete source damage with MSD**

Experimental Verification of Rose's Constant K Solution in Bonded Crack Patching

Dr. Richard Müller
Major Robert Fredell
Professor James Dally
Mr. Cornelis Guijt
Center for Aircraft Structural Life Extension
Department of Engineering Mechanics
United States Air Force Academy, Colorado

ABSTRACT

Bonded composite patches have been used for two decades to extend the lives of fatigue-damaged F-16, F-111, B-1B, C-141B, and many other aircraft. One of the key features of the technology is extremely slow crack growth under the bonded repair. Researchers have performed hundreds of experiments on repaired cracked panels, and have reported near-constant crack growth rates for a variety of relatively thin sheet ($t < 3$ mm or 0.125 inch) configurations and constant amplitude load cases. Constant crack growth rates rely on the existence of a constant crack tip cyclic stress intensity factor, ΔK , underneath the patch.

The paper describes the results of experimental stress analyses carried out on cracked aluminum panels with bonded composite patch repairs. Experimental strain gage and photoelastic measurements of K underneath a bonded repair validated Westergaard's analytical stress field description. These measurements, combined with fatigue crack growth studies, have verified that a constant K condition (predicted by L.R.F. Rose) indeed exists for cracks under bonded repairs. For the configuration tested, this held true while the crack size was less than roughly 80% of the repair width. These results are key to providing accurate predictions of crack growth rates and subsequent nondestructive inspection intervals in service.

KEY WORDS: Aging aircraft, bonded repair, crack patching, damage tolerance, Rose model, stress intensity factor K

Introduction

Bonded composite repairs to fatigue-damaged aircraft safely extend useful lives by slowing crack growth by orders of magnitude compared with the unrepaired case. Numerous experimental studies on repaired cracked panels have reported near-constant crack growth rates for a variety of configurations under constant amplitude loading. L.R.F. Rose was the first to publish a theory attributing these constant crack growth rates to a constant cyclic stress intensity factor, ΔK , underneath a bonded composite doubler [1]. However, researchers have not uniformly agreed on the validity of the Rose theory, particularly concerning short cracks ($2a < 10$ mm or 0.4 inches).

It was Irwin who in 1957 first suggested the use of strain gages for the prediction of the stress intensity near the tip of a crack. However, little progress has been made in implementing this suggestion. Dally and Sanford [2] successfully experimented with the problems of accurate measurements around strain gradients, the magnitude of the strain to be measured if the gage were placed in close proximity to the tip, and the size of the gage relative to the size of the near field region. They succeeded in reducing the theory to practice, and by setting boundaries for the gage locations, derived equations for determination of K .

Verifications of these stress intensities came with the experimental methods of Kobayashi [3] based on compliance measurements and photoelasticity. Mannog [4] and Theocaris [5] demonstrated the application of shadow caustics in a wide range of plane bodies containing cracks, and finally Barker et al. [6] have shown an accurate numerical technique for determining the stress intensity factor from full-field displacement data which can be obtained with either Moiré or speckle photography. Rosakis and Ravi-Chandra [7] have shown experimentally that the state of stress at the crack tip is three-dimensional in region I (see figure 1) and is not represented by either plane stress or plane strain. Plane stress conditions only exist when the radial distance from the crack tip exceeds half the skin thickness.

The validity of these techniques have demonstrated that strain gages can be effectively employed to measure the stress intensity factor in a cracked sheet. However, the determination of the opening mode in a cracked panel containing a bonded repair by

strain gages cannot be employed directly without proving the validity of the Westergaard equations underneath the patch, which form the basis for the stress intensity models.

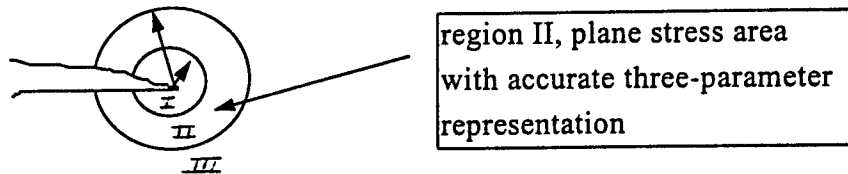


Figure 1. Schematic representation of regions surrounding crack tip (after [2]).

The area adjacent to the crack tip is divided into three regions, as shown in figure 1. After accounting for the valid ranges for this strain approach, the closest valid location to crack should be chosen. The inner boundary of validity is equal to a radius around the crack tip of the sheet thickness divided by two, while the outer radius is bounded by three-tenths of the half crack length (figure 1) and is theoretically based on truncation of the higher order terms of the strain field multi-parameter theory [2].

The error due to strain gradient is minimized by placing the strain gages sufficiently far from the crack tip and is then eliminated by a simple integration procedure.

Theoretical Multiparametric Representation of the Strain Field

Sanford [8] showed that the Westergaard equations [9] should be generalized to solve fracture mechanics problems where the stress field in the neighborhood of the crack tip is influenced by the proximity of boundaries and points of load application. The stresses expressed in this generalized form are given by:

$$\begin{aligned}\sigma_{xx} &= \text{Re}Z - y \text{Im}Z' - y \text{Im}Y' + 2 \text{Re}Y \\ \sigma_{yy} &= \text{Re}Z + y \text{Im}Z' + y \text{Im}Y' \\ \tau_{xy} &= -y \text{Re}Z' - y \text{Re}Y' - \text{Im}Y'\end{aligned}\tag{1}$$

For a single-ended crack, the stress functions Z and Y can be represented by:

$$\begin{aligned} Z(z) &= \sum_{n=0}^N A_n z^{n-1/2} \\ Y(z) &= \sum_{m=0}^M B_m z^m, \end{aligned} \quad (2)$$

with $z = x + iy$

By substituting equation (1) into the plane stress-strain relations, the following generalized equations for the strain field are obtained:

$$\begin{aligned} E\varepsilon_{xx} &= (1-\nu)\operatorname{Re} Z - (1+\nu)y\operatorname{Im} Z' - (1+\nu)y\operatorname{Im} Y' + 2\operatorname{Re} Y \\ E\varepsilon_{yy} &= (1-\nu)\operatorname{Re} Z + (1+\nu)y\operatorname{Im} Z' + (1+\nu)y\operatorname{Im} Y' - 2\nu\operatorname{Re} Y \\ \gamma_{xy} &= \frac{1}{\mu}\tau_{xy} \end{aligned} \quad (3)$$

The stress field can be expressed exactly by using the infinite series representations of the stress functions Z and Y given in equation (2). The exact approach cannot be used in practice due to the infinite number of unknown coefficients A_n and B_m , and consecutively an infinite number of strain gages. For a four-term representation the next expression for ε_{xx} is obtained if Z and Y are determined for $n = 0, 1$ and $m = 0, 1$:

$$\begin{aligned} E\varepsilon_{xx} &= A_0 r^{-1/2} \cos \frac{\theta}{2} [(1-\nu) - (1+\nu) \sin \frac{\theta}{2} \sin \frac{3\theta}{2}] + 2B_0 + \\ &\quad A_1 r^{1/2} \cos \frac{\theta}{2} [(1-\nu) + (1+\nu) \sin^2 \frac{\theta}{2}] + 2B_1 r \cos \theta \\ E\varepsilon_{yy} &= A_0 r^{-1/2} \cos \frac{\theta}{2} [(1-\nu) + (1+\nu) \sin \frac{\theta}{2} \sin \frac{3\theta}{2}] - 2\nu B_0 + \\ &\quad A_1 r^{1/2} \cos \frac{\theta}{2} [(1-\nu) - (1+\nu) \sin^2 \frac{\theta}{2}] - 2\nu B_1 r \cos \theta \\ \mu_{xy} &= \frac{A_0}{2} r^{1/2} \sin \theta \cos \frac{3\theta}{2} - \frac{A_1}{2} r^{1/2} \sin \theta \cos \frac{\theta}{2} - 2B_1 r \sin \theta, \\ &\quad \text{with } K_I = \sqrt{2\pi} A_0 \end{aligned} \quad (4)$$

By considering the orientation of the strain gages at an arbitrary angle α according to the coordinate transformation presented in figure 2, some of the terms in the strain field representation can be eliminated.

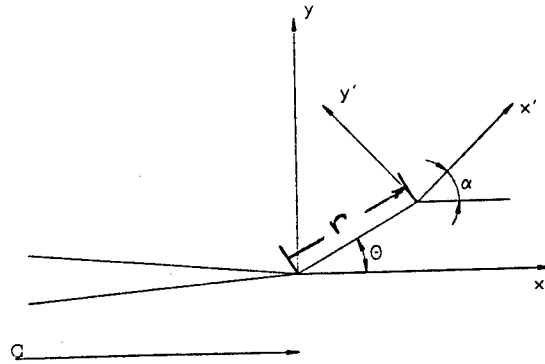


Figure 2. Coordinate system used in described crack, strain gage geometry.

The strains related to the rotated coordinate system shown in figure 2 are determined from the first invariant of strain,

$$\epsilon_{x'x'} + \epsilon_{y'y'} = \epsilon_{xx} + \epsilon_{yy} \quad (5)$$

For the complex of the strain transformation holds,

$$\epsilon_{y'y} - \epsilon_{x'x'} + i\gamma_{x'y'} = (\epsilon_{yy} - \epsilon_{xx} + i\gamma_{xy})e^{2i\alpha} \quad (6)$$

Substituting in equation (3) results for the transformed strain in x-direction:

$$\begin{aligned} 2\mu\epsilon_{x'x'} = & A_0 r^{\frac{1}{2}} \left[k \cos \frac{\theta}{2} - \frac{1}{2} \sin \theta \sin \frac{3\theta}{2} \cos 2\alpha + \frac{1}{2} \sin \theta \cos \frac{3\theta}{2} \sin 2\alpha \right] + \\ & B_0 (k + \cos 2\alpha) + A_1 r^{\frac{1}{2}} \cos \frac{\theta}{2} \left[k + \sin^2 \frac{\theta}{2} \cos 2\alpha - \frac{1}{2} \sin \theta \sin 2\alpha \right] + \\ & B_1 r \left[(k + \cos 2\alpha) \cos \theta - 2 \sin \theta \sin 2\alpha \right], \end{aligned} \quad (7)$$

where

$$k = \frac{1-\nu}{1+\nu}$$

Equation (7) gives the relation between K_I and the strain $\epsilon_{x'x'}$, measured with a single strain gage oriented at an angle α , with respect to the $P(x'y')$ coordinate system.

Strain Gage Location and Orientation

While six parameters are considered to represent an exact solution [10], a three-parameter solution (using A_0 , B_0 , A_1) still gives sufficient accuracy (in the order of $\pm 5\%$) with the use of a single gage [2]. Starting from the three-parameter solution, some terms can be eliminated by gage positioning and orientation. B_0 can be eliminated from equation (7) by setting

$$\cos 2\alpha = -k = -\frac{1-\nu}{1+\nu} \quad (8)$$

Setting A_1 to zero,

$$k + \sin^2 \frac{\theta}{2} \cos 2\alpha - \frac{1}{2} \sin \theta \sin 2\alpha = 0,$$

which can be satisfied if

(9)

$$\tan \frac{\theta}{2} = -\cot 2\alpha$$

The results show that a single element strain gage can be used to provide the data necessary for a three parameter solution. The relation between ν , θ and α is presented in table 1, from [2].

Poisson's ratio ν	θ (deg)	α (deg)
0.250	73.74	63.64
0.300	65.16	61.29
0.333	60.00	60.00
0.400	50.76	57.69
0.500	38.97	54.74

Table 1. Offset angles α and θ as function of Poisson's ratio ν from [2].

For an aluminum sheet with $\nu = 1/3$, $\alpha = \theta = 60^\circ$. If the gage is placed in region II, equation 7 reduces to:

$$K_I = E \cdot \sqrt{\frac{8}{3}} \cdot \pi \cdot r \cdot \epsilon_{xx} \quad (10)$$

Experimental Verification of Strain Field Representation for Bonded Repairs

The validity of the above-described analysis can be verified using the steps described in the approach. With the strain field described by equations (4) and a single strain gage, as shown in figure 3, in the vicinity of the crack tip, the strains of model and experiment can be compared. With increasing crack length, the strain results should show a similar trend.

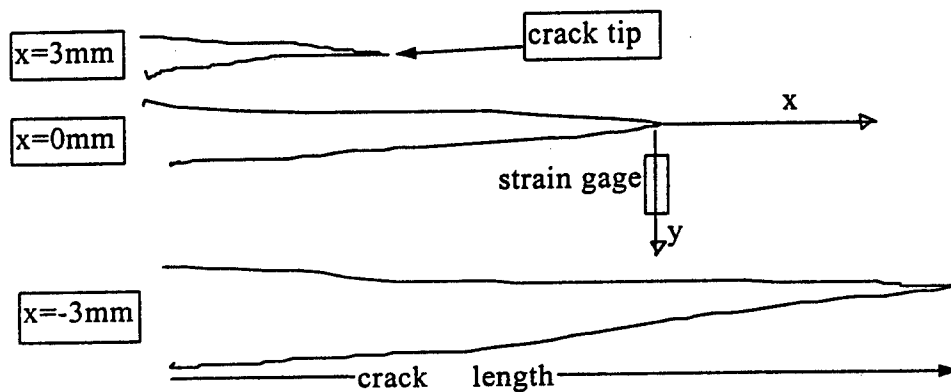


Figure 3. Strain gage location in y direction (parallel to the crack) as a function of the crack length.

For an aluminum sheet with $\nu=1/3$, and simplifying the equation for the strain field representation parallel to the crack, the following relation for ϵ_{yy} is obtained:

$$\frac{E\epsilon_{yy}}{A_0} = r^{-\frac{1}{2}} \cos \frac{\theta}{2} \left[\frac{2}{3} + \frac{4}{3} \sin \theta \sin \frac{3\theta}{2} \right] \quad (11)$$

The analytical results for the strains at a fixed location as a function of the crack length can be determined from figure 4.

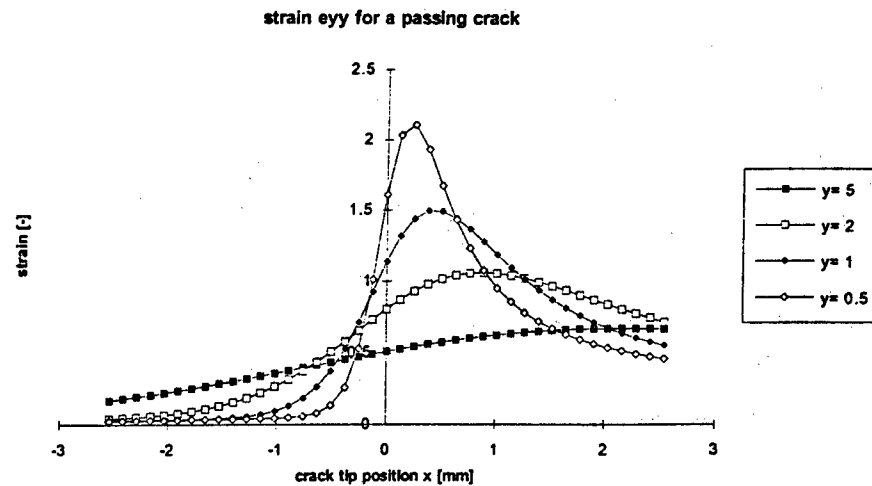


Figure 4. Strains parallel to the crack flank as function of crack length.

As crack length increases, the strain will increase to a maximum when the crack tip is close to the gage. However, the maximum is not achieved when the crack is just in line with the gage. The vertical displacement of the gage from the crack alters the trend, resulting in the maximum strain being displayed 2 mm before the crack tip is in line with the gage, both according to the prediction and measurement. If the same results can be obtained with strains underneath patches, the complex higher order equations remain valid to describe the stress field. A similarity approach is used: similar strains, K values, and crack opening displacements imply similar crack growth rates. Moreover, this experiment demonstrates that both the location of the crack and the onset of crack extension can be determined using strain gages.

Figure 4 demonstrated the change in theoretical strain as crack tip location changes with respect to the strain gage, while figure 5 compares experimental results with the theoretical curve for a single gage location ($y = 4.2$ mm).

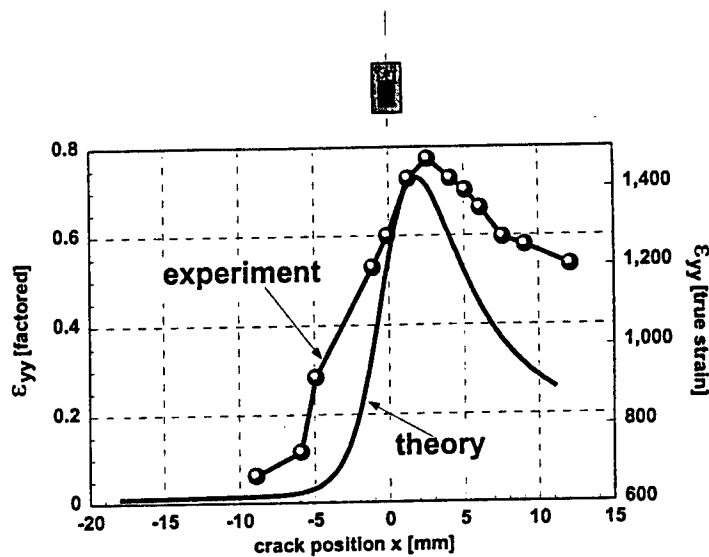


Figure 5. Strain ϵ_{yy} in the vicinity of a crack tip as function of the crack position.

Both curves display the same order of magnitude and trend (curve shape). This approach is used to validate the use of the K-approach with strain gages underneath a patch, but this strain gage measurement also can locate the crack tip with respect to the gage: if the strain is increasing, the crack tip is approaching the gage, while if the strain is decreasing, the crack tip has already passed the gage. Considering the valid ranges for this strain approach, the closest possible location to the crack should be chosen. Gages must be located close to the crack tip for optimum results, without violating the Zone I/Zone II boundary at half the sheet thickness from the crack tip, as introduced in the theory.

In work to be reported separately [11], an isochromatic fringe pattern study using photoelastic materials showed a reduction in the stress field underneath the repair compared to the unrepaired situation, and again the strain field representation by Westergaard can be used for determining the stress intensity K_I . The fringe patterns at the crack tip stay similar in shape and orientation (implying no significant change in shear stress or biaxiality).

Hence, the strain field representation derived in this report to describe the K is valid for unpatched cracked thin sheets and for bonded repairs, as demonstrated by strain gage measurements and photoelastic measurements.

Experimental Measurements of Stress Intensity Factor in a Bonded Repair

The strain gage analysis was verified using a center-cracked aluminum alloy 2024-T3 alclad sheet 1.0 mm (0.040 inches) thick with length by width dimensions 500 x 152 mm (20 x 6 inches). An equivalent stiffness, rectangular glass/epoxy/aluminum composite doubler 1.1 mm (0.044 inches) thick with length by width dimensions 92 x 77 mm (3.6 x 3.0 inches) was adhesively bonded over the crack using a rubber-toughened epoxy film cured at 120°C (250°F). Six strip gages were used and interpolation of the strains at the gages was performed. The strip gages had grid dimensions of 0.062", type EA-13-062MW-120 and were installed along the $\theta = \alpha = 60^\circ$ line, as shown in figure 6. Static strain measurements were taken from 0 to 105 MPa uniaxial tension.

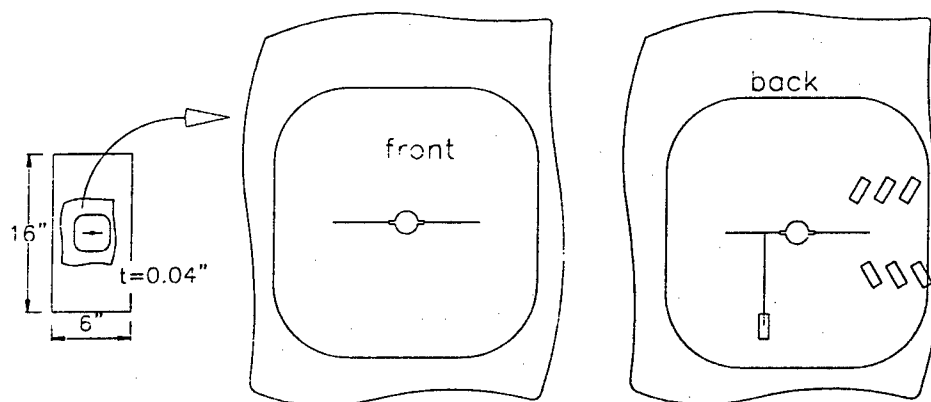


Figure 6. Schematic representation of single-sided repair and strain gages for stress intensity measurements ($\theta = \alpha = 60$ degrees, strain field analysis gage \perp crack).

Properly designed bonded composite repairs can increase the life of cracked components by two or three orders of magnitude. Figure 7 shows results of two typical constant amplitude fatigue tests carried out in support of this paper. Test conditions were as follows: $\sigma_{\max} = 130$ MPa, $R = 0.05$, room temperature, $f = 10$ Hertz. In the repaired case, 200,000 fatigue cycles passed without any crack growth, followed by several hundred thousand cycles of very slow crack growth.

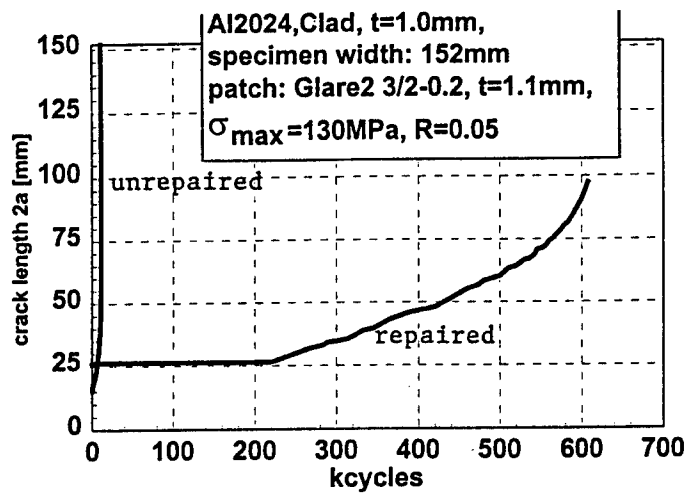


Figure 7. Repaired and unrepaired constant amplitude fatigue crack growth curves.

Figure 8 shows the measured reduction in K_I achieved by applying a bonded repair to the cracked adherend. Static strain measurements were taken at six separate crack lengths from 25 to 80 mm. Strip gages containing five grids at 1.3 mm (0.050 inch) pitch were used. The gages were 1.6 mm (0.062 inches) long and the first gage was placed 5 mm from the crack tip.

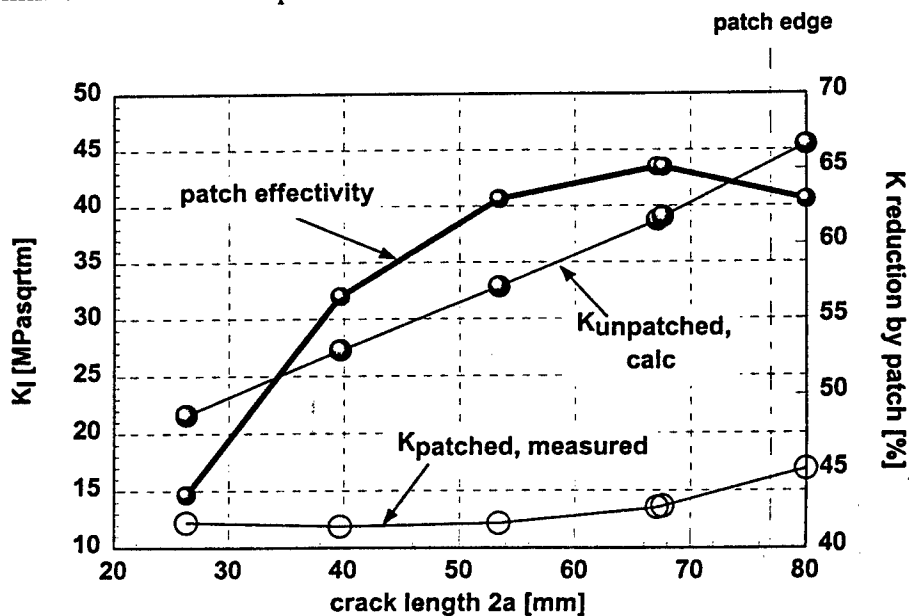


Figure 8. Reduction in stress intensity due to the application of a bonded repair.

Figure 8 clearly shows the significant reduction in K_I that accompanies the bonded repair. With increasing crack length, K remains constant until the crack length reaches about 80% of the patch width. (No data were taken for cracks shorter than $2a = 25$ mm.) Although K_{apparent} (measured by the strain gages) remained constant, the absolute reduction in K increased as the crack grew longer. With increasing crack length, the patch bridges the crack more efficiently because of larger restraint on crack opening displacement. Once the crack approached the edge of the repair, K was still reduced significantly, but by a smaller percentage.

The measured crack growth rates are shown in figure 9, where $d(2a)/dN$ is plotted as function of the crack length. A constant crack growth rate ($d2a/dN = 1.2 \times 10^{-7}$ m/cycle) is clearly evident up to $2a = 60$ mm. This crack growth rate corresponds to an effective ΔK value (based on observed crack growth rate) of between 7 and 9 MPa $\sqrt{\text{m}}$ (from [12] and the authors, respectively). The apparent ΔK values (experimentally measured with strain gages) were 13.0 ± 0.3 MPa $\sqrt{\text{m}}$ over the range $25 \text{ mm} < 2a < 60 \text{ mm}$.

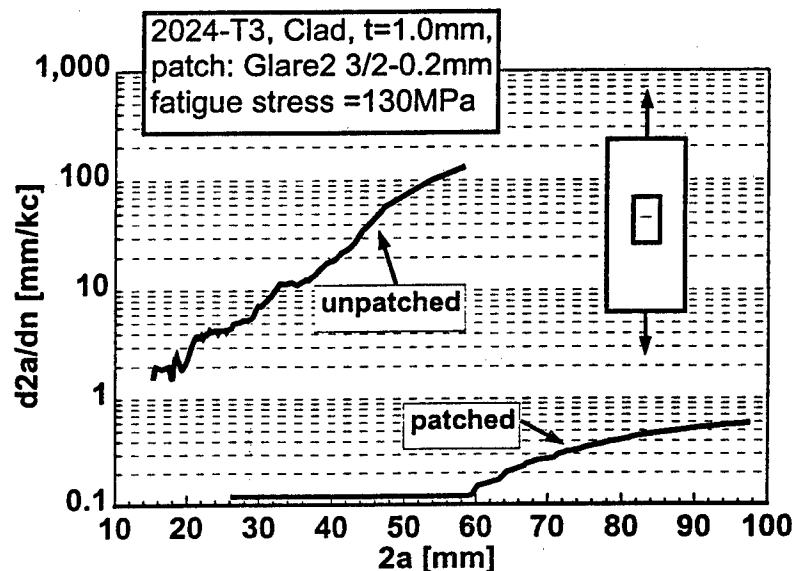


Figure 9. Plot of repaired and unrepaired crack growth rates versus crack length.

Discussion

The data show clearly how effective a bonded repair is in reducing the stress intensity factor and the crack growth rates for cracks longer than 25 mm in thin aluminum sheets. Reductions in K_I of more than 60% are easily achievable, corresponding to reductions in crack growth rates of one to two orders of magnitude over the unrepaired case. Most significantly, K and crack growth rates remain constant for a large portion of the life of the crack after repair, making inspection intervals easy to calculate.

In the configuration tested, when the crack length exceeded about 80% of the patch width, the constant K condition ceased to exist, and some acceleration was seen in the crack growth rate. However, this higher growth rate remained substantially slower than in the unrepaired case. Thus, even when a crack extends beyond the repair, it is easily detectable over a reasonable and safe period of time. Even more significantly, the critical flaw size required for fracture is significantly lengthened. Paris-type integration techniques can be used to convert the measured stress intensities into crack growth rates.

The approximately 4 MPa \sqrt{m} (30%) difference between $\Delta K_{\text{apparent}}$ (as measured by the strain gages) and $\Delta K_{\text{effective}}$ (experimentally observed crack growth rate) indicates that a substantial part of the fatigue cycle must be spent in crack closure. This is probably a thermally induced phenomenon, as the measured stress intensities beneath the repair were too low to produce significant crack tip plasticity and subsequent closure. Strain gages were applied after the bonded repair was cured. Hence, the gages could not measure any residual thermal stresses. The complex interaction between repair and substrate materials with different coefficients of thermal expansion and restraint caused by local heating in a stiffened structural repair is explained more completely in [13] and [14]. However, most simply,

$$\Delta K_{\text{effective}} = \Delta K_{\text{apparent}} + \Delta K_{\text{residual, thermal}} \quad (11)$$

where $\Delta K_{\text{residual, thermal}}$ represents the residual thermal stress from the bonding process (in this case, compressive) that acts on the crack tip. In the case presented here, the thermal stress acts to reduce $\Delta K_{\text{effective}}$ by shifting the fatigue ratio R from +0.05 to a negative value.

Additional investigations are necessary to determine the effectiveness of bonded repairs on short cracks at higher stress levels. Further study of the observed temporary complete stopping of crack growth after repair (not observed with all composite repair materials) is also needed.

Summary and Conclusions

The results of experimental stress analyses carried out on cracked aluminum panels with bonded composite patch repairs were presented. Experimental strain gage measurements of the stress intensity factor K beneath a bonded composite repair validated Westergaard's analytical strain field description. These measurements, in combination with fatigue crack growth studies, verified Rose's prediction of a constant K condition for cracks repaired with bonded composite patches. These results will aid accurate predictions of crack growth rates and subsequent nondestructive inspection intervals in service.

In this study of bonded repairs to cracked aluminum sheets, the key conclusions are:

- The Westergaard multi-coefficient strain field representation can be used to accurately determine stress intensity factors using strain gages in cracked panels containing bonded repairs.
- Measured stress intensity reductions up to 65% were achieved with the application of a bonded composite repair, correlating to more than ten times slower crack growth rates than in the unrepaired situation.
- As predicted by Rose, the repaired crack tip cyclic stress intensity is independent of crack length over a range of crack lengths as observed by crack growth rates and strain gage measurements. The apparent difference between the two measurements is attributed to residual thermal effects.
- Calculated or measured stress intensity factors can easily provide the relation to crack growth can be easily made with help of the Paris-type calculations.
- Repair effectiveness declines somewhat when the crack length approaches the repair width.

Acknowledgments

The authors wish to express their appreciation for the strong support of the U.S. Air Force Wright Laboratory's Flight Dynamics Directorate and the U. S. Air Force Academy's Department of Engineering Mechanics.

References

1. Rose, L.R.F., *Int. J. Fracture*, **18**, pp. 135-144, 1982.
2. Dally J.W. and R.J. Sanford, Strain Gage Methods for Measuring the Opening-Mode Stress-Intensity Factor, K_I , *Experimental Mechanics Proc.* 1985 Soc. of Exp. Mech. Spring Conf. on Exp. Mech., pp. 851-860, June 1985.
3. Kobayashi, ed., *Experimental Techniques in Fracture Mechanics*, SEM Monograph, Iowa State University Press, 1973.
4. Mannog, P., "Schattenoptische Messung der spezifischen bruchenergy wahrend des brugvorgangs bei plexiglas," *Proc. Int. Conf. on the Physics of Non-Crystalline Solids*, Delft, The Netherlands, pp. 481-490, 1964.
5. Theocaris, P.S., *J. Applied Mechanics*, **37**, pp. 409-415, 1970.
6. Barker D.B., R.J. Sanford, and Chona, R., *Experimental Mechanics*, **25** (4), pp. 399-406, 1985.
7. Rosakis, A.J. and K. Ravi-Chandra, "On Crack Tip Stress States and Experimental Evaluation of Three-Dimensional Effects," *Cal. Inst. of Tech.*, Report FM-84-2, March 1984.
8. Sanford, R.J., A critical Re-examination of the Westergaard [x-1] Method for Solving Opening Mode Crack Problems, *Mech. Res. Comm.*, **6** (5), 1979.
9. Westergaard, H.M., *J. Appl Mech.*, **6**, 1939.
10. Chona, R., G.R. Irwin, and R.J. Sanford, "Influence of Specimen Size and Shape on the Singularity-Dominated Zone", *Fracture Mechanics*, 14th Symp., Vol. 1: Theory and Analysis, ASTM STP 791, eds. J.C. Lewis and G. Sines, Amer. Soc. Test and Mat., I-3-I-23, 1983.

11. Hastie R., R. Fredell, and J. Dally, "A Photoelastic Study of Crack Repair" to be published in *J. Exp. Mech.*
12. Paris, P.C., "Fatigue--An Interdisciplinary Approach," Proc. 10th Sagamore Conf., Syracuse, NY, p. 107, 1964.
13. Rose, L.R.F., "Residual Thermal Stresses," in *Bonded Repair of Aircraft Structures*, Baker, Jones, editors. Dordrecht: Kluwer Academic Publishers, pp. 90-91, 1988.
14. Fredell, R., W. van Barneveld and A. Vlot, "Analysis of Composite Crack Patching of Fuselage Structures: High Patch Elastic Modulus Isn't the Whole Story," Proc. 39th Int. SAMPE Symp., Anaheim, pp. 610-623, April 1994.

SESSION IV

CORROSION/FATIGUE

Chairman: *D. Nieser*, OC-ALC/LACRA

Prediction of the Intergranular Corrosion/Fatigue Interaction Effect in Thin-Webbed Stiffening Members

R. W. Bush, A. J. Hinkle, R. J. Bucci and M. Kulak
Alcoa Technical Center, Alcoa Center, PA 15069

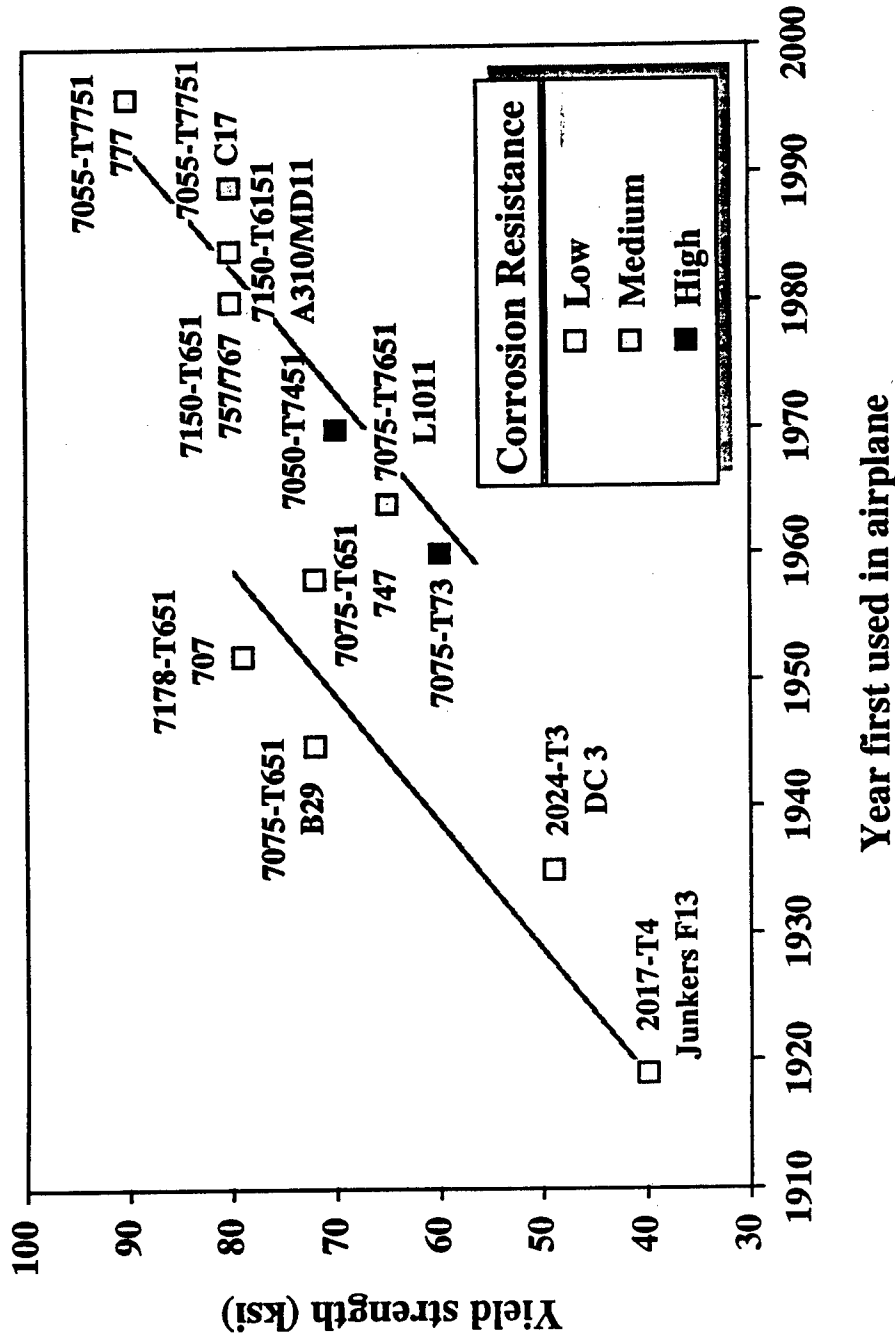
1996 USAF Aircraft Structural Integrity Program Conference
San Antonio, TX
December 3-5, 1996

Abstract

Certain high strength 7XXX aluminum alloy products can be susceptible to intergranular corrosion (IGC) attack during interim manufacturing steps between solution heat treatment ("W" condition) and final aging to a more corrosion resistant (T7X-type) temper.

This presentation is directed at the assessment of potential interaction effects between IGC and fatigue in thin-webbed stiffening members. A representative small airplane wing stiffener was chosen as the baseline part configuration for evaluation. Cyclic life data and crack-initiating feature demographics derived from over 90 tested specimens excised from parts containing varying degrees of IGC are described. The initial flaw size distribution data was then utilized in concert with conventional fatigue crack growth information to validate fracture mechanics based prediction of cyclic life degradation linked to IGC. The potential use of the evolving test and evaluation process as a basis for integrating design and material acquisition strategies is discussed in terms of the investigation findings.

Corrosion resistance has been a prominent factor in aluminum development chronology.



While prevention is the main line of corrosion defense, controls are needed to safeguard against long-term consequences of corrosion.

- Consideration must be given to the potential for corrosion to combine with fatigue and produce undetected cracks.
- Wide area corrosion must be avoided to keep cracks from becoming widespread.
- Optimized material and manufacturing process selections can go a long way toward easing the economic burden of corrosion.
- Predictive capability is needed to facilitate all of the above.

Study scope

Problem:

- Some Al alloys experience intergranular corrosion (IGC) attack that can lead to fissuring along surface and near-surface metal grain boundaries; work is needed to quantify the potential impact of IGC on fatigue life.
- Though the benefit potential of a damage-based lifing approach is clear,
 - The methodology is still developing for corrosion use.
 - Application is relatively untested.
 - Corrosion microfeature population data is sparse.

Objective:

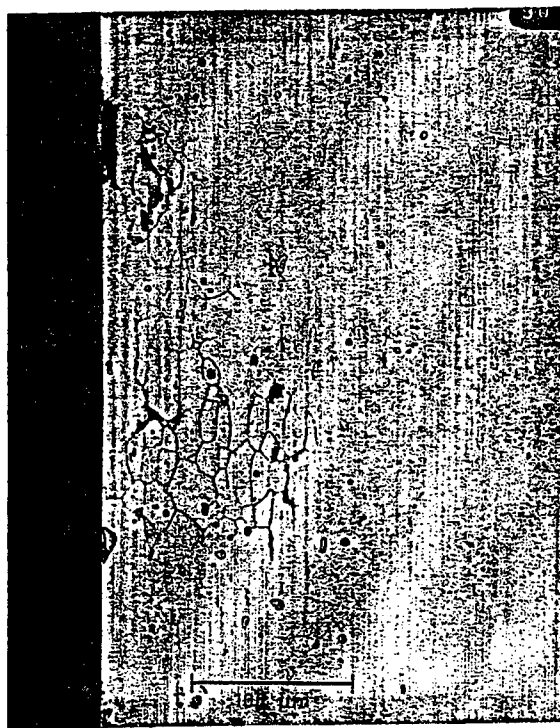
- Evaluate impact of IGC on aluminum alloy fatigue performance.
- Assess plausibility of treating total life as crack growth from an equivalent initial flaw size (EIFS) based on IGC demographics.

Approach:

- Select material with known IGC condition.
- Establish flaw population data from coupon tests.
- Validate analytic premise from contrast of predictions with test results.

Intergranular corrosion (IGC) may not be evident without special inspection methods.

- IGC characterized by preferential attack at or adjacent to grain boundaries.
- Encountered in all Aluminum heat treatable products.
- Related to electrochemical reactions associated with Cu-depleted zones and/or anodic precipitates.
- While applied stress is not a precursor for IGC, damage accrual is exacerbated in a stress environment.



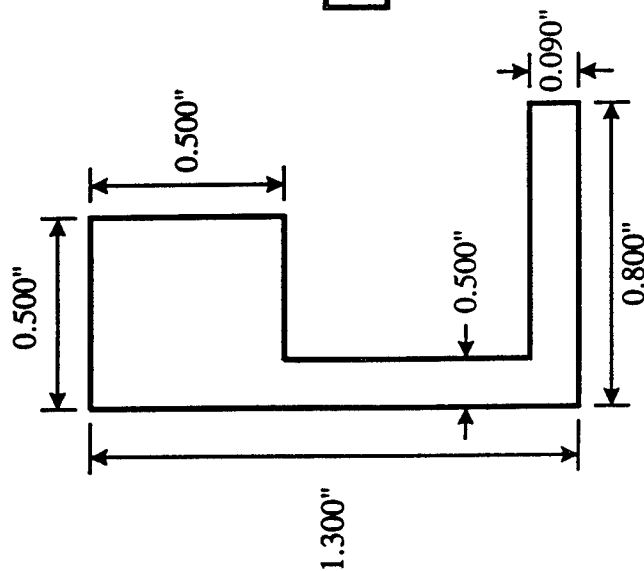
7xxx aluminum alloy are more vulnerable to IGC in their manufacturing sequence.

- Condition can occur between solution heat treatment and final aging to a more stable and corrosion resistant temper.
- IGC susceptibility is greatest for as-fabricated materials in the W and F conditions, but O, T6 and T7X temper materials may also experience the problem to lesser degree.
- With special processing the condition is controllable in a production environment.
- Analytic tools are being developed to optimize the manufacturing/control process and to evaluate fitness of suspect parts.

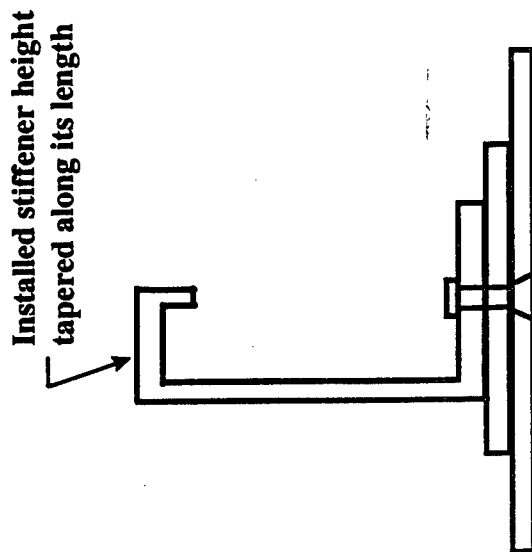
A recent field problem gave opportunity to study fracture mechanics based prediction of fatigue crack growth originating from IGC.

- 7150-T77511 extruded stiffeners possessing IGC condition in portions of final parts not machined.
- Testing conducted to link cyclic performance with IGC.
- Over 90 fatigue tests on specimens excised from parts with varying degrees of IGC.
- Fractography conducted to determine life-limiting feature demographics.
- Fatigue origin sizes used in combination with FCG data to validate equivalent flaw life prediction approach.

Extruded stiffener detail before and after installation

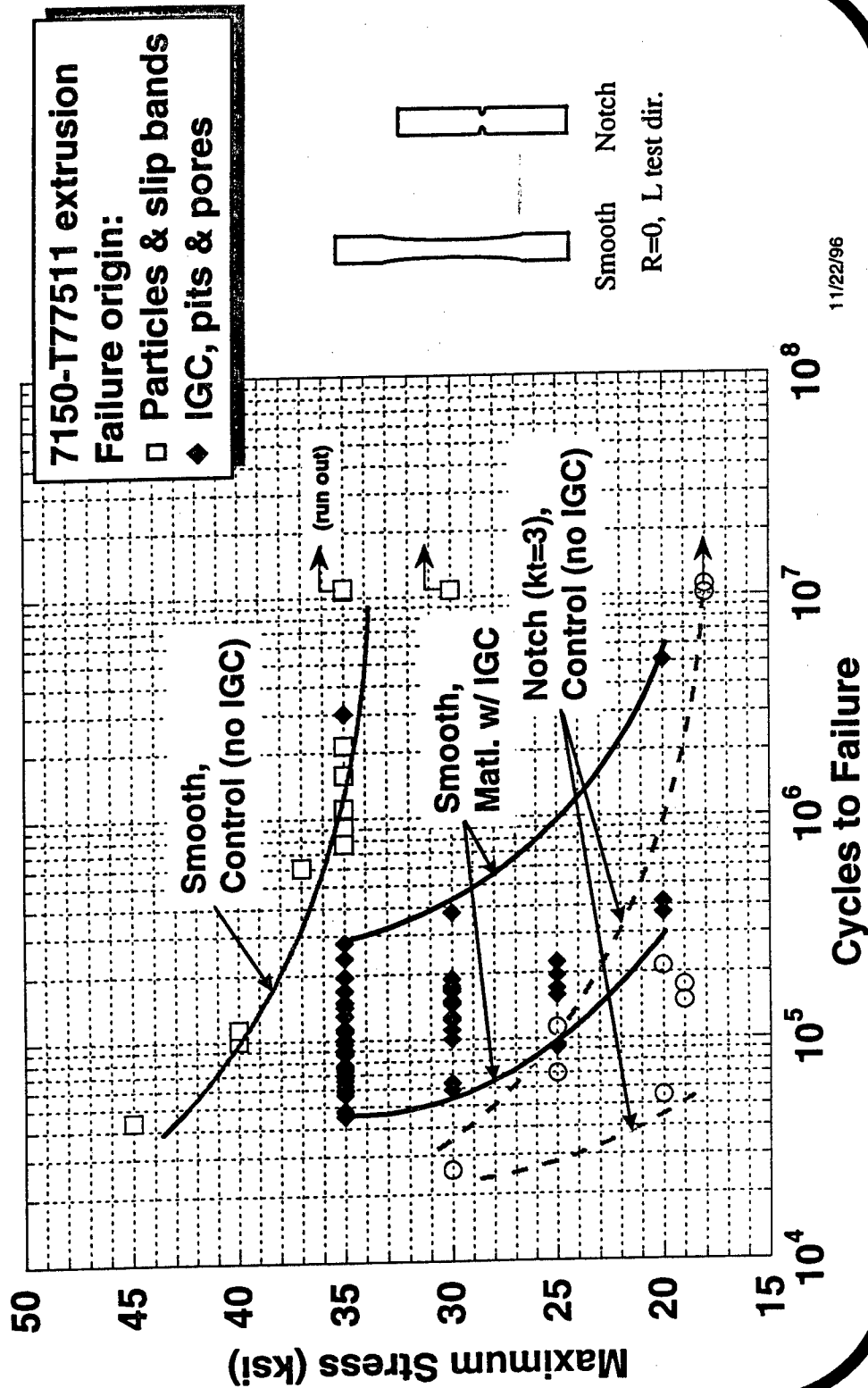


Original extruded cross section
(prior to finish machining)



Stiffened design detail with
machined stiffener installed

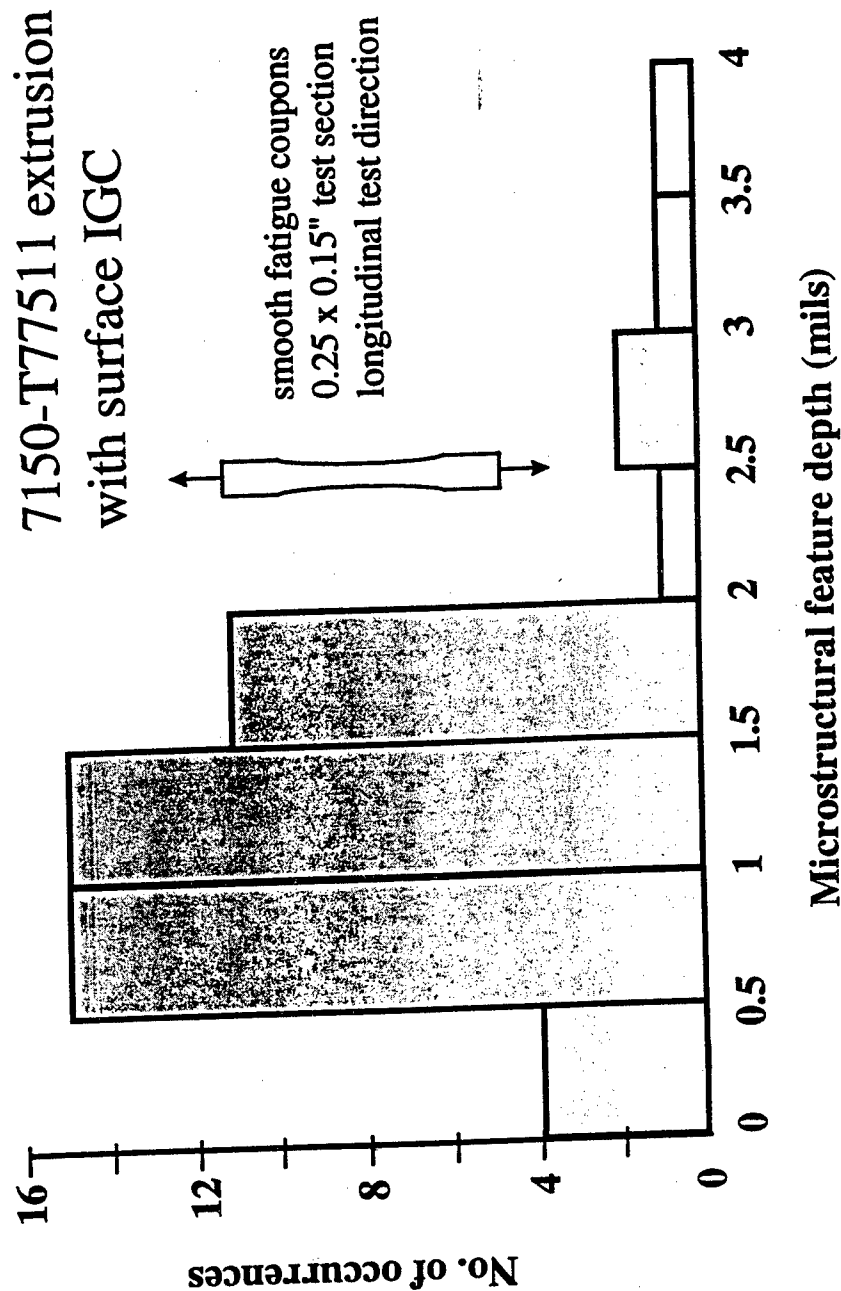
Fatigue performing links with crack originating microfeature type.



Implications of Test Results

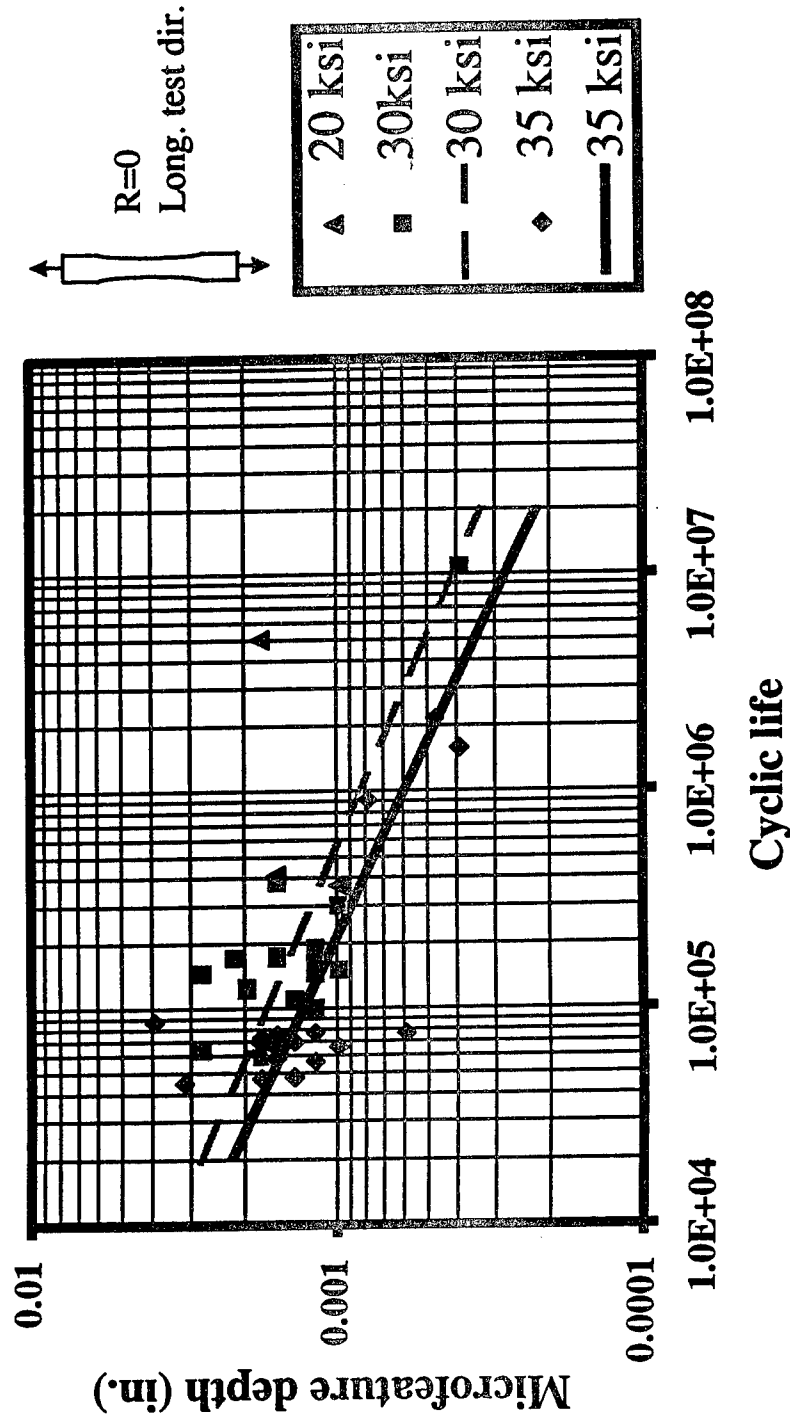
- IGC suspect material exhibited substantial smooth specimen fatigue strength knockdown from results of control tests.
- Not all failures were from IGC even though specimens were taken from locations with IGC condition.
- The smooth specimen knockdown less than that of a $kt=3$ notch.
- While the latter is comforting, additional work is needed to assess impact of wide area IGC on the following:
 - Notch fatigue allowables, including the notch size effect.
 - Safety margin and adequacy of inspection intervals for large lead cracks.
- Smooth specimen test ideal for generation of initial flaw data.

Typical crack originating microfeatures were < 2 mils, but depths to 4 mils were found.

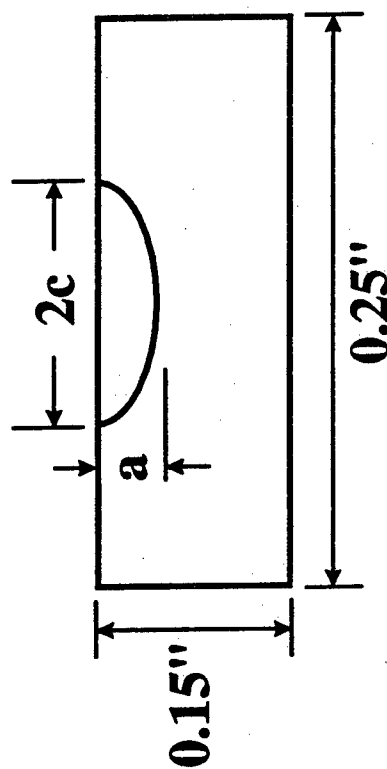


Cyclic performance correlates with scale of the life-limiting microfeature.

7150-T77511 extrusion with surface IGC

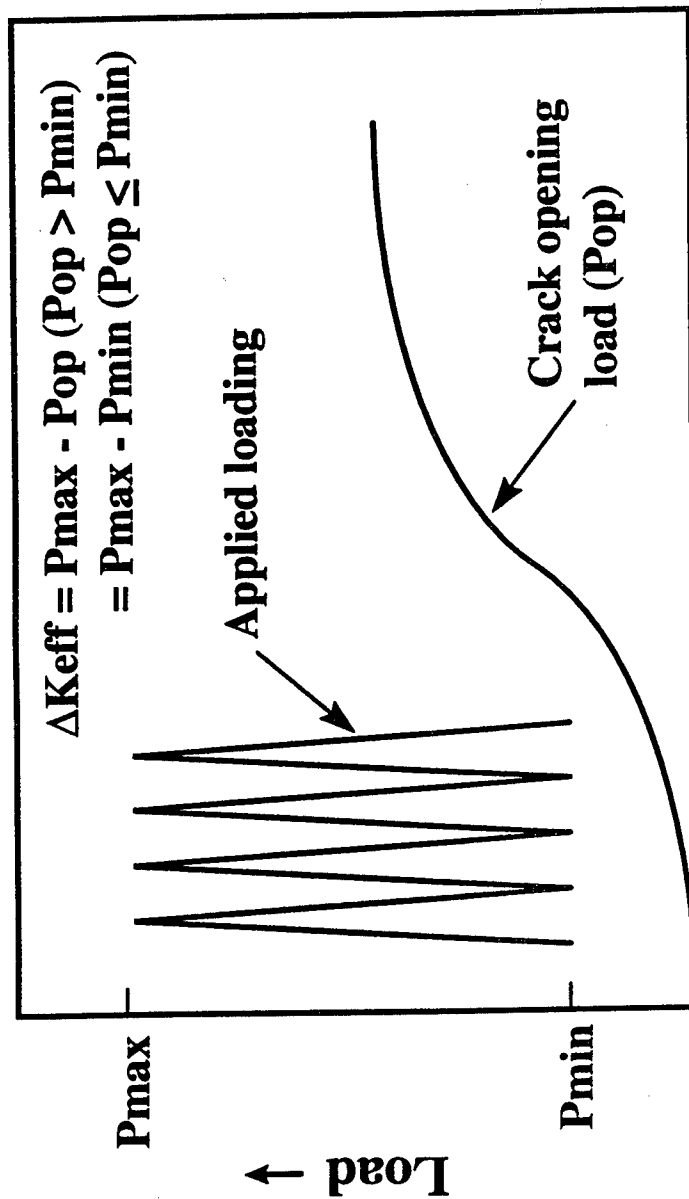


Measured flaw population data was used to validate the equivalent flaw approach to fatigue life prediction approach.



Assumed equivalent initial flaw geometry
(equilibrium shape: $a/2c = 0.3$)

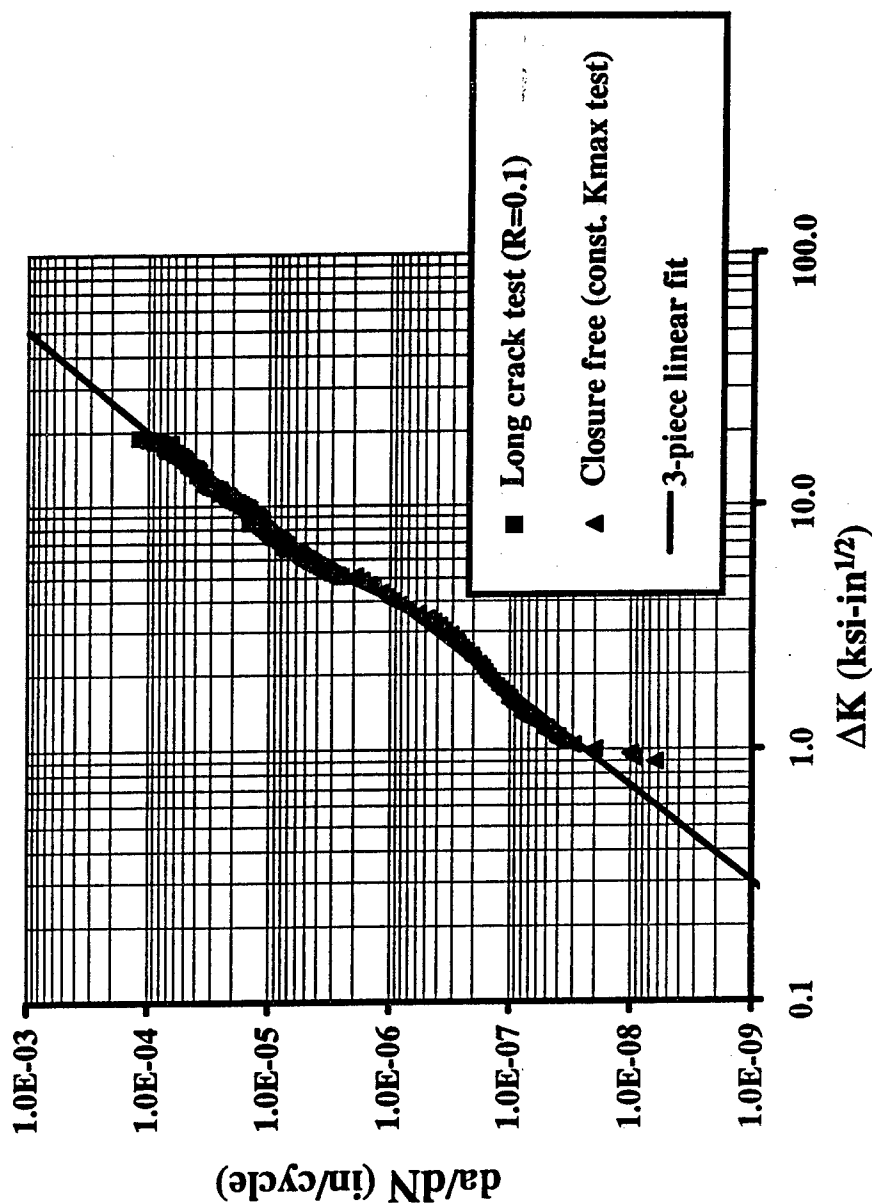
Evaluation of small crack growth requires closure free FCGR data.



Crack opening load transition with crack evolution and growth

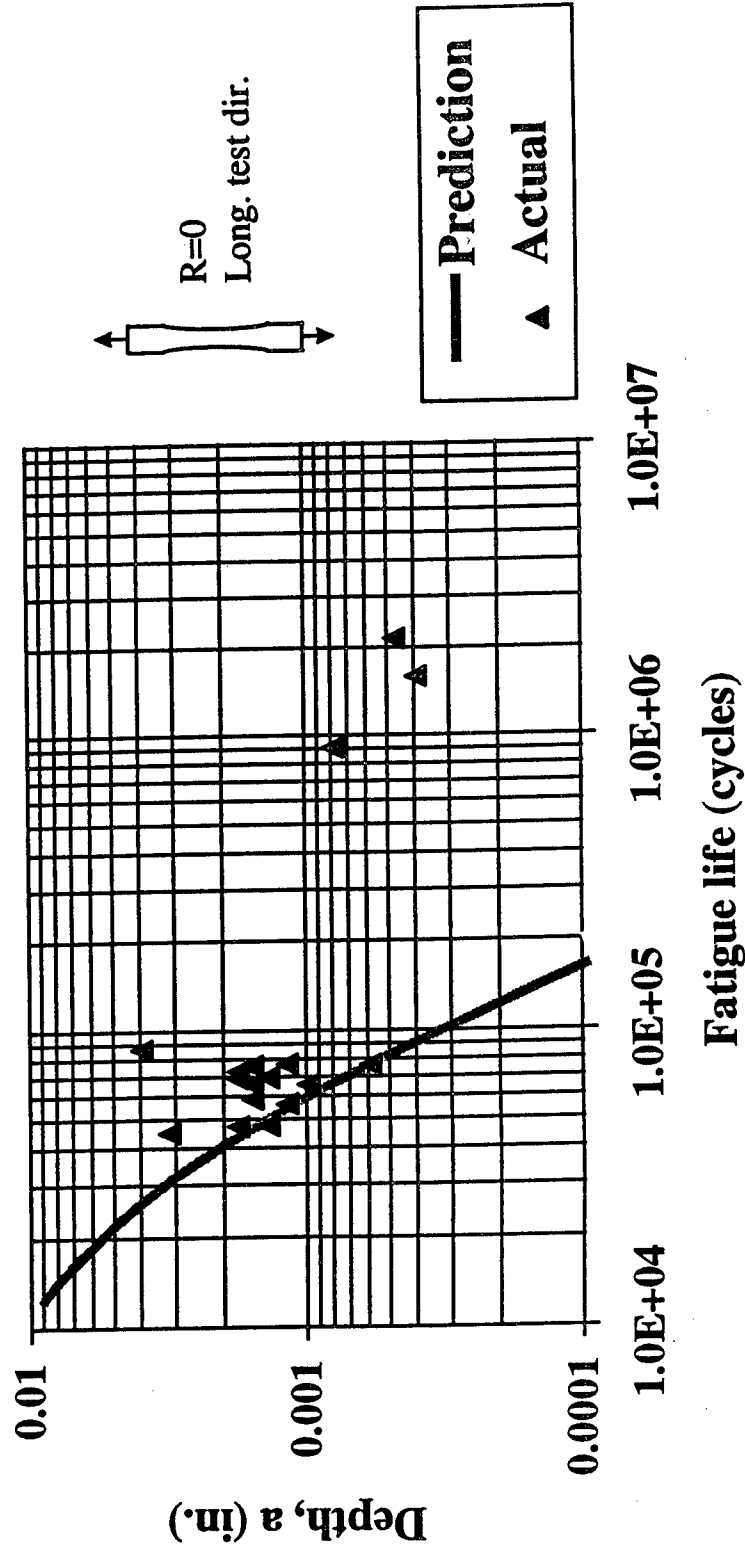
FCGR law built from splice of closure free and conventional long crack data.

7150-T77511 Extrusion, L-T test direction



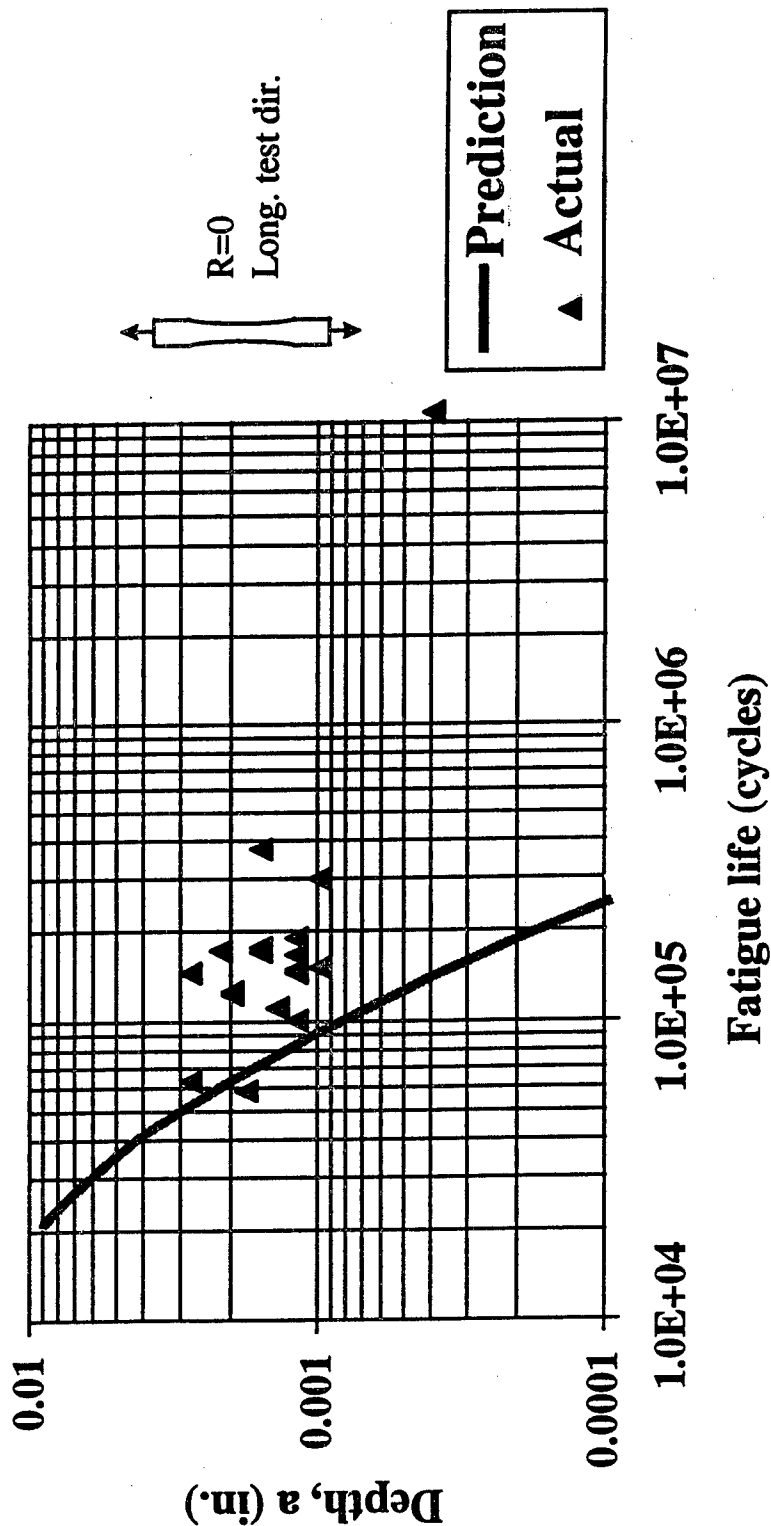
35 ksi: microfeature depth vs. cyclic life

7150-T77511 extrusion with surface IGC



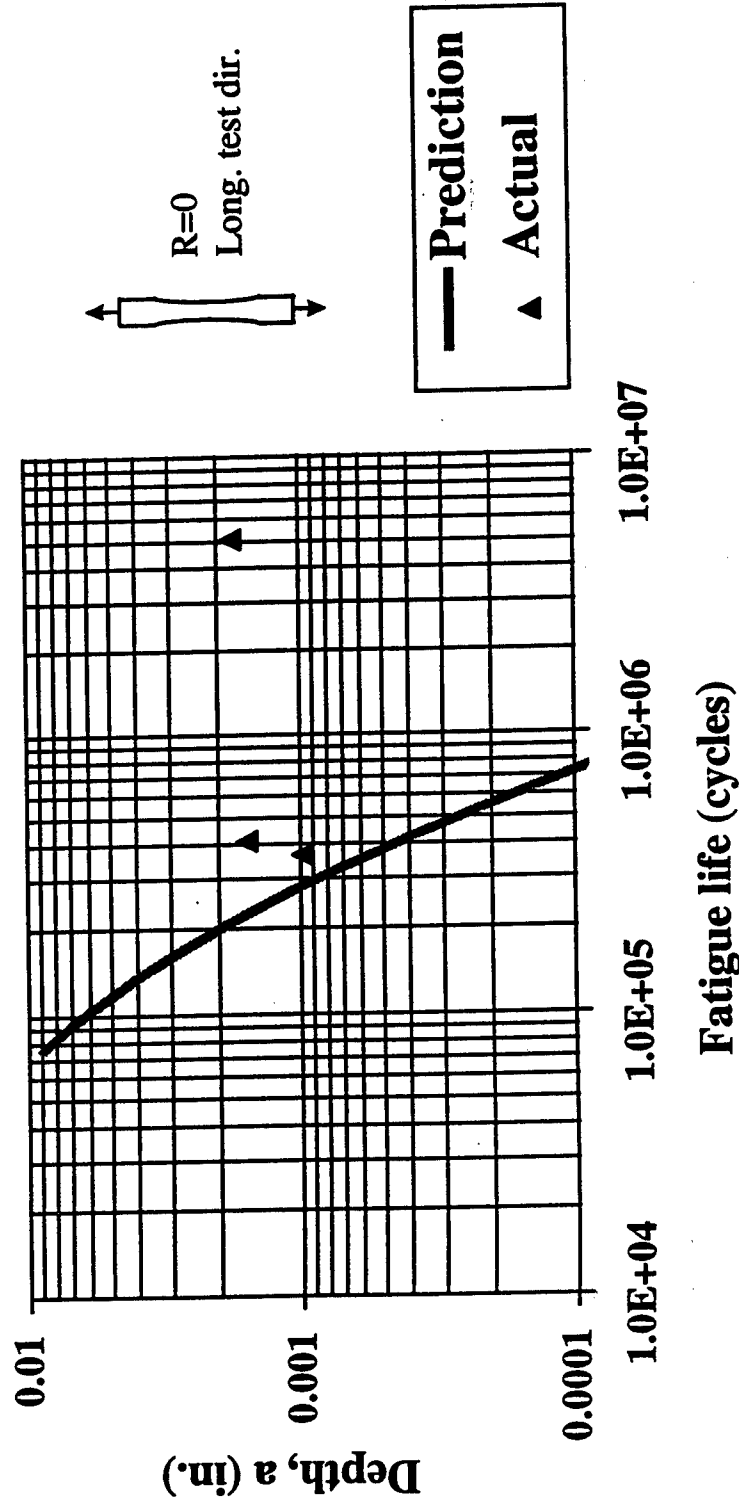
30 ksi: microfeature depth vs. cyclic life

7150-T77511 extrusion with surface IGC

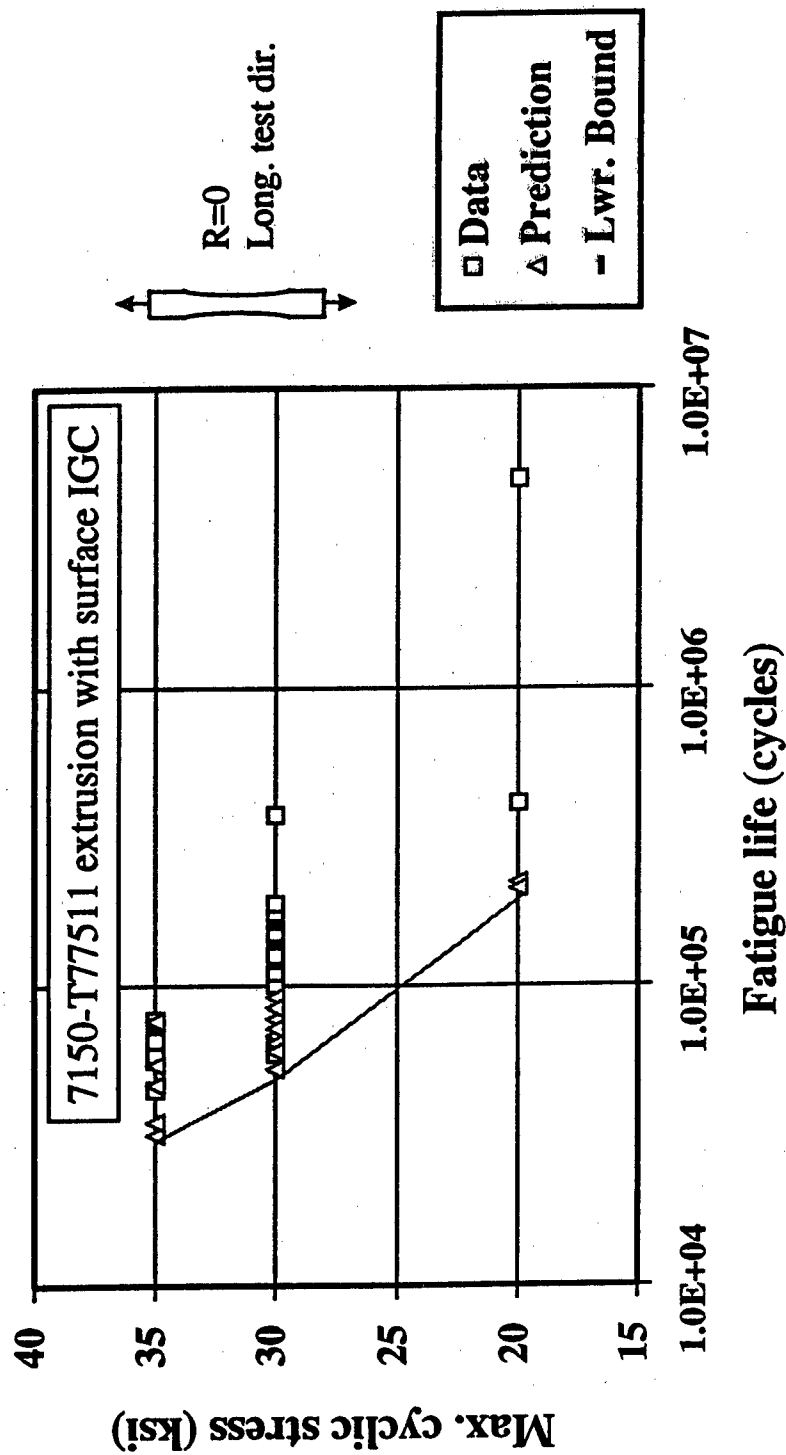


20 ksi: microfeature depth vs. cyclic life

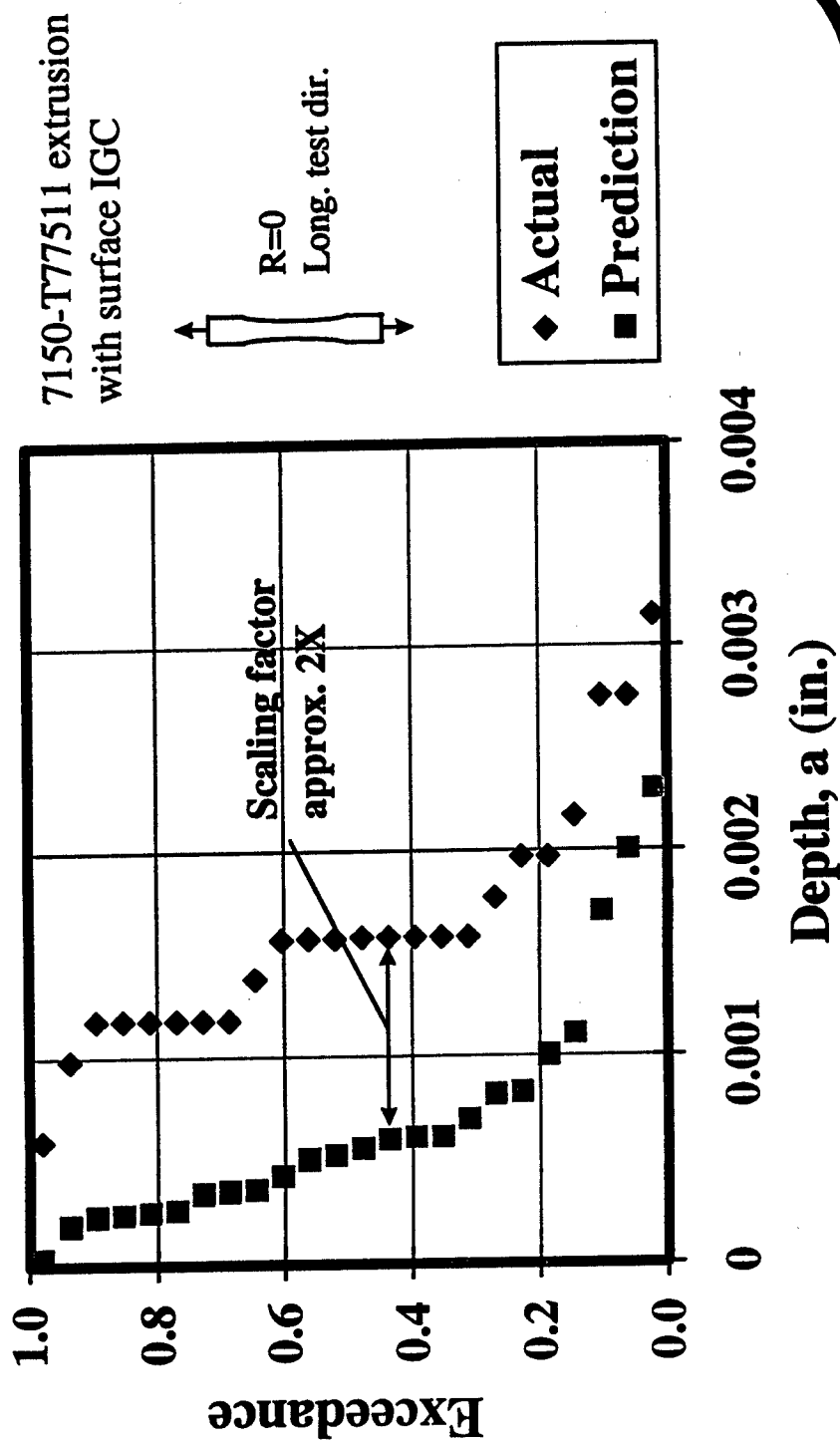
7150-T77511 extrusion with surface IGC



S-N test results compare favorably with the equivalent initial flaw based predictions.



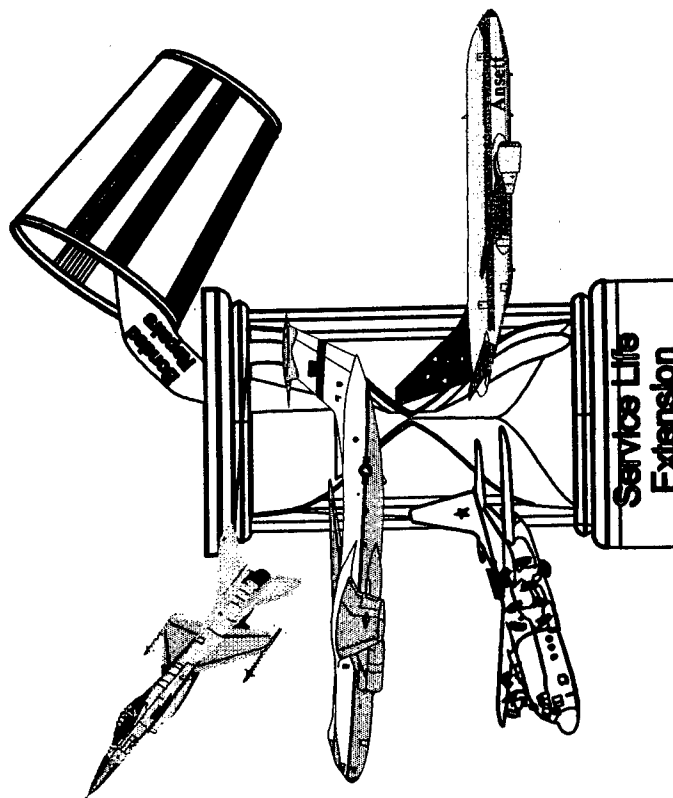
Backcalculation from coupon tests offers a means to reduce cost of generating life-limiting microfeature population data.



Summary

- Corrosion prevention/control begins with proper selection of materials and manufacturing processes along with practices for the continued quality assurance of same.
- Impact of IGC on the fatigue performance of a representative 7xxx Al extrusion has been investigated.
- Applicability of fracture mechanics based lifing tools has been validated to the scale of representative IGC features.
- The implications of IGC on widespread damage (aging aircraft) and monolithic structure (low cost manufacturing) scenarios merits further study.

Advantageous Applications of Bonded Repairs for Corrosion Damage



ASIP 96 Presentation

by

Alan Kerr

Chief Design Engineer

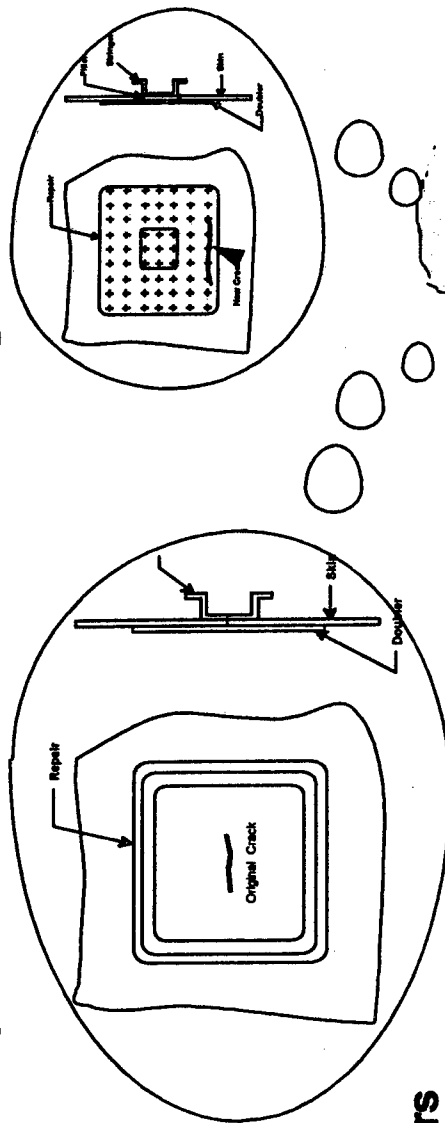
Advanced Repair Technology International

Co-Authored by

Dr. Alan Baker

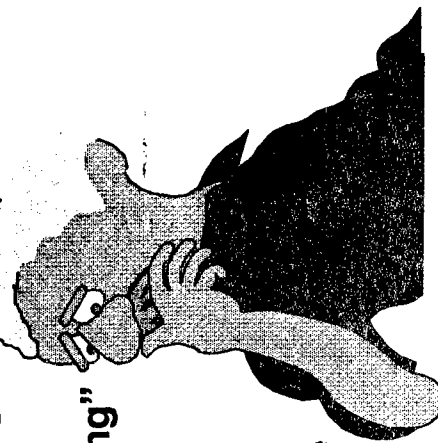
Aeronautical and Maritime Research Laboratories
Australia

We Have a Vision of the Potential for Bonded Repairs and Crack Patching

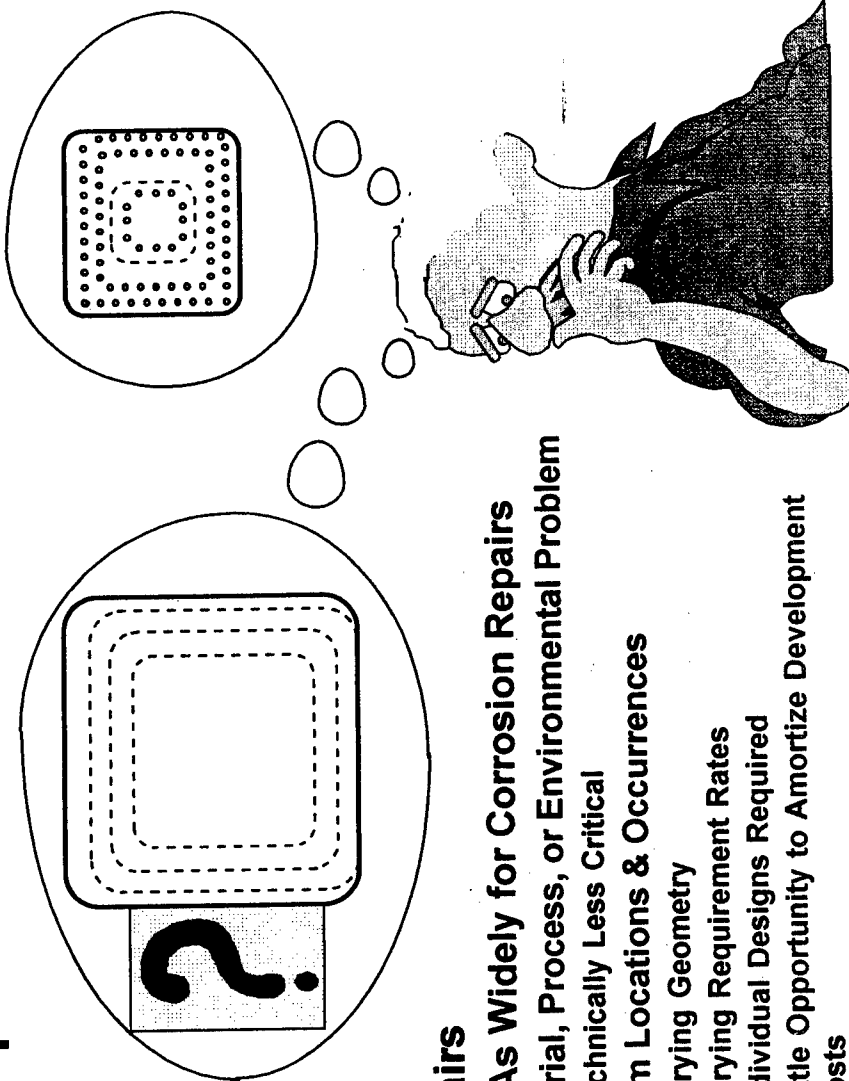


- **Bonded Repairs**

- ◇ **Successful in Service for 20 Years**
- ◇ **Traditional Focus Has Been Towards "Crack Patching"**
 - A Structural Problem
 - Technically More Critical
 - Commonality of Repair Across a Fleet
 - Repairs Individually Justified
 - Development Costs Easily Amortized Across Fleet Wide Applicability
 - Large Economic Gains in Particular Cases



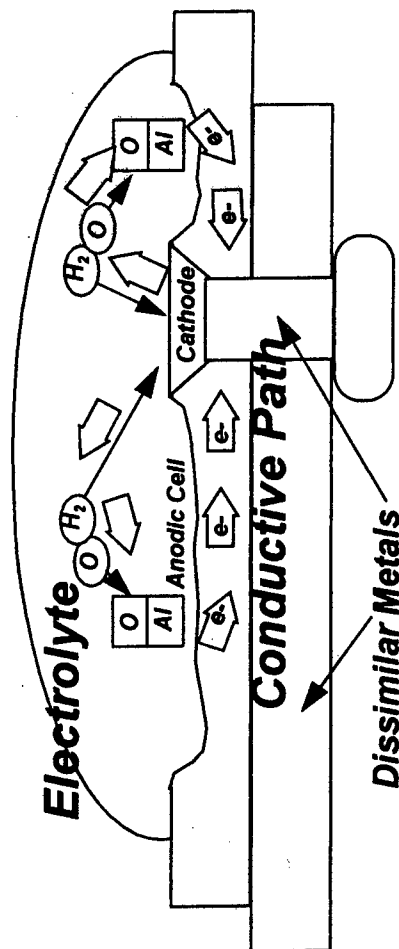
We Don't Yet Have a Vision of the Potential of Bonded Repairs for Corrosion Refurbishment



● Bonded Repairs

- ◇ Not Used As Widely for Corrosion Repairs
 - A Material, Process, or Environmental Problem
 - Technically Less Critical
 - Random Locations & Occurrences
 - Varying Geometry
 - Varying Requirement Rates
 - Individual Designs Required
 - Little Opportunity to Amortize Development Costs

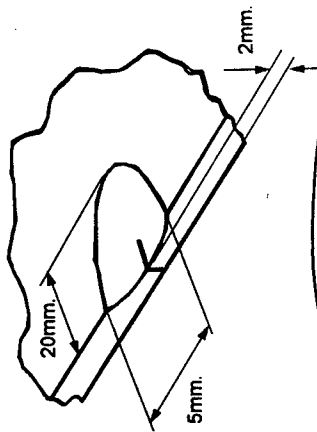
About Corrosion



- **Complex Electro-Chemical Reaction**
 - ◇ Reduces Refined Metals Back to Metal Oxides
 - Natural Laws of Entropy
- **Occurs "Randomly" Throughout the Structure**
 - ◇ A Distinct Difference to Fatigue Failures Which
 - Will Tend to Localize to Similar Places on Different Airframes
- **A More Benign Failure Mode Than Fatigue Problems**
 - ◇ More of a Material/ Process Problem
 - Which Leads to a Structural Problem
 - Rather Than Fatigue, Which Is a Structural Design Problem

Structural Effects of Corrosion

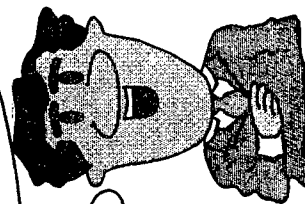
- **Reduced Static Strength**
 - ◇ Loss of Load Bearing Material
 - ◇ Introduction of Stress Concentrations
- **Reduced Fatigue Strength**
 - ◇ Higher Stresses Due to Material Loss
 - ◇ High Stress Intensities at Base of Pits,
- **Re-Occurrence of Corrosion**
 - ◇ After Repair



True!

But We are Changing Rules
And Requiring More of Repairs &
Airframes Than We
Ever Have Before

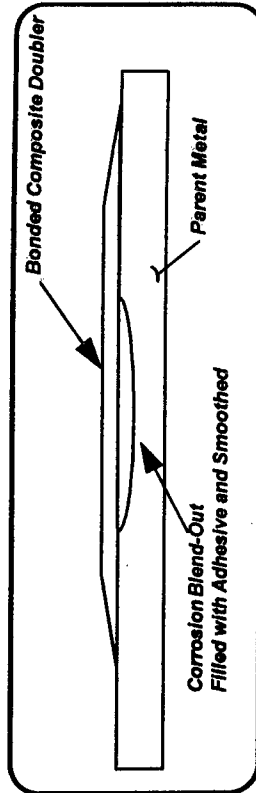
What's New About This?
We've Been Dealing
With This For Years
And Doing Just Fine!



Basic Bonded Repair Concepts

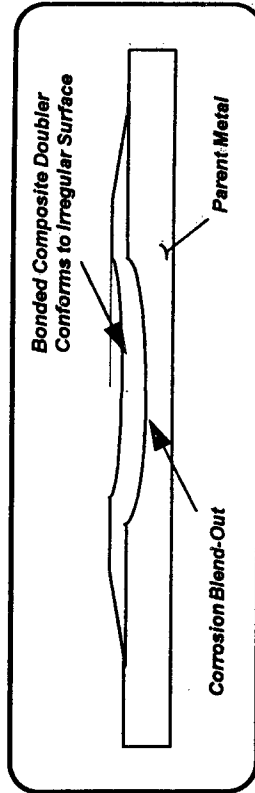
◇ Filled Repairs

- Comparable to Metallic Repairs but Without the Added Burden of Holes Etc.



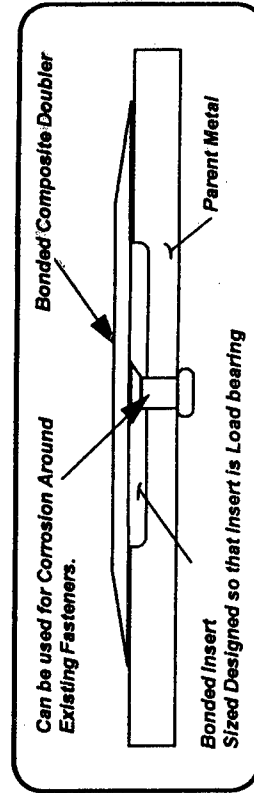
◇ Conformal Repairs

- No Direct Comparison With Conventional Repair Techniques
- Reinforcement Molded to Irregular Shape of Grind-out



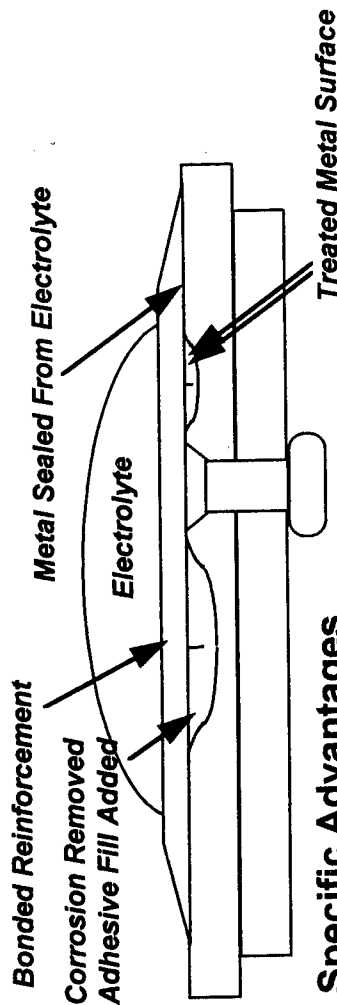
◇ Insert Repairs

- Structural Load Bearing Insert
- Extends the Capability of the Bonded Repair Into Thicker Sections



Conceptual Advantages of Bonded Repairs Applied To Corrosion Damage

- The Same Advantages of We Saw in Crack Patching
 - ◇ Benign Application
 - ◇ Much Improved Inspectability of the Sub Structure
 - ◇ Reduced Stress Concentration
- Corrosion Specific Advantages
 - ◇ Surface Preparation
 - A Closely Controlled Corrosion Inhibiting Process
 - ◇ Complete Sealing of the Repair Breaking Electrical Path
 - ◇ Ability to Conform to Irregular Surfaces Left After Grind-outs
 - ◇ No Added Potential for Galvanic Action With Correct Choice of Reinforcement

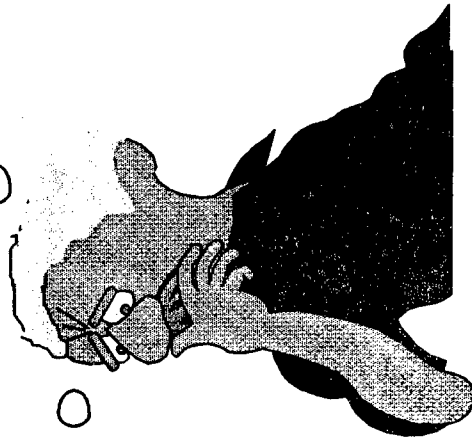


Concerns !

**Fatigue Life
of Corroded
Area After
Bonding?**

**Behavior of
corroded
Surface After
Bonding ?**

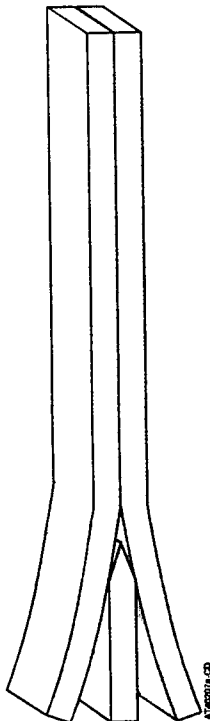
**Maintainability
of a Bonded
Repair?**



R

ARTI 000370C

Behavior of Corroded Surface After Repair Application



- **Concerns**

- ◇ Possible to Achieve an Acceptable Bond
- ◇ Long Term Durability of Repair

- **AMRL Wedge Test Results**

- ◇ Repairs Applied Directly Onto a Surface Conditioned in a Salt Spray Environment
- ◇ Used Only the Standard Grit Blast/Silane Surface Preparation
- ◇ Results Show No Discernible Difference in Behavior
(Continuing Research With Results Still to Be Published)

- **Reoccurrence of Corrosion**

- ◇ Prevented Because of the Sealing Effects
- ◇ Greater Ability to Detect Corrosion Under Bonded Repair
 - Using Standard NDI Processes

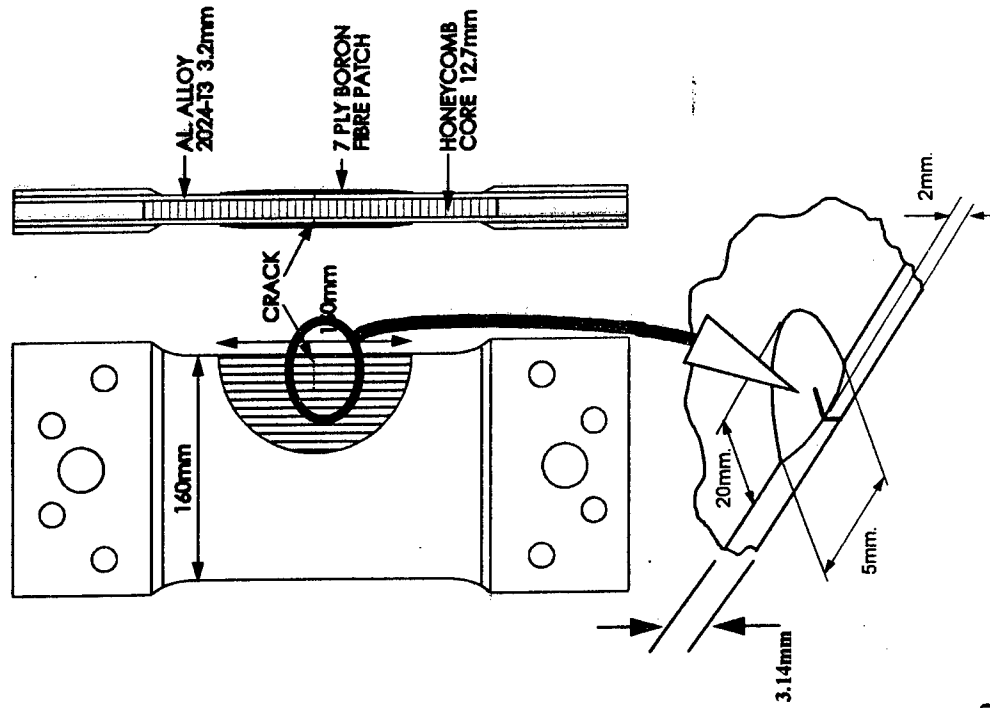
Fatigue Life Behavior

● Concerns

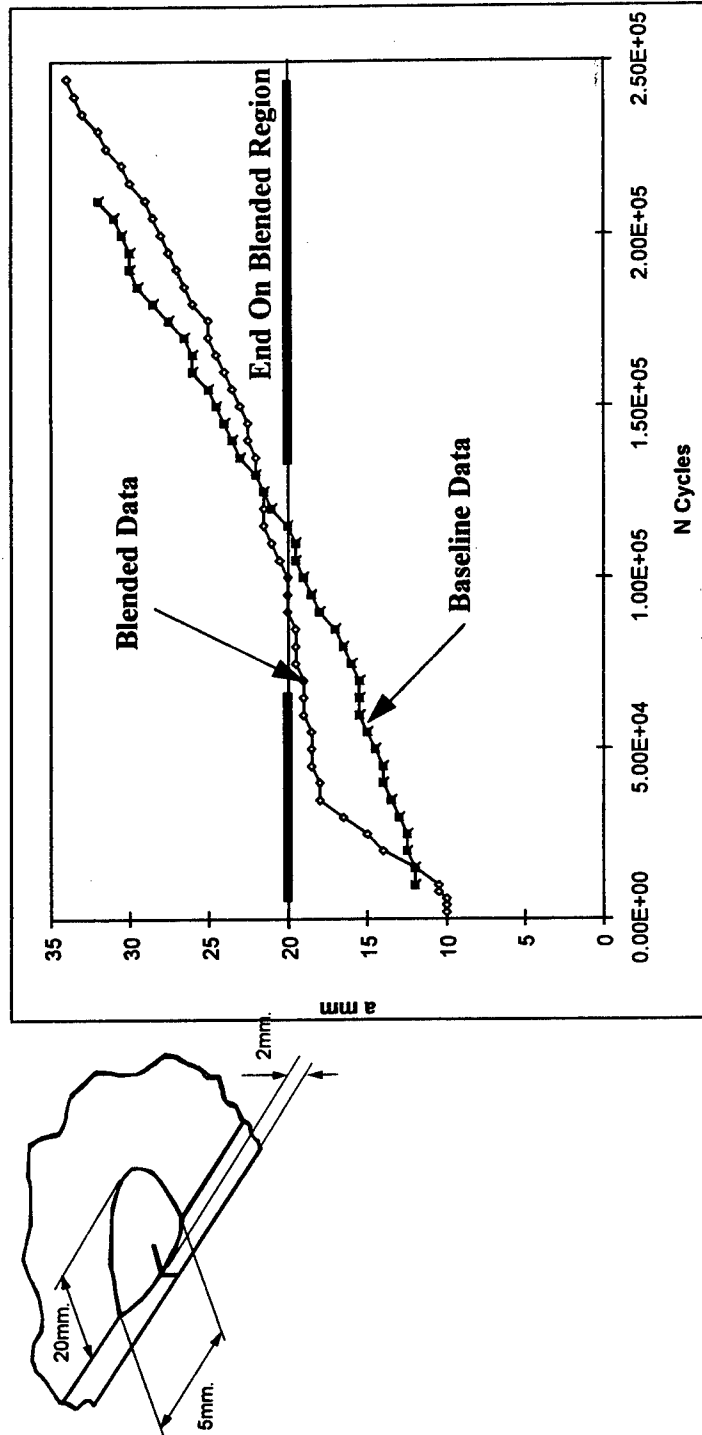
- ◇ Crack Growth Behavior in Blended Areas With Reinforcements
- ◇ Fatigue Behavior Caused by Isolated Pit Left Behind
 - Initiate Crack
 - Potential for Multiple Cracks and MSD

● AMRL Test Results

- ◇ Crack Growth Underneath Reinforced Corrosion Grind-Out
- ◇ MSD on Riveted Lap Joints

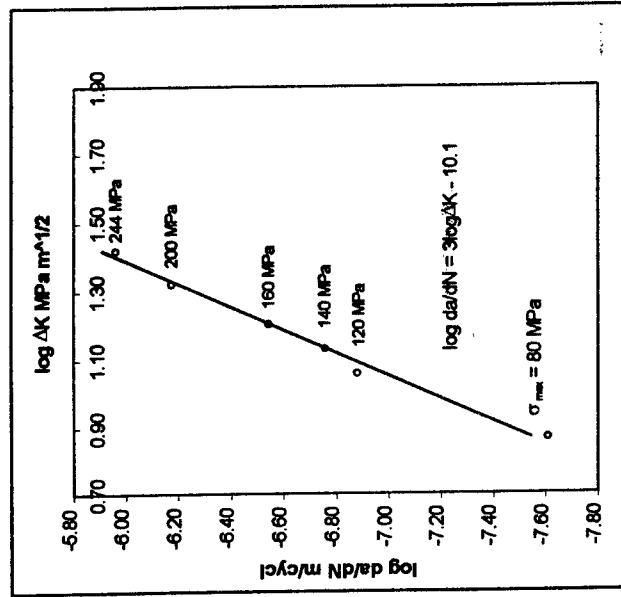
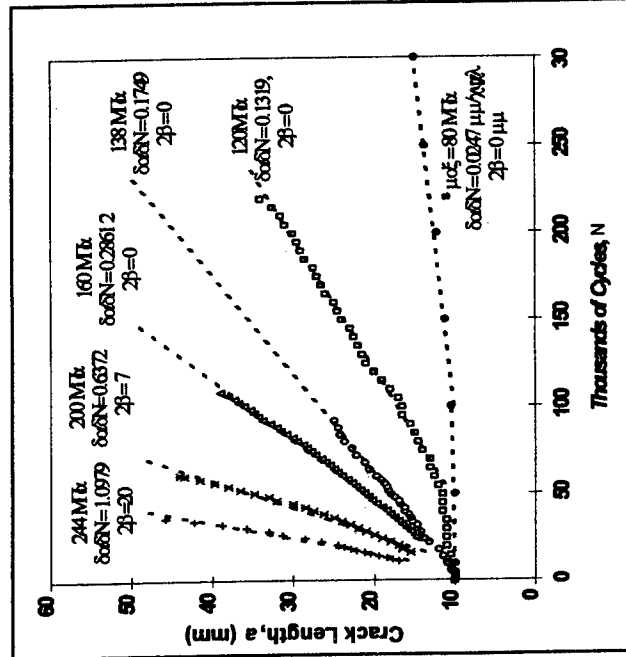


Crack Growth Test Results



- Crack Growth Rate Effected Only in The Blend-Out Region
- Stable Predictable (Comparable) Crack Growth Outside of Blend Region

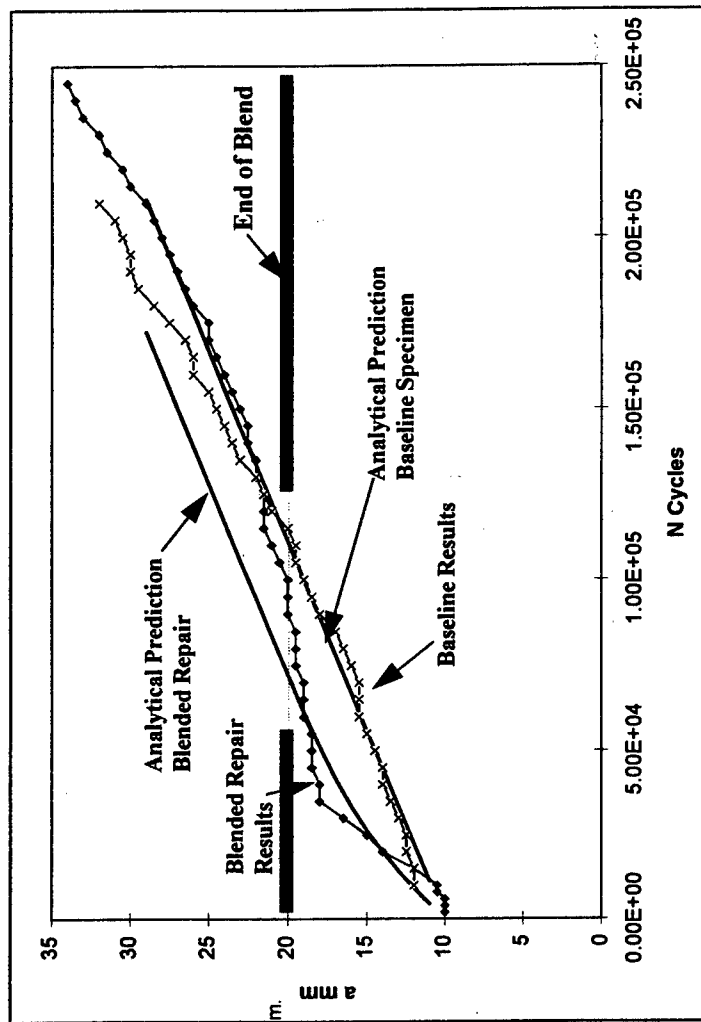
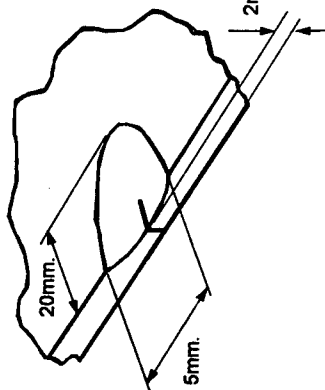
AMRL Crack Growth Prediction Studies



- Crack Growth Independent of Crack Length

$$a = A_R \int_0^N (\Delta K_\infty)^{n_R} dN$$

Blend-out Crack Growth Results



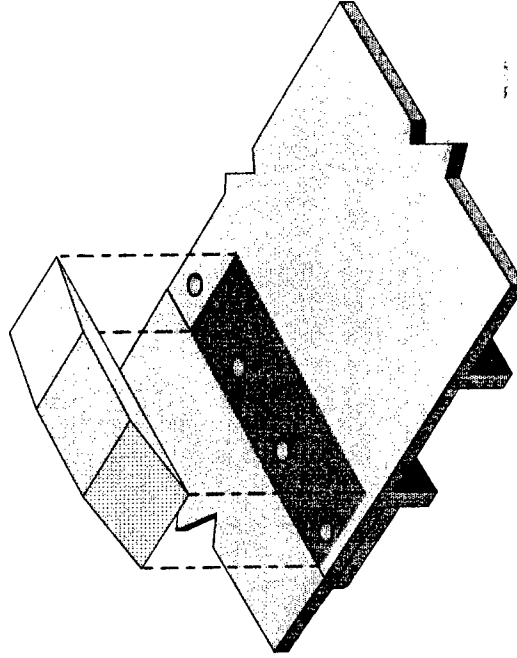
- Simplified Predictive Methods

- ◇ Based on Stress Levels in Metal With Blend
- ◇ Correlate with Trend

Maintainability of Bonded Repairs

- The same as for crack patching

- ◇ C-130
 - 20 years in service
- ◇ B-767 keel beam repair
 - > 8,300 hrs (5,900 ldgs)
- ◇ B-747 demonstrator repairs.
 - 20155 hrs (3692 cycles)
- ◇ Routine Inspections
 - All with no evidence of failure apart from some minor erosion damage



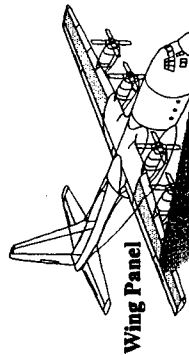
Case Study #1 : C-130 Outer Wing Planks

◆ Problem:

- Stress Corrosion Cracking in Stiffeners
- Induced By Fasteners

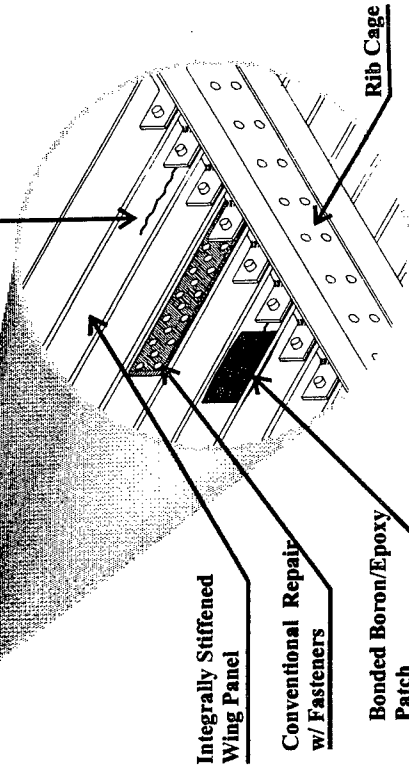
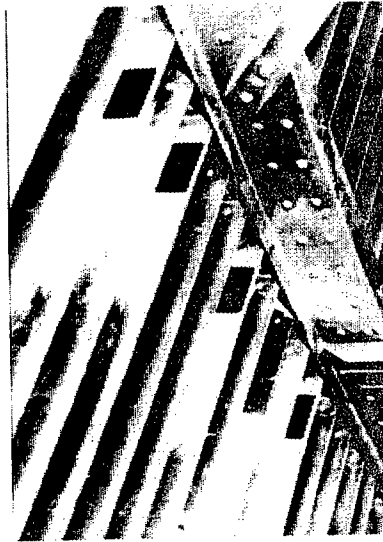
◆ Solution:

- Boron/Epoxy Bonded Repair Applied Inside the Wet Wing
- Over 1000 Repairs Applied With No Crack Growth in 20 Years
- Estimated Savings \$67 Million



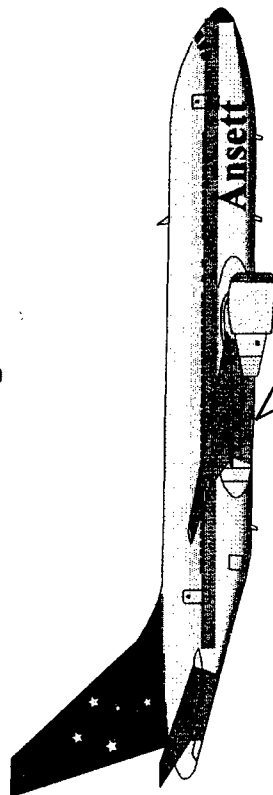
Stress Corrosion Cracking

Completed Repair

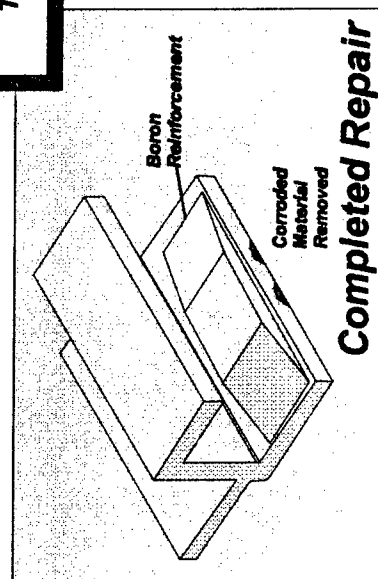


Case Study #2 : B-767 Keel Beam

- ◆ Problem:
 - Severe Pitting Corrosion
- ◆ Solution:
 - Boron/Epoxy Reinforcement
 - Beam Replacement the Only Alternative



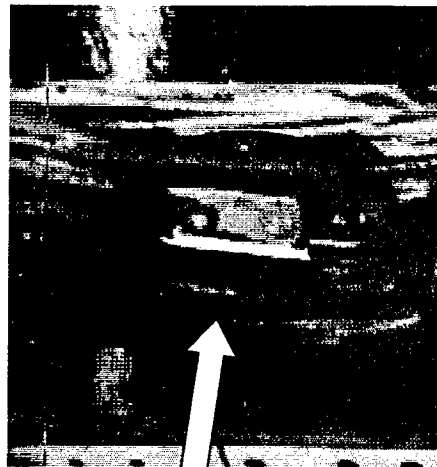
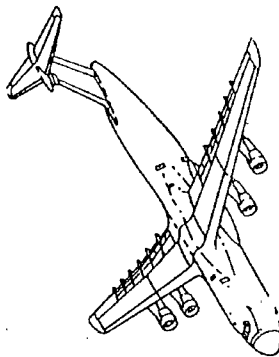
One Day Downtime
Vs
Three Weeks



Case Study #3 : C-5 Horizontal Stabilizer Corrosion

◆ Problem:

- 5 Corrosion Grind-outs

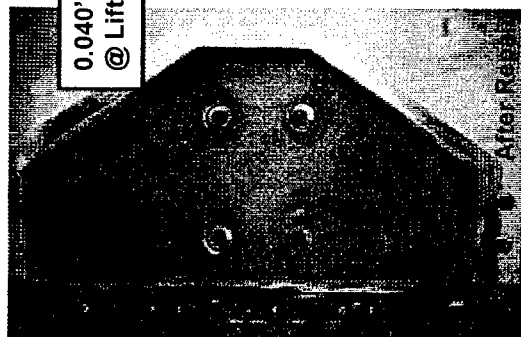


Before

Grind Out Through Skin
@ Lift Point

0.040" Grind-out
@ Lift Point

Surface Grind-outs
0.030" 3 Places

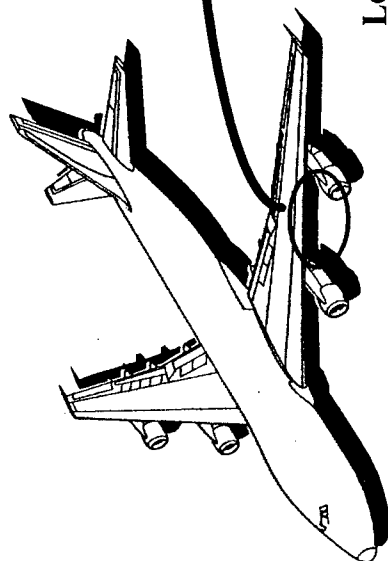


After Repair

Solution:

- 5 Boron/Epoxy Bonded Repairs
- Design, and Installation in 10 Days

Case Study #4 : B-747 Lower Wing Skin



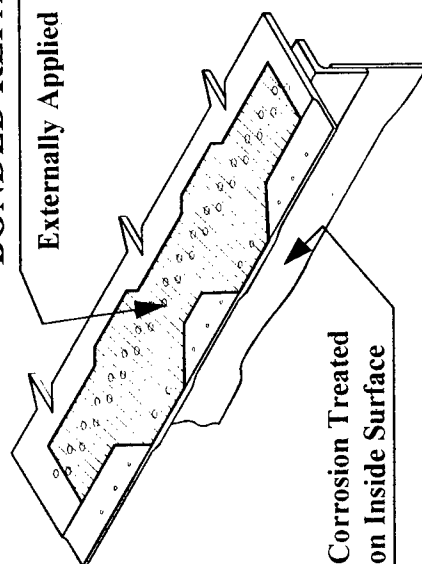
Front Spar

Corrosion

Lower Wing Skin

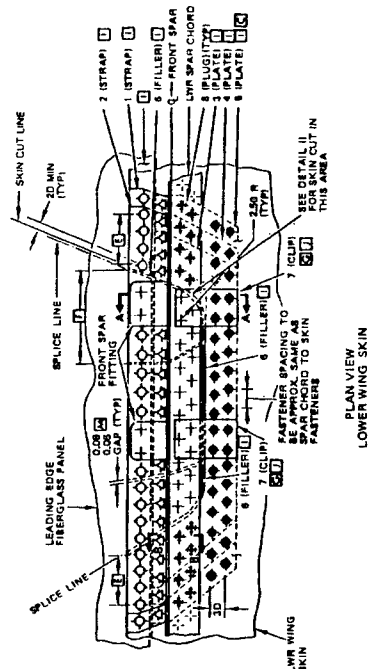
BONDED REPAIR

Externally Applied



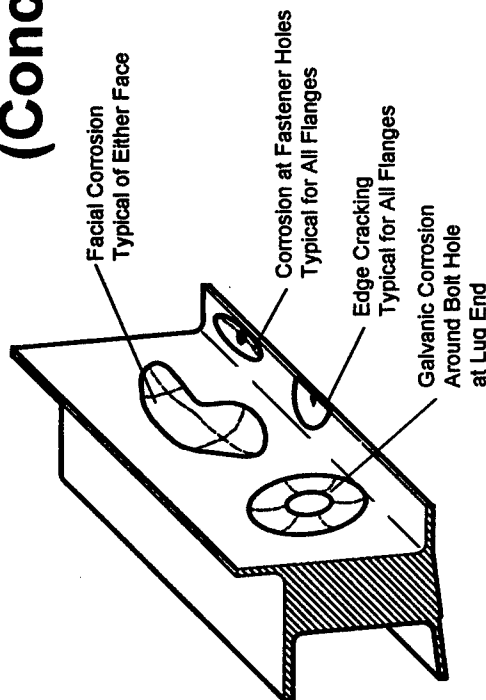
Corrosion Treated on Inside Surface

View Looking Onto Lower Wing Skin

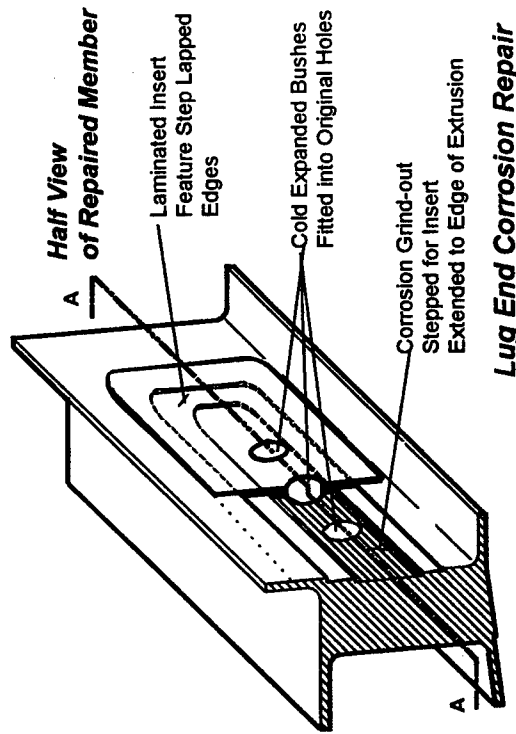


SRM Repair

Case Study #5 :B707 Keel Beam Repair (Concept)



General Damage Description on Keel Beam Chord



Lug End Corrosion Repair

- **Problem**
 - ◇ Corrosion Beyond Allowable Limits
- **Solution**
 - ◇ Bonded Insert Repair
 - ◇ In-Situ Application

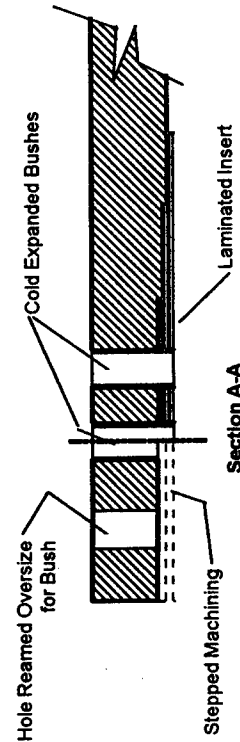
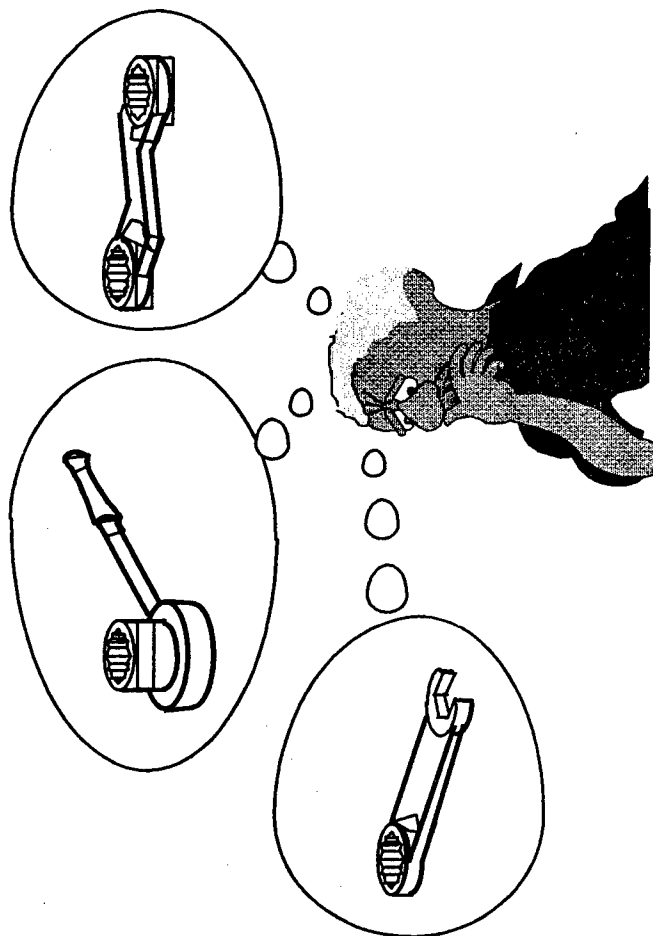


Figure 3-8

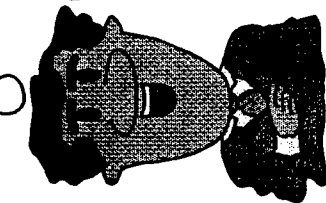


Choices!

- Each of the Tools Does Essentially the Same Operation
- Ideally The Choice Is Based on Advantages
- Practically Choice Is Based
 - ◇ Convenience , Familiarity, & Availability
- Similarly, the Choice of Repair Technique Is Based On
 - ◇ Confidence, Familiarity, & Availability

Confidence A Low Risk Approach

Comfortable
With Use on Secondary
Structure

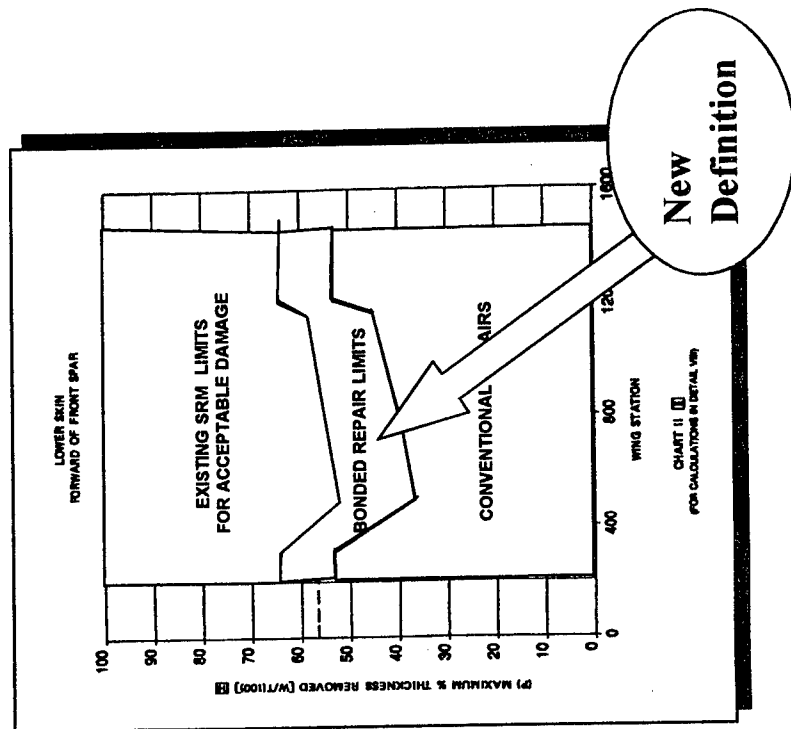


But Maximum Gains
With Use on Primary
Structure

- Incremental Extension
of the SRM "Grind-
Out" Limits

- ◇ Define "Repairable Using Bonded
Repairs" Band
- ◇ Level of Justification Greatly
Reduced From "Crack Patching"
 - Good Response Time
- ◇ Opportunity to Build Confidence
Through Use
- ◇ Economic Gains
 - Even With This Cautious
Approach

ARTI Proprietary



Familiarity

- **Will Come Through Use and Exposure**
- **Technology Accepted By Airworthiness Bodies & Design Authorities**
 - ◇ **Generic Design Principals**
 - ◇ **Revised Allowable/Repairable Damage Limits**
- **Technology Transfer Programs**
 - ◇ **CRMS**
 - ◇ **CRAS**
- **Training Programs**
 - ◇ **Design**
 - ◇ **Application**
- **RAAF Has Worked to Build This Situation**
 - ◇ **Experience and Confidence with the Technology Over the Last 20 years**

Availability

- Technology is Available and In Use
 - ◇ WR-ALC
 - ◇ OO-ALC
 - ◇ Commercial Groups
 - ARTI, Boeing, Lockheed, Northrop
- Need For Co-Ordination and Standardization Being Addressed Through Wright Labs Initiatives
 - ◇ Acceptable Design Standards
 - ◇ Acceptable Application Standards

Conclusion

- **Bonded Repairs**
 - ◇ Advantages Which Can Be Useful For Addressing Corrosion Damage
 - ◇ A Strong Baseline Group Of Existing Examples to Provide Confidence
 - ◇ Current Levels of Concern
 - Addressable With Existing State of the Art Data
 - ◇ Need More Applications to Build Familiarity and Develop Availability
- **Bonded Repairs**
 - ◇ Are Not A Panacea for Every Repair Situation
 - ◇ Another Resource to Be Considered
 - ◇ Vast Potential
 - Limited Only by Lack of Innovation



National Research
Council Canada

Conseil national
de recherche Canada

NRC - CNRC

***Damage Tolerance Implications of Corrosion
Pillowing on Fuselage Lap Joints***

N.C. Bellinger and J.P. Komorowski*
Structures, Materials and Propulsion Laboratory
National Research Council Canada

* presenter

Canada

1996 USAF Structural Integrity
Program Conference
3-5 December, 1996
San Antonio, Texas

Acknowledgments

- This work had been funded by
 - » USAF nondevelopmental Airlift Aircraft program (NDAA), Federal Aviation Administration (FAA), Transport Canada (TC) and National Research Council Canada (NRCC)

NRC-CNRC

Outline of Presentation

- **Background**
- **Objectives**
- **Finite Element Technique**
- **Model Verification**
- **Finite Element Results**
- **Specimen Teardown**
- **Discussion**
- **Conclusions**

NRC-CNRC

Background

- **1995 ASIP presentation:**
 - demonstrated finite element technique for corrosion pillowing simulation,
 - results indicated that a significant increase in stress occurred in a lap joint caused by the volumetric increase associated with corrosion by-products.
- **Indicated the need for damage tolerance study of the problem.**

NRC-CNRC

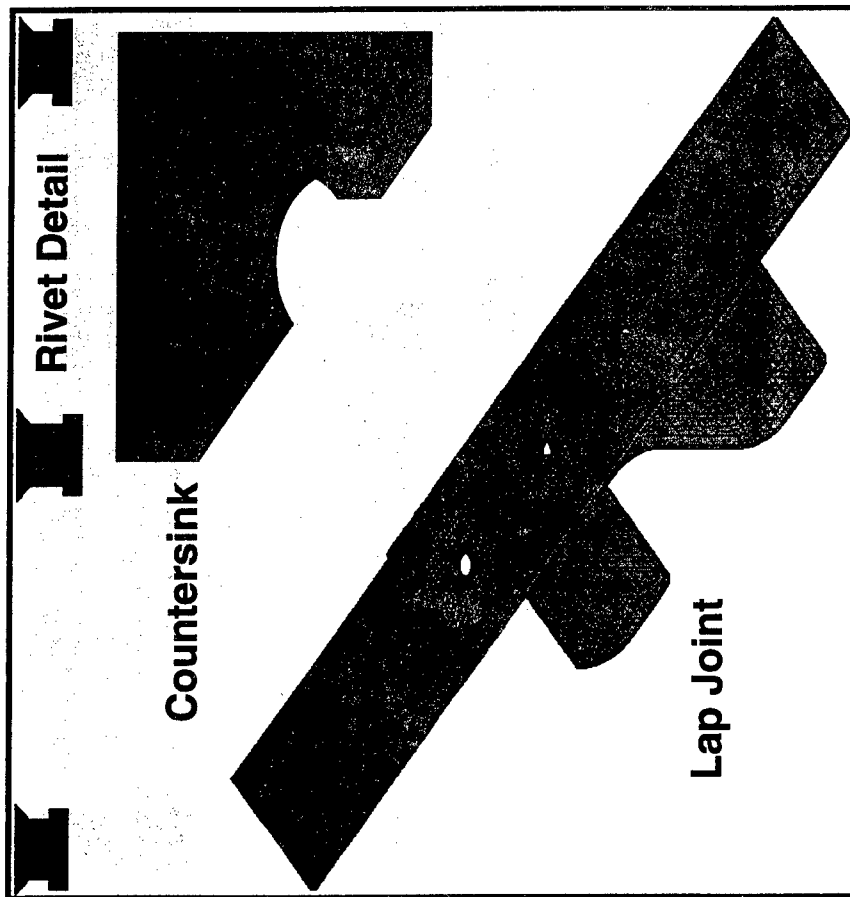
Objectives

- To use finite element techniques to determine the effect of pillowings on the stress distribution in fuselage lap joints.
- To verify the numerical analysis by carrying out simulated corrosion tests.
- To evaluate the effect of these stress changes on structural integrity/damage tolerance.

NRC-CNRC

Finite Element Model

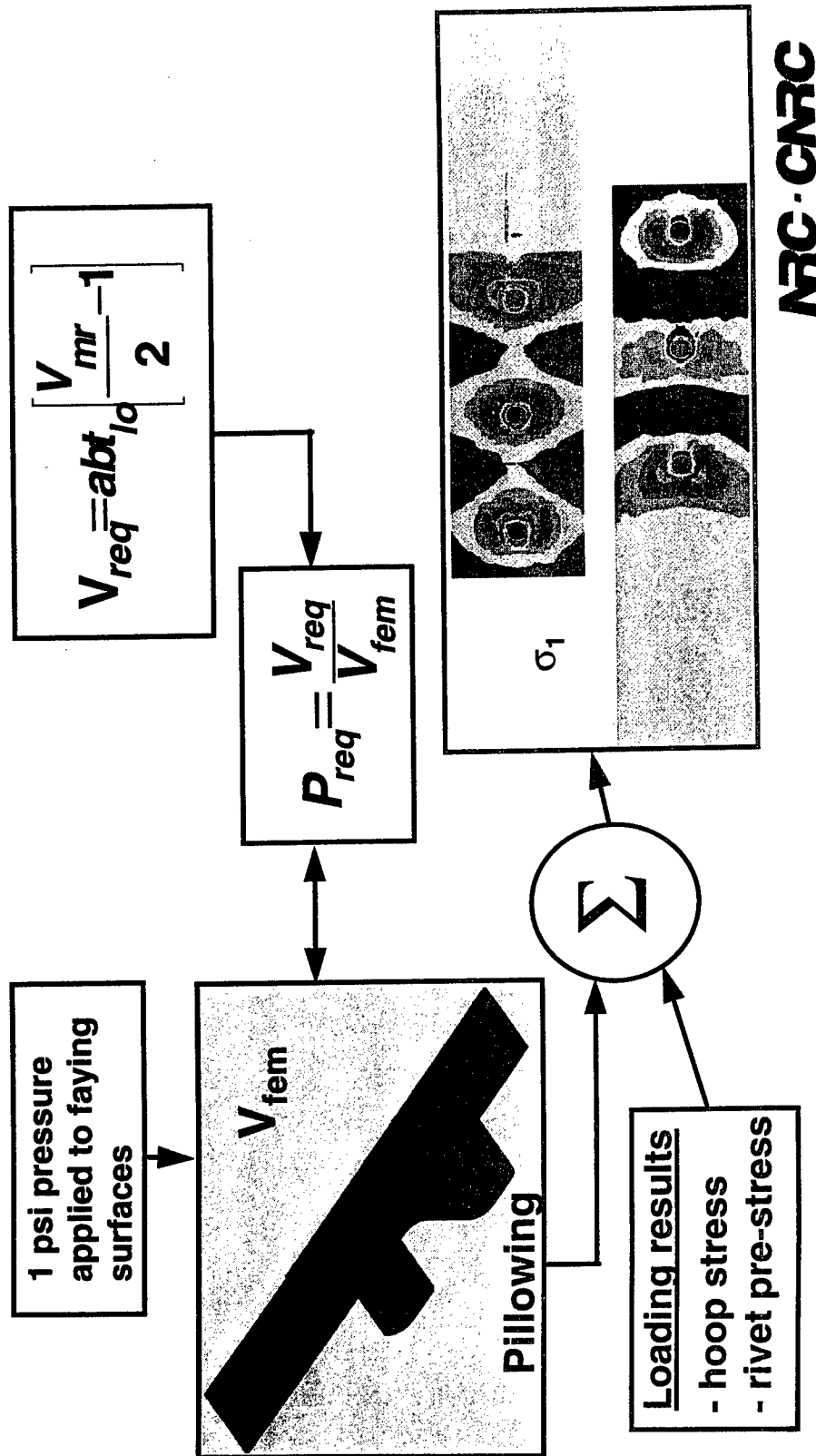
Stress Analysis



- 3D finite element analysis.
- Rivet/skin interaction simulated using nonlinear gap elements.
- Three separate loading conditions:
 - 1) hoop stress
 - 2) rivet pre-stress
 - 3) corrosion pillowing

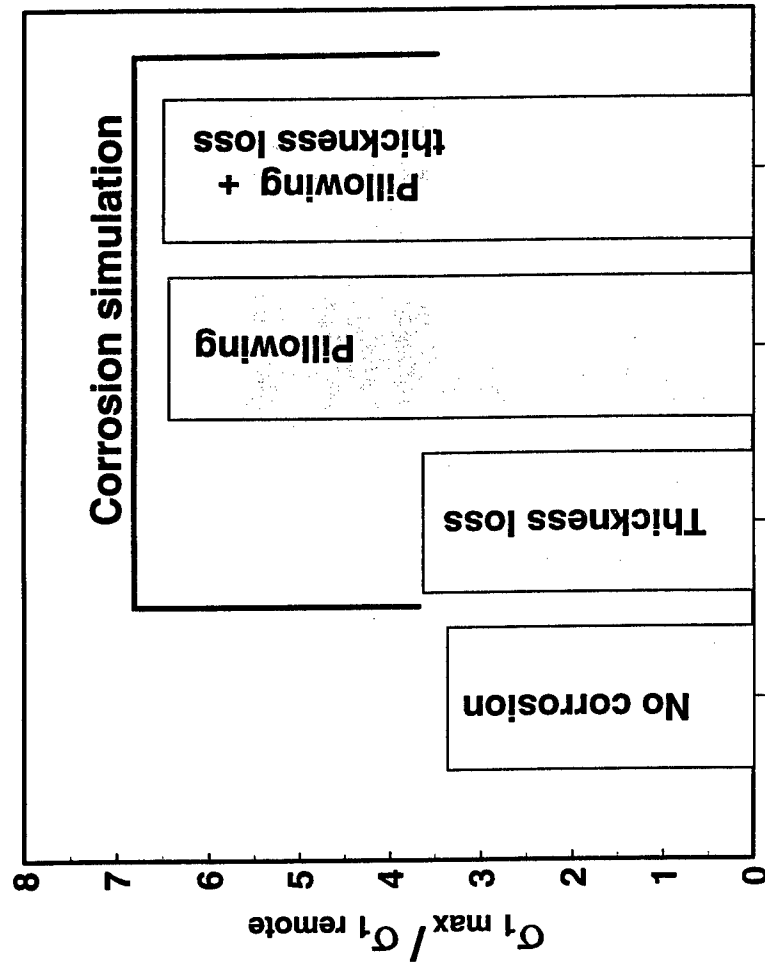
NRC-CARC

Finite Element Technique



Effect of Pillowing and Thickness Loss

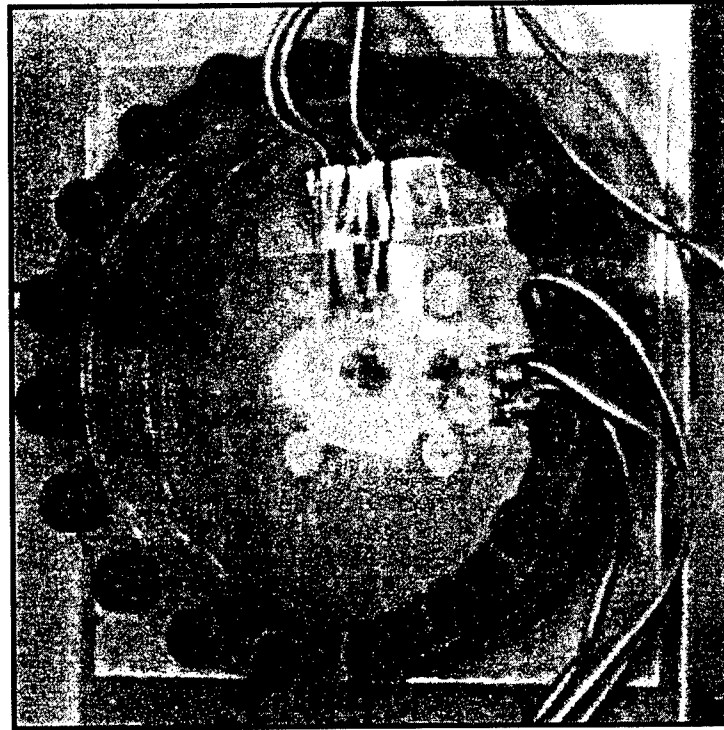
10% material loss



- Finite element models generated with and without thickness loss.
- Results show significant increase caused by pillowing as compared to thickness loss effect.

NRC · CNRC

Corrosion Pillowing Model Verification

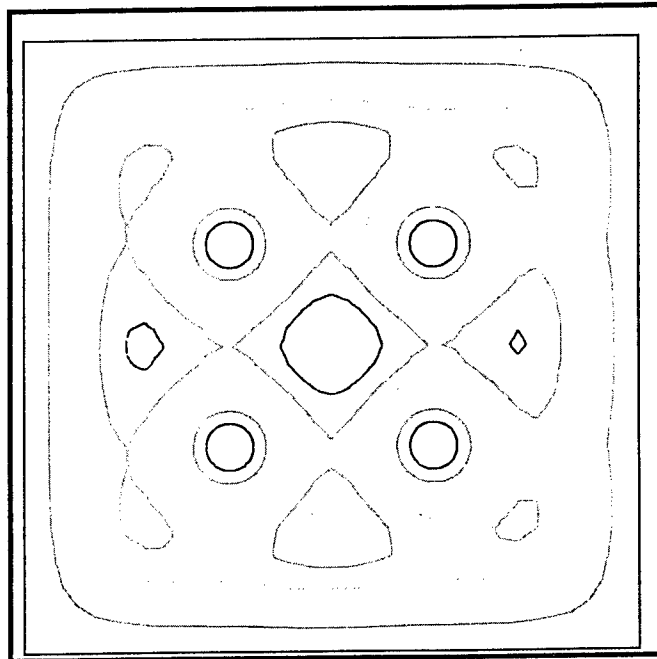


- four countersunk rivets
- 0.040" thick top skin
- hydraulically pressurized
- strain gauged
- shadow moiré

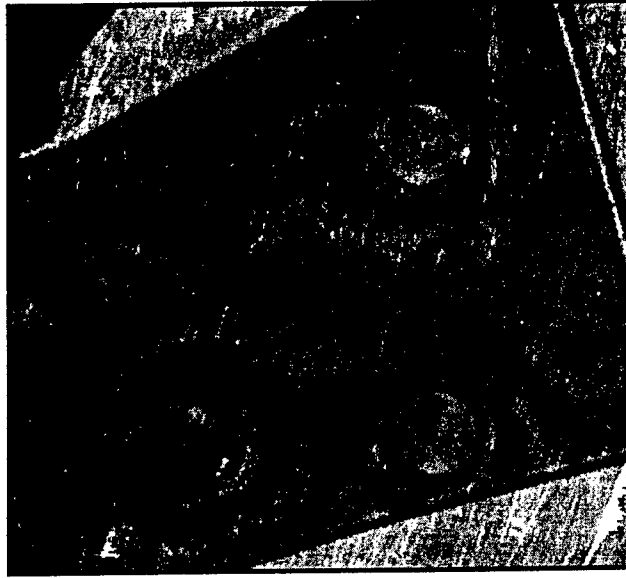
NRC · CNRC

Corrosion Pillowing Model Verification

Contour plots



Finite Element Results

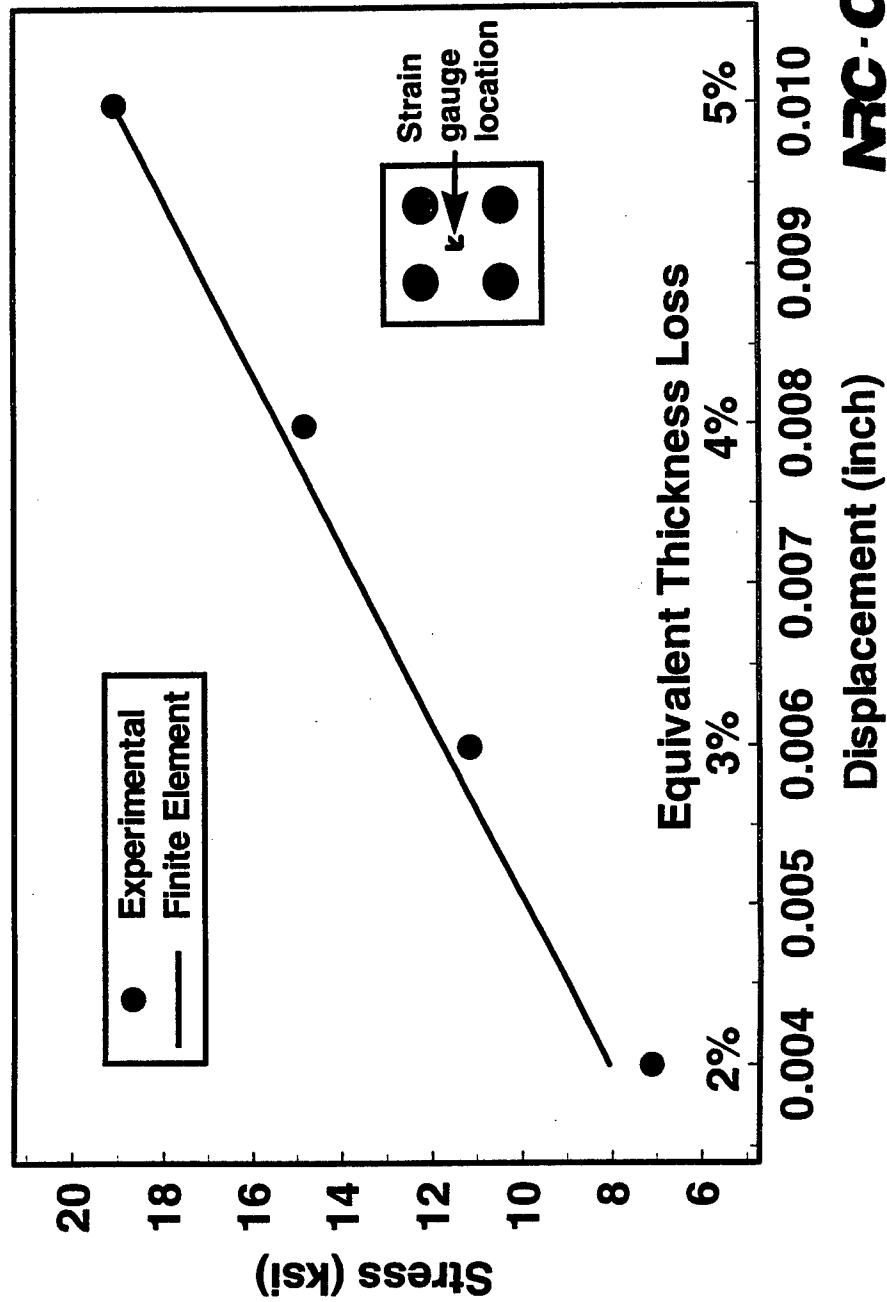


Shadow Moiré

NRC-CNRC

Corrosion Pillowing Model Verification

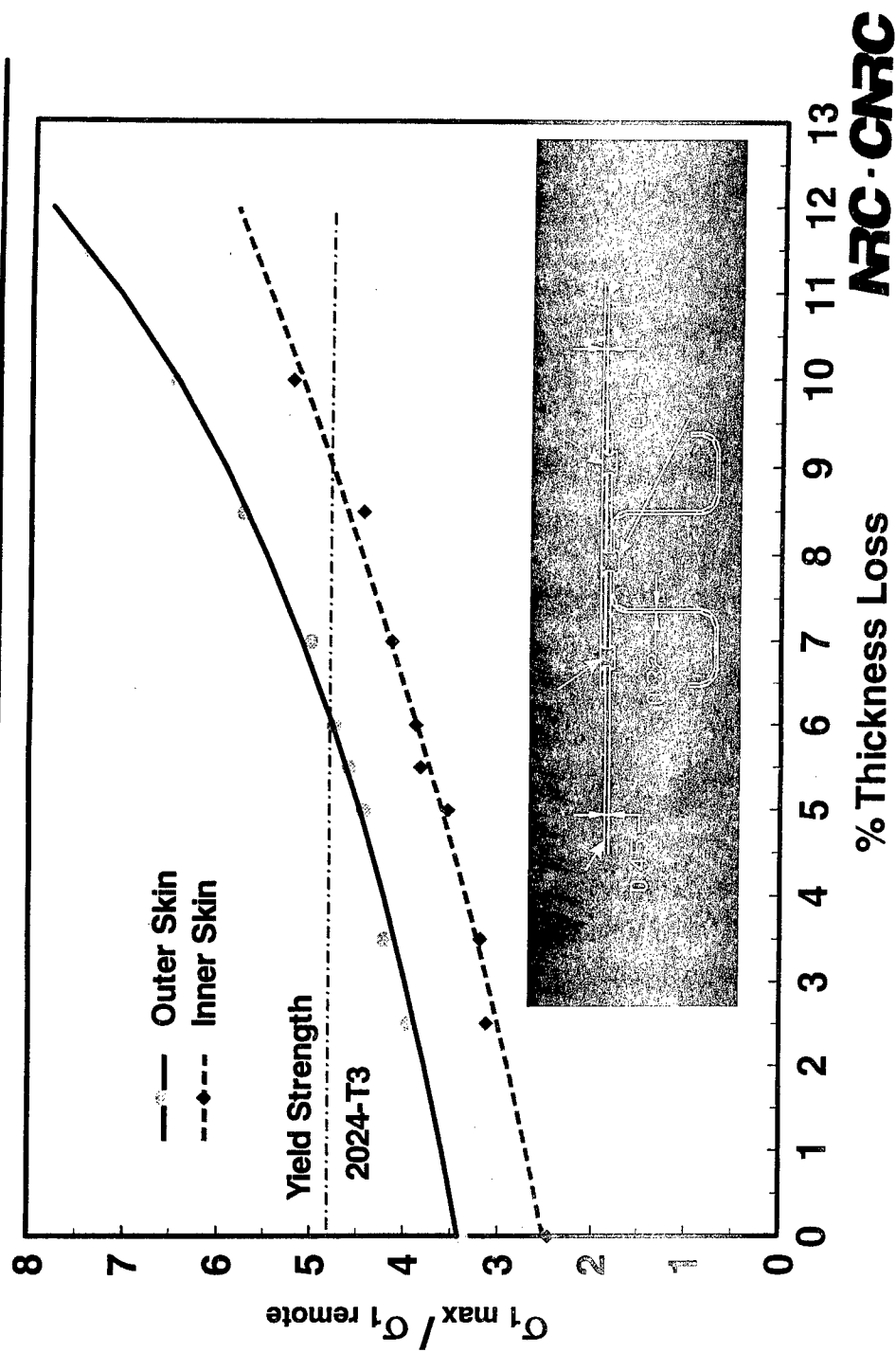
Outer surface results at maximum pillowing deflection



NRC-CNRC

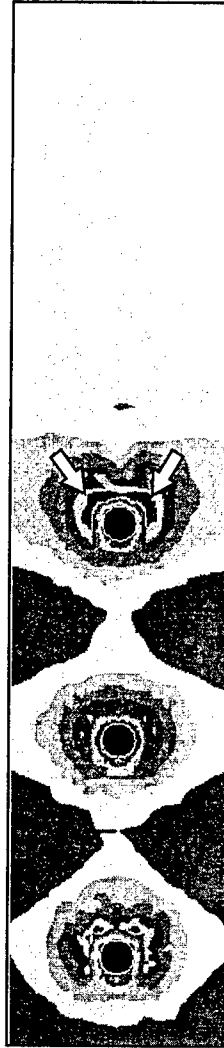
Effect of Pillowing

Two layer lap joint - upper rivet row

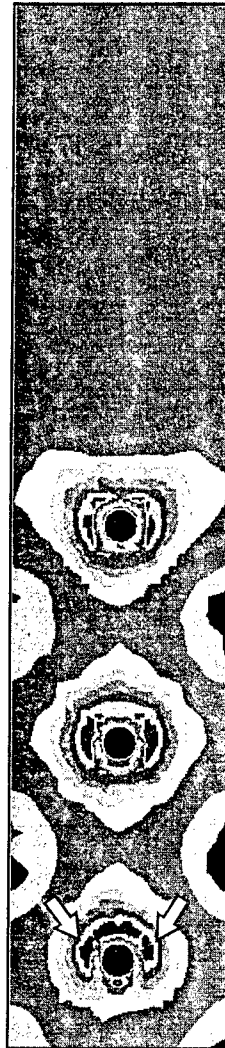


Location of Maximum Stress

2.5% Thickness loss



6% Thickness loss



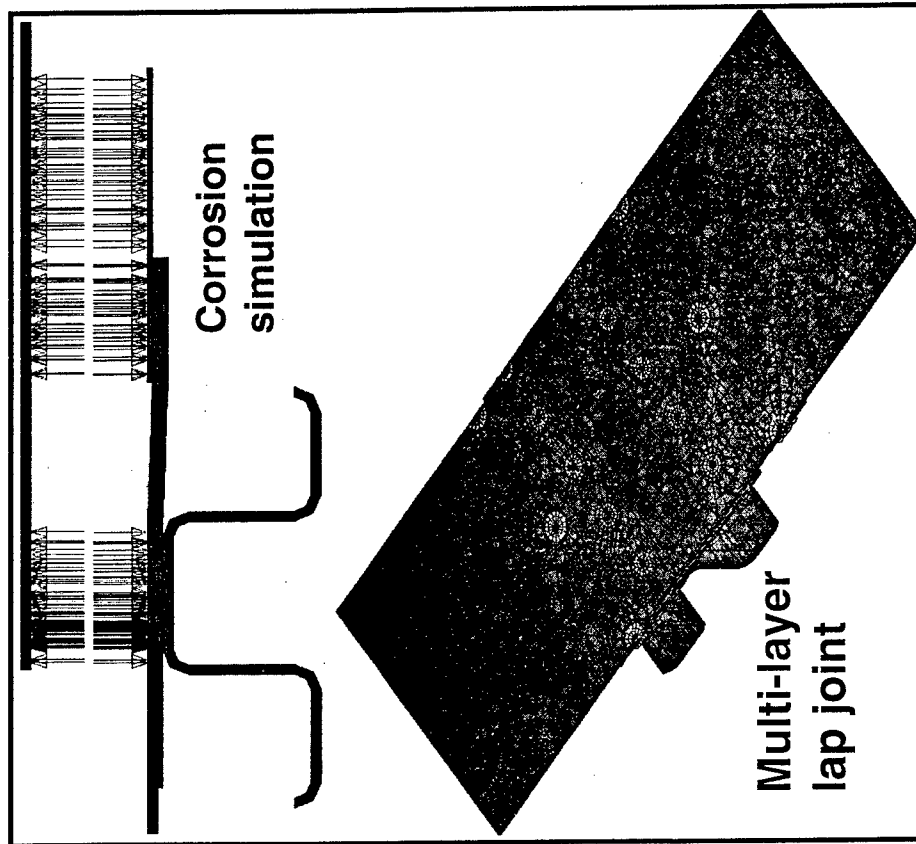
Arrows indicate location of maximum stress

- Depending on location of corrosion and severity of pilling in rivet area, maximum stress in joint may shift rivet holes or occur in other skins.

NRC - CNRC

Finite Element Model

Stress Analysis - Multi-layer lap joint

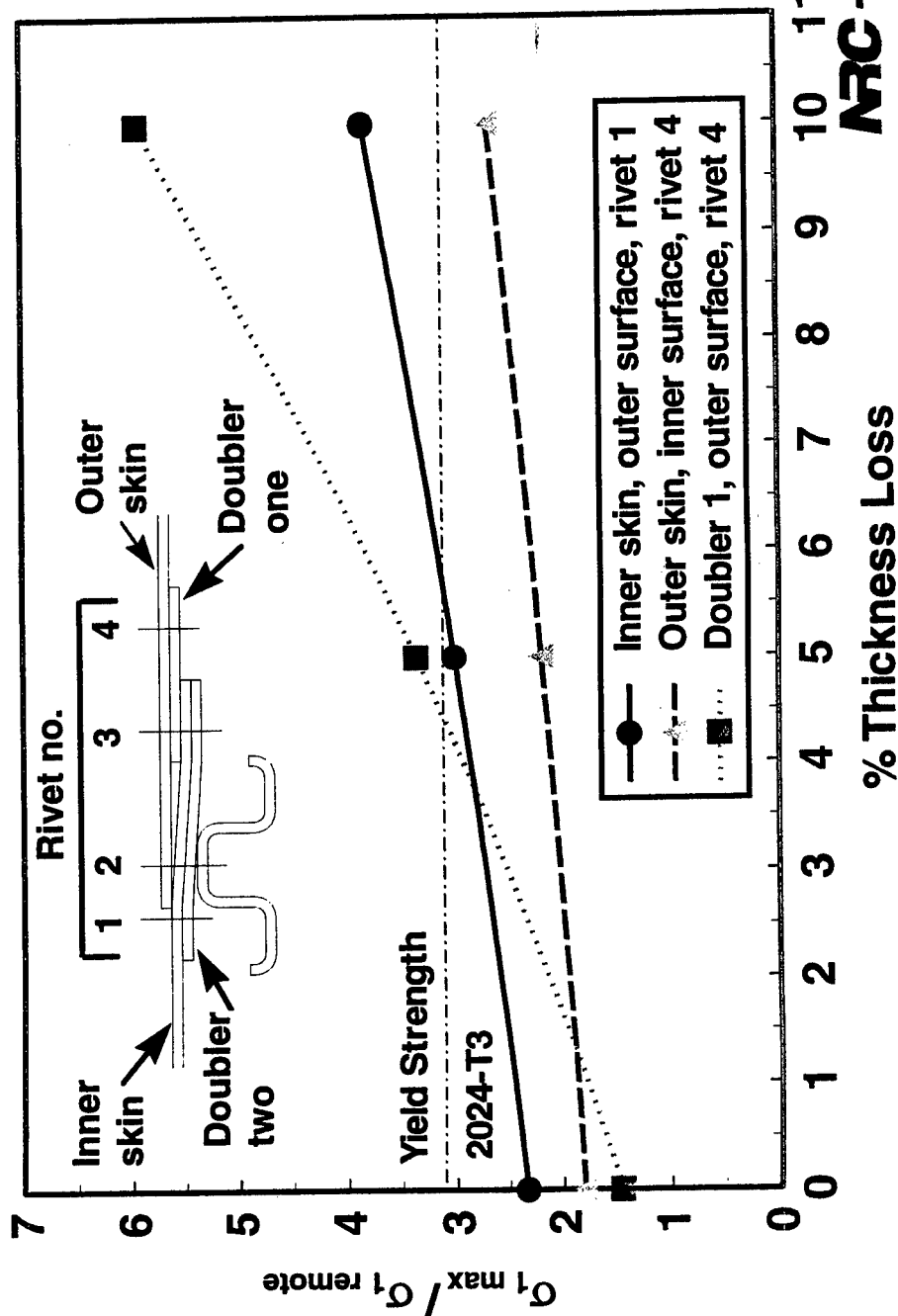


- 3D finite element analysis.
- Rivet/skin interaction simulated using nonlinear gap elements.
- Three separate loading conditions:
 - 1) hoop stress
 - 2) rivet pre-stress
 - 3) corrosion pillowing

ARC-CARC

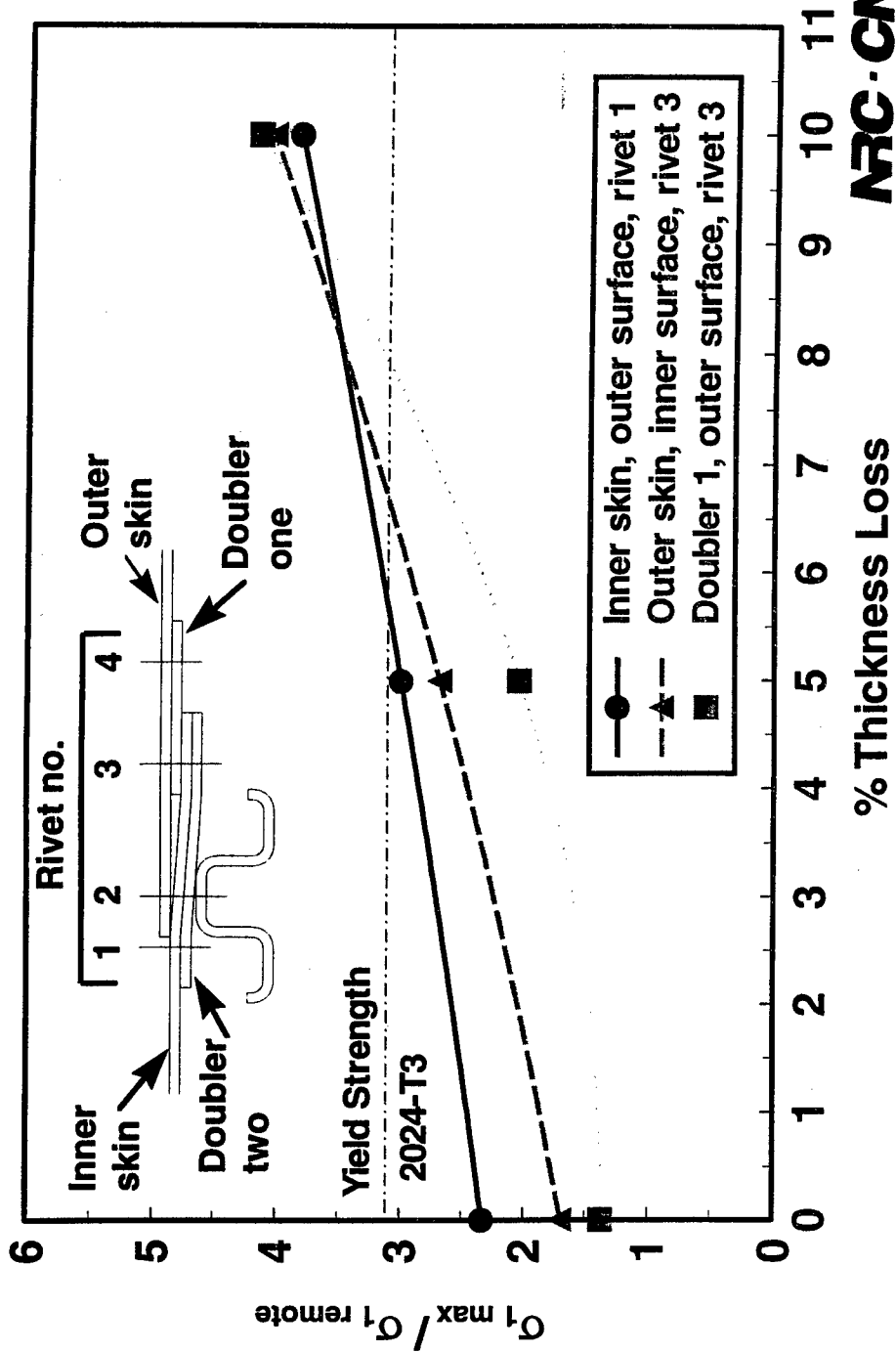
Effect of Pillowing

Multi-layer lap joint



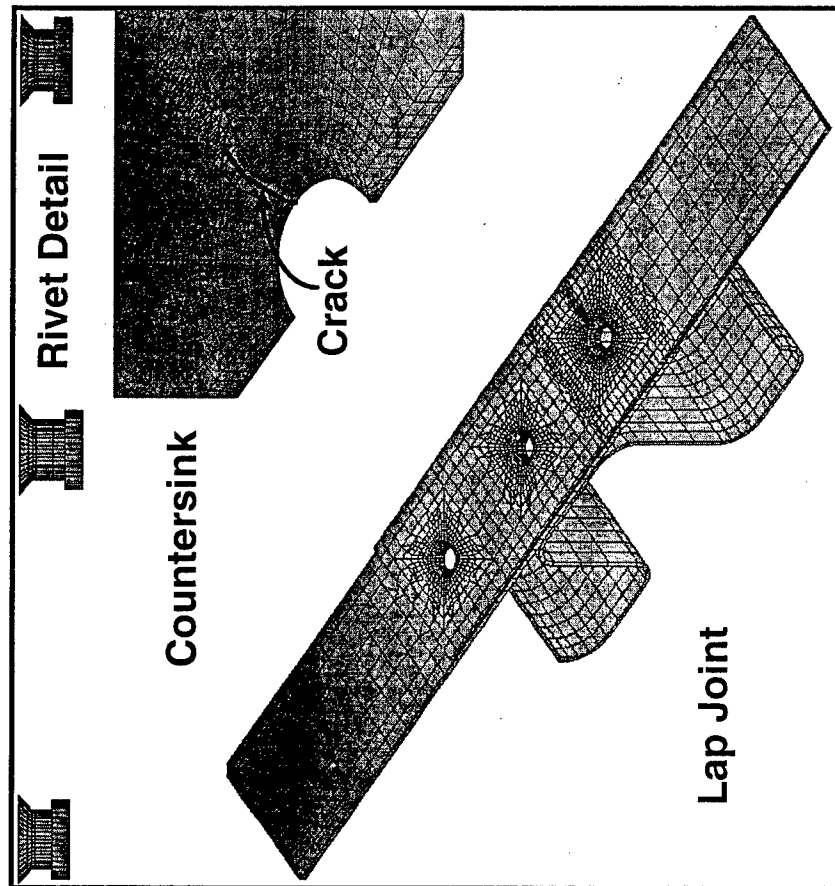
Effect of Pillowing

Multi-layer lap joint



Finite Element Model

Fracture Mechanics Analysis



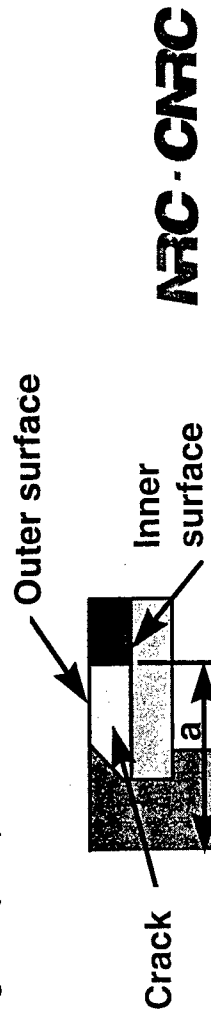
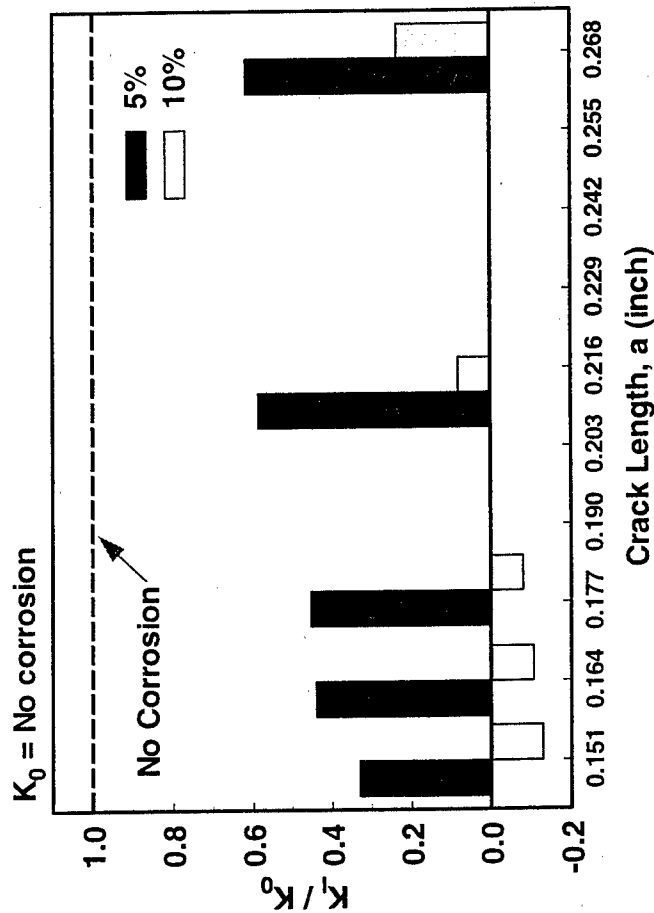
- Stress analysis model except for:
 - Second order elements in area of critical rivet row.
 - Mid-side nodes at crack tip moved to quarter point to simulate stress singularity.

NRC-CNRC

Fracture Mechanics Analysis

Stress intensity for crack edge along outer surface

- Stress intensity for crack edge along outer surface decreases as corrosion pilling increases.
- Pilling has significant influence on crack in hole vicinity:
 - may arrest crack growth if present before corrosion.

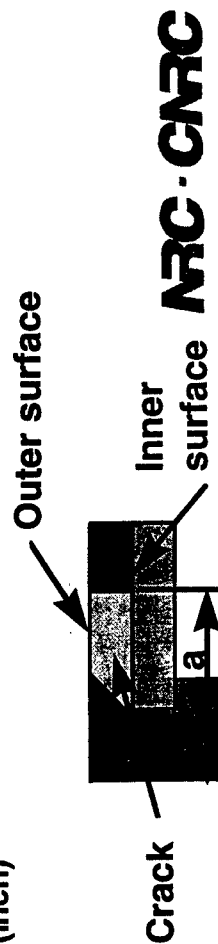
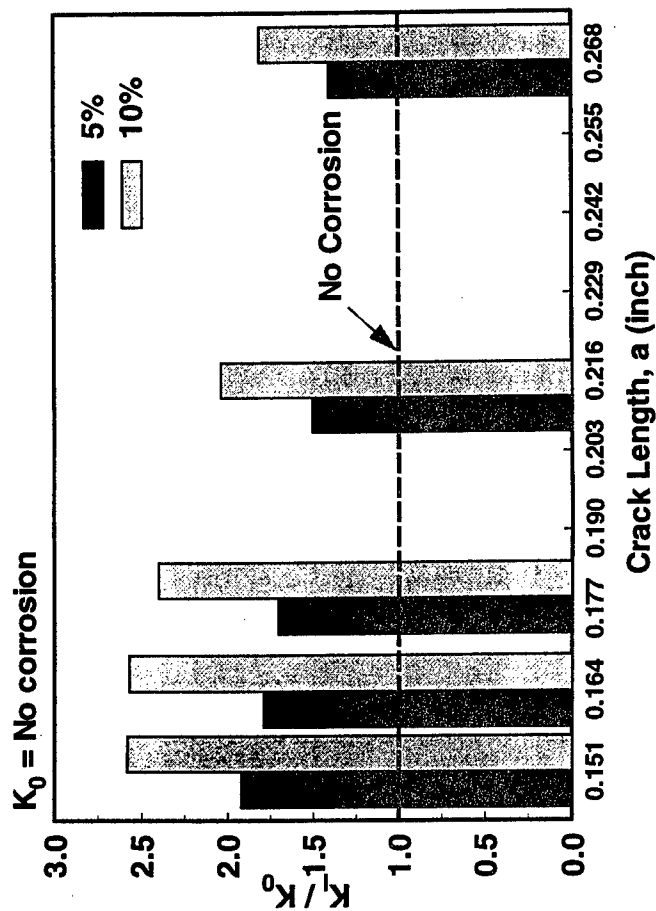


ARC-CARC

Fracture Mechanics Analysis

Stress intensity for crack edge along inner surface

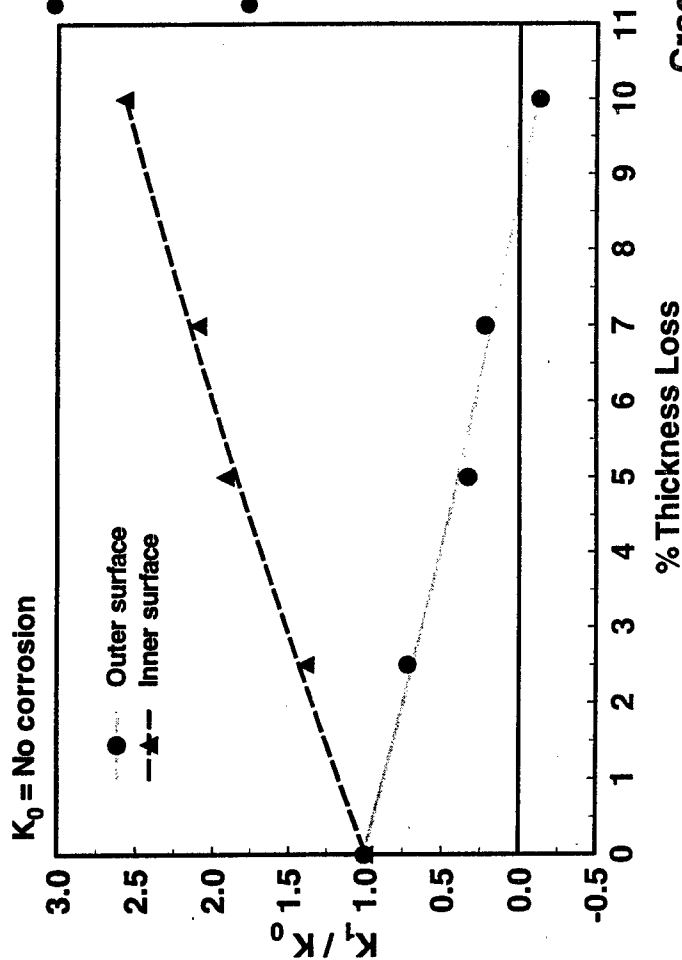
- Indicates a crack would grow faster along inner faying surface resulting in an elliptical crack with a high aspect ratio.
- Decreasing stress intensity suggests influence of pillowing is reduced (but still significant) away from hole.



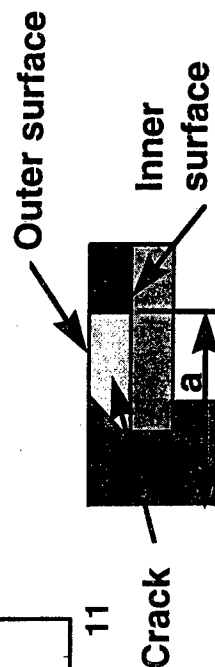
NRC-CARC

Fracture Mechanics Analysis

Single crack length, $a = 0.15125$ inch

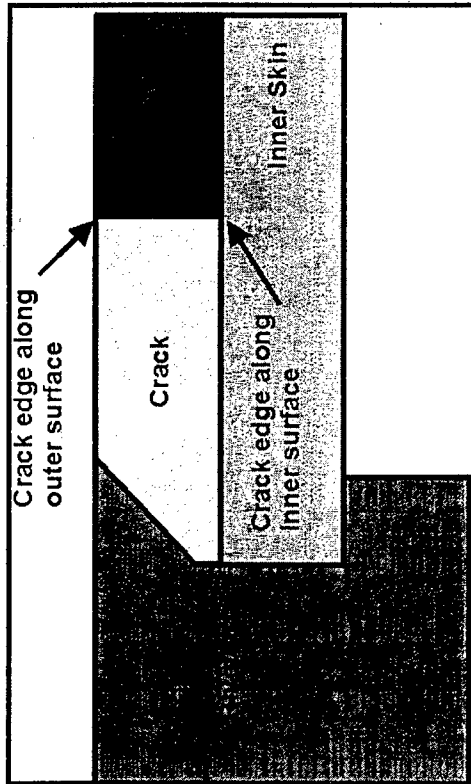


- Suggests semi-elliptical crack with high aspect ratio.
- Crack could be present along inner surface which has not yet penetrated through thickness.

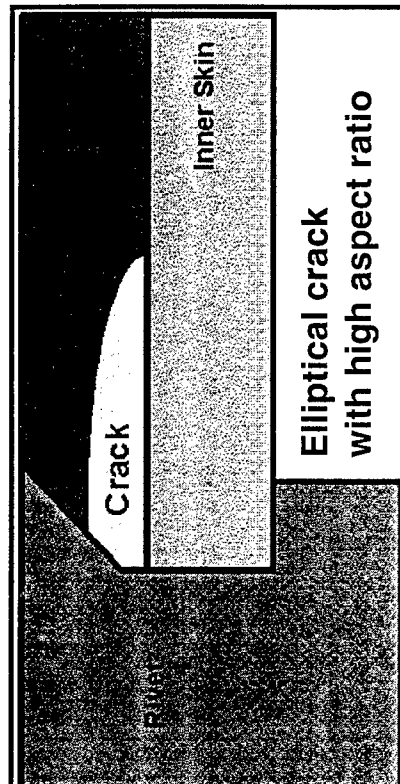


NRC-CARC

Fracture Mechanics Analysis



Crack shape used in model



Elliptical crack
with high aspect ratio

Predicted crack shape due to
corrosion pitting

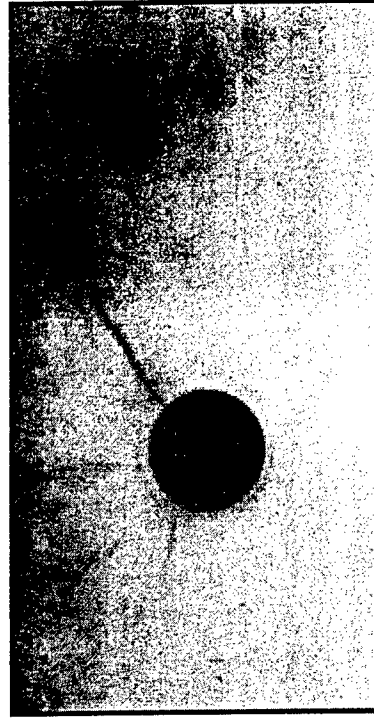
NRC - CNRC

Specimen Teardown

47-18A, Boeing 727-200 N4747, S4R - BS1020



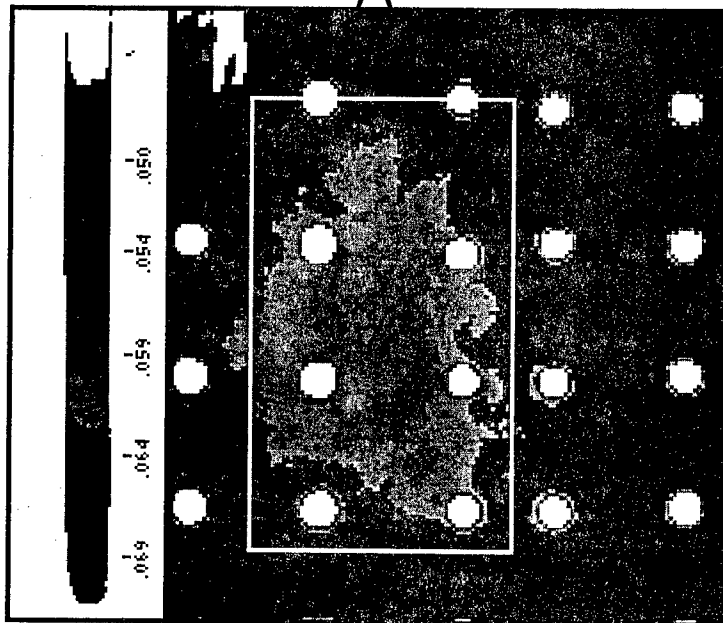
- Upper rivet row inner skin, faying surface (non-critical area).
- Dark areas contain ~10% thickness loss maximum.
- Cracks in the areas adjacent to maximum corrosion pilling.



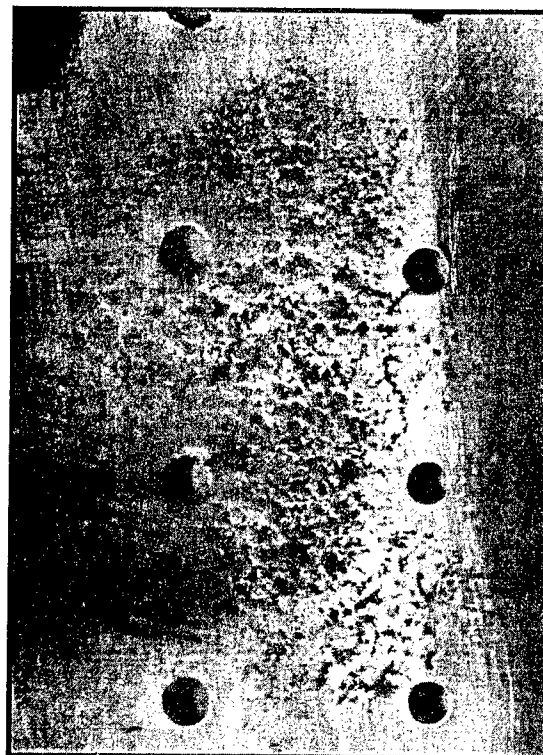
NRC-CNRC

Specimen Teardown

1D, Lockheed L1011, S33R - BS529-589



Colorized thickness
loss map

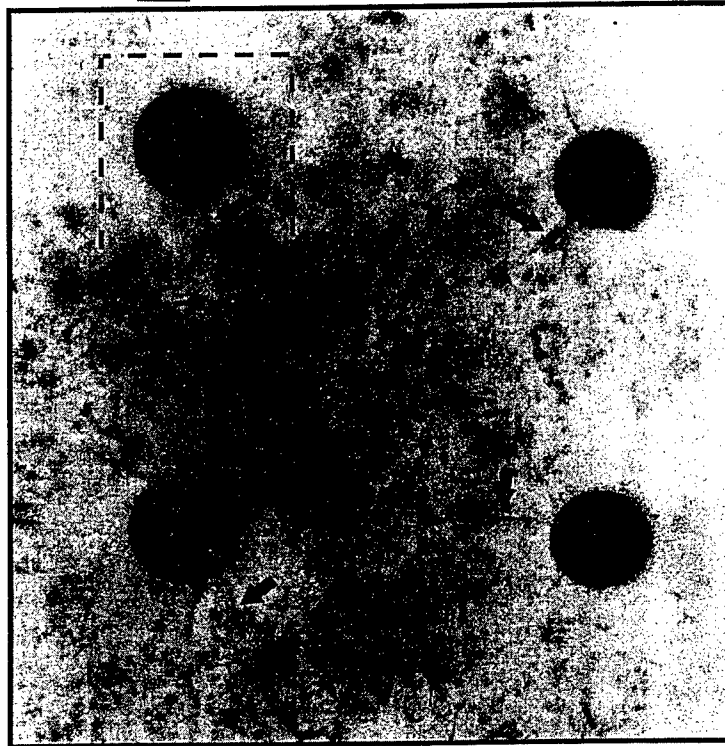


Photograph of
Specimen L1011-1D

NRC-CNRC

Specimen Teardown

1D, Lockheed L1011, S33R - BS529-589



X-ray image



Photo

- Outer skin, faying surface (non-critical rivet rows).
- Average 14% thickness loss.
- No crack penetrates outer surface.

NRC · CNRC

Residual Strength Capability

Possible effect of pillowing on inspection actions

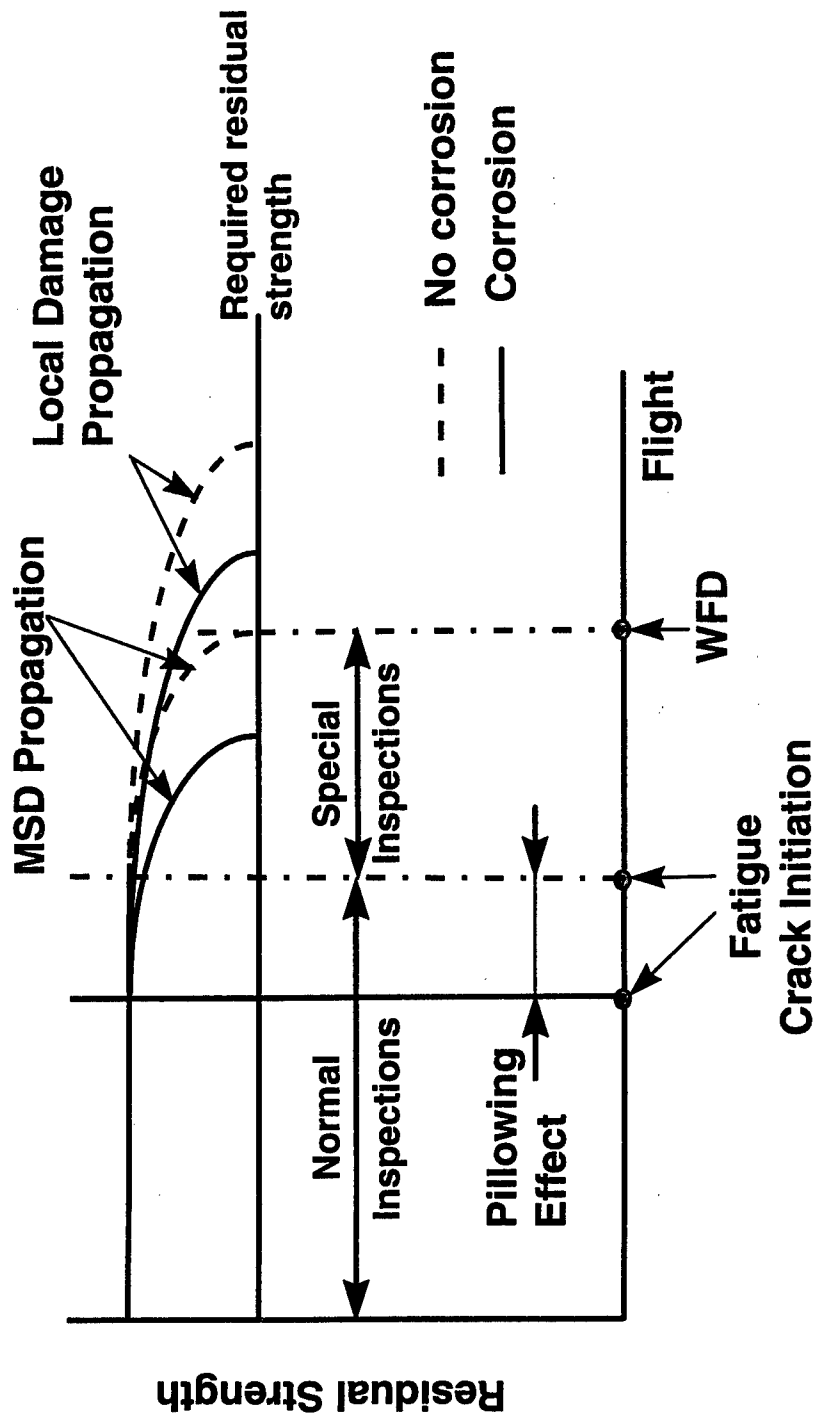


Chart modified from T. Swift, NASA CP 3274

NRC-CNRC

Conclusions

Finite Element Modeling verified or supported through:

- Hydro-pillowing experiment (deformations and strains)
- Permanent deformation observed in corroded joints after disassembly (yielding - predicted)
- Corrosion pillowing stress leads to non surface breaking cracks (several examples from retired and operational aircraft found)

NRC - CNRC

Damage Tolerance Implications

Conclusions

- **Shift in location of maximum stress;**
 - not concentrating inspections in new critical area.
- **Pillowing could cause a high aspect ratio crack to grow which may not penetrate through the thickness until the crack length is quite large;**
 - these types of cracks would be difficult to detect.
- **Corrosion pillowing may initiate cracks prematurely;**
 - special inspections to detect multi-site damage may have to be initiated earlier if corrosion present.

NRC-CNRC



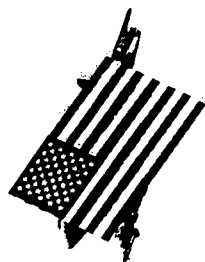
Full Scale AV-8B Wing Test with Known Delaminations

Troy S. Hullander
H. Wriley Gay
Scott C Bledsoe

AV-8B In Service Support Team
MCAS Cherry Point, NC

4 December 1996
USAF Aircraft Structural
Integrity Program Conference

San Antonio, Texas



Test Program Team

United States

AV-8B In Service Support Team

Troy S. Hullander, H. Wriley Gay, Scott C. Bledsoe

McDonnell Douglas Aerospace

Daryl Carpenter, Al Maiuro, Henry Fry, Terry Fornash, John Roberts
Naval Air Systems Command

Jim Candela, Troy S. Hullander

United Kingdom

British Aerospace Corporation

Peter Gates, Andy Crane

Defense Research Agency

Ian Sandell



Presentation Outline

- AV-8B Harrier Overview
- Statement of Problem
- Wing Substructure Delaminations
- Type of Delaminations
- Laboratory Test Program
- Laboratory Test Program Results
- Other Data Supporting Test Program
- Fatigue Spectrum Development
- Fatigue Test Spectrum
- Test Article Description
- Full Scale Test Set-up
- Test Results



AV-8B Overview



AV-8B Harrier Overview

- The AV-8B Harrier Is a Close Ground Support Attack Fighter With Vertical / Short Takeoff and Landing (V/STOL) Capabilities.
- The Aircraft Is Built Jointly by McDonnell Douglas Aerospace and British Aerospace.
- The Harrier Is Flown by the United States Marine Corps, British Royal Air Force, Italian Navy and Spanish Navy.
- Due to Its V/STOL Capabilities, This Aircraft Can Operate From Short Airfields, Roadways, or Small Ships.
- The Harrier Carries a Wide Range of Armament and Enough Fuel That Allows a Combat Radius Comparable to Any Other Light Fighter/Attack Aircraft
- The Harrier Has Full Capabilities for Air Intercept, Anti-Ship, Air to Ground Attack During All Weather Operations

AV-8B Harrier Overview- Structure



- The Structure of the Harrier Is a Combination of Carbon/Epoxy Composites and Metal.
- The AV-8B Is 26% Composite Materials.

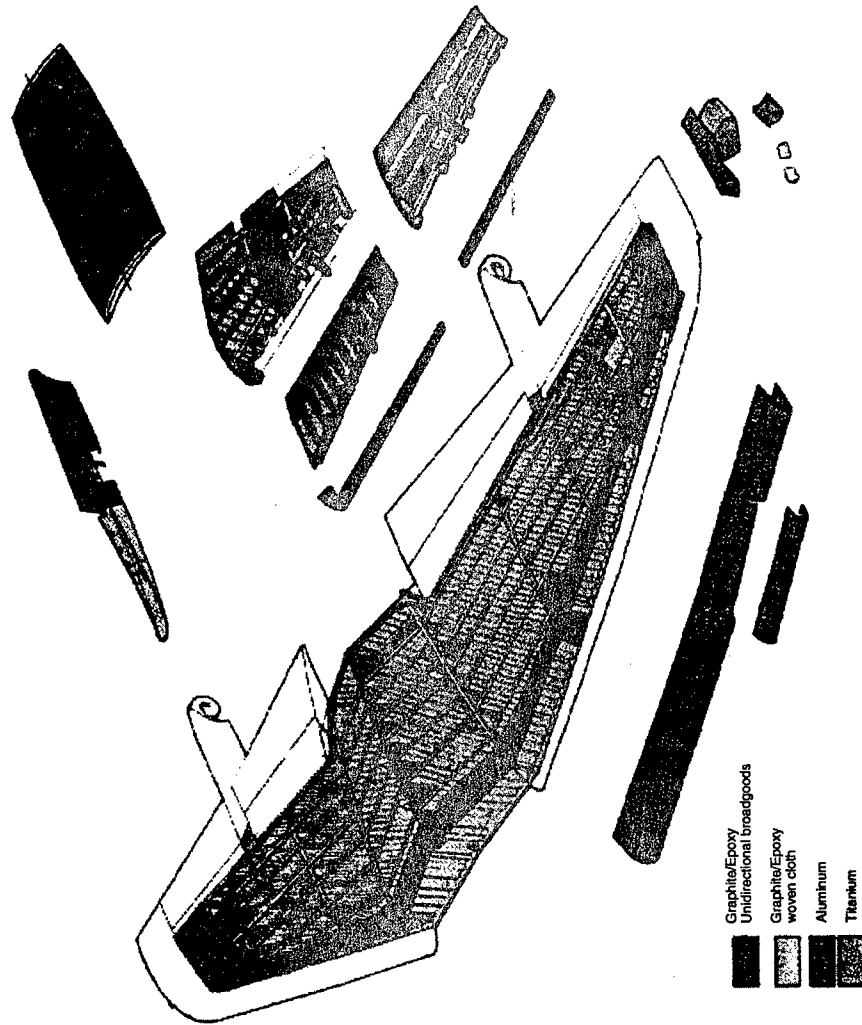
AV-8B Material Usage



AV-8B Harrier Overview - Wing



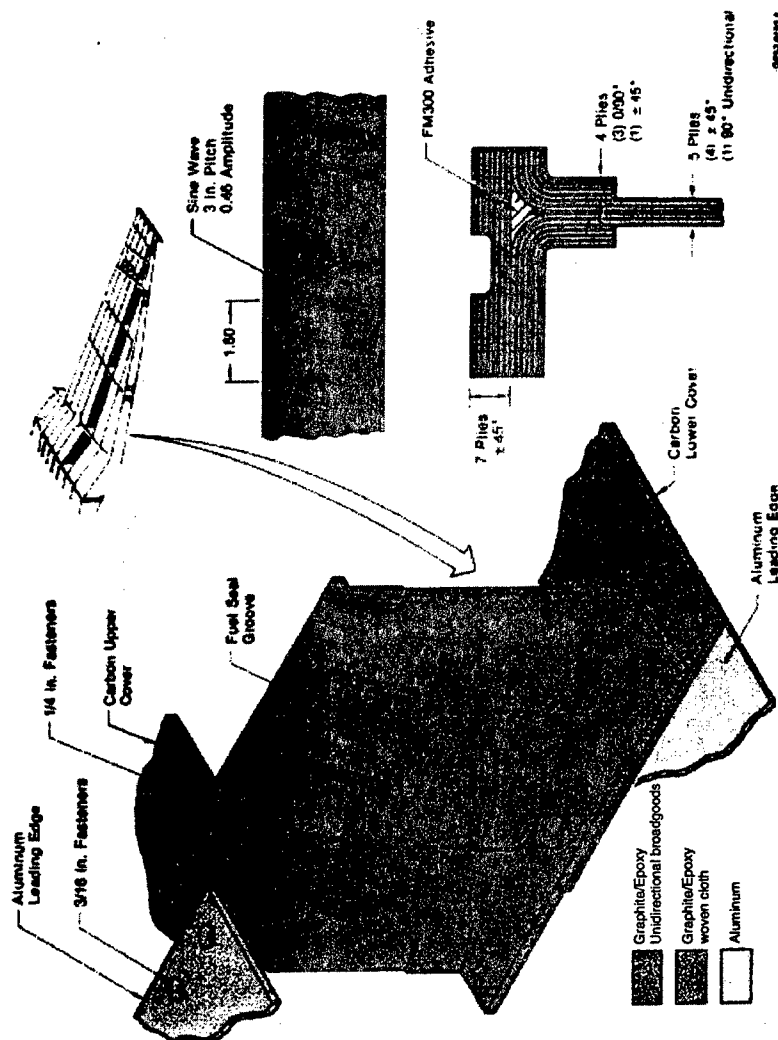
- The Wing Torque Box Has a Monolithic Composite Skin and Sine Wave Composite Substructure
- Only Primary Attachment Points (Wing to Fuselage, Pylons, Landing Gear) Are Metal



AV-8B Harrier Overview - Composite Substructure



- The AV-8B Wing Substructure Is Molded Carbon/Epoxy Sine Wave Spars and Caps
- The Sine Wave Spars are Lighter in Weight and More Efficient Than Conventional Stiffened Sections





Statement of Problem



Statement of Problem

- During the Manufacture of the AV-8B Wing, the Substructure Intersections May Require Shimming.
- Failure to Shim Adequately May Result in Delaminations When Fasteners are Installed.
- McDonnell Douglas Aerospace Discovered Delaminations in Production Wings and Changed the Manufacturing Process to Alleviate Future Occurrences of Delaminations.
- Approximately 150 Wings in the AV-8B Fleet Were Suspected of Having These Substructure Delaminations.
- To Minimize Delamination Growth, Flight Loads Were Restricted to 2/3 Limit Load on All Affected Aircraft.
- A Test Program was established to Investigate the Growth of Delaminations Common to the Affected AV-8B Wings.

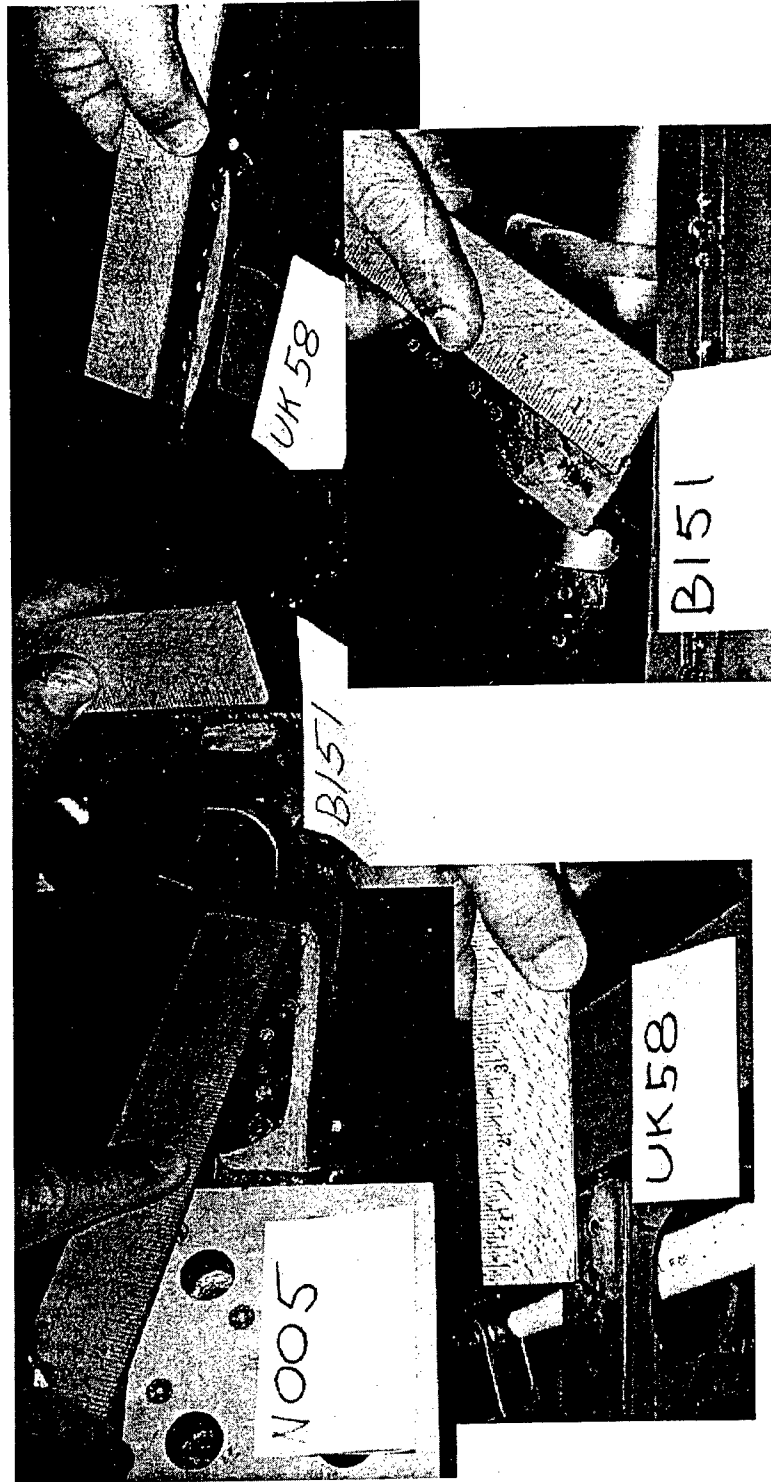


Wing Substructure Delaminations



Wing Substructure Delaminations

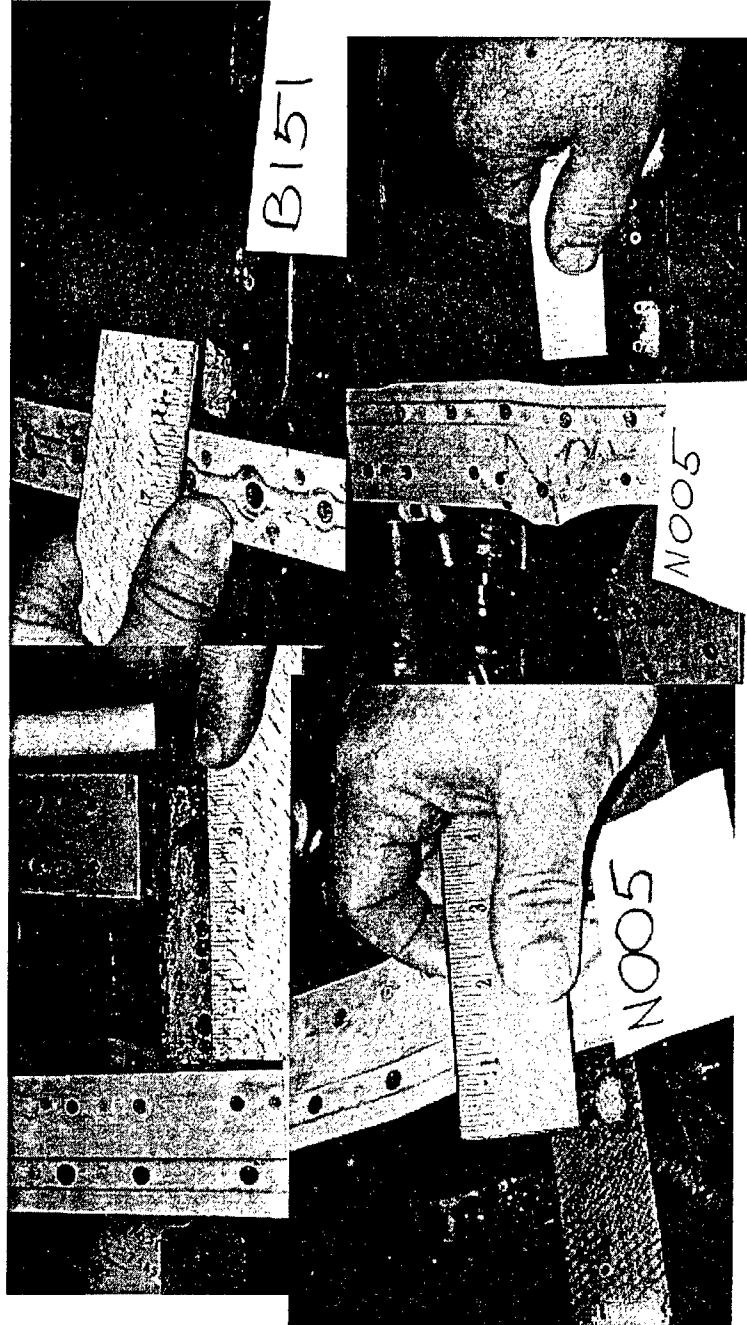
- Delaminations at Composite to Metal Substructure Joints





Wing Substructure Delaminations

- More Delaminations at Composite to Metal Substructure Joints at Structure with Sealant Grooves.





Types of Delaminations

Types of Delaminations



- Two Types of Delaminations Occur in Carbon/Epoxy Laminates

- Single Level Delaminations

- Caused by Foreign Objects Between Plies, Disbonds During Unbagging, Thermal Stresses During Cure, Trapped Volatiles, Etc..

- Multilevel Delaminations

- Caused by Interlaminar Shear Failures - Impact or Unshimmed Gap Pull-up During Fastener Installation

Analytical Techniques



- Test Data Available for Single Level Delaminations for Development of Semi-Empirical Equations to Calculate the Effects of Delaminations and Propagation Effects
 - If the Laminate Compression Load Is High Enough for the Laminate on Either Side of the Delamination to Buckle - the Energy Released From the Buckled Plies Will Propagate the Delamination
 - Failure Modes - Static Compression Failure or Overall Panel Buckling
- Trends Are Similar for Multilevel Delamination. As for Single Level Delaminations, However, There Is Not Enough Test Data Available to Develop Semi-Empirical Equations for Analysis and Propagation Predictions.



Laboratory Test Program



Laboratory Test Program

- Multilevel Delaminations Test Program
- Specifically Addressed Wing C/E Skin and Substructure Delaminations Induced by Installing the Fasteners Where Unshimmed Gaps Exist Between Wing Skin and Substructure
 - Generally Spar and Rib Intersections
- All Delaminations MDC Found on AV-8B Wings That Occurred During Wing Assembly Were Multilevel Delaminations

Laboratory Test Program

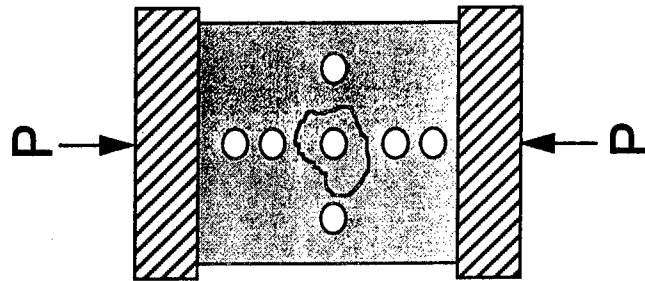


- Test Program Included Element and Component Static and Fatigue Tests for Typical Unidirectional Wing Skin and Woven Substructure With Induced Delaminations
- Strength Reduction Factors for Hot/Wet and Cold/Dry Environmental Conditions Were Developed for Delaminated Laminates of Varying Thickness
- In-Plane Compression, Bearing, Compression and Tension/Bearing Interaction, Interlaminar Shear, Sine Wave Spar Shear, and Out of Plane Tension Modes of Failure Were Examined and Allowables Developed.
- Over 500 Specimens Were Tested.

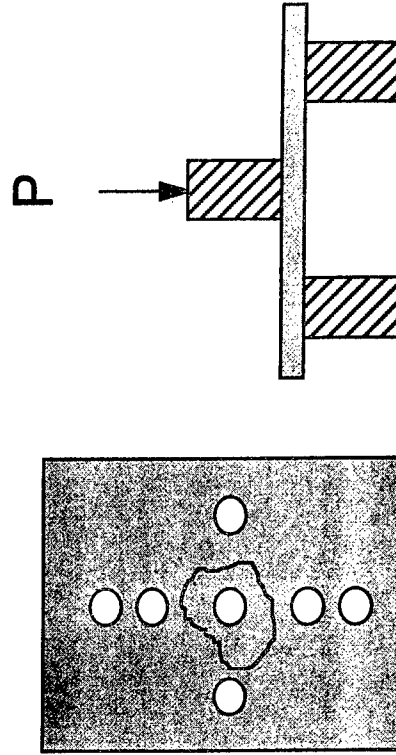


Test Specimen Configurations

Compression Test



Interlaminar Shear Test

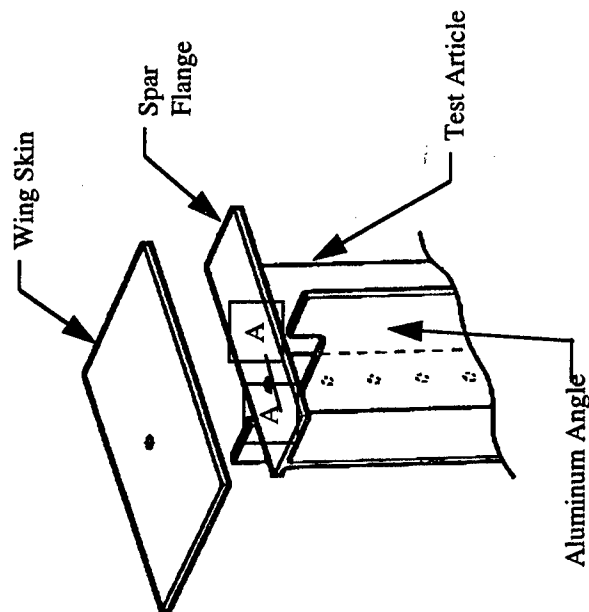
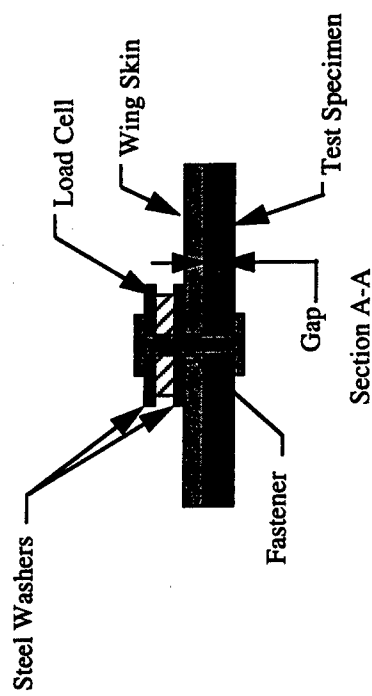
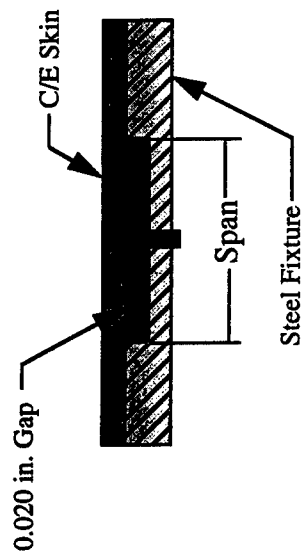


Delamination Inductions into Test Specimens



- Delaminations in Test Specimens Were Created by Installing a Fastener Over Unshimmed Gaps Between Specimen Laminates and Simulated Substructure
- The Unshimmed Gaps Varied From 0.020 to 0.080 inches thick over a span of 3 to 6 inches.
- Fastener Torque Versus Clamp-up Force Was Recorded.
- Fastener Torque Applied Were Same As Required in Production.

Delamination Inductions into Test Specimens





Laboratory Test Program Results

Laboratory Test Program Results

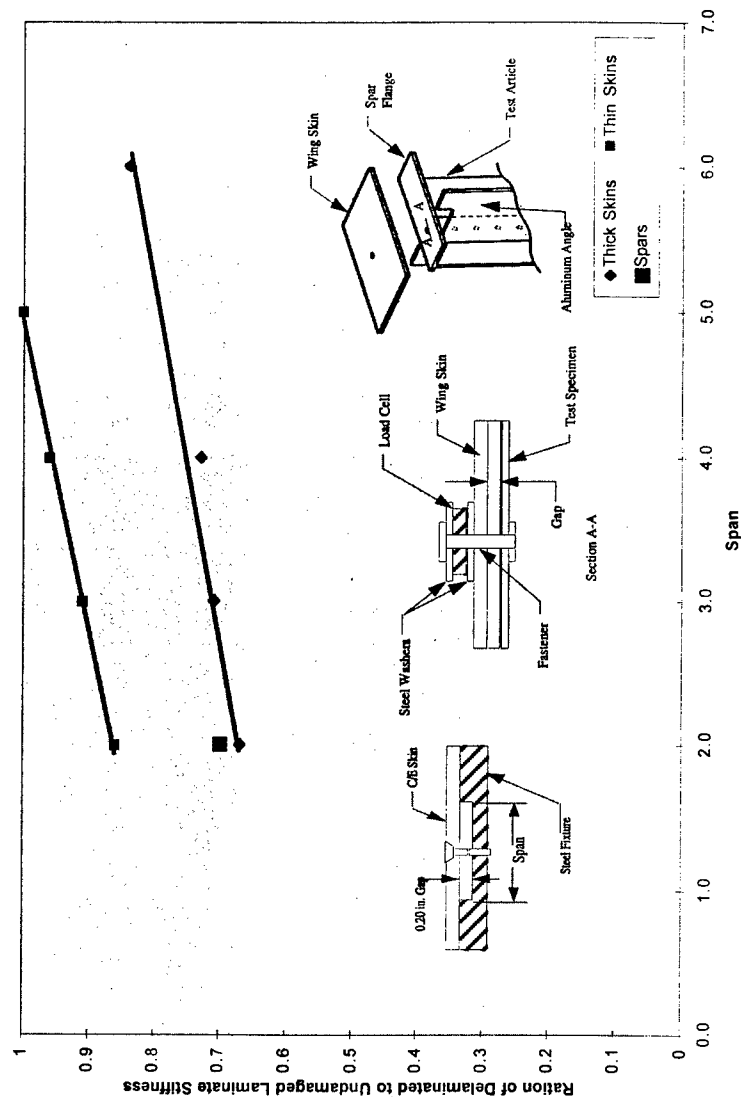


- The Following Aspects of Composite Properties Were Reviewed for the Test Spectrum Development.
 - Delamination Stiffness Reduction
 - In-Plane Compression
 - Interlaminar Shear
 - Sine Wave Spar Shear
 - Out-of-Plane Loads
 - Composite Fatigue
 - Delaminations Influence on Fatigue



Laboratory Test Program Results

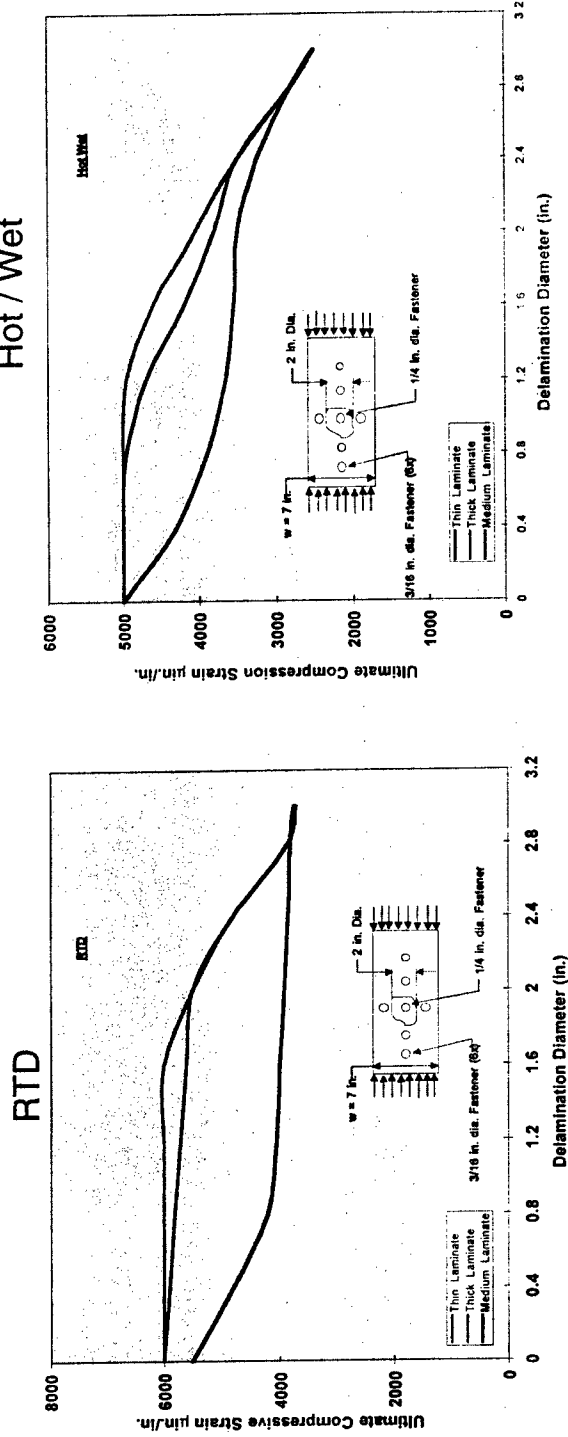
● Delamination Influence on Stiffness





Laboratory Test Program Results

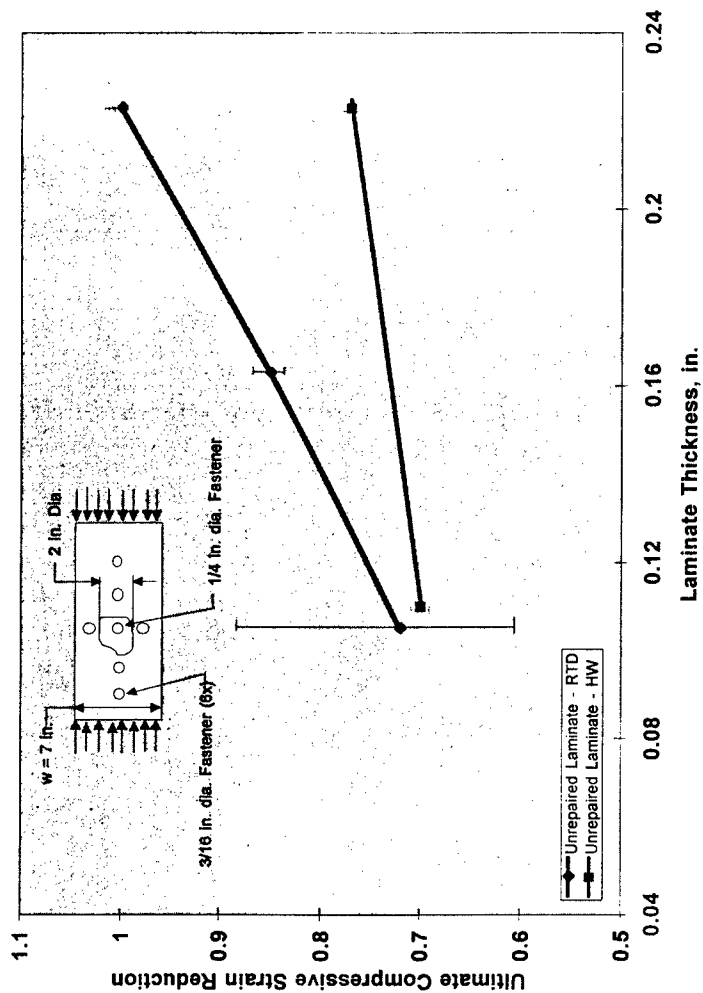
- Test Data Supporting the Reduction of In-plane Compression Strength of Delaminated Laminates





Laboratory Test Program Results

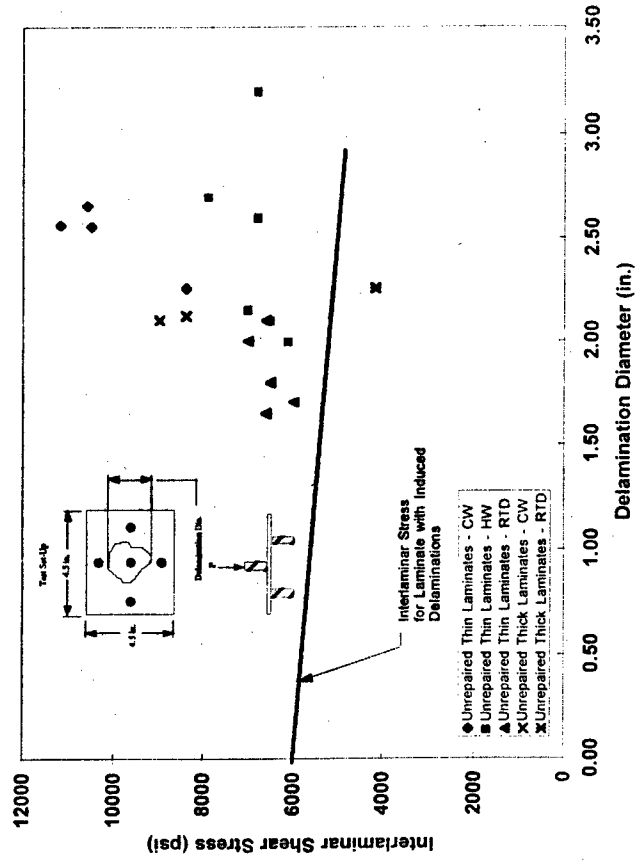
- Compression Strength Reduction Versus Laminate Thickness





Laboratory Test Program Results

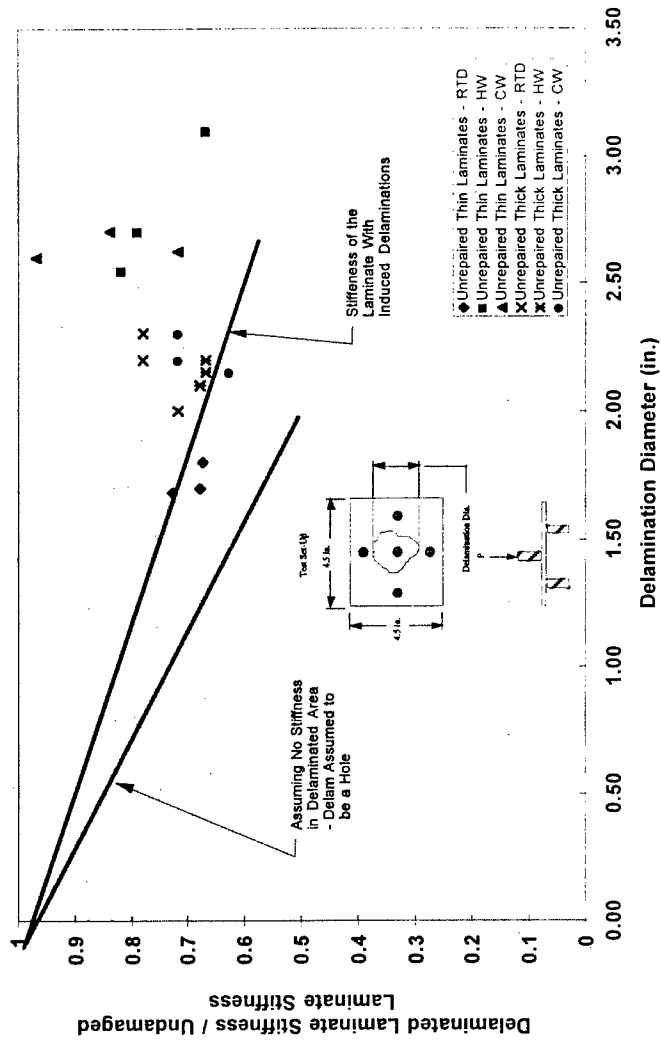
- Test Data Supporting the Reduction of Interlaminar Shear Strength in Delaminated Laminates





Laboratory Test Program Results

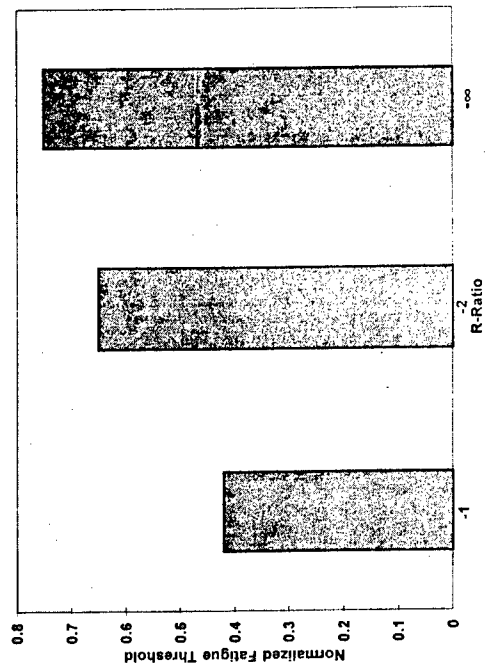
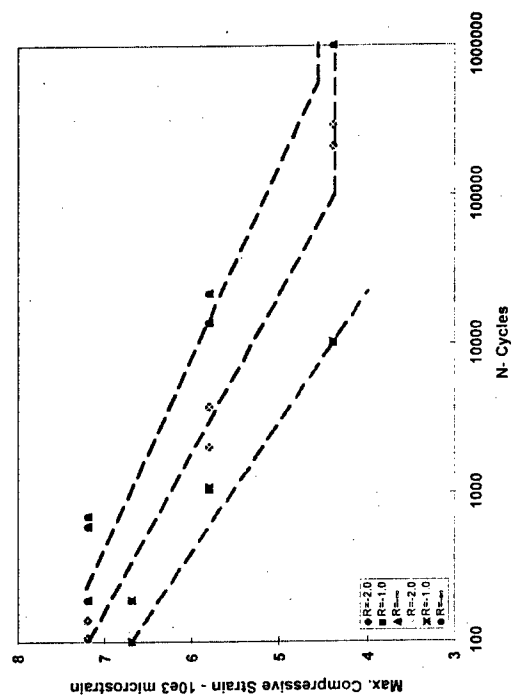
- Test Data in Support of Reduction of Out-of-plane Compression Strength of Delaminated Laminates





Laboratory Test Program Results

- The Effects of Composite Fatigue
 - Primarily Compression - Compression Dominated Spectrum
 - Test Data Shows That Tension Compression Can Be More Damaging to Delaminated Laminates



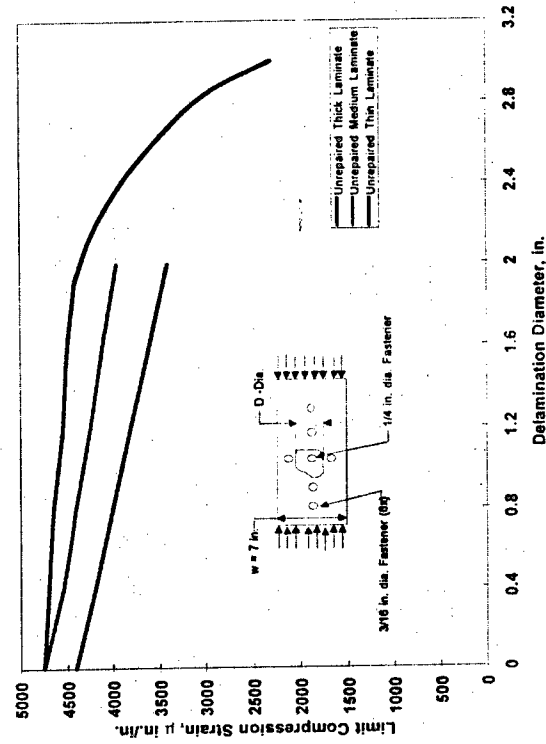
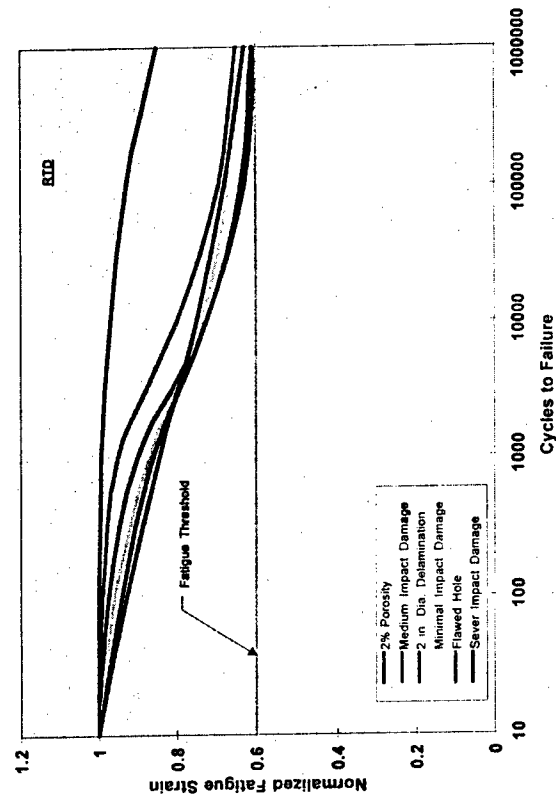


Other Data Supporting Test Program



Other Data Supporting Test Program

- Test Data That Shows the Influence of Delaminations on Fatigue Strength





Fatigue Spectrum Development

33

Fatigue Spectrum Development



- Original Full Scale Development Test Performed for 12,000 Spectrum Fatigue Hours (SFH). (Two Lifetimes)
- MDA Proposed a Truncated Fatigue Spectrum in Order to Compress the Test Time and Cost.
- Only the Fatigue Cycles That Were of High Enough Magnitude to Be Damaging to Composite Materials Were Included for the Test Spectrum.
- A Static Residual Stress Test to Ultimate Load Was Planned

Fatigue Spectrum Development



- Delaminations Produced Significant Out-of-Plane Stiffness Reductions
 - ~30% Reduction in Spar Cap
 - ~5-35% Reduction in Skin
- Interlaminar Shear Strength Reductions Are Less Pronounced
- Stiffness Reductions Allows Load Redistribution
- Out-of-Plane Loads Weaken Matrix Near Delamination Making Them Susceptible to Increased Delamination Growth Under In-Plane Compression.
- Test Program Included Fuel Pressurization Cycles in Fatigue Spectrum

Fatigue Spectrum Development



- Tension / Compression (T/C) Loading Has Greater Fatigue Effect Than Either Tension / Tension (T/T) or Compression / Compression (C/C) Loadings.
- The Influence of Tension Loads
 - They Do Not Directly Cause Delamination Propagation
 - They Can Cause Laminate Matrix Damage (Subcracking / Crazeing)
 - Laminate Matrix Damage May Lower Compression Load Levels Needed for Delamination Propagation
- Test Program Retained All Tension Fatigue Cycles in Fatigue Spectrum

Fatigue Spectrum Development



- Maximum AV-8B Limit Wing Skin Strain = 2700 $\mu\text{In.} / \text{In.}$
- AV-8B Tests Show That a 2.0 Inch Delamination Could Reduce the Hot/Wet Static Compression Strength of the Wing by up to 30%.
 - Damage Compression Strain = 3500 $\mu\text{In.} / \text{In.}$
- Fatigue Endurance Limit for Laminates Historically Set at ~60% of the Damaged Static Strength.
 - Tests Indicate That This Could Be As High As 90% for AV-8B, However, These Tests Utilized Compression Only Cycle, Teflon Lined Support Plated, and Uniaxial Loading.
- Assume 60% of 3500 $\mu\text{In.} / \text{In.}$ = 2100 $\mu\text{In.} / \text{In.}$
- 2100 / 2700 = 0.78 Design Limit Load
- Test Program Retained All Compression Fatigue Cycles Greater Than 78%



Fatigue Test Spectrum

38



Fatigue Test Spectrum

- The Full-Scale Development (FSD) Fatigue Spectrum

AV-8B FTV1 FATIGUE SPECTRUM
Per 1000 Hours

Max. % DLL	Min % DLL			% DLL	Occur.
	14.3	0	-14.3 -28.6		
47.1	1859	1331	45	47.1	360
55.7	1702	983	29	55.7	302
65.0	1605	658	12	65.0	254
75.0	1190	128	4	75.0	146
85.0	477	63	2	80.0	84
95.0	150	29	1	88.0	4
105.0	46	3			
110.0	13				
118.0	7				
128.5	1				

Coupled with 1g
(14.3% DLL)



Fatigue Test Spectrum

- The Delamination Test Program Truncated FSD Fatigue Spectrum for Composite Laminate

AV-8B FTV1 FATIGUE SPECTRUM
Per 1000 Hours

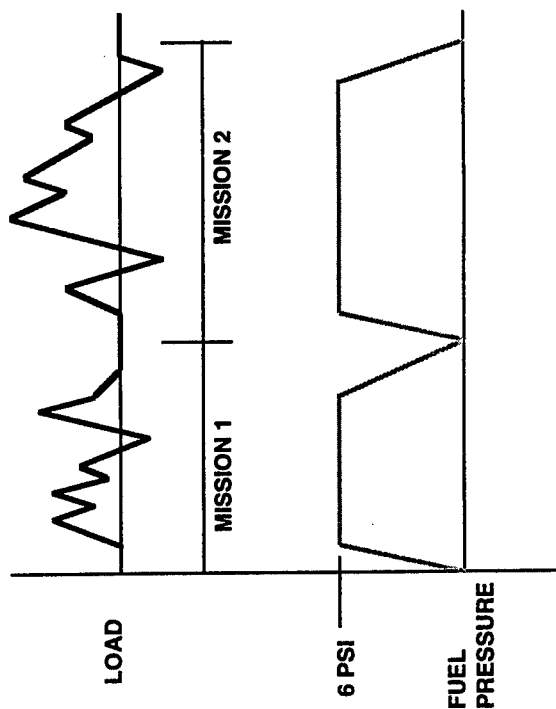
Max. % DLL	Min % DLL			% DLL	Occur.
	14.3	0	-14.3 -28.6		
47.1	Eliminated	45	5	47.1	Eliminated
55.7	Eliminated	29	4	55.7	Eliminated
65.0	Eliminated	12	2	65.0	Eliminated
75.0	1190	128	4	75.0	146
85.0	477	63	2	80.0	84
95.0	150	29	1	88.0	4
105.0	46	3			
110.0	13				
118.0	7				
128.5	1				

Coupled with 1g
(14.3% DLL)



Fatigue Test Spectrum

- Out-of-Plane Cyclic Loading:
- Fuel Pressurization Cycles



WING PRESSURE/LOAD RELATIONSHIP



Test Article Description

Test Article Description

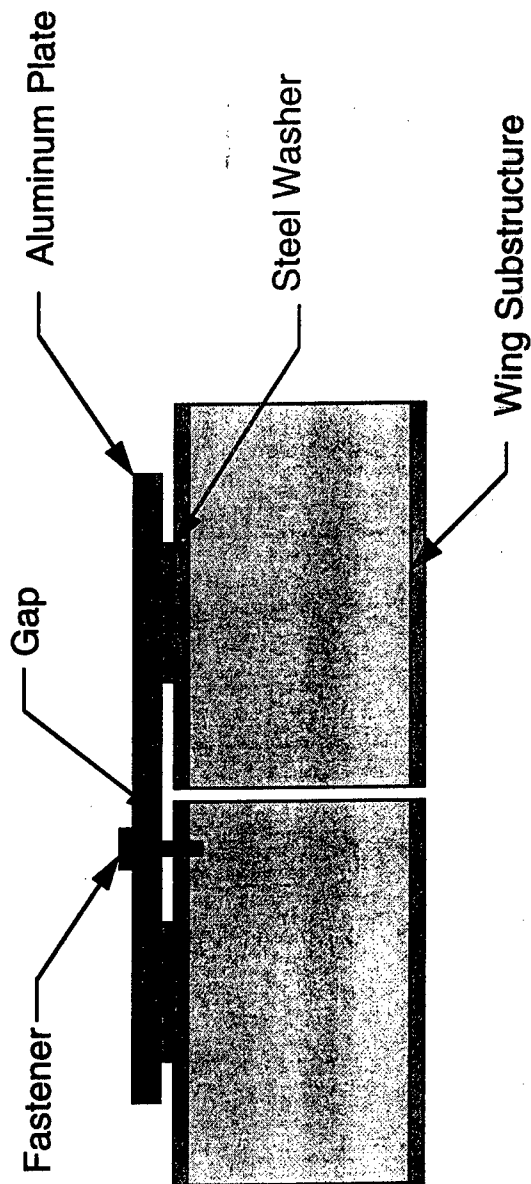


- The Test Article Is a Production AV-8B Wing Designated UK58.
- The Test Article Included Leading Edge, Inboard Pylons, Flaps, Ailerons, and Over Wing Fairing.
- The Wing Was Placed in a Test Fixture Which Replicated the Loads and Deflections at the Wing-to-Fuselage Attach Points.
- The Fuel Cell Was Filled With Water and Pressurized with Air to Replicate Fuel in the Wing During the Test

Test Article Description



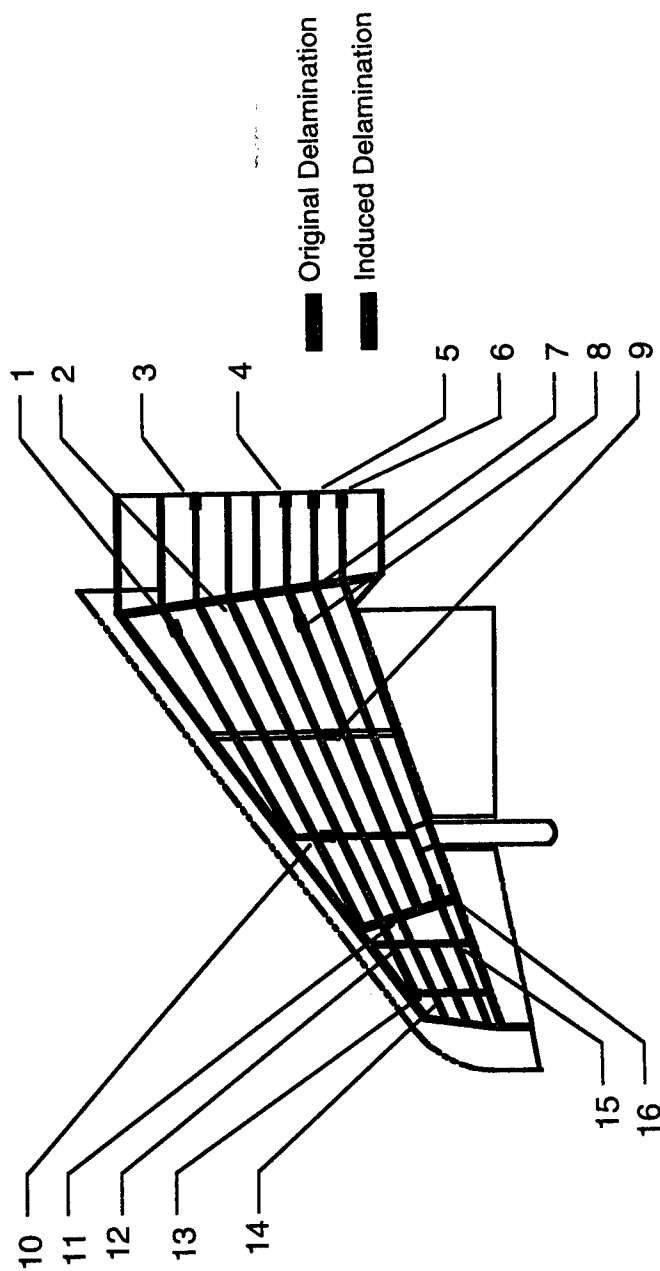
- Delaminations Induced Into UK58 Test Article
 - The Wing was Deskinned
 - Delaminations Induced by Creating Artificial Gaps and installing Fasteners per Production Specification.



Test Article Description



- Delaminations Induced Into UK58 Test Article
 - Six Original Delaminations Plus 10 Additional Delaminations Based on Findings From Production Wing Inspections





Test Article Description

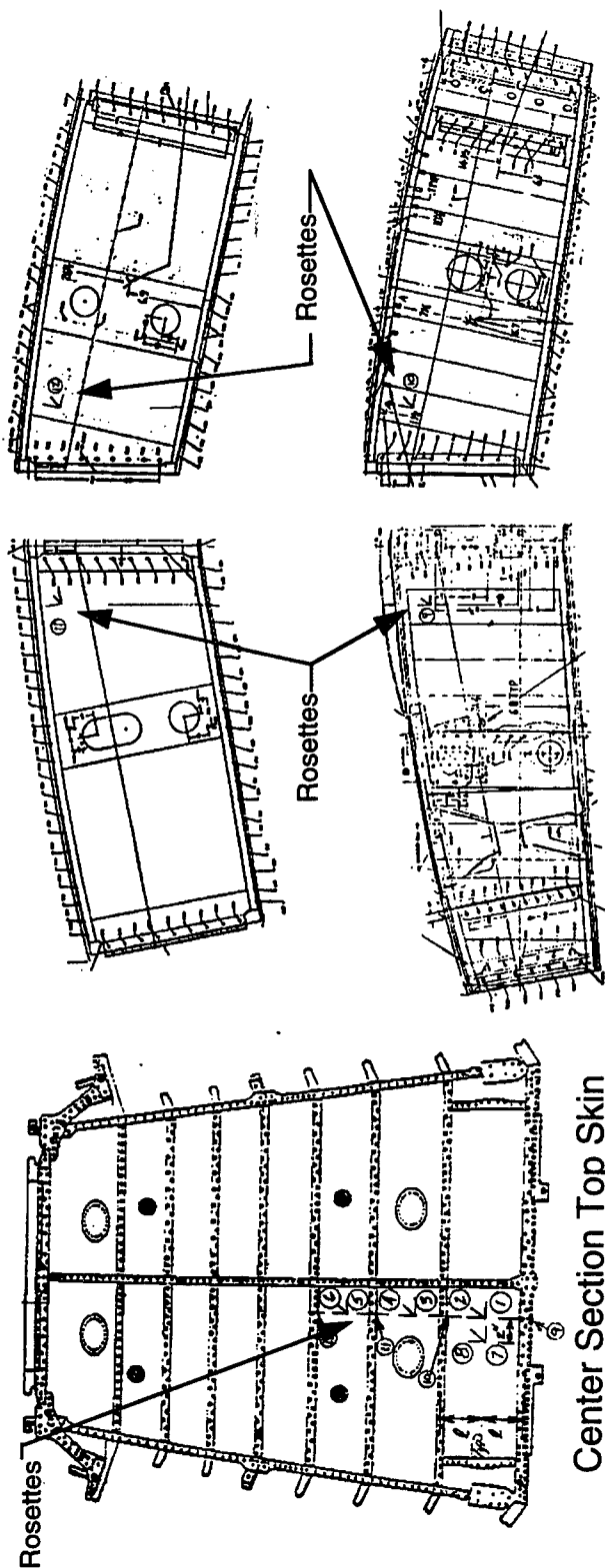
- Delaminations Induced Into UK58 Test Article
 - Sizes of the Delaminations Found During the Production Line Inspection and the NDI Measurements of the Induced Delaminations

Delam #	Delamination Size, in.	Delam #	Delamination Size, in.
1	1.24 x 4.66 x 0.053	9	0.70 x 2.0 x 0.077
2	0.18 x 0.62	10	0.54 x 1.12 x 0.042
3	0.45 x 0.95 x 0.059	11	0.20 x 0.60
4	0.43 x 1.1 x 0.070	12	0.20 x 0.60
5	0.35 x 0.85	13	0.40 x 1.1 x 0.057
6	0.28 x 0.79 x 0.051	14	0.50 x 4.00
7	0.30 x 4.50	15	0.80 x 1.60
8	0.35 x 0.75 x 0.053	16	0.50 x 0.99 x 0.050



Test Article Description

- Test Article Instrumentation - Center Section and Spars
 - Area Were FSD Wing Static Test Failed.
 - Linear Strain Gages and Rosettes Placed in Critical Load Paths.

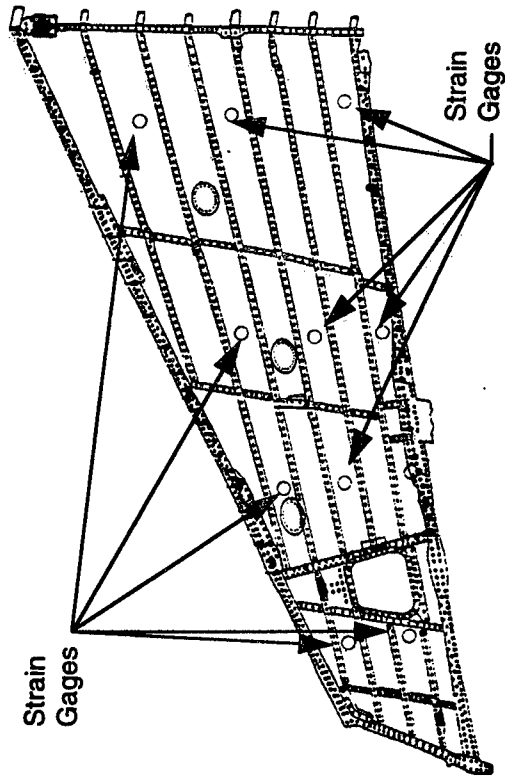
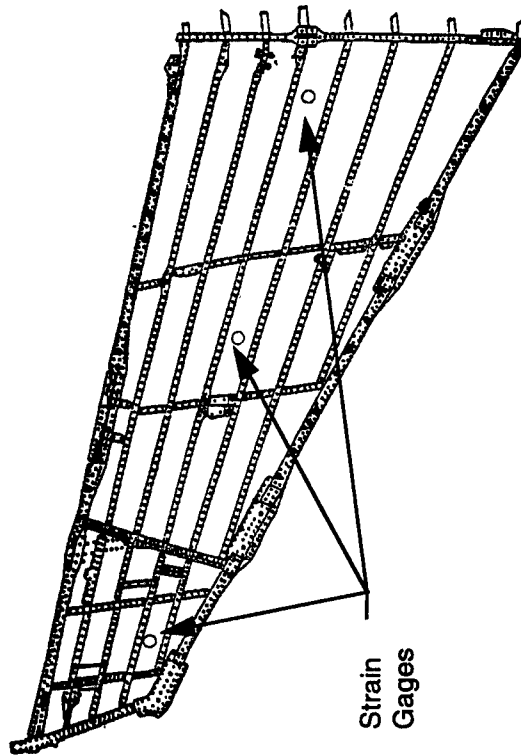


Center Section Top Skin



Test Article Description

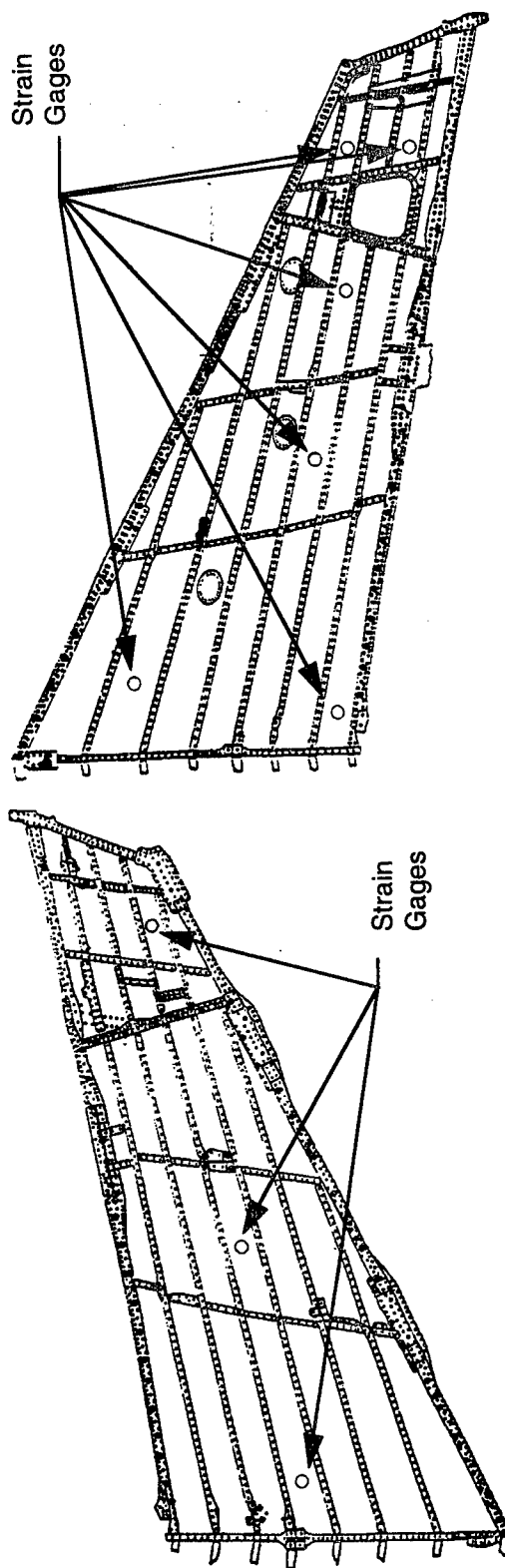
- Test Article Instrumentation - LH Side Skins
 - Linear Strain Gages and Rosettes Placed in Critical Load Paths.





Test Article Description

- Test Article Instrumentation - RH Side Skins
 - Linear Strain Gages and Rosettes Placed in Critical Load Paths.



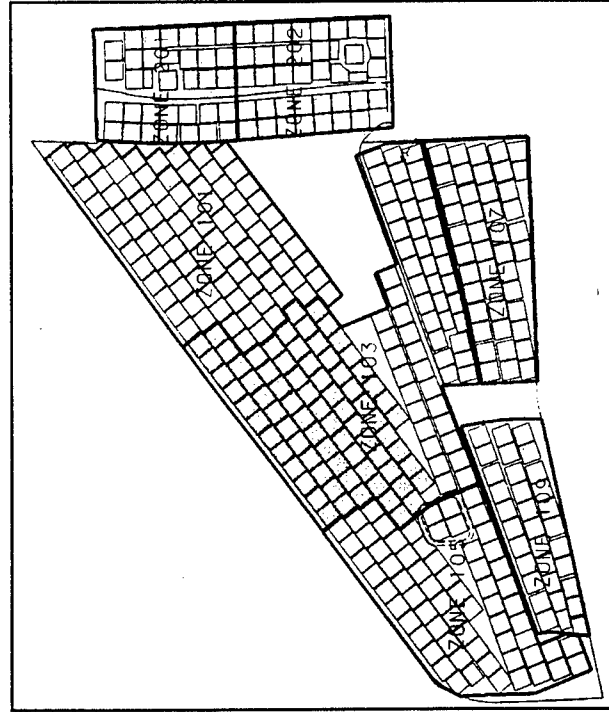
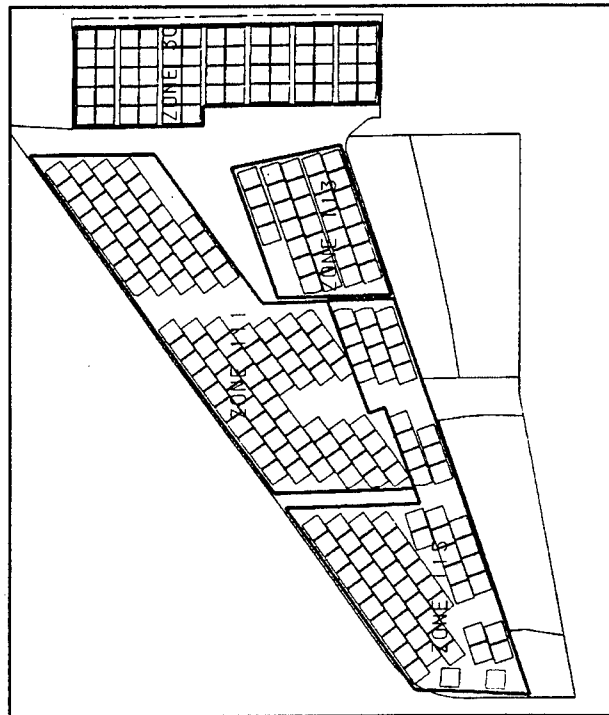


Full Scale Test Set-Up

Full Scale Test Setup



- Test Article Tension Pad Installation - Typical





Full Scale Test Set-up

- Test Article in Fixture at McDonnell Douglas Aerospace Corporation





Test Results

53

Test Results

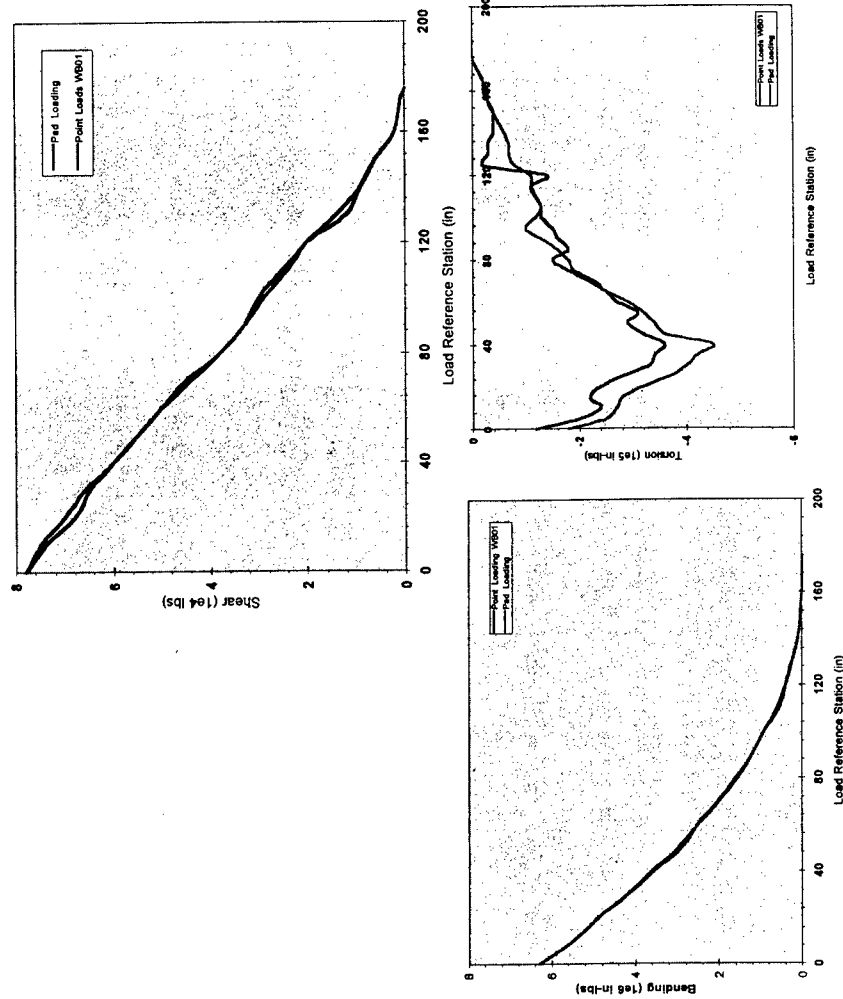


- The UK58 Test Article Was Cycled to 12,000 Effective Spectrum Flight Hours
 - No Leaks Occurred in the Fuel Cell
 - Strain Surveys Taken During the Test Showed No Anomalies in Strains
- Static Residual Stress Test to 150% DLL With No Significant Strain Anomalies.
- Test Fixture Limit Was Set to 200% DLL
- Failure Test Went to 200% DLL Before Shutting Down
 - Test Fixture Beam Buckled at 200% DLL Causing Shut Down

Static Test Load Cases



- Load Case for Ultimate Load (1.5 X Limit) for Worst Point in the Sky.
- Shear, Bending, and Torsion Graphs
- Test Loads Correlated Well With Design Loads





AV-8B Program Results

- Test Was a Success
- No Adverse Strength Reductions Were Experienced Due to the Inclusion of Delaminations in the Wing Skin and Wing Substructure.
 - The Flight Restriction on the USMC AV-8B Aircraft was removed.
- Post Teardown of the Wing Skin and Substructure Is Underway at Naval Aviation Depot Cherry Point. Preliminary Results:
 - No Visual Signs of Wing Skin and/or Substructure Failure.
 - Detailed Ultrasonic Inspection is Forthcoming.
- The AV-8B Age Exploration Program Routinely Inducts Aircraft and Performs C-Scans of Wing Skins to Monitor Delamination Growth.

GLARE®, Reducing Weight and Improving Structural Integrity

Ir. Jan Willem Gunnink*
Structural Laminates Company
Kluyverweg 4, 2629 HT Delft, The Netherlands

Prof. Boud Vogelesang
Delft University of Technology
Kluyverweg 1, 2629 HS Delft, The Netherlands

Introduction

While flying aircraft structures are vulnerable to corrosion, fatigue as well as damage tolerance problems, it is certain that these problems will increase significantly due to (anticipated) life extension of the current fleet.

To achieve this life extension a significant amount of effort is going on, especially in the field of repair. New repair methods are being developed. Bonding joining technique is extensively promoted over standard riveting procedures. New materials like boron and GLARE® are introduced as preferred patch materials.

Previous ASIP Conferences indicated that these new materials are excellent to repair damaged aircraft structures. However, it is not known very well that some of them can improve the structural integrity and simultaneously reduce weight by using them as primary structural materials.

In this paper will be shown that GLARE® can be used as a primary structural material offering increased durability and damage tolerance capability at a 20-30% weight reduction compared to currently applied materials. The main emphasize will be on the application in the fuselage. In this respect some sub- as well as large scale GLARE® components will be shown and (test) results will be discussed briefly. This will include large scale fuselage as well as bulkhead components.

Advantages of GLARE®

In several publications the advantages of GLARE® are stated ^[1,2,3]. In this section these benefits will be summarized:

- weight (density)
- strength
- fatigue
- damage tolerance
- impact resistance
- flame resistant
- lightning strike
- thermal insulation
- corrosion resistant
- repairability
- maintenance.

Some of these characteristics will be mentioned briefly.

Disadvantages of GLARE®

In most reports and discussions, three disadvantages of GLARE® are addressed, i.e.

- cost
- stiffness
- workshop properties.

During the course of this paper it will be shown that by proper design as well as taking advantages of the ability of the material, these disadvantages can be minimized and can even be turned into their opposite.

Applications of GLARE®

Due to its characteristics GLARE® is considered for fatigue and damage tolerance critical structures. It is therefore applicable in large primary components like fuselage skins and bulkheads as well as lowerwing and flap skins. Some research results on fuselages will be shown.

Due to its flame resistant capabilities GLARE® offers potential to further increase the safety of aircraft. Several new aircraft programs are looking at GLARE® from this perspective. In combination with the fatigue and damage tolerance capabilities it will offer increased safety, reduced weight as well as reduced maintenance cost (less or no inspection!!).

The higher impact performance of GLARE® makes it an attractive material for impact prone areas like the cockpit crown, front bulkheads, leading edges, flaps, undercarriage doors and cargo floors. Its impact capabilities together with its flame resistant characteristics makes it suitable for cargo linings as well as "blast resistant" containers. Up to this moment a GLARE® container built by Galaxy Scientific Co.^[4] is the only container which meets the blast and fire requirements of the FAA (Fig. 1).

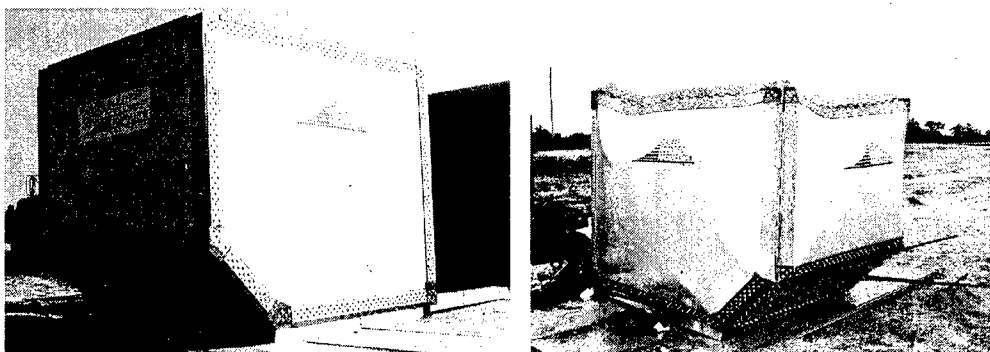


Fig. 1 GLARE® ECOS³ before and after FAA-conducted explosive testing (courtesy Galaxy Scientific Co.)

GLARE® has lower stiffness compared to aluminum alloy. Studies and research programs mainly performed by the US Airforce have shown that this is one of the aspects, which makes GLARE® an excellent material to repair damaged aluminum structures^[5]. Several US Airforce airplanes are currently fly-testing GLARE® patch repairs, a.o. the fuselage of the C-5A. Also Daimler-Benz Aerospace Airbus (DBAA) has shown in its certification test article for the A-330 the improved repairability aspects with GLARE® over conventional aluminum alloys.

Airbus A-340 fuselage barrel test^[6]

Daimler-Benz Aerospace Airbus has performed a fuselage barreltest using GLARE® in the crown of this section. The application of GLARE® resulted in a more than 20% weight reduction over the standard aluminum structure (skin to skin). It resulted also in a reduction of parts as well as a less complicated part compared to its aluminum baseline. The reduction of parts was obtained by the deletion of Ti-crackstoppers. This was a natural consequence of applying an almost fatigue insensitive material. Due to the good fatigue behaviour of GLARE® joints it is not a prerequisite to have increased skin thicknesses at the joints as well as at stringer locations. Both aspects have contributed to complexity reduction of the part.

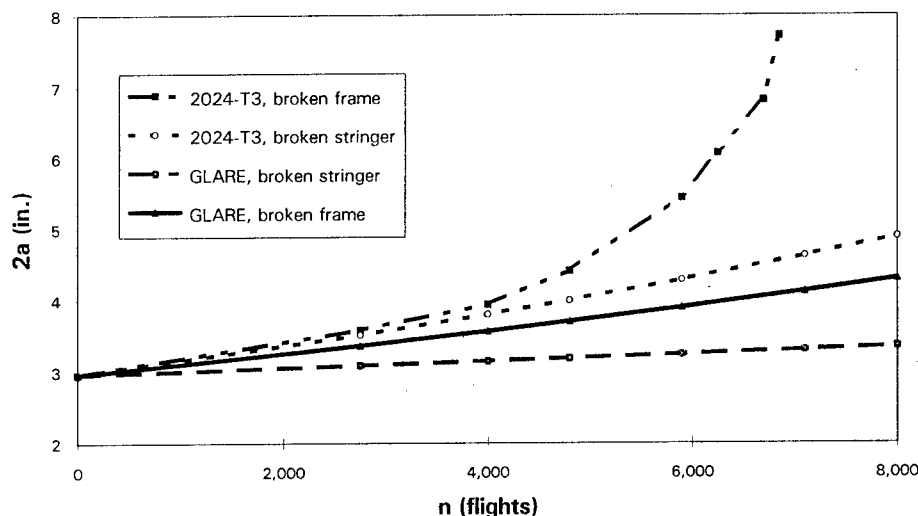


Fig. 2 Crackgrowth in the Airbus A-340 barreltest^[6]

The results of the damage tolerance test on this fuselage section was extremely good. Figure 2 shows the crackgrowth behaviour of a central broken member (frame or stringer) including skin fracture with a starter crack of 75 mm (~ 3.0 " in) in an all aluminum section compared to the GLARE® section. It clearly indicates that a crack in the aluminum section over a broken frame becomes critical in about 6,500 flights,

whereas the same crack configuration in GLARE[®] grows slowly and turns out to become critical only after more than 40,000 flights.

Airbus A-330 rear pressure bulkhead^[7]

DBAA has installed a GLARE[®] dome section in the rear pressure bulkhead in its certification testarticle for the A-330. This part is rather complex because of its double curvature as well as the application of the so-called splicing concept^[3]. The latter one is developed by SLC to avoid the problem of limited aluminum width. The application of this concept effectively results in theoretically an unlimited sheet width capability. It turns out that the available autoclave and pretreatment equipment are the only dimensional constraints.

Consequently, the rear pressure bulkhead has a reduced number of parts, i.e. less number of bulkhead sections and also no Ti-crackstoppers and less number of stringers.

Compared to the standard aluminum bulkhead the GLARE[®] bulkhead offers more than 25% weightreduction. Furthermore the damage tolerance test shows that the GLARE[®] bulkhead has almost no crackgrowth at all (Fig. 3). It also clearly shows the fast crackgrowth in the aluminum part as well as the temporary crackstop capability of the Ti-strap and a GLARE[®] strap.

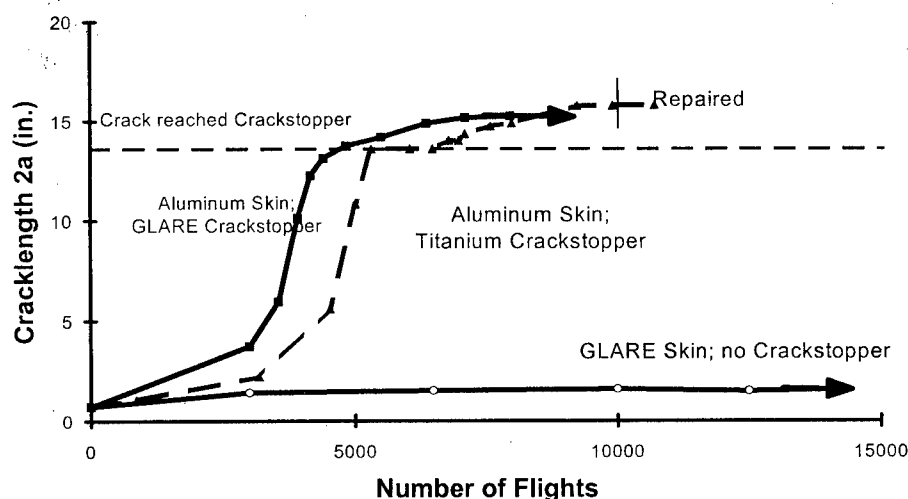


Fig. 3 Fatigue crackgrowth in the A-330 rear pressure bulkhead^[7]

While this part has difficult access and therefore is hard to inspect, it can be understood that the damage tolerance behaviour of the GLARE® bulkhead will have a significant positive impact on operational performance and cost.

Lear 45 radome front bulkhead in GLARE®^[8]

Extensive testing of GLARE® justified its good impact performance. In a research program between Shorts Brothers and SLC^[8] is shown that GLARE® is outperforming all other considered options, i.e. aluminum alloys and composites, glass as well as graphite. This resulted in a low weight and low cost application for the radome front bulkhead of the Lear 45. Fig. 4 shows the GLARE® component after the bird impact test.

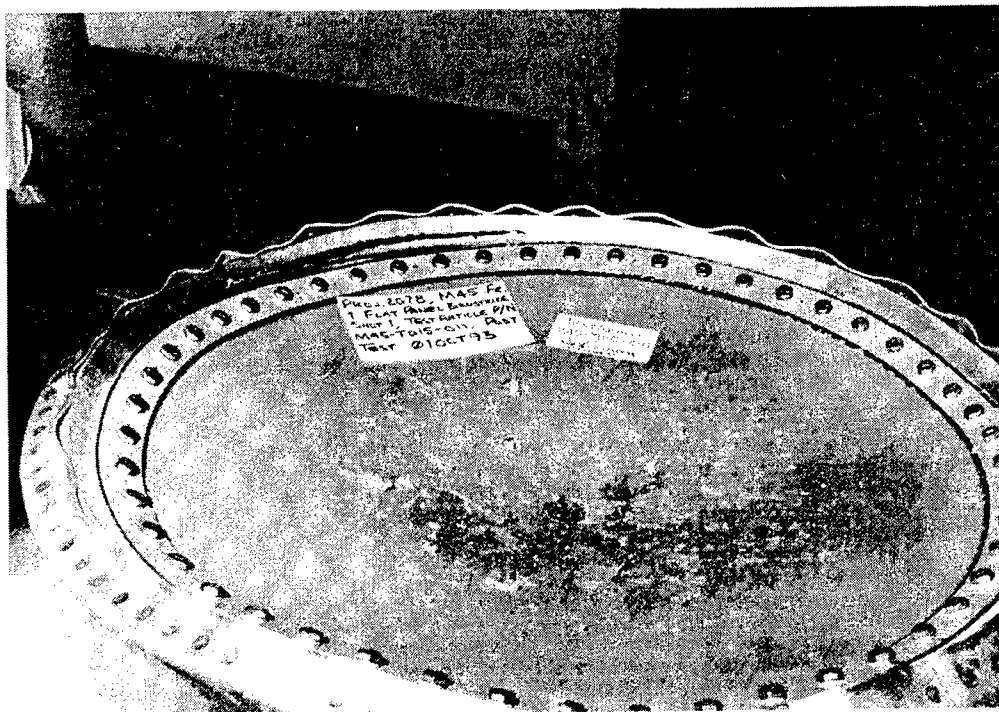


Fig. 4 GLARE® radome front bulkhead test^[8]

Workshop properties of GLARE®

Extensive research, especially at Delft University and at several OEM's, makes clear that GLARE® can be machined almost equally to aluminum alloys. In certain cases some adjusted tooling is recommended. Workshop experience showed that the learning process is simple and fast. It turns out that GLARE® can be easily drilled, milled, sheared and waterjet cutted. Forming of GLARE® has some limitation, due to the elongation of the fibres. Also springback angles after forming are different compared to aluminum alloys. However, like machining, the learning process is simple and fast. Even very complex parts can be made, which is, among others, demonstrated by Aerospatiale performing a stretch formed GLARE® cockpit crown (Fig. 5).

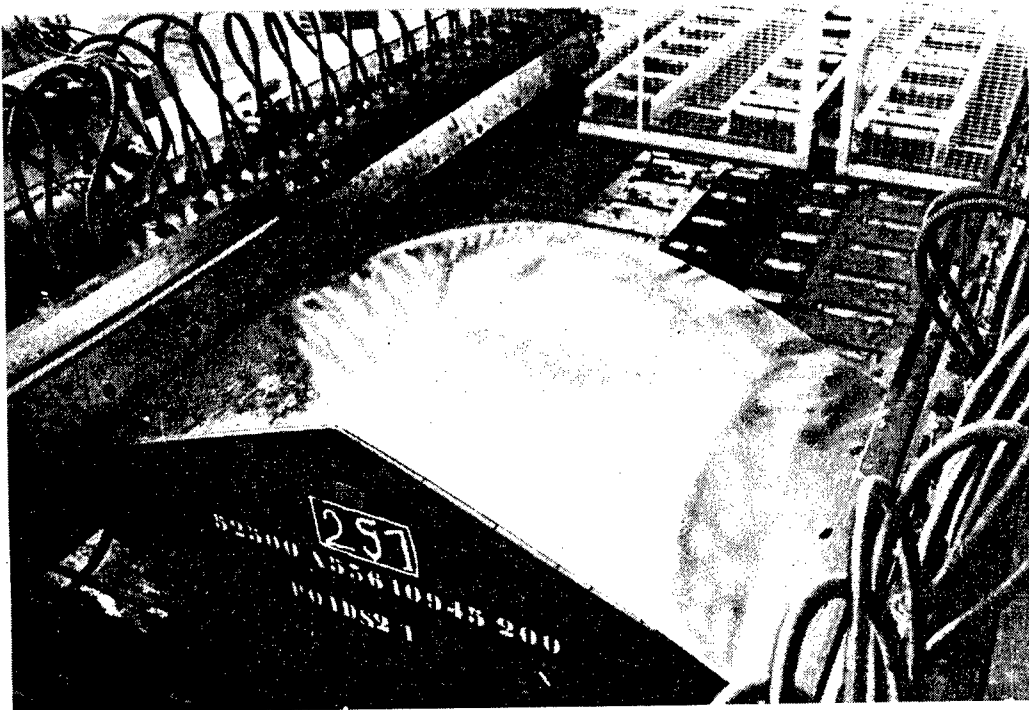


Fig. 5 Stretch formed GLARE® cockpit crown
(Courtesy Aerospatiale)

The nature of GLARE® allows for shapes not possible or very difficult to achieve with aluminum alloys.

The layered concept of GLARE® applied in a complex tool creates components not (easy) achievable in aluminum alloys (thickparts, AS

cockpit crown, etc.). It is obvious that this aspect can reduce the cost of a component/part significantly.

Cost of GLARE® components

It is clear that due to the nature of the product, GLARE® is more expensive per unit area compared to aluminum alloys. However, as is mentioned in the section above, the characteristics of GLARE® makes it possible to reduce the cost ratio significantly. Moreover, recent studies and analyses indicate that with proper design and production methods even cost reduction is possible. Important elements in this process are weight reduction, buy/flight ratio, simplified components and reduction of parts. In the previous sections some of these aspects have been addressed. Part reduction in fuselages and bulkhead by eliminating the Ti-straps is one aspect to obtain cost minimization. Less number of longitudinal lapjoints through the splicing concept is another significant cost reduction factor for fuselage sections. Simplification of parts can be achieved a.o. by deleting the thickness steps at joints and stringers. Finally it turns out that the buy/fly ratio of GLARE® fuselage components is more than a factor two less compared to their aluminum counterparts. This means that more than twice the amount of material is required for the aluminum part compared to the GLARE® part. Taking into account these factors combined with usage of the specific GLARE® characteristics into the production process can result in the above mentioned cost savings.

Conclusions

It is clear that GLARE® offers significant weight reduction for primary aircraft structures. Weight savings in the range of 15% - 25% are possible.

Moreover, extensive testing by several institutes as well as OEM's, including flight evaluation, show that the application of GLARE® will enhance the structural integrity of the aircraft and on top of that can improve the safety of the crew and passengers.

Finally it can be concluded that these benefits can be achieved at relative small cost increase or for certain components, with proper use of the characteristics even cost reduction can be obtained.

References

1. "GLARE® for skin materials?; Example: A-3XX fuselage", J.W. Gunnink, L. Schwarmann, SLC-report TD-M-96-005, 1996.
2. "GLARE®; A Structural Material for Fire Resistant Aircraft Fuselages", G.H.J.J. Roebroeks, Presentation AGARD Conference, Dresden, October 1996.
3. "Fibre Metal Laminates and the Very Large Civil Transport", J.W. Gunnink, L.B. Vogelesang, In: "50 Years of Advanced Materials" or "Back to the Future", SAMPE-Europe Conference Proceedings, Toulouse, June 1994, ISBN 3-9520477-1-6.
4. ECOS³ Luggage Container, Explosive Containment Systems, Brochure, Galaxy Scientific Corporation, New Jersey, USA, 1996.
5. "Design Development of a Bonded Fuselage Repair for the C-5A", Major R. Fredell, HQ USAFA/DFEM, 1995 USAF Structural Integrity program Conference.
6. On the application of GLARE® for Airbus Fuselage Structures, L. Schwarmann, N. Ohrloff, T. Beumler, In: Fatigue of Aircraft Materials, pp. 191 - 197, Delft University Press 1992.
7. "Application of GLARE® material on Fuselage Structures with Special Regard to Repair and Inspection", T. Beumler, J.W. Gunnink, 25th European Aircraft Maintenance Conference, Athens, November 1995.
8. "Impact properties and related applications of Fiber Metal Laminates", K. Poston, A.C. Mattousch, T.J. Matway, In: "50 Years of Advanced Materials" or "Back to the Future", SAMPE-Europe Conference Proceedings, Toulouse, June 1994.

An Experimental Evaluation of Fatigue Crack Growth Prediction Models

*Prof. Luigi Lazzeri
Prof. Attilio Salvetti
Department of Aerospace Engineering
University of Pisa
Via Diotisalvi, 2 - 56126 Pisa - Italy

Abstract

Damage tolerance analysis relies on Fracture Mechanics design tools, and among these the methods for crack growth analysis have an outstanding relevance. Considerable efforts have been dedicated in the last decades to the development of models, at first of a rather semi-empirical character, later on grounded on more physical basis, to explain the interactions between load cycles of different amplitude. From this point of view, the closure phenomenon is unanimously considered by the scientific community as the most important in explaining the various effects that may be present in a crack propagation process under variable amplitude loading. The paper analyses the main models, commonly used by the aircraft community, on the basis of the comparison of the predictions with experimental results which have been specifically generated in a research program carried out at the Department of Aerospace Engng. of Pisa. Flight-by-flight load spectra have been used, of the gust dominated type, as well as simple Variable Amplitude sequences (overload, underload, ..). The 2024 aluminium alloy has been used, with two thicknesses: 2.54 mm in the T3 condition and 12.5 mm in the T351 condition. Some results have already been presented elsewhere, while others, e.g. those relevant to the plate material, have never been presented before. The paper discusses the performance of various models, with emphasis on the semi-empirical and analytical crack closure models, giving also indications about the spectrum sensitivity of the various models.

A copy of the view-graphs of the presentation is reported in the following. Particular care has been taken in keeping the information as clear as possible. The paper presents the results of a research program that has been going on at the Department of Aerospace Engineering of Pisa since mid 1992

and consequently some of the results have already been presented in two previous Conferences. Therefore, the reader can find more details of the research in:

A. Salvetti, L. Lazzeri, A. Pieracci: "An assessment of fatigue crack growth prediction models for aerospace structures", in AGARD Report 797, Sept. 1993.

L. Lazzeri, A. Pieracci, A. Salvetti: "An evaluation of fatigue crack growth prediction methods used in aircraft design", in 'Estimation, enhancement and control of aircraft fatigue performance', Proceedings of the 18th ICAF Symposium, pp. 615-645, EMAS publ., 1995.



**AN EXPERIMENTAL EVALUATION OF
FATIGUE CRACK GROWTH
PREDICTION METHODS**

**L. Lazzeri and A. Salvetti
Department of Aerospace Engng.
University of Pisa - Italy**

**1996 USAF Structural Integrity Program Conference
San Antonio, 3/5 December 1996**



INDEX OF PRESENTATION

MODELS FOR CRACK GROWTH PREDICTION UNDER SPECTRUM LOADING

EXPERIMENTAL PROGRAM

COMPARISON OF TEST RESULTS WITH PREDICTIONS

a vs. F PLOTS

da/dF - Kmax PLOTS

Nex/Ncalc DISTRIBUTION

DISCUSSION

CONCLUSIONS



FATIGUE CRACK GROWTH MODELS

- NON INTERACTIVE MODEL
- CHARACTERISTIC K CONCEPT
- YIELD ZONE MODELS
- CRACK CLOSURE MODELS

SEMIEMPIRICAL MODELS:

- CORPUS
- ONERA
- PREFFAS
- MODGRO/AFGROW

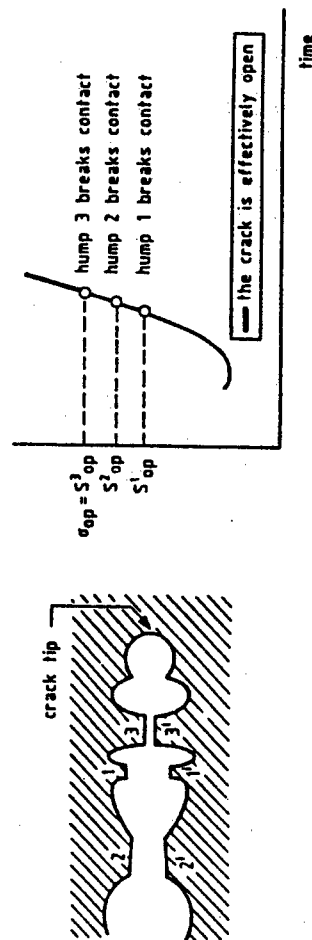
ANALYTICAL MODELS (STRIP YIELD MODELS):

- FASTRAN-II
- STRIPY-93



CORPUS

CRACK CLOSURE IS RELATED WITH THE FORMATION OF HUMPS ON THE CRACK FACES:



- PRIMARY AND SECONDARY PLASTIC ZONES
- PLANE STRESS OPENING FUNCTION
- PLANE STRAIN/PLANE STRESS TRANSITION CONSIDERED ONLY FOR WHAT CONCERNS THE PLASTIC ZONE SIZE
- MULTIPLE OVERLOAD EFFECT



ONERA

- PREVIOUS STRESS HISTORY ---> EQUIVALENT LOAD CYCLE
- PLANE STRAIN/PLANE STRESS TRANSITION: RATIO OF IRWIN PLASTIC ZONE SIZE/THICKNESS
- THICKNESS EFFECT: RELAXATION OF THE INFLUENCE OF K_{min} ON THE INTERACTION RULE
- OPENING FUNCTION: WEIGHTED AVERAGE OF TWO VALUES:
C.A. LOAD AND SINGLE O.L. EFFECT

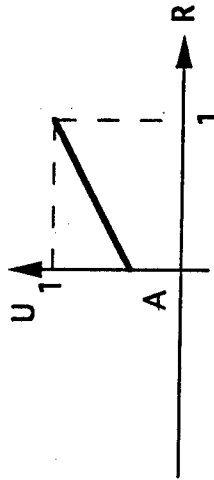


PREFAS

INITIALLY PROPOSED FOR SHORT LOAD SEQUENCES, i.e. THE CRACK GROWS INSIDE THE PLASTIC ZONE GENERATED BY THE HIGHEST PEAK IN THE BLOCK

- COMPRESSIVE STRESSES ARE SET EQUAL TO ZERO

- $\Delta K_{eff}/\Delta K_{nom} = U(R) = A + B R$



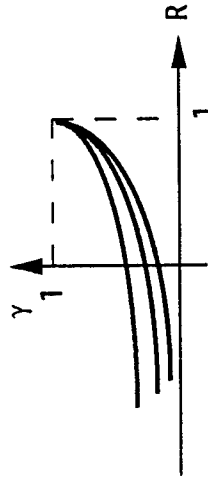
- A SPECIFIC TEST ($R=0.1 + 1 \text{ O.L. AT } 1.7 S_{max}$ EVERY 1000 CYCLES) IS REQUIRED

- NO PLANE STRAIN/PLANE STRESS TRANSITION



MODGRO/AFGROW

- OVERLOAD EFFECT IS ACTIVE FOR A GIVEN FRACTION (25%) OF THE PRIMARY PLASTIC ZONE SIZE (IRWIN FORMULATION: $r = \frac{1}{\alpha \Pi} \left(\frac{K_{\max}}{\sigma_y} \right)^2$)
- THE SHAPE OF THE OPENING FUNCTION IS CONSIDERED INDEPENDENT FROM THE MATERIAL



- NO PLANE STRAIN/PLANE STRESS TRANSITION IS CONSIDERED



STRIP YIELD MODELS

- YIELDING IS CONFINED IN A NARROW STRIP AHEAD OF THE CRACK TIP AND ON THE CRACK FLANKS
- PLASTIC ZONE SIZE AND CRACK SURFACE DISPLACEMENTS ARE OBTAINED BY SUPERPOSITION OF TWO ELASTIC PROBLEMS:
 - (a) A CRACK IN A PLATE SUBJECTED TO A REMOTE UNIFORM STRESS;
 - (b) A CRACK IN A PLATE SUBJECTED TO A UNIFORM STRESS ACTING OVER A SEGMENT OF THE CRACK SURFACE.
- BARS YIELD IN TENSION WHEN THE STRESS EXCEEDS $\alpha \sigma_0$
- σ_0 IS THE FLOW STRESS, AVERAGE BETWEEN YIELD AND ULTIMATE STRESS
- THE CONSTRAINT FACTOR, α , KEEPS THE THREE-AXIALITY OF THE STRESS STATE INTO ACCOUNT



EXPERIMENTAL PROGRAM

2024-T3 ALCLAD, T=2.54 MM, CCT SPECIMENS, W=160 MM

- FLIGHT-BY-FLIGHT SEQUENCES:

MINITWIST (S_{1g} = 60, 65, 70, 75, 80 MPa)

ATR-42 (S_{1g} = 65, 70, 75 MPa)

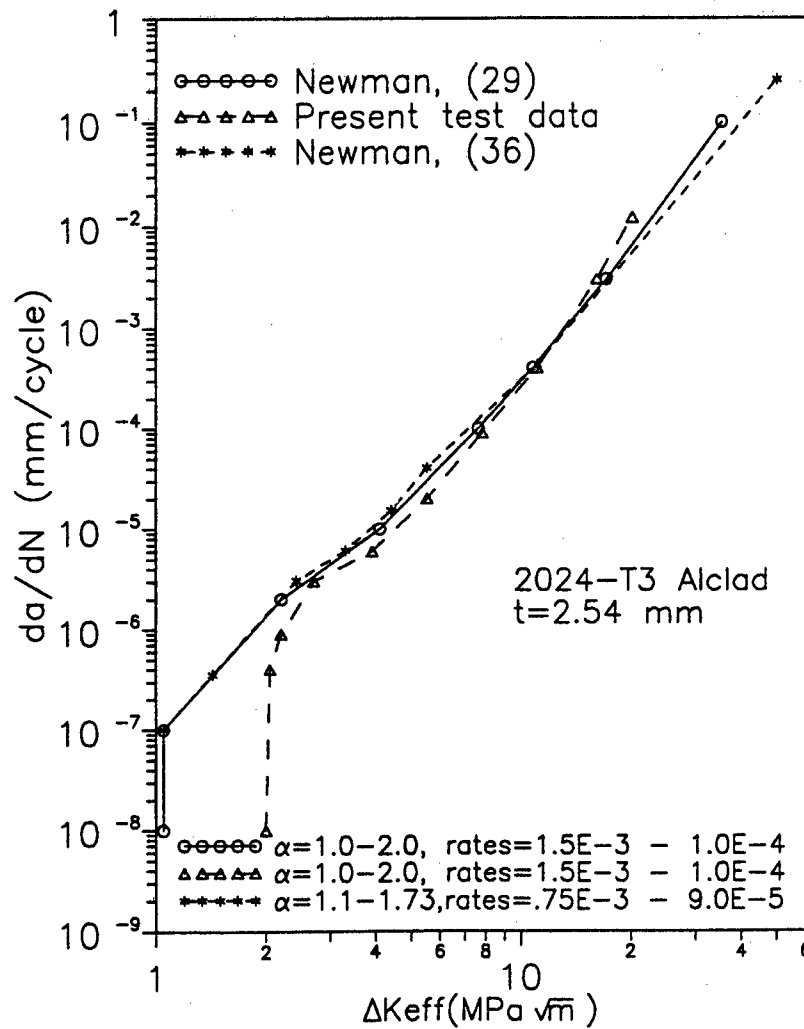
PIAGGIO P.180 (S_{max} = 160, 180, 200 MPa)

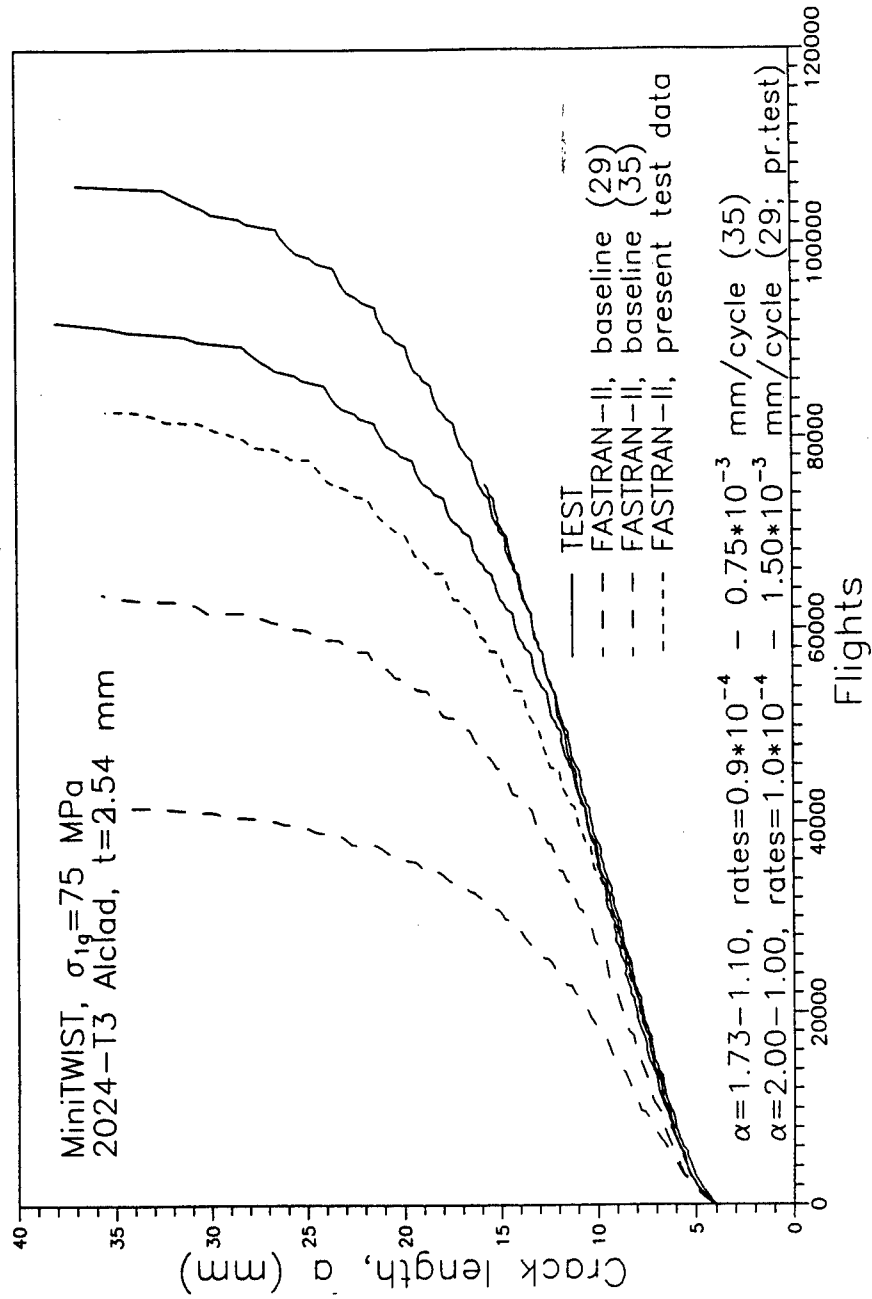
- SIMPLE VARIABLE AMPLITUDE LOAD SEQUENCES, OBTAINED INTERSPERSING A C.A. SEQUENCE WITH OL AND/OR UL AT REGULAR INTERVALS:

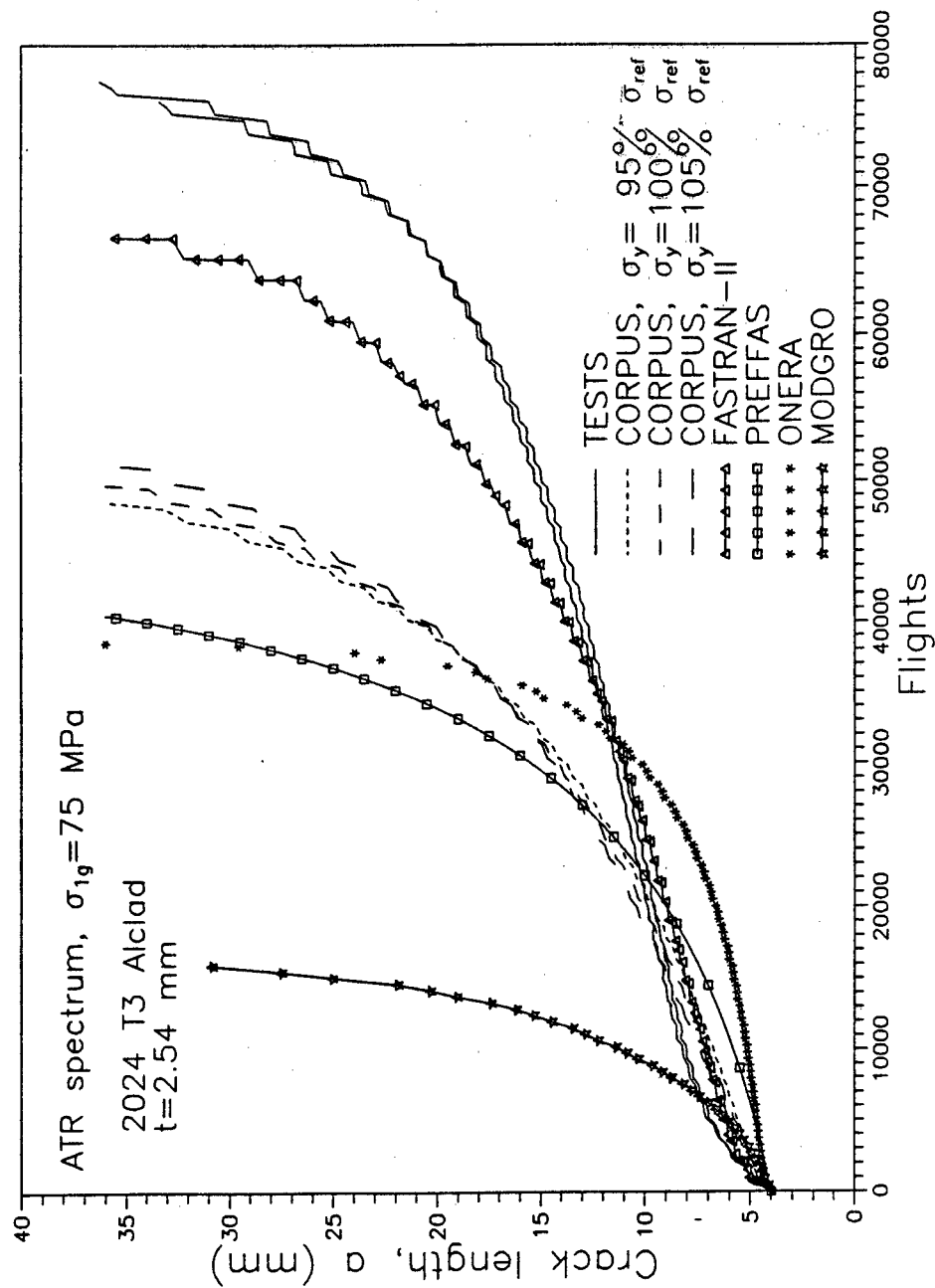
- (45-85 MPa) PLUS UL-OL EVERY 100 OR 200 CYCLES
- (45-85 MPa) PLUS UL-4OLs EVERY 200 CYCLES
- (50-100 MPa) PLUS OL (140 OR 180 MPa) EVERY 200 OR 1000 CYCLES
- (50-100 MPa) PLUS UL (0 OR -50 MPa) EVERY 200 OR 1000 CYCLES
- (50-100 MPa) PLUS 5OLs AT 140 MPa (PLUS UL)

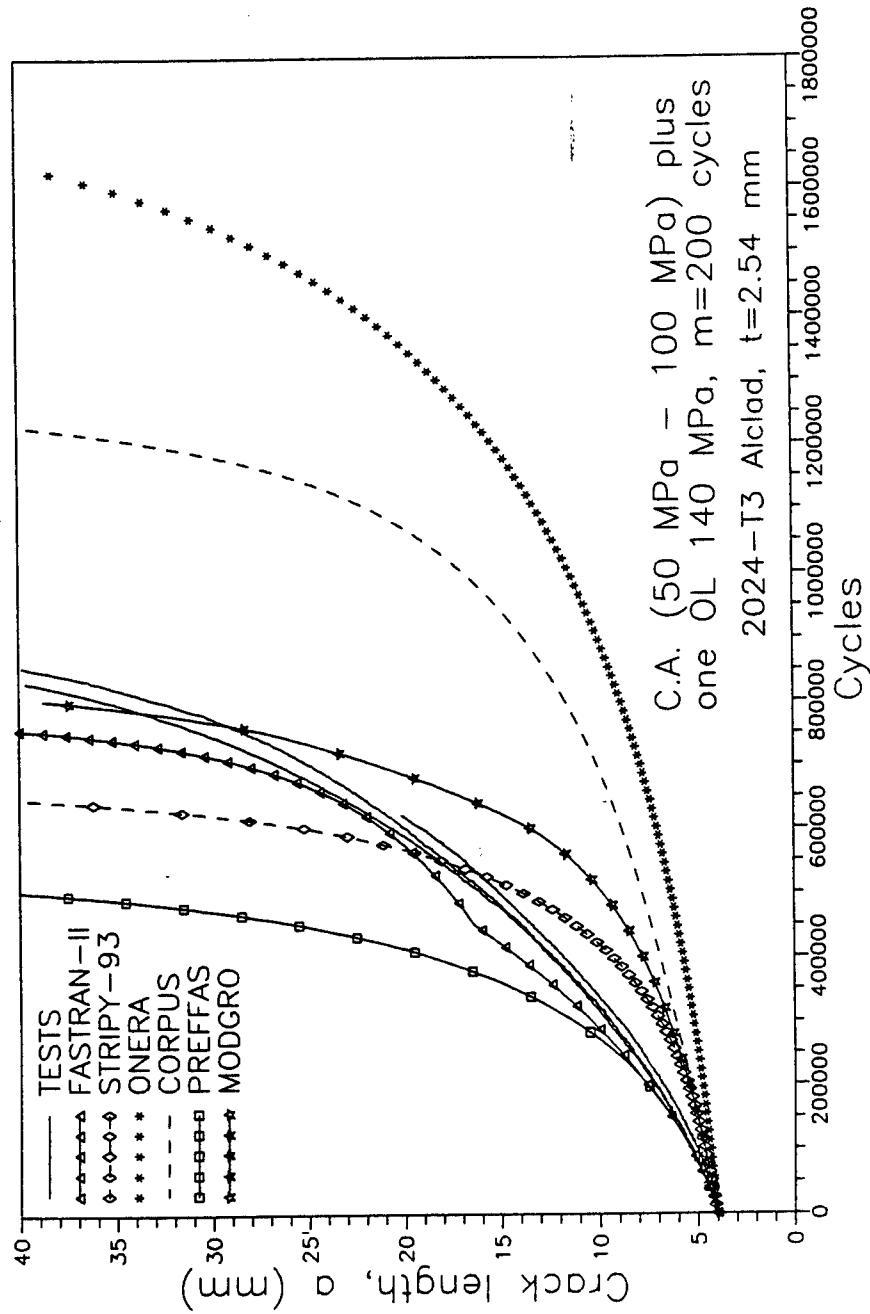
2024-T351, T=12.5 MM, CT SPECIMENS, W=36 MM

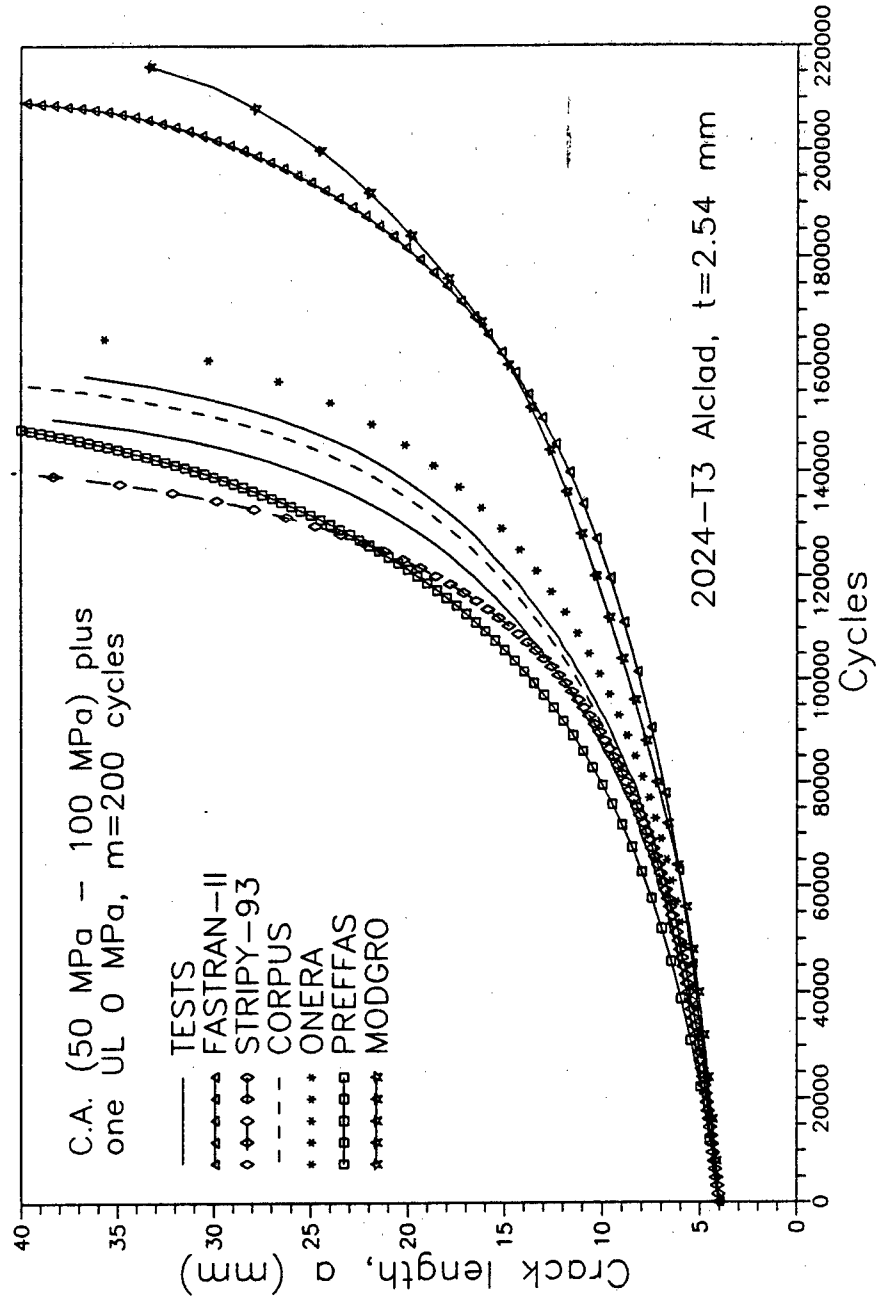
- SIMPLE V. A. LOAD SEQUENCES, SIMILAR TO THOSE DESCRIBED ABOVE

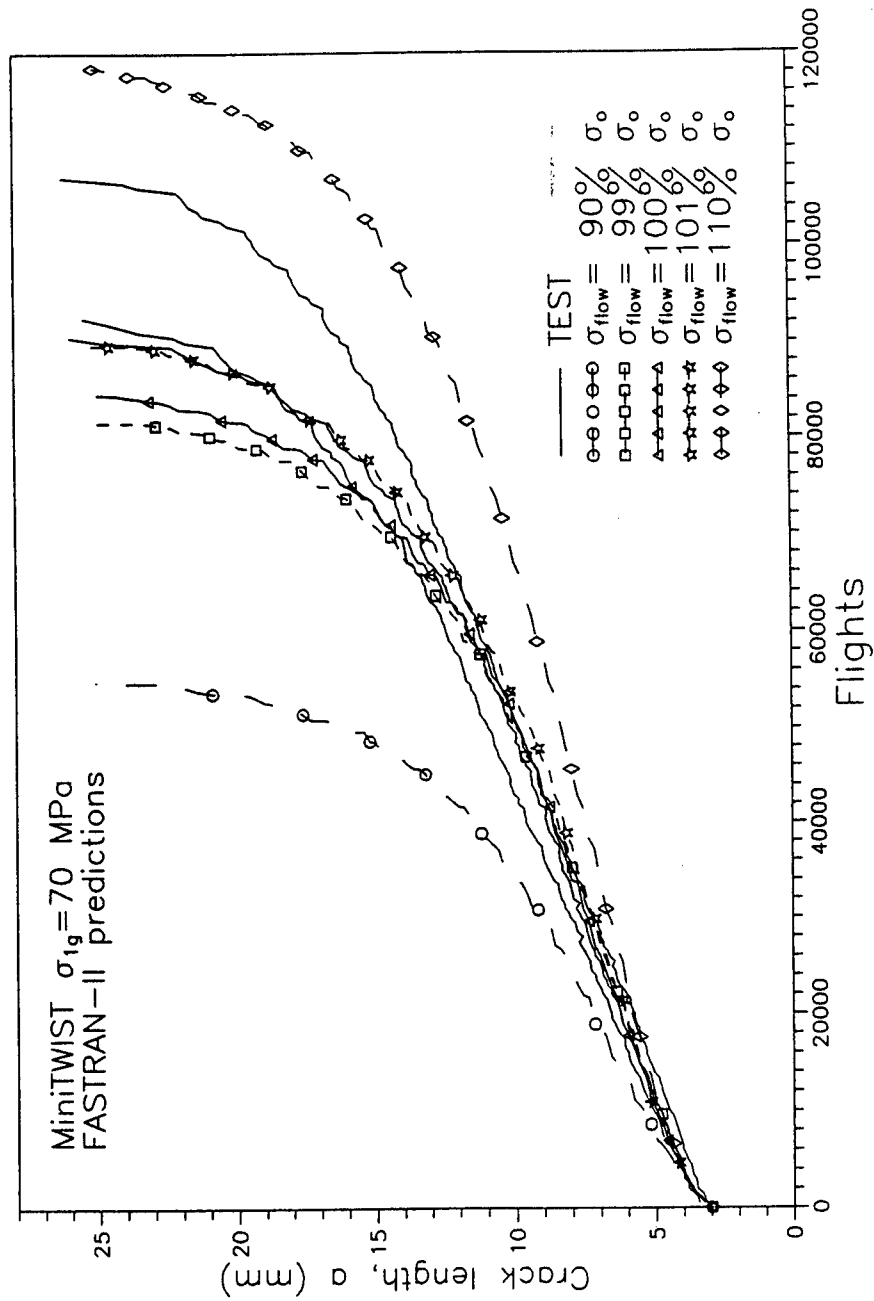


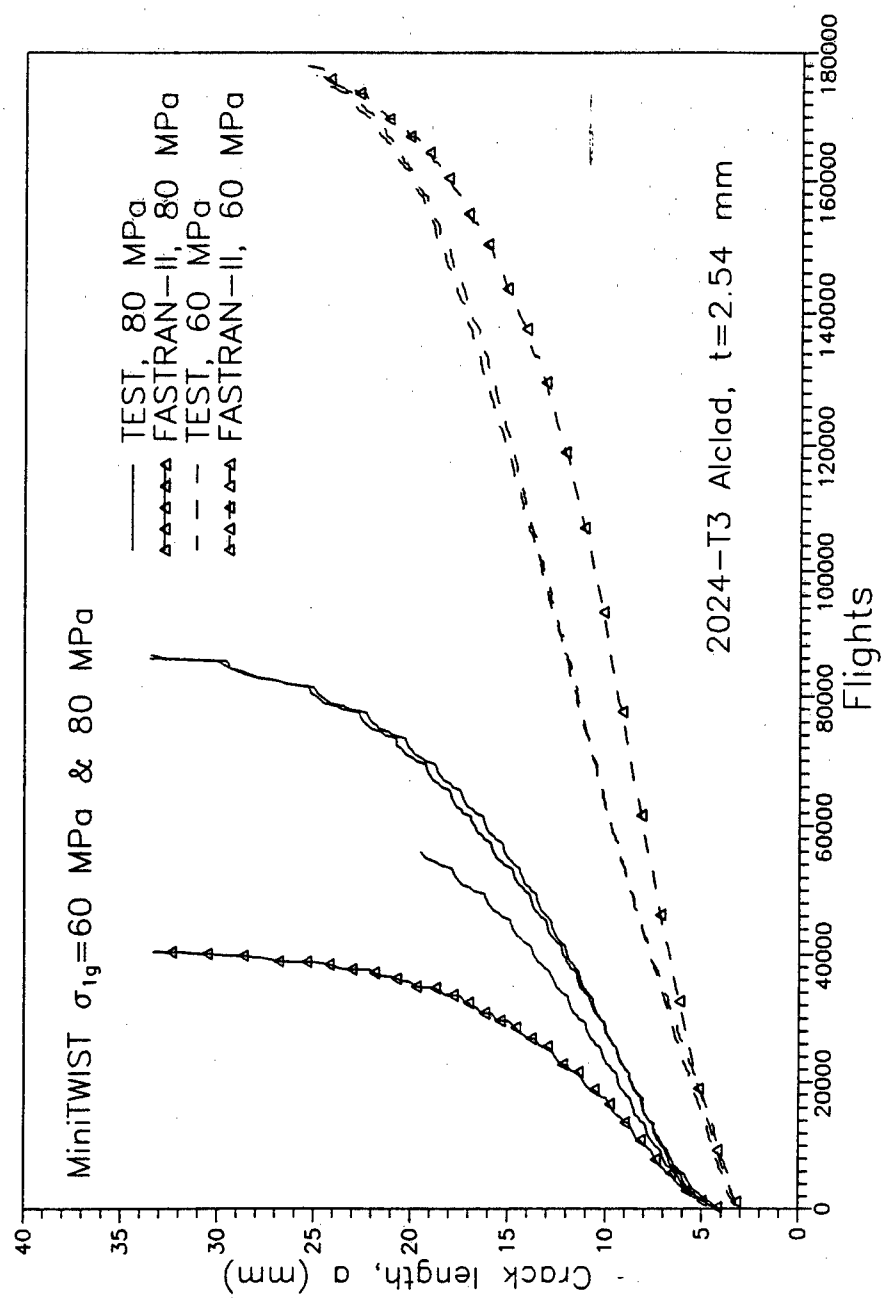


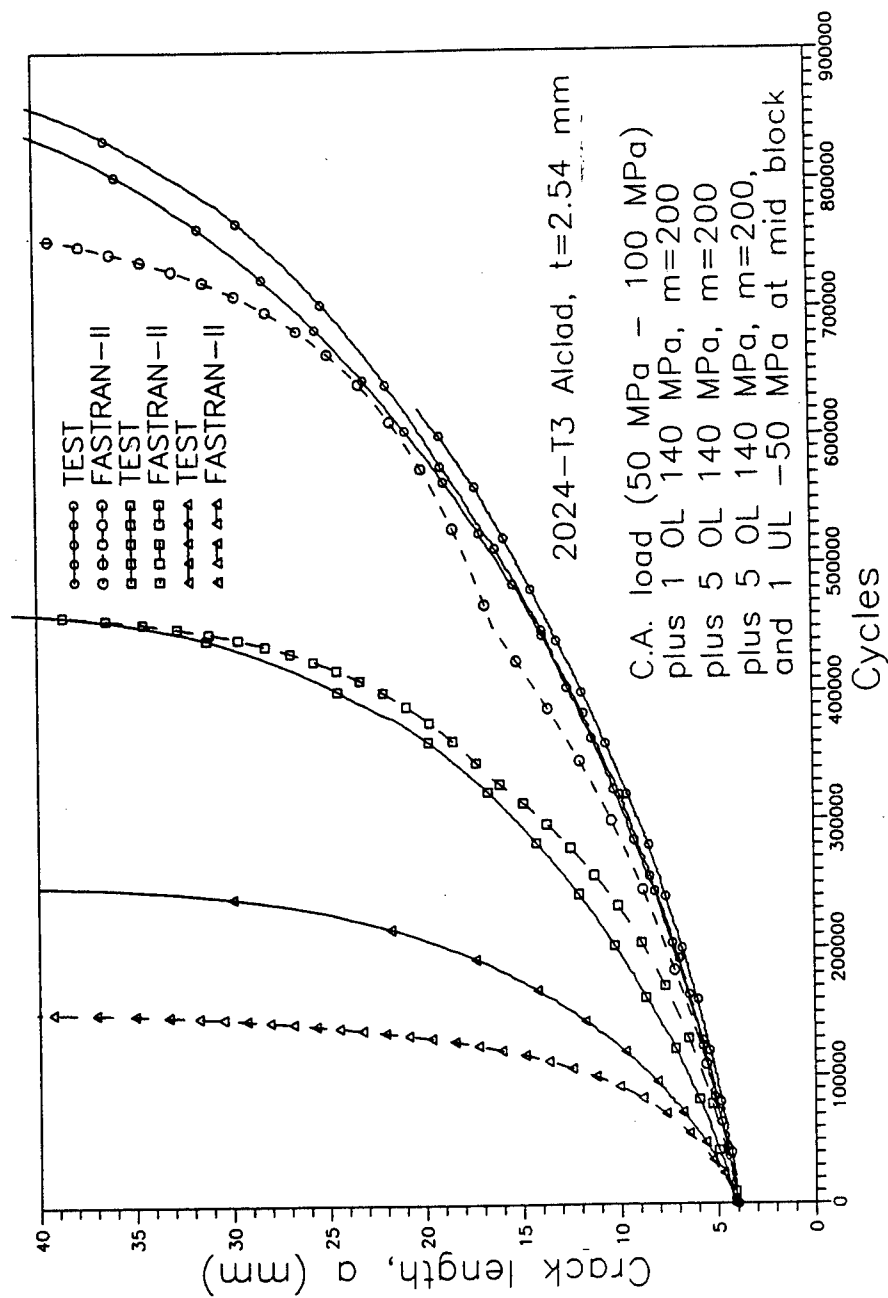


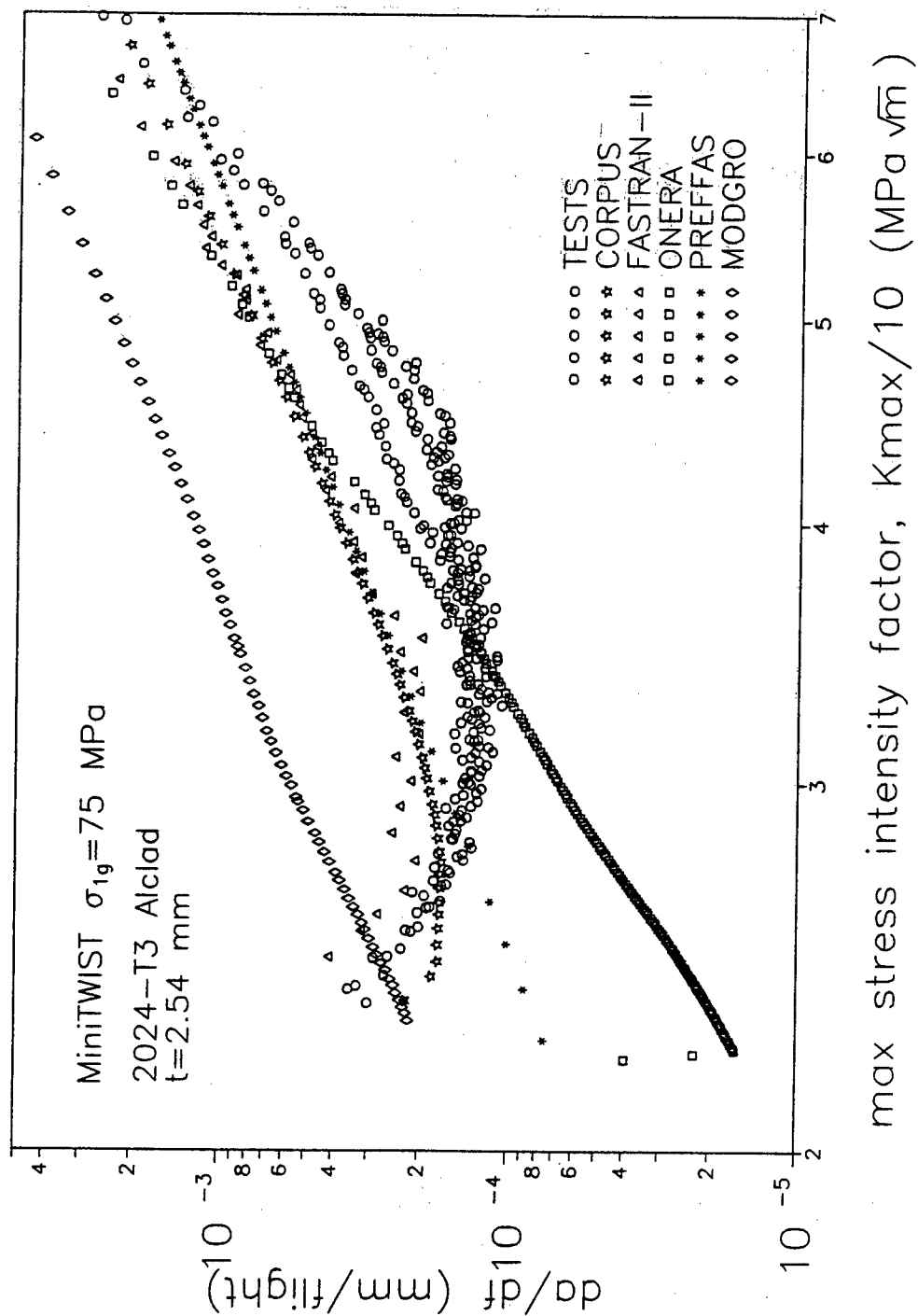


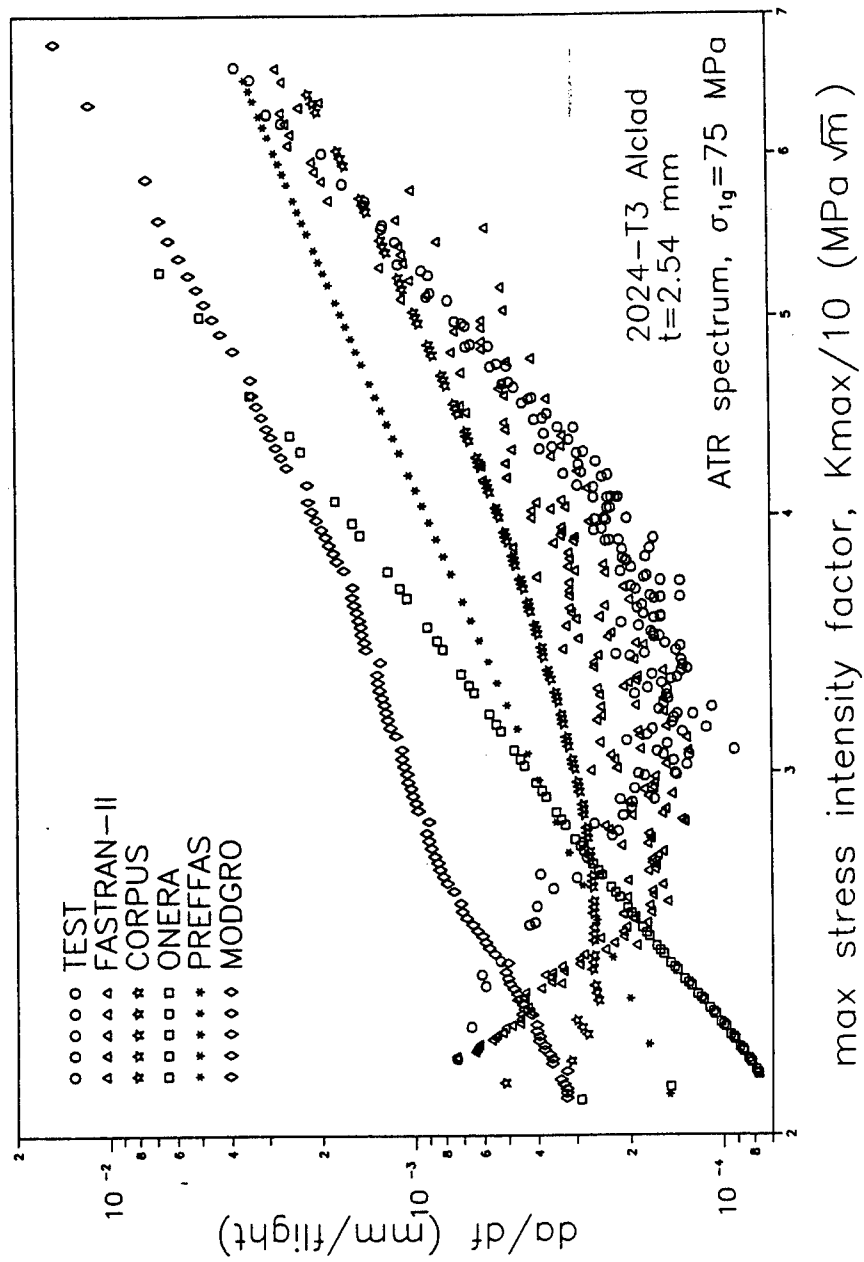


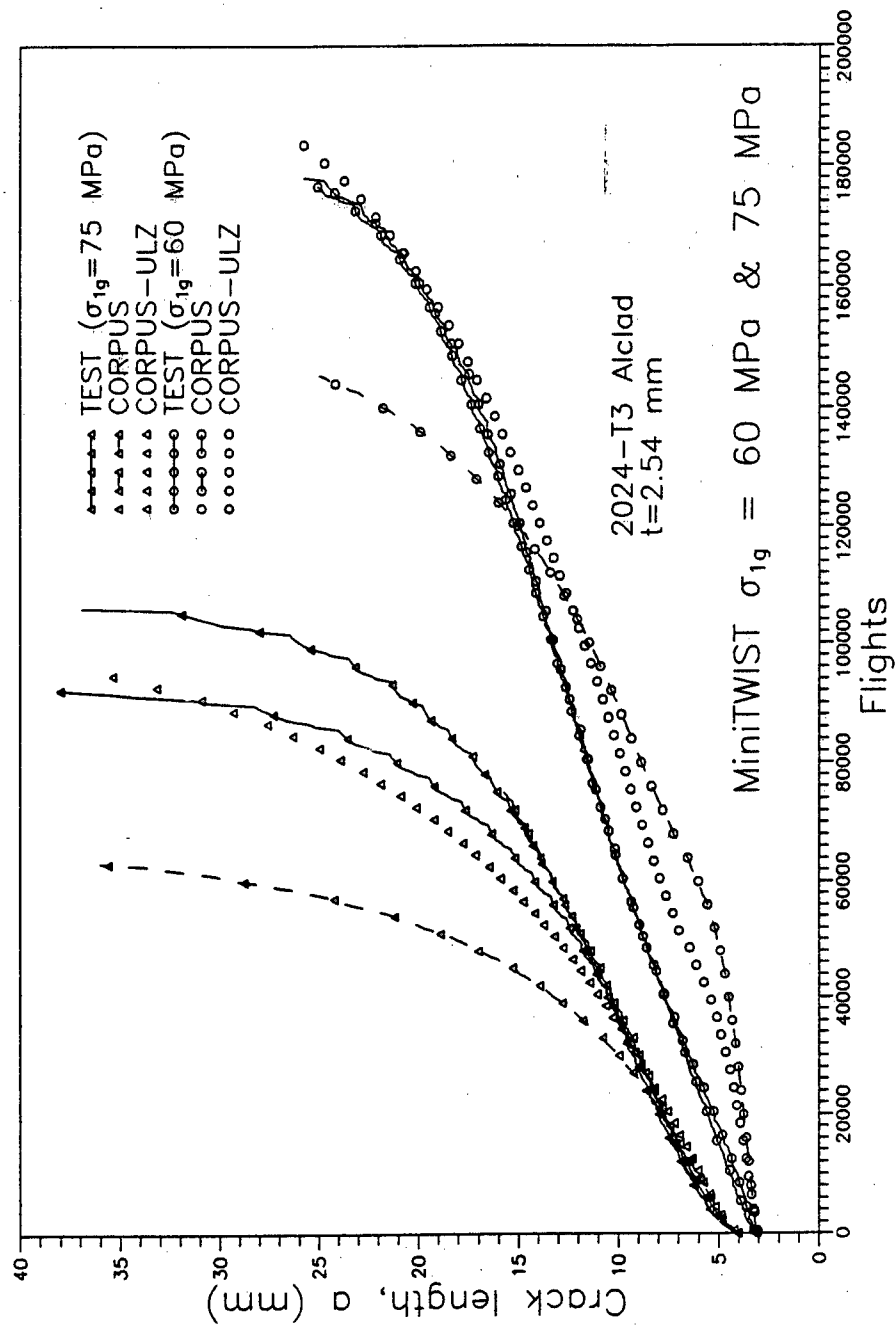


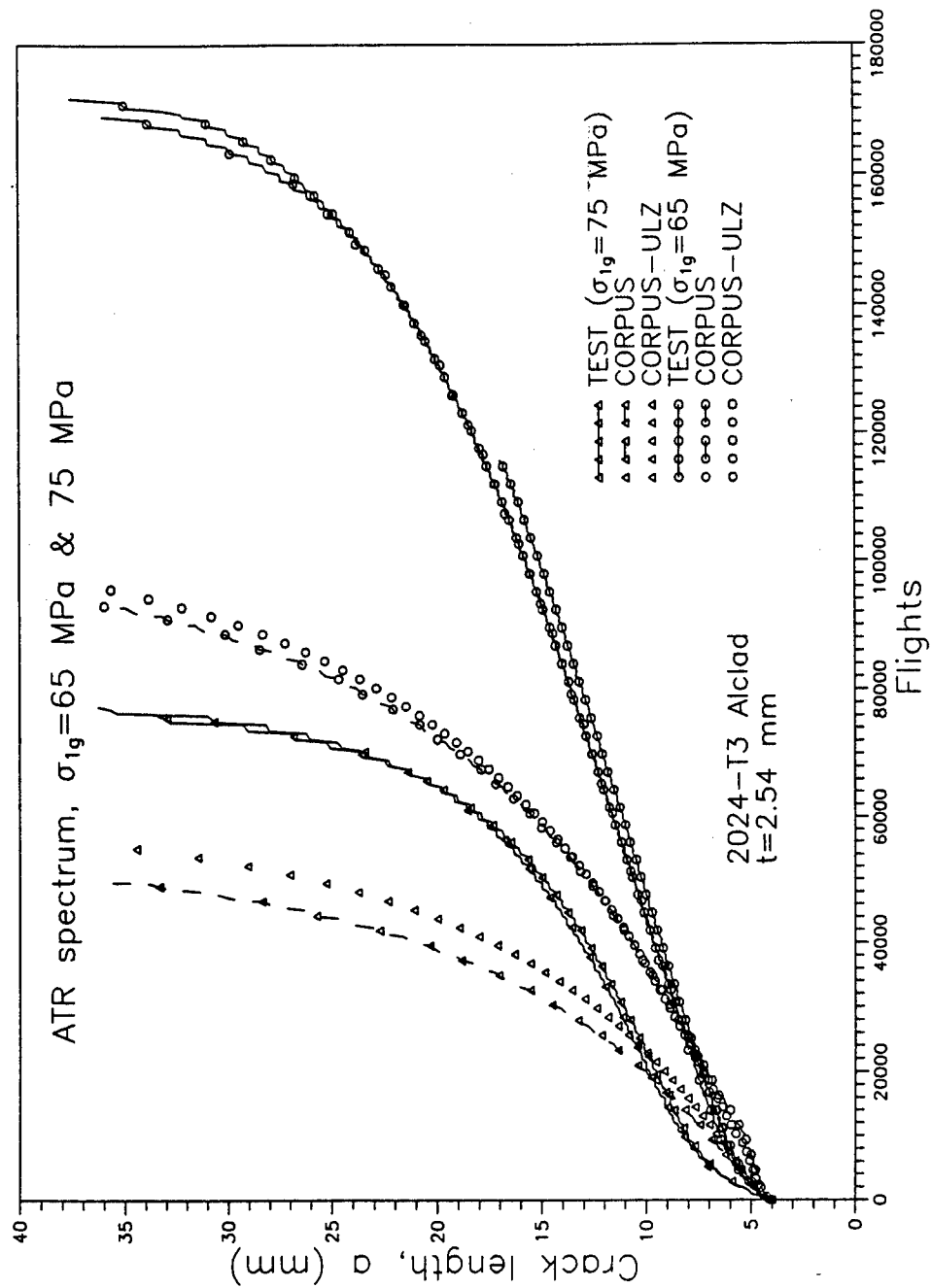


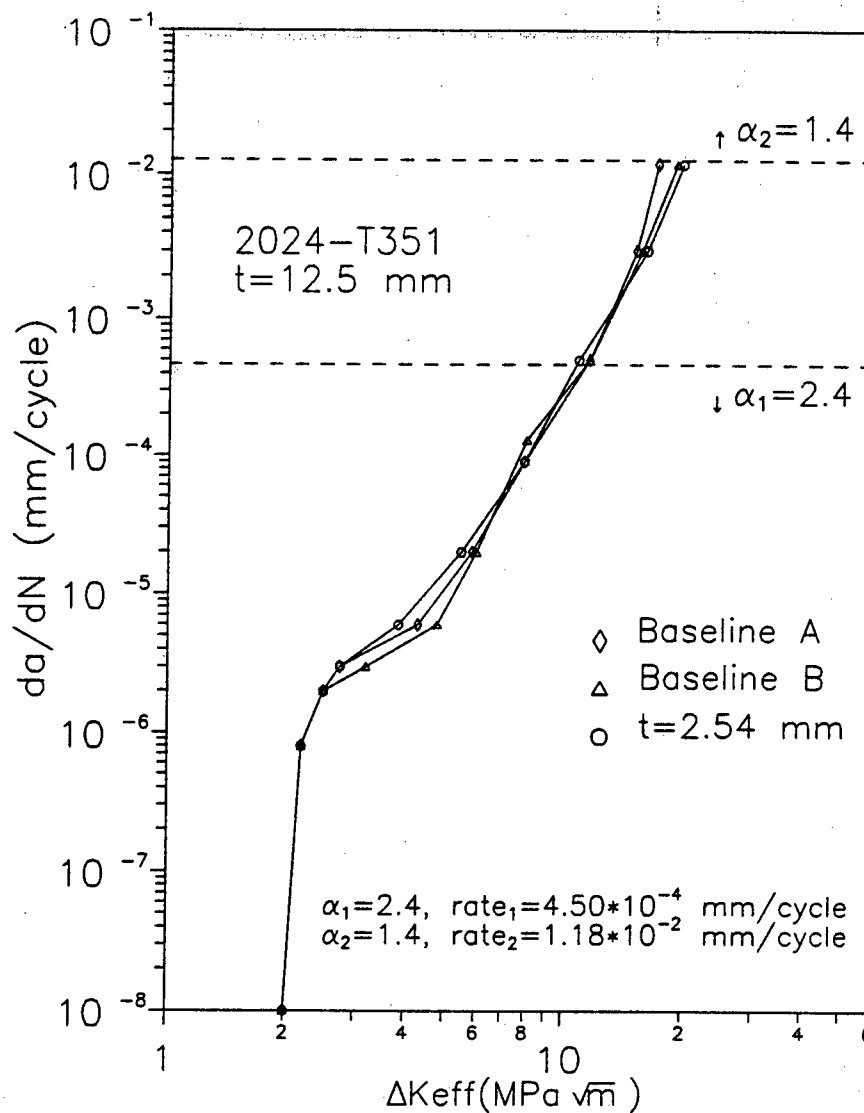


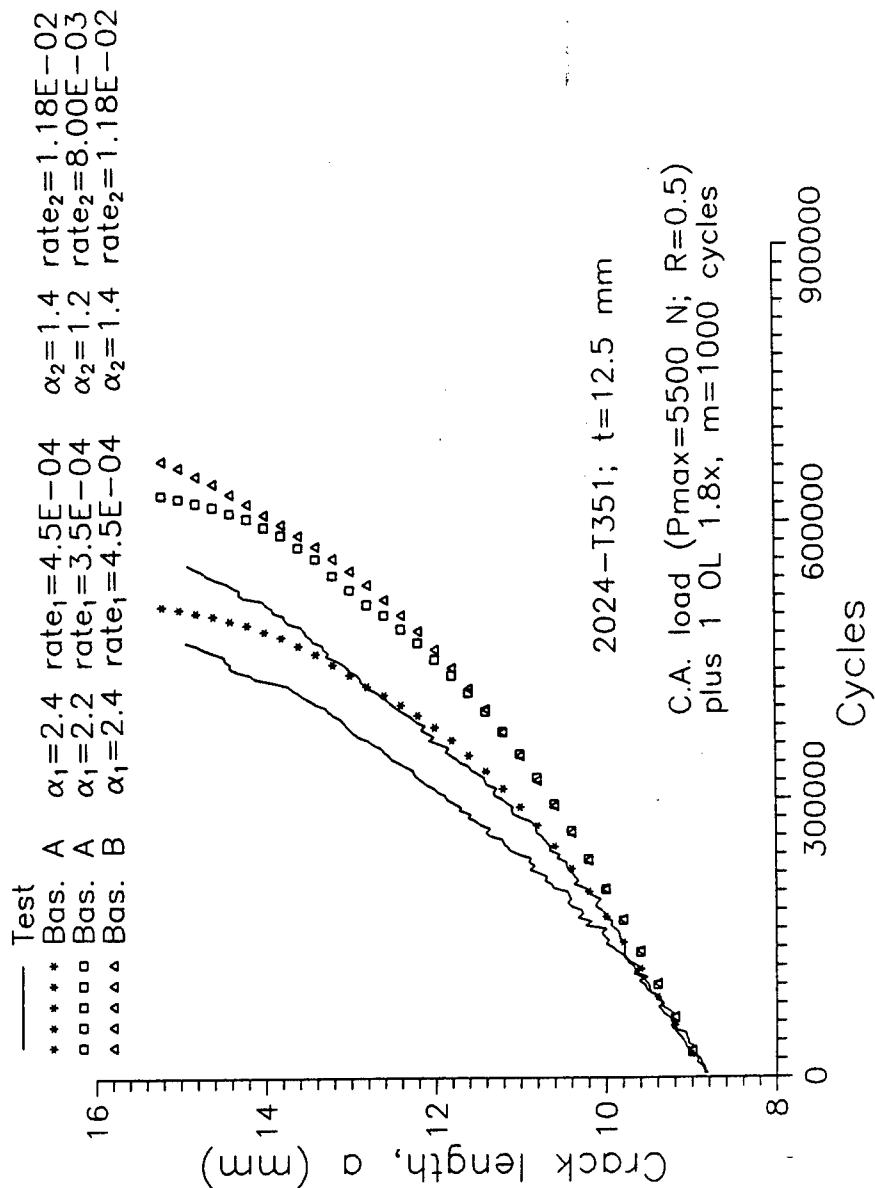


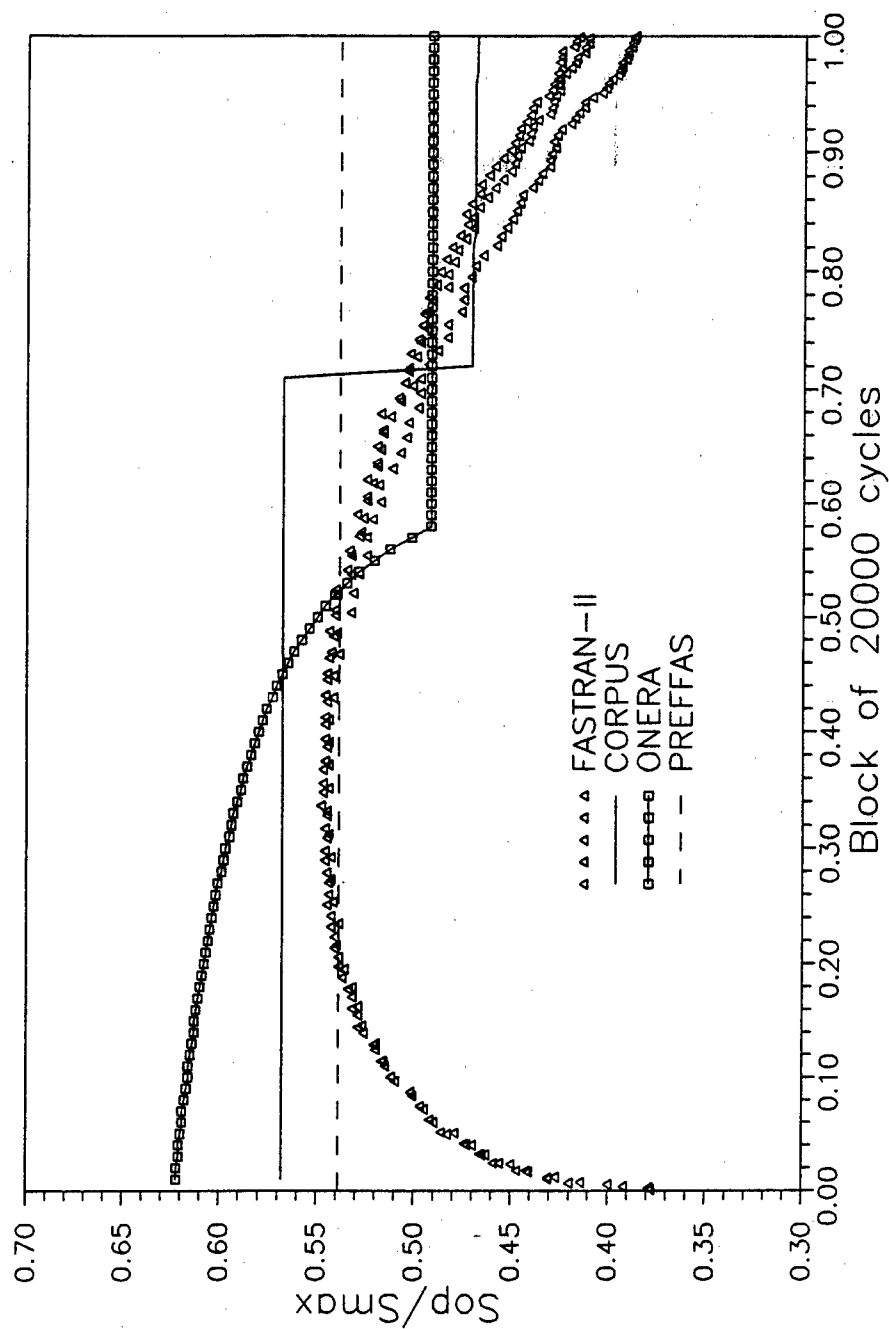


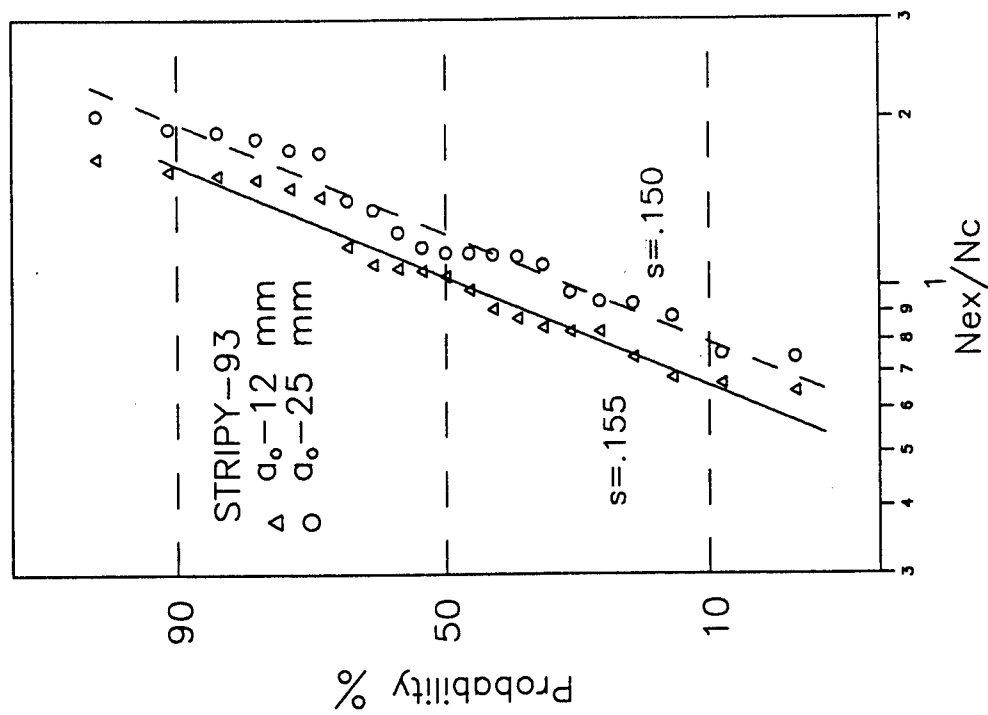
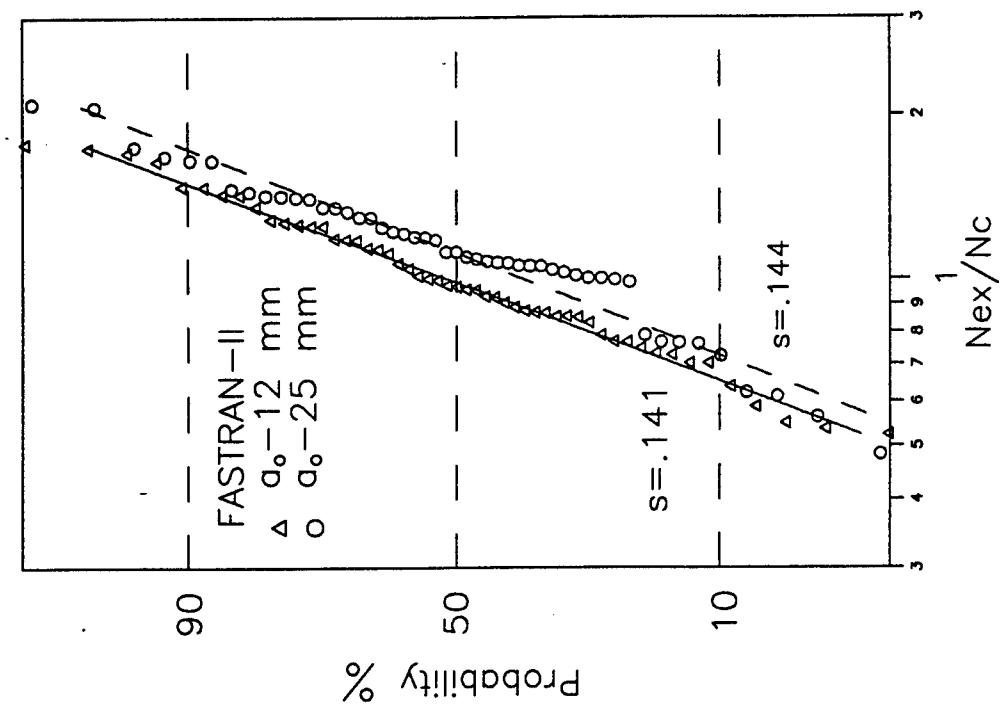


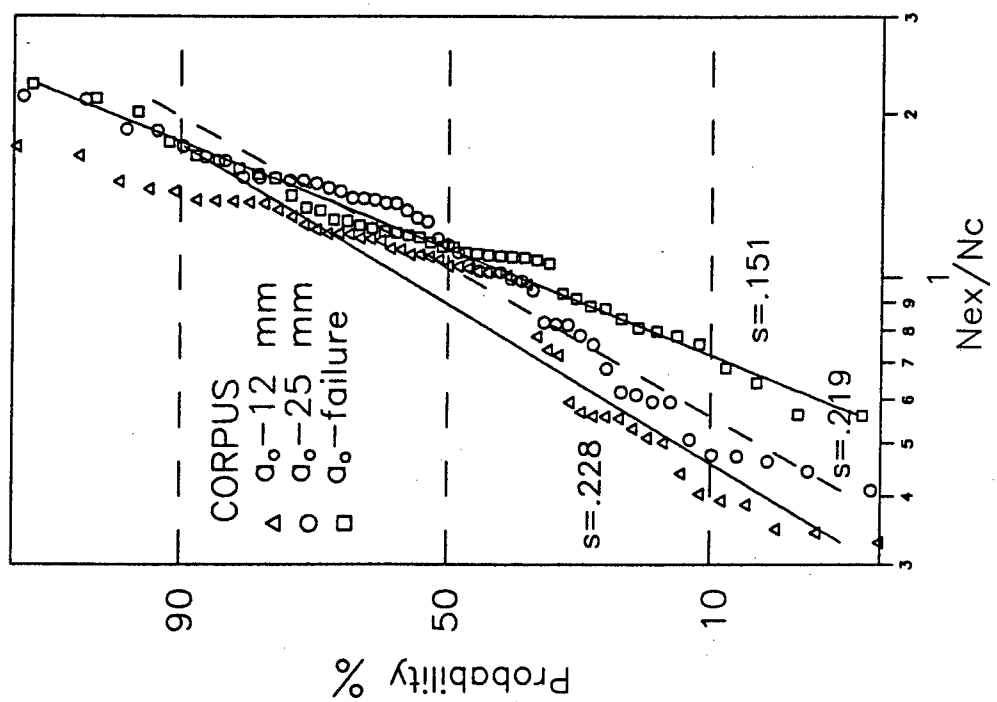
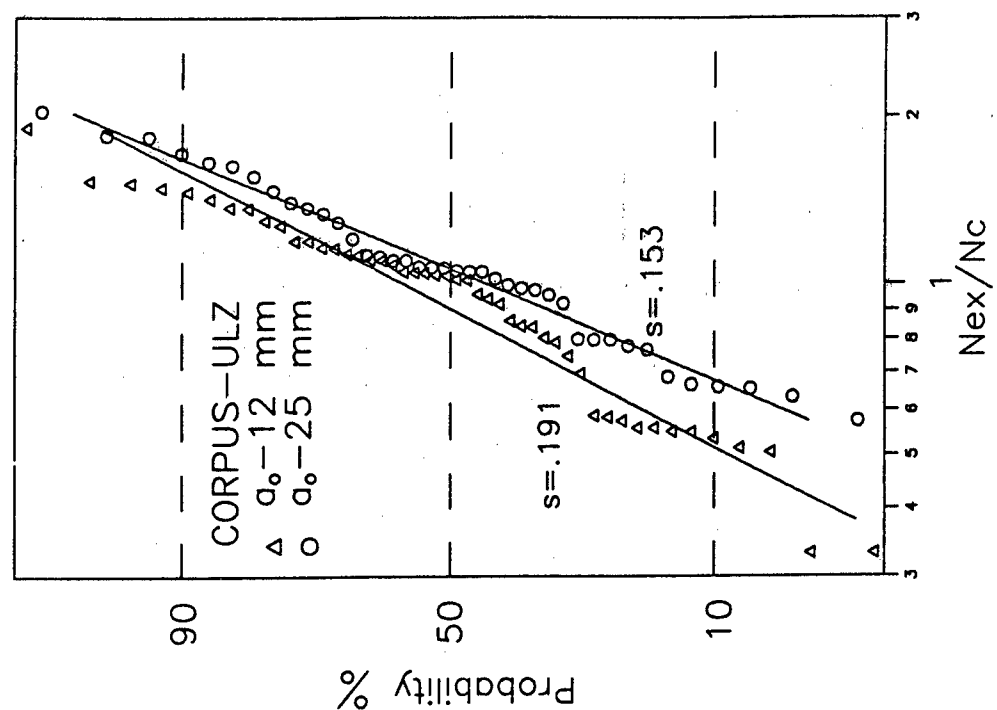


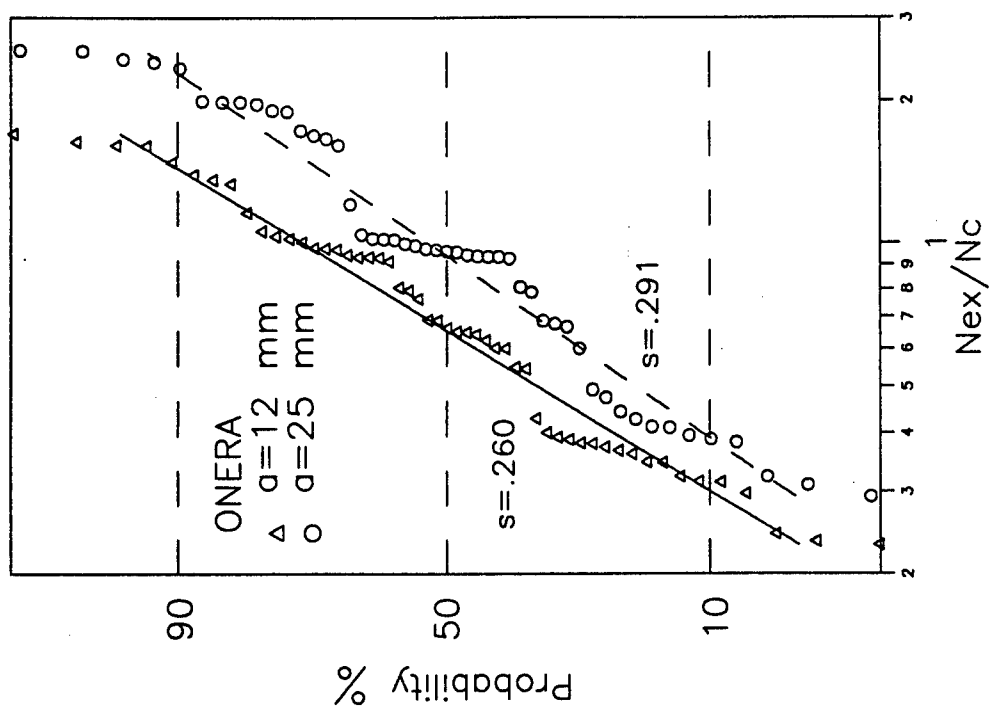
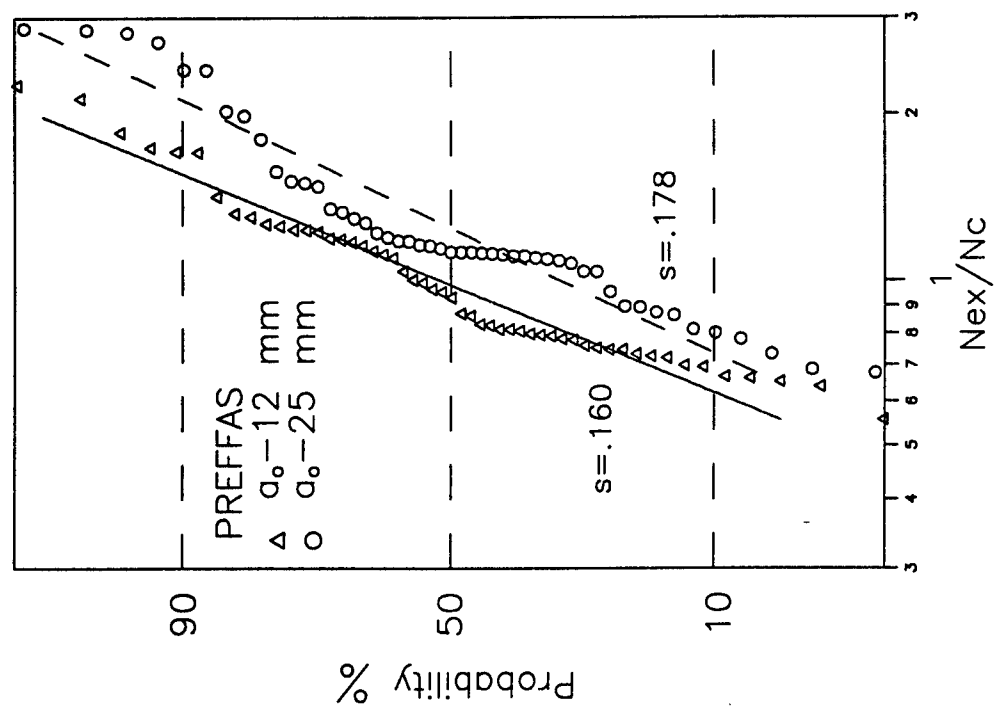


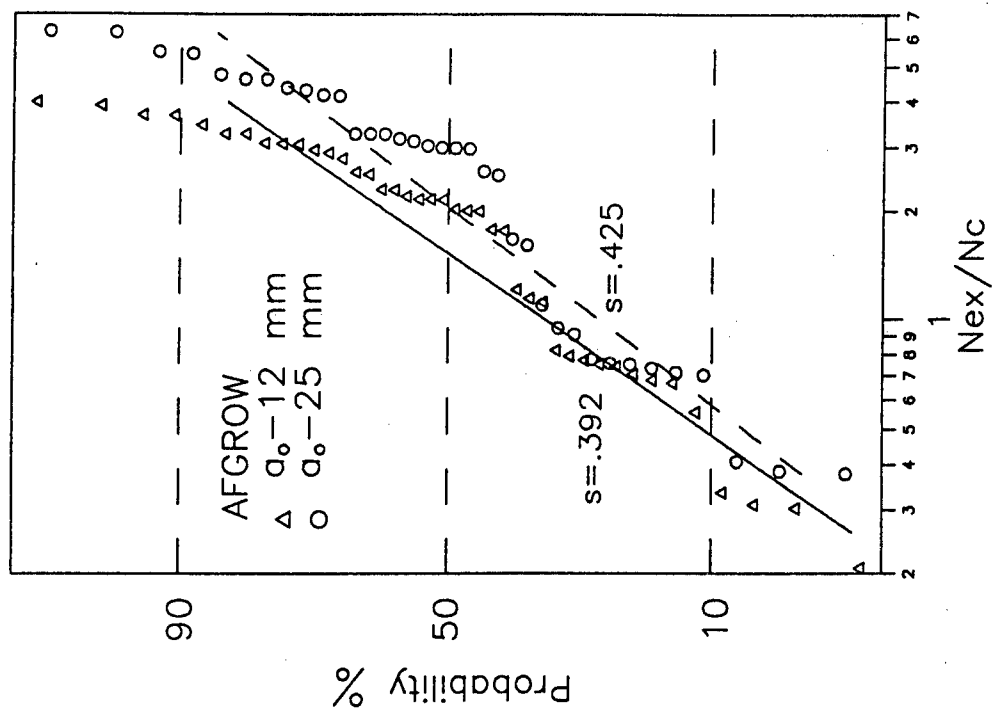
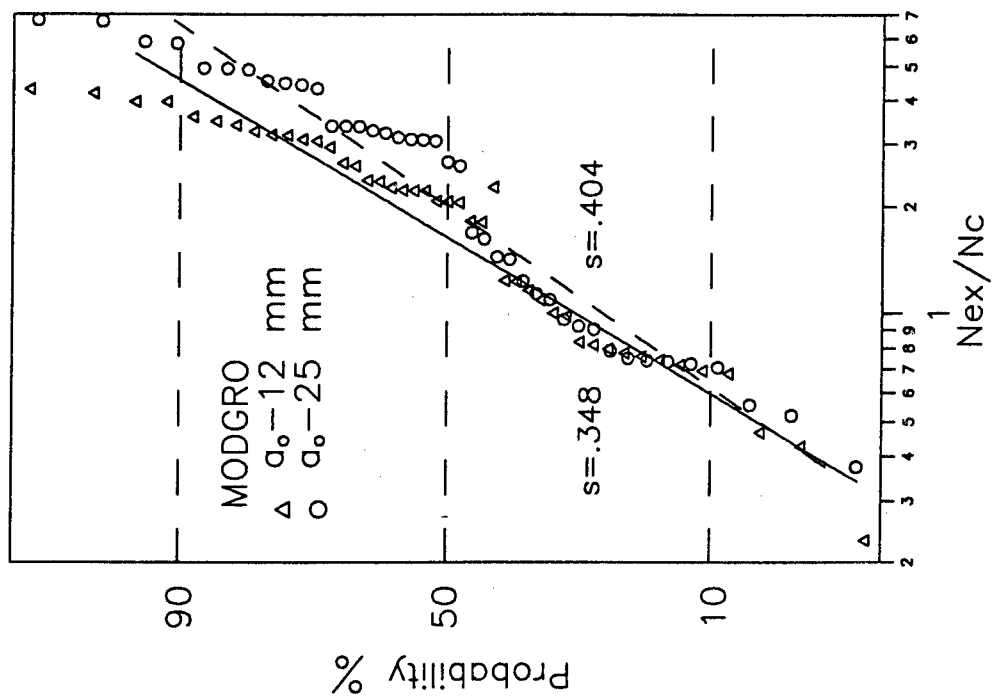














CONCLUSIONS

- THE INFLUENCE OF THE USE OF CRACK PROPAGATION LAW CONSTANTS BASED ON PRESENT TEST ACTIVITY ON PREDICTIONS IS SMALL FOR CORPUS, BUT IN OTHER CASES BRINGS TO MEANINGFUL DIFFERENCES
- STRIP-YIELD MODELS PROVED TO BE THE MOST RELIABLE METHODS
- A RELATIVELY SIMPLE METHOD, LIKE PREFFAS, IS ABLE TO PROVIDE RATHER ACCURATE PREDICTIONS, IN A SIGNIFICANT RANGE OF SPECTRA AND STRESS LEVELS
- THE MODIFIED CORPUS MODEL, WHICH CONSIDERS AN UNDERLOAD AFFECTED ZONE, INCREASES THE QUALITY OF THE PREDICTIONS, TO A GREATER OR MINOR EXTENT ACCORDING TO THE LOAD SPECTRUM
- CORPUS AND FASTRAN-II MODELS ARE CAPABLE OF PROVIDING THE SAME TREND OF CRACK GROWTH RATES VS. CRACK LENGTH OBSERVED IN TEST DATA
- TRANSITION FROM PLANE STRAIN TO PLANE STRESS CONDITIONS PLAYS AN IMPORTANT ROLE AND IS VERY DIFFICULT TO BE MODELLED CORRECTLY

Lower Wing Disassembly and Inspection Results of Two High Time USAF B707 Aircraft

Joe Luzar *

Senior Specialist Engineer - Durability & Damage Tolerance
Boeing Defense & Space Group - Product Support Division
Wichita, Kansas

Anthony Hug *

Principle Engineer - Materials and Processes Technology
Boeing Commercial Airplane Group
Wichita, Kansas

Summary

This study assessed the extent of cracking and corrosion damage in typical B707-100 and -300 lower wing aircraft structure in support of a USAF risk assessment of the lower wing structure of the E-8C Joint STARS aircraft. High stressed areas along the front and rear spars, near the main landing gear fittings, and at the WS360 chordwise wing splice joint were specifically excluded as these areas are subject to existing service bulletin inspection/rework requirements and are not "typical". Lower wing skin panels (2024 clad aluminum) and stringers (7075 clad aluminum) from two retired USAF B707 aircraft were disassembled, paint stripped, etched, and inspected. All occurrences of cracking and corrosion damage were documented. The cracking data was further analyzed to yield histograms of equivalent single corner crack sizes.

All wing skin and stringer fastener holes were inspected with a 20x optical microscope and crack indications were found in 2631 fastener holes. A small sampling of crack indications were metallurgically examined to characterize the through thickness extent of cracking. Stress intensity factors were calculated for each actual stringer crack indication site and used to calculate equivalent single corner crack sizes in an assumed analytical geometry. Resulting histograms of

stringer cracking occurrences verses equivalent single corner crack size are reported for each aircraft.

Background

The United States Air Force is converting retired B707 aircraft into E-8C Joint STARS aircraft. At the time of conversion, the select aircraft have logged approximately 40000 to 65000 flight hours and 17000 to 22000 cycles. Cracking and corrosion data from this task will support a USAF risk assessment of the lower wing structure of the E-8C Joint STARS aircraft. Teardown inspection data was obtained from select lower wing sections cut from two B707 aircraft having the same or similar lower wing structure. Left-hand lower wing sections from aircraft CZ-180 (B707-123, s/n #17635, line #15, 78416 flight hours, 36359 cycles) and aircraft CZ-184 (B707-321B, s/n #19266, line #531, 57382 flight hours, 22533 cycles) were inspected. (Note, the respective CZ numbers were the then current USAF designated airframe identification numbers and will be used throughout this paper.). Aircraft CZ-180 was selected as being the highest time B707 aircraft available for disassembly and aircraft CZ-184 was selected as being a same model with similar flight hours as the current E-8C fleet. The as-received panels were trimmed to remove areas not to be inspected resulting in the final disassembly and inspection sections shown in Figures 1a and 1b.

Disassembly and Inspection Procedure

The seven as-received sections were photographed to document the initial configuration and to aid parts identification after disassembly. Each section was completely disassembled and each component vibro-engraved with an identifying tracking number. When required, components were cut into smaller pieces for subsequent processing. All components were stripped of sealant and paint, etched with sodium hydroxide to remove approximately 0.0002 inch of surface material to enhance visual detection capabilities, and deoxidized.

All fastener holes were visually inspected with a 20x wide field hand held microscope. Crack indications having fatigue crack characteristics and surface lengths greater than 0.01 inch were recorded. Surface lengths were measured directly from the microscope scale to the nearest 0.005 inch. Down hole lengths were estimated using the microscope scale as a reference. The types of crack indications found included:

- 1) Hole wall indications which did not reach either end of the hole.
- 2) Hole edge indications with dimensions in the hole and on one surface.
- 3) Through thickness indications.
- 4) Surface indications near the hole but not extending into the hole.
- 5) Indications in countersinks.

Illustrations of the types of crack indications found and associated descriptive codes used to characterize the crack indications are summarized in Figure 2.

Clock position, hole diameter, and part thickness were recorded for all crack indications. Clock position for most indications were determined using 12:00 o'clock forward perpendicular to the stiffeners and 3:00 o'clock inboard parallel to the stiffeners. On vertical surfaces, 12:00 o'clock is up and 3:00 o'clock is inboard or forward when viewed looking forward or outboard respectively.

Total flange widths and short ligament hole distances (noted as edge margin in the data tables) were recorded for all stiffener crack indications. In addition, the flange half width (flange edge to web center line) was recorded for holes with cracks in unsymmetric sections.

Additional qualitative information describing the location and extent of hole wall crack indications were recorded as "Field Bias" and "Field Vert. Size". Field Bias data indicates where in the hole wall the inspector observes most the crack indications. The codes are T = top, M = middle, or B = bottom of the hole. Field Vert Size data indicates the extent of crack indications in the hole wall and is presented as a percentage of the overall hole wall thickness. This information was useful in subsequent analysis to categorize the typical presence of many hole wall crack indications as a single or double embedded, corner, or through-thickness cracks.

Wing skin hole crack indications are also cross referenced to the corresponding stringer hole where applicable.

Example data for wing skin and stiffener crack indications are presented in Figures 3a and 3b.

The locations of wing skin fastener holes with crack indications were marked on the skin panels and photographs taken. For stiffeners and other internal structure

common to the wing skin, the hole locations of crack indications common to the wing skin were marked on the skin panels and photographed a second time.

All surfaces of the wing components were visually examined for corrosion damage. Some of the larger areas of corrosion damage were marked on the individual components and photographs taken. Skin panel corrosion damage areas were marked and photographed at the same time as the panels were photographed to document cracked hole data. When corrosion damage was local or less than severe, a written description of it was reported including extent and depth. Metallographic cross section examinations were performed on some of the more severe corrosion damage areas and reported. Corrosion damage quantification follows the same descriptions as prior teardowns and inspections with light corrosion being defined as penetration depths less than 0.001 inch, moderate corrosion between 0.001 and 0.010 inch, and severe corrosion greater than 0.010 inch.

A representative photograph of a skin panel exhibiting skin hole crack indications and corrosion damage is presented in Figure 4a. The same skin panel remarked with stringer hole crack indication data is presented in Figure 4b.

Disassembly and Inspection Results

Fatigue Cracks

Crack indications with the typical characteristics of fatigue cracking were identified and described at a total of 2631 hole locations in the inspected structure. The majority of crack indications were detected in the stiffeners rather than the skin (1675 vs 869). As expected, crack indications were observed more frequently at holes common to the wing skin spanwise splice stiffeners (ie S4, S8, S14, and S18) and the heavy spanwise stiffeners on either side of the wing access holes (ie S5 and S7). In addition, the majority of crack indications were found in the high stress areas in and around S4 to S8 with diminishing occurrences forward of S8 or aft of S4. The larger number of crack indications found in CZ-184 is attributed to inspecting a larger portion of the wing relative to CZ-180 and not to any differences of usage, wing loads, or flight history. The fatigue crack indication totals by airplane, section, and component are summarized in Figure 5.

The largest stiffener cracks found are presented in Figure 6 and Figures 7a thru 7c. The largest crack of the three was found in the splice stiffener S8 of the high time aircraft. Two of these three cracks initiated from a fastener hole common to the stiffener base flange and wing skin while the third crack initiated from a stiffener web drain hole.

The longest fatigue crack in the wing skin was common to stiffener S6, Section 5 of CZ-184 and shown in Figure 8. The crack had a length of 0.28 inch on one side of the hole and a total length of 0.77 inch including the 0.31 inch hole diameter.

The inspection results showed that cracked holes tended to be grouped together in various locations of the structure. It was also common for both skin and stiffener to be cracked at the same fastener location. Of the 869 wing skin fastener holes with crack indications, 519 fastener locations also had crack indications in the mating stringers.

Another characteristic was that the crack indications almost always occurred in multiples. The most common crack description in the tables was MHWC - multiple hole wall cracks. In most cases this description did not mean two or three or even ten indications but more like dozens of individual indications (ref. Figure 9a).

Most of the stiffener crack indications occurred in the skin attach flange holes but there were groups of stiffener web holes that had some of the longer indications. These were web holes that served as fuel dam attach holes or fuel drain holes. A total of 40 of these holes were identified with crack indications (34 in CZ-180 and 6 in CZ-184). The stiffener free flange rib attach holes were cracked at 6 scattered locations throughout the inspected structure.

Opening select fastener holes to observe the extent of through thickness cracking confirmed that the cracks were due to fatigue. Direct observation also confirmed the presence of multiple initiation sites at almost all of the opened holes and also confirmed previously observed surface crack length dimensions. When there were large numbers of small cracks partially grown together to form larger cracks either as hole wall cracks, hole wall with edge cracks, or as surface cracks, it was more difficult to characterize cracking and estimate depths. Typical examples of multiple hole cracks that have partially grown together and multiple surface cracks are shown in Figures 9a and 9b. These examples show the difficulty in exactly characterizing the extent of cracking.

Corrosion Damage

Scattered areas of severe corrosion damage were identified on all examined sections except Section 4/3 from CZ-180 which only had moderate corrosion damage. The most extensive severe corrosion occurred on Sections 1, 2, and 5 of CZ-184. The most numerous areas of corrosion damage on the skin exterior occurred around the countersink edge of fastener holes which contained steel fasteners. All of these fastener holes had some corrosion and a large percentage of them had "typical" amounts comparable to that shown in Figure 10a. Figure 10a shows a countersink cross section of a fastener hole which held a steel fastener. The photograph shows pitting in the countersink and initial stages of exfoliation. The exfoliation is 0.007 inch deep and extends 0.12 inch from the edge of the countersink. The most severe corrosion of this type is shown in Figure 10b. Very few other holes, if any, had comparable corrosion in the countersink area.

Engineering Data Reduction and Analysis

Engineering reduction of the site specific inspection data was simplified by using typical cross section stringer/skin geometry. The analysis geometry was of stringers S7, S8, and S9, and the lower wing skin inboard of the chordwise splice joint at Wing Station 360 as shown in Figure 11. This geometry is representative of typical structure and is located in a fairly uniform ground-air-ground stress area. Skin and stringer material callouts and plane stress fracture toughness values are noted. Stringer S7 is typical of stringers S5 and S7 which are on either side of the access panel row. Stringer S8 is typical of skin splice stringers at S4, S8, S14, and S18. Stringer S9 is typical of all other stringers.

Stringer crack indication inspection data from both aircraft was reduced to equivalent single corner cracks in the analytical geometry (Figure 11) based on equivalent stress intensity factors. The inspection data was first characterized as being either single or double, corner, embedded or through thickness and a resulting stress intensity value calculated based on actual geometry. The resulting stress intensity value was then used to back-calculate the equivalent single corner crack size in the analytical geometry. A total of 1653 stringer crack indications out of 1675 reported were evaluated with this process. The difference of 22 crack indications represented unique configuration details that were not typical of the

general structure and were excluded. All splice stringer data was equivalenced to S8 (1258 holes). All data from stringers adjacent to the access holes was equivalenced to S7 (308 holes). And all other stringer data was equivalenced to S9 (87 holes).

Histogram plots of occurrence frequency and cumulative percentages versus equivalent single corner crack sizes for each analysis stringer (S7, S8, and S9) are presented in Figures 12a, 12b, and 12c and again (reduced scale) in Figures 13a, 13b, and 13c.

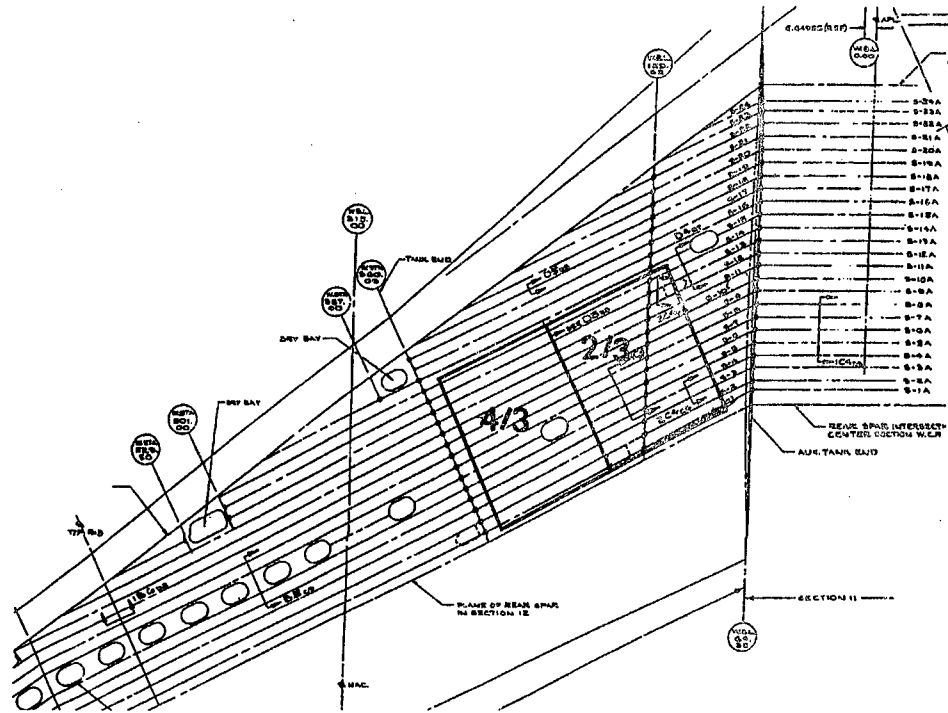


Figure 1a: CZ-180 (B707-123) Lower Wing Teardown and Inspection Sections

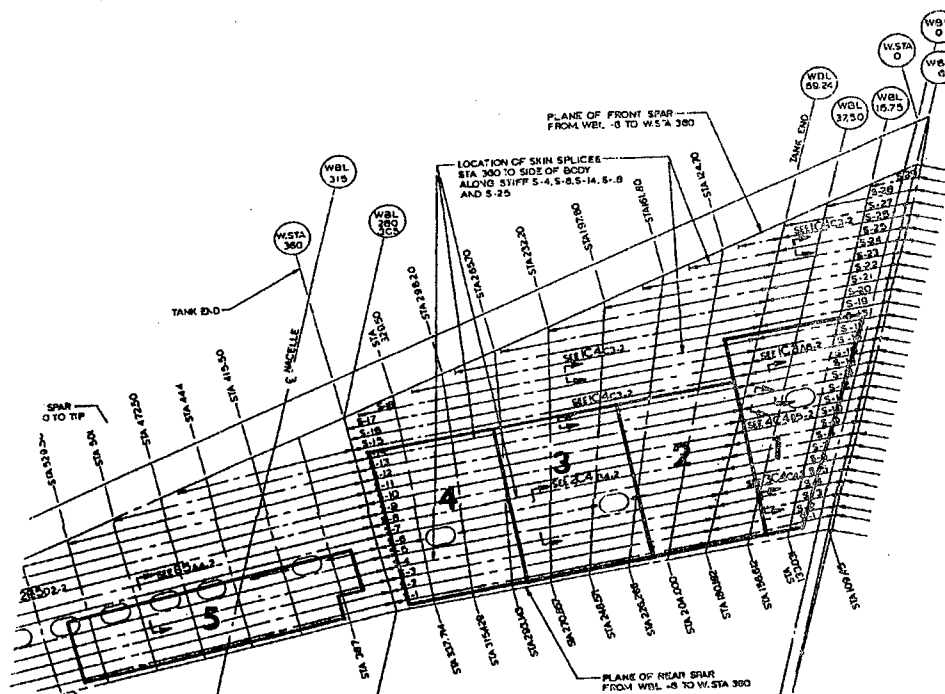
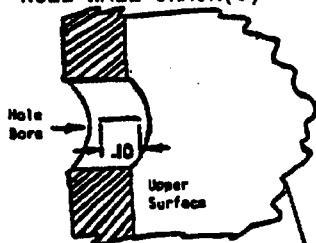
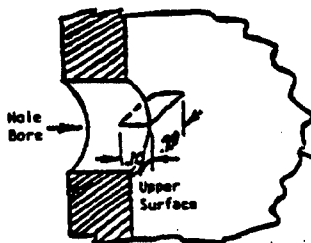


Figure 1b: CZ-184 (B707-321B) Lower Wing Teardown and Inspection Sections

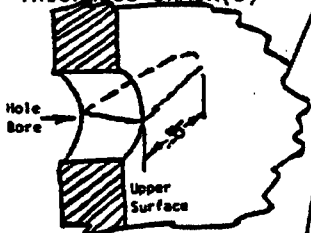
HOLE WALL CRACK(S)



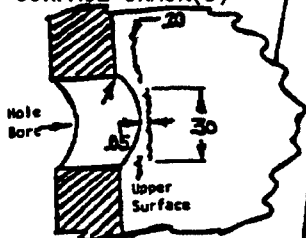
HOLE EDGE CRACK(S)



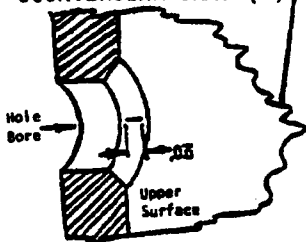
THRU THE THICKNESS CRACK(S)



SURFACE CRACK(S)



COUNTERSINK CRACK(S)



The crack description code in the tables utilizes the following abbreviations:

A - aft	L - lower
C - crack(s)	M - multiple
E - edge	S - surface
F - forward	T - thru thickness
H - hole	U - upper
K - countersink	W - wall

EXAMPLES		
CRACK 1/ DESCRIPTION CODE	CRACK DIMENSIONS (INCH)	
HWC	.10	2/
USEC	.10-.20	3/
TC	.35	4/
MUSC	.30-.05/.20	5/
KC	.03	6/

- 1/ M precedes code for multiple cracks.
- 2/ Dimension shown is maximum individual crack axial length in hole bore.
- 3/ First dimension is maximum individual crack axial length in hole bore. Second dimension shown is maximum individual crack surface radial length from the hole edge.
- 4/ Dimension shown is maximum individual crack radial length.
- 5/ First dimension shown is maximum individual crack surface length. Second dimensions are minimum/maximum radial distance of crack(s) from hole edge.
- 6/ Dimension shown is maximum individual crack length in countersink surface.

Figure 2: Crack Indication Types, Description Codes, and Dimensioning Procedures

Hole No.	Crack Clock Position	Crack Description Code	Crack Dimensions (inch)	Field Bias	Field Vert. Size (% t)	Hole Diameter (inch)	Part Thickness (inch)	Stiffener Hole No.
1	12	MUSEC	0.015-0.010	TM TB	30 30	0.50	0.64	-
	12	MHWC	0.020					
	6	MHWC	0.020					
2	1	USEC	0.020-0.020			0.50	0.64	-
3	7	MHWC	0.020	T	15	0.37	0.63	-
4	12	MHWC	0.015	M	10	0.50	0.63	-
	6	MHWC	0.030	T	20			
5	12	MHWC	0.020	T	5	0.50	0.63	-
	6	MHWC	0.020	T	20			
6	12	MHWC	0.010	TM	20	0.50	0.63	-
	6	MUSEC	0.015-0.015					
	6	MHWC	0.030	T				
7	12	USEC	0.07-0.02			0.37	0.31	6

Figure 3a: Example Lower Wing Skin Crack Indication Inspection Data

Hole No.	Crack Clock Position	Crack Description Code	Crack Dimensions (inch)	Field Bias	Field Vert. Size (% t)	Hole Diameter (inch)	Part Thickness (inch)	Flange Width (inch)	Edge Margin (inch)
Stiffener 1									
1	3-4	MLSC	.08-.01/.03			0.31	0.30	1.45	0.49
Stiffener 3									
2 *	6 6	FSEC MHWC	0.05-0.05 0.06	F	30	0.25	0.21		
Stiffener 4									
3	12	HWC	0.02	B	5	0.38	0.75/0.51	6.20	1.36
4	12 5-7	MHWC MLSC	0.02	B	5	0.38	0.51	6.20	2.07
5	12	MLSEC	.05-0/.18			0.38	0.51	6.20	1.41

* Cracking is at a drain hole in the stiffener web

Figure 3b: Example Lower Wing Stringer Crack Indication Inspection Data

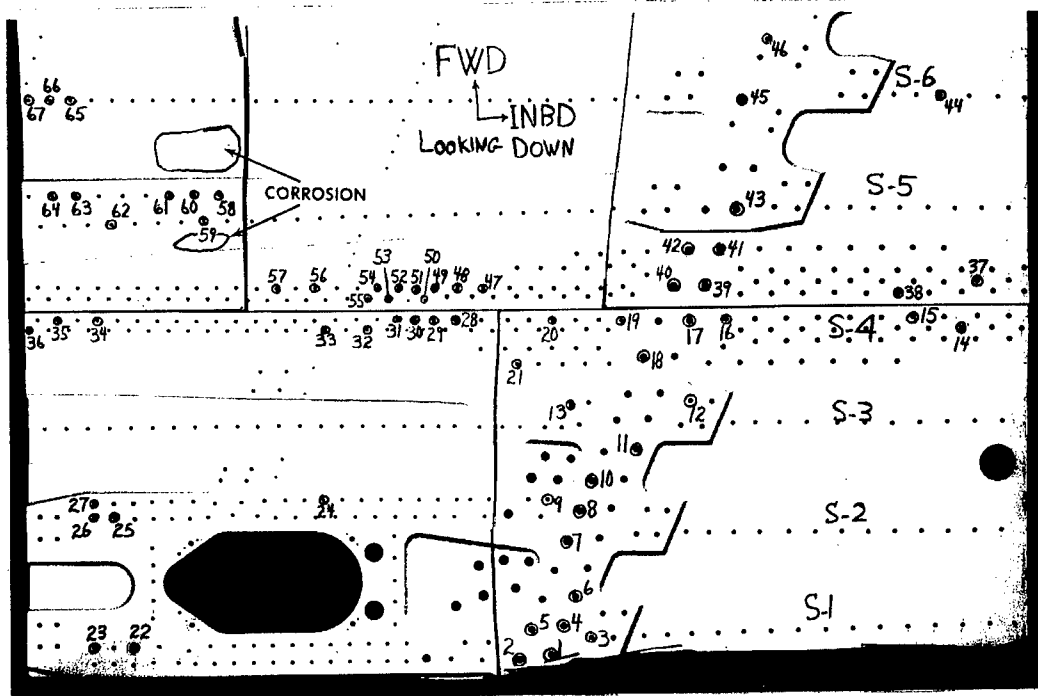
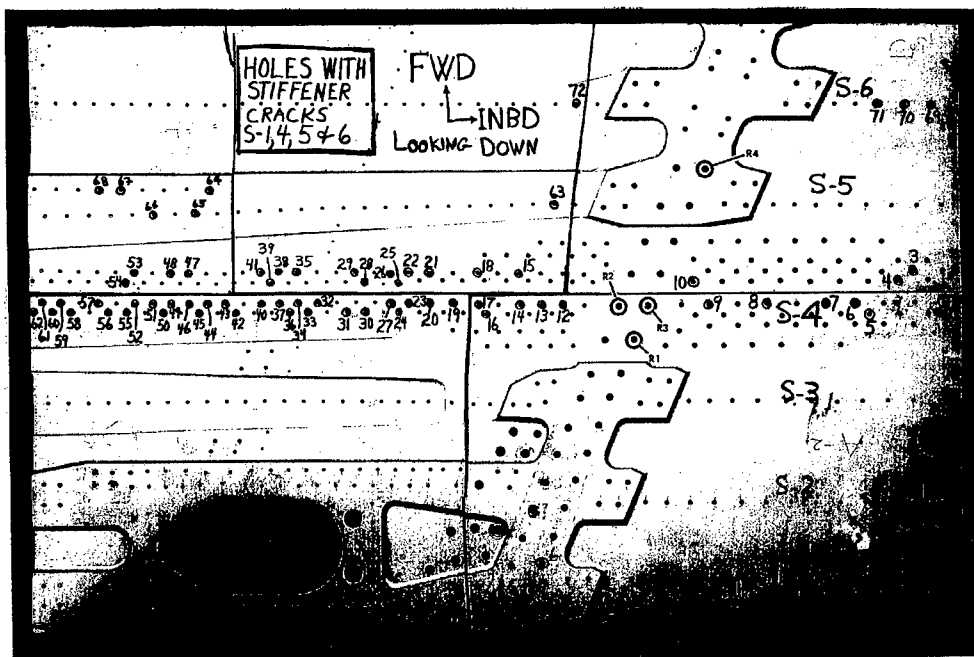


Figure 4a: Wing Skin Hole Crack Indication Locations



The hole numbers with "R" prefixes are located in the rib chord.

Figure 4b: Stiffener Hole Crack Indication Locations

Component	Number of Fastener Holes with Crack Indications							All Sections
	CZ-180 Sections		CZ-184 Sections					
	2/3	4/3	1	2	3	4	5	
SKIN:								
at S4	34	57	22	27	40	47	23	250
at S5	1	4	0	7	20	18	36	86
at S7	5	4	0	13	45	40	-	107
at S8	45	43	8	15	13	32	-	156
at S14	0	2	7	16	9	24	-	58
at S18	-	-	1	-	-	-	-	1
Other	71	12	40	48	7	23	10	211
Sub-Totals	156	122	78	126	134	184	69	869
STIFFENERS:								
S4	65	97	28	60	104	117	176	647
S5	5	2	0	6	41	38	83	175
S7	6	1	0	12	72	51	-	142
S8	91	74	8	65	65	92	-	395
S14	11	7	2	70	71	51	-	212
S18	-	-	17	-	-	-	-	17
Others	31	5	17	20	2	8	4	87
Sub-Totals	209	186	72	233	355	357	263	1675
Other Components	38	5	5	23	-	16	-	87
Grand Totals	403	313	155	382	489	557	332	2631
Airplane Totals	716		1915					

Figure 5: Fatigue Crack Summary by Airplane, Section, and Component

Stiffener	Crack Length (inch)	Hole ID Number	Airplane and Section ID	Photograph
8	2.38	37	CZ-180, 4/3	Figure 7a
7	1.44	65	CZ-184, 3	Figure 7b
9	0.42+, 0.84	32	CZ-180, 4/3	Figure 7c

Figure 6: Largest Stiffener Fatigue Cracks Found

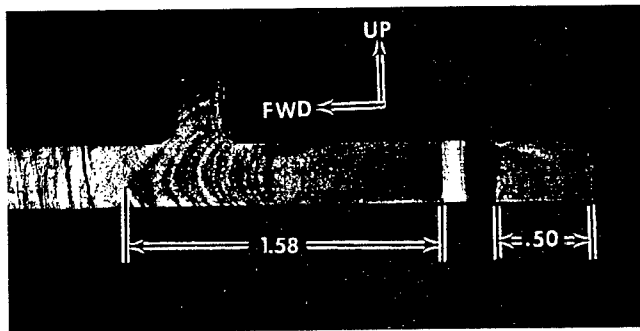


Figure 7a: CZ-180, Stiffener S8, Hole 37, Base Flange Crack

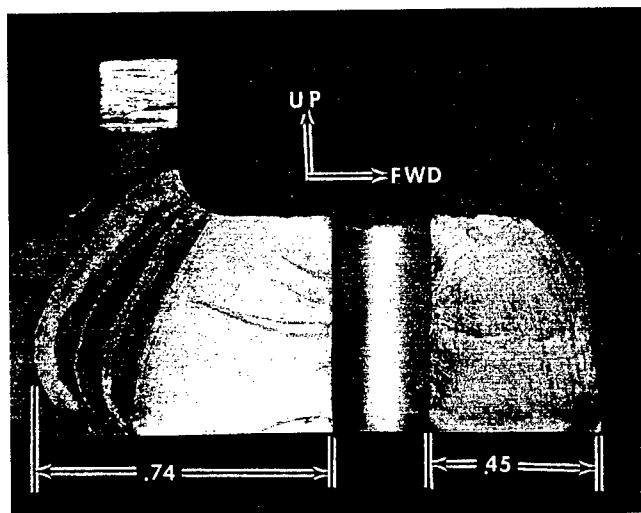


Figure 7b: CZ-184, Stiffener S7, Hole 65, Base Flange Crack

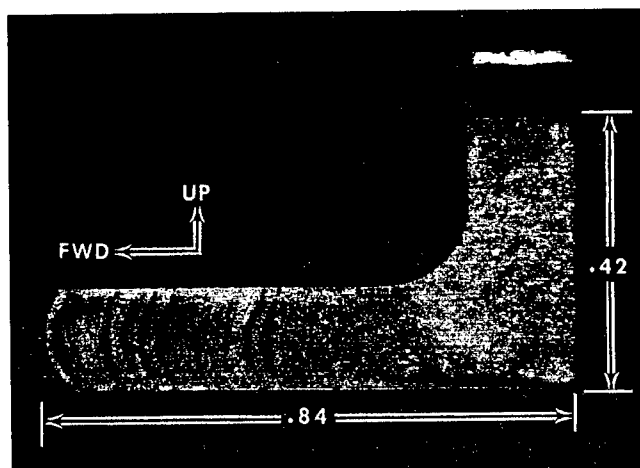


Figure 7c: CZ-180, Stiffener S9, Hole 32, Web Drain Hole Crack

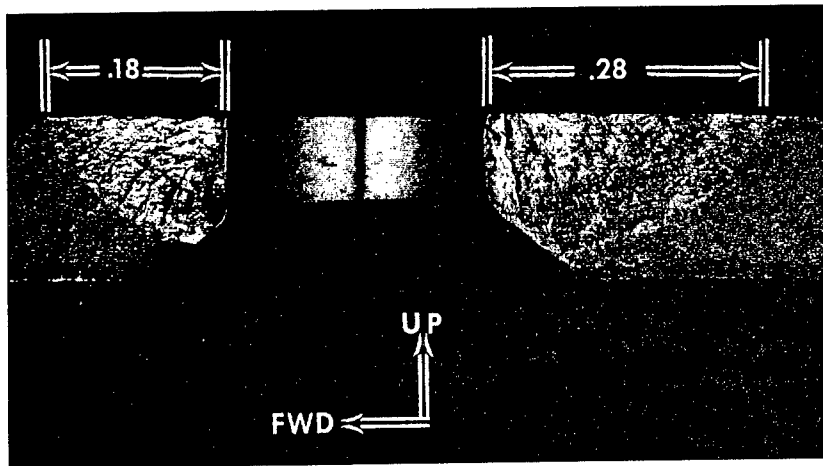


Figure 8: Largest Skin Crack, Hole 26, Section 5, CZ-184

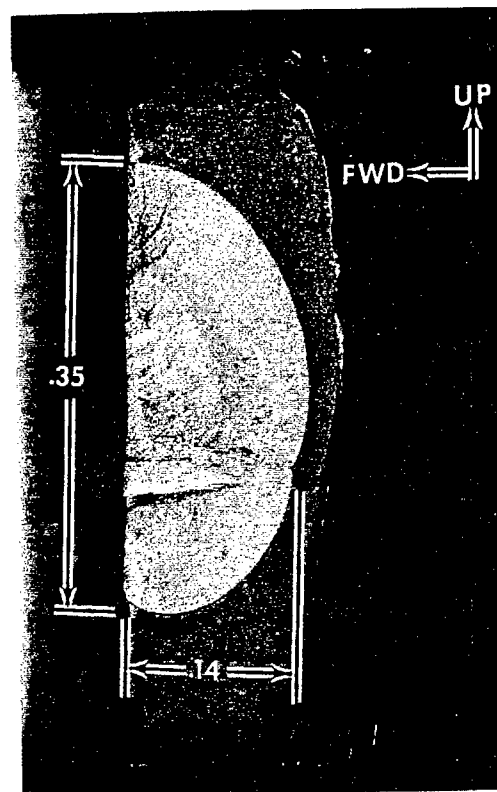


Figure 9a: Multiple Hole Wall Crack Pattern and Extent after Opening

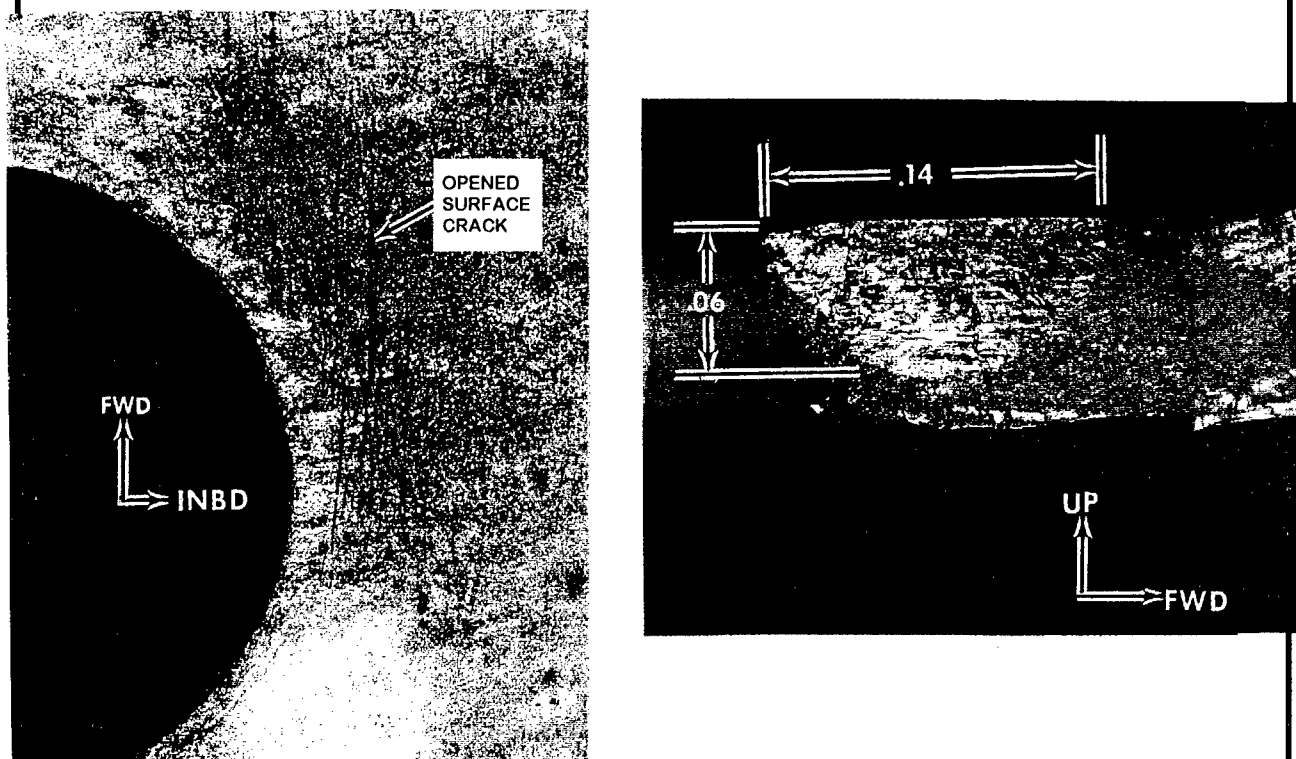


Figure 9b: Typical Surface Crack Pattern and Extent after Opening

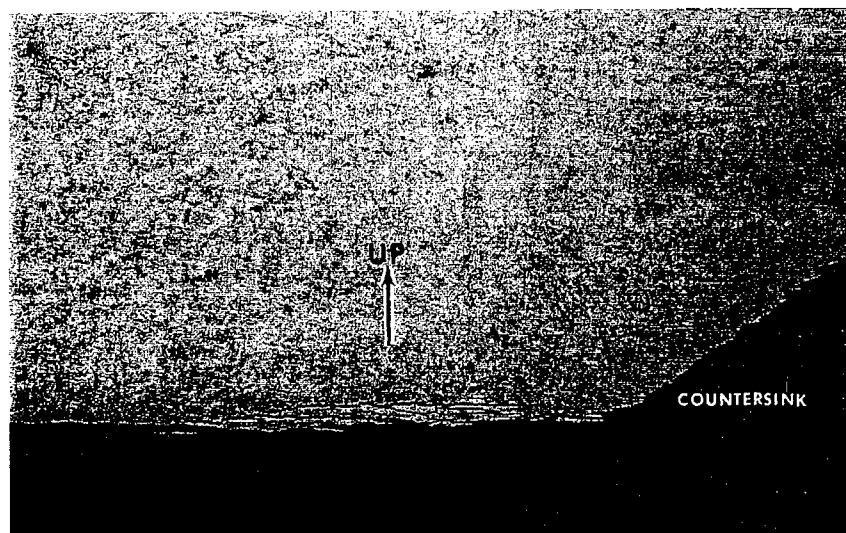


Figure 10a: "Typical" Wing Skin Countersink Degree and Extent of Corrosion

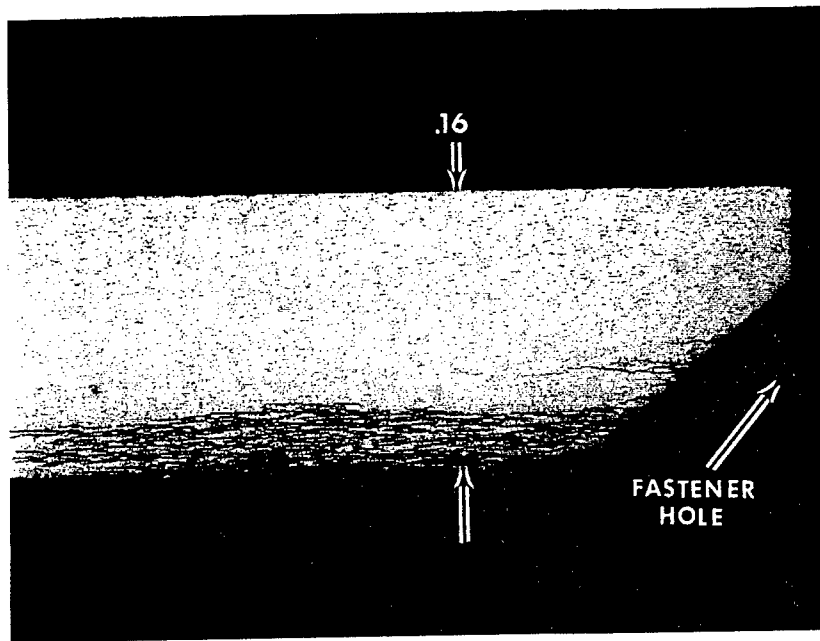


Figure 10b: Severe Wing Skin Countersink Degree and Extent of Corrosion

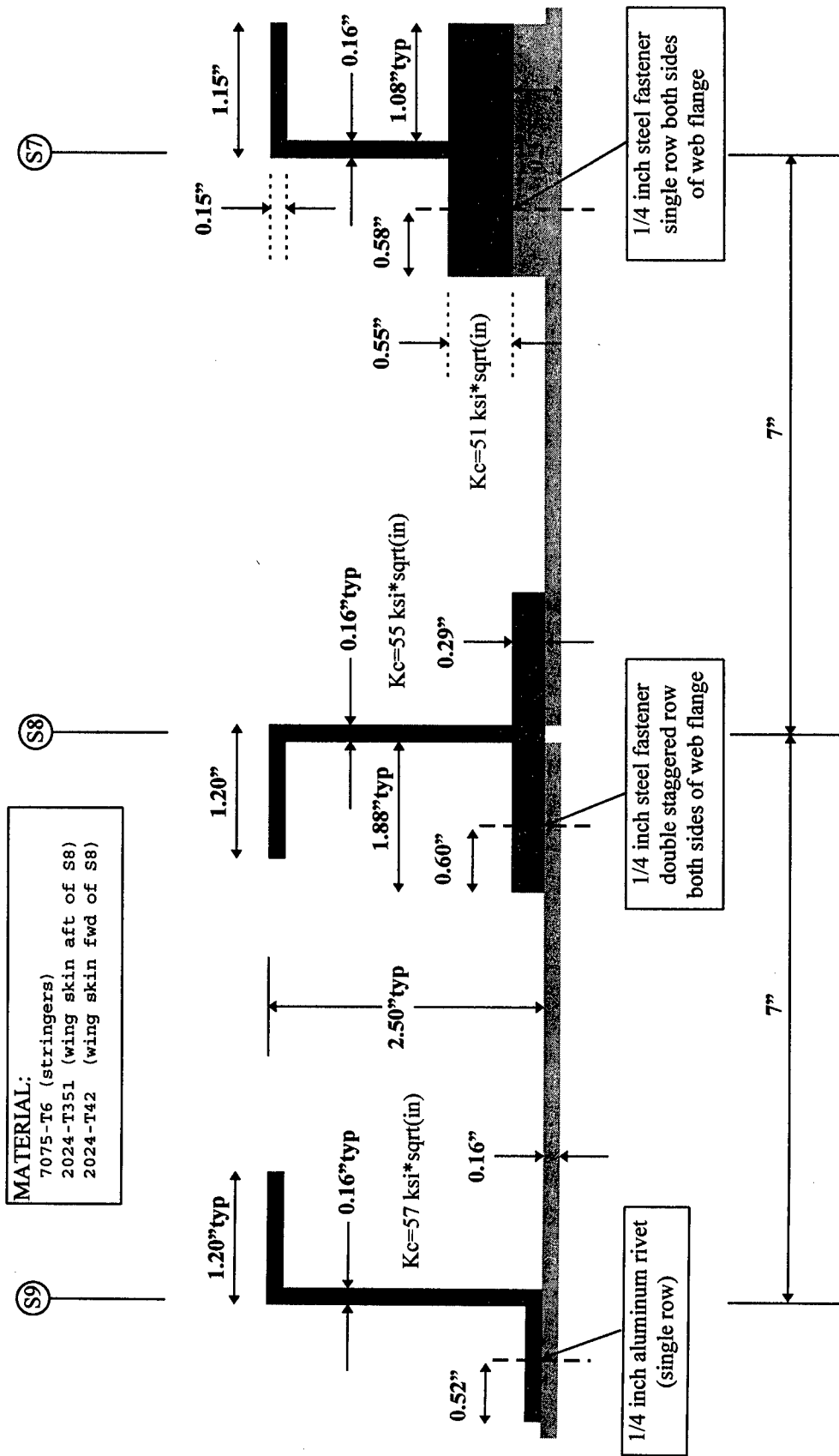


Figure 11: Typical Stringer Lower Wing Skin Cross Section Inboard of Wing Station 360
 (NO SCALE)

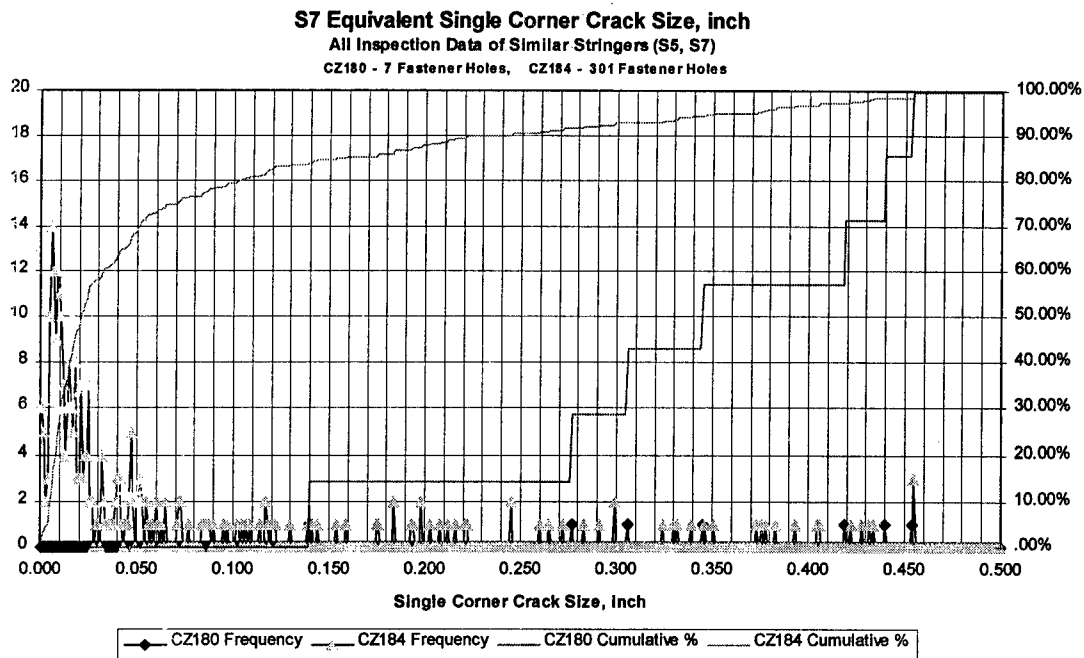


Figure 12a

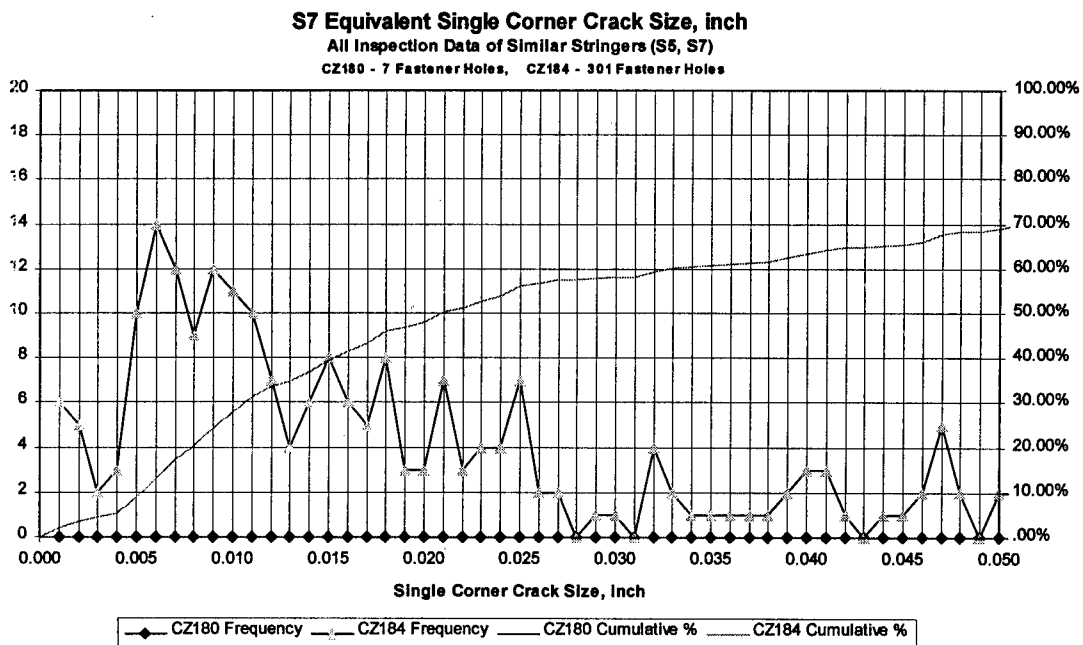


Figure 13a

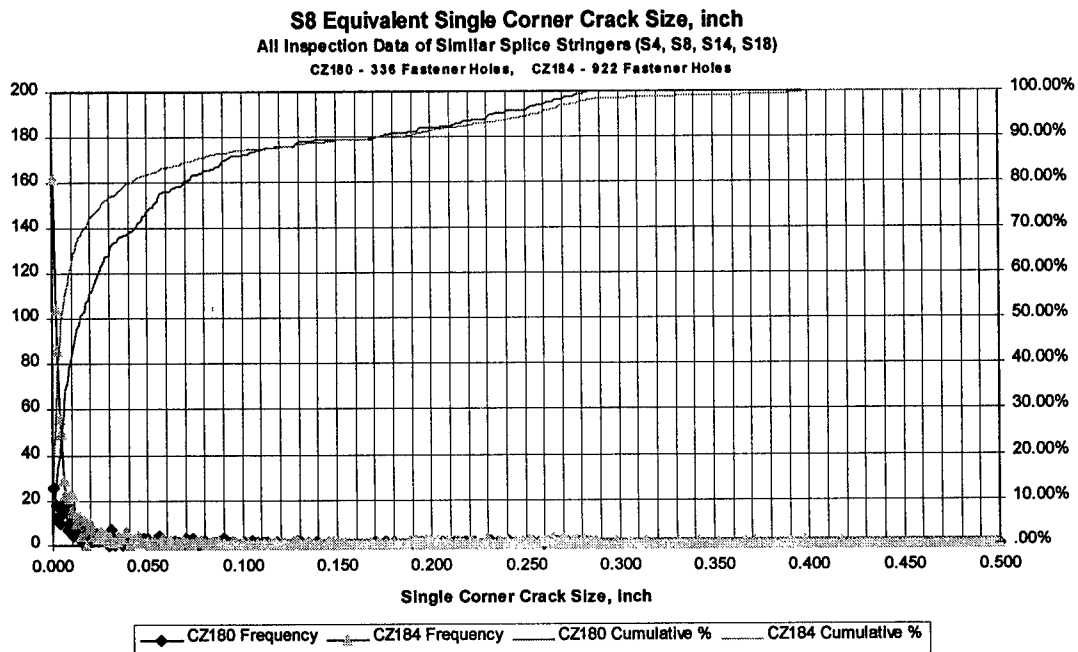


Figure 12b

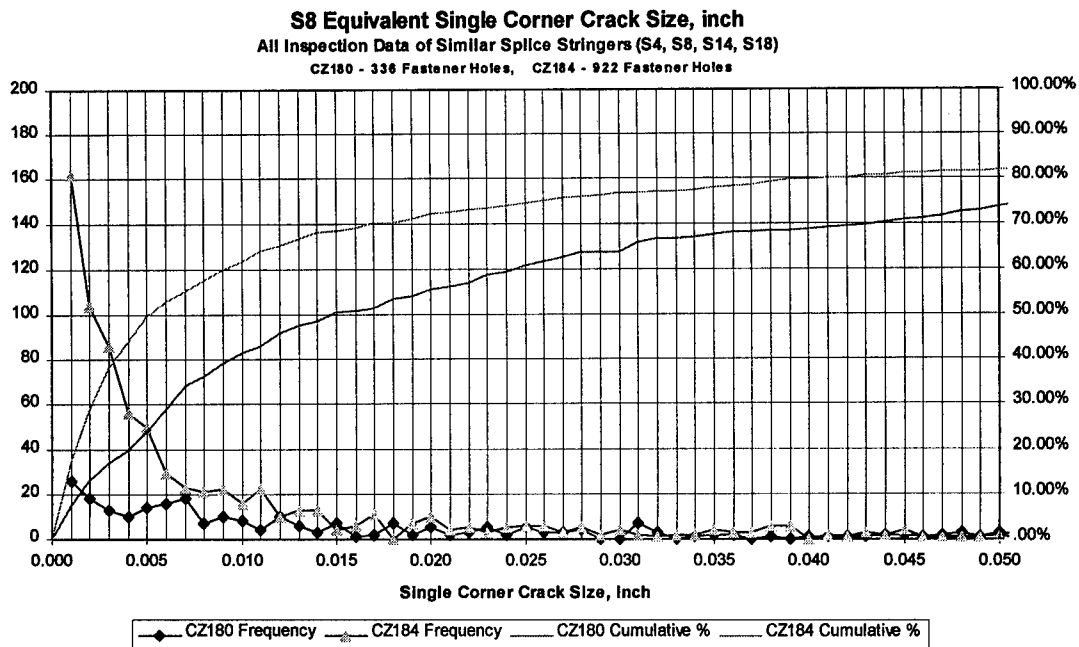


Figure 13b

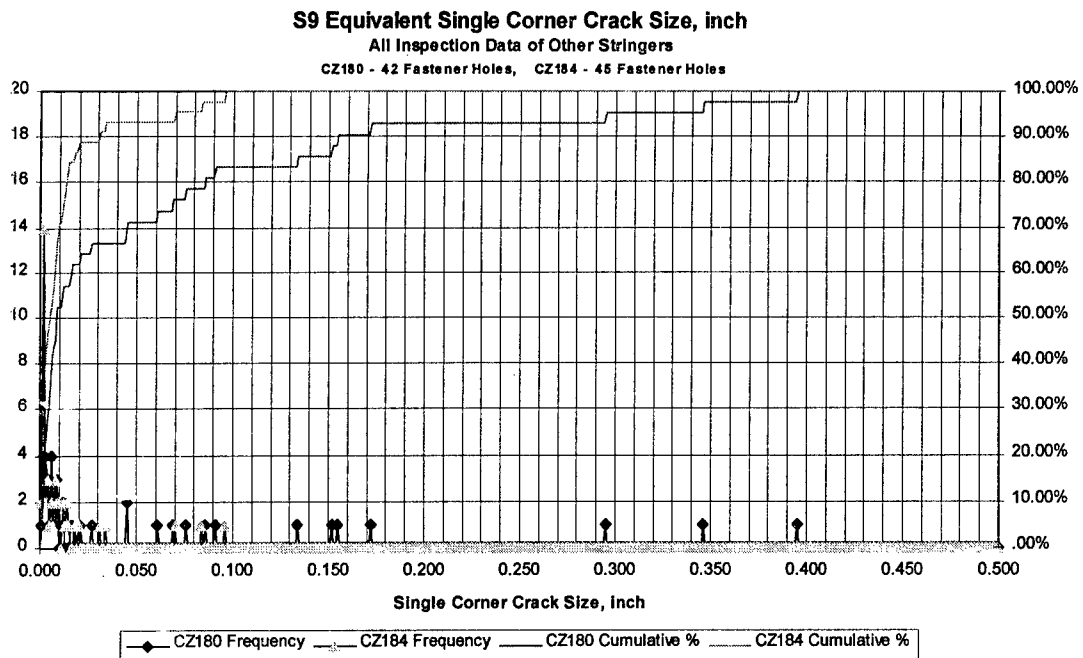


Figure 12c

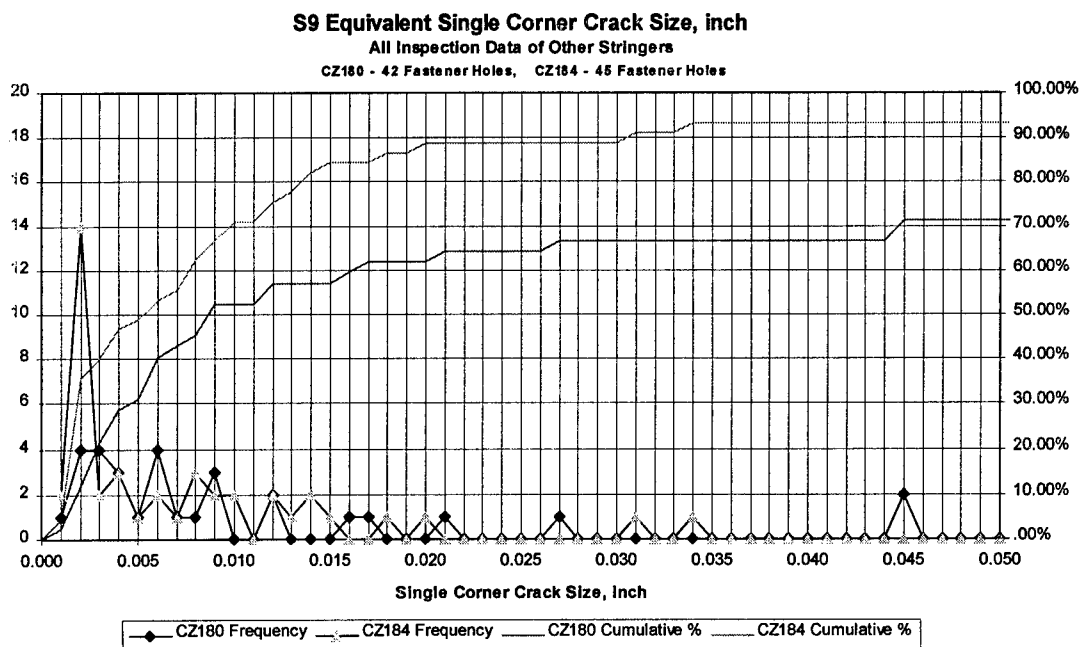


Figure 13c

Thoughts on Risk Analysis of an Aging Aircraft

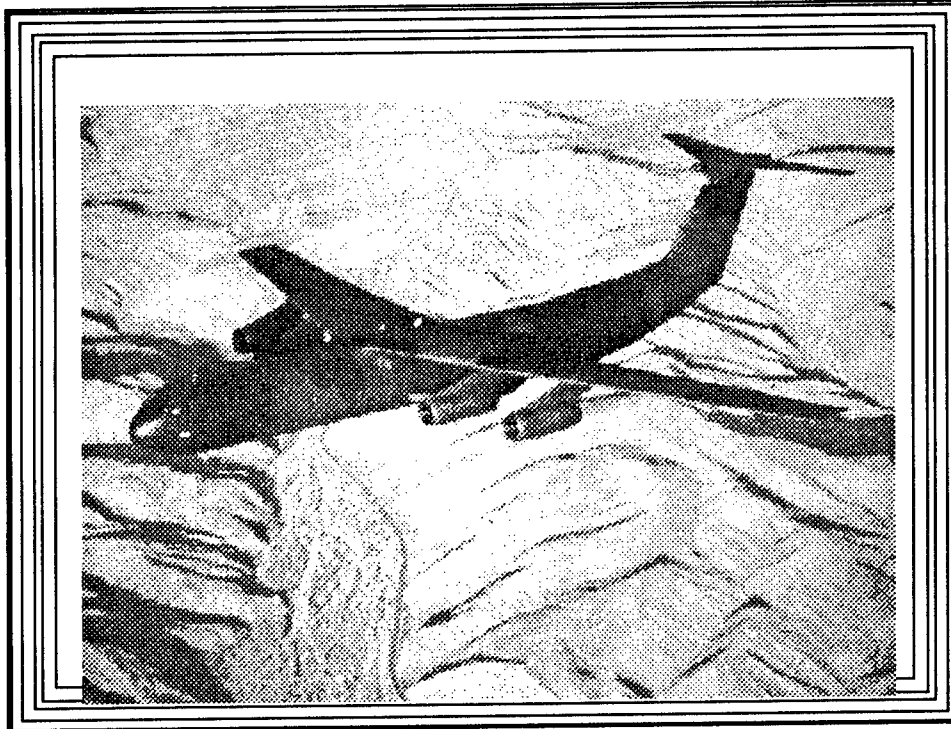
Presented At The 1996 USAF Structural Integrity
Program Conference, San Antonio, Texas

3-5 December 1996

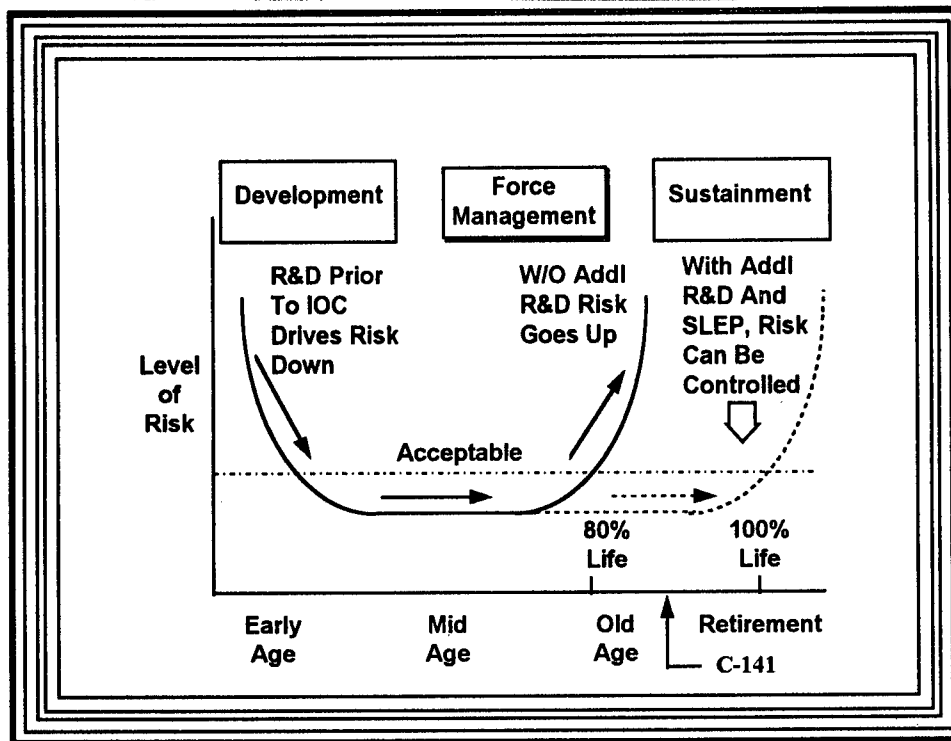
R.P. Bell
K.M. Jones
Lockheed Martin
Marietta, Georgia

R.E. Alford
WR-ALC/LJLEA
Robins AFB, Georgia

Safe operation of an aging aircraft is a primary concern of both civilian and military operators. This presentation gives an overview of one additional tool that can be used to quantify, or at least to relatively quantify, safety. This presentation will be built around our experiences on the C-141, but the lessons and tools should be applicable to any aging aircraft. It also gives a historical account of some of our more important analysis with a discussion of the methods used and, in hind sight, lessons learned. It has been most useful on the C-141 for selecting practical courses of action for solving short term structural problems.

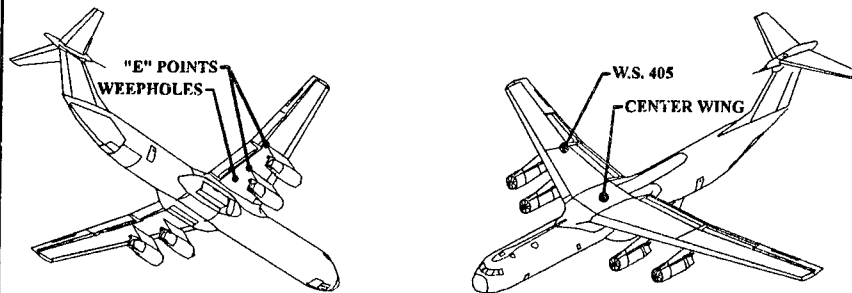


The C-141A was produced and delivered to the Air Force in the 1960's. The aircraft is mostly constructed of 7075 T6 aluminum alloys and was designed for 30000 flight hours of service. Stretched during the 1970s and with the addition of aerial refueling capability , this C-141B configuration became the work horse of MAC. Presently, there are 218 C-141s flying, some of which will fly into the 21st century. The Force is currently averaging 37500 damage hours and the present goal is 45000 damage hours on the lower surface spanwise splices.



As the above slide shows the C-141 is reaching the end of its useful life. Because of this, additional tools are necessary to provide effective and safe Force Management. One of these tools is that of Risk Analysis methodology.

Risk Analysis Major Areas Completed



This slide shows the major risk analyses that will be covered during this presentation. There have been others, but these will serve to illustrate the things that caused us problems. The same methodology can also be applied to fuselage structure, but our emphasis has been on wings. So, the context of this presentation will be in those terms.

Risk Analysis

What is It?

- Risk is derived from an Italian word which means "To Dare"
- On the C-141, it refers to the probability of catastrophic failure to major components of the aircraft when flying standard missions and usage
- It is not a calculation of uncertainty, which refers to an unknown event taking place

All of life is uncertain. No one can predict the future. However, it is possible to make calculations about certain actions. This is where Risk becomes useful. In the 17th Century, the concept was beginning to be understood. These early studies were the forerunners of our present methods of analysis.

The word risk is derived from an Italian word which means "To Dare". There are a number of definitions of Risk. However, in the context of the C-141, it refers to the probability of losing a major component or components which could cause catastrophic failure. It does not refer to uncertainty, which refers to the probability of an unknown event happening. It is concerned only with the fixed engineering probability calculations of things which could happen to the aircraft while flying standard missions and usage.

However, it is not as exact a calculation as it seems. One problem is that the data received for estimating flight hours, inspections, etc., is not exact. So, in addition to the calculations, judgments must be made about the validity of the answers.

Risk Analysis Why Do It?

- Field Data indicates a problem which has developed or is developing
- Cracking has reached a generalized state or is showing up in adjacent components
- Questions about what is the real chance of having a catastrophic failure
- Can look at various Force Management scenarios and determine course of action

Why do risk analysis when the slow crack growth method is available for managing the aircraft? Suppose that statistical analysis of inspection data indicates that there may be cracks in the Force that are greater than the critical crack length. Then the question is what do we do? In most cases this condition has existed for some time on some aircraft. If the answer is to ground aircraft, then which aircraft should be grounded. What inspections need to be performed and when? Will these inspections actually decrease the risk? Do we need to send out field teams for a special inspection? All of these questions can be answered to some degree by performing a risk analysis.

[illegible]

535

Risk Analysis

What does it Tell Us

- Which Aircraft, if any, need to be Grounded
- Parts that absolutely have to be protected
- Implications of adding inspections on reducing the overall risk
- Degree of fail-safety that the aircraft may or may not have

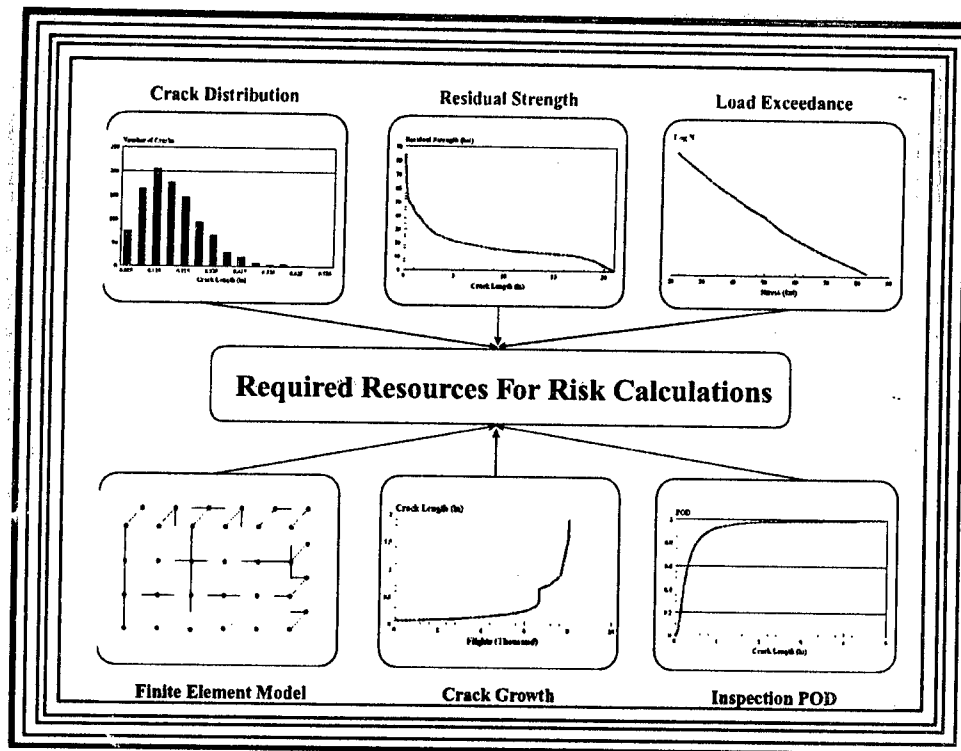
Risk analysis helps us to make decisions about what Force management actions to take. A possible question on the C-141 would be, "What is the risk of flying beyond 45000 damage hours?" Another question on an aging aircraft is does it still have the inherent fail-safety that stands behind the slow crack growth method.

Risk Analysis

What Programs are Available

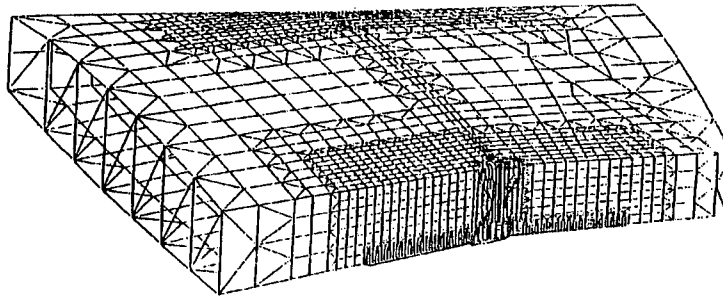
- Risky - Lincoln - AFMC/ASC/ENFS
- Prof - Behrens/Burns - Wright Labs/UDRI
- SAIFE - Anderjaska - FAA
- In House programs - all of our LMASC programs are based on the methodology developed by Dr. John Lincoln of the Wright Labs

There are a number of programs available for doing probabilistic analysis. I've listed three of the ones at which we've looked. LMASC uses the methodology that was developed and programmed in Risky by Dr. John Lincoln of the AFMC/ASC/ENFS. Generally, we use an in house program called DICE which runs on a main frame IBM system. Presently, Risky resides on the a VMS VAX system. PROF is similar to our program in that it uses almost the same inputs, but uses a slightly different method of inputting the loads. SAIFE is a comprehensive force management simulation program which uses Monte Carlo sampling to determine inspection intervals. We used the Monte Carlo method when generating the distributions and probabilities of failure in one of our first analysis attempts, and SAIFE gave some insight into this method.



The above slide shows in graphic form most of the resources that are needed for a C-141 or any Risk analysis. Details will be covered in the next few slides. Two of the above resources are deterministic. The others have a degree of uncertainty associated within themselves that had to be considered in judging the results of the final answers.

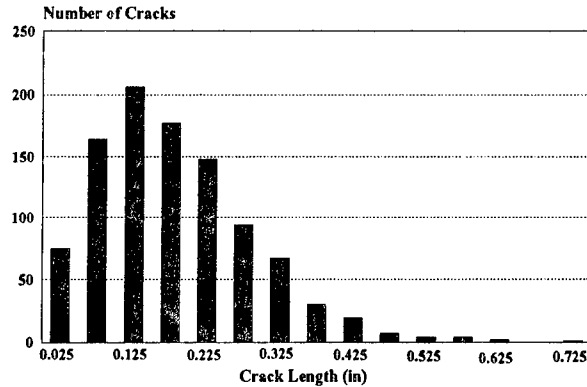
Risk Analysis Finite Element Model



This shows the C-141 WS 405 finite element model used in one of our Risk Analyses. A model with this level of similar detail is probably required to perform risk studies. This model was originally built for analysis related to a composite repair program. It was available for our Risk studies, and we were able to modify it by constructing non-linear fastener elements.

Risk

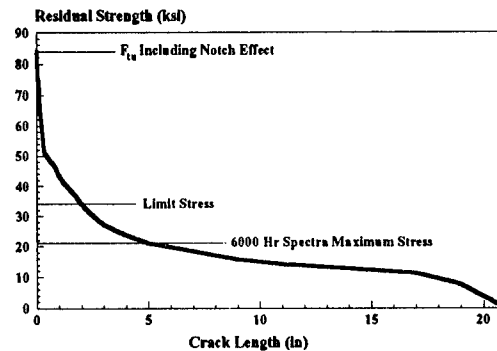
WS405 CRACK SIZE DISTRIBUTION



Crack size distributions can be derived from field inspection data, teardown results, or an assumed initial flaw distribution. Field inspection data should be detailed, providing information on the number of sites inspected, the size and direction of flaws, and the flight hours or cycles at the time of the inspection. In general, a better fit to a continuous distribution (Weibull, log-normal, etc.) will be obtained if the flaws are grouped by location and direction. All flaws should also be adjusted to a particular baseline flight hour value using the mean crack growth curve. Now having said that, it is a well known fact that field data will not be this complete. The data will be grouped around certain lengths, but crack depths will not be available and so on. An example of this can be seen in the crack data obtained from an inspection of the beam cap later.

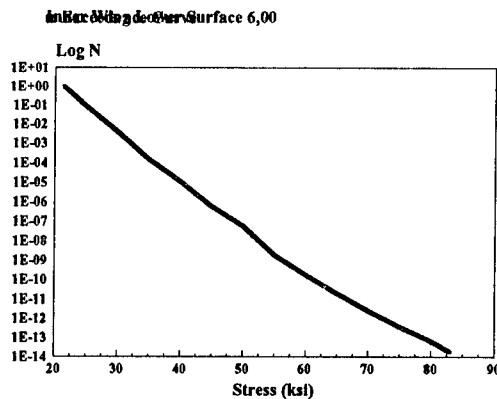
Risk Residual Strength

FIGURE 10



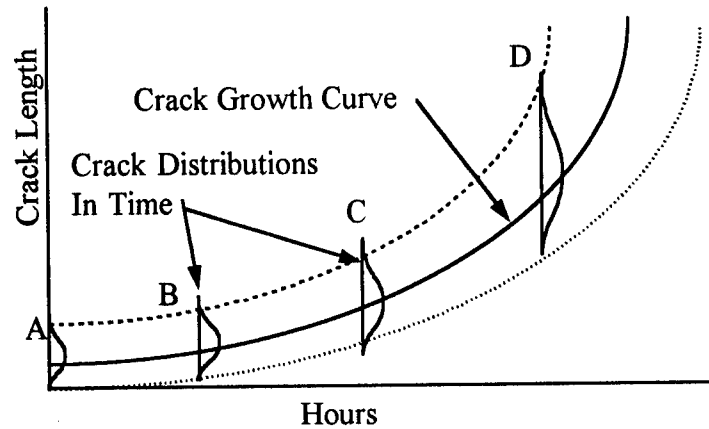
The residual strength of the affected components is required for both the primary structure and the alternate load-path structure after the primary has failed. Linear fracture mechanics provides accurate predictions in crack range where the plastic radius is not more than 10% of the crack length. For the small crack range, test data or Feddersen's method have been used. This is particularly true when determining the residual strength of the alternate load-path structure after the primary failure, as it usually involves yielding and large bearing loads. Non-linear finite element models are necessary to predict the net-section stresses that can be compared to test results to determine the failing stresses of small cracks.

Risk Loads vs Probability



C-141 risk analysis has typically employed two approaches to obtain the spectra for this type of analysis. One of these methods is to select the worst mission of the Baseline Missions set and calculate the risk for it. The second method is to pick a reasonable time of usage such as between PDM. cycles (6,000 hours). Longer intervals are more conservative, but may be unreasonable for the short-term. Assuming single flight stresses for "return-to-base" or fail-safe capability could be unconservative, there can often be wide variations in stresses on a single flight. However, the idea is to provide the risk for an average aircraft during the time period of the analysis. Otherwise, the answer will come back the same as the standard deterministic methods of analysis. During our initial program evaluation, we looked at an in-house program that gave the same answers as the slow crack growth method.

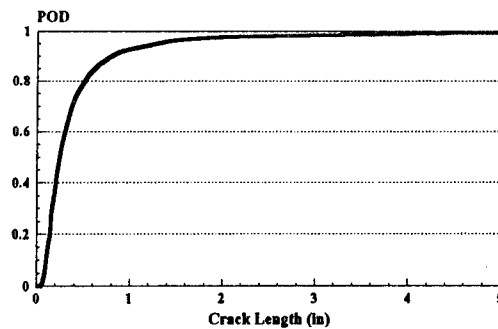
Risk Analysis Effect of Time



This slide shows a typical crack growth curve used in the analysis. This curve is sometimes referred to as the Master Crack Growth curve. We've also included cartoons which represent the distributions of cracks at points A, B, C and D. As the curve extends out in time, the standard deviation also increases meaning that there is much more spread in the answers. Typically, for our analysis, the inspections and points of interest are close to the time that the cracking data was obtained. A rule of thumb used by other disciplines is that the standard deviation should vary as the square root of time.

Risk Analysis

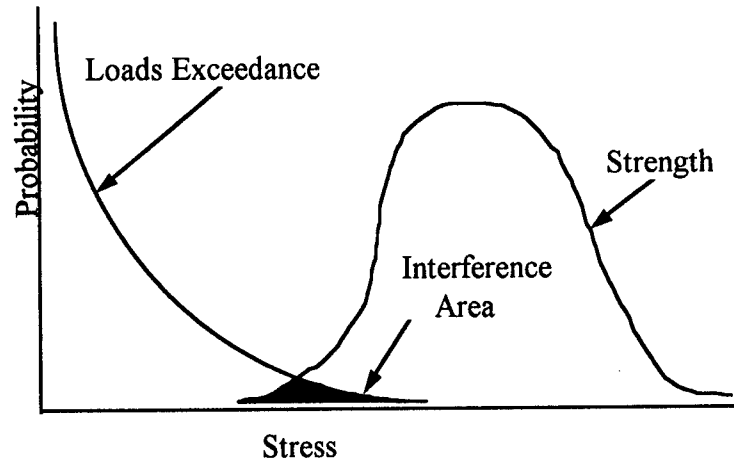
SPANWISE SPLICE OUTER TAB ECSS P



One primary objective of a risk analysis is the determination of an inspection interval which provides adequate safety as an aircraft ages. Inspection data must be in the form of a POD curve which reasonably describes the inspection performance under field conditions. "Have Cracks" data has generally been found to be acceptable for existing methods. Emerging inspection technologies need to have POD curves developed to be useful, not only for risk analysis, but for comparing NDI methods.

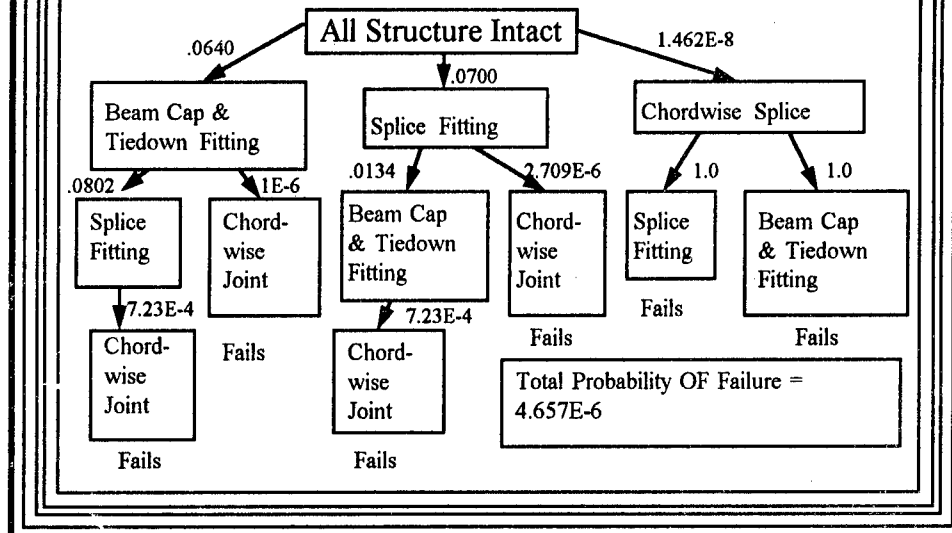
Risk Analysis

What is the Overall Method



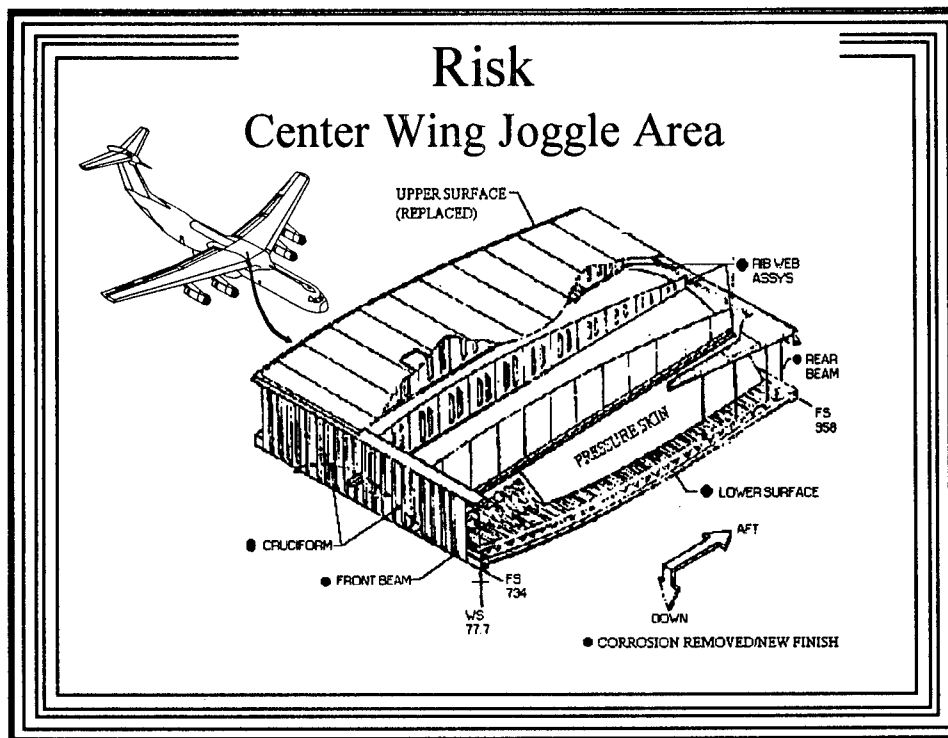
The above graphic portrays the method by which the Risk is calculated. However, it is over simplified in that the risk is not the area of the intersection, but rather the probability of the load exceeding the strength in this area. However, it is this calculation carried out at points in time that is used to quantify the risk. When these distributions standard, the answer can be directly calculated.

Risk Analysis Failure Sequences or Trees



This slide shows a typical failure tree generated for the WS 405 inner to outer wing joint on the C-141.. Our first analysis attempts did not take into account the inherent fail-safety of the aircraft and were overly conservative. There is a reliability program called CAFTA for generating these trees.

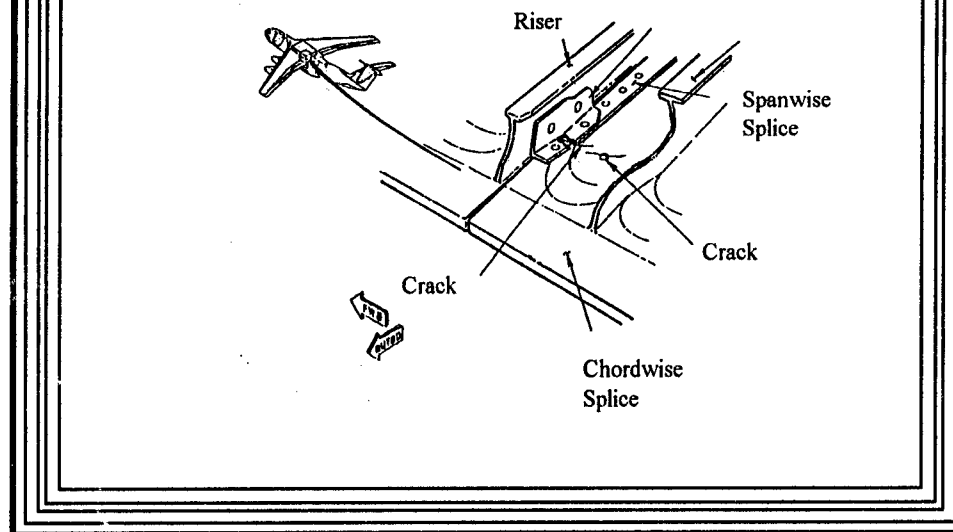
The total risk of failure in redundant structure is a combination of single element failures. A failure tree should be developed that takes into account as many possible failure paths. However, economics and time dictate how many can be examined, since a full blown analysis has to be carried out for each of the above blocks, i.e. FEM runs, crack growth, probability of failure calculations, etc. Dropping conditional failure modes is conservative, but often not realistic.



This shows the center wing box. Presently, about half of the C-141 Force is having new wing boxes installed. At the time of this original analysis this was not the case. Cracking had developed in the area near the joint on one of the early wing fatigue tests, and a fix had been incorporated which solved the problem during its original design lifetime of 30000 hours. However, as the aircraft passed 30000 damage hours, cracking again began to develop in this area.

A risk analysis was conducted as a point of interest at the time. It was done to get some feel for the magnitude of the problem. Subsequent analyses of this area have incorporated all of the tools developed to date. However, it is interesting to look back at this analysis and see what can be learned.

Risk Analysis Center Wing Joggle Detail



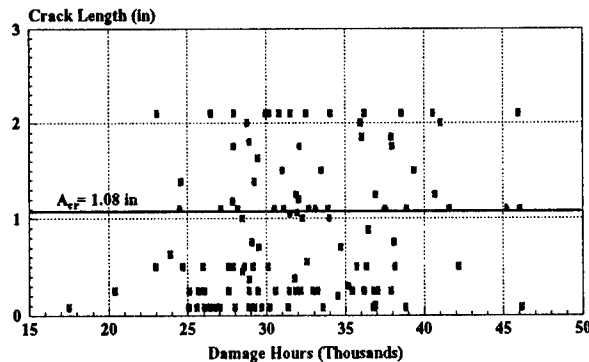
This shows a detail of the joggle area and points of associated cracking. One of the problems associated with analyzing this area was the difficulty in obtaining strength values in the tapering area which was also undergoing bending stresses. The area is typical of most integrally stiffened panel construction. The panels are connected spanwise and cracks in adjacent structure may mean fail-safety is lost with failure of the first panel. This was the major concern of the Air Force and LMASC.

Summarizing this analysis:

1. No failure trees were used so any answers were overly conservative.
2. Did not need or use a non-linear model since second panel failure was assumed and not examined.
3. Very few cracking sites so suspended data (sites that were of the same type, but where no cracks were found) was not a problem.
4. Cut the strength curve off at 80% of F_{tu} .
5. Did use PODs from "Have Cracks"

Risk Analysis

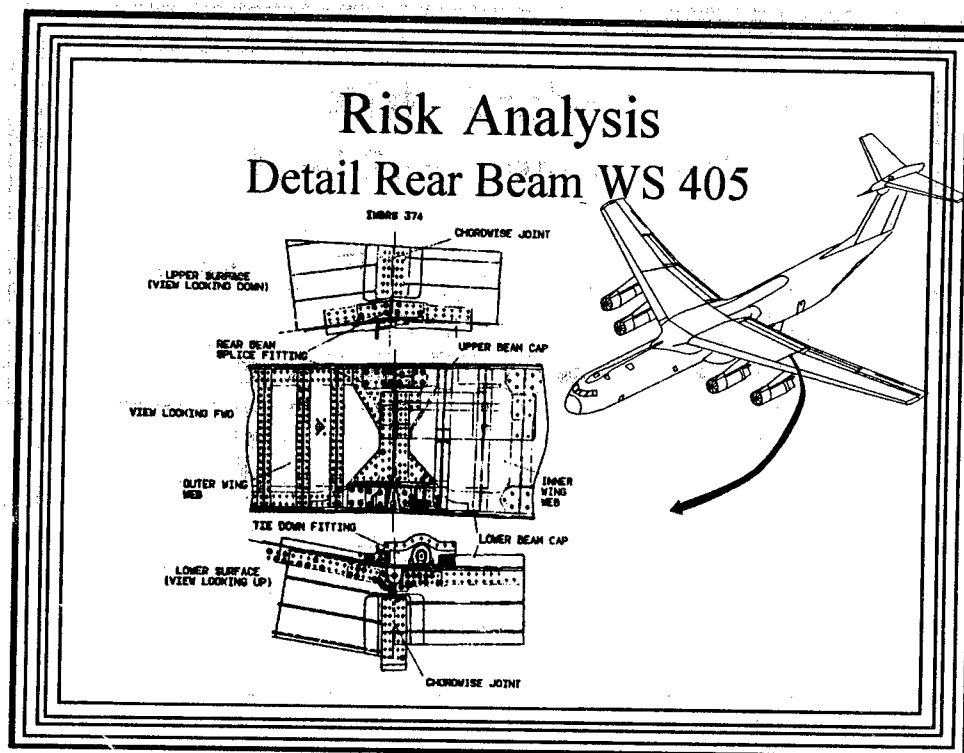
WS405 CRACK DISTRIBUTION



This slide shows the results of inspections carried out at the WS 405 Rear beam area. This inspection was precipitated by the discovery of two beam caps failed in this area on force aircraft. The risk analysis of the WS 405 inner to outer wing joint was precipitated by these discoveries.

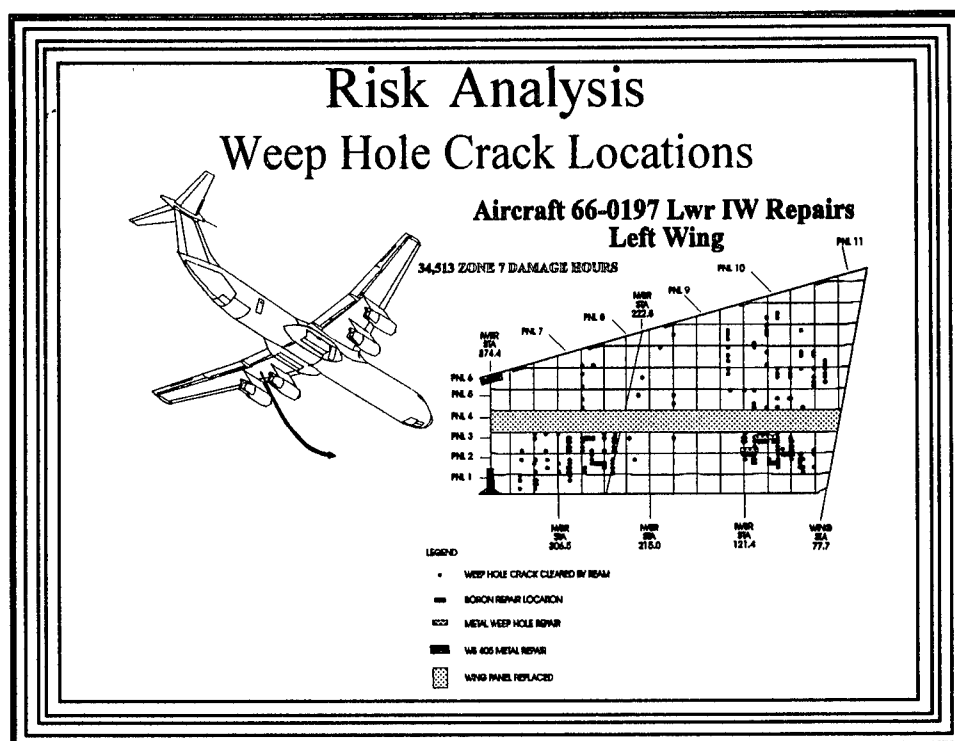
The original risk was carried out in the same fashion as the center wing risk and only examined failure of one element. This gave a very conservative answer and gave no insight into the proper procedures to put in place to guarantee the safety of the Force until repairs could be installed. Out of this came the need to produce a more realistic analysis which would take into account the fail-safety of the joint.

One of the problems with analyzing multi element structure is that of analyzing for the worst case, wherein the aircraft will theoretically have to be grounded. This does not take into account the real residual strength of the structure. Consequently, decisions are often made on "gut" feel, since the worst case option is usually rejected when it does not conform to reality, especially in times of crisis. However, it does relieve the analyst of any supposed responsibility. The failure tree concept gives at least a relative idea of what the risk really is. Note the grouping of the inspection data.



This shows the results of additional inspections carried out after the original risk analysis was concluded. These inspections verified the extent of cracking that had been hypothesized by the distributions used in the original risk analysis. The following were the major issues in this analysis.

1. For the final analysis, non-linear bolt loads were used in the Finite element model. Our first attempts used linear loads and it was felt that the distribution of stresses after first panel failure was inaccurate.
2. The worst mission of the average missions was used for the exceedance curves. There has been criticism of this because the projected design usage did not show that this particular mission was flown that often. However, force usage forms indicated that there was a high probability of this mission being flown.
3. The residual strength curve for the small cracks region was closed out by straight lining the data from 80% average yield stress to average yield stress.
4. Suspensions were not a problem since the number of replicates was a fairly high percentage of the total fasteners involved.
5. The POD curves were obtained from the 50% confidence curve of "Have Cracks".



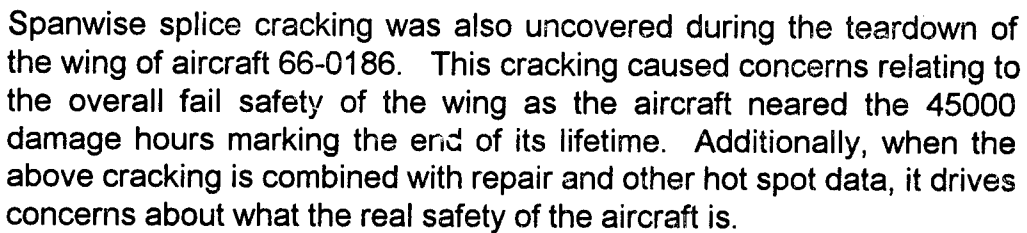
The weep hole problem came to light as a result of the appearance of large cracks on six aircraft. This prompted a teardown of a C-141 wing on a high damage aircraft (AC 66-0186). This data was then used to refine the original Risk calculations.

The risk analysis of the weep holes used the following methodology:

1. 6000 Hour spectra which was equivalent to the worst mission.
2. A linear overall model and several detail models were used to calculate the fail-safe stresses
3. Suspended data was not a factor since such a large number of the holes were cracked and inspection data was of superior quality since it was done in a laboratory type environment.
4. The Probability of Detection data was taken from "Have Cracks" and was based on the 50% confidence curve in this report. Additionally, this data was semi verified since it was possible to look at the original on aircraft data and compare it to the lab data after the wing was disassembled.
5. Failure trees were used and consideration was given to the effects of repairs on the risk.
6. A teardown of a high damage aircraft confirmed the original risk estimate

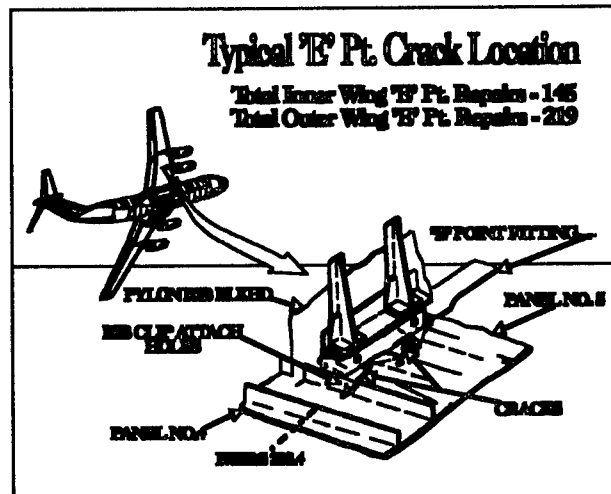
This analysis resulted in a force wide panel replacement and Boron repair program to ensure the operational capability of the C-141 Force.

Typical Spanwise Splice Cracking



552

Pylon E Point



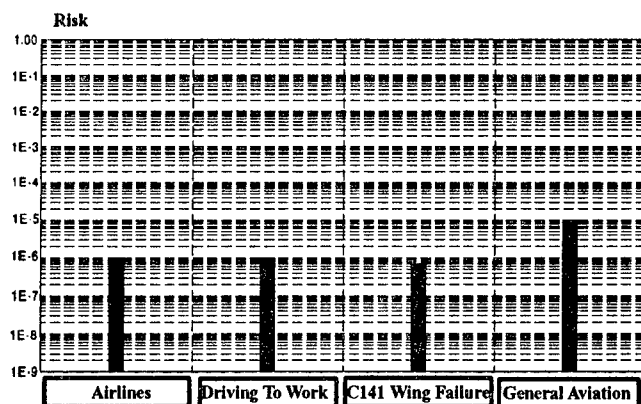
This shows the pylon E point. This area was included because cracking of the E point area has caused complete failures of wing panels on two aircraft. Inspection of the adjacent panel revealed no damage in the spanwise splices. The real danger to the spanwise splices occurs after the first panel failure which is more likely to be precipitated by other stress risers. This was demonstrated on the Specimen A failure picture shown earlier.

The analysis of the spanwise splices brought into play most of our methods. This included:

1. Failure trees, which included not only adjacent panels, but also repairs and other points affecting the spanwise splices.
2. Non-linear model combined with small crack test data for the fail-safe calculation.
3. Spectra which accounted for time and the effect of flying the worst mission.
4. Used "Have Cracks" PODs.
5. Suspensions were taken into account to give an apparent initial flaw distribution. Suspensions were input as flight hours before the distributions were turned.

Risk Analysis

RISK COMPARISONS



This table presents the different levels of risk in graphical form. Generally, the risk of a major accident while driving to and from work is 1E-6 (1 in a million). The probability of a fatal accident in a light plane is 1E-5 (1 in one hundred thousand). For safe operations of military aircraft the risk should not be greater than 1E-7 (1 in ten million). When the risk starts to exceed 1E-6 (1 in a million), consideration should be given to repair or replacement, and the risk can only exceed 1E-5 (1 in a hundred thousand) for a very short period of time (generally the time to bring corrective action to closure).

Risk Analysis Lessons Learned

- Failure Trees
- Need for better POD Data
- Non-Linear Finite Element Models
- Small Crack Data

The major lessons learned are as follows:

1. For multi element structure it is imperative to look at the overall probability of failure to get an accurate estimation of the Risk
2. There is a need for better and more accurate POD data, not only for Risk analysis, but also to be used in determining the correct detectable length for slow crack growth methods.
3. To do proper second element failure analysis and also to do regular fail-safe analysis, non-linear finite element models are required to determine the proper load distributions.
4. Small crack data is also needed for the same reasons as given in number three above.

Risk Analysis

Conclusions

- Useful for looking at Total Safety near the end of an Aircraft's useful Life
- Not for setting general Inspection Intervals
- Management tool for addressing unanticipated Force Problems

Risk analysis can be a useful tool for Structural Integrity Program managers. It is a tool for quantifying the actual state of health of an aircraft when it is faced with a short term problem. It definitely does not replace the present methods of slow crack growth for general Force Management. However, it may be useful for addressing aging aircraft problems in the future.